Topics in vortex methods for the computation of three- and two-dimensional incompressible unsteady flows

Thesis by
Grégoire Stéphane Winckelmans

In Partial Fulfillment of the Requirements
for the Degree of
Doctor of Philosophy

California Institute of Technology
Pasadena, California
1989
(Submitted February 24, 1989)

In memory of my father,

Marc Winckelmans

Acknowledgements

I wish to express my deepest gratitude to my advisor, Professor Anthony Leonard, for his guidance and support during my graduate studies. His dedication to research and education combined with his kindness and sense of humor were always appreciated.

I would also like to thank my friends at GALCIT for their contributions and encouragements, both personally and professionally.

Special thanks to my mother and father for their support during my studies. My only regret is that my father is not alive to share this accomplishment with me.

Many institutions helped with the completion of this work. I am also very grateful to them. The Belgian American Educational Foundation made it possible for me to obtain my Master's degree at Caltech. The research leading to this thesis was financially supported, for the first two years, by the NASA Ames Research Center under the university consortium agreement NCA2-90 and, for the last two years, by the Air Force under the AFOSR contract No. F49620-86-C-0134. The San Diego Supercomputer Center provided the computing support. This work would not have been possible if it were not for the possibility of using extensively their CRAY XMP-48.

Finally, special thanks to Karen Post for her patience and caring. I wish her the best for her future doctoral work.

Abstract

Contributions to vortex methods for the computation of incompressible unsteady flows are presented. Three methods are investigated, both theoretically and numerically.

The first method to be considered is the inviscid method of vortex filaments in three dimensions, and the following topics are presented: (a) review of the method of regularized vortex filaments and of convergence results for multiple-filament computations, (b) modeling of a vortex tube by a single filament convected with the regularized Biot-Savart velocity applied on the centerline: velocity of the thin filament vortex ring and dispersion relation of the rectilinear filament, and (c) development of a new regularization of the Biot-Savart law that reproduces the lowest mode dispersion relation of the rectilinear vortex tube in the range of large to medium wavelengths.

Next the method of vortex particles in three dimensions is investigated, and the following contributions are discussed: (a) review of the method of singular vortex particles: investigation of different evolution equations for the particle strength vector and weak solutions of the vorticity equation, (b) review of the method of regularized vortex particles and of convergence results, and introduction of a new algebraic smoothing with convergence properties as good as those of Gaussian smoothing, (c) development of a new viscous method in which viscous diffusion is taken into account by a scheme that redistributes the particle strength vectors, and application of the method to the computation of the fusion of two vortex rings at $Re = 400$, and (d) investigation of the particle method with respect to the conservation laws and derivation of new expressions for the evaluation of the quadratic diagnostics: energy, helicity and enstrophy.

The third method considered is the method of contour dynamics in two dimensions. The particular efforts presented are (a) review of the classical inviscid method and development of a new regularized version of the method, (b) development of a new vector particle version of the method, both singular and regularized: the method of *particles of vorticity gradient*, (c) development of a viscous version of the method of regularized particles and application of the method to computation of the reconnection of two vortex patches of same sign vorticity, and (d) investigation of the particle method with respect to the conservation laws and derivation of new expressions for the evaluation of linear and quadratic diagnostics.

Contents

Title Page i

Copyright ii

Dedication iii

Acknowledgements iv

Abstract v

Table of Contents vi

List of Figures xv

List of Tables xvi

1 Introduction 1

2 Three-dimensional vortex filaments 6

2.1 Some background 7

2.2 The method of vortex filaments 9

2.2.1 Singular vortex filaments 9

2.2.2 Regularized vortex filaments 11

2.3 The velocity of thin vortex rings 17

2.3.1 The general case 17

2.3.2 Some examples 19

2.4 Linearized perturbations of a straight vortex filament 22

2.4.1 Some background 22

2.4.2 Linearized perturbations of a vortex filament evolving under its own induced velocity applied on the centerline 24

2.4.2.1 The general case 24

2.4.2.2 Some examples 27

2.4.3 A three-dimensional velocity smoothing that reproduces Kelvin's lowest mode dispersion relation 30

2.5 Numerical results 38
2.5.1 Numerical verification of the dispersion relation 39
2.5.2 Results on vortex rings. 40
2.5.2.1 The velocity of the single-filament vortex ring 40
2.5.2.2 The stability of the single-filament vortex ring 40
2.5.3 Results on solitary waves on a rectilinear vortex filament . . . 42
2.5.4 Results on the interaction between vortex rings 45
2.5.4.1 The problem of the fusion of two vortex rings computed using the method of regularized vortex filaments 46
2.5.4.2 The problem of the two vortex rings in a "knot" configuration computed using the method of regularized vortex filaments 46

3 Three-dimensional vortex particles **47**
3.1 Singular vortex particles and weak solution of the vorticity equation . 48
3.2 Regularized vortex particles 54
3.3 Representation of viscous effects by the redistribution of particle strengths 59
3.4 The method of vortex particles with respect to the conservation laws 62
3.5 Numerical results 68
3.5.1 The problem of the fusion of two vortex rings: motivation and review of previous investigations 69
3.5.1.1 Experimental investigations 69
3.5.1.2 Numerical investigations 70
3.5.2 Some points that are common to all computations 71
3.5.3 The problem of the fusion of two vortex rings computed using the method of singular vortex particles 73
3.5.4 The problem of the fusion of two vortex rings computed using the inviscid version of the method of regularized vortex particles 74
3.5.5 The computation of a single vortex ring, inviscid and viscous: a test case for the convergence of the method of regularized vortex particles 75
3.5.6 The problem of the fusion of two vortex rings computed using the viscous version of the method of regularized vortex particles 82
3.5.7 The problem of the two vortex rings in a "knot" configuration: a test case for the consistency of the method of regularized vortex particles 87

4 Two-dimensional particles of vorticity gradient: an alternative to the method of contour dynamics **93**
4.1 An evolution equation for the vorticity gradient in two-dimensional flows 94
4.2 The method of contour dynamics or method of filaments of vorticity curl 95
4.2.1 The classical method of contour dynamics 95
4.2.2 A regularized version of the method of contour dynamics . . . 96
4.3 A particle method for the vorticity gradient 99
4.3.1 Singular particles of vorticity gradient 99
4.3.2 Singular particles of vorticity curl 101
4.3.3 Regularized particles of vorticity gradient 103
4.3.4 Representation of viscous effects by the redistribution of particle strengths 106
4.4 The method of filaments of vorticity curl and the method of particles of vorticity gradient with respect to the conservation laws 107
4.5 Numerical results 109
4.5.1 The short time diffusion of a circular vortex patch of uniform vorticity 110
4.5.2 The short time interaction between two vortex patches of uniform and same sign vorticity 113

5 Summary and conclusions **116**

A Conservation laws for two- and three-dimensional incompressible unbounded flows **119**
A.1 Three-dimensional unbounded flows 119
A.2 Two-dimensional unbounded flows 120

B The connection between regularized three-dimensional vortex filaments and regularized two-dimensional vortex particles **122**
B.1 The general case 122
B.2 Some examples 123

C Mathematical derivations needed in the development of a three-dimensional velocity smoothing that reproduces Kelvin's lowest mode dispersion relation. **129**

D The numerical computation of an infinite periodic vortex filament **137**

E The numerical computation of an infinite, non-periodic vortex filament 140

F The evolution equations for a set of vortex particles 142

G The evaluation of quadratic diagnostics when using vortex filaments or vortex particles 145

G.1 The singular case 145

G.1.1 Singular vortex filaments 145

G.1.2 Singular vortex particles 146

G.2 The regularized case 149

G.2.1 A note on quadratic diagnostics and regularized filament or particle methods 149

G.2.2 Regularized vortex filaments 151

G.2.3 Regularized vortex particles 151

H Three-dimensional vortex-dipoles 158

H.1 Singular vortex-dipoles 158

H.2 Regularized vortex-dipoles 159

H.3 The vortex-dipole as the limit of four vortex particles 162

H.4 Two-dimensional vortex-dipoles 163

I The evaluation of quadratic diagnostics when using filaments of vorticity curl or particles of vorticity gradient 167

I.1 The singular case 167

I.1.1 Singular filaments of vorticity curl 167

I.1.2 Singular particles of vorticity gradient 169

I.2 The regularized case 172

I.2.1 Regularized filaments of vorticity curl 172

I.2.2 Regularized particles of vorticity gradient 173

I.3 Some important remarks 176

References 178

J Figures 187

List of Figures

J.1 Some three-dimensional regularization functions: low order algebraic (short dash), high order algebraic (short chain-dot), Gaussian (solid), $e^{-\rho^3}$ (long chain-dot), $\mathrm{sech}^2(\rho^3)$ (long dash), Super-Gaussian (medium dash), constant (dot). 188

J.2 Roots of the dispersion relation for angular mode $m = +1$ (dot) and $m = -1$ (solid) for rectilinear vortex with uniform vorticity core. Circles indicate unstable crossing points and crosses stable crossing points in weak strain. (From Robinson & Saffman 1984). 188

J.3 Dispersion relation for a rectilinear vortex. Exact result for uniform vortex (solid). Vortex filaments using low order algebraic smoothing with $\beta = e^{-3/4}$ (dash), Gaussian with $\beta = (1/2^{1/2})\, e^{(\gamma/2-3/4)}$ (chain-dot), constant with $\beta = (1/2)\, e^{7/12}$ (dot). 189

J.4 Dispersion relation for a rectilinear vortex. Exact result of Kelvin (1880) for uniform vortex (solid). Approximation of exact result for different values of c^2 (chain-dot). Exact result for regularized vortex filament using the new simple algebraic velocity smoothing $q(\rho)$ with $\beta = e^{1/4}$ (dot). 190

J.5 New velocity smoothings $q(\rho)$: new velocity smoothing that reproduces the approximation of Kelvin's exact result (chain-dot), new simple algebraic velocity smoothing with $\beta = e^{1/4}$ (dot). For comparison, low order algebraic smoothing $g(\rho)$ with $\beta = e^{-3/4}$ (dash). 190

J.6 Numerical decoupling of the new velocity smoothing $q(\rho)$: $q(\rho)/\rho$ (solid), $q_\epsilon(\rho)/\rho$ for different values of ϵ (chain-dot). For comparison, low order algebraic smoothing $g(\rho)/\rho$ with $\beta = e^{-3/4}$ (dash). 191

J.7 Dispersion relation for a rectilinear vortex. Exact result of Kelvin (1880) (solid) and numerical results with new velocity smoothing $q(\rho)$ (diamond). Exact result for low order algebraic smoothing $g(\rho)$ and $\beta = e^{-3/4}$ (dash) and numerical results (square). 191

J.8 Dispersion relation for a rectilinear vortex. Exact result of Kelvin (1880) (solid). Numerical results using new velocity smoothing $q(\rho)$ with fixed N_λ and different values of ϵ (symbols). 192

J.9 Dispersion relation for a rectilinear vortex. Exact result of Kelvin (1880) (solid). Numerical results using new velocity smoothing $q(\rho)$ with fixed ϵ and different values of N_λ (symbols). 192
J.10 Velocity of a vortex ring. Lamb's asymptotic result for uniform vorticity core (solid), Fraenkel's asymptotic result (dot), Norbury's numerical result (short dash), low order algebraic $g(\rho)$ (dash) and new $q(\rho)$ (chain-dot). 193
J.11 Stability of a single-filament vortex ring ($\Gamma = 1.0$, $R = 1.0$, $\sigma_K = .50$): low order algebraic velocity smoothing $g(\rho)$ with $\beta = e^{-3/4}$ (left), new smoothing $q(\rho)$ (right). 194
J.12 The Hasimoto soliton for different values of the torsion parameter: (a) $T = 2.0$, (b) $T = 1.0$, (c) $T = .50$ (from Hasimoto 1972). 195
J.13 Perspective view of a solitary wave on a filament evolving under the full Biot-Savart velocity ($\Gamma = 1.0$, $T = .50$, $\sigma_K = .20$): low order algebraic smoothing $g(\rho)$ with $\beta = e^{-3/4}$ (left), new smoothing $q(\rho)$ (right). . . . 196
J.14 Perspective view of a solitary wave on a filament evolving under the full Biot-Savart velocity ($\Gamma = 1.0$, $T = .50$, $\sigma_K = .40$): low order algebraic smoothing $g(\rho)$ with $\beta = e^{-3/4}$ (left), new smoothing $q(\rho)$ (right). . . . 197
J.15 Perspective view of the collision of opposite but otherwise identical solitons on a filament evolving under LIA. Frames not uniformly spaced in time (from Aref & Flinchem 1984). 198
J.16 Perspective view of the collision of opposite but otherwise identical solitary waves on a filament evolving under the full Biot-Savart velocity. ($\Gamma = 1.0$, $T = .50$, $\sigma_K = .10$, new velocity smoothing $q(\rho)$). 199
J.17 The fusion of two vortex rings computed with the method of regularized vortex filaments. Perspective view of the filaments. 201
J.18 The "knot" problem computed with the method of regularized vortex filaments. Perspective view of the filaments. 203
J.19 Contour of integration for the evaluation of the inverse Fourier transform of $\hat{P}_1(l)$. 204
J.20 Contour of integration for the evaluation of the inverse Fourier transform of $\hat{P}_2(l)$. 204
J.21 The computation of an infinite periodic vortex filament. 205
J.22 The computation of an infinite non-periodic vortex filament. 205
J.23 Vorticity and velocity fields for an isolated regularized vortex particle (left) and for a infinite array of particles with $\sigma/h = 2.0$ (right) (The low order algebraic smoothing has been used). 207

J.24 The fusion and fission of two laminar vortex rings in water. Dye is used as a marker. (a) front view, (b) side view. Photographs from Schatzle (1987) and private communication. 209
J.25 Initial condition for the computation of the fusion of two vortex rings. 210
J.26 Discretization of the core of a vortex tube. Each cell has an equal area πr_l^2. 210
J.27 The fusion of two vortex rings computed with the method of singular vortex particles and using the transpose scheme. Perspectives view of the particle strength vectors α^p. 211
J.28 The fusion of two vortex rings computed with the method of singular vortex particles. Diagnostics I, E and E_f (dash). Transpose scheme (solid), classical scheme (chain-dash) and mixed scheme (chain-dot). . . 212
J.29 The fusion of two vortex rings computed with the inviscid method of regularized vortex particles. Perspectives view of the particle strength vectors α^p: (a) classical scheme, (b) transpose scheme. 213
J.30 The fusion of two vortex rings computed with the inviscid method of regularized vortex particles. $x-y$ projection of the particle strength vectors α^p: (a) classical scheme, (b) transpose scheme. 214
J.31 The fusion of two vortex rings computed with the inviscid method of regularized vortex particles. Diagnostics I, E_f. Transpose scheme (solid), classical scheme (chain-dash). 215
J.32 The single vortex ring computed with the inviscid method of regularized vortex particles. $n_c = 5$. Perspective view of the particle strength vectors α^p. 216
J.33 The single vortex ring computed with the viscous method of regularized vortex particles. $Re = 400$ and $n_c = 6$. Perspective view of the particle strength vectors α^p. 217
J.34 The single vortex ring computed with the method of regularized vortex particles. Vorticity contours: inviscid with $n_c = 5$ (left), viscous with $Re = 400$ and $n_c = 6$ (right). 220
J.35 The single vortex ring computed with the inviscid method of regularized vortex particles. $n_c = 5$. Diagnostics I, dX_c/dt, $\tilde{E}$ (solid) and $\tilde{E}_f$ (dash), $\tilde{\mathcal{E}}$ (solid) and $\tilde{\mathcal{E}}_f$ (dash). 221
J.36 The single vortex ring computed with the viscous method of regularized vortex particles. $Re = 400$ and $n_c = 6$. Diagnostics I, dX_c/dt, $\tilde{E}$ (solid) and $\tilde{E}_f$ (dash), $\tilde{\mathcal{E}}$ (solid) and $\tilde{\mathcal{E}}_f$ (dash). 222

J.37 The fusion of two vortex rings computed with the viscous method of regularized vortex particles. $Re = 400$. Perspective view of the particle strength vectors α^p. 227
J.38 The fusion of two vortex rings computed with the viscous method of regularized vortex particles. $Re = 400$. $x - y$ projection of the particle strength vectors α^p. 232
J.39 The fusion of two vortex rings computed with the viscous method of regularized vortex particles. $Re = 400$. $x - z$ projection of the particle strength vectors α^p. 237
J.40 The fusion of two vortex rings computed with the viscous method of regularized vortex particles. $Re = 400$. $y - z$ projection of the particle strength vectors α^p. 242
J.41 The fusion of two vortex rings computed with the viscous method of regularized vortex particles. $Re = 400$. Contours of out of plane vorticity: ω_y in $x - z$ plane (left), ω_x in $y - z$ plane (right). 247
J.42 The fusion of two vortex rings computed with the viscous method of regularized vortex particles. $Re = 400$. Contours of out of plane strain-rate: $\partial v/\partial y$ in $x - z$ plane (left), $\partial u/\partial x$ in $y - z$ plane (right). . 252
J.43 The fusion of two vortex rings computed with the viscous method of regularized vortex particles. $Re = 400$. Diagnostics I, Γ, $\tilde{E}$ (solid) and $\tilde{E}_f$ (dash), $\tilde{\mathcal{E}}$ (solid) and $\tilde{\mathcal{E}}_f$ (dash). 254
J.44 The fusion and fission of two vortex rings computed with the viscous method of regularized vortex particle. Low resolution computation with transpose scheme. Perspective view of the particle strength vectors α^p. 255
J.45 The fusion and fission of two vortex rings computed with the viscous method of regularized vortex particle. Low resolution computation with transpose scheme. Diagnostics I, $\tilde{E}$ (solid) and $\tilde{E}_f$ (dash). 256
J.46 Remeshing strategy for regularized vortex particles. 257
J.47 The "knot" problem computed with the method of regularized vortex particles. No remeshing and no relaxation of the vorticity divergence. Perspective view of the particle strength vectors α^p. 258
J.48 The "knot" problem computed with the method of regularized vortex particles. Remeshing but no relaxation of the vorticity divergence. Perspective view of the particle strength vectors α^p. 259

J.49 The "knot" problem computed with the method of regularized vortex particles. No remeshing but relaxation of the vorticity divergence. Perspective view of the particle strength vectors α^p. 260
J.50 The "knot" problem computed with the method of regularized vortex particles. Remeshing and relaxation of the vorticity divergence. Perspective view of the particle strength vectors α^p. 261
J.51 The "knot" problem computed with the method of regularized vortex particles. No remeshing and no relaxation of the vorticity divergence. Diagnostics I, A, $\tilde{E}$ (solid) and $\tilde{E}_f$ (dash), $\tilde{\mathcal{H}}$. 262
J.52 The "knot" problem computed with the method of regularized vortex particles. Remeshing but no relaxation of the vorticity divergence. Diagnostics I, A, $\tilde{E}$ (solid) and $\tilde{E}_f$ (dash), $\tilde{\mathcal{H}}$. 263
J.53 The "knot" problem computed with the method of regularized vortex particles. No remeshing but relaxation of the vorticity divergence. Diagnostics I, A, $\tilde{E}$ (solid) and $\tilde{E}_f$ (dash), $\tilde{\mathcal{H}}$. 264
J.54 The "knot" problem computed with the method of regularized vortex particles. Remeshing and relaxation of the vorticity divergence. Diagnostics I, A, $\tilde{E}$ (solid) and $\tilde{E}_f$ (dash), $\tilde{\mathcal{H}}$. 265
J.55 Vorticity and velocity fields for an isolated three-dimensional regularized vortex-dipole (The low order algebraic smoothing has been used). 266
J.56 (a) Two-dimensional regularized vortex-dipole as the limit of two two-dimensional regularized vortex particles. (b) Three-dimensional regularized vortex-dipole as the limit of four three-dimensional regularized vortex particles. 267
J.57 The short time diffusion of a circular vortex patch of uniform vorticity computed with the method of regularized particles of vorticity gradient: Vectors $\alpha^p \wedge \hat{\mathbf{e}}_z$ (left) , Vorticity contours (right). 268
J.58 Diagnostics for the short time diffusion of a circular vortex patch of uniform vorticity computed with the method of regularized particles of vorticity gradient: Ω, A, $\tilde{\mathcal{E}}$, $\tilde{E}$ (solid), E (dash) and E_{cd} (chain-dash).269
J.59 The short time interaction between two vortex patches of uniform and same sign vorticity computed with the method of regularized particles of vorticity gradient. Vectors $\alpha^p \wedge \hat{\mathbf{e}}_z$: inviscid (left), viscous (right). . . 272
J.60 Diagnostics for the short time inviscid interaction between two vortex patches of uniform and same sign vorticity computed with the method of regularized particles of vorticity gradient: Ω, A, $\tilde{\mathcal{E}}$, $\tilde{E}$ (solid), E (dash) and E_{cd} (chain dash). 273

J.61 Diagnostics for the short time viscous interaction between two vortex patches of uniform and same sign vorticity computed with the method of regularized particles of vorticity gradient: Ω, A, $\tilde{\mathcal{E}}$, $\tilde{E}$ (solid), E (dash) and E_{cd} (chain dash). 274

List of Tables

3.1 Parameters and numerical results at $t = 0$ for the computation of a single vortex ring with the method of regularized vortex particles. . . . 79
3.2 Parameters for the computation of the knot problem with the method of regularized vortex particles. 90

B.1 Three-dimensional regularization functions 127
B.2 Two-dimensional regularization functions 128

Chapter 1

Introduction

This thesis is concerned with the numerical computation, using vortex methods, of unsteady vortical flows of an incompressible fluid. This work originally focused on three-dimensional vortex methods. Insights gained during those investigations naturally led to the development of a new two-dimensional method as well. This explains why "three-dimensional" precedes "two-dimensional" in the title of this thesis.

Vortex methods are an alternative to Eulerian methods, i.e grid methods. They are Lagrangian methods that only require computational elements where the "action" is, i.e., where the vorticity is. In many flows of physical interest, only a small fraction of the entire flow volume is occupied by fluid that contains vorticity. The rest of the flow is essentially vorticity free. For an incompressible fluid, it is sufficient to follow only the evolution of the vorticity field because the velocity field can be computed from the vorticity field (the so-called Biot-Savart induction law) and from boundary conditions. The evolution of the vorticity field depends on whether the flow is inviscid or viscous.

For inviscid flows, it is known from the theorems of Kelvin and Helmholtz that vortex tubes retain their identity and simply move as material volumes. Inviscid flows can thus be represented with Lagrangian computational elements that are, roughly speaking, sections of a vortex tube. Each element is convected with the fluid velocity, and the vorticity vector associated to that element is strained by the local velocity gradient. This is essentially the method of three-dimensional vortex filaments which is reviewed in detail by Leonard (1980b,1985) (see also Saffman & Baker (1979) for a general review of vortex interactions). When the filaments are rectilinear, then only the projection of the filaments in the plane has to be considered. This is the method of two-dimensional vortex particles also called method of *vortex blobs*.

Two-dimensional vortex blobs have been and still are widely used. They are computationally more affordable than three-dimensional vortex filaments and have been used to investigate many interesting problems such as the time-developing shear layer (Nakamura, Leonard & Spalart 1982) and the space-developing shear layer (Ashurst 1979, Inoue 1985). The computation of separated flows has also been stud-

ied. Examples are Spalart & Leonard (1981), Spalart (1982) and Spalart, Leonard & Baganoff (1983). These efforts are still in progress (Chua K., private communication).

For two-dimensional problems with piecewise constant vorticity, the method of contour dynamics introduced by Zabusky & Hughes (1979) can be used instead of the method of vortex particles (Zabusky & Overman 1983, Dritschel 1985,1986, 1988). In this method, the boundaries of patches of uniform vorticity are convected by the fluid velocity. Because of the uniformity of the vorticity within each patch, the determination of the velocity field reduces to integrals along the patch boundaries only. This method is inviscid because it relies on the vorticity remaining uniform within each vortex patch.

For three-dimensional problems, the method of vortex filaments has been used to investigate already fairly complex vortical flows. Leonard (1980a,1981) used the method to investigate the evolution of a turbulent spot in a laminar boundary layer. Ashurst (1983) used it to study the evolution of the time-developing round jet. More recently, the method was used by Ashurst & Meiburg (1985) for the study of the time-developing three-dimensional shear layer and by Meiburg & Lasheras (1986) for the study of the time-developing three-dimensional plane wake. One must keep in mind that the method of vortex filaments is essentially inviscid and that only problems where the viscosity plays a minor role can be investigated using that method. Moreover, the method has problems when a single filament is used to model a physical tube of vorticity. The equations of motion, with proper rescaling, lead to a correct description of the dynamics of the vortex tube only when the perturbation wavelength is much bigger than the core size of the vortex tube. For wavelengths that are of the order of the core size, the dynamics are not resolved properly (Moore & Saffman 1972, Leonard 1985).

For viscous flows, the vorticity field is still convected by the velocity field, but it also diffuses. Vortex tubes do not necessarily retain their identity in time because of the possibility of reconnection of vortex lines by viscous diffusion. The method of vortex filaments cannot be used to compute such processes unless some form of filament surgery is used. A major contribution of this thesis will be the development of a viscous method of vortex particles that can take into account complex vortex tube interactions where the viscous diffusion plays an important role.

The body of this thesis is divided into three chapters. Each chapter covers a different method and can almost be read independently. Moreover, each chapter has its own introduction, which contains additional details not included in the present global introduction. The outline of the thesis is as follows:

- Chapter 2 is concerned with the method of three-dimensional vortex filaments.

The method of regularized filaments (Leonard 1980b, 1985) is reviewed in detail. In particular, two issues related to the modeling of a vortex tube with a single vortex filament evolving under the Biot-Savart velocity applied on the centerline are investigated: 1) the velocity of the single-filament vortex ring and 2) the dispersion relation of the perturbed rectilinear vortex filament (Leonard 1985). Both issues are closely related. The analysis provides the appropriate scaling that reproduces the correct velocity of the thin ring and the correct dispersion relation of the thin vortex tube. This scaling is applied to many vorticity distributions of numerical interest, and the numerical values for the scaling factors are also provided. It is shown however that the vortex filament does not reproduce the correct dispersion relation of the vortex tube as soon as the perturbation wavelength is smaller than five times or so the vortex tube core size. This failure is responsible for the development of spurious instabilities in numerical computations. A new regularization of the Biot-Savart integral is proposed. This regularization forces the single filament to correctly reproduce the exact dispersion relation of the vortex tube of uniform vorticity in the range of large to medium perturbation wavelengths.

- Chapter 3 is concerned with the method of three-dimensional vortex particles, also commonly called *vortex sticks* or *vortons* (Rehbach 1978, Beale & Majda 1982a, 1982b, Novikov 1983, Aksman, Novikov & Orszag 1985, Mosher 1985, Beale 1986b, Saffman & Meiron 1986, Choquin & Cottet 1988). These vortex particles are vector elements (vorticity vector $\times$ volume). The element is convected with the fluid velocity, and the strength vector is stretched in accordance with the velocity gradient tensor. Different evolution equations for the strength vector are investigated. This chapter is related to Chapter 2 because a vortex particle is, to a certain extent, a discretization of a vortex filament. Vortex particles are however not "connected" to neighbor particles for all times as opposed to the situation for vortex filaments, where adjacent computational points are always connected by the filament itself. The lack of connectivity introduces consistency problems, because the vorticity field represented by a collection of vortex particles does not necessarily remain divergence free for all times. However, there is an advantage in that one can introduce viscous diffusion in the method. In this thesis, a new viscous method is proposed in which viscous diffusion is taken into account by a scheme that redistributes the particle strength vectors in a way that is consistent with viscous diffusion. The treatment of viscous diffusion in such a manner was introduced by Mas-Gallic (1987) and Degond & Mas-Gallic (1988a,1988b) (see also Cottet & Mas-Gallic 1983,1987) in the general frame-

work of solving a convection-diffusion equation using a particle method. Their theoretical developments are applied to the method of three-dimensional vortex particles. It is shown numerically that the method is indeed consistent with viscous diffusion at a quantitative level, and that complex problems can be computed using this method. In particular, the viscous fusion of two vortex rings at a Reynolds number of 400 is computed, and the numerical results are compared not only qualitatively, but also quantitatively with the experimental results of Schatzle & Coles (1987 and private communication). Numerical evidence is also provided that the viscous method helps reduce the consistency problems of the method of vortex particles by keeping the divergence of the particle vorticity field at a low level.

- Finally, Chapter 4 is concerned with vortex methods for two-dimensional flows. Both filament (i.e., contour) and vector particle methods are investigated. The filament method is the now classical inviscid method of contour dynamics introduced by Zabusky & Hughes (1979) (see also Zabusky 1981, Zabusky & Overman 1983, Dritschel 1985, 1986). It is an inviscid method in which the boundaries of vortex patches of constant vorticity are convected by the velocity field. The velocity field only depends on the position of the boundaries. A regularized version of the method of contour dynamics is proposed that should help solve some of the problems encountered with the classical method, such as excessive generation of contour length and subsequent need for *contour surgery* (Dritschel 1988). This regularized version of the method of contour dynamics is also inviscid. A new particle version of the method is also proposed, and both the inviscid and viscous versions of the method are developed. These particles are vector elements (gradient of vorticity vector $\times$ area). The element is convected by the velocity field, and the strength vector is subjected to the two-dimensional evolution equation for the vorticity gradient. This method is, to the method of contour dynamics, what the method of vortex particles is, in three dimensions, to the method of vortex filaments. In particular, it is shown that the viscous version of the method can account for the process of reconnection of vortex patches by viscous diffusion. This reconnection process, although two-dimensional, is very similar to the three-dimensional process of vortex tube reconnection (as encountered in the problem of the fusion of two vortex rings).

Some remarks that apply to all three chapters:

- The present thesis is devoted to the improvement of vortex methods per se, i.e., to the development of vortex methods that are accurate and that correctly

reproduce the physics of vorticity in free space, both inviscid and viscous. The problems related to boundary conditions and to the creation of vorticity at the wall are of course of great physical interest but are not addressed in this thesis. Only unbounded problems are considered.

- A particular effort is placed on the correct evaluation of diagnostics. These diagnostics are used extensively to measure the performance of the numerical computations.

- The computation of the velocity field (from the vorticity field in three dimensions and from the vorticity gradient field in two dimensions) is always carried by summing over all the computational elements. If there are N such elements, the computational effort is thus $\mathcal{O}(N^2)$ at every time step. It is understood that this scheme is simple but costly and is not viable as soon as the number of computational elements becomes large. Even on the CRAY XMP-48, the available resources tend to limit the number of computational elements to $N \simeq 10,000$. Two-dimensional schemes that require a grid and are only $\mathcal{O}(M \log M) + \mathcal{O}(N)$ (where the grid is $M \times M$) already exist (Anderson 1986). Fast methods that are grid free have also been developed (Appel 1985). and are still under investigation (Pepin, F., private communication). In three-dimensions, fast methods are just emerging (Greengard 1987). The theoretical developments have been completed but the method has not yet been implemented. The implementation of fast algorithms should be the next important step in the development of three-dimensional vortex methods for very large scale scientific computations. This thesis work is however oriented towards the development of accurate, widely applicable vortex methods, not towards the development of fast vortex methods. It is hoped that both efforts will meet eventually, and that a fast algorithm will be combined with the three-dimensional viscous method of vortex particles presented in this thesis.

Chapter 2

Three-dimensional vortex filaments

This chapter is concerned with the computation of three-dimensional incompressible inviscid flows using the method of vortex filaments. It also serves the purpose of introducing the notation used throughout the thesis. Earlier reviews of the method along with some applications may be found in Leonard (1980b,1985).

The justification of the method of vortex filaments and the necessary background are reviewed in Section 2.1. The method itself is reviewed in detail in Section 2.2. It is shown that singular filaments cannot be used, and that a regularization of some sort is necessary. In particular, the regularized method of Leonard (1975,1980a,1980b,1981,1985) is reviewed. A generalized Hamiltonian formulation (Agishtein & Migdal 1986) is also presented. The behavior of the method with respect to the conservation laws is reviewed as well (Leonard 1980b,1985), together with convergence results (Greeengard 1986) related to multiple-filament computations. A new regularization function that is algebraic but has convergence properties similar to the Gaussian regularization is also introduced.

In the next two sections, Section 2.3 and Section 2.4, the modeling of a vortex tube with a single filament subjected to the Biot-Savart velocity applied on the centerline is examined. In Section 2.3, the velocity of the single-filament vortex ring is examined. The asymptotic velocity formula for the thin filament vortex ring (Leonard 1985) is compared with the asymptotic formula for the thin tube vortex ring (Saffman 1970). Many vorticity distributions are investigated in detail. (The connection between three- and two-dimensional vorticity distributions is also examined in detail in Appendix B, and tables of three- and two-dimensional regularization functions are provided). A matching procedure that correctly reproduces the asymptotic velocity of the thin tube vortex ring (Moore & Saffman 1972, Leonard 1985) is reviewed. This procedure amounts to a rescaling of the filament core size with respect to the tube core size. In Section 2.4, a related problem is examined: the linearized perturbations of the rectilinear vortex tube (Kelvin 1880, Widnall, Bliss & Tsai 1974, Moore & Saffman 1972, 1975, Tsai & Widnall 1976, Widnall & Tsai 1977, Robinson & Saffman 1984) and the linearized perturbations of the rectilinear vortex filament

evolving under the centerline velocity (Leonard 1985). In particular, the dispersion relation for the vortex filament is computed for three typical vorticity distributions over the full range of wavelengths. It is shown that the centerline scheme, together with the rescaling of the core size, correctly reproduces the dispersion relation of the vortex tube when the perturbation wavelength is large compared with the core size. However, it is also shown that the scheme does not reproduce the dispersion relation of the vortex tube (for the lowest order perturbation mode, i.e., the mode with unperturbed core structure) as soon as the perturbation wavelength is smaller than roughly five times the core size. This behavior is related to the appearance of spurious numerical instabilities when performing single-filament computations. A new regularization scheme for the dynamics of the vortex filament is proposed. This scheme forces the single vortex filament to correctly reproduce the dispersion relation of the vortex tube for the lowest perturbation mode.

Finally, Section 2.5 is reserved for the numerical results obtained using usual regularization schemes as well as this new regularization scheme. Several problems are analyzed: dispersion relation of the straight filament, velocity and stability of the single-filament vortex ring, and solitary waves on a straight filament. Some multiple-filament computations that involve vortex ring interactions are also discussed.

2.1 Some background

The three-dimensional momentum equation for a constant-density fluid can be written as

$$\frac{\partial \mathbf{u}}{\partial t} + \boldsymbol{\omega} \wedge \mathbf{u} = -\nabla \left(\frac{p}{\rho} + \frac{\mathbf{u} \cdot \mathbf{u}}{2} \right) + \nu \nabla^2 \mathbf{u} \,, \tag{2.1}$$

where $\mathbf{u}(\mathbf{x}, t)$ is the velocity field, $\boldsymbol{\omega}(\mathbf{x}, t) = \nabla \wedge \mathbf{u}(\mathbf{x}, t)$ is the vorticity field, p is the pressure field, ρ is the density and ν is the kinematic viscosity. The three-dimensional vorticity equation is obtained by taking the curl of Equation (2.1). This gives

$$\frac{\partial \boldsymbol{\omega}}{\partial t} + \nabla \wedge (\boldsymbol{\omega} \wedge \mathbf{u}) = \nu \nabla^2 \boldsymbol{\omega} \,, \tag{2.2}$$

Using the properties that $\nabla \cdot \mathbf{u} = 0$ and $\nabla \cdot \boldsymbol{\omega} = \nabla \cdot (\nabla \wedge \mathbf{u}) = 0$, Equation (2.2) can be rewritten as

$$\frac{\partial \boldsymbol{\omega}}{\partial t} + (\mathbf{u} \cdot \nabla)\, \boldsymbol{\omega} = (\boldsymbol{\omega} \cdot \nabla)\, \mathbf{u} + \nu \nabla^2 \boldsymbol{\omega} \,, \tag{2.3}$$

or

$$\frac{\partial \boldsymbol{\omega}}{\partial t} + \nabla \cdot (\boldsymbol{\omega}\, \mathbf{u}) = (\boldsymbol{\omega} \cdot \nabla)\, \mathbf{u} + \nu \nabla^2 \boldsymbol{\omega} \,, \tag{2.4}$$

or

$$\frac{\partial \boldsymbol{\omega}}{\partial t} + \nabla \cdot (\boldsymbol{\omega}\, \mathbf{u}) = \nabla \cdot (\mathbf{u}\, \boldsymbol{\omega}) + \nu \nabla^2 \boldsymbol{\omega} \,. \tag{2.5}$$

Recalling that the evolution equation for a material line element $\delta\mathbf{l}$ is given by (Batchelor 1967)

$$\frac{\partial \delta\mathbf{l}}{\partial t} + (\mathbf{u}\cdot\nabla)\,\delta\mathbf{l} = (\delta\mathbf{l}\cdot\nabla)\,\mathbf{u}\,, \tag{2.6}$$

it follows that, for inviscid flows, vortex lines move as material lines (Helmholtz).

A vortex tube is defined as the collection of vortex lines that pierce a given surface patch S. The circulation of a vortex tube is defined as

$$\Gamma = \int_S \boldsymbol{\omega}\cdot d\mathbf{x} = \int_{\partial S} \mathbf{u}\cdot d\mathbf{x}\,, \tag{2.7}$$

where the last equality is obtained by the use of Stokes' theorem with ∂S the contour bounding the curve S. Because $\nabla\cdot\boldsymbol{\omega} = 0$, the circulation of a vortex tube is the same for all oriented surface patches that define the vortex tube (Helmholtz).

Using Equation (2.1), it is easy to show that

$$\frac{d}{dt}\Gamma = \nu \int_{\partial S} \nabla^2\mathbf{u}\cdot d\mathbf{x} = -\nu \int_{\partial S} \nabla\wedge\boldsymbol{\omega}\cdot d\mathbf{x} = \nu \int_S \nabla^2\boldsymbol{\omega}\cdot d\mathbf{x}\,, \tag{2.8}$$

where Stoke's theorem and the identity $\nabla\wedge(\nabla\wedge) = -\nabla^2 + \nabla(\nabla\cdot)$ have been used. For inviscid flows, Equation (2.8) reduces to

$$\frac{d}{dt}\Gamma = 0\,, \tag{2.9}$$

and the circulation of a vortex tube is conserved (Kelvin).

Vortex tubes are thus interesting entities in inviscid flows: they move as material volumes, and they retain their circulation, i.e., they preserve their identity. These facts form the basis for the method of vortex filaments.

For viscous flows, the concept of a vortex tube is not as useful. Of course one can define vortex tubes at every instant and associate to each vortex tube a unique circulation which is still independent of where it is measured along the vortex tube. This is kinematics only. Unfortunately, vortex tubes do not retain their identity because of viscous diffusion. Indeed, according to Equation (2.8), the rate of change of the circulation in one section of a vortex tube is not necessarily the same as the rate of change in any other section. This fact and the concept of vortex tubes with unique circulation are incompatible unless vortex tubes are allowed to reconnect.

2.2 The method of vortex filaments

2.2.1 Singular vortex filaments

Singular vortex filaments are space curves of zero cross-sectional area but finite circulation. They define the vorticity field

$$\boldsymbol{\omega}(\mathbf{x},t) = \sum_p \Gamma^p \int_{\mathcal{C}^p(t)} \delta(\mathbf{x}-\mathbf{x}^p)\,\frac{\partial \mathbf{x}^p}{\partial s}\,ds\,, \tag{2.10}$$

where $\mathbf{x}^p$ stands for $\mathbf{x}^p(s,t)$, s is a Lagrangian coordinate (not necessarily a length coordinate!), Γ^p is the circulation of the p filament and $\delta(\mathbf{x})$ is the three-dimensional δ-function.

The velocity field $\mathbf{u}(\mathbf{x},t)$ is computed from the filament representation of the vorticity field as the curl of a streamfunction which solves $\nabla^2\boldsymbol{\psi}(\mathbf{x},t) = -\boldsymbol{\omega}(\mathbf{x},t)$. Recalling that the Green's function for $-\nabla^2$ in a three-dimensional unbounded domain is given by $G(\mathbf{x}) = 1/(4\pi\,|\mathbf{x}|)$, one obtains, for the streamfunction,

$$\boldsymbol{\psi}(\mathbf{x},t) = G(\mathbf{x}) * \boldsymbol{\omega}(\mathbf{x},t) = \frac{1}{4\pi}\sum_p \Gamma^p \int_{\mathcal{C}^p(t)} \frac{1}{|\mathbf{x}-\mathbf{x}^p|}\,\frac{\partial \mathbf{x}^p}{\partial s}\,ds\,, \tag{2.11}$$

where $*$ stands for the convolution product. The velocity is taken as the curl of (2.11) and is given by

$$\begin{aligned}
\mathbf{u}(\mathbf{x},t) &= \nabla\wedge\boldsymbol{\psi}(\mathbf{x},t) \\
&= \frac{1}{4\pi}\sum_p \Gamma^p \int_{\mathcal{C}^p(t)} \nabla\left(\frac{1}{|\mathbf{x}-\mathbf{x}^p|}\right)\wedge\frac{\partial \mathbf{x}^p}{\partial s}\,ds \\
&= -\frac{1}{4\pi}\sum_p \Gamma^p \int_{\mathcal{C}^p(t)} \frac{1}{|\mathbf{x}-\mathbf{x}^p|^3}(\mathbf{x}-\mathbf{x}^p)\wedge\frac{\partial \mathbf{x}^p}{\partial s}\,ds \\
&= \sum_p \Gamma^p \int_{\mathcal{C}^p(t)} \mathbf{K}(\mathbf{x}-\mathbf{x}^p)\wedge\frac{\partial \mathbf{x}^p}{\partial s}\,ds = (\mathbf{K}(\mathbf{x})\wedge) * \boldsymbol{\omega}(\mathbf{x},t)\,,
\end{aligned} \tag{2.12}$$

where $\mathbf{K}(\mathbf{x})\wedge = -\left(1/\left(4\pi|\mathbf{x}|^3\right)\right)\,\mathbf{x}\wedge$ and is known as the Biot-Savart kernel.

It can be shown that the vorticity and the streamfunction are divergence free. This comes as a consequence of the fact that the contours $\mathcal{C}^p(t)$ are closed. The velocity is also divergence free because it is taken as the curl of a streamfunction. In the most general case, a potential velocity field, $\nabla\phi$, must be added to the above velocity field in order to satisfy boundary conditions (such as a free-stream velocity or a flow tangency condition at a solid boundary). The problems associated with boundary conditions are not investigated in this thesis. Only unbounded problems are considered.

The singular vortex filaments presented above are not useful in numerical computations. They simply are too singular. Indeed, it is easily seen that the velocity

induced by a singular filament diverges like $1/|\mathbf{x}-\mathbf{x}(s,t)|$ for points approaching the filament from a direction other than the direction of the filament itself. This divergence is similar to the $1/r$ divergence of point vortices in two dimensions. Moreover, a singular filament has an infinite self-induced velocity everywhere its curvature is non-zero (Batchelor 1967). Indeed, a Taylor series expansion of $\mathbf{x}(s',t)$ about $\mathbf{x}(s,t)$ leads to

$$\begin{aligned}(\mathbf{x}-\mathbf{x}')\wedge\frac{\partial\mathbf{x}'}{\partial s'} &= \frac{(s'-s)^2}{2}\left(\frac{\partial^2\mathbf{x}}{\partial s^2}\wedge\frac{\partial\mathbf{x}}{\partial s}\right)+\frac{(s'-s)^3}{3}\left(\frac{\partial^3\mathbf{x}}{\partial s^3}\wedge\frac{\partial\mathbf{x}}{\partial s}\right)+\mathcal{O}\left((s'-s)^4\right)\,,\\ |\mathbf{x}-\mathbf{x}'|^2 &= (s'-s)^2\left(\frac{\partial\mathbf{x}}{\partial s}\cdot\frac{\partial\mathbf{x}}{\partial s}\right)+(s'-s)^3\left(\frac{\partial^2\mathbf{x}}{\partial s^2}\cdot\frac{\partial\mathbf{x}}{\partial s}\right)+\mathcal{O}\left((s'-s)^4\right)\,,\end{aligned} \tag{2.13}$$

so that the self-induced velocity becomes

$$\frac{\partial}{\partial t}\mathbf{x}(s,t)=-\frac{\Gamma}{8\pi}\left[\frac{\left(\frac{\partial^2\mathbf{x}}{\partial s^2}\wedge\frac{\partial\mathbf{x}}{\partial s}\right)}{\left(\frac{\partial\mathbf{x}}{\partial s}\cdot\frac{\partial\mathbf{x}}{\partial s}\right)^{\frac{3}{2}}}\int^{s'}\frac{ds'}{|s'-s|}+\mathcal{O}(1)\right]\,, \tag{2.14}$$

which results in a logarithmic divergence. Notice that a two-dimensional point vortex is the projection, in the plane, of a singular filament that is straight and perpendicular to the plane. Consequently, a point vortex has zero self-induced velocity since the equivalent filament has no curvature.

There is an interesting point about filaments which is reported in Agishtein & Migdal (1986): one can define the generalized Hamiltonian (i.e., the kinetic energy)

$$E=\frac{1}{2}\int\boldsymbol{\psi}\cdot\boldsymbol{\omega}\,d\mathbf{x}=\frac{1}{8\pi}\sum_{p,q}\Gamma^p\,\Gamma^q\int_{\mathcal{C}^p(t)}\int_{\mathcal{C}^q(t)}\frac{1}{|\mathbf{x}^p-\mathbf{x}^q|}\left(\frac{\partial\mathbf{x}^p}{\partial s}\cdot\frac{\partial\mathbf{x}^q}{\partial s'}\right)ds\,ds'\,, \tag{2.15}$$

and write, for the equations of motion,

$$\frac{2}{\Gamma^p}\frac{\delta E}{\delta x_i^p}=\left(\frac{\partial\mathbf{x}^p}{\partial s}\,ds\wedge\frac{\partial\mathbf{x}^p}{\partial t}\right)_i\,. \tag{2.16}$$

This is very similar to point vortices in two dimensions for which the Hamiltonian is given by

$$E=\frac{1}{2}\int\psi\,\omega\,d\mathbf{x}=-\frac{1}{4\pi}\sum_{\substack{p,q\\p\neq q}}\Gamma^p\,\Gamma^q\,\log\left(\frac{|\mathbf{x}^p-\mathbf{x}^q|}{a}\right)\,, \tag{2.17}$$

with the property that

$$\frac{2}{\Gamma^p}\frac{\delta E}{\delta x_i^p}=\left(\hat{\mathbf{e}}_z\wedge\frac{d\mathbf{x}^p}{dt}\right)_i\,. \tag{2.18}$$

Notice that the $q=p$ term has been excluded in Equation (2.17). The Hamiltonian is thus finite, and Equation (2.18) indeed defines the dynamics of point vortices with zero

self-induced velocity. In Equation (2.15), the $q = p$ term cannot be excluded because this would amount to excluding entire filaments. Consequently, the Hamiltonian is infinite, and Equation (2.16) defines the dynamics of vortex filaments with infinite self-induced velocity. The Hamiltonian formulation of singular vortex filaments is thus not very useful.

The only way to obtain a finite Hamiltonian and a zero local contribution to the self-induced velocity is to exclude parts of the filament $d\mathbf{x}^p = d\mathbf{x}^q$ in the Hamiltonian. This is essentially the *cut-off* method as used by Hama (1962,1963) and others (see also Leonard (1980b,1985)). In the next section, the method of regularized vortex filaments as used by Moore(1972), Leonard (1975,1980a,1980b,1985), Ashurts & Meiburg (1985), Meiburg & Lasheras (1986) and others is presented. In this method, the vorticity distribution along the filament is regularized. The Hamiltonian is well defined and the local contribution to the self-induced velocity is zero.

2.2.2 Regularized vortex filaments

Regularized vortex filaments yield the vorticity field

$$\boldsymbol{\omega}_\sigma(\mathbf{x},t) = \zeta_\sigma(\mathbf{x}) * \boldsymbol{\omega}(\mathbf{x},t) = \sum_p \Gamma^p \int_{\mathcal{C}^p(t)} \zeta_\sigma(\mathbf{x}-\mathbf{x}^p)\,\frac{\partial \mathbf{x}^p}{\partial s}\,ds\ , \tag{2.19}$$

where ζ_σ is an appropriate regularization function (i.e., an approximation to the δ-function) which is usually taken as radially symmetric, and σ is a smoothing radius (i.e., a cut-off length or core size), i.e.,

$$\zeta_\sigma(\mathbf{x}) = \frac{1}{\sigma^3}\,\zeta\left(\frac{|\mathbf{x}|}{\sigma}\right)\ , \tag{2.20}$$

with the normalization

$$4\pi \int_0^\infty \zeta(\rho)\,\rho^2\,d\rho = 1\ . \tag{2.21}$$

The function ζ_σ defines the vorticity distribution within the core of the vortex filament.

The velocity field is computed from the filament representation of the vorticity field as the curl of a streamfunction which solves $\nabla^2\boldsymbol{\psi}_\sigma(\mathbf{x},t) = -\boldsymbol{\omega}_\sigma(\mathbf{x},t)$. Defining $\chi(\rho)$ such that

$$-\zeta(\rho) = \nabla^2\chi(\rho) = \frac{1}{\rho^2}\frac{d}{d\rho}\left(\rho^2\frac{d\chi}{d\rho}\right) = \frac{1}{\rho}\frac{d^2}{d\rho^2}\left(\rho\,\chi(\rho)\right)\ , \tag{2.22}$$

one obtains, for the streamfunction,

$$\begin{aligned}\boldsymbol{\psi}_\sigma(\mathbf{x},t) &= G(\mathbf{x}) * \boldsymbol{\omega}_\sigma(\mathbf{x},t) = \chi_\sigma(\mathbf{x}) * \boldsymbol{\omega}(\mathbf{x},t)\\ &= \sum_p \Gamma^p \int_{\mathcal{C}^p(t)} \chi_\sigma(\mathbf{x}-\mathbf{x}^p)\,\frac{\partial \mathbf{x}^p}{\partial s}\,ds\ ,\end{aligned} \tag{2.23}$$

where

$$\chi_\sigma(\mathbf{x}) = \frac{1}{\sigma}\,\chi\left(\frac{|\mathbf{x}|}{\sigma}\right) . \tag{2.24}$$

A function $g(\rho)$ is now defined as

$$g(\rho) = \int_0^\rho \zeta(t)\, t^2\, dt . \tag{2.25}$$

This function will be needed extensively in the present Chapter as well as in Chapter 3. From the normalization condition (2.21), it follows that $4\pi\, g(\rho) \to 1$ as $\rho \to \infty$. Since $\zeta(\rho)$ is $\mathcal{O}(1)$ for small ρ, it follows that $g(\rho)$ is $\mathcal{O}(\rho^3)$ for small ρ.

The following relations between $g(\rho)$, $\chi(\rho)$ and $\zeta(\rho)$ will also prove very useful. First, from the definition of $g(\rho)$,

$$\frac{g'(\rho)}{\rho^2} = \zeta(\rho) . \tag{2.26}$$

Second, from the definition of $g(\rho)$ and $\chi(\rho)$,

$$g(\rho) = \int_0^\rho \zeta(t)\, t^2\, dt = -\int_0^\rho \frac{d}{dt}\left(t^2\,\frac{d\chi}{dt}\right) dt = -\rho^2\,\chi'(\rho) , \tag{2.27}$$

so that

$$\frac{\chi'(\rho)}{\rho} = -\frac{g(\rho)}{\rho^3} . \tag{2.28}$$

Finally, from Equation (2.26),

$$\frac{1}{\rho}\frac{d}{d\rho}\left(\frac{g(\rho)}{\rho^3}\right) = \frac{g'(\rho)}{\rho^4} - 3\,\frac{g(\rho)}{\rho^5} = \frac{1}{\rho^2}\left(\zeta(\rho) - 3\,\frac{g(\rho)}{\rho^3}\right) . \tag{2.29}$$

From Equation (2.28), it follows that $\chi(\rho)$ is $\mathcal{O}(\rho^2)$ for small ρ and that $\chi(\rho) \to 1/(4\pi\rho)$ as $\rho \to \infty$.

Now, consider the velocity given by the curl of the streamfunction (2.23). Recalling that $\rho = |\mathbf{x}|/\sigma$, with $\partial\rho/\partial x_i = x_i/(\sigma^2\rho)$, one obtains, with the help of Equation (2.28),

$$\begin{aligned}
\frac{\partial}{\partial x_i}\,\chi_\sigma(\mathbf{x}) &= \frac{1}{\sigma}\,\frac{\partial}{\partial x_i}\,\chi(\rho) = \frac{1}{\sigma}\,\frac{\partial\rho}{\partial x_i}\,\chi'(\rho) = \frac{1}{\sigma^3}\,x_i\,\frac{\chi'(\rho)}{\rho} \\
&= -\frac{1}{\sigma^3}\,x_i\,\frac{g(\rho)}{\rho^3} = -\frac{g(\rho)}{|\mathbf{x}|^3}\,x_i ,
\end{aligned} \tag{2.30}$$

so that the velocity finally becomes

$$\begin{aligned}
\mathbf{u}_\sigma(\mathbf{x},t) &= \nabla\wedge\boldsymbol{\psi}_\sigma(\mathbf{x},t) = \sum_p \Gamma^p \int_{C^p(t)} \nabla\left(\chi_\sigma(\mathbf{x}-\mathbf{x}^p)\right)\wedge\frac{\partial\mathbf{x}^p}{\partial s}\,ds \\
&= -\sum_p \Gamma^p \int_{C^p(t)} \frac{g_\sigma(\mathbf{x}-\mathbf{x}^p)}{|\mathbf{x}-\mathbf{x}^p|^3}(\mathbf{x}-\mathbf{x}^p)\wedge\frac{\partial\mathbf{x}^p}{\partial s}\,ds \\
&= \sum_p \Gamma^p \int_{C^p(t)} \mathbf{K}_\sigma(\mathbf{x}-\mathbf{x}^p)\wedge\frac{\partial\mathbf{x}^p}{\partial s}\,ds = (\mathbf{K}_\sigma(\mathbf{x})\wedge) * \boldsymbol{\omega}(\mathbf{x},t) ,
\end{aligned} \tag{2.31}$$

where

$$g_\sigma(\mathbf{x}) = g\left(\frac{|\mathbf{x}|}{\sigma}\right) , \tag{2.32}$$

and

$$\mathbf{K}_\sigma(\mathbf{x})\wedge = -(g_\sigma(\mathbf{x})/|\mathbf{x}|^3)\,\mathbf{x}\wedge \tag{2.33}$$

is the regularized Biot-Savart kernel. At large distances compared with σ, the velocity induced by a regularized vortex filament is the same as if the filament were singular since $4\pi\, g(\rho) \to 1$ as $\rho \to \infty$. The induced velocity goes to zero as $r \to 0$ since $g(\rho)$ is $\mathcal{O}(\rho^3)$ for small ρ. In particular, the local contribution to the self-induced velocity is proportional to $\int (s'-s)^2\, ds'$.

The vorticity and the streamfunction are divergence free as a consequence of the facts that the contours $\mathcal{C}^p(t)$ are closed and that σ is constant for each filament. The velocity is also divergence free since it is taken as the curl of a streamfunction.

The evolution equation for the vortex filaments is usually taken as

$$\frac{\partial}{\partial t}\mathbf{x}^p(s,t) = \mathbf{u}_\sigma(\mathbf{x},t)\Big|_{\mathbf{x}=\mathbf{x}^p(s,t)} . \tag{2.34}$$

There is also a generalized Hamiltonian formulation which produces the evolution equation (2.34) (Agishtein & Migdal 1986), i.e.,

$$\tilde{E} = \frac{1}{2}\int \boldsymbol{\psi}_\sigma\cdot\boldsymbol{\omega}\, d\mathbf{x} = \frac{1}{2}\sum_{p,q}\Gamma^p\,\Gamma^q \int_{\mathcal{C}^p(t)}\int_{\mathcal{C}^q(t)} \chi_\sigma(\mathbf{x}^p-\mathbf{x}^q)\left(\frac{\partial \mathbf{x}^p}{\partial s}\cdot\frac{\partial \mathbf{x}^q}{\partial s'}\right) ds\, ds' , \tag{2.35}$$

and

$$\frac{2}{\Gamma^p}\frac{\delta \tilde{E}}{\delta x_i^p} = \left(\frac{\partial \mathbf{x}^p}{\partial s}\, ds \wedge \frac{\partial \mathbf{x}^p}{\partial t}\right)_i . \tag{2.36}$$

The Hamiltonian $\tilde{E}$ is a motion invariant. In fact, this formulation is very similar to the Hamiltonian formulation for two-dimensional regularized vortex particles, with

$$\tilde{E} = \frac{1}{2}\int \psi_\sigma\,\omega\, d\mathbf{x} = -\frac{1}{2}\sum_{p,q}\chi_\sigma(\mathbf{x}^p-\mathbf{x}^q) \tag{2.37}$$

and

$$\frac{2}{\Gamma^p}\frac{\delta \tilde{E}}{\delta x_i^p} = \left(\hat{\mathbf{e}}_z \wedge \frac{d\mathbf{x}^p}{dt}\right)_i . \tag{2.38}$$

Notice that the Hamiltonian $\tilde{E} = \frac{1}{2}\int \boldsymbol{\psi}_\sigma\cdot\boldsymbol{\omega}\, d\mathbf{x}$ is not equal to the kinetic energy of the system which is given by $E = \frac{1}{2}\int \boldsymbol{\psi}_\sigma\cdot\boldsymbol{\omega}_\sigma\, d\mathbf{x}$. If one takes E instead of $\tilde{E}$ as the Hamiltonian, then this produces the evolution equation

$$\frac{\partial}{\partial t}\mathbf{x}^p(s,t) = \Big(\zeta_\sigma(\mathbf{x}) * \mathbf{u}_\sigma(\mathbf{x},t)\Big)\Big|_{\mathbf{x}=\mathbf{x}^p(s,t)} \tag{2.39}$$

with the kinetic energy E as motion invariant (Leonard 1980b). In other words, subjecting the vortex filaments to the evolution equation (2.34) or (2.39) leads to conservation of $\tilde{E}$ or E, respectively. The only problem with the choice of E instead of $\tilde{E}$ as Hamiltonian is that E cannot, in general, be evaluated, except with some rare choices of the regularization function $\zeta(\rho)$. The reader is referred to Appendix G, Section G.2.1 for more information on this subject.

The reader is also referred to Appendix A, Section A.1 for a review of the conservation laws in three-dimensional unbounded inviscid flows and to Appendix G, Section G.2.2 for the expressions of the semi-regularized helicity $\tilde{\mathcal{H}} = \int \mathrm{u}_\sigma \cdot \boldsymbol{\omega}\, d\mathbf{x}$ and the semi-regularized enstrophy $\tilde{\mathcal{E}} = \int \boldsymbol{\omega}_\sigma \cdot \boldsymbol{\omega}\, d\mathbf{x}$ of a system of regularized vortex filaments. The expressions for the linear impulse $\mathbf{I}$ and the angular impulse $\mathbf{A}$ are easily obtained. They are given by

$$\mathbf{I} = \frac{1}{2} \sum_p \Gamma^p \int_{C^p(t)} \mathbf{x}^p \wedge \frac{\partial \mathbf{x}^p}{\partial s}\, ds\,, \tag{2.40}$$

$$\mathbf{A} = \frac{1}{2} \sum_p \Gamma^p \int_{C^p(t)} \mathbf{x}^p \wedge \left(\mathbf{x}^p \wedge \frac{\partial \mathbf{x}^p}{\partial s} \right) ds\,. \tag{2.41}$$

$\mathbf{I}$ and $\mathbf{A}$ are conserved with any of the two choices for the evolution equation (Leonard 1980b,1985).

The convergence of the regularized vortex filament method has been investigated by Greengard (1986). He has shown convergence, at least for some finite time T, to the solution of the three-dimensional vorticity equation. The convergence is as follows: the appropriate error norm for the vorticity and velocity fields goes to zero as the number of filaments increases, and the core size σ decreases subjected to the constraint that the cores overlap (i.e., $\sigma/h > 1$ where h is a typical distance between filaments). The condition of core overlapping is natural. Indeed, the representation of a smooth function by a sum of smooth distributions, each of extent σ, can only be achieved if the typical distance between the centers of each distribution is less than σ. The error is usually composed of two terms: one term which is $\mathcal{O}(\sigma^r)$ and another term which is $\mathcal{O}(\sigma(h/\sigma)^m)$. The exponent m is related to the number of derivatives that exist of the smoothing function $\zeta(\rho)$. For most of the functions used in practice, m is large so that it is essential that the cores do overlap (i.e., $\sigma/h > 1$) for the second error term to vanish as $\sigma \to 0$. The exponent r is related to the moment properties of the smoothing function, that is $\zeta(\rho)$ has to satisfy the normalization constraint (2.21) together with

$$\int_0^\infty \zeta(\rho)\, \rho^{2+s}\, d\rho = 0\,, \qquad 2 \le s \le r-1 \qquad s \text{ even}\,, \tag{2.42}$$

$$\int_0^\infty |\zeta(\rho)|\, \rho^{2+r}\, d\rho < \infty\,. \tag{2.43}$$

In particular, it can be shown that $r \geq 2$ as soon as $\int_0^\infty |\zeta(\rho)|\, \rho^4\, d\rho < \infty$. If, moreover, $\zeta(\rho)$ is positive, then $r = 2$. A list of smoothing functions $\zeta(\rho)$, together with the associated $g(\rho)$ and $\chi(\rho)$ functions, is given in Table B.1. Notice that the smoothings that are $r > 2$, such as the super-Gaussian, are also not strictly positive. Plots of these regularization functions are given in Figure J.1.

For instance, the *Gaussian smoothing* (B.8)

$$\zeta(\rho) = \frac{1}{(2\pi)^{3/2}}\, e^{-\rho^2/2} \tag{2.44}$$

corresponds to $m = \infty$, $r = 2$. The *low order algebraic smoothing* (B.10) proposed by Rosenhead (1930) and used by Moore (1972) and others

$$\zeta(\rho) = \frac{3}{4\pi}\, \frac{1}{(\rho^2+1)^{5/2}} \tag{2.45}$$

gives $m = \infty$ but $r = 0$ because the inequality (2.43) is not satisfied. So, although this smoothing has been used extensively because of its numerical convenience (it is algebraic !), the theoretical error estimates show that this may be a poor choice because the first component of the error $\mathcal{O}(\sigma^r)$ does not vanish as $\sigma \to 0$.

A new smoothing is proposed which will be referred to as the *high order algebraic smoothing* (B.12):

$$\zeta(\rho) = \frac{15}{8\pi}\, \frac{1}{(\rho^2+1)^{7/2}}\,. \tag{2.46}$$

This smoothing has the same convergence properties as the Gaussian smoothing (B.8) since it corresponds to $m = \infty$, $r = 2$, but it is much easier to use in numerical computations. Indeed, the associated $\chi(\rho)$ and $g(\rho)$ functions that are needed for the evaluation of the streamfunction (2.23) and the velocity (2.31) have elegant and compact forms and are cheaper and more convenient to use than the $\chi(\rho)$ and $g(\rho)$ functions associated with the Gaussian smoothing. This smoothing will also prove very useful in Chapter 3.

In the above regularized vortex filament method, the core size σ was taken constant for all filaments and all times. Of course, it does not have to be that way. Each filament can be assigned its own core size σ^p which may depend on time. For instance, conservation of the total volume of vorticity can be achieved with the use of the following model equation (Leonard 1980b,1985)

$$\frac{d}{dt}\left((\sigma^p(t))^2\, \mathcal{L}^p(t)\right) = 0\,, \tag{2.47}$$

where $\mathcal{L}^p(t)$ is the total length of the vortex filament. This scheme produces a local increase in the amplitude of the vorticity within the core of the filament as $\mathcal{L}^p(t)$

increases due to vortex stretching. When each vortex filament has its own core size $\sigma^p(t)$, it is useful to symmetrize the evolution Equations (2.34) or (2.39) using $\sigma^{pq} = \sigma^{qp}$ where σ^{pq} is the core size used to compute the influence of filament q on filament p and conversely. This ensures conservation of the linear impulse and the angular impulse (Leonard 1980b,1985). This also preserves the Hamiltonian structure of the method, and hence ensures conservation of the Hamiltonian. Simple symmetrization schemes are $\sigma^{pq\,2} = \sigma^p \sigma^q$ or $\sigma^{pq\,2} = \left(\sigma^{p\,2} + \sigma^{q\,2}\right)/2$.

Finally, it may be desirable to account for gradients of stretching rates along the filament. This can be achieved with a core size that is also a function of the coordinate s, i.e., $\sigma^p = \sigma^p(s,t)$ and with a model equation for the conservation of local volume of vorticity of the form

$$\frac{d}{dt}\left(\left(\sigma^p(s,t)\right)^2 \mathcal{L}^p(s,t)\right) = 0\,, \tag{2.48}$$

where $\mathcal{L}^p(s,t) = \int \left(\frac{\partial \mathbf{x}^p}{\partial s} \cdot \frac{\partial \mathbf{x}^p}{\partial s}\right)^{1/2} ds$ is the local length of the vortex filament. Moore & Saffman (1972) argued that variations of σ^p along the filament produce helical vortex lines and hence axial flow that tends to eliminate these variations. Proceeding nevertheless, it is found that this choice does not conserve linear impulse and angular impulse. Moreover, the Hamiltonian structure of the method is lost. The vorticity field (2.19) and the streamfunction (2.23) are no longer divergence free. The velocity field (2.31) is still divergence free since it is still taken as the curl of a streamfunction. In fact, the situation is now very similar to the situation that will be encountered with vortex particles, Chapter 3. The divergence free vorticity field that corresponds to the curl of the velocity field is given by

$$\begin{aligned}\omega_\sigma^N(\mathbf{x},t) \;=\; \sum_p \Gamma^p \int_{C^p(t)} \Bigg[& \zeta_\sigma(\mathbf{x}-\mathbf{x}^p)\frac{\partial \mathbf{x}^p}{\partial s} \\ & + \nabla\left(\frac{\partial \mathbf{x}^p}{\partial s} \cdot \nabla\left(\chi_\sigma(\mathbf{x}-\mathbf{x}^p)\right)\right)\Bigg] ds\,. \end{aligned} \tag{2.49}$$

This vorticity field is divergence free because the integrand itself is divergence free. The reader is referred to Chapter 3 for the justification of this expression.

In conclusion, the choice $\sigma^p = \sigma^p(s,t)$ leads to a loss of many nice properties and is probably not a good choice. If intense vortex stretching is to be expected during the course of a computation, it is probably wiser to represent the initial core structure of a vortex tube with many filaments, each with a small core size $\sigma^p(t)$. Then, when intense stretching occurs, the core size of the vortex tube can become as small as the core size of each individual filament and the physics is modeled properly together with the conservation of the linear impulse, the angular impulse and the Hamiltonian.

2.3 The velocity of thin vortex rings

The motion of thin vortex rings has been a subject of interest for some time. Lamb (1932) gave a proof of Kelvin's formula for the velocity of a thin vortex ring with uniform vorticity within the core. Saffman (1970) and Fraenkel (1970) gave the expression for the velocity of a thin ring with arbitrary vorticity distribution. Fraenkel (1972) also gave higher order asymptotic formulas that describe the shape and overall properties of rings with uniform ω/r for quite substantial cross-sections. Norbury (1973) computed numerically the exact shape and other properties for the same case but over the whole range of cross-sections (from the thin vortex ring with uniform vorticity to the Hill's spherical vortex ring).

In the present section, the velocity of thin rings of general vorticity distribution is examined, and the numerical results obtained with two different approaches are compared. The correct results obtained with Saffman's formula are compared with the incorrect result obtained by translating the vortex ring with the centerline velocity. The matching procedure which produces the asymptotically correct vortex ring velocity is reviewed. Quite a variety of vorticity distributions are examined in detail.

2.3.1 The general case

Consider a thin vortex ring with the centerline of the vortex core given by $\mathbf{x}(\theta) = R\cos\theta\hat{\mathbf{e}}_x + R\sin\theta\hat{\mathbf{e}}_y$. The velocity induced by the vortex ring is

$$\mathbf{u}(\mathbf{x},t) = -\Gamma\int_0^{2\pi}\frac{g\left(\frac{|\mathbf{x}-\mathbf{x}(\theta)|}{\sigma}\right)}{|\mathbf{x}-\mathbf{x}(\theta)|^3}(\mathbf{x}-\mathbf{x}(\theta))\wedge\frac{\partial\mathbf{x}}{\partial\theta}d\theta\,. \tag{2.50}$$

If the ring velocity is taken as the self-induced velocity on the centerline, one obtains (Leonard 1985)

$$\begin{aligned} U_R &= -\frac{\Gamma}{R}\int_0^{2\pi}\frac{g\left(\frac{2R}{\sigma}|\sin(\theta/2)|\right)}{(2R|\sin(\theta/2)|)^3}(-2R^2\sin^2(\theta/2))d\theta \\ &= \frac{\Gamma}{R}\int_0^{\pi/2}\frac{g\left(\frac{2R}{\sigma}\sin\varphi\right)}{\sin\varphi}d\varphi = \frac{\Gamma}{R}\int_0^1\frac{g\left(\frac{2R}{\sigma}t\right)}{t(1-t^2)^{\frac{1}{2}}}dt\,, \end{aligned} \tag{2.51}$$

where $\varphi = \theta/2$, $t = \sin\varphi$ and U_R stands for the translational velocity. For thin rings, the asymptotic limit of Equation (2.51) as $\sigma/R \to 0$ is examined by writing

$$U_R = \frac{\Gamma}{R}\left[\int_0^1\frac{g\left(\frac{2R}{\sigma}t\right)}{t}dt + \int_0^1\frac{g\left(\frac{2R}{\sigma}t\right)}{t}\left(\frac{1}{(1-t^2)^{\frac{1}{2}}}-1\right)dt\right]\,. \tag{2.52}$$

The first integral in Equation (2.52) is evaluated by parts

$$\begin{aligned}\int_0^1 \frac{g\left(\frac{2R}{\sigma}t\right)}{t}dt &= -\left(\frac{2R}{\sigma}\right)\int_0^1 g'\left(\frac{2R}{\sigma}t\right)\log t\,dt = -\int_0^{2R/\sigma} g'(\rho)\log\left(\frac{\sigma}{2R}\rho\right)\,d\rho \\ &= \log\left(\frac{2R}{\sigma}\right)\int_0^{2R/\sigma} g'(\rho)d\rho - \int_0^{2R/\sigma} g'(\rho)\log\rho\,d\rho \\ &\simeq \log\left(\frac{2R}{\sigma}\right)\int_0^{\infty} g'(\rho)d\rho - \int_0^{\infty} g'(\rho)\log\rho\,d\rho \\ &= \frac{1}{4\pi}\log\left(\frac{2R}{\sigma}\right) - \int_0^{\infty} g'(\rho)\log\rho\,d\rho\,. \end{aligned} \tag{2.53}$$

For the second integral in Equation (2.52), it is appropriate to take $g(2Rt/\sigma) = 1/4\pi$ since $R/\sigma \to \infty$. This integral then becomes

$$\begin{aligned}\frac{1}{4\pi}\int_0^1 \frac{1}{t}\left(\frac{1}{(1-t^2)^{\frac{1}{2}}} - 1\right)dt &= \frac{1}{4\pi}\int_0^{\pi/2}\frac{(1-\cos u)}{\sin u}du = \frac{1}{4\pi}\int_0^{\pi/2}\tan(u/2)du \\ &= \frac{1}{4\pi}\left[-2\log\left(\cos(u/2)\right)\right]_0^{\pi/2} = \frac{1}{4\pi}\log 2\,. \end{aligned} \tag{2.54}$$

Thus, when the velocity of the thin ring is taken as the velocity on the centerline, one finally obtains (Leonard 1985)

$$U_R = \frac{\Gamma}{4\pi R}\left[\log\left(\frac{4R}{\sigma}\right) - 4\pi\int_0^{\infty} g'(\rho)\log\rho\,d\rho\right]\,. \tag{2.55}$$

where $g'(\rho) = \rho^2\zeta(\rho)$.

A more careful analysis by Saffman (1970) and Fraenkel (1970) leads to the following expression for the velocity of a thin vortex ring

$$U_R = \frac{\Gamma}{4\pi R}\left[\log\left(\frac{8R}{\sigma}\right) - \frac{1}{2} + \left(\int_0^1 (2\pi g_2(\rho))^2\frac{d\rho}{\rho} + \int_1^{\infty}\left((2\pi g_2(\rho))^2 - 1\right)\frac{d\rho}{\rho}\right)\right]\,, \tag{2.56}$$

where $2\pi g_2(\rho)$ is the fraction of circulation of the two-dimensional vorticity distribution $\zeta_2(\rho)$ within a dimensional radius $\rho = r/\sigma$. The connection between three-dimensional vorticity and velocity smoothings, $\zeta(\rho)$ and $g(\rho)$, and two-dimensional vorticity and velocity distributions, $\zeta_2(\rho)$ and $g_2(\rho)$, is examined in details in Appendix B.

If the two formulas are to agree, the following integral constraint must be satisfied:

$$4\pi\int_0^{\infty} g'(\rho)\log\rho\,d\rho = \frac{1}{2} - \log 2 - \left(\int_0^1 (2\pi g_2(\rho))^2\frac{d\rho}{\rho} + \int_1^{\infty}\left((2\pi g_2(\rho))^2 - 1\right)\frac{d\rho}{\rho}\right)\,. \tag{2.57}$$

It will be shown in Section 2.3.2 that the integral constraint is not satisfied in general. This is due to the fact that the velocity of a vortex ring cannot be taken as the velocity

on the centerline, even when $\sigma/R \to 0$. Of course, as proposed by Leonard (1985), one can reproduce numerically the correct velocity of a thin vortex ring of given vorticity and velocity distribution, $\zeta_2(\rho)$ and $g_2(\rho)$, by choosing an appropriate smoothing of the Biot-Savart integral in such a way as to satisfy the integral constraint (2.57). This point will be examined further at the end of Section 2.3.2.

2.3.2 Some examples

In this section, the results obtained when using Equations (2.55) and (2.56) with usual three-dimensional smoothings and their corresponding two-dimensional smoothings as given in Appendix B are examined. The reader is referred to that appendix for the details on the velocity and vorticity smoothings.

If the three-dimensional exponential smoothing (B.8) is considered, and Equation (2.55) is used, one then obtains

$$\begin{aligned} U_R &= \frac{\Gamma}{4\pi R}\left[\log\left(\frac{4R}{\sigma}\right) - \left(\frac{2}{\pi}\right)^{\frac{1}{2}} \int_0^\infty \rho^2\, e^{-\rho^2/2} \log\rho\, d\rho\right] \\ &= \frac{\Gamma}{4\pi R}\left[\log\left(\frac{8R}{\sigma}\right) - \left(\frac{1}{2}\log 2 + 1 - \frac{\gamma}{2}\right)\right] \\ &= \frac{\Gamma}{4\pi R}\left[\log\left(\frac{8R}{\sigma}\right) - 1.05796576\right] , \end{aligned} \tag{2.58}$$

where γ is the Euler constant, $\gamma = .577215664$. Use of Equation (2.56), with the corresponding two-dimensional Gaussian distribution (B.9) leads to

$$\begin{aligned} \int_0^1 (2\pi g_2(\rho))^2 \frac{d\rho}{\rho} &= \int_0^{1/\sqrt{2}} \left(1 - e^{-t^2}\right)^2 \frac{dt}{t} = \frac{1}{2}\int_0^{1/2} \left(1 - e^{-u}\right)^2 \frac{du}{u} \\ &= \int_0^{1/2} \left(1 - e^{-u}\right)\frac{du}{u} - \frac{1}{2}\int_0^{1/2}\left(1 - e^{-2u}\right)\frac{du}{u} \\ &= \mathrm{E_i}(1/2) - \frac{1}{2}\mathrm{E_i}(1) + \frac{\gamma}{2} - \log 2 \\ \int_1^\infty \left((2\pi g_2(\rho))^2 - 1\right)\frac{d\rho}{\rho} &= \int_{1/\sqrt{2}}^\infty \left(\left(1 - e^{-t^2}\right)^2 - 1\right)\frac{dt}{t} \\ &= \frac{1}{2}\int_{1/2}^\infty e^{-2u}\frac{du}{u} - \int_{1/2}^\infty e^{-u}\frac{du}{u} \\ &= \frac{1}{2}\mathrm{E_i}(1) - \mathrm{E_i}(1/2) , \end{aligned} \tag{2.59}$$

with $\mathrm{E_i}(x) = \int_x^\infty e^{-u}/u\, du = -\gamma - \log x + \int_0^x (1 - e^{-u})/u\, du$, so that

$$\begin{aligned} U_R &= \frac{\Gamma}{4\pi R}\left[\log\left(\frac{8R}{\sigma}\right) - (\log 2 + \frac{1}{2} - \frac{\gamma}{2})\right] \\ &= \frac{\Gamma}{4\pi R}\left[\log\left(\frac{8R}{\sigma}\right) - .90453935\right] . \end{aligned} \tag{2.60}$$

Thus, the centerline ring velocity (2.58) does not agree with the correct ring velocity as given by Saffman's formula (2.60).

A similar problem occurs when the three-dimensional smoothing (B.16), which corresponds to the two-dimensional constant vorticity core (B.17) is considered. Using Equation (2.55), one obtains

$$\begin{aligned} 4\pi \int_0^\infty g'(\rho) \log \rho \, d\rho &= \frac{4}{\pi} \int_0^1 \frac{\rho^2}{(1-\rho^2)^{\frac{1}{2}}} \log \rho \, d\rho \\ &= \frac{2}{\pi} \left(\left[\left(\arcsin \rho - \rho(1-\rho^2)^{\frac{1}{2}} \right) \log \rho \right]_0^1 \right. \\ &\qquad \left. + \int_0^1 \left((1-\rho^2)^{\frac{1}{2}} - \frac{\arcsin \rho}{\rho} \right) d\rho \right) \\ &= \frac{2}{\pi} \left(0 + \frac{1}{2} \left[\rho(1-\rho^2)^{\frac{1}{2}} + \arcsin \rho \right]_0^1 - \int_0^1 \frac{\arcsin \rho}{\rho} d\rho \right) \\ &= \frac{2}{\pi} \left(\frac{\pi}{4} - \frac{\pi}{2} \log 2 \right) = \frac{1}{2} - \log 2 \, , \end{aligned} \tag{2.61}$$

leading to

$$U_R = \frac{\Gamma}{4\pi R} \left[\log \left(\frac{8R}{\sigma} \right) - \frac{1}{2} \right] \, . \tag{2.62}$$

Use of Saffman's formula (2.56), with the corresponding two-dimensional constant vorticity distribution (B.17), leads to

$$\begin{aligned} U_R &= \frac{\Gamma}{4\pi R} \left[\log \left(\frac{8R}{\sigma} \right) - \frac{1}{2} + \int_0^1 \rho^3 d\rho \right] \\ &= \frac{\Gamma}{4\pi R} \left[\log \left(\frac{8R}{\sigma} \right) - \frac{1}{4} \right] \, , \end{aligned} \tag{2.63}$$

which is the correct expression for the ring velocity (Lamb 1932).

Actually, there exists a three-dimensional smoothing which is such that the use of Equation (2.55) leads to the same result as the use of Equation (2.56) with the corresponding two-dimensional smoothing. This is the case of the low order algebraic smoothing (B.10). Indeed, the use of Equation (2.55) and [43] leads to

$$\begin{aligned} U_R &= \frac{\Gamma}{4\pi R} \left[\log \left(\frac{4R}{\sigma} \right) - 3 \int_0^\infty \frac{\rho^2}{(\rho^2+1)^{\frac{5}{2}}} \log \rho \, d\rho \right] \\ &= \frac{\Gamma}{4\pi R} \left[\log \left(\frac{4R}{\sigma} \right) - 3 \left(\frac{1}{3} (1 - \log 2) \right) \right] \\ &= \frac{\Gamma}{4\pi R} \left[\log \left(\frac{8R}{\sigma} \right) - 1 \right] \, , \end{aligned} \tag{2.64}$$

and the use of Equation (2.56), with the coresponding two-dimensional smoothing (B.11) leads to

$$\int_0^1 (2\pi g_2(\rho))^2 \frac{d\rho}{\rho} = \int_0^1 \left(\frac{\rho^2}{\rho^2+1} \right)^2 \frac{d\rho}{\rho} = \frac{1}{2} \int_0^1 \left(1 - \frac{1}{t+1} \right)^2 \frac{dt}{t}$$

$$
\begin{aligned}
&= \frac{1}{2}\left(\log 2 - \frac{1}{2}\right) \\
\int_1^\infty \left((2\pi g_2(\rho))^2 - 1\right)\frac{d\rho}{\rho} &= \int_1^\infty \left(\left(\frac{\rho^2}{\rho^2+1}\right)^2 - 1\right)\frac{d\rho}{\rho} \\
&= \frac{1}{2}\int_1^\infty \left(\left(1 - \frac{1}{t+1}\right)^2 - 1\right)\frac{dt}{t} \\
&= -\frac{1}{2}\left(\log 2 + \frac{1}{2}\right) , \qquad (2.65)
\end{aligned}
$$

so that one finally obtains

$$
U_R = \frac{\Gamma}{4\pi R}\left[\log\left(\frac{8R}{\sigma}\right) - 1\right] . \qquad (2.66)
$$

This is thus a very special case where both formulas lead to the same result so that the integral constraint (2.57) is satisfied. This is also a special case for another reason: it is a case for which Equation (2.51) can be integrated in closed form so that the velocity of a ring moving with the centerline velocity can be computed for any value of the ratio σ/R. Indeed,

$$
\begin{aligned}
U_R &= \frac{\Gamma}{R}\int_0^{\pi/2} \frac{g\left(\frac{2R}{\sigma}\sin\varphi\right)}{\sin\varphi} d\varphi = \frac{\Gamma}{4\pi R}\left(\frac{2R}{\sigma}\right)^3 \int_0^{\pi/2} \frac{\sin^2\varphi}{\left((2R/\sigma)^2\sin^2\varphi + 1\right)^{\frac{3}{2}}} d\varphi \\
&= \frac{\Gamma}{4\pi R}\frac{1}{(1+p^2)^{\frac{1}{2}}}\left[\mathrm{K}\left(\frac{1}{(1+p^2)^{\frac{1}{2}}}\right) - \mathrm{E}\left(\frac{1}{(1+p^2)^{\frac{1}{2}}}\right)\right] , \qquad (2.67)
\end{aligned}
$$

where $p = \sigma/2R$, $\mathrm{K}(x)$ and $\mathrm{E}(x)$ are the complete elliptic integrals of the first and second kind, respectively. This result is of great numerical interest as it can be used to check the accuracy of a numerical code that makes use of the low order algebraic smoothing. The validity of the asymptotic formula (2.55) with respect to the exact formula (2.51) can also be verified by examining the behavior of Equation (2.67) as $p \to 0$. Recalling that [1]

$$
\begin{aligned}
\mathrm{K}(x) &\sim \log\left(\frac{4}{x'}\right) + \mathcal{O}(x'^2 \log x') \\
\mathrm{E}(x) &\sim 1 + \mathcal{O}(x'^2 \log x') , \qquad (2.68)
\end{aligned}
$$

as $x \to 1$, with $x'^2 = 1 - x^2$, one obtains

$$
U_R = \frac{\Gamma}{4\pi R}\left[\log\left(\frac{8R}{\sigma}\right) - 1 + \mathcal{O}\left(\left(\frac{\sigma}{R}\right)^2 \log\left(\frac{\sigma}{R}\right)\right)\right] , \qquad (2.69)
$$

which confirms (2.64).

Finally, the three-dimensional constant smoothing (B.14) leads, with the use of Equation (2.55), to

$$\begin{aligned} U_R &= \frac{\Gamma}{4\pi R}\left[\log\left(\frac{4R}{\sigma}\right) - 3\int_0^1 \rho^2 \log\rho\, d\rho\right] \\ &= \frac{\Gamma}{4\pi R}\left[\log\left(\frac{8R}{\sigma}\right) - \left(\log 2 - \frac{1}{3}\right)\right] . \end{aligned} \tag{2.70}$$

Equation (2.56) with the corresponding two-dimensional vorticity distribution (B.15) could not be integrated in closed form.

In conclusion, the approach of computing the velocity of a vortex ring with the centerline velocity yields the wrong result for most vorticity distributions. However, if the asymptotically correct velocity of a thin vortex ring of given core size σ_2 and vorticity distribution $\zeta_2(\rho)$ and $g_2(\rho)$ is desired, it can be obtained by taking the velocity of the ring as the Biot-Savart velocity applied on the centerline with some three-dimensional smoothing $\zeta(\rho)$ and $g(\rho)$ and with a core size $\sigma = \beta\sigma_2$ so as to satisfy (Leonard 1985)

$$\begin{aligned} &\log\beta + 4\pi\int_0^\infty g'(\rho)\log\rho\, d\rho \\ &= \frac{1}{2} - \log 2 - \left(\int_0^1 (2\pi g_2(\rho))^2 \frac{d\rho}{\rho} + \int_1^\infty \left((2\pi g_2(\rho))^2 - 1\right)\frac{d\rho}{\rho}\right) . \end{aligned} \tag{2.71}$$

For instance, the values of β that correctly reproduce the asymptotic velocity of the ring of uniform vorticity core σ_K are given by

$$\beta = \begin{cases} (1/2^{1/2})\, e^{(\gamma/2 - 3/4)} & \text{for the Gaussian smoothing} \\ e^{-1/4} & \text{for the constant vorticity smoothing} \\ e^{-3/4} & \text{for the low order algebraic smoothing} \\ (1/2)\, e^{7/12} & \text{for the constant smoothing} \end{cases} \tag{2.72}$$

2.4 Linearized perturbations of a straight vortex filament

2.4.1 Some background

The linearized perturbations of a straight vortex filament with a uniform vorticity distribution within the core were analyzed by Kelvin (1880). He also gave the analysis corresponding to a hollow vortex tube where the vorticity is concentrated on a cylindrical sheet. His results apply only in the absence of a straining field and are reviewed by Robinson & Saffman (1984). The perturbed shapes are helical disturbances proportional to $f(r)\exp(ikx + im\theta + i\Omega t)$, where m is the azimuthal mode in cylindrical coordinates, k is the axial wave number and Ω is the circular frequency.

The dispersion relation giving $\Omega(l;m)$ implicitly is

$$\frac{\mathrm{J}'_{|m|}(\delta)}{\delta\,\mathrm{J}_{|m|}(\delta)} + \frac{m}{\delta^2 c} = -\frac{\mathrm{K}'_{|m|}(l)}{l\,\mathrm{K}_{|m|}(l)}\ , \tag{2.73}$$

where

$$\begin{cases} l & = k\sigma_K \text{ is the dimensionless wave number,} \\ \sigma_K & \text{is the core radius,} \\ c & = 1/2m + \Omega/\omega_0 \text{ with } \Gamma = \pi\sigma_K^2\omega_0\ , \\ \delta^2 & = l^2(1-c^2)/c^2\ , \\ \mathrm{J}_m & \text{is the Bessel function of the first kind and order } m\ , \\ \mathrm{K}_m & \text{is the modified Bessel function of the second kind and order } m\ . \end{cases}$$

According to Kelvin, the roots of Equation (2.73) are purely real and give the angular frequency of stable bending modes of the vortex tube with c in $[-1,1]$ so that Ω/ω_0 lies in $[-1-m/2, 1-m/2]$. There is an infinite number of roots for each m and l. The case where the angular mode $m = \pm 1$ corresponds to azimuthal perturbations of the form $\exp(\pm i\theta)$ and is shown in Figure J.2 from Robinson & Saffman (1984). Notice that the figure is symmetrical with respect to the l axis because there are modes corresponding to $m = 1$ and modes corresponding to $m = -1$. The first radial bending mode (i.e., the lowest order mode) has no node in the velocity perturbation and its dispersion curve does not cross the l axis. Higher order bending modes have a more complex core structure with one or more nodes in the perturbation velocity depending on the mode order. Their dispersion relation also crosses the l axis so that there is a certain wave number l_0 for which the perturbation does not rotate. Widnall, Bliss & Tsai (1974) conjectured that instability for both the pair of straight vortex filaments of opposite sign circulation and the vortex ring occurs whenever the wave number l of the perturbation corresponds to that wave number l_0. The basic mechanism was confirmed by Moore & Saffman (1975) and by Tsai & Widnall (1976) for the related problem of the line vortex in a uniform plane strain and confirmed in detail by Widnall & Tsai (1977) for the thin vortex ring of uniform vorticity core. The general mathematical analysis of Moore & Saffman (1975) actually shows that the necessary condition for instability of the line vortex is that the dispersion relation is degenerate, i.e., that modes of same wave number l but different angular dependence have same circular frequency $\pm\Omega$. The explanation goes as follows: each mode corresponds to an helical wave (as will also be seen in Section 2.4.2) of circular frequency $\pm\Omega$. The superposition of two modes of same wave number l but opposite circular frequency Ω produces a sine wave that does not rotate and is thus unstable in the presence of a strain field.

The dispersion relation for the lowest bending mode was generalized to arbitrary vorticity distribution, $\zeta_2(\rho)$, by Moore & Saffman (1972) for the case of long bending waves (i.e., for $l \to 0$). If $2\pi g_2(\rho)$ is the fraction of circulation within the dimensional radius ρ, the asymptotic behavior of the dispersion relation is given by

$$\begin{aligned} D(l) &= \frac{\pi\sigma^2\Omega(l)}{\Gamma} \\ &= \pm\left(\frac{l}{2}\right)^2\left[\log\left(\frac{l}{2}\right)+\gamma-\left(\int_0^1(2\pi g_2(\rho))^2\frac{d\rho}{\rho}+\int_1^\infty\left((2\pi g_2(\rho))^2-1\right)\frac{d\rho}{\rho}\right)\right. \\ &\qquad \left.+\mathcal{O}(l^2\log l)\right]. \end{aligned} \tag{2.74}$$

as $l \to 0$. This expression has a term similar to the expression for the asymptotic velocity of thin vortex rings, Equation (2.56). Refer to Section 2.3.2 for the values of the integrals of Equation (2.74) with some typical vorticity distributions. For instance, the Gaussian distribution (B.9) gives

$$D(l) = \pm\left(\frac{l}{2}\right)^2\left[\log\left(\frac{l}{2}\right)+\left(\log 2+\frac{\gamma}{2}\right)\right]. \tag{2.75}$$

The low order algebraic distribution (B.11) gives

$$D(l) = \pm\left(\frac{l}{2}\right)^2\left[\log\left(\frac{l}{2}\right)+\left(\gamma+\frac{1}{2}\right)\right], \tag{2.76}$$

and the uniform distribution (B.17) gives

$$D(l) = \pm\left(\frac{l}{2}\right)^2\left[\log\left(\frac{l}{2}\right)+\left(\gamma-\frac{1}{4}\right)\right]. \tag{2.77}$$

2.4.2 Linearized perturbations of a vortex filament evolving under its own induced velocity applied on the centerline

2.4.2.1 The general case

The dispersion relation for linearized perturbations on a rectilinear vortex filament that is subjected to its self-induced velocity applied on the centerline will be examined. Of course, this analysis is much more restrictive than the full analysis conducted by Kelvin (1880) because it will only reproduce the dispersion relation for the lowest order mode of the case $m = \pm 1$. This is to be expected because the vorticity disturbance is fixed when representing a vortex tube with a single filament. Nevertheless, this analysis will be of great numerical interest because it will provide, for the whole range of wave numbers l, the numerical dispersion relation of the type of vortex filaments that one actually uses in numerical computations.

Recall the dynamics of a vortex filament evolving under its self-induced velocity applied on the centerline

$$\frac{\partial}{\partial t}\mathbf{x}(s,t) = -\Gamma \int_{-\infty}^{\infty} \frac{g\left(\frac{|\mathbf{x}-\mathbf{x}'|}{\sigma}\right)}{|\mathbf{x}-\mathbf{x}'|^3}(\mathbf{x}-\mathbf{x}') \wedge \frac{\partial \mathbf{x}'}{\partial s'} ds' \,, \tag{2.78}$$

where $\mathbf{x}-\mathbf{x}'$ stands for $\mathbf{x}(s,t)-\mathbf{x}(s',t)$, $g(\rho)$ is the three-dimensional velocity smoothing and s is a material coordinate which is taken here as a length coordinate. The scaling of Equation (2.78) is done by defining $\mathbf{y} = \mathbf{x}/\sigma$ and $\eta = s/\sigma$. This leads to

$$\frac{\partial}{\partial t}\mathbf{y}(\eta,t) = -\frac{\Gamma}{\sigma^2} \int_{-\infty}^{\infty} \frac{g(|\mathbf{y}-\mathbf{y}'|)}{|\mathbf{y}-\mathbf{y}'|^3}(\mathbf{y}-\mathbf{y}') \wedge \frac{\partial \mathbf{y}'}{\partial \eta'} d\eta' \,, \tag{2.79}$$

where $\mathbf{y}-\mathbf{y}'$ stands for $\mathbf{y}(\eta,t)-\mathbf{y}(\eta',t)$. Linearization of Equation (2.79) about a straight filament aligned with the x axis, with $\mathbf{y}(\eta,t) = \eta\hat{\mathbf{e}}_x + \delta\mathbf{y}(\eta,t)$, leads to

$$\begin{aligned}
\frac{\partial}{\partial t}\delta\mathbf{y}(\eta,t) &= -\frac{\Gamma}{\sigma^2} \int_{-\infty}^{\infty} \frac{g(|\eta-\eta'|)}{|\eta-\eta'|^3} \left[(\eta-\eta')\hat{\mathbf{e}}_x \wedge \frac{\partial \delta\mathbf{y}'}{\partial \eta'} + (\delta\mathbf{y}-\delta\mathbf{y}') \wedge \hat{\mathbf{e}}_x \right] d\eta' \\
&= -\frac{\Gamma}{\sigma^2}\, \hat{\mathbf{e}}_x \wedge \int_{-\infty}^{\infty} \frac{g(|\eta-\eta'|)}{|\eta-\eta'|^3} \left[(\eta-\eta')\frac{\partial \delta\mathbf{y}'}{\partial \eta'} - (\delta\mathbf{y}-\delta\mathbf{y}') \right] d\eta' \,.
\end{aligned} \tag{2.80}$$

Noticing that

$$(\eta-\eta')\frac{\partial \delta\mathbf{y}'}{\partial \eta'} - (\delta\mathbf{y}-\delta\mathbf{y}') = -(\eta-\eta')^2 \frac{\partial}{\partial \eta'}\left(\frac{\delta\mathbf{y}-\delta\mathbf{y}'}{\eta-\eta'}\right) \,, \tag{2.81}$$

one obtains

$$\frac{\partial}{\partial t}\delta\mathbf{y}(\eta,t) = \frac{\Gamma}{\sigma^2}\, \hat{\mathbf{e}}_x \wedge \int_{-\infty}^{\infty} \frac{g(|\eta-\eta'|)}{|\eta-\eta'|} \frac{\partial}{\partial \eta'}\left(\frac{\delta\mathbf{y}-\delta\mathbf{y}'}{\eta-\eta'}\right) d\eta' \,. \tag{2.82}$$

Equation (2.82) can be integrated by parts to give, using the fact that $g(\rho) \to 1/4\pi$ as $\rho \to \infty$,

$$\frac{\partial}{\partial t}\delta\mathbf{y}(\eta,t) = -\frac{\Gamma}{\sigma^2}\, \hat{\mathbf{e}}_x \wedge \int_{-\infty}^{\infty} \frac{1}{(\eta-\eta')} \frac{\partial}{\partial \eta'}\left(\frac{g(|\eta-\eta'|}{|\eta-\eta'|}\right)(\delta\mathbf{y}-\delta\mathbf{y}')d\eta' \,. \tag{2.83}$$

Defining

$$Q(\rho) = -4\pi \frac{1}{\rho}\frac{d}{d\rho}\left(\frac{g(\rho)}{\rho}\right) \,, \tag{2.84}$$

Equation (2.83) becomes

$$\frac{\partial}{\partial t}\delta\mathbf{y}(\eta,t) = \frac{\Gamma}{4\pi\sigma^2}\, \hat{\mathbf{e}}_x \wedge \left[C\,\delta\mathbf{y}(\eta,t) + \int_{-\infty}^{\infty} Q(|\eta-\eta'|)\delta\mathbf{y}(\eta',t)d\eta' \right] \,, \tag{2.85}$$

where

$$C = -\int_{-\infty}^{\infty} Q(|\eta|)d\eta = -2\int_0^{\infty} Q(\rho)d\rho = 8\pi \int_0^{\infty} \frac{1}{\rho}\frac{d}{d\rho}\left(\frac{g(\rho)}{\rho}\right) d\rho \,. \tag{2.86}$$

Notice that C is properly defined as soon as $g(\rho)$ is $\mathcal{O}(\rho)$ for small ρ. This property will be of importance in Section 2.4.3. For usual velocity smoothings (i.e., when $g(\rho)$ is $\mathcal{O}(\rho^3)$ for ρ small), there are two alternative formulas that can be used to evaluate C and that are obtained through integration by parts:

$$\begin{aligned} C &= 8\pi \int_0^\infty \frac{1}{\rho}\frac{d}{d\rho}\left(\frac{g(\rho)}{\rho}\right) d\rho = -8\pi \int_0^\infty \frac{g(\rho)}{\rho^3} d\rho + 8\pi \int_0^\infty \frac{g'(\rho)}{\rho^2} d\rho \\ &= 8\pi \int_0^\infty \frac{g(\rho)}{\rho^3} d\rho \\ &= 4\pi \int_0^\infty \frac{g'(\rho)}{\rho^2} d\rho \,. \end{aligned} \tag{2.87}$$

However, when $g(\rho)$ is $\mathcal{O}(\rho)$ for small ρ, only Equation (2.86) can be used.

Equation (2.86) is now in an appropriate form that one can take its Fourier transform. Defining

$$\widehat{\delta \mathbf{y}}(l,t) = \int_{-\infty}^{\infty} \delta \mathbf{y}(\eta,t) e^{-il\eta} d\eta \,, \tag{2.88}$$

where $l = k\sigma$ is the dimensionless wave number, one obtains, with the use of the convolution theorem,

$$\begin{aligned} \frac{\partial}{\partial t}\widehat{\delta \mathbf{y}}(l,t) &= \frac{\Gamma}{4\pi\sigma^2}\left[C + \hat{Q}(l)\right] \hat{\mathbf{e}}_x \wedge \widehat{\delta \mathbf{y}}(l,t) \\ &= \frac{\Gamma}{4\pi\sigma^2} \hat{G}(l)\, \hat{\mathbf{e}}_x \wedge \widehat{\delta \mathbf{y}}(l,t) \,, \end{aligned} \tag{2.89}$$

where $\hat{Q}(l)$ is the Fourier transform of $Q(\rho)$ and $\hat{G}(l) = C + \hat{Q}(l)$. It is now easy to find the eigenvalues and eigenvectors of Equation (2.89). Indeed,defining

$$\widehat{\delta \mathbf{y}}(l,t) = \widehat{\delta \mathbf{y}}_0(l) e^{i\,\Omega(l)\,t} \,, \tag{2.90}$$

one obtains the following equation for the eigenvectors:

$$\left(\left(\frac{\Gamma}{4\pi\sigma^2}\hat{G}(l)\,\hat{\mathbf{e}}_x\wedge\right) - i\,\Omega(l)\right)\, \widehat{\delta \mathbf{y}}_0(l) = 0 \,. \tag{2.91}$$

The eigenvalues are solutions of

$$\Omega(l)\left(\Omega^2(l) - \left(\frac{\Gamma}{4\pi\sigma^2}\hat{G}(l)\right)^2\right) = 0 \,. \tag{2.92}$$

The trivial eigenvalue, $\Omega = 0$, corresponds to a simple translation of the vortex filament along its own axis. The non-trivial eigenvalues correspond to stable helical modes rotating at angular velocity $\Omega(l)$

$$\begin{aligned} &\Omega_+(l) = \Omega(l) = \tfrac{\Gamma}{4\pi\sigma^2}\hat{G}(l)\,; \qquad \widehat{\delta \mathbf{y}}_0(l) = A_+(\hat{\mathbf{e}}_y - i\hat{\mathbf{e}}_z)e^{i\Omega(l)t} \\ &\Omega_-(l) = -\Omega(l) = -\tfrac{\Gamma}{4\pi\sigma^2}\hat{G}(l)\,; \quad \widehat{\delta \mathbf{y}}_0(l) = A_-(\hat{\mathbf{e}}_y + i\hat{\mathbf{e}}_z)e^{-i\Omega(l)t} \,. \end{aligned} \tag{2.93}$$

The dispersion relation for a vortex filament subjected to its own induced velocity applied on the centerline is thus finally given by

$$\begin{aligned} D(l) &= \frac{\pi\sigma^2\Omega(l)}{\Gamma} \\ &= \pm\frac{1}{4}\hat{G}(l) = \pm\frac{1}{4}(C+\hat{Q}(l)) \\ &= \pm\frac{1}{4}\left[-\int_{-\infty}^{\infty} Q(|\eta|)d\eta + \int_{-\infty}^{\infty} Q(|\eta|)e^{-il\eta}d\eta\right] \\ &= \pm\frac{1}{4}\left[-2\int_0^{\infty} Q(\rho)d\rho + 2\int_0^{\infty} Q(\rho)\cos(l\rho)d\rho\right] \\ &= \pm 2\pi\int_0^{\infty}\frac{1}{\rho}\frac{d}{d\rho}\left(\frac{g(\rho)}{\rho}\right)(1-\cos(l\rho))d\rho\,. \end{aligned} \tag{2.94}$$

The most general perturbed mode can be written as

$$\begin{aligned} \delta\mathbf{y}(\eta,t) = \Re\Bigg[\frac{1}{2\pi}\int_{-\infty}^{\infty}\Big(&A_+(l)(\hat{\mathbf{e}}_y - i\hat{\mathbf{e}}_z)e^{i\Omega(l)t} \\ &+A_-(l)(\hat{\mathbf{e}}_y + i\hat{\mathbf{e}}_z)e^{-i\Omega(l)t}\Big)e^{il\eta}dl\Bigg]\,. \end{aligned} \tag{2.95}$$

For a single-wavelength perturbation, a typical mode is given by

$$\delta\mathbf{y}(\eta,t) = \Re\left[\left(B_+(\hat{\mathbf{e}}_y - i\hat{\mathbf{e}}_z)e^{i\Omega(l)t} + B_-(\hat{\mathbf{e}}_y + i\hat{\mathbf{e}}_z)e^{-i\Omega(l)t}\right)e^{il\eta}\right]\,. \tag{2.96}$$

In the special case where $B_+ = B_- = B/2$, the two helical modes add up to give a simple plane wave perturbation

$$\delta\mathbf{y}(\eta,t) = B\cos(l\eta)\left(\cos(\Omega(l)t)\,\hat{\mathbf{e}}_y + \sin(\Omega(l)t)\,\hat{\mathbf{e}}_z\right)\,. \tag{2.97}$$

Finally, by analogy with the formula obtained for the velocity of a thin filament vortex ring subjected to the self-induced velocity applied on the centerline (Section 2.3.1), the following asymptotic expression for the dispersion relation of a vortex filament also exists:

$$D(l) = \pm\left(\frac{l}{2}\right)^2\left[\log l + \left(\gamma - \frac{1}{2}\right) + 4\pi\int_0^{\infty} g'(\rho)\,\log\rho\,d\rho\right]\,. \tag{2.98}$$

This expression corresponds to the asymptotic value of Equation (2.94) as $l \to 0$.

2.4.2.2 Some examples

In this section, the dispersion relation $\Omega(l)$ given by the analysis of Section 2.4.2.1 is examined for the case of some common three-dimensional velocity smoothings $g(\rho)$.

In what follows, the Fourier transform of $Q(|\eta|)$ is evaluated using

$$\begin{aligned}\hat{Q}(l) &= 2\int_0^\infty Q(\rho)\cos(l\rho)d\rho \\ &= 8\pi\left[\int_0^\infty \frac{g(\rho)}{\rho^3}\cos(l\rho)d\rho - \int_0^\infty \frac{g'(\rho)}{\rho^2}\cos(l\rho)d\rho\right] . \end{aligned} \tag{2.99}$$

The three-dimensional Gaussian smoothing (B.8) leads, with the use of Equations (2.87), (2.99) and [43], to

$$\begin{aligned}
C &= 4\pi\int_0^\infty \frac{g'(\rho)}{\rho^2}d\rho = \left(\frac{2}{\pi}\right)^{\frac{1}{2}}\int_0^\infty e^{-\rho^2/2}d\rho = 1 , \\
4\pi\int_0^\infty \frac{g'(\rho)}{\rho^2}\cos(l\rho)d\rho &= \left(\frac{2}{\pi}\right)^{\frac{1}{2}}\int_0^\infty e^{-\rho^2/2}\cos(l\rho)d\rho = e^{-l^2/2} , \\
&4\pi\int_0^\infty \frac{g(\rho)}{\rho^3}\cos(l\rho)d\rho \\
&= \frac{1}{2}\left[\int_0^\infty \frac{g'(\rho)}{\rho^2}\cos(l\rho)d\rho - l\int_0^\infty \frac{g'(\rho)}{\rho}\sin(l\rho)d\rho + l^2\int_0^\infty g'(\rho)\,\mathrm{Ci}(l\rho)d\rho\right] \\
&= \frac{1}{2}\left(\frac{2}{\pi}\right)^{\frac{1}{2}}\left[\int_0^\infty e^{-\rho^2/2}\cos(l\rho)d\rho - l\int_0^\infty \rho\, e^{-\rho^2/2}\sin(l\rho)d\rho + l^2\int_0^\infty \rho^2 e^{-\rho^2/2}\mathrm{Ci}(l\rho)d\rho\right] \\
&= \frac{1}{2}\left[e^{-l^2/2} - l^2e^{-l^2/2} + l^2\int_0^\infty \rho^2e^{-\rho^2/2}\left(\gamma + \log(l\rho) + \sum_{n=1}^\infty \frac{(-1)^n(l\rho)^{2n}}{2n(2n)!}\right)\right] \\
&= \frac{1}{2}\Bigg[(1-l^2)e^{-l^2/2} + l^2\Bigg(\gamma\int_0^\infty \rho^2e^{-\rho^2/2}d\rho + \int_0^\infty \log(l\rho)\rho^2e^{-\rho^2/2}d\rho \\
&\qquad + \sum_{n=1}^\infty \frac{(-1)^n}{2n(2n)!}\int_0^\infty (l\rho)^{2n}\rho^2e^{-\rho^2/2}d\rho\Bigg)\Bigg] \\
&= \frac{1}{2}\left[(1-l^2)e^{-l^2/2} + l^2\left(\frac{1}{2}\left(2+\gamma-\log 2+\log l^2\right) + \sum_{n=1}^\infty \frac{(-1)^n(2n+1)!!\,l^{2n}}{2n(2n)!}\right)\right] , \\
&\hat{Q}(l) \\
&= -(1+l^2)e^{-l^2/2} + l^2\left(\frac{1}{2}\left(2+\gamma-\log 2+\log l^2\right) + \sum_{n=1}^\infty \frac{(-1)^n(2n+1)!!\,l^{2n}}{2n(2n)!}\right) ,
\end{aligned} \tag{2.100}$$

where $\mathrm{Ci}(x)$ is the Cosine Integral, $\mathrm{Ci}(x) = -\int_x^\infty \cos t/t\,dt = \gamma + \log x + \int_0^x(\cos t - 1)/t\,dt = \gamma + \log x + \sum_{n=1}^\infty(-1)^n x^{2n}/2n(2n)!$. Notice that uniform convergence of the infinite series has been assumed so as to be allowed to switch the order of the sum and integral. Notice also the usual notation $(2n+1)!! = 1\cdot 3\cdots(2n+1)$.The expression for the dispersion relation finally becomes

$$\begin{aligned}D(l) &= \pm\frac{1}{4}\Bigg[1-(1+l^2)e^{-l^2/2} + l^2\Bigg(\frac{1}{2}\left(2+\gamma-\log 2+\log l^2\right) \\ &\qquad + \sum_{n=1}^\infty \frac{(-1)^n(2n+1)!!\,l^{2n}}{2n(2n)!}\Bigg)\Bigg] . \end{aligned} \tag{2.101}$$

The expansion of the dispersion relation (2.101) for small l leads to

$$D(l) = \pm \left(\frac{l}{2}\right)^2 \left[\log\left(\frac{l}{2}\right) + \frac{1}{2}(\log 2 + \gamma + 1) + \mathcal{O}(l^2 \log l)\right] , \tag{2.102}$$

which does not agree with Equation (2.75) obtained using Saffman's formula (2.74) with the corresponding two-dimensional vorticity distribution (B.9).

The three-dimensional low order algebraic smoothing (B.10) leads to

$$\begin{aligned}
C &= 4\pi \int_0^\infty \frac{g'(\rho)}{\rho^2} d\rho = 3 \int_0^\infty \frac{1}{(\rho^2+1)^{\frac{5}{2}}} d\rho = 2 , \\
4\pi \int_0^\infty \frac{g'(\rho)}{\rho^2} \cos(l\rho) d\rho &= 3 \int_0^\infty \frac{\cos(l\rho)}{(\rho^2+1)^{\frac{5}{2}}} d\rho = \frac{3\sqrt{\pi}}{4\Gamma(5/2)} l^2 \, \mathrm{K}_2(l) \\
&= l^2 \, \mathrm{K}_2(l) , \\
4\pi \int_0^\infty \frac{g(\rho)}{\rho^3} \cos(l\rho) d\rho &= \int_0^\infty \frac{\cos(l\rho)}{(\rho^2+1)^{\frac{3}{2}}} d\rho = \frac{\sqrt{\pi}}{2\Gamma(3/2)} l \, \mathrm{K}_1(l) \\
&= l \, \mathrm{K}_1(l) , \\
\hat{Q}(l) &= 2\left(l \, \mathrm{K}_1(l) - l^2 \, \mathrm{K}_2(l)\right) ,
\end{aligned} \tag{2.103}$$

where K_m is the modified Bessel function of the second kind and order m. The dispersion relation then becomes

$$D(l) = \pm \frac{1}{2}\left(1 + l \, \mathrm{K}_1(l) - l^2 \, \mathrm{K}_2(l)\right) , \tag{2.104}$$

and the expansion for small l leads to

$$D(l) = \pm \left(\frac{l}{2}\right)^2 \left[\log\left(\frac{l}{2}\right) + \left(\gamma + \frac{1}{2}\right) + \mathcal{O}(l^2 \log l)\right] . \tag{2.105}$$

which agrees with Equation (2.76) obtained using Saffman's formula (2.74) with the corresponding two-dimensional vorticity distribution (B.11). This is a very special case where both formulas lead to the same result.

The three-dimensional constant smoothing (B.14) leads to

$$\begin{aligned}
C &= 4\pi \int_0^\infty \frac{g'(\rho)}{\rho^2} d\rho = 3 \int_0^1 d\rho = 3 , \\
4\pi \int_0^\infty \frac{g'(\rho)}{\rho^2} \cos(l\rho) d\rho &= 3 \int_0^1 \cos(l\rho) d\rho = 3 \frac{\sin l}{l} , \\
4\pi \int_0^\infty \frac{g(\rho)}{\rho^3} \cos(l\rho) d\rho &= \int_0^1 \cos(l\rho) d\rho + \int_1^\infty \frac{\cos(l\rho)}{\rho^3} d\rho \\
&= \frac{\sin l}{l} + \frac{l^2}{2}\left(\frac{1}{l}\left(\frac{\cos l}{l} - \sin l\right) + \mathrm{Ci}(l)\right) \\
&= \frac{\sin l}{l} + \frac{1}{2}\left(\cos l - l \sin l + l^2 \mathrm{Ci}(l)\right) , \\
\hat{Q}(l) &= \cos l - l \sin l + l^2 \, \mathrm{Ci}(l) - 4\frac{\sin l}{l} ,
\end{aligned} \tag{2.106}$$

so that the dispersion relation finally becomes

$$D(l) = \pm\frac{1}{4}\left(3 + \cos l - l\,\sin l + l^2\,\mathrm{Ci}(l) - 4\,\frac{\sin l}{l}\right) . \tag{2.107}$$

The expansion for small l gives

$$D(l) = \pm\left(\frac{l}{2}\right)^2\left[\log\left(\frac{l}{2}\right) + \left(\log 2 + \gamma - \frac{5}{6}\right) + \mathcal{O}(l^2\log l)\right] . \tag{2.108}$$

It was not possible to integrate Saffman's formula (2.74) in closed form with the corresponding two-dimensional vorticity distribution (B.15).

The same conclusion as in Section 2.3 applies here. The approach of computing the dispersion relation of a straight vortex filament by considering the velocity on the centerline does not, in general, reproduce the results obtained with the more careful analysis of Saffman, except in the very particular case of the low order algebraic smoothing. However, if mimicking the correct behavior of the dispersion relation for small l is desired, it can be done by rescaling the core size in the same way as explained in Section 2.3.2.

In Figure J.3, the dispersion relation for the three smoothings considered above is given, together with Kelvin's lowest mode dispersion relation. The core size of each smoothing was appropriately redefined so that all dispersion relations follow the uniform vorticity dispersion relation as $l \to 0$. In other words, if σ_K is the core radius of the constant vorticity distribution, then the core size of the three-dimensional smoothing was taken as $\sigma = \beta\sigma_K$ with β given by (2.72). Notice that there is only one set of curves drawn, the other set being the mirror image with respect to the l axis as in Figure J.2 from Robinson & Saffman (1984). It is interesting to note that all curves fail to reproduce Kelvin's dispersion relation as soon as $l = k\sigma_K \geq 1$. Kelvin's dispersion relation does not cross the l axis. Instead, it approaches $1/2$ asymptotically as $l \to \infty$. All curves obtained with the three-dimensional velocity smoothings do cross the l axis at a value of l of around 2. There is thus a typical wavelength for which a vortex filament subjected to its self-induced velocity applied on the centerline does not rotate. Such a mode is very likely to become unstable in the presence of strain. Notice also that all dispersion curves approach the negative value $-C/4$ as $l \to \infty$, instead of Kelvin's value of $1/2$.

2.4.3 A three-dimensional velocity smoothing that reproduces Kelvin's lowest mode dispersion relation

It was shown in Section 2.4.2 that all common three-dimensional velocity smoothings lead to a dispersion relation that does not follow Kelvin's lowest mode dispersion

relation as soon as $l = k\sigma_K \geq 1$. This means that, as soon as $\lambda \leq 2\pi\sigma_K$, the dynamics of a vortex filament are poorly modeled by moving the filament with its own velocity field applied on the centerline.

The problem of interest in the present section is the following: Is there a three-dimensional velocity smoothing, call it $q(\rho)$, which reproduces Kelvin's lowest mode dispersion relation for all wave numbers l ? Of course very large values of l are not of much interest because a vortex tube perturbed with a very short wavelength undergoes core deformations that cannot be represented with a single vortex filament as is the case for Kelvin's lowest mode. So, if large wave numbers (i.e., wavelengths that are small with respect to the core size of the vortex tube) are of interest, one has to use many filaments, each of which with a small core size σ^p to represent accurately the core structure of a vortex tube of core size σ. After all, the method of vortex filaments converges as the number of filaments $p \to \infty$ and $\sigma^p \to 0$. Nevertheless, it is thought that there is a range of dimensionless wave numbers, say l up to 3 or 4 for which it still is of interest to obtain a numerical scheme that is able to reproduce Kelvin's lowest mode dispersion relation with only one vortex filament. Such a scheme might help eliminate spurious numerical instabilities. This problem is investigated in what follows.

The three-dimensional smoothing of interest $q(\rho)$ will not be constrained to be derived from a vorticity smoothing $\zeta(\rho)$, i.e., $q(\rho) \neq \int_0^\rho \zeta(t)t^2dt$. Indeed, if $q(\rho)$ is constrained in that way, then it will be $\mathcal{O}(\rho^3)$ for small ρ, since a *physically acceptable* vorticity smoothing is $\mathcal{O}(1)$ for small ρ (cfr. Table B.1). $q(\rho)$ should not be $\mathcal{O}(\rho^3)$ for small ρ because this is the behavior of all common smoothings $g(\rho)$, and they all fail to reproduce Kelvin's lowest mode dispersion relation.

Thus, the following inverse problem is considered: Given Kelvin's lowest mode dispersion relation for the uniform vorticity core $D_K(l) = \pi\sigma_K^2\Omega(l)/\Gamma$ for all l, it is desired to find a function $q(\rho)$ such that

$$D_K(l) = -\frac{1}{4}(C + \hat{Q}(l)) \,, \tag{2.109}$$

where

$$C = -2\int_0^\infty Q(\rho)d\rho = 8\pi\int_0^\infty \frac{1}{\rho}\frac{d}{d\rho}\left(\frac{q(\rho)}{\rho}\right)d\rho \,, \tag{2.110}$$

and $\hat{Q}(l)$ is the Fourier transform of $Q(|\eta|)$,

$$\hat{Q}(l) = \int_\infty^\infty Q(|\eta|)e^{-il\eta}d\eta = 2\int_0^\infty Q(\rho)\cos(l\rho)d\rho = -8\pi\int_0^\infty \frac{1}{\rho}\frac{d}{d\rho}\left(\frac{q(\rho)}{\rho}\right)\cos(l\rho)d\rho \,. \tag{2.111}$$

Notice that the upper curve of the dispersion relation is assumed when writing Equation (2.109). This convention will be kept in all that follows, remembering that there

are two curves that are the mirror image of each other with respect to the l axis. Now, since it is known that Kelvin's dipersion relation approaches $1/2$ when $l \to \infty$, this gives $C/4 = -1/2$. Thus, the following integral constraint needs to be satisfied:

$$4\pi \int_0^\infty \frac{1}{\rho}\frac{d}{d\rho}\left(\frac{q(\rho)}{\rho}\right) d\rho = -1 \ . \tag{2.112}$$

Equation (2.112) already shows that $q(\rho)$ cannot have any $\mathcal{O}(\rho^2)$ term for small ρ, but does not rule out the possibility of an $\mathcal{O}(\rho)$ term. Moreover, Equation (2.109) gives

$$\hat{Q}(l) = -C - 4\, D_K(l) = 2 - 4\, D_K(l) \ , \tag{2.113}$$

so that $\hat{Q}(l)$ is known provided $D_K(l)$ is known. The inverse Fourier transform of $\hat{Q}(l)$ produces $Q(\rho)$ which can then be integrated to obtain $q(\rho)$

$$4\pi\frac{q(\rho)}{\rho} = -\int_0^\rho Q(t)\, t\, dt + \text{constant} \ , \tag{2.114}$$

where the constant of integration is chosen so that $4\pi q(\rho) \to 1$ as $\rho \to \infty$. The principles of the method for finding $q(\rho)$ are thus completely defined. The only problem with the above is that Kelvin's dispersion relation for the lowest mode is not known explicitly in the form $D_K = D_K(l)$. Instead it is given by an implicit relation of the form $F(D_K, l) = 0$ as is shown by Equation (2.73). Kelvin's exact dispersion relation is therefore approximated using an expression that has the same behavior as the exact result for small l, Equation (2.77), and that approaches $1/2$ as $l \to \infty$. An expression of the form

$$D_K(l) = \frac{1}{2} - \frac{1}{2}\left(\frac{1 + \left(\frac{l}{2}\right)^2 \log\left(\frac{l}{2}\right)^2}{\left(\frac{cl}{2}\right)^4 + \left(\frac{1}{2} - 2\gamma\right)\left(\frac{l}{2}\right)^2 + 1}\right) \tag{2.115}$$

is assumed, where c^2 is an adjustable parameter that is real and positive. This expression approaches $1/2$ asymptotically and gives, for small l,

$$\begin{aligned} D_K(l) &\simeq -\frac{1}{2}\left(\frac{l}{2}\right)^2 \log\left(\frac{l}{2}\right)^2 - (\gamma - \frac{1}{4})\left(\frac{l}{2}\right)^2 + \mathcal{O}(l^4 + l^4 \log l) \\ &= -\left(\frac{l}{2}\right)^2 \left[\log\left(\frac{l}{2}\right) + \left(\gamma - \frac{1}{4}\right) + \mathcal{O}(l^2 \log l)\right] \end{aligned} \tag{2.116}$$

which is identical to Equation (2.77). In Figure J.4, a comparison between Kelvin's lowest mode exact dispersion relation and the approximation (2.115) for different values of the free parameter c^2 is given. The best fit is obtained with $c^2 = 1.43$, at least in the range of interest with wave numbers that are small to moderate.

Use of Equation (2.115) with Equation (2.113) leads to the following approximation for $\hat{Q}(l)$,

$$\hat{Q}(l) = 2\left(\frac{1+\left(\frac{l}{2}\right)^2 \log\left(\frac{l}{2}\right)^2}{\left(\frac{cl}{2}\right)^4 + \left(\frac{1}{2}-2\gamma\right)\left(\frac{l}{2}\right)^2 + 1}\right) . \tag{2.117}$$

The evaluation of the inverse Fourier transform of $\hat{Q}(l)$ and the subsequent integration of $Q(\rho)$ to obtain $q(\rho)$ from Equation (2.114) are mathematically involved and are given in Appendix C. The expression for $q(\rho)$ that comes from the analysis is lengthy and is also given in Appendix C, together with a listing of the Fortran program that evaluates $q(\rho)$.

One main result is that $q(\rho)$ behaves like

$$4\pi q(\rho) = A\,\rho + B\,\rho^3 + \cdots \tag{2.118}$$

for small ρ, as opposed to usual velocity smoothings that are $\mathcal{O}(\rho^3)$ for small ρ.

In Figure J.5, plots of $q(\rho)$ for different values of the parameter c^2 are given. It is remarkable that the $q(\rho)$ function behaves very smoothly when the parameter c^2 is the one that leads to the best fit of Kelvin's dispersion relation (i.e., $c^2 = 1.43$), and does not behave that smoothly otherwise. This leads to a strong belief that this $q(\rho)$ function, obtained from an inverse problem with an approximation of Kelvin's exact dispersion relation, is very close to the exact $q(\rho)$ function that would be obtained if Kelvin's dispersion relation were known explicitly.

Now the use of the new velocity smoothing function $q(\rho)$ for numerical computations is examined. Recall the dynamics of a vortex filament evolving under the regularized Biot-Savart velocity integral applied on the centerline

$$\frac{\partial}{\partial t}\mathbf{x}(s,t) = -\Gamma \int_c \frac{q\left(\frac{|\mathbf{x}-\mathbf{x}'|}{\sigma_K}\right)}{|\mathbf{x}-\mathbf{x}'|^3}(\mathbf{x}-\mathbf{x}') \wedge \frac{\partial \mathbf{x}'}{\partial s'}\, ds' , \tag{2.119}$$

where $\mathbf{x}-\mathbf{x}'$ stands for $\mathbf{x}(s,t)-\mathbf{x}(s',t)$, $q(\rho)$ is the three-dimensional velocity smoothing and s is a material coordinate which is not necessarily a length coordinate. With $q(\rho)$ of the form (2.118), one might suspect that the new velocity smoothing cannot be used and that the integral diverges when $s \to s'$. Fortunately, this is not the case, due to the presence of the cross-product in the integrand. Indeed, recalling the Taylor series expansion of $\mathbf{x}(s',t)$ about $\mathbf{x}(s,t)$, Equation (2.13), the limit of the integrand is obtained as

$$\frac{q\left(\frac{|\mathbf{x}-\mathbf{x}'|}{\sigma_K}\right)}{|\mathbf{x}-\mathbf{x}'|^3}(\mathbf{x}-\mathbf{x}') \wedge \frac{\partial \mathbf{x}'}{\partial s'} = \frac{A}{2\sigma_K}\frac{\left(\frac{\partial^2 \mathbf{x}}{\partial s^2} \wedge \frac{\partial \mathbf{x}}{\partial s}\right)}{\left(\frac{\partial \mathbf{x}}{\partial s}\cdot\frac{\partial \mathbf{x}}{\partial s}\right)^{\frac{3}{2}}} + \mathcal{O}(s'-s) . \tag{2.120}$$

Thus the remarkable result is obtained that, in addition to the far field velocity contribution that would be obtained with any usual velocity smoothing, the use of the new $q(\rho)$ smoothing also leads to a non-zero velocity contribution due to the local curvature (with usual velocity smoothings, there is no local contribution to the self-induced velocity since the Biot-Savart law is proportional to $\int (s'-s)^2\, ds'$).

An important remark has to be made at this point: the fact that the integrand is finite when $\mathbf{x}(s,t) \rightarrow \mathbf{x}(s',t)$ in Equation (2.120) is due to the fact that the approach to $\mathbf{x}(s',t)$ is made on the filament. The integrand diverges like $1/r$ when approaching $\mathbf{x}(s',t)$ from any other direction. This is not surprising because the new velocity smoothing $q(\rho)$ was *designed* to only correctly reproduce the behavior of one filament evolving under the regularized Biot-Savart integral applied on the centerline. Consequently, the $q(\rho)$ function should not be used for multiple-filament computations, unless the interaction in between filaments is done using some common $g(\rho)$ smoothing, reserving the $q(\rho)$ smoothing for the influence of the filament on itself. However, there is no theoretical support for this procedure, and it is recommended that multiple-filament computations be done using only $g(\rho)$ smoothings. For instance, a vortex filament computation of a vortex tube with core deformation should be performed using multiple filaments with overlapping of the individual cores so that the sum of the individual vorticity distributions is capable of representing the core structure of the vortex tube.

For single-filament computations, the use of the new velocity smoothing $q(\rho)$ as given by Equation (C.18) in Appendix C is costly. As an alternative, $q(\rho)$ is stored in a table for $\rho = 0$ to $\rho = 20$ by increment $\Delta\rho = .01$, and a table look up with linear interpolation between data points is used. This method was found to give $q(\rho)$ to less than .01 % error. For ρ larger than 20, $q(\rho)$ is approximated using an expression of the type $4\pi q(\rho) = 1 + c_1/\rho + c_2/\rho^2$, where c_1 and c_2 are taken as the best fit.

It is also useful to decouple numerically the local velocity contribution due to the local curvature from the far field contribution. Failure to do so might introduce numerical problems when the vortex filament loops back on itself, i.e., when $\mathbf{x}(s,t) \rightarrow \mathbf{x}(s',t)$ without $s \rightarrow s'$. An easy way of decoupling the local influence from the far field is to write

$$\begin{aligned} 4\pi q(\rho) &= A\,\rho + B\,\rho^3 + \cdots \\ &= A\rho\, e^{-\rho^2/\epsilon^2} + 4\pi q_\epsilon(\rho)\,, \end{aligned} \tag{2.121}$$

where $q_\epsilon(\rho)$ is a function similar to usual $g(\rho)$ smoothings, i.e., $q_\epsilon(\rho)$ is $\mathcal{O}(\rho^3)$ for small ρ. At this point, the parameter ϵ is purely arbitrary. Whatever does not go into $q_\epsilon(\rho)$ goes into the first term. The advantage of writing $q(\rho)$ in this form is that the first

term velocity contribution to the velocity can be evaluated analytically for small ϵ. The remaining part $q_\epsilon(\rho)$ is handled numerically in the same way as usual smoothings $g(\rho)$ are handled. One just has to store $q_\epsilon(\rho)/\rho^3$ in a table and use a table look up with linear interpolation between data points as explained above. In Figure J.6, both $q(\rho)/\rho$ and $q_\epsilon(\rho)/\rho$ are shown, together with $g(\rho)/\rho)$ for the case of the low order algebraic smoothing with the proper scaling (i.e., with $\beta = e^{-3/4}$). Notice the similar behaviors of $q_\epsilon(\rho)/\rho$ and $g(\rho)/\rho$. With $q(\rho)$ given by Equation (2.121), the dynamics of the vortex filament become

$$\begin{aligned}\frac{\partial}{\partial t}\mathbf{x}(s,t) &= -\Gamma\left[\frac{A}{4\pi\sigma_K}\int_C \frac{\exp\left(-\frac{|\mathbf{x}-\mathbf{x}'|^2}{\epsilon^2\sigma_K^2}\right)}{|\mathbf{x}-\mathbf{x}'|^2}(\mathbf{x}-\mathbf{x}')\wedge\frac{\partial\mathbf{x}'}{\partial s'}\,ds'\right.\\ &\left.+\int_C \frac{q_\epsilon\left(\frac{|\mathbf{x}-\mathbf{x}'|}{\sigma_K}\right)}{|\mathbf{x}-\mathbf{x}'|^3}(\mathbf{x}-\mathbf{x}')\wedge\frac{\partial\mathbf{x}'}{\partial s'}\,ds'\right]. \qquad (2.122)\end{aligned}$$

The first integral is now approximated by Laplace's method for asymptotic behavior of integrals [19]. Using Equation (2.13), it is found that

$$\begin{aligned}&\frac{1}{2}\frac{\left(\frac{\partial^2\mathbf{x}}{\partial s^2}\wedge\frac{\partial\mathbf{x}}{\partial s}\right)}{\left(\frac{\partial\mathbf{x}}{\partial s}\cdot\frac{\partial\mathbf{x}}{\partial s}\right)}\int^{s'}\left[\frac{\left(1+\frac{2}{3}(s'-s)\left(\frac{\partial^3\mathbf{x}}{\partial s^3}\wedge\frac{\partial\mathbf{x}}{\partial s}\right)/\left(\frac{\partial^2\mathbf{x}}{\partial s^2}\wedge\frac{\partial\mathbf{x}}{\partial s}\right)+\cdots\right)}{\left(1+(s'-s)\left(\frac{\partial^2\mathbf{x}}{\partial s^2}\cdot\frac{\partial\mathbf{x}}{\partial s}\right)/\left(\frac{\partial\mathbf{x}}{\partial s}\cdot\frac{\partial\mathbf{x}}{\partial s}\right)+\cdots\right)}\times\right.\\ &\left.\exp\left(-\frac{(s'-s)^2}{\epsilon^2\sigma_K^2}\left(\frac{\partial\mathbf{x}}{\partial s}\cdot\frac{\partial\mathbf{x}}{\partial s}\right)\left(1+(s'-s)\left(\frac{\partial^2\mathbf{x}}{\partial s^2}\cdot\frac{\partial\mathbf{x}}{\partial s}\right)/\left(\frac{\partial\mathbf{x}}{\partial s}\cdot\frac{\partial\mathbf{x}}{\partial s}\right)+\cdots\right)\right)\right]ds'. \qquad (2.123)\end{aligned}$$

Using only the leading term above, it is found that Laplace's method gives, as $\epsilon\to 0$,

$$\begin{aligned}&\int^{s'}\exp\left(-\frac{(s'-s)^2}{\epsilon^2\sigma_K^2}\left(\frac{\partial\mathbf{x}}{\partial s}\cdot\frac{\partial\mathbf{x}}{\partial s}\right)\right)ds' \sim \int_\infty^\infty \ldots ds' = 2\int_0^\infty \ldots ds'\\ &= \frac{\epsilon\sigma_K}{\left(\frac{\partial\mathbf{x}}{\partial s}\cdot\frac{\partial\mathbf{x}}{\partial s}\right)^{1/2}}\int_0^\infty t^{-1/2}e^{-t}\,dt = \frac{\sqrt{\pi}\epsilon\sigma_K}{\left(\frac{\partial\mathbf{x}}{\partial s}\cdot\frac{\partial\mathbf{x}}{\partial s}\right)^{1/2}}. \qquad (2.124)\end{aligned}$$

An analysis of the second term asymptotic shows an error of $\mathcal{O}(\epsilon^2)$. The approximation to Equation (2.122) finally becomes

$$\frac{\partial}{\partial t}\mathbf{x}(s,t) \simeq -\Gamma\left[\frac{A\sqrt{\pi}\epsilon}{8\pi}\frac{\left(\frac{\partial^2\mathbf{x}}{\partial s^2}\wedge\frac{\partial\mathbf{x}}{\partial s}\right)}{\left(\frac{\partial\mathbf{x}}{\partial s}\cdot\frac{\partial\mathbf{x}}{\partial s}\right)^{3/2}}+\int_C\frac{q_\epsilon\left(\frac{|\mathbf{x}-\mathbf{x}'|}{\sigma_K}\right)}{|\mathbf{x}-\mathbf{x}'|^3}(\mathbf{x}-\mathbf{x}')\wedge\frac{\partial\mathbf{x}'}{\partial s'}\,ds'\right]. \qquad (2.125)$$

Numerical accuracy dictates the choice of the parameter ϵ. ϵ has to be small enough for the asymptotic value of the first integral above to be acceptable. However ϵ cannot be too small because it then becomes difficult to capture numerically the contribution of the integral that involves $q_\epsilon(\rho)$.

Consider the velocity of a thin vortex ring that is subjected to the new velocity smoothing. The asymptotic analysis presented in Section 2.3.1 remains valid when $q(\rho)$ is $\mathcal{O}(\rho)$ for small ρ. In particular, Equation (2.55) remains valid and leads to

$$\begin{aligned} U_R &= \frac{\Gamma}{4\pi R}\left[\log\left(\frac{4R}{\sigma_K}\right) - 4\pi\int_0^\infty q'(\rho)\log\rho\, d\rho\right] \\ &= \frac{\Gamma}{4\pi R}\left[\log\left(\frac{4R}{\sigma_K}\right) - .4440\right] \\ &\simeq \frac{\Gamma}{4\pi R}\left[\log\left(\frac{8R}{\sigma_K}\right) - \frac{1}{4}\right], \end{aligned} \tag{2.126}$$

where the integral has been evaluated numerically with $c^2 = 1.43$. Thus, within the accuracy of the numerical integration and evaluation of $q'(\rho)$, the correct velocity of the vortex ring with uniform core vorticity is recovered. This was to be expected because of the strong analogy between Equation (2.55) and Equation (2.99) and the fact that the new $q(\rho)$ function was designed to reproduce Kelvin's dispersion relation for small l, wathever the value of c^2 is. In other words, this result comes as a consequence of the constraint

$$4\pi\int_0^\infty q'(\rho)\log\rho\, d\rho = \frac{1}{4} - \log 2\,, \tag{2.127}$$

related to the behavior of the dispersion relation for small l and enforced for all values of c^2.

This section is concluded by developing a simplified velocity smoothing $q(\rho)$ that reproduces Kelvin's lowest mode dispersion relation to a reasonable approximation. There is no term of $\mathcal{O}(\rho^2)$ because of the need to satisfy the integral constraint (2.112) but an $\mathcal{O}(\rho)$ term is required. One therefore considers

$$q(\rho) = \frac{1}{4\pi}\frac{\rho}{(\rho^2+1)^{\frac{1}{2}}}\,, \tag{2.128}$$

which is $\mathcal{O}(\rho+\rho^3)$ for small ρ. The associated vorticity smoothing

$$\zeta(\rho) = \frac{q'(\rho)}{\rho^2} = \frac{1}{4\pi}\frac{1}{\rho^2(\rho^2+1)^{\frac{3}{2}}} \tag{2.129}$$

is $\mathcal{O}(1/\rho^2)$ for small ρ and cannot be thought of as a physical vorticity distribution, even when integrated along a filament. Indeed, if a straight filament is considered, one obtains, for the equivalent two-dimensional distributions,

$$\begin{aligned} q_2(\rho) &= \rho^2\int_{-\infty}^{\infty}\frac{q\left((\rho^2+t^2)^{\frac{1}{2}}\right)}{(\rho^2+t^2)^{\frac{3}{2}}}\,dt \\ &= \frac{1}{4\pi}\rho^2\int_{-\infty}^{\infty}\frac{1}{(\rho^2+t^2+1)^{\frac{1}{2}}(\rho^2+t^2)}\,dt \end{aligned}$$

$$= \frac{1}{4\pi}\rho^2\left[\frac{1}{\rho}\arctan\left(\frac{1}{\rho}\frac{t}{(\rho^2+t^2+1)^{\frac{1}{2}}}\right)\right]_{-\infty}^{\infty}$$

$$= \frac{1}{2\pi}\rho\arctan\left(\frac{1}{\rho}\right), \tag{2.130}$$

$$\zeta_2(\rho) = \frac{q_2'(\rho)}{\rho} = \frac{1}{2\pi}\left(\frac{1}{\rho}\arctan\left(\frac{1}{\rho}\right) - \frac{1}{\rho^2+1}\right). \tag{2.131}$$

Notice that $q_2(\rho)$ is $\mathcal{O}(\rho+\rho^2)$ for small ρ and $\zeta_2(\rho)$ is $\mathcal{O}(1/\rho)$ for small ρ. Thus, as $r \to 0$, the two-dimensional vorticity distribution diverges like $1/r$ and the circumferential velocity goes to a constant ($= \Gamma/4\sigma$ in this case). These are thus not physical velocity and vorticity distributions. However it might be that the $q(\rho)$ smoothing used to define the dynamics of a vortex filament evolving under the centerline velocity correctly reproduces the dynamics a physical vortex tube.

The dispersion relation for a filament subjected to the velocity taken on the centerline is obtained using Equations (2.109), (2.110), and (2.111):

$$\begin{aligned}
C &= 2\int_0^\infty \frac{1}{\rho}\frac{d}{d\rho}\left(\frac{1}{(\rho^2+1)^{\frac{1}{2}}}\right)d\rho \\
&= -2\int_0^\infty \frac{1}{(\rho^2+1)^{\frac{3}{2}}}\,d\rho = -2\,, \\
\hat{Q}(l) &= -2\int_0^\infty \frac{1}{\rho}\frac{d}{d\rho}\left(\frac{1}{(\rho^2+1)^{\frac{1}{2}}}\right)\cos(l\rho)\,d\rho\,, \\
&= \frac{\sqrt{\pi}}{\Gamma(3/2)}\,l\,\mathrm{K}_1(l) = 2\,l\,\mathrm{K}_1(l) \\
D(l) &= \mp\frac{1}{4}\left(C+\hat{Q}(l)\right) \\
&= \pm\frac{1}{2}\left(1-l\,\mathrm{K}_1(l)\right)\,,
\end{aligned} \tag{2.132}$$

where K_1 is the modified Bessel function of the second kind and order 1. Notice that $D(l) \to \pm 1/2$ as $l \to \infty$, thus showing that the dispersion relation approaches asymptotically the same value as Kelvin's lowest mode dispersion relation. However, the behaviors for small l do not match. Indeed, the expansion of $D(l)$ for small l gives

$$D(l) = \pm\left(\frac{l}{2}\right)^2\left[\log\left(\frac{l}{2}\right) + \left(\gamma - \frac{1}{2}\right) + \mathcal{O}\left(l^2\log l\right)\right], \tag{2.133}$$

which is not equivalent to Equation (2.116). If the core size σ is rescaled so as to obtain the same expansion of the dispersion relation for small l, $\sigma = \beta\sigma_K$ with $\beta = e^{1/4}$ is obtained. The dispersion relation of this simple smoothing is given in Figure J.4. Notice that, although $D(l) = \pi\sigma^2\Omega(l)/\Gamma$ approaches $1/2$ asymptotically, the rescaled

dispersion relation $D_K(l) = \pi\sigma_K^2\Omega(l)/\Gamma$ approaches $1/(2\beta^2)$ asymptotically. A plot of $q(\rho)$ is also given in Figure J.5, with the core size rescaled, i.e., with $\rho = r/\sigma_K = \beta r/\sigma$.

If the velocity of a thin vortex ring subjected to that velocity smoothing is computed using Equation (2.55), one obtains

$$\begin{aligned} U_R &= \frac{\Gamma}{4\pi R}\left[\log\left(\frac{4R}{\sigma}\right) - \int_0^\infty \frac{1}{(\rho^2+1)^{\frac{3}{2}}}\log\rho\, d\rho\right] \\ &= \frac{\Gamma}{4\pi R}\left[\log\left(\frac{4R}{\sigma}\right) + \log 2\right] \\ &= \frac{\Gamma}{4\pi R}\left[\log\left(\frac{8R}{\sigma}\right) - 0\right] . \end{aligned} \tag{2.134}$$

Again, the scaling of the core size to obtain the correct ring velocity of a uniform vorticity core leads to $\sigma = \beta\sigma_K$ with $\beta = e^{1/4}$.

In conclusion, this very simple three-dimensional smoothing can, with proper scaling, be used instead of the algebraically complicated one. It has a similar behavior, at least in the range of small to medium values of l. In fact, one might suspect that any smoothing which is $\mathcal{O}(\rho + \rho^3)$ for small ρ has a dispersion relation that does not cross the l axis and can thus be used to model Kelvin's lowest mode dispersion relation.

2.5 Numerical results

In this section, the numerical results that were obtained using the method of vortex filaments described in the previous sections are presented.

The space curves $\mathbf{x}^p(s,t)$ are always described using parametric cubic splines. The filaments thus have a continuous second derivative, $\partial^2\mathbf{x}/\partial s^2$, at each computational point. The integration of the Biot-Savart law is done using the information from the cubic splines and the trapezoidal rule. The trapezoidal integration rule has spectral convergence when the integrand is known exactly and is periodic, i.e., when the vortex filaments are infinite periodic curves or closed curves. Here, the trapezoidal rule is only third order because of the cubic splines approximation of the integrand. The parametric coordinate, s, is always taken as a Lagrangian coordinate and not a length coordinate. The time integration is done using the classical Runge-Kutta scheme of order 4 (RK4). The computations involving usual velocity smoothings, $g(\rho)$, are performed using the low order algebraic smoothing (B.10). The reason for this choice is that, at the time the computations were performed, the new high order algebraic smoothing (B.12) was not yet discovered. For multiple-filament computations, the error estimates presented in Section 2.2.2 show however that it is

important, for convergence, to consider high order regularization functions such as the Gaussian smoothing (B.8) or our high order algebraic smoothing (B.12).

Finally, the plots of vortex filaments are done by simply connecting the computational points with straight line segments instead of using the spline fits.

2.5.1 Numerical verification of the dispersion relation

An important first step in the use of the new velocity smoothing, $q(\rho)$, presented in Section 2.4.3 is to verify numerically the correctness of the lengthy mathematical derivations of Section 2.4.3 and Appendix C. Does the new $q(\rho)$ smoothing reproduce indeed Kelvin's lowest mode dispersion relation when used numerically ?

The numerical computation of an infinite periodic vortex filament evolving under the Biot-Savart integral applied on the centerline is done following a procedure that was first introduced by Moore (1972), but that has been modified for better accuracy when the wavelength λ of interest is not much bigger than the core size σ of the filament. The procedure is presented in detail in Appendix D.

Figure J.7 shows the numerical results obtained with an infinite periodic vortex filament perturbed by a sine wave (i.e., the sum of two helical waves as discussed in Section 2.4.2). $N_\lambda = 40$ computational points per wavelength have been used. The numerical data obtained with the low order algebraic smoothing (B.10) fall exactly on the theoretical curve given by Equation (2.103). The data obtained with the new smoothing $q(\rho)$ and $c^2 = 1.43$ fall almost exactly on Kelvin's lowest mode curve (actually, they fall exactly on the approximation (2.115) to Kelvin's curve). These results are very comforting because they imply that the mathematical developments of Section 2.4.3 and Appendix C are indeed correct.

Figure J.8 shows the effect of the splitting of the new velocity function $q(\rho)$ as explained in Section 2.4.3. Different values of the splitting parameter, ϵ, have been investigated numerically for a fixed number, $N_\lambda = 40$, of computational points per wavelength. The choice $\epsilon = .1$ gives the best results up to $l = k\sigma_K \simeq 5$. The choice $\epsilon = .15$ gives good results up to $l \simeq 4$. Taking $\epsilon = .25$ leads to poor results as soon as $l \simeq 2$. Of course, the smaller ϵ, the better the numerical result (assuming that the contribution of $q_\epsilon(\rho)$ is correctly captured by the discretization, i.e., that N is large enough !).

Figure J.9 shows the effect of the discretization, i.e., the effect of N_λ for a fixed value of the splitting parameter $\epsilon = .15$. It appears that a poor discretization of the filament leads very quickly to a wrong numerical dispersion relation. For instance, $N_\lambda = 5$ is obviously not sufficient.

One conclusion of this investigation is that $N_\lambda = 10$ with $\epsilon = .15$ is a fair choice

if the range of interest is $l \leq 3$. Another conclusion is that, if the filament is not expected to loop back on itself, then the full $q(\rho)$ function should be used instead of the split expression (2.125).

2.5.2 Results on vortex rings.

2.5.2.1 The velocity of the single-filament vortex ring

Another problem of interest is the determination of the velocity of a single-filament vortex ring subjected to the Biot-Savart velocity applied on the centerline, and the comparison with some known results. The results of this investigation are summarized in Figure J.10. The exact result for the velocity of a vortex ring with the low order algebraic smoothing (B.10), Equation (2.67), is plotted for the full range of values of σ_K/R. The numerical results obtained using the new velocity smoothing $q(\rho)$ with $N = 200$ computational points are also plotted. These results can be compared with the results of Lamb (1932), Fraenkel (1972) and Norbury (1973). The asymptotic result of Lamb (1932) for the thin vortex ring with uniform vorticity is given by Equation (2.63). The higher order asymptotic result of Fraenkel (1972) for the ring with uniform ω/r is, in the present notation, given by

$$U_R = \frac{\Gamma}{4\pi R}\left[\left(\log\left(\frac{8R}{\sigma_K}\right) - \frac{1}{4}\right) - \frac{3}{8}\left(\frac{\sigma_K}{R}\right)^2\left(\log\left(\frac{8R}{\sigma_K}\right) - \frac{5}{4}\right)\right] . \qquad (2.135)$$

Notice that the definitions $A = \pi\sigma_K^2$ for the area $\Gamma = \pi U_R R$ for the circulation have been used in order to present his results with the present notation. For instance, the Hill's spherical vortex corresponds to $\sigma_K/R = \sqrt{2}$.

The results of Norbury (1973) are both analytical and numerical. He gives the computed shape and overall properties of the ring with uniform ω/r over the full range of values of σ_K/R and compares these results with asymptotic formulas. His results for the velocity of the ring are also plotted in Figure J.10. Because the circulation Γ is not a constant in his numerical computation, it was rescaled properly so as to be consistent with the above definitions of A and Γ.

Notice that the ring velocity obtained with the low order algebraic smoothing $g(\rho)$ is closer to Norbury's result than the ring velocity obtained with the new velocity smoothing $q(\rho)$, although the differences are small.

2.5.2.2 The stability of the single-filament vortex ring

As discussed in Section 2.4.1, the instability of a vortex ring is related to the dispersion relation of the rectilinear vortex filament (Widnall, Bliss & Tsai 1974, Moore &

Saffman 1975, Tsai & Widnall 1976, Widnall & Tsai 1977). Modes that do not rotate or that rotate slowly are unstable in the presence of a weak strain. The flow near the core of a thin vortex ring of radius R and core size σ is close to that near a rectilinear vortex in a uniform strain, the weak strain at some location along the torus being due to the velocity field induced by the rest of the ring (Widnall, Bliss & Tsai 1974). The principal axes of the strain are at 45° with respect to the plane of the ring, roughly speaking. Modes that do not rotate are convected away from their disturbed position with a velocity that is proportional to their displacement and hence become unstable. Saffman (1978) gives formulas for the number of waves to expect on a thin ring. For the thin ring of uniform vorticity within the core σ_K, the dispersion relation of Kelvin (1880) has an enumerable infinity of zeroes (see Figure J.2 from Robinson & Saffman 1984). The first two occur at the value of $l_1 = k_1\sigma_K \simeq 2.5$ (mode 1) and $l_2 = k_2\sigma_K \simeq 4.35$ (mode 2). The dispersion relation associated with the lowest mode (mode 0) has no zero. Mode 1 is more likely to occur than mode 2. According to Saffman's estimate, the number of waves on the vortex ring is an integer N_w approximated by

$$N_w = k\,R = .40\,e^{\tilde{U}}\,, \tag{2.136}$$

where

$$\tilde{U} = \frac{4\pi R}{\Gamma}\,U_R = \log\left(\frac{8R}{\sigma_K}\right) - \frac{1}{4}\,. \tag{2.137}$$

For instance, with $R = 1.0$ and $\sigma_K = .50$, $k = 5 \simeq 4.98$ is obtained for mode 1. Such a ring is thus expected to go unstable in mode 1 and with $N_w = 5$ wavelengths along the torus.

The dispersion relation corresponding to usual velocity smoothing, $g(\rho)$, has a zero for mode 0 at a value of $l_0 = k_0\sigma_K \simeq 2\ldots3$ ($l_0 = 2.37$ for the low order algebraic smoothing). A single-filament vortex ring subjected to one of these smoothings is thus expected to become unstable in mode 0 with approximately the correct wavelength. On the other hand, the dispersion relation for the new velocity smoothing, $q(\rho)$, has no zero since it reproduces Kelvin's dispersion relation for mode 0. A single-filament vortex ring subjected to that smoothing is thus expected to be stable.

The results of a numerical computation presented in Figure J.11 show that this is indeed the case. These computations are done using one filament discretized with $N = 64$ computational points. Each filament has circulation $\Gamma = 1.0$, radius $R = 1.0$ and core size $\sigma_K = .50$ (i.e., $\sigma = \beta\sigma_K$ with $\beta = e^{-3/4}$ for the low order algebraic smoothing $g(\rho)$ and $\beta = 1$ for the new smoothing $q(\rho)$). At $t = 0$, the position of each computational point is perturbed with a random amplitude $\leq .0025$. The direction of the perturbation is also randomized. Both computations are started using the same initial condition and are done with $\Delta t = .10$. The core size is subjected to

Equation (2.48). According to Saffman's formula (2.136), it is also expected to obtain $N_w = 5$ wavelengths along the filament when the low order algebraic smoothing is used. This is indeed the case as can be seen from Figure J.11 ($\sigma_K(t = 50.) = .43178$). On the other hand, the single-filament vortex ring that is subjected to the new velocity smoothing remains stable for all times ($\sigma_K(t = 120.) = .50003$). This is consistent with the fact that a vortex ring cannot go unstable in mode 0, i.e., when there is no degree of freedom to describe the core structure .

The conclusion of this section is that one has to be careful when computing problems where the physics strongly depends on the core structure of vortex tubes. In the above, it is pure luck that the numerical unstable mode at $l_0 \simeq 2.37$ almost identically matches the physical unstable mode at $l_1 \simeq 2.5$.

In fact, the correct way of computing the instability of a vortex ring is to use a usual smoothing $g(\rho)$ that is convergent (such as the high order algebraic smoothing) and to discretize the core structure σ_K with many filaments p and $\sigma^p << \sigma_K$. Then, if one obtains instability at $l_1 = k_1\sigma_K \simeq 2.5$ with $k_1\sigma^p << 1$, one expects that the physics of the problem is correctly captured because of the convergence of the method of vortex filaments.

2.5.3 Results on solitary waves on a rectilinear vortex filament

It was shown in Section 2.4.3 that the new velocity smoothing $q(\rho)$ leads to a non-zero local contribution to the self-induced velocity of the vortex filament everywhere its curvature is non-zero. This is in contrast with usual velocity smoothings $g(\rho)$ for which the local contribution to the self-induced velocity is zero since $g(\rho)$ is $\mathcal{O}(\rho^3)$ for small $\rho = r/\sigma$. The large differences in their dispersion relation were also shown in Section 2.4.3.

It is interesting to compare the usual smoothings and the new smoothing with the so-called *Localized Induction Approximation* (LIA), an asymptotic theory in which the self-induced velocity of a vortex filament is solely due to the local curvature. Before doing so, both the LIA approximation and the theoretical results that are associated with it are briefly reviewed.

The LIA approximation was introduced to understand the nonlinear behavior of a very thin vortex filament (Sante Da Rios 1906, Hama 1962, 1963 , Arms & Hama 1965). In that approximation, it is assumed that the core size, σ, of the vortex filament is so small than the only self-induced velocity is that due to the local curvature. More specifically, from examining the Biot-Savart induction law with a usual smoothing (or

cut-off), it is found that

$$\frac{\partial}{\partial t}\mathbf{x}(s,t) \simeq -\frac{\Gamma}{4\pi}\left(\log\left(\frac{L}{\sigma}\right)+\mathcal{O}(1)\right)\frac{\left(\frac{\partial^2\mathbf{x}}{\partial s^2}\wedge\frac{\partial\mathbf{x}}{\partial s}\right)}{\left(\frac{\partial\mathbf{x}}{\partial s}\cdot\frac{\partial\mathbf{x}}{\partial s}\right)^{\frac{1}{2}}}, \tag{2.138}$$

where L is a large scale cut-off not fully specified. In the LIA approximation, the term $\log(L/\sigma)$ is taken as constant, neglecting the slow variation of the log compared with its argument. This gives

$$\frac{\partial}{\partial t}\mathbf{x}(s,t) = C\,\frac{\left(\frac{\partial\mathbf{x}}{\partial s}\wedge\frac{\partial^2\mathbf{x}}{\partial s^2}\right)}{\left(\frac{\partial\mathbf{x}}{\partial s}\cdot\frac{\partial\mathbf{x}}{\partial s}\right)^{\frac{3}{2}}}, \tag{2.139}$$

where $C \simeq (\Gamma/4\pi)\log(L/\sigma)$. Of course, the LIA approximation only captures the behavior of the Biot-Savart induction law for the large scale bending of thin vortex filaments. It is however an interesting approximation because there exists a number of exact solutions to Equation (2.139).

The dynamics of a filament evolving under the LIA is usually described with s as an arclength (i.e., $\frac{\partial\mathbf{x}}{\partial s}\cdot\frac{\partial\mathbf{x}}{\partial s}=1$) and using a Frenet-Serret reference frame, an orthonormal frame composed of the local tangent vector $\hat{\mathbf{t}}=\frac{\partial\mathbf{x}}{\partial s}$, the principal normal $\hat{\mathbf{n}}=\frac{\partial^2\mathbf{x}}{\partial s^2}/\kappa$, and the binormal $\hat{\mathbf{b}}=\hat{\mathbf{t}}\wedge\hat{\mathbf{n}}$ (Betchov 1965). $\kappa(s,t)=\left(\frac{\partial^2\mathbf{x}}{\partial s^2}\cdot\frac{\partial^2\mathbf{x}}{\partial s^2}\right)^{1/2}$ is the curvature. Equation (2.139) can then be written as

$$\begin{aligned}\frac{\partial\mathbf{x}}{\partial t} &= C\,\hat{\mathbf{t}}\wedge(\kappa\,\hat{\mathbf{n}}) = C\,\kappa\,\hat{\mathbf{b}}\,,\\ \dot{\mathbf{x}} &= \kappa\,\hat{\mathbf{b}}\,,\end{aligned} \tag{2.140}$$

where the overdot stands for differentiation with respect to a new time, $C\,t$ (which has the dimension of the square of a length). The coordinate vectors vary according to Frenet-Serret formulas

$$\hat{\mathbf{t}}' = -\kappa\,\hat{\mathbf{n}}\quad,\ \hat{\mathbf{n}}' = \tau\,\hat{\mathbf{b}}-\kappa\,\hat{\mathbf{t}}\quad,\ \hat{\mathbf{b}}' = -\tau\,\hat{\mathbf{n}}\,, \tag{2.141}$$

where the prime stands for differentiation with respect to s. τ, defined by the last equation in (2.141), is called the torsion. $\kappa(s,t)$ and $\tau(s,t)$ are enough to completely specify the space curve $\mathbf{x}(s,t)$. Appropriate differentiation of Equation (2.140) and Equation (2.141) leads to a coupled system of partial differential equations for κ and τ

$$\dot{\kappa}+(\kappa\,\tau)'+\kappa'\,\tau = 0\,, \tag{2.142}$$

$$\dot{\tau}-\left(\frac{\kappa''}{\kappa}-\tau^2+\frac{\kappa^2}{2}\right)' = 0\,. \tag{2.143}$$

Hasimoto (1972) gave solutions to Equations (2.142) and (2.143) that are solitons on a straight filament with

$$\tau(s,t) = \tau_0 = c/2 \qquad \text{a constant} \;\; ; \;\; \kappa(s,t) = 2\,\nu\,\mathrm{sech}(\nu\,(s-ct))\,. \tag{2.144}$$

These solitons have constant torsion, τ, and propagate with a constant velocity that is twice the torsion. ν is the inverse of a length scale and only defines the global size of the solitary wave. Given ν and τ_0, and defining $T = \tau_0/\nu$, the shape and position of the soliton is given by (Hasimoto 1972):

$$\begin{aligned} x &= s - \frac{2}{\nu(1+T^2)}\,\tanh(\nu(s-ct))\,, \\ y + i\,z &= \frac{2}{\nu(1+T^2)}\,\mathrm{sech}(\nu(s-ct))\,e^{i\left[T\,\nu(s-ct)+\nu^2(1+T^2)t\right]}\,. \end{aligned} \tag{2.145}$$

Figure J.12 from Hasimoto (1972) illustrates the shape of these solitons for different values of the torsion parameter, T.

More recently, Cieśliński (1985) also gave solutions to Equations (2.142) and (2.143) that are solitons for which the generating vortex filament (of infinite or finite length) remains in the interior of a torus moving with constant velocity.

Now the results which were obtained by subjecting an Hasimoto solitary wave of torsion $T = .50$ to the full Biot-Savart induction law are presented. Two cases are considered, a thin vortex filament with $\sigma_K = .20$ and a fat vortex filament with $\sigma_K = .40$. Each case is computed twice, once with the low order algebraic smoothing (B.10) ($\beta = e^{-3/4}$) and once with the new velocity smoothing (without splitting). The numerical details associated with the computation of an infinite vortex filament are presented in Appendix E. The computations are done with $N = 600$, $\Gamma = 1.0$ and $\Delta t = .05$. The results are shown in Figure J.13 and Figure J.14. With $\sigma_K = .20$, there is a clear tendency to preserve the shape of the initial condition in both computations. This is consistent with the solitary wave behavior of a thin vortex filament as predicted by the LIA theory. The results are very much alike, and the new velocity smoothing gives a slightly lower wave speed. This slight difference is due to the small difference, for small $l = k\,\sigma_K$, in the behavior of the dispersion relation of the two smoothings (Figure J.7). With $\sigma_K = .40$, the vortex filaments do not behave at all in accordance with the LIA theory. The vortex filament is too fat to support solitary waves, and the initial shape is not retained. Moreover, the two computations yield very different results. This is to be expected, at least qualitatively, from the large differences, for medium to large l, in the dispersion relation of the two smoothings. Of course, the case with $\sigma_K = .40$ is not of great physical significance. The vortex tube is simply too fat with respect to the size of the wave to be represented with a single filament.

One should really use a collection of thin filaments in order to capture the internal structure of the vortex core. But this is another subject, and it is still felt that it is of some interest to understand the numerical behavior of isolated vortex filaments, thin or fat.

Finally, the collision of solitary waves is considered. The Hasimoto solitary waves are really solitons. This means, among other things, that, when two or more of these waves collide, each emerges from the collision in its previous form. This process is illustrated in Figure J.15 from Aref & Flinchem (1984). One might however be concerned about the physical significance of these collisions. Indeed, the process of collision is such that different segments of the same vortex filament come very close to each other. When this occurs, the assumption of localized induction fails. No matter how small the core size σ_K, the velocity cannot anymore be only function of the local curvature. Segments which are very close strongly influence each other through the usual Biot-Savart interaction, and it seems very unlikely for the contribution from this interaction to be negligible with respect to the LIA contribution. Computations performed with the full Biot-Savart law confirm these suspicions. Figure J.16 illustrates the collision of two identical waves of torsion $T = .50$. This computation is done with $N = 600$, $\sigma_K = .10$, $\Gamma = 1.0$, $\Delta t = .10$ and the splitting of $q(\rho)$ with $\epsilon = .15$. It is clearly seen that two waves evolving under the full Biot-Savart law do not survive a collision. The outcome of this particular collision seems to be the production of an elongated vortex ring that moves away from the main filament.

2.5.4 Results on the interaction between vortex rings

In this section, the numerical results that were obtained with multiple-filament computations are presented. Both computations presented here involve a strong interaction between two vortex rings. The motivation for these computations is given in detail in Chapter 3, Section 3.5. One should thus refer to that section for additional information. The present results are only qualitative and are presented only for comparison purposes with the quantitative results obtained with the method of vortex particles.

The parameters which are common to both computations are the radius $R = 1.0$ and circulation $\Gamma = 1.0$ of each ring, the number of filaments $P = 9$ per ring (with $\Gamma^p = 1.0/9$), the core size $\sigma^p = .20$ of each filament, and the geometrical parameter $r_l = .04$ (see Figure J.26). The computations are done using the low order algebraic smoothing (B.10) with $\beta = e^{-3/4}$. The core radius of the equivalent uniform vorticity ring is thus roughly $\sigma_K \simeq \sigma^p/\beta + 2\,r_l \simeq .50$. The core size $\sigma^p(t)$ is also subjected to Equation (2.48), and the interaction in between filaments is symmetrized as explained

in Section 2.2.2.

2.5.4.1 The problem of the fusion of two vortex rings computed using the method of regularized vortex filaments

This computation is initialized in the configuration showed in Figure J.25 with the two rings at a spacing $s = 3.0$ center to center and at an angle $\theta_0 = 12.5°$ with respect to the vertical. The number of computational points per filament is $N_\varphi = 128$ for a total of $N = 2304$. The time step is $\Delta t = .05$

The time evolution of the vortex filaments is presented in Figure J.17. Notice the development of helical waves near the reconnection region. These waves correspond to regions of axial flow. It is clearly seen that the fusion process cannot occur because of the inviscid nature of the filament method. Vortex filaments are indeed closed curves (that support constant circulation) for all times and cannot be disconnected (except artificially). It will be seen in Chapter 3, Section 3.5 that the viscous version of the method of vortex particles is able to account for the process of viscous reconnection of vortex tubes.

2.5.4.2 The problem of the two vortex rings in a "knot" configuration computed using the method of regularized vortex filaments

This computation is initialized with the two rings in a knot configuration and a spacing $s = 1.0$ center to center. The number of computational points per filament is $N_\varphi = 64$ for a total of $N = 1152$. The time step is $\Delta t = .09$

The time evolution of the vortex filaments is presented in Figure J.18. The interaction between the two rings is very violent, and the vortex tubes become quickly very convoluted. Concentrated regions with helical waves and hence axial flow are also present. Again, due to the inviscid nature of the filament method, the computation cannot lead to viscous reconnection of vortex tubes and has to be aborted at some point.

Chapter 3

Three-dimensional vortex particles

In the present chapter, the use of vortex particles for computing three-dimensional, incompressible vortical flows is examined. Vortex particles, also commonly called *vortex sticks* or *vortons*, are an alternative to the use of the vortex filaments presented in Chapter 2. They are vector elements. A position vector, a strength vector (= vorticity $\times$ volume), and in some cases a core size are associated to each element. Each element can thus be thought of as a little section of a vortex tube (= circulation $\times$ length). The element is convected with the local velocity, and the evolution of the strength vector is in accordance with Helmholtz equation. The method has the advantage that these particles are somewhat independent. They do not belong to a specific vortex filament for all times. This property makes the method attractive because an explicit treatment of viscous diffusion using a general scheme proposed by Mas-Gallic (1987) and Degond & Mas-Gallic (1988a,1988b) can be incorporated in the method. With that scheme, it is hoped that processes such as vortex tube reconnection can be modeled. The method of vortex particles present however a consistency problem: the particle vorticity field is not guaranteed to be divergence free for all times as it should be. This is an issue of serious concern which has to be addressed.

The following issues are investigated: use of δ-function particles and weak solutions of the vorticity equation (Section 3.1); use of regularized particles and choice of the regularization function (Section 3.2); representation of viscous effects by the redistribution of element strengths (Section 3.3); and conservation laws - how to evaluate them ? - are they satisfied ? (Section 3.4 and Appendix G). The last section, Section 3.5, contains the numerical results. The new algebraic regularization function, introduced in Chapter 2, is used extensively because of its good convergence properties and its computational efficiency. This regularization function is also a prime choice for the evaluation of the quadratic diagnostics: energy, helicity and enstrophy. The convergence of the method, both inviscid and viscous, is investigated on the problem of the axisymmetric vortex ring. Particular emphasis is also placed on the numerical computation of the viscous fusion of two vortex rings and on the comparison of the numerical results with the experimental results of Schatzle and Coles

(1987). It is shown that the viscous method can indeed lead to the entire process of vortex ring fusion and that the method can produce quantitative results. It is also shown numerically that the viscous diffusion helps reduce the inconsistency problems of the method, and that the particle vorticity field remains almost divergence free during the entire course of the computation. Finally, a relaxation scheme is proposed that forces the particle vorticity field to remain almost divergence free for all times, regardless of the effect of viscous diffusion.

As a parenthesis, the use of three-dimensional vortex-dipoles is also investigated theoretically. Since no numerical computations were performed using these vortex-dipoles, the theoretical investigation is reported in an appendix (Appendix H).

3.1 Singular vortex particles and weak solution of the vorticity equation

The three-dimensional vorticity equation for an incompressible flow is given by Equation (2.4). If $\mathbf{u}(\mathbf{x},t)$ is considered to be given, then Equation (2.4) is an hyperbolic evolution equation for the vorticity field, which is the right form to be solved using particle methods for hyperbolic equations (see Raviart 1985, 1987). Indeed, these methods have been developed to solve equations of the type

$$\frac{\partial \mathbf{f}}{\partial t} + \nabla\cdot(\mathbf{f}\,\mathbf{u}) = A(\mathbf{u})\,\mathbf{f}\,, \tag{3.1}$$

where $\mathbf{u}(\mathbf{x},t)$ is a given velocity field and $A(\mathbf{u})$ is a matrix function of $\mathbf{u}$. In the vorticity Equation (2.4), $(\boldsymbol{\omega}\cdot\nabla)\mathbf{u}$ stands for $(\nabla\mathbf{u})\,\boldsymbol{\omega}$, and thus, $A(\mathbf{u}) = \nabla\mathbf{u}$.

Now the vortex particle method is examined more specifically. The vorticity field is discretized onto vortex particles, also called *vortex sticks* or *vortons* (Rehbach 1978, Beale & Majda 1982a, 1982b, Novikov 1983, Aksman, Novikov & Orszag 1985, Mosher 1985, Beale 1986b, Saffman & Meiron 1986, Choquin & Cottet 1988),

$$\boldsymbol{\omega}(\mathbf{x},t) = \sum_p \boldsymbol{\omega}^p(t)\,vol^p\,\delta(\mathbf{x}-\mathbf{x}^p(t)) = \sum_p \boldsymbol{\alpha}^p(t)\,\delta(\mathbf{x}-\mathbf{x}^p(t)) = \sum_p \boldsymbol{\omega}^p\,. \tag{3.2}$$

Here, of course, the velocity field $\mathbf{u}(\mathbf{x},t)$ is not given. It is computed from the particle representation of the vorticity field as the curl of a streamfunction which solves $\nabla^2\boldsymbol{\psi}(\mathbf{x},t) = -\boldsymbol{\omega}(\mathbf{x},t)$, namely

$$\boldsymbol{\psi}(\mathbf{x},t) = G(\mathbf{x}) * \boldsymbol{\omega}(\mathbf{x},t) = \sum_p G(\mathbf{x}-\mathbf{x}^p(t))\,\boldsymbol{\alpha}^p(t) = \frac{1}{4\pi}\sum_p \frac{\boldsymbol{\alpha}^p(t)}{|\mathbf{x}-\mathbf{x}^p(t)|}\,, \tag{3.3}$$

where $*$ stands for the convolution product. The velocity is taken as the curl of (3.3) and is given by

$$\mathbf{u}(\mathbf{x},t) \;=\; \nabla\wedge\boldsymbol{\psi}(\mathbf{x},t) = \sum_p \nabla\left(G(\mathbf{x}-\mathbf{x}^p(t))\right)\wedge\boldsymbol{\alpha}^p(t)$$

$$
\begin{aligned}
&= \frac{1}{4\pi}\sum_p \nabla\left(\frac{1}{|\mathbf{x}-\mathbf{x}^p(t)|}\right)\wedge\boldsymbol{\alpha}^p(t)\\
&= -\frac{1}{4\pi}\sum_p \frac{1}{|\mathbf{x}-\mathbf{x}^p(t)|^3}(\mathbf{x}-\mathbf{x}^p(t))\wedge\boldsymbol{\alpha}^p(t)\\
&= -\frac{1}{4\pi|\mathbf{x}-\mathbf{x}^p(t)|^3}(\mathbf{x}-\mathbf{x}^p(t))\wedge\boldsymbol{\alpha}^p(t)+\mathbf{u}^p(\mathbf{x},t)\\
&= \sum_p \mathbf{K}(\mathbf{x}-\mathbf{x}^p(t))\wedge\boldsymbol{\alpha}^p(t)=(\mathbf{K}(\mathbf{x})\wedge)*\boldsymbol{\omega}(\mathbf{x},t)\,, \qquad (3.4)
\end{aligned}
$$

where $\mathbf{u}^p(\mathbf{x},t)$ stands for the velocity field without the contribution of the p particle, and $\mathbf{K}(\mathbf{x})\wedge = -\left(1/\left(4\pi|\mathbf{x}|^3\right)\right)\,\mathbf{x}\wedge$ is the Biot-Savart kernel.

The evolution equations for the particle position and strength vector are usually taken as

$$
\frac{d}{dt}\mathbf{x}^p(t) = \mathbf{u}^p(\mathbf{x}^p(t),t)\,, \qquad (3.5)
$$

$$
\frac{d}{dt}\boldsymbol{\alpha}^p(t) = (\boldsymbol{\alpha}^p(t)\cdot\nabla)\,\mathbf{u}^p(\mathbf{x}^p(t),t)\,, \qquad (3.6)
$$

which will be referred to as the *classical scheme.*

A few remarks should be made at this point:

- The particle vorticity field (3.2) is not generally divergence free. Indeed,

$$
\nabla\cdot(\boldsymbol{\omega}(\mathbf{x},t)) = \sum_p \nabla(\delta(\mathbf{x}-\mathbf{x}^p(t)))\cdot\boldsymbol{\alpha}^p(t)\,. \qquad (3.7)
$$

  This fact makes the method inconsistent in some sense because a basis which is not divergence free is used to represent a vector field that should be divergence free for all times. In other word, the particle method is only solving for some field $\boldsymbol{\omega}$ according to the hyperbolic equation (2.4). In addition, it shall be seen that the field $\boldsymbol{\omega}(\mathbf{x},t)$ can, as time evolves, become a poor representation of the real vorticity field, even when the initial condition $\boldsymbol{\omega}(\mathbf{x},0)$ is a good representation of the initial vorticity field.

- The streamfunction (3.3) is also not generally divergence free. Indeed,

$$
\nabla\cdot(\boldsymbol{\psi}(\mathbf{x},t)) = -\frac{1}{4\pi}\sum_p \frac{1}{|\mathbf{x}-\mathbf{x}^p(t)|^3}\left((\mathbf{x}-\mathbf{x}^p(t)\cdot\boldsymbol{\alpha}^p(t)\right)\,. \qquad (3.8)
$$

  This result is a direct consequence of the fact that $\nabla^2\boldsymbol{\psi} = -\boldsymbol{\omega}$ is solved with $\boldsymbol{\omega}$ not generally divergence free.

- The velocity field (3.4) is divergence free since it is the curl of a streamfunction. Indeed,

$$
\nabla\cdot(\mathbf{u}(\mathbf{x},t)) = \frac{3}{4\pi}\sum_p \frac{1}{|\mathbf{x}-\mathbf{x}^p(t)|^5}(\mathbf{x}-\mathbf{x}^p(t))\cdot((\mathbf{x}-\mathbf{x}^p(t))\wedge\boldsymbol{\alpha}^p(t)) = 0\,, \qquad (3.9)
$$

since $(\mathbf{x}-\mathbf{x}^p)$ is orthogonal to $(\mathbf{x}-\mathbf{x}^p)\wedge\boldsymbol{\alpha}^p$. At $\mathbf{x}=\mathbf{x}^p$, the singularity is of removable type so that $\nabla\cdot\mathbf{u}=0$.

- As noted by Novikov (1983), one can reconstruct a divergence free vorticity field from the particles by writing

$$\boldsymbol{\omega}^N(\mathbf{x},t)=\sum_p\left[\boldsymbol{\alpha}^p(t)\,\delta(\mathbf{x}-\mathbf{x}^p(t))+\nabla\left(\boldsymbol{\alpha}^p(t)\cdot\nabla\left(\frac{1}{4\pi|\mathbf{x}-\mathbf{x}^p(t)|}\right)\right)\right]\ . \quad (3.10)$$

The added term corresponds to that which is needed to close the vortex lines (i.e., make $\boldsymbol{\omega}$ divergence free), and it decays only as $1/r^3$. Making use of suffix notation, one obtains, for the components of this vorticity field,

$$\begin{aligned}\omega_i^N(\mathbf{x},t) &= \sum_p\left[\alpha_i^p(t)\,\delta(\mathbf{x}-\mathbf{x}^p(t))+\frac{\partial}{\partial x_i}\left(\alpha_j^p(t)\frac{\partial}{\partial x_j}\left(\frac{1}{4\pi|\mathbf{x}-\mathbf{x}^p(t)|}\right)\right)\right]\\ &= \sum_p\left[\alpha_i^p(t)\,\delta(\mathbf{x}-\mathbf{x}^p(t))-\frac{\partial}{\partial x_i}\left(\alpha_j^p(t)\frac{(x_j-x_j^p(t))}{4\pi|\mathbf{x}-\mathbf{x}^p(t)|^3}\right)\right]\\ &= \sum_p\Bigg[\alpha_i^p(t)\,\delta(\mathbf{x}-\mathbf{x}^p(t))\\ &\quad-\left(\frac{\alpha_i^p(t)}{4\pi|\mathbf{x}-\mathbf{x}^p(t)|^3}-3\,\frac{\alpha_j^p(t)(x_j-x_j^p(t))}{4\pi|\mathbf{x}-\mathbf{x}^p(t)|^5}(x_i-x_i^p(t))\right)\Bigg]\ , \quad (3.11)\end{aligned}$$

so that

$$\begin{aligned}\boldsymbol{\omega}^N(\mathbf{x},t) &= \sum_p\Bigg[\left(\delta(\mathbf{x}-\mathbf{x}^p(t))-\frac{1}{4\pi|\mathbf{x}-\mathbf{x}^p(t)|^3}\right)\boldsymbol{\alpha}^p(t)\\ &\qquad+3\,\frac{((\mathbf{x}-\mathbf{x}^p(t))\cdot\boldsymbol{\alpha}^p(t))}{4\pi|\mathbf{x}-\mathbf{x}^p(t)|^5}(\mathbf{x}-\mathbf{x}^p(t))\Bigg]\ . \quad (3.12)\end{aligned}$$

- If the curl of the velocity field (3.4) is taken, one obtains the vorticity field (3.10). Indeed, making use of suffix notation, one obtains

$$\begin{aligned}(\nabla\wedge\mathbf{u})_i &= \epsilon_{ijk}\frac{\partial}{\partial x_j}\left[\sum_p\epsilon_{klm}\frac{\partial}{\partial x_l}\left(\frac{1}{4\pi|\mathbf{x}-\mathbf{x}^p(t)|}\right)\alpha_m^p(t)\right]\\ &= \sum_p(\delta_{im}\delta_{jl}+\delta_{il}\delta_{jm})\frac{\partial}{\partial x_j}\frac{\partial}{\partial x_l}\left(\frac{1}{4\pi|\mathbf{x}-\mathbf{x}^p(t)|}\right)\alpha_m^p(t)\\ &= \sum_p\frac{\partial}{\partial x_j}\frac{\partial}{\partial x_j}\left(\frac{1}{4\pi|\mathbf{x}-\mathbf{x}^p(t)|}\right)\alpha_i^p(t)\\ &\qquad+\frac{\partial}{\partial x_i}\left(\alpha_j^p(t)\,\frac{\partial}{\partial x_j}\left(\frac{1}{4\pi|\mathbf{x}-\mathbf{x}^p(t)|}\right)\right)\\ &= \sum_p\left[\boldsymbol{\alpha}^p(t)\,\delta(\mathbf{x}-\mathbf{x}^p(t))+\nabla\left(\boldsymbol{\alpha}^p(t)\cdot\nabla\left(\frac{1}{4\pi|\mathbf{x}-\mathbf{x}^p(t)|}\right)\right)\right]_i\\ &= \left(\boldsymbol{\omega}^N\right)_i\ . \quad (3.13)\end{aligned}$$

Thus, $\boldsymbol{\omega}^N = \nabla\wedge\mathbf{u} = \nabla\wedge(\nabla\wedge\boldsymbol{\psi}) = -\nabla^2\boldsymbol{\psi}+\nabla(\nabla\cdot\boldsymbol{\psi})$. Recalling that $\nabla^2\boldsymbol{\psi} = -\boldsymbol{\omega}$, it follows that $\nabla(\nabla\cdot\boldsymbol{\psi}) = \boldsymbol{\omega}^N - \boldsymbol{\omega}$.

- The second term in Equation (3.10) does not contribute to the velocity field as computed by the Biot-Savart law since it is the gradient of a scalar field. In other words, inserting Equation (3.2) or Equation (3.10) in the Biot-Savart integral yields the same velocity field (3.4).

Saffman & Meiron (1986) have shown that the formulation Equation (3.5), and Equation (3.6) does not constitute a weak solution of Equation (2.4).

As noticed by Rehbach (1978) (see also Cantaloube & Huberson 1984 and Choquin & Cottet 1988), alternative forms of the three-dimensional vorticity equation (2.4) can be written as follows:

$$\frac{\partial\boldsymbol{\omega}}{\partial t} + \nabla\cdot(\boldsymbol{\omega}\,\mathbf{u}) = (\boldsymbol{\omega}\cdot\nabla)\mathbf{u}\,, \tag{3.14}$$

$$= \left(\boldsymbol{\omega}\cdot\nabla^T\right)\mathbf{u}\,, \tag{3.15}$$

$$= \frac{1}{2}\left(\boldsymbol{\omega}\cdot\left(\nabla+\nabla^T\right)\right)\mathbf{u}\,. \tag{3.16}$$

This is so because $\left(\boldsymbol{\omega}\cdot\left(\nabla-\nabla^T\right)\right)\mathbf{u} = (\nabla\wedge\mathbf{u})\wedge\boldsymbol{\omega} = 0$ since $\nabla\wedge\mathbf{u} = \boldsymbol{\omega}$. The formulation (3.14) leads to the *classical scheme* (3.6) for the evolution equation of the particle strength vector. The formulation (3.15) suggests the evolution equation

$$\frac{d}{dt}\boldsymbol{\alpha}^p(t) = \left(\boldsymbol{\alpha}^p(t)\cdot\nabla^T\right)\mathbf{u}^p(\mathbf{x}^p(t),t)\,. \tag{3.17}$$

This scheme will be referred to as the *transpose scheme*. The formulation (3.16) suggests the evolution equation

$$\frac{d}{dt}\boldsymbol{\alpha}^p(t) = \frac{1}{2}\left(\boldsymbol{\alpha}^p(t)\cdot\left(\nabla+\nabla^T\right)\right)\mathbf{u}^p(\mathbf{x}^p(t),t)\,. \tag{3.18}$$

This scheme will be referred to as the *mixed scheme*. This scheme was favored by Rehbach because the symmetry of the matrix $\frac{1}{2}\left(\nabla\mathbf{u}+\nabla^T\mathbf{u}\right)$ yields computational savings.

All three schemes would be equivalent if the vorticity field defined by Equation (3.2) were equal to the curl of the velocity field (3.4). Unfortunately for the particle method, this is not the case, as a consequence of the non-zero divergence of the field (3.2). So, although Equations (3.14), (3.15) and (3.16) are equivalent when $\boldsymbol{\omega} = \nabla\wedge\mathbf{u}$, they are not equivalent otherwise. Consequently, Equations (3.6), (3.17) and (3.18) lead to different results when solving the three-dimensional vorticity equation with vortex particles.

The transpose scheme Equation (3.17) is very special. First of all, it leads to the exact conservation of the total vorticity as will be seen in Section 3.4, a property not satified by the classical scheme (3.6) or the mixed scheme (3.18). Moreover, it leads to a weak solution of Equation (3.15) as shown by Winckelmans & Leonard (1988). The proof is done using the same procedure as in Saffman & Meiron (1986).

First, since $\mathbf{u}^p(\mathbf{x},t)$ is smooth in the neighborhood of $\mathbf{x}^p$, Equations (3.5) and (3.17) imply that

$$\frac{\partial}{\partial t}\boldsymbol{\omega}^p + (\mathbf{u}^p \cdot \nabla)\,\boldsymbol{\omega}^p - \left(\boldsymbol{\omega}^p \cdot \nabla^T\right)\mathbf{u}^p = 0 \tag{3.19}$$

at all points including $\mathbf{x} = \mathbf{x}^p$. It remains to consider whether

$$((\mathbf{u} - \mathbf{u}^p) \cdot \nabla)\,\boldsymbol{\omega}^p - \left(\boldsymbol{\omega}^p \cdot \nabla^T\right)(\mathbf{u} - \mathbf{u}^p) = 0 \tag{3.20}$$

at $\mathbf{x}^p$ in a weak sense. A local coordinate system with the origin at $\mathbf{x}^p$ is considered and use is made of suffix notation. The superscript, p, of the particle is dropped. It thus remains to consider whether the following integral vanishes for an arbitrary smooth function $f(\mathbf{x})$:

$$\int f(\mathbf{x}) \left[\epsilon_{ljk}\frac{\alpha_j x_k}{r^3}\frac{\partial}{\partial x_l}(\alpha_i\,\delta(\mathbf{x})) - \delta(\mathbf{x})\,\alpha_l\frac{\partial}{\partial x_i}\left(\epsilon_{ljk}\frac{\alpha_j x_k}{r^3}\right)\right] d\mathbf{x}\,. \tag{3.21}$$

The first term is integrated by parts, and Equation (3.21) becomes

$$-\int \delta(\mathbf{x}) \left[\epsilon_{ljk}\,\alpha_i\alpha_j\frac{\partial}{\partial x_l}\left(\frac{f\,x_k}{r^3}\right) + \epsilon_{ljk}\,\alpha_j\alpha_l\,f\frac{\partial}{\partial x_i}\left(\frac{x_k}{r^3}\right)\right] d\mathbf{x}\,. \tag{3.22}$$

The second term in Equation (3.22) is different from the one obtained using the evolution Equations (3.5) and (3.6) as in Saffman & Meiron (1986), namely

$$-\int \delta(\mathbf{x}) \left[\epsilon_{ljk}\,\alpha_i\alpha_j\frac{\partial}{\partial x_l}\left(\frac{f\,x_k}{r^3}\right) + \epsilon_{ijk}\,\alpha_j\alpha_l\,f\frac{\partial}{\partial x_l}\left(\frac{x_k}{r^3}\right)\right] d\mathbf{x}\,. \tag{3.23}$$

As pointed out by Greengard & Thomann (1988), one needs to assume a radially symmetric regularization of the δ-function for the integrals above, interpreted in the principal value sense, to be well-defined. Such a regularization is assumed in the present context.

Being smooth, $f(\mathbf{x})$ has a Taylor series

$$f(\mathbf{x}) = f(0) + x_r\,f_r(0) + \frac{1}{2}\,x_r\,x_s\,f_{rs}(0) + \cdots\,. \tag{3.24}$$

From the symmetry of the integrand in (3.22) and (3.23), it follows that only even powers of the coordinates need to be considered. Moreover, terms of order 4 and

higher vanish sufficiently fast so as to cancel the δ-function contribution. Thus only the constant term and the quadratic terms need to be considered. The first part of Equation (3.22) (or (3.23)) gives

$$\begin{aligned} f(0)\left(\epsilon_{kjk}\,\alpha_i\alpha_j\int\frac{\delta(\mathbf{x})}{r^3}d\mathbf{x} - 3\,\epsilon_{ljk}\,\alpha_i\alpha_j\int\frac{\delta(\mathbf{x})}{r^3}x_kx_l\,d\mathbf{x}\right) \\ +f_{rs}(0)\Bigg(\epsilon_{kjk}\,\alpha_i\alpha_j\int\frac{\delta(\mathbf{x})}{r^3}x_rx_s\,d\mathbf{x} \\ +\epsilon_{rjk}\,\alpha_i\alpha_j\int\frac{\delta(\mathbf{x})}{r^3}x_sx_k\,d\mathbf{x} \\ +\epsilon_{sjk}\,\alpha_i\alpha_j\int\frac{\delta(\mathbf{x})}{r^3}x_rx_k\,d\mathbf{x} \\ -3\,\epsilon_{ljk}\,\alpha_i\alpha_j\int\frac{\delta(\mathbf{x})}{r^3}x_rx_sx_kx_l\,d\mathbf{x}\Bigg)\,. \end{aligned} \tag{3.25}$$

The first and third term in Equation (3.25) vanish since $\epsilon_{kjk} = 0$. The second term vanishes since $\epsilon_{ljk}\,x_kx_l = 0$. The fourth and fifth terms are identical since $f_{rs}(0) = f_{sr}(0)$; they are found to be zero as follows [53]:

$$f_{rs}(0)\,\epsilon_{rjk}\,\alpha_i\alpha_j\int x_sx_k\,dS \propto f_{rs}(0)\,\epsilon_{rjk}\,\alpha_i\alpha_j\,\delta_{sk} = f_{rs}(0)\,\epsilon_{rjs}\,\alpha_i\alpha_j = 0\,. \tag{3.26}$$

The last term is proportional to

$$f_{rs}(0)\,\epsilon_{ljk}\,\alpha_i\alpha_j\int x_rx_sx_kx_l\,dS\,. \tag{3.27}$$

Using the result [53] that

$$\int x_ix_jx_kx_l\,dS \propto \delta_{ij}\delta_{kl} + \delta_{ik}\delta_{jl} + \delta_{il}\delta_{jk}\,, \tag{3.28}$$

it is easily seen that this term also vanishes. Thus, the first term of Equation (3.22) (or (3.23)) vanishes. The term that does not vanish in Equation (3.23) is the second term. It is proportional to (Saffman & Meiron 1986)

$$f_{rs}(0)\,(\epsilon_{ijr}\,\alpha_j\alpha_s + \epsilon_{ijs}\,\alpha_j\alpha_r)\,, \tag{3.29}$$

which does not vanish in general, thus showing that the classical scheme does not constitute a weak solution of the three-dimensional vorticity equation (3.14).

With the transpose scheme, the second term in Equation (3.22) vanishes trivially even before integration since $\epsilon_{ljk}\,\alpha_j\alpha_l = 0$. Thus, the transpose scheme constitutes a weak solution of the three-dimensional vorticity equation (3.15). That property and the conservation of total vorticity leads to the belief that the transpose scheme is more suited than the classical scheme to the representation of three-dimensional

vortical flows with a limited number of vortex particles. This point will be examined further when presenting numerical results in Section 3.5

Important remarks made by Greengard & Thomann (1988) should be mentioned:

- The above proof that singular vortex particles evolving under the transpose scheme form weak solutions of the vorticity equation is "fragile" and depends on the type of regularization of the δ-function. Only for a radially symmetric regularization of the δ-function are the integrals, evaluated in the principal value sense, bounded.

- The vorticity field associated with three-dimensional singular vortex particles is not divergence free. Consequently, a finite sum of particles cannot represent a divergence free vorticity field. This fact is in opposition with two-dimensional singular vortex particles (i.e., point vortices) for which the particle vorticity field is divergence free, and is a serious obstacle to the validity of finitely many singular particles as models for the solution of the three-dimensional vorticity equation.

- A more important notion than the concept of weak solution with singular vortex elements is the concept of convergence to a smooth solution with regularized vortex elements. As will be seen in Section 3.2, the method of regularized vortex particles has been shown to converge both in two and three dimensions, at least for some finite time T. When the number of elements goes to infinity and the smoothing goes to zero in an appropriate way, the solution of the differential equations that govern the particle trajectories in the discrete system converges to the exact particle trajectories, and the vorticity and velocity fields converge as well.

In the next section, the method of regularized vortex particles is examined more closely.

3.2 Regularized vortex particles

In this section, the regularized version of the method of vortex particles is considered. More specifically, the vorticity field is now represented as follows:

$$\boldsymbol{\omega}_\sigma(\mathbf{x},t) = \zeta_\sigma(\mathbf{x}) * \boldsymbol{\omega}(\mathbf{x},t) = \sum_p \boldsymbol{\alpha}^p(t)\,\zeta_\sigma(\mathbf{x}-\mathbf{x}^p(t))\,. \tag{3.30}$$

The three-dimensional regularization function $\zeta_\sigma(\mathbf{x})$ was already introduced in Chapter 2, Section 2.2.2, together with the regularization functions for the streamfunction $\chi_\sigma(\mathbf{x})$ and the velocity $g_\sigma(\mathbf{x})$. The useful relations between these functions were also introduced in that chapter.

The velocity field is computed from the particle representation of the vorticity field as the curl of a streamfunction which solves $\nabla^2\boldsymbol{\psi}_\sigma(\mathbf{x},t) = -\boldsymbol{\omega}_\sigma(\mathbf{x},t)$. Following the same procedure as with vortex filaments, one obtains, for the streamfunction,

$$\begin{aligned}\boldsymbol{\psi}_\sigma(\mathbf{x},t) &= G(\mathbf{x}) * \boldsymbol{\omega}_\sigma(\mathbf{x},t) = \chi_\sigma(\mathbf{x}) * \boldsymbol{\omega}(\mathbf{x},t) \\ &= \sum_p \chi_\sigma(\mathbf{x}-\mathbf{x}^p(t))\,\boldsymbol{\alpha}^p(t)\,, \end{aligned} \tag{3.31}$$

and, for the velocity,

$$\begin{aligned}\mathbf{u}_\sigma(\mathbf{x},t) &= \nabla\wedge\boldsymbol{\psi}_\sigma(\mathbf{x},t) = \sum_p \nabla\left(\chi_\sigma(\mathbf{x}-\mathbf{x}^p(t))\right)\wedge\boldsymbol{\alpha}^p(t) \\ &= -\sum_p \frac{g_\sigma(\mathbf{x}-\mathbf{x}^p(t))}{|\mathbf{x}-\mathbf{x}^p(t)|^3}(\mathbf{x}-\mathbf{x}^p(t))\wedge\boldsymbol{\alpha}^p(t) \\ &= \sum_p \mathbf{K}_\sigma(\mathbf{x}-\mathbf{x}^p(t))\wedge\boldsymbol{\alpha}^p(t) = (\mathbf{K}_\sigma(\mathbf{x})\wedge) * \boldsymbol{\omega}(\mathbf{x},t)\end{aligned} \tag{3.32}$$

where $\mathbf{K}_\sigma(\mathbf{x})\wedge = -(g_\sigma(\mathbf{x})/|\mathbf{x}|^3)\,\mathbf{x}\wedge$ is the regularized Biot-Savart kernel. At large distances compared with σ, the velocity induced by a regularized vortex particle is the same as if the particle were singular since $4\pi\, g(\rho) \to 1$ as $\rho \to \infty$. The induced velocity goes to zero as $r \to 0$ since $g(\rho)$ is $\mathcal{O}(\rho^3)$ for small ρ.

The evolution equations for the particle position and strength vector are, with the classical scheme, taken as

$$\frac{d}{dt}\mathbf{x}^p(t) = \mathbf{u}_\sigma(\mathbf{x}^p(t),t)\,, \tag{3.33}$$

$$\frac{d}{dt}\boldsymbol{\alpha}^p(t) = (\boldsymbol{\alpha}^p(t)\cdot\nabla)\,\mathbf{u}_\sigma(\mathbf{x}^p(t),t)\,. \tag{3.34}$$

Again, the transpose scheme

$$\frac{d}{dt}\boldsymbol{\alpha}^p(t) = \left(\boldsymbol{\alpha}^p(t)\cdot\nabla^T\right)\mathbf{u}_\sigma(\mathbf{x}^p(t),t)\,, \tag{3.35}$$

or the mixed scheme

$$\frac{d}{dt}\boldsymbol{\alpha}^p(t) = \frac{1}{2}\left(\boldsymbol{\alpha}^p(t)\cdot\left(\nabla+\nabla^T\right)\right)\mathbf{u}_\sigma(\mathbf{x}^p(t),t) \tag{3.36}$$

can be used instead of Equation (3.34). Again, the transpose scheme is the only one that conserves total vorticity as will be seen in Section 3.4.

In Appendix F, the details of the evolutions equations for any of the above choices are given. They are presented in the form that is actually programmed when performing numerical computations with these vortex particles.

Remarks made in Section 3.1 concerning singular vortex particles are also relevant here:

- The particle vorticity field (3.30) is not generally divergence free. Indeed,

$$\nabla\cdot(\boldsymbol{\omega}_\sigma(\mathbf{x},t)) = \sum_p \nabla(\zeta_\sigma(\mathbf{x}-\mathbf{x}^p(t)))\cdot\boldsymbol{\alpha}^p(t)\ . \tag{3.37}$$

  The regularized vortex particle method is thus also inconsistent, because a basis which is not divergence free is used to represent a vector field that should be divergence free for all times. $\boldsymbol{\omega}_\sigma(\mathbf{x},0)$ can be set to be initially a very good representation of the real vorticity field but nothing guarantees that, as time evolves, $\boldsymbol{\omega}_\sigma(\mathbf{x},t)$ remains a good representation of that field. This point will be examined numerically in Section 3.5.

- The streamfunction (3.31) is also not generally divergence free. Indeed,

$$\nabla\cdot(\boldsymbol{\psi}_\sigma(\mathbf{x},t)) = -\sum_p \frac{g_\sigma(\mathbf{x}-\mathbf{x}^p(t))}{|\mathbf{x}-\mathbf{x}^p(t)|^3}\left((\mathbf{x}-\mathbf{x}^p(t))\cdot\boldsymbol{\alpha}^p(t)\right)\ . \tag{3.38}$$

  This result is a direct consequence of the fact that $\nabla^2\boldsymbol{\psi}_\sigma = -\boldsymbol{\omega}_\sigma$ is solved with $\boldsymbol{\omega}_\sigma$ not generally divergence free.

- The velocity field (3.32) is divergence free since it is the curl of a streamfunction.

- A divergence free vorticity field can be reconstructed from the particles by writing

$$\boldsymbol{\omega}_\sigma^N(\mathbf{x},t) = \sum_p\Big[\boldsymbol{\alpha}^p(t)\,\zeta_\sigma(\mathbf{x}-\mathbf{x}^p(t)) + \nabla\Big(\boldsymbol{\alpha}^p(t)\cdot\nabla\Big(\chi_\sigma(\mathbf{x}-\mathbf{x}^p(t))\Big)\Big)\Big]\ . \tag{3.39}$$

  The added term corresponds to that which is needed to close the vortex lines (i.e., to make $\boldsymbol{\omega}_\sigma$ divergence free) and it decays only like $1/r^3$. Following the same steps as in Section 3.1, Equation (3.10), and using Equations (2.26) through (2.29), it is easy to show that

$$\begin{aligned}\boldsymbol{\omega}_\sigma^N(\mathbf{x},t) \;=\; \sum_p\Bigg[&\left(\zeta_\sigma(\mathbf{x}-\mathbf{x}^p(t)) - \frac{g_\sigma(\mathbf{x}-\mathbf{x}^p(t))}{|\mathbf{x}-\mathbf{x}^p(t)|^3}\right)\boldsymbol{\alpha}^p(t)\\ &+\left(3\frac{g_\sigma(\mathbf{x}-\mathbf{x}^p(t))}{|\mathbf{x}-\mathbf{x}^p(t)|^3} - \zeta_\sigma(\mathbf{x}-\mathbf{x}^p(t))\right)\frac{((\mathbf{x}-\mathbf{x}^p(t))\cdot\boldsymbol{\alpha}^p(t))}{|\mathbf{x}-\mathbf{x}^p(t)|^2}(\mathbf{x}-\mathbf{x}^p(t))\Bigg]\ .\end{aligned} \tag{3.40}$$

- If the curl of the velocity field (3.32) is taken, then one obtains the vorticity field (3.39). This property is easy to show following the same steps as in Section 3.1, Equation (3.13) but replacing $G(\mathbf{x}) = 1/(4\pi|\mathbf{x}|)$ by $\chi_\sigma(\mathbf{x})$ and recalling that $\nabla^2\chi(\rho) = -\zeta(\rho)$. In particular, $\boldsymbol{\omega}_\sigma^N = \nabla\wedge\mathbf{u}_\sigma = \nabla\wedge(\nabla\wedge\boldsymbol{\psi}_\sigma) = -\nabla^2\boldsymbol{\psi}_\sigma + \nabla(\nabla\cdot\boldsymbol{\psi}_\sigma)$. Recalling that $\nabla^2\boldsymbol{\psi}_\sigma = -\boldsymbol{\omega}_\sigma$, it follows that $\nabla(\nabla\cdot\boldsymbol{\psi}_\sigma) = \boldsymbol{\omega}_\sigma^N - \boldsymbol{\omega}_\sigma$.

- The second term in Equation (3.39) does not contribute to the velocity field as computed by the Biot-Savart law since it is the gradient of a scalar field. In other words, inserting Equation (3.30) or Equation (3.39) in the Biot-Savart integral yields the same velocity field (3.32).

The particle vorticity field (3.30), the divergence free vorticity field (3.39), and the velocity field (3.32) are shown in Figure J.23 for two cases: an isolated vortex particle, and an infinite array of vortex particles with $\sigma/h = 2.0$, where h is the distance between particles. It is seen that, when the particles are nicely aligned and the cores overlap sufficiently, the particle vorticity field $\boldsymbol{\omega}_\sigma$ is a very good representation of the divergence free vorticity field $\boldsymbol{\omega}_\sigma^N$. This is to be expected, since these particles essentially represent computational points on a vortex filament. This illustration of course does not address situations in which the particles are not nicely aligned, as could happen in the course of a numerical computation.

Beale & Majda (1982a,1982b), Beale (1986a,1986b), Cottet (1988) and Choquin & Cottet (1988) have shown convergence of the regularized vortex particle method, at least for some finite time T, to the solution of the three-dimensional vorticity equation (3.14), (3.15) or (3.16) with any of the choices (3.34), (3.35) or (3.36). Beale (1986b) has also obtained improved error estimates when using the mixed scheme (3.36), due to the symmetry of the stretching operator. It is not intended, in the present thesis, to review their work. It is only recalled that, according to their convergence proofs, the appropriate error norm for the vorticity and velocity fields goes to zero as the number of particles increases and the core size σ decreases subjected to the constraint that the cores overlap (i.e., $\sigma/h > 1$ where h is a typical distance in between particles). As is the case with the regularized method of vortex filaments, Section 2.2.2, the error norm for the vorticity is composed of two terms: one term which is $\mathcal{O}(\sigma^r)$ and another term which is $\mathcal{O}(\sigma(h/\sigma)^m)$. The reader is referred to Chapter 2, Section 2.2.2 for the relationship between the smoothing function $\zeta(\rho)$ and the convergence exponents m and r.

A number of typical smoothing functions $\zeta(\rho)$ and their associated $g(\rho)$ and $\chi(\rho)$ functions are collected in Table B.1. Notice that the smoothings that are $r > 2$, such as the super-Gaussian, are also not strictly positive. This property will be of

importance in Section 3.3 where the inclusion of the viscous effects in the vortex particle method will be examined. Notice also that some smoothings have $\zeta(\rho) > 0$ but $\eta(\rho) = -\zeta'(\rho)/\rho \not> 0$. These smoothings are also poor choices when including the viscous terms as will be seen in Section 3.3.

In the context of vortex particles, the new high order algebraic smoothing (B.12) is very special in many respects:

- It has convergence properties that are as good as those of Gaussian smoothing (B.8).
- The associated $\chi(\rho)$ and $g(\rho)$ functions that are needed for the evaluation of the streamfunction (3.31) and the velocity (3.32) have elegant and compact forms and are cheaper and more convenient to use than the $\chi(\rho)$ and $g(\rho)$ functions associated with Gaussian smoothing (B.8).
- The gradients of the velocity field (3.32) that are needed in the computation of the stretching term using Equations (3.34), (3.35) or (3.36) also take a simple compact form. The final form of the evolution equations that are obtained when using that smoothing is given in Appendix F.
- Finally, as will be seen in Appendix G, this smoothing is also the only one for which one can write closed form expressions for the semi-regularized quadratic diagnostics such as the kinetic energy $\tilde{E}$, the helicity $\tilde{\mathcal{H}}$ and the enstrophy $\tilde{\mathcal{E}}$ of a system of regularized vortex particles.

All these *qualities* of the high order algebraic smoothing make it a prime choice for numerical computations.

A important remark on the method of regularized vortex particles: what really lacks in the convergence proofs is an error estimate for the divergence of the particle vorticity field, $\nabla\cdot\boldsymbol{\omega}_\sigma$. Indeed, the method of vortex particles has no built-in control on keeping this divergence small. It will be shown in Section 3.5 that this lack of consistency is precisely what gets the method into trouble after some time. A relaxation scheme will also be proposed that forces the particle vorticity field to be almost divergence free for all times, and hence makes the method suited for long time computations.

Finally, as is the case with the method of regularized vortex filaments, Section 2.2.2, each particle can be assigned its own core size σ^p which may also depend on time. For instance, the model equation

$$\frac{d}{dt}\left((\sigma^p(t))^2\ |\boldsymbol{\alpha}^p(t)|\right) = 0 \tag{3.41}$$

ensures conservation of volume of vorticity (provided that the discretization is fine enough that cores still overlap after stretching has occurred!). With that choice, the evolution equations for the particles position and strength vector are symmetrized with $\sigma^{pq} = \sigma^{qp}$ where σ^{pq} is the core size used to compute the influence of particle q on particle p and conversely. When the transpose scheme is used (see Section 3.4), this choice ensures the conservation of total vorticity.

As mentioned at the begining of this chapter, the use of regularized vortex-dipoles for the computation of three-dimensional incompressible flows was also examined. The conservation of the linear invariants was investigated as well. Since no numerical experiments were carried out with that method, this theoretical investigation is presented in Appendix H.

3.3 Representation of viscous effects by the redistribution of particle strengths

Despite the weaknesses of the vortex particle method, there is one feature that such a method allows for and that cannot be achieved with a vortex filament method: the possibility of taking into account viscous diffusion. This property is of course very attractive since viscous diffusion is a necessary ingredient for the reconnection of vortex tubes.

For viscous incompressible flows, the three-dimensional vorticity equation becomes

$$\frac{\partial \omega}{\partial t} + \nabla\cdot(\omega\,\mathbf{u}) = (\omega\cdot\nabla^T)\mathbf{u} + \nu\,\nabla^2\omega\,, \tag{3.42}$$

where the stretching term $(\omega\cdot\nabla^T)\mathbf{u}$ can be replaced by any of the equivalent forms $(\omega\cdot\nabla)\,\mathbf{u}$ or $(1/2)\left(\omega\cdot\left(\nabla+\nabla^T\right)\right)\mathbf{u}$ as explained in Section 3.1. The treatment of the stretching term when using a vortex particle method was examined in Section 3.2. The treatment of the diffusion term is examined in the this section.

The diffusion term is treated using a deterministic approach in which the strength vectors $\boldsymbol{\alpha}^p(t)$ are redistributed among particles in a manner that is consistent with viscous diffusion. This approach was introduced by Mas-Gallic (1987) and Degond & Mas-Gallic (1988a,1988b) (see also Cottet & Mas-Gallic 1983, 1987 and Choquin & Huberson 1988) in the general framework of solving convection-diffusion equations using particle methods. Their work will not be reviewed, but some of the results that are relevant in the present context will be mentioned. The theoretical results will also be applied to the method of regularized vortex particles.

In essence, they have shown that the diffusion operator (i.e., the Laplacian) can be approximated by an integral operator which can, in turn, be discretized using the

particle representation of the function of interest. The results apply to a function in R^d but will only be written here in R^3.

Consider a smoothing function with radial symmetry as described in Section 3.2 and which satisfies the integral constraints (2.21), (2.42) and (2.43) together with

$$\int_0^\infty |\zeta'(\rho)|\, \rho^{3+r}\, d\rho < \infty \,. \tag{3.43}$$

Define

$$\eta_\sigma(\mathbf{x}) = \frac{1}{\sigma^5}\, \eta\left(\frac{|\mathbf{x}|}{\sigma}\right) \,, \tag{3.44}$$

with

$$\eta(\rho) = -\frac{\zeta'(\rho)}{\rho} \,. \tag{3.45}$$

Then a good approximation to $\nabla^2 f(\mathbf{x})$ is given by

$$\nabla^2 f(\mathbf{x}) \simeq 2 \int (f(\mathbf{y}) - f(\mathbf{x}))\, \eta_\sigma(\mathbf{x}-\mathbf{y})\, d\mathbf{y} \tag{3.46}$$

in the sense that, in the appropriate norm, the difference between $\nabla^2 f(\mathbf{x})$ and Equation (3.46) is $\mathcal{O}(\sigma^r)$. Again, notice that the classical smoothing (B.10) does not satisfy the constraint (3.43) and is therefore a poor choice for the diffusion term as well.

The function $\eta_\sigma(\mathbf{x})$ which appears in Equation (3.46) is essentially an approximation to the kernel for the heat equation. The nature of the approximation may be understood as follows. For the purpose of illustration, consider the Gaussian smoothing (B.8) which is such that $\eta(\rho) = \zeta(\rho)$. Then, the Fourier transform of Equation (3.46) gives

$$\begin{aligned} 2\,(\hat{\eta}_\sigma(\mathbf{k}) - 1)\, \hat{f}(\mathbf{k}) &= \frac{2}{\sigma^2}\left(e^{-k^2\sigma^2/2} - 1\right) \hat{f}(\mathbf{k}) \\ &\simeq -k^2 \left(1 + \mathcal{O}\left(k^2\sigma^2\right)\right) \hat{f}(\mathbf{k}) \qquad \text{for small } \mathbf{k} \\ &\simeq \mathcal{F}\left(\nabla^2 f(\mathbf{x})\right) \,, \end{aligned} \tag{3.47}$$

thus showing that, in the Fourier space, the integral operator is a second order approximation to the Laplacian when $\eta(\rho)$ is the Gaussian. This conclusion is consistent with the above error estimate since the Gaussian smoothing corresponds to $r = 2$.

Consider now the convection-diffusion equation

$$\frac{\partial f}{\partial t} + \nabla\cdot(f\,\mathbf{u}) = \nu\, \nabla^2 f \,, \tag{3.48}$$

and the equation approximating (3.48)

$$\frac{\partial f}{\partial t} + \nabla\cdot(f\,\mathbf{u}) = 2\,\nu \int (f(\mathbf{y}) - f(\mathbf{x}))\, \eta_\sigma(\mathbf{x}-\mathbf{y})\, d\mathbf{y} \,. \tag{3.49}$$

Acceptable error estimates are obtained for the difference in time between the solutions of the two problems for all ν, provided that $\eta(\rho) \geq 0$ for all ρ (which implies that $r \leq 2$). When $\eta(\rho)$ is not positive for all ρ, acceptable errors can be obtained only if ν is small enough ($\nu = \mathcal{O}(\sigma^2)$).

Consider a particle approximation of $f(\mathbf{x}, t)$,

$$f_\sigma(\mathbf{x}, t) = \sum_p \left(f^p(t)\, vol^p(t)\right) \zeta_\sigma(\mathbf{x} - \mathbf{x}^p(t)) \,, \tag{3.50}$$

and solve the approximate convection-diffusion problem (3.49) using a particle discretization of the integral operator. This leads to

$$\begin{aligned} \frac{d}{dt}\mathbf{x}^p(t) &= \mathbf{u}(\mathbf{x}^p(t), t) \,, \\ \frac{d}{dt} vol^p(t) &= vol^p(t)\, \nabla\cdot\mathbf{u}(\mathbf{x}^p(t), t) \,, \\ \frac{d}{dt}\left(f^p(t)\, vol^p(t)\right) &= 2\,\nu\, vol^p(t) \sum_q vol^q(t)\left(f^q(t) - f^p(t)\right) \eta_\sigma(\mathbf{x}^p(t) - \mathbf{x}^q(t)) \,. \end{aligned} \tag{3.51}$$

Then, for $\eta(\rho) \geq 0$, the error estimates show that the replacement of the integral operator by a discrete sum leads to an error of $\mathcal{O}(h^m/\sigma^{m+1})$. This error component is in addition to the error of $\mathcal{O}(\sigma^r)$ due to the replacement of the Laplacian by the integral operator. Thus, the particle approximation of the diffusion term leads to a global error of $\mathcal{O}(\nu(\sigma^r + h^m/\sigma^{m+1}))$. For arbitrary ν, this error is higher than the error $\mathcal{O}(\sigma^r + h^m/\sigma^m)$ due the the particle approximation of the convective term, but for small ν ($\nu = \mathcal{O}(\sigma^2)$), this error is lower than the error due to the convective term. Finally, for $\eta(\rho)$ not positive for all ρ and $\nu = \mathcal{O}(\sigma^2)$, one can obtain an error estimate of $\mathcal{O}(\nu(\sigma^{r-2} + h^m/\sigma^{m+1}))$ which is still smaller than the error due to the convective term.

An important remark: $\zeta(\rho) \not> 0$ implies that $\eta(\rho) \not> 0$ but $\zeta(\rho) > 0$ does not guarantee that $\eta(\rho) > 0$. Refer to Table B.1 for examples. When computing viscous problems, it is probably a good policy to use functions for which both $\zeta(\rho) > 0$ and $\eta(\rho) > 0$ (such as the high order algebraic smoothing (B.12)). This limits the choice to functions that have $r = 2$, but it leaves the freedom of having any value for the viscosity!

Degond & Mas-Gallic (1988b) have generalized the formulation to an operator of the form $\nabla\cdot(\nu(\mathbf{x}, t)\nabla\,)$ instead of $\nu\,\nabla^2$ with ν constant. This generalization could prove very useful if one thinks of using this method in the context of large eddy simulation with a subgrid turbulent eddy viscosity.

A straightforward application of the above method to solving Equation (3.42) with regularized vortex particles leads to the following scheme

$$\frac{d}{dt}\mathbf{x}^p(t) = \mathbf{u}_\sigma(\mathbf{x}^p(t),t)\,, \tag{3.52}$$

$$\frac{d}{dt}\boldsymbol{\alpha}^p(t) = \left(\boldsymbol{\alpha}^p(t)\cdot\nabla^T\right)\mathbf{u}_\sigma(\mathbf{x}^p(t),t) + 2\,\nu\sum_q\left(vol^p\,\boldsymbol{\alpha}^q(t) - vol^q\,\boldsymbol{\alpha}^p(t)\right)\eta_\sigma(\mathbf{x}^p(t)-\mathbf{x}^q(t))\,. \tag{3.53}$$

Again, the stretching term in Equation (3.53) can be treated in alternative ways using the classical scheme (3.34) or the mixed scheme (3.35). The evolution equations when using the high order algebraic smoothing (B.12) are given in Appendix F.

An important consequence of the particle discretization of the integral operator is that it is conservative, i.e.,

$$\frac{d}{dt}\sum_p\boldsymbol{\alpha}^p(t) = 0 \tag{3.54}$$

for the viscous part. The total vorticity is thus not affected by the treatment of the diffusion term. Only the treatment of the stretching term can affect the total vorticity. It will be seen in Section 3.4 that the only scheme that conserves total vorticity is the transpose scheme (as in Equation (3.53)).

3.4 The method of vortex particles with respect to the conservation laws

In the present section, the behavior of the vortex particles method with respect to the conservation laws is examined. These conservation laws are reviewed in Appendix A.

The first consideration here is to examine the conservation of the linear invariants. These will be referred to as *invariants* when the real physical flow is understood and as *diagnostics* when the flow is actually computed with the method of vortex particles.

For a system of singular vortex particles, with the particle vorticity field defined by (3.2), the linear diagnostics (A.1), (A.2) and (A.3) become

$$\boldsymbol{\Omega} = \sum_p\boldsymbol{\alpha}^p(t)\,, \tag{3.55}$$

$$\mathbf{I} = \frac{1}{2}\sum_p\mathbf{x}^p(t)\wedge\boldsymbol{\alpha}^p(t)\,, \tag{3.56}$$

$$\mathbf{A} = \frac{1}{2}\sum_p\mathbf{x}^p(t)\wedge\left(\mathbf{x}^p(t)\wedge\boldsymbol{\alpha}^p(t)\right)\,. \tag{3.57}$$

For a system of regularized vortex particles, with the particle vorticity field defined by (3.30), the above expressions for the total vorticity (3.55) and the linear impulse (3.56) still hold. The expression for the angular impulse (3.57) has to be replaced by

$$\mathbf{A} = \frac{1}{2}\sum_p \mathbf{x}^p(t) \wedge (\mathbf{x}^p(t) \wedge \boldsymbol{\alpha}^p(t)) - \frac{1}{3} C\, \sigma^2\, \boldsymbol{\Omega}\ , \tag{3.58}$$

where

$$C = 4\pi \int_0^\infty \zeta(\rho)\, \rho^4\, d\rho\ . \tag{3.59}$$

Notice that Equation (3.58) reduces to Equation (3.57) when $\boldsymbol{\Omega} = 0$. With the high order algebraic smoothing (B.12), $C = 3/2$. With the low order algebraic smoothing (B.10), C does not converge so that the angular impulse is not defined unless $\boldsymbol{\Omega} = 0$.

Equation (3.58) is obtained by taking a local coordinate system centered at $\mathbf{x}^p$. Then, defining $\mathbf{x}' = \mathbf{x} - \mathbf{x}^p$, one obtains

$$\begin{aligned}
\int \mathbf{x} \wedge (\mathbf{x} \wedge \boldsymbol{\omega})\, d\mathbf{x} &= \int (\mathbf{x}^p + \mathbf{x}') \wedge ((\mathbf{x}^p + \mathbf{x}') \wedge \boldsymbol{\alpha}^p)\ \zeta_\sigma(\mathbf{x}')\, d\mathbf{x}' \\
&= \mathbf{x}^p \wedge (\mathbf{x}^p \wedge \boldsymbol{\alpha}^p) + \int \mathbf{x}' \wedge (\mathbf{x}^p \wedge \boldsymbol{\alpha}^p)\, \zeta_\sigma(\mathbf{x}')\, d\mathbf{x}' \\
&\quad + \int \mathbf{x}^p \wedge (\mathbf{x}' \wedge \boldsymbol{\alpha}^p)\, \zeta_\sigma(\mathbf{x}')\, d\mathbf{x}' + \int \mathbf{x}' \wedge (\mathbf{x}' \wedge \boldsymbol{\alpha}^p)\, \zeta_\sigma(\mathbf{x}')\, d\mathbf{x}'\ .
\end{aligned} \tag{3.60}$$

The second and third integrals in Equation (3.60) vanish due to symmetry of the integrand. The fourth integral is evaluated by considering a spherical coordinate system with $d\mathbf{x}' = dr\ r\, d\theta\ r \sin\theta\, d\varphi$. In that coordinate system, $\mathbf{x}'$ is written as

$$\mathbf{x}' = r\sin\theta\, \cos\varphi\, \hat{\mathbf{e}}_1 + r\sin\theta\, \sin\varphi\, \hat{\mathbf{e}}_2 + r\cos\theta\, \hat{\mathbf{e}}_3\ , \tag{3.61}$$

where $\hat{\mathbf{e}}_1 = \mathbf{x}^p/|\mathbf{x}^p|$, $\hat{\mathbf{e}}_2 = \boldsymbol{\alpha}^p/|\boldsymbol{\alpha}^p|$ and $\hat{\mathbf{e}}_3 = \hat{\mathbf{e}}_1 \wedge \hat{\mathbf{e}}_2$. With $\rho = |\mathbf{x}'|/\sigma$, one then obtains

$$\begin{aligned}
\int \mathbf{x}' \wedge (\mathbf{x}' \wedge \boldsymbol{\alpha}^p)\, d\mathbf{x}' &= \sigma^2 \int_0^\infty \zeta(\rho)\, \rho^4\, d\rho\ \times \\
&\quad \Bigg[\int_0^{2\pi} \cos^2\varphi\, d\varphi \int_0^\pi \sin^3\theta\, d\theta\ \hat{\mathbf{e}}_1 \wedge (\hat{\mathbf{e}}_1 \wedge \boldsymbol{\alpha}^p) \\
&\quad + \int_0^{2\pi} \sin^2\varphi\, d\varphi \int_0^\pi \sin^3\theta\, d\theta\ \hat{\mathbf{e}}_2 \wedge (\hat{\mathbf{e}}_2 \wedge \boldsymbol{\alpha}^p) \\
&\quad + \int_0^{2\pi} d\varphi \int_0^\pi \cos^2\theta\, \sin\theta\, d\theta\ \hat{\mathbf{e}}_3 \wedge (\hat{\mathbf{e}}_3 \wedge \boldsymbol{\alpha}^p) \Bigg] \\
&= \sigma^2 \int_0^\infty \zeta(\rho)\, \rho^4\, d\rho\ \times \left[\frac{4\pi}{3}\, (-2\,\boldsymbol{\alpha}^p) \right]\ ,
\end{aligned} \tag{3.62}$$

and this result leads to Equation (3.58) for the angular impulse of a system of regularized particles.

The conservation of the total vorticity and the linear impulse of a system of vortex particles is now examined. It will be shown that the transpose scheme is the only one that performs well.

First define the notation

$$\mathbf{K}^{pq} = \mathbf{K}(\mathbf{x} - \mathbf{x}^q(t))\Big|_{\mathbf{x}=\mathbf{x}^p(t)} ; \qquad \frac{\partial \mathbf{K}^{pq}}{\partial x_i} = \frac{\partial}{\partial x_i}\mathbf{K}(\mathbf{x} - \mathbf{x}^q(t))\Big|_{\mathbf{x}=\mathbf{x}^p(t)} , \tag{3.63}$$

where $\mathbf{K}$ is the Biot-Savart kernel (Equation (3.4) for singular particles, and Equation (3.32) for regularized particles). Notice that $\mathbf{K}^{pq} = -\mathbf{K}^{qp}$ and that $\partial \mathbf{K}^{pq}/\partial x_i = \partial \mathbf{K}^{qp}/\partial x_i$.

With the use of the transpose scheme, the evolution equations for the particle position and strength vector become

$$\frac{d}{dt}x_i^p = \sum_q (\mathbf{K}^{pq} \wedge \boldsymbol{\alpha}^q)_i , \tag{3.64}$$

$$\frac{d}{dt}\alpha_i^p = \boldsymbol{\alpha}^p \cdot \left(\sum_q \frac{\partial \mathbf{K}^{pq}}{\partial x_i} \wedge \boldsymbol{\alpha}^q\right) = -\sum_q \frac{\partial \mathbf{K}^{pq}}{\partial x_i} \cdot (\boldsymbol{\alpha}^p \wedge \boldsymbol{\alpha}^q) . \tag{3.65}$$

The total vorticity is conserved by the transpose sheme as noted by Choquin & Cottet (1988). Indeed,

$$\frac{d}{dt}\boldsymbol{\Omega} = \frac{d}{dt}\left(\sum_p \alpha_i^p\right) = -\sum_{p,q} \frac{\partial \mathbf{K}^{pq}}{\partial x_i} \cdot (\boldsymbol{\alpha}^p \wedge \boldsymbol{\alpha}^q) = 0 , \tag{3.66}$$

since one sums on all pairs (p, q) and $\partial \mathbf{K}^{pq}/\partial x_i = \partial \mathbf{K}^{qp}/\partial x_i$.

The investigation of the linear impulse is more complicated. One must investigate

$$\frac{d}{dt}\mathbf{I} = \frac{d}{dt}\left(\frac{1}{2}\sum_p \mathbf{x}^p \wedge \boldsymbol{\alpha}^p\right) = \frac{1}{2}\sum_p \left(\frac{d}{dt}\mathbf{x}^p \wedge \boldsymbol{\alpha}^p\right) + \frac{1}{2}\sum_p \left(\mathbf{x}^p \wedge \frac{d}{dt}\boldsymbol{\alpha}^p\right) . \tag{3.67}$$

The first term in Equation (3.67) is equal to

$$\frac{1}{2}\sum_{p,q} (\mathbf{K}^{pq} \wedge \boldsymbol{\alpha}^q) \wedge \boldsymbol{\alpha}^p = -\frac{1}{2}\sum_{p,q} \boldsymbol{\alpha}^p \wedge (\mathbf{K}^{pq} \wedge \boldsymbol{\alpha}^q) . \tag{3.68}$$

The second term of Equation (3.68) must be examined in more detail. Using suffix notation, this term is given by

$$\begin{aligned}
&\frac{1}{2}\sum_p \left(\mathbf{x}^p \wedge \frac{d}{dt}\boldsymbol{\alpha}^p\right)_i \\
&\quad = -\frac{1}{2}\sum_{p,q} \epsilon_{ijk}\, x_j^p \frac{\partial \mathbf{K}^{pq}}{\partial x_k} \cdot (\boldsymbol{\alpha}^p \wedge \boldsymbol{\alpha}^q) \\
&\quad = -\frac{1}{4}\sum_{p,q} \epsilon_{ijk}\,(x_j^p - x_j^q)\frac{\partial \mathbf{K}^{pq}}{\partial x_k} \cdot (\boldsymbol{\alpha}^p \wedge \boldsymbol{\alpha}^q) - \frac{1}{4}\sum_{p,q} \epsilon_{ijk}\,(x_j^p + x_j^q)\frac{\partial \mathbf{K}^{pq}}{\partial x_k} \cdot (\boldsymbol{\alpha}^p \wedge \boldsymbol{\alpha}^q) \\
&\quad = -\frac{1}{4}\sum_{p,q} \epsilon_{ijk}\,(x_j^p - x_j^q)\frac{\partial \mathbf{K}^{pq}}{\partial x_k} \cdot (\boldsymbol{\alpha}^p \wedge \boldsymbol{\alpha}^q) .
\end{aligned} \tag{3.69}$$

The second sum in Equation (3.69) has vanished since one sums on all pairs (p,q) and $\partial \mathbf{K}^{pq}/\partial x_k = \partial \mathbf{K}^{qp}/\partial x_k$.

Recalling that, for singular particles,

$$\frac{\partial K_l}{\partial x_k} = \frac{\partial}{\partial x_k}\left(-\frac{x_l}{4\pi|\mathbf{x}|^3}\right) = -\frac{\delta_{lk}}{4\pi|\mathbf{x}|^3} + 3\frac{x_l x_k}{4\pi|\mathbf{x}|^5}\ , \tag{3.70}$$

one obtains

$$\begin{aligned}
&\frac{1}{2}\sum_p \left(\mathbf{x}^p \wedge \frac{d}{dt}\boldsymbol{\alpha}^p\right)_i \\
&\quad = \frac{1}{4}\sum_{p,q} \epsilon_{ijk}\frac{(x_j^p - x_j^q)}{4\pi|\mathbf{x}^p - \mathbf{x}^q|^3}(\boldsymbol{\alpha}^p \wedge \boldsymbol{\alpha}^q)_k \\
&\qquad\qquad -\frac{3}{4}\sum_{p,q} \epsilon_{ijk}\frac{(x_j^p - x_j^q)(x_k^p - x_k^q)}{4\pi|\mathbf{x}^p - \mathbf{x}^q|^5}((\mathbf{x}^p - \mathbf{x}^q)\cdot(\boldsymbol{\alpha}^p \wedge \boldsymbol{\alpha}^q)) \\
&\quad = \frac{1}{4}\sum_{p,q} \epsilon_{ijk}\frac{(x_j^p - x_j^q)}{4\pi|\mathbf{x}^p - \mathbf{x}^q|^3}(\boldsymbol{\alpha}^p \wedge \boldsymbol{\alpha}^q)_k \qquad (\text{since } \epsilon_{ijk}\, x_j x_k = 0\,) \\
&\quad = -\frac{1}{4}\sum_{p,q}(\mathbf{K}^{pq} \wedge (\boldsymbol{\alpha}^p \wedge \boldsymbol{\alpha}^q))_i \\
&\quad = -\frac{1}{2}\sum_{p,q}(\boldsymbol{\alpha}^p \wedge (\mathbf{K}^{pq} \wedge \boldsymbol{\alpha}^q))_i\ ,
\end{aligned} \tag{3.71}$$

where the last equality has been obtained using the symmetry property $\mathbf{K}^{pq} = -\mathbf{K}^{qp}$ and the vector identity $\mathbf{a}\wedge(\mathbf{b}\wedge\mathbf{c}) + \mathbf{b}\wedge(\mathbf{c}\wedge\mathbf{a}) + \mathbf{c}\wedge(\mathbf{a}\wedge\mathbf{b}) = 0$.

For regularized vortex particles, one obtains, using properties presented in Section 3.2,

$$\begin{aligned}
\frac{\partial K_l}{\partial x_k} &= \frac{\partial}{\partial x_k}\left(-\frac{g_\sigma(\mathbf{x})}{|\mathbf{x}|^3}x_l\right) \\
&= -\frac{g_\sigma(\mathbf{x})}{|\mathbf{x}|^3}\delta_{lk} + \left(3\frac{g_\sigma(\mathbf{x})}{|\mathbf{x}|^3} - \zeta_\sigma(\mathbf{x})\right)\frac{x_l x_k}{|\mathbf{x}|^2}\ ,
\end{aligned} \tag{3.72}$$

so that the same result as for singular vortex particles is obtained, namely

$$\frac{1}{2}\sum_p \left(\mathbf{x}^p \wedge \frac{d}{dt}\boldsymbol{\alpha}^p\right) = -\frac{1}{2}\sum_{p,q} \boldsymbol{\alpha}^p \wedge (\mathbf{K}^{pq} \wedge \boldsymbol{\alpha}^q)\ . \tag{3.73}$$

Finally, combining Equations (3.68) and (3.73), one obtains, for both singular or regularized vortex particles,

$$\frac{d}{dt}\mathbf{I} = \frac{d}{dt}\left(\frac{1}{2}\sum_p \mathbf{x}^p \wedge \boldsymbol{\alpha}^p\right) = -\sum_{p,q} \boldsymbol{\alpha}^p \wedge (\mathbf{K}^{pq} \wedge \boldsymbol{\alpha}^q)\ . \tag{3.74}$$

The right hand side of Equation (3.74) is essentially a particle discretization of $-\int \boldsymbol{\omega}\wedge\mathbf{u}\,d\mathbf{x}$ and should be small (at least as long as the particles representation of

the vorticity field is a good approximation of an actual vorticity field (cfr. Sections 3.1 and 3.2)). Indeed, if the alternative form of the momentum equation, Equation (2.1), is recalled and integrated over an unbounded volume, then $\int \boldsymbol{\omega} \wedge \mathbf{u}\, d\mathbf{x} = 0$. The linear impulse is thus conserved by the transpose scheme as long as the particle discretization of the vorticity field is almost divergence free, i.e., as long as $\boldsymbol{\omega}_\sigma \simeq \nabla \wedge \mathbf{u}_\sigma$.

Because of the complexity of the terms involved, the conservation of the angular impulse was not investigated theoretically. Numerical experiments in Section 3.5 will show that the angular impulse is not conserved exactly by the method.

It is easy to see the classical scheme or the mixed scheme do not conserve any of the linear invariants. In this respect, the transpose scheme is superior to the other choices. For instance, with the classical scheme, Equation (3.65) is replaced by

$$\frac{d}{dt}\alpha_i^p = \alpha_l^p \frac{\partial}{\partial x_l}\left(\sum_q (\mathbf{K}^{pq} \wedge \boldsymbol{\alpha}^q)_i\right) . \tag{3.75}$$

This leads, after some algebra, to

$$\frac{d}{dt}\boldsymbol{\Omega} = \sum_{p,q} 3\,\frac{((\mathbf{x}^p - \mathbf{x}^q)\cdot\boldsymbol{\alpha}^p)}{4\pi|\mathbf{x}^p - \mathbf{x}^q|^5}(\mathbf{x}^p - \mathbf{x}^q) \wedge \boldsymbol{\alpha}^q \tag{3.76}$$

for singular vortex particles, and to

$$\frac{d}{dt}\boldsymbol{\Omega} = \sum_{p,q}\left(3\,\frac{g_\sigma(\mathbf{x}^p - \mathbf{x}^q)}{|\mathbf{x}^p - \mathbf{x}^q|^3} - \zeta_\sigma(\mathbf{x}^p - \mathbf{x}^q)\right)\frac{((\mathbf{x}^p - \mathbf{x}^q)\cdot\boldsymbol{\alpha}^p)}{|\mathbf{x}^p - \mathbf{x}^q|^2}(\mathbf{x}^p - \mathbf{x}^q) \wedge \boldsymbol{\alpha}^q \tag{3.77}$$

for regularized vortex particles. The right-hand sides above do not vanish in general.

Notice that, with any of the three schemes, there is a rate of change of the vorticity associated with the presence of an external potential flow ϕ

$$\frac{d}{dt}\alpha_i^p(t) = \alpha_j^p(t)\,\frac{\partial^2}{\partial x_i x_j}\phi(\mathbf{x}^p(t), t) , \tag{3.78}$$

and that this has a non-zero contribution to the total vorticity, i.e.,

$$\frac{d}{dt}\left(\sum_p \alpha_i^p(t)\right)_{\text{potential}} = \sum_p \alpha_j^p(t)\,\frac{\partial^2}{\partial x_i x_j}\phi(\mathbf{x}^p(t), t) . \tag{3.79}$$

So far, the conservation of the linear invariants with the inviscid method of vortex particle, both singular and regularized, has been examined. One must now investigate the conservation of the linear invariants when the viscous method presented in Section 3.3 is used.

First, it is easy to see that the viscous integral operator (3.46) is conservative (i.e., conserves total vorticity). Indeed,

$$\int\int (\boldsymbol{\omega}(\mathbf{y}) - \boldsymbol{\omega}(\mathbf{x}))\,\eta_\sigma(\mathbf{x} - \mathbf{y})\, d\mathbf{y}\, d\mathbf{x} = 0 . \tag{3.80}$$

The particle discretization (3.53) of the integral operator is also conservative since

$$\sum_{p,q} (vol^p \, \boldsymbol{\alpha}^q - vol^q \, \boldsymbol{\alpha}^p) \, \eta_\sigma(\mathbf{x}^p - \mathbf{x}^q) = 0 \, . \tag{3.81}$$

The total vorticity is thus not affected by the treatment of the diffusion term.

Second, as pointed out by Mas-Gallic (private communication 1988), the linear impulse is not affected by the viscous integral operator but is affected by the particle discretization of the integral operator. Indeed, since

$$0 = \int \mathbf{x}' \, \eta_\sigma(\mathbf{x}') \, d\mathbf{x}' = \int (\mathbf{x} - \mathbf{y}) \, \eta_\sigma(\mathbf{x} - \mathbf{y}) \, d\mathbf{x} \, , \tag{3.82}$$

so that

$$\int \mathbf{x} \, \eta_\sigma(\mathbf{x} - \mathbf{y}) \, d\mathbf{x} = \int \mathbf{y} \, \eta_\sigma(\mathbf{x} - \mathbf{y}) \, d\mathbf{x} \, , \tag{3.83}$$

one obtains

$$\begin{aligned}
&\int \mathbf{x} \wedge \left[\int (\boldsymbol{\omega}(\mathbf{y}) - \boldsymbol{\omega}(\mathbf{x})) \, \eta_\sigma(\mathbf{x} - \mathbf{y}) \, d\mathbf{y} \right] d\mathbf{x} \\
&\quad = \int \left[\int \mathbf{x} \, \eta_\sigma(\mathbf{x} - \mathbf{y}) \, d\mathbf{x} \right] \wedge \boldsymbol{\omega}(\mathbf{y}) \, d\mathbf{y} - \int \int \mathbf{x} \wedge \boldsymbol{\omega}(\mathbf{x}) \, \eta_\sigma(\mathbf{x} - \mathbf{y}) \, d\mathbf{y} \, d\mathbf{x} \\
&\quad = \int \left[\int \mathbf{y} \, \eta_\sigma(\mathbf{x} - \mathbf{y}) \, d\mathbf{x} \right] \wedge \boldsymbol{\omega}(\mathbf{y}) \, d\mathbf{y} - \int \int \mathbf{x} \wedge \boldsymbol{\omega}(\mathbf{x}) \, \eta_\sigma(\mathbf{x} - \mathbf{y}) \, d\mathbf{y} \, d\mathbf{x} \\
&\quad = \int \int \mathbf{y} \wedge \boldsymbol{\omega}(\mathbf{y}) \, \eta_\sigma(\mathbf{x} - \mathbf{y}) \, d\mathbf{x} \, d\mathbf{y} - \int \int \mathbf{x} \wedge \boldsymbol{\omega}(\mathbf{x}) \, \eta_\sigma(\mathbf{x} - \mathbf{y}) \, d\mathbf{y} \, d\mathbf{x} \\
&\quad = 0 \, ,
\end{aligned} \tag{3.84}$$

by interchanging the role of $\mathbf{x}$ and $\mathbf{y}$ in the first integral. If one now considers the particle discretization of the integral operator, one obtains

$$\begin{aligned}
&\sum_p \mathbf{x}^p \wedge \left[\sum_q (vol^p \, \boldsymbol{\alpha}^q - vol^q \, \boldsymbol{\alpha}^p) \, \eta_\sigma(\mathbf{x}^p - \mathbf{x}^q) \right] \\
&\quad = \frac{1}{2} \sum_{p,q} (\mathbf{x}^p - \mathbf{x}^q) \wedge (vol^p \, \boldsymbol{\alpha}^q - vol^q \, \boldsymbol{\alpha}^p) \, \eta_\sigma(\mathbf{x}^p - \mathbf{x}^q) \\
&\quad \neq 0
\end{aligned} \tag{3.85}$$

in general. It is thus a matter of discretization to conserve linear impulse with the particle approximation of the integral operator, and it is reasonable to assume that, as the number of particles increases, the linear impulse is better conserved. This will be checked numerically in some of the computations presented in Section 3.5.

In conclusion, the use of the transpose scheme for the stretching term and of the viscous operator for the diffusion term leads to

$$\frac{d}{dt} \boldsymbol{\Omega} \;=\; 0 \tag{3.86}$$

$$\frac{d}{dt}\mathbf{I} = -\sum_{p,q} \boldsymbol{\alpha}^p \wedge (\mathbf{K}^{pq} \wedge \boldsymbol{\alpha}^q) + \frac{\nu}{2} \sum_{p,q} (\mathbf{x}^p - \mathbf{x}^q) \wedge (vol^p\, \boldsymbol{\alpha}^q - vol^q\, \boldsymbol{\alpha}^p) \ . \qquad (3.87)$$

Total vorticity is conserved. Linear impulse is not conserved in general. The first term in the rate of change of the linear impulse nearly vanishes when it is a good representation of $-\int \boldsymbol{\omega} \wedge \mathbf{u}\, d\mathbf{x}$, i.e., when the particle vorticity field is almost divergence free. The second term in the rate of change of the linear impulse vanishes when the number of particles increases, i.e., when the particle discretization of the viscous integral operator is accurate.

The above analysis of the conservation of the linear invariants carries through when each particle has its own core size $\sigma^p(t)$ provided that the evolution equations for the particles position and strength vector are symmetrized.

The evaluation of the semi-regularized quadratic diagnostics, such as energy $\tilde{E}$, helicity $\tilde{\mathcal{H}}$ and enstrophy $\tilde{\mathcal{E}}$ is difficult. The difficulty comes from the fact that the particle representation of the particle vorticity field is not generally divergence free. The derivation of the appropriate expressions is presented in detail in Appendix G. It is also shown, in that appendix, that the high order algebraic smoothing (B.12) is a prime choice as far as the evaluation of the quadratic diagnostics is concerned.

The inviscid method of vortex particles, both singular and regularized, does not conserve kinetic energy and helicity exactly with any of the choices for the stretching term. These quantities are thus used as diagnostics to measure the performance of the method on a particular problem. With singular particles, it will be shown numerically in Section 3.5 that the transpose scheme performs best on the conservation of kinetic energy.

In viscous computations, the decay of the kinetic energy is used as a diagnostic to check if Equation (A.8) is satisfied.

3.5 Numerical results

In this section, the numerical results that were obtained with the method of vortex particles are examined. The use of singular and regularized particles are investigated numerically. For the method of regularized particles, both the inviscid and viscous versions of the method are investigated. The linear and quadratic diagnostics are used extensively to measure the performance of the numerical computations.

Special emphasis is made on the investigation of the method for the computation of the fusion of two vortex rings. Before presenting the computational strategy and the

numerical results, the motivation for studying this problem is given in Section 3.5.1, together with a review of previous work, both experimental and numerical.

3.5.1 The problem of the fusion of two vortex rings: motivation and review of previous investigations

The problem of the fusion of two vortex rings that are initially side by side has received, in the past ten years, much attention. It has been widely investigated, both experimentally and numerically. This problem is of special interest for many reasons. It is closely related to the understanting of the interaction between three-dimensional vortex structures, a fundamental step towards the understanding of turbulent flows. It is also an elegant problem that is somewhat well defined at time $t = 0$ and that contains many of the ingredients which are present in more complex flows, such as intense vortex stretching, interaction between regions of opposite sign vorticity and viscous reconnection of vortex tubes.

Previous investigations, both experimental and numerical are briefly reviewed.

3.5.1.1 Experimental investigations

Many of the experiments that involve the fusion of two vortex rings are purely qualitative and are limited to flow vizualization. The only experiments that also provide quantitative information are the experiments by Schatzle & Coles (1987) and Izutsu, Oshima K. & Oshima Y. (1987).

The experiment by Schatzle & Coles is done in water. Two laminar vortex rings, initially at a slight angle with respect to each other, collide. Both the fusion and the fission processes are observed. These processes are illustrated in the series of photographs from Schatzle & Coles (1987 and private communication) reproduced in Figure J.24. Dye is used as a material line marker to vizualize the reconnection of the vortex tubes. One must however keep in mind that the location of the dye is not necessarily the location of the vorticity. There are two reasons: first, the vortex cores are not completely filled with dye and second, in viscous flows, vorticity does not behave as a material line but dye nearly does. For the fusion process, the velocity field is measured using laser-Doppler velocimetry. The measurements are in the plane of symmetry of the collision and are used to provide many quantitative results prior to and during the fusion process: velocity, vorticity and strain rates contours, contours of the different terms of the vorticity equation and global data such as the time history of the circulation. The geometry and the vorticity profiles of each ring prior to collision are also provided and are proposed as initial conditions for numerical computations. Finally, time scale estimates for the reconnection process are discussed. The results

of the numerical computations done using the viscous method of vortex particles will be compared to the experimental results of Schatzle & Coles.

The experiment by Izutsu, Oshima K. & Oshima Y. is done in air. Velocities are measured in the entire three-dimensional space using a X-wire probe. Computer animations of the vorticity field computed from the measured velocity field are provided. Although their results cover a larger portion of space, their resolution is not as good as the resolution of the experiment by Schatzle & Coles.

3.5.1.2 Numerical investigations

Early investigations of the process of the fusion of two vortex rings were done using inviscid methods. Because the process of vortex tubes reconnection requires the presence of some viscous dissipation, intervention of some sort is needed to force the vortex tubes to reconnect. The earliest computation using the method of regularized vortex filaments is by Leonard (1975). When the cores of filaments of opposite sign vorticity overlap significantly, the geometry of the filaments is redefined so as to mimic the reconnection process. The same type of procedure is used in the computation by Yamashita & Oshima (1988). In the total absence of viscosity, the process of reconnection can never fully occur since vortex lines remain connected for all times. This is illustrated by the numerical experiment, Chapter 2, Section 2.5.4.1.

A related subject of great interest is the investigation, both theoretically and numerically, of the possibility of a singularity developing in the inviscid vorticity equation in finite time. Refer to Siggia (1984) and Pumir & Siggia (1987) for such investigations using the method of vortex filaments.

The simulation of the fusion of two vortex rings using the method of regularized vortex particle has also been tried by several investigators (Anderson & Greengard 1984, Shirayama & Kuwahara 1984). In earlier studies, flow diagnostics were not computed and the numerical results appear questionable. In the computation by Anderson & Greengard, the particles are subjected to a random walk that simulates viscous diffusion. In the computation by Shirayama & Kuwahara, the method is inviscid, and intervention of some sort is still needed to force the vortex tubes to reconnect. Some inviscid computations are presented in Section 3.5.3 and Section 3.5.4.

A few authors have attempted direct simulations of the Navier-Stokes equation on this problem. Two such efforts are known: the simulation by Ashurst & Meiron (1987), and the simulation by Chen & Oshima (1988). Ashurst & Meiron use the method of regularized vortex filaments to start their computation. The rings are initially co-planar. When the cores of filaments of opposite sign vorticity overlap significantly, the computation is interrupted. A $32 \times 32 \times 32$ grid is then placed in

the collision area and the Navier-Stokes equations are solved on that grid with fixed boundary conditions. The argument is that the fusion process occurs so rapidly that it is a good approximation to freeze the rest of the vortex rings while computing the time evolution of the fusion process inside the box only. They perform computations over a wide range of Reynolds numbers ($Re = \Gamma/\nu = 10$, 100 and 1,000, where Γ is the circulation of one vortex ring). For the simulations at $Re = 100$ and 1,000, they conclude that the time scale for the disappearance of circulation in the plane of collision scales like the convective time scale σ_K^2/Γ, where σ_K is the core radius of the equivalent vortex ring of uniform vorticity.

In the computation by Chen & Oshima, both rings are included in the computational domain. The grid is $61 \times 42 \times 42$ and the Reynolds number is $Re = 200$. Although the number of mesh points is larger than that used by Ashurst & Meiron, the resolution is lower since the entire problem is computed at once. For that reason, the results are mostly qualitative (although plots of the circulation in all planes of interest are provided).

It will be shown in Section 3.5.6 that the new viscous version of the method of regularized vortex particles is able to produce satisfactory results without having to reduce the computational domain to a small region.

Spectral computations of the viscous reconnection of antiparallel vortex tubes have also been achieved (Pumir & Kerr 1987, Meiron et al. 1988). These computations are carried out using a pseudospectral code with periodic boundary conditions. They are part of an effort to understand the reconnection of vortex tubes in general but also to explore the possibility of a singularity developing in the Euler equations in finite time.

Finally, some analytical work by Takaki & Hussain (1986) should also be mentioned. In their analysis, the local flow field is expanded into polynomials of the coordinates, and the coefficients, which are functions of time, are obtained by substituting the expansions into the vorticity equation. They conclude that the entire process of vortex reconnection is completed within the convective time scale σ_K^2/Γ, but that the presence of viscosity is necessary for the occurrence of the process.

3.5.2 Some points that are common to all computations

The fluid mechanical aspects of the fusion of two vortex rings are studied in detail in Section 3.5.6. Before then, the fusion of two vortex rings is only used as a test problem for the method of singular vortex particles (Section 3.5.3) and for the inviscid version of the method of regularized vortex particles (Section 3.5.4). In the present section, the details that are common to all computations presented in the next five

sections are given.

All computations are performed using the simple, but costly $\mathcal{O}(N^2)$ algorithm where the influence of each particle on all other particles is computed explicitly.

The ordinary differential equations for the time evolution of the particles position and strength vector are presented in detail in Appendix F. For the regularized method, our new high order algebraic smoothing (B.12) is used consistently for the reasons mentioned in Section 3.2 and Section 3.3.

The time integration of the evolution equations is done using the low storage Runge-Kutta scheme of order 3 (WRK3) introduced by Williamson (1980).

All computations presented below involve two circular vortex rings as initial condition. The parameters that are common to all computations are the radius $R = 1.0$ and circulation $\Gamma = 1.0$ of each ring. The core structure of each ring is discretized using a scheme that allocates to each vortex particle an equal area normal to the vorticity vector. This scheme is illustrated in Figure J.26. One vortex particle is placed at the center of the circle of radius r_l. If $n_c = 0$ then no other layer of particles is used. If $n_c \neq 0$, then $1 \leq n \leq n_c$ additional layers are used, the nth such layer being made of $8\,n$ particles and each particle being placed at the centroid $r_c = ((1 + 12\,n^2)/6n)\,r_l$ of its own cell. Each cell has an area $\pi\,r_l^2$. The maximum radius reached by this discretization is $r_{max} = (2\,n_c + 1)\,r_l$. The number of particles per cross section is $N_s = 1 + 4\,n_c\,(n_c + 1)$. N_φ such sections are used to discretize the torus itself.

In three dimensions, each vortex particle has to be assigned a volume, not an area. If φ is the azimuthal angle along the torus, it is easy to see that $d\mathbf{x} = ((R + r\cos\theta)\,d\varphi)\,(r\,d\theta\,dr)$. If θ_1 and θ_2 are the angles associated with a particular cell and $r_1 = (2\,n - 1)\,r_l$ and $r_2 = (2\,n + 1)\,r_l$ are the lower and upper radius of that cell, one obtains, integrating the infinitesimal volume $d\mathbf{x}$ for $\Delta\varphi = 2\pi/N_\varphi$, that the volume of that cell is given by

$$vol = \Delta\varphi\,(r_2 - r_1)\left[(\theta_2 - \theta_1)\,R\left(\frac{r1 + r2}{2}\right) + (\sin\theta_2 - \sin\theta_1)\left(\frac{r_1^2 + r_1 r_2 + r_2^2}{3}\right)\right]. \tag{3.88}$$

The other parameters for the ring discretization and initial vorticity distribution are specific to each computation. This condition is partially due to the fact that these computations were done over a long period of time and were refined from experience.

When presenting numerical results, both linear and quadratic diagnostics (when they are not trivially zero) are provided. For the linear diagnostics, the linear impulse $\mathbf{I}$ and the angular impulse $\mathbf{A}$ are given. The conservation of total vorticity $\boldsymbol{\Omega} = 0$ is guaranteed for all times due to the symmetry of the problems that are considered. When presenting quadratic diagnostics, $E = \frac{1}{2}\int \mathbf{u}\cdot\mathbf{u}\,d\mathbf{x}$, $E_f = \frac{1}{2}\int \boldsymbol{\psi}\cdot\boldsymbol{\omega}\,d\mathbf{x}$ and

$\mathcal{H} = \int \boldsymbol{\omega}^N \cdot \mathbf{u}\, d\mathbf{x} = \int \boldsymbol{\omega} \cdot \mathbf{u}\, d\mathbf{x} = \mathcal{H}_f$ are given for singular particles. In the evaluation of E and E_f, the singularity is removed by avoiding the infinite self-energy of the particle. The reader is reminded that only E is the (desingularized) kinetic energy of the system, and that the approximation E_f is equal to E (up to some constant) only when the particle vorticity field $\boldsymbol{\omega}$ is a good representation of the divergence free field $\boldsymbol{\omega}^N$. For regularized vortex particles, $\tilde{E} = \frac{1}{2} \int \mathbf{u}_\sigma \cdot \mathbf{u}\, d\mathbf{x}$ and $\tilde{E}_f = \frac{1}{2} \int \boldsymbol{\psi}_\sigma \cdot \boldsymbol{\omega}\, d\mathbf{x}$, $\tilde{\mathcal{H}} = \int \boldsymbol{\omega}^N \cdot \mathbf{u}_\sigma\, d\mathbf{x} = \int \boldsymbol{\omega} \cdot \mathbf{u}_\sigma\, d\mathbf{x} = \tilde{\mathcal{H}}_f$, $\tilde{\mathcal{E}} = \int \boldsymbol{\omega}^N \cdot \boldsymbol{\omega}_\sigma^N\, d\mathbf{x}$ and $\tilde{\mathcal{E}}_f = \int \boldsymbol{\omega} \cdot \boldsymbol{\omega}_\sigma\, d\mathbf{x}$ are given. The reader is reminded that only $\tilde{E}$ is the exact semi-regularized kinetic energy of the system, and that the approximation $\tilde{E}_f$ is equal to $\tilde{E}$ only when the particle vorticity field $\boldsymbol{\omega}_\sigma$ is a good representation of the divergence free vorticity field $\boldsymbol{\omega}_\sigma^N$. The same remark applies to the exact semi-regularized enstrophy $\tilde{\mathcal{E}}$ and the approximation $\tilde{\mathcal{E}}_f$.

3.5.3 The problem of the fusion of two vortex rings computed using the method of singular vortex particles

The first step towards the understanding of the performance of the method of vortex particles is the computation, using singular particles as presented in Section 3.1, of the fusion of two vortex rings. The different choices for the evolution equation of the particle strength vector are compared: classical scheme, transpose scheme and mixed scheme.

All three computations are performed using the same initial condition. They are initialized in the configuration shown in Figure J.25 with the two rings at a spacing $s = 3.0$ center to center and at an angle $\theta_0 = 10.0°$ with respect to the vertical. The discretization parameters are $r_l = .08$, $n_c = 2$ and $N_\varphi = 44$. Therefore, $N_s = 25$ particles per section for a total of $N = 2200$. The distance between particles in the radial direction is $h \simeq 2r_l = .16$. This distance is roughly equal to the distance between particles along the torus itself, with $h \simeq 2\pi R/N_\varphi = .14$.

The symmetry of the problem is used, and only the particles in one half of one ring are actually computed. This choice reduces the computational effort by 1/4 and also ensures that the symmetry is preserved for all times. The particle strengths are in the ratio [1 : .54 : .16] from the center to the outer layer for a total circulation $\Gamma = 1.0$. The time step is initially $\Delta t = .008$ and is reduced towards the end of the computation to $\Delta t = .0016$.

The results are shown in Figure J.27 for the plots of strength vectors and in Figure J.28 for the diagnostics. All computations fail to lead to the fusion process. The transpose scheme is the one that goes farthest in time, up to $t \simeq 4.2$. The computation blows up when the strength vectors of some particles are suddenly out of alignment from the vortex tube itself. The diagnostics are instructive. They indicate

that the transpose scheme performs better than the two other schemes, with regard to the conservation of linear impulse I (with $I(0) = 1.054936$) and energy (with $E(0) = 3.749091$ and $E_f(0) = 3.675169$). The transpose scheme nearly conserves linear impulse and energy up to the time at which the computation blows up. The classical scheme does a poor job at conserving the linear impulse and the energy. Finally, the mixed scheme stands in between the other two as far as the conservation of the linear impulse is concerned. Notice also that the curves for E and E_f follow each other up to times that are very close to the time of the singularity, thus indicating that, up to then, the particle vorticity field ω is a good representation of a divergence free field.

The conclusion is clear: for singular vortex particles, the transpose scheme is superior to the other ones. However, the singular nature of these particles leads to a divergence in the computation of the interaction between vortex tubes of opposite sign vorticity. Singular particles are thus not useful in a general situation.

3.5.4 The problem of the fusion of two vortex rings computed using the inviscid version of the method of regularized vortex particles

In this section, the performance of the inviscid method of regularized vortex particles presented in Section 3.2 is examined on the problem of the fusion of two vortex rings.

As far as the particle locations and strengths are concerned, the initial conditions are identical to the ones used in Section 3.5.3. The core of each particle is taken as $\sigma = .20$ which satisfies the overlaping constraint since $h \simeq .15$. The time step is $\Delta t = .08$. Only the classical scheme and the transpose scheme are investigated.

The results are shown in Figure J.29 and Figure J.30 for the plots of strength vectors, and in Figure J.31 for the diagnostics. As opposed to singular particles, the use of regularized particles allows a computation much farther in time with numerical divergence at about $t \simeq 11.0$. Although both computations fail to go through the entire fusion process (which is to be expected since they are inviscid!), it appears that the reconnection of vortex tubes has nearly occurred. The choices, classical and transpose schemes, do not however lead to equivalent results. The solution at $t = 11.09$ is noticeably different depending on which choice is used. It would be interesting to repeat these computations with many more particles to see whether or not both computations converge to the same result.

The diagnostics are presented in Figure J.31. As in Section 3.5.3, one still has $I(0) = 1.054936$. For the semi-regularized energy, one now obtains $\tilde{E}(0) \simeq \tilde{E}_f(0) = 8.884598 \times 10^{-3}$. Both schemes perform equally well (or equally badly), with a slight plus on the conservation of linear impulse for the transpose scheme and a slight plus

on the conservation of energy for the classical scheme, at least up to $t \simeq 8.0$. It will be shown in Section 3.5.5, Section 3.5.6 and Section 3.5.7 that the transpose scheme indeed performs well on the conservation of linear impulse, at least as long as the particle vorticity field ω_σ remains a good representation of the divergence free field ω_σ^N. It is thus suspected that, in the present case, ω_σ becomes a poor representation of ω_σ^N at about $t \simeq 8.0$.

The conclusion is not as clear as with singular vortex particles. In very smooth situations, all schemes (including the mixed scheme) perform well as long as the particle vorticity field ω_σ remains almost divergence free (since all schemes are then equivalent as seen in Section 3.2). The "inviscid fusion" of vortex rings is however not a smooth situation. That the converged solution obtained with the inviscid method of regularized vortex particles is indeed the solution (if it exists!) of the inviscid vorticity equation is hard to believe. Nevertheless, the general picture of the flow seems to be correct, at least up to when the computation diverges. What is really missing in the method is the presence of viscous dissipation. It will be shown, in the next two sections, that the viscous version of the method of regularized vortex particles introduced in Section 3.3 indeed solves the viscous vorticity equation in the limit, and that this method can be used to compute, with very acceptable results, the viscous fusion of two vortex rings.

3.5.5 The computation of a single vortex ring, inviscid and viscous: a test case for the convergence of the method of regularized vortex particles

The goal is to compute the viscous fusion of two vortex rings and to obtain quantitative information that can be compared with the experiment of Schatzle & Coles (1987). This will be done in Section 3.5.6. Before doing so, one needs to investigate the performance of the method of regularized vortex particles, inviscid and viscous on a simple but instructive problem: the single vortex ring.

This problem is axisymmetric. Consequently, only one section of the torus has to be computed. Of course, it is still necessary to compute the influence of all particles in all other section on the particles of that section. Nevertheless, the computational effort is now reduced by a factor of $1/N_\varphi$. Because of that reduction, computations that involve up to $n_c = 6$ layers of particles per section for a total of $N \simeq 20,000$ vortex particles can be carried out.

The initial vorticity field that is discretized using the vortex particles is given

by

$$\boldsymbol{\omega}(\mathbf{x},0) = \omega(r,\theta,0)\,\hat{\mathbf{e}}_\varphi = \frac{\Gamma}{2\pi\,{\sigma_R}^2}\left(1+\frac{r}{R}\cos\theta\right) e^{-r^2/2\sigma_R{}^2}\,\hat{\mathbf{e}}_\varphi\,, \tag{3.89}$$

where σ_R is the core size of the vortex ring. The term in parenthesis in Equation (3.89) is a first order correction term which accounts for the vorticity stretching. Indeed, if the vortex lines go in almost circular trajectories about the center of the ring (which is true for thin rings), then the vorticity is modified according to that term. Since the rings considered here are neither very thin nor very fat, it is reasonable to initialize the vorticity field using the correction term.

With the above initial condition, the initial enstrophy can be evaluated exactly. This will be used as a diagnostic at time $t = 0$ to verify that the kinetic energy of the viscous computation indeed decays according to $dE/dt = -\nu\,\mathcal{E}$, as seen in Appendix A, Equation (A.8). The enstrophy of the initial condition is given by

$$\begin{aligned}
\mathcal{E}(0) &= \int \boldsymbol{\omega}(\mathbf{x},0)\cdot\boldsymbol{\omega}(\mathbf{x},0)\,d\mathbf{x} \\
&= \left(\frac{\Gamma}{2\pi\,{\sigma_R}^2}\right)^2 \int_{\varphi=0}^{2\pi}\int_{\theta=0}^{2\pi}\int_{r=0}^{\infty}\left(e^{-r^2/2\sigma_R{}^2}\left(1+\frac{r}{R}\cos\theta\right)\right)^2 \\
&\qquad\qquad \left(1+\frac{r}{R}\cos\theta\right) R\,d\varphi\,r\,d\theta\,dr \\
&= \frac{\Gamma^2\,R}{{\sigma_R}^4}\int_0^\infty\left(1+\frac{3}{2}\frac{r^2}{R^2}\right) e^{-r^2/\sigma_R{}^2}\,r\,dr \\
&= \frac{\Gamma^2\,R}{2\,{\sigma_R}^2}\left(1+\frac{3}{2}\frac{{\sigma_R}^2}{R^2}\right)
\end{aligned} \tag{3.90}$$

In the above integration, it has been assumed that the integral in r can be extended to ∞, independently of θ. This is valid only when the ring is thin enough that the vorticity at $r = R$ is very small (i.e., when $\sigma_R << R$).

The initialization of the vortex particles is done as follows. For each particle placed at the centroid $\mathbf{x}^p(0)$ of its own cell of volume vol^p, the particle strength is taken as $\boldsymbol{\alpha}^p_{old}(0) = vol^p \times \boldsymbol{\omega}(\mathbf{x}^p(0),0)$. At this point, the particle vorticity field $\boldsymbol{\omega}_\sigma(\mathbf{x},0)$ is not a good representation of the exact vorticity field $\boldsymbol{\omega}(\mathbf{x},0)$. For instance, $\boldsymbol{\omega}_\sigma(\mathbf{x}^p(0),0) \neq \boldsymbol{\omega}(\mathbf{x}^p(0),0)$. In order to obtain a good initial condition, one then solves for new particle strengths $\boldsymbol{\alpha}^p_{new}(0)$ by imposing that $\boldsymbol{\omega}_\sigma(\mathbf{x}^p(0),0) = \boldsymbol{\omega}(\mathbf{x}^p(0),0)$, namely

$$\sum_q \boldsymbol{\alpha}^q_{new}(0)\,\zeta_\sigma(\mathbf{x}^p(0)-\mathbf{x}^q(0)) = \boldsymbol{\alpha}^p_{old}(0)/vol^p \tag{3.91}$$

In the following, this procedure will be referred to as the *relaxation of the initial condition.* Equation (3.91) is essentially a system of linear equations for the new particle strengths and is easy to solve. Indeed, since the initial strength vector $\boldsymbol{\alpha}^p_{old}$ is close to the objective $\boldsymbol{\alpha}^p_{new}$, this system is of the form $A\,\alpha_{new} = \alpha_{old}$ where A is

almost equal to the identity matrix. Writing $A = (A - I) + I$, the following iterative method can be written to solve this system

$$\begin{aligned} \alpha_{new}^{(0)} &= \alpha_{old} && \text{initialization} \\ \alpha_{new}^{(n)} &= \alpha_{old} + (I - A)\,\alpha_{new}^{(n-1)} && 1 \leq n \leq niter\,. \end{aligned} \tag{3.92}$$

It is found that the iteration process converges in typically $niter = 5$ iterations.

Notice that there is still an arbitrary parameter in defining the initial condition of a specific numerical computation: the choice of the core size σ of the regularized vortex particles. In the present stategy, σ is chosen so as to be consistent with the correct decay of the kinetic energy at $t = 0$. The procedure is as follows:

- Choose a core size σ which satisfies the overlaping constraint, typically $\sigma/h \simeq 1.3$.
- Relax the inital condition as explained above so as to have a particle vorticity field ω_σ that is close to the exact vorticity field ω.
- Perform two computational time steps so as to obtain numerically $\tilde{E}(0)$, $\tilde{E}(\Delta t)$ and $\tilde{E}(2\,\Delta t)$. The numerical decay of the semi-regularized kinetic energy is then given, to second order, by

$$\frac{d}{dt}\tilde{E}(0) = \frac{(-\tilde{E}(2\,\Delta t) + 4\,\tilde{E}(\Delta t) - 3\,\tilde{E}(0))}{2\,\Delta t}\,. \tag{3.93}$$

- Verify that $d\tilde{E}/dt = -\nu\,\mathcal{E}(0)$ where $\mathcal{E}(0)$ is given by Equation (3.90). If the comparison is not sufficiently close, change the core size σ slightly and iterate on this process.

Notice that the exact kinetic energy E and not the semi-regularized energy $\tilde{E}$ should be used for the above process to be totally justified. Recall however, that the semi-regularized energy $\tilde{E}$ is an excellent approximation to the exact energy E when the number of particles is large (cfr. Appendix G, Section G.2.1). This is not true for the approximation of the enstrophy $\mathcal{E}$ by the semi-regularized enstrophy $\tilde{\mathcal{E}}$ as will be seen in the numerical results. Notice also that the above procedure cannot be used during the course of the computation to verify that the kinetic energy continues to decrease at the proper rate. This is precisely due to the fact that the computed semi-regularized enstrophy $\tilde{\mathcal{E}}(t)$ is not a good approximation of the exact unknown enstrophy $\mathcal{E}(t)$ unless the number of computational particles is very very large.

The strategy for the particle discretization, the relaxation of the initial condition, and the choice of the particle core size is now defined. The numerical computations, both inviscid and viscous, are now examined. As usual, $R = 1.0$, $\Gamma = 1.0$.

The inital ring radius is taken as $\sigma_R = .10$. The initial velocity of the ring is thus given asymptotically by Equation (2.60), i.e., $U_R = .2767296$. The maximum radius reached by the discretization is $r_{max} = (2\,n_c + 1)\,r_l = .35$. This defines r_l as a function of n_c, the number of layers used to discretized the inital vorticity field. The cases $n_c = 4$, $n_c = 5$ and $n_c = 6$ are examined. The number of sections N_φ is chosen in such a way that the distance between neighbor particles is the same in all directions, i.e., $h \simeq 2\,r_l \simeq 2\pi\,R/N_\varphi$. All computations are done with $\Delta t = .025$ and using the transpose scheme. For the viscous computations, the viscosity is chosen so that the Reynolds number based on circulation is $Re = \Gamma/\nu = 400$. This corresponds to $\nu = 2.50 \times 10^{-3}$. Roughly speaking, viscous diffusion will bring vorticity to the last layer of discretization $n = n_c$ at about $t = 3.0 \ldots 4.0$. This estimate is based on the two-dimensional spreading of a Gaussian distribution with $\sigma_R{}^2 = 2\nu t$. The inviscid computations are done with the same inital discretization as those of the viscous computations. With the above choices, one obtains, for the exact enstrophy given by Equation (3.90), $\mathcal{E}(0) = 50.75000$. The exact initial rate of decay of the kinetic energy is thus given by $dE/dt(0) = -\nu\,\mathcal{E}(0) = -.1268750$. In addition to the usual diagnostics, the centroid velocity $d\,X_c/dt$ is also monitored, with Lamb (1932) and Saffman's (1970) definition of the vorticity centroid

$$X_c = \frac{\int \omega_y\, x\, z^2\, d\mathbf{x}}{\int \omega_y\, z^2\, d\mathbf{x}} \,. \tag{3.94}$$

The parameters that are specific to each computation and the numerical results at $t = 0$ are summarized in Table 3.1.

Notice how close the numerical values of $\tilde{E}(0)$ and $\tilde{E}_f(0)$ are. This closeness is a numerical confirmation that the particle vorticity field $\boldsymbol{\omega}_\sigma$ is a good representation of the divergence free field $\boldsymbol{\omega}_\sigma^N$. The numerical values of $\tilde{\mathcal{E}}(0)$ and $\tilde{\mathcal{E}}_f(0)$ are not as close. As the level of discretization increases, the semi-regularized energy $\tilde{E}(0)$ converges to the exact value $E(0)$ much faster than the enstrophy does. For instance, with $n_c = 6$, one obtains convergence of the energy up to 3 or 4 digits, but one still has $\tilde{\mathcal{E}}(0) = 56.61$, instead of the theoretical value $\mathcal{E}(0) = 50.75$. These results are consistent with the remarks made in Appendix G, Section G.2.1 concerning the convergence of the semi-regularized energy and semi-regularized enstrophy to the exact energy and enstrophy.

The viscous computations were done for $n_c = 4$, 5 and 6. The inviscid computations were done for $n_c = 4$ and 5. The results are presented in Figure J.32 & Figure J.33 for plots of the strength vectors, Figure J.34 for the vorticity contours and Figure J.35 & Figure J.36 for the diagnostics.

	$n_c = 4$	$n_c = 5$	$n_c = 6$
r_l	.03889	.03182	.02692
N_φ	80	100	117
N_s	81	121	169
N	6,480	12,100	19,773
$I(0)$	3.213919	3.215482	3.218423
$\tilde{E}(0)$	1.047552	1.036491	1.031477
$\tilde{E}_f(0)$	1.047634	1.036526	1.031498
$\tilde{\mathcal{E}}(0)$	61.34640	58.30524	56.61377
$\tilde{\mathcal{E}}_f(0)$	62.38420	58.99072	57.16328
$dX_c/dt(0)$	.26605	.26607	.26620
σ	.1000	.0840	.0735
$d\tilde{E}/dt(0)$ (viscous only)	−.1276	−.12684	−.12687

Table 3.1: Parameters and numerical results at $t = 0$ for the computation of a single vortex ring with the method of regularized vortex particles.

First, the results of the inviscid computations are examined. As seen in Figure J.35, the linear impulse I and the semi-regularized energy $\tilde{E}$ are very well conserved up to $t = 5.0$. The vorticity contour plots given in Figure J.34 show that the core structure remains almost circular up to $t \simeq 2.0$, but then an instability is evident. At time $t \simeq 3.5$, the core structure has two local vorticity maxima. This structural instability of the core also shows up in the time history of the enstrophy $\tilde{\mathcal{E}}$, Figure J.35, with a sudden increase in $\tilde{\mathcal{E}}$ at about $t \simeq 2.0$. Recall that the enstrophy is not generally conserved in three-dimensional or even axisymmetric inviscid flows because of the possibility of vortex stretching. It is not clear whether the results of this computation are correct or not. There are no other inviscid computations to which these results may be compared. Examining Figure J.32, one might suspect that the origin of the core structure instability is purely numerical and is due to the accumulation of vortex filaments in some region and to the lack of vortex filaments in other regions (*vortex filaments*, in the present context, are defined as a collection of regularized vortex particles that indeed discretize a closed vortex filament). On the other hand, recalling that vortex lines move as material lines, one might think that this behavior is physically correct. There is however a subtle point here. The fact that vortex lines move as material lines does not necessarily mean that vortex filaments move as material entities with their centerline velocity. In other words, it could be that the process of convecting the filaments with the centerline velocity leads to small

errors that slowly accumulate in time until the point at which the computation ceases to be valid. Notice that this remark does not contradict the convergence proofs that only state that the method converges as $\sigma \to 0$ and $N \to \infty$ with $\sigma/h > 1$. A diagnostic which is very sensitive to the core structure is the centroid X_c and even more sensitive its time derivative, the centroid velocity dX_c/dt. In Figure J.35, dX_c/dt is given for different levels of discretization, $nc = 4$ and $n_c = 5$. Notice that the solution is not fully converged since both curves do not lie on top of each other (the other diagnostics, linear impulse, energy and enstrophy are identical for both cases $n_c = 4$ and $n_c = 5$, at least up to $t = 4.0$ and are thus only plotted for $n_c = 5$). Nevertheless, both curves do overlap for short time, and it appears that the tendency of structural instability of the core is present no matter what level of discretization is used. It could thus very well be that the solution of the inviscid vorticity equation with the initial vorticity field given by Equation (3.89) indeed leads to a structural instability of the vortex core. One must keep in mind that the initial condition of the computation is not a solution of the inviscid vorticity equation and hence might be unstable. Judging from the conservation of the linear impulse and the semi-regularized energy, one might think that the solution given by this computation is correct. A solution that conserves the linear impulse and the semi-regularized energy is however not necessarily the correct one. In conclusion, it appears that the method converges, but very slowly.

The results of the viscous computations are now examined. Figure J.33 illustrates the viscous diffusion of the ring. It can be seen that the vortex particles that have little or no strength at $t = 0$ obtain increased strength at the expense of the particles that have some strength. This is precisely the role of viscous diffusion. Recall that the viscous method is conservative (see Section 3.3). The circulation of the vortex ring is thus conserved (except for the exponentially small amount of cancellation due to the viscous interaction between sections of the torus that are far apart but have opposite sign vorticity). As seen in Figure J.35, the linear impulse I is almost conserved with a slight degradation starting at $t \simeq 1.50$. As explained in Section 3.4, the transpose scheme for the stretching of the particle strengths conserves linear impulse as long as ω_σ remains almost divergence free which is the case here as seen from the overlaping of the curves $\tilde{E}$ and $\tilde{E}_f$, and $\tilde{\mathcal{E}}$ and $\tilde{\mathcal{E}}_f$. The slight degradation of I is thus not due to the stretching term but to the viscous term. As also explained in Section 3.4, the viscous integral operator conserves linear impulse, but the discretization of the operator onto particles does not. In the present case, the discretization is fine enough (r_l is small enough) that the linear impulse is conserved up to the time $t \simeq 1.50$ at which viscous diffusion reaches the maximum radius of

discretization $r = r_{max}$. This argument is consistent with the fact that the same behavior is observed when the number of layers $n_c = 4$, 5 or 6 is increased, but r_{max} is kept fixed. If this computation is continued much further in time, the particle strengths will tend towards the same constant (except for the effect of vortex stretching as they go in orbit around the center of the vortex core). This is clearly incorrect, and what is required is more layers extending to larger values of r_{max}. However such a luxury could not be afforded (the present computation at $n_c = 6$ already requires $N = 19,773$ particles!).

The other diagnostics are now examined. The semi-regularized energy $\tilde{E}$ initially decays at the proper rate (see Table 3.1). It is believed that $\tilde{E}$ continues to decay at the proper rate, at least up to times at which the maximum radius of discretization $r = r_{max}$ starts to "fill up", but no proof can be offered. Notice also that, due to viscous diffusion, the enstrophy $\tilde{\mathcal{E}}$ decreases and hence the kinetic energy $\tilde{E}$ decreases more slowly. The vorticity contour plots given in Figure J.34 show that the core develops an instability. Viscous diffusion acts as a smoothing and the solution is not as irregular as in the inviscid case. As was the case with the inviscid computation, it is not clear whether or not the results given by the numerical computation are correct. The only independent reliable numerical computations that are known are the spectral computations by Stanaway, Cantwell & Spalart (1988). Among their cases, they provide the results of a numerical computation of a viscous vortex ring at $Re = 400$. Unfortunately, in their initial condition, they use $\sigma_R = .250/\sqrt{2} = .177$ whereas, in the present initial condition, $\sigma_R = .100$. The present initial vorticity profile is thus much steeper than theirs. With their initial condition, they do not observe a structural instability of the vortex core. Actually, in their very long time computation, the vorticity field smoothly evolves from the initial Gaussian distribution to the asymptotic solution given by the Stokes ring as $t \to \infty$. They are not able to decrease σ_R much below .177 because their computation is done on a grid and they have grid size restrictions. In the present case, σ_R cannot be increased much above .100 because the computation is Lagrangian. To reach a large discretization radius (say $r_{max} = .35 * (.177/.100) = .62$) with a good level of discretization (i.e., r_l not too big) would require more layers of discretization than can be afforded, at least with the $\mathcal{O}(N^2/N_\varphi)$ scheme. Again, the conclusion is unclear. It could be that, for the same reasons as in the inviscid case, the process of convecting vortex filaments with the centerline velocity leads to cummulative errors and hence that the computation ceases to be valid after some time. It could also be that the vortex ring with $\sigma_R = .177$ is structurally stable and that the vortex ring with $\sigma_R = .100$ is unstable. It must be remembered that the initial condition of the computation is not a solution

of the viscous vorticity equation. Depending on the steepness of the initial condition (i.e., the vorticity gradient) and the Reynolds number, the solution might be stable or unstable. If the very sentive diagnostic dX_c/dt is considered, Figure J.36, it is seen that the computation is again not fully converged even with $n_c = 6$ (again, the other diagnostics, linear impulse, energy and enstrophy are identical for the cases $n_c = 4$, $n_c = 5$ and $n_c = 6$ and are only plotted for $n_c = 6$). It can also be seen that the time at which the core stucture begins to go unstable is delayed when the level of discretization is increased. Whether or not the ring is structurally stable as $N \to \infty$ is a mystery that would require a scheme faster than $\mathcal{O}(N^2/N_\varphi)$ to be resolved.

In conclusion, the above investigation of the method of regularized vortex particles, both inviscid and viscous, on the problem of the single vortex ring, is very instructive. The results show that the inviscid regularized method is able, at least for some time, to capture the physics of the problem, with the appropriate conservation of the linear impulse and the semi-regularized energy. The results also show that the viscous version of the method can indeed account for viscous diffusion in a consistent way, with the appropriate conservation of the linear impulse and the appropriate decay of the semi-regularized energy. The potential problems that still remain are, in our opinion, associated with poor long time convergence of the method. One variation that might help convergence for longer times would be to use an average velocity for the time evolution of the particle position and strength vector. The idea was proposed by Leonard (1980b) in the context of the vortex filament method (cfr. Chapter 2, Section 2.2.2 and Appendix G, Section G.2.1), and can easily be applied to the vortex particle method. Such a scheme would, on the inviscid ring problem, conserve the exact kinetic energy E instead of conserving the semi-regularized energy $\tilde{E}$ and hence would be superior to the above method, at least for a fixed level of discretization (Again, as $N \to \infty$ and $\sigma \to 0$, all choices converge to the same result since the vortex filaments then become vortex lines and are properly convected as material lines).

3.5.6 The problem of the fusion of two vortex rings computed using the viscous version of the method of regularized vortex particles

In Section 3.5.3, the performance of the method of singular vortex particles was investigated on the problem of the fusion of two vortex rings. In Section 3.5.4, the performance of the inviscid method of regularized vortex particles was investigated on the same problem. In Section 3.5.5, experience was acquired with the inviscid and viscous versions of the method of regularized vortex particles by considering the single vortex ring. Some refinements were developed that improve the initial condition and

the initial decay of the kinetic energy. All the ingredients necessary for the viscous computation of the fusion of two vortex rings are now available.

The perfectly symmetric viscous collison of two vortex rings is considered. The symmetry of the problem is exploited, and the evolution of only one half of one ring is computed . The computational effort is thus reduced by 1/4. The computation is started in the configuration shown in Figure J.25 with the two rings at a spacing $s = 2.70$ center to center and at an angle $\theta_0 = 15.0°$ with respect to the vertical. As usual each ring has $R = 1.0$ and $\Gamma = 1.0$. Each vortex ring is initially identical to the Gaussian vortex ring studied in Section 3.5.5, i.e., $\sigma_R = .10$, $r_{max} = .35$ with the asymptotic ring velocity $U_R = .2767296$. As seen in Chapter 2, Section 2.3.2, the core radius of the corresponding vortex ring with uniform vorticity is $\sigma_K = \sigma_R/\beta = .1924$. The core discretization of the ring is limited to $n_c = 3$ layers of particles because the computation is now $\mathcal{O}(N^2/4)$ instead of being $\mathcal{O}(N^2/N_\varphi)$. Thus $N_s = 49$ vortex particles per cross section with $r_l = .050$. The number of sections N_φ is again chosen so that the distance between neighbor particles is the same in all directions, i.e., $h \simeq 2\,r_l \simeq 2\pi\,R/N_\varphi$. This gives $N_\varphi = 64$ sections of particles per ring for a total of $N = 6,272$ particles. The viscosity is again $\nu = 2.50 \times 10^{-3}$ and the Reynolds number based on the circulation of one ring is $Re = \Gamma/\nu = 400$.

The parameters of an initial computation suggested by the experiment of Schatzle & Coles (1987) are, when normalized to have $R = 1.0$ and when averaged on the left and right rings: $s \simeq 2.70$, $\sigma_R \simeq .16$, $\theta_0 \simeq 13.3°$ and $Re \simeq 1800$. Their rings are thus fairly fat with the corresponding uniform vorticity core $\sigma_K \simeq .31$. Such fat rings cannot be discretized in the present computation for the reasons explained in Section 3.5.5. The Reynolds number cannot be matched either. Computations at Reynolds number higher than $Re = 400$ were tried, but discretization problems were encountered. To resolve the scales of a high Reynolds number flow requires many more particles than can be afforded. The present discretization is thus a compromise between what one would like to do and what one can do.

As explained in Section 3.5.5, the initial particle vorticity field is relaxed so as to obtain the desired inital vorticity field. As also explained in that section, the core size of the particles is adjusted so that the semi-regularized energy initially decays according to $d\tilde{E}/dt(0) = -\nu\,\mathcal{E}(0)$. For each ring, $\mathcal{E}(0)$ is given by Equation (3.90). Since the vorticity distributions of both rings do not overlap significantly at $t = 0$, it is reasonable to take $\mathcal{E}(0) = 2 \times 50.7500 = 101.500$. This enstrophy corresponds to a theoretical value of $dE/dt(0) = -\nu\,\mathcal{E}(0) = -.2537500$. With the particle core size $\sigma = .0650$, one obtains numerically $\tilde{E}(0) = 2.057761$, $\tilde{E}_f(0) = 2.058030$ and $d\tilde{E}/dt(0) = -.2546135$ which is taken to be sufficiently close to the theoretical

value. The other numerical results at $t = 0$ are $I(0) = 6.156745$, $\tilde{\mathcal{E}}(0) = 133.9288$ and $\tilde{\mathcal{E}}_f(0) = 136.0653$. As was the case in Section 3.5.5, $\tilde{E}(0) \simeq \tilde{E}_f(0)$, which indicates that the initial particle vorticity field ω_σ is indeed a good representation of the divergence free field ω_σ^N. Also, the semi-regularized enstrophy $\tilde{\mathcal{E}}(0)$ is again a poor approximation to the exact enstrophy $\mathcal{E}(0)$.

The transpose scheme is used for the evolution equation of the particles strength vector. The time step is $\Delta t = .05$, and the time integration is done up to $t = 8.0$. By that time, viscous diffusion has moved significant amounts of vorticity out to the maximum radius of discretization $r_{max} = .35$, and additional layers would be needed in order to proceed in time. The time $t = 8.0$ is however sufficient for the fusion process to be completed as will be seen from the numerical results.

From the point of view of fluid mechanics, this computation is more important than others described in this thesis. Consequently, many plots of the results are provided. The plots of the particle strength vectors are given in Figure J.37 for the perspective view and in Figure J.38, Figure J.39 & Figure J.40 for the three two-dimensional projections. In addition, contour plots of the out of plane vorticity field and of the out of plane strain-rate are given for both the $x - z$ and the $y - z$ planes of symmetry. For the vorticity field, $\omega_\sigma^N = \nabla \Lambda \mathbf{u}_\sigma$ which is divergence free is plotted. Thus, there are plots of ω_y and $\partial v/\partial y$ for the $x - z$ plane and plots of ω_x and $\partial u/\partial x$ for the $y - z$ plane. The $x - z$ data can be compared with the experimental data of Schatzle & Coles (1987). The $y - z$ data are new. They are given in Figure J.41 for the vorticity contours and in Figure J.42 for the strain-rate contours.

Finally, the diagnostics of the computation, I, $\tilde{E}$ and $\tilde{E}_f$, $\tilde{\mathcal{E}}$ and $\tilde{\mathcal{E}}_f$ are provided in Figure J.43, together with the circulation Γ_y in half of the plane $x - z$ and the circulation Γ_x in half of the plane $y - z$.

First, the diagnostics are discussed. The linear impulse is well conserved, at least up to $t \simeq 3.0$. It then starts to degrade very slowly. At the end of the computation, roughly 98% of the initial linear impulse is left. This slight degradation of the linear impulse was explained in detail in Section 3.5.5. The semi-regularized energy $\tilde{E}$ initially decays at the proper rate. Moreover, the curves $\tilde{E}$ and $\tilde{E}_f$ as well as the curves $\tilde{\mathcal{E}}$ and $\tilde{\mathcal{E}}_f$ remain very close to each other. This is an indication that the particle vorticity field ω_σ remains, during the entire course of the computation, a good approximation of a divergence free field. This result is very comforting as it indicates that the computation remains consistent for all times, and that the explicit treatment of viscous diffusion helps to keep ω_σ nearly divergence free. Again, due to viscous diffusion, the enstrophy $\tilde{\mathcal{E}}$ decreases, and hence the kinetic energy $\tilde{E}$ decreases more slowly. It is also interesting to notice that the process of vortex reconnection

does not lead to very dramatic variations in the kinetic energy and enstrophy.

The perspective view of the particle strength vectors, Figure J.37, together with the two-dimensional projections, Figure J.38, Figure J.39 and Figure J.40, clearly illustrate the fusion process and the viscous reconnection of the vortex tubes. In particular, the $x - z$ projection and the $y - z$ projection compare very well with the photographs of Schatzle & Coles (1987 and private communication), Figure J.24. The fusion process essentially occurs between $t \simeq 2.0$ and $t \simeq 6.0$. By $t = 6.0$, the vortex tubes have nearly completely reconnected. Some pairs of opposite sign strength vectors are still present in the interaction region, but these pairs behave as weak vortex dipoles. Their vorticity is small but the linear impulse they represent is non-negligeable (recall that the strength of a vortex dipole (i.e., its linear impulse) is proportional to $\alpha \times h$).

The vorticity contours, Figure J.41, and the strain-rate contours, Figure J.42, together with the circulations Γ_y and Γ_x, Figure J.43, provide some of the quantitative information that is available. Notice that Γ_y is not exactly equal to unity at $t = 0$. This is due to the fact that the Gaussian vorticity distributions of the two rings overlap very slightly at $t = 0$. Γ_y starts decreasing very rapidly as soon as $t \simeq 2.0$ and is essentially zero by $t \simeq 6.0$. The time history of Γ_x is almost exactly the mirror image of that of Γ_y. Whatever is lost in Γ_y appears in Γ_x and the sum $\Gamma_y + \Gamma_x$ is nearly conserved as it should be (it is believed that the small amount of $\Gamma_y + \Gamma_x$ that is lost is contained in the weak vortex dipoles that leave the domain in which ω_y is integrated to obtain Γ_y). The contour plots, Figure J.41 and Figure J.42 illustrate the vanishing of ω_y to the profit of ω_x and the importance of the role played by the strain-rate field $\partial v/\partial y$. For future reference, recall that the value of the vorticity at the center of the original vortex tubes is $\Gamma/2\pi\,\sigma_R{}^2 = 15.91$. The vortex tube corresponding to ω_x starts forming very early and remains close to the z axis up to $t \simeq 4.5$ so. After that time, reconnection is nearly completed and the vortex tube slowly migrates towards its final position at about $y \simeq 1.3$. Notice the presence of multiple maxima in ω_x at early times. The core of the vortex tubes corresponding to ω_y remains fairly circular up to $t \simeq 1.5$. After that time, the vortex tubes start getting pushed toward each other by the strain-rate field ($\partial u/\partial x < 0$ and $\partial v/\partial y > 0$). The vorticity contours become elongated in the z direction and eventually split into two entities. These elongated shapes are also reported in Schatzle (1987) as well as the splitting of the vorticity regions. In the experiment, the collision of the two rings is however not perfectly symmetric, and the splitting of the vorticity regions results in alternate regions of opposite sign vorticity roughly aligned along the z axis. The numerical computation shows that the splitting process also occurs in perfectly symmetric collisions.

The contours given in Figure J.42 show that $\partial v/\partial y$ in the $x-z$ plane is small for some time but that it then increases dramatically starting at $t \simeq 1.5$. From $t \simeq 2.5$ to $t \simeq 5.0$, $\partial v/\partial y$ has values around $1.0 \ldots 1.5$. After $t \simeq 5.5$, $\partial v/\partial y$ decreases also very rapidly. This is in good agreement with the data of Schatzle (1987). If ϵ denotes some rough time and space average strain-rate $\partial v/\partial y$, in the vicinity of the collision region, then $\epsilon \simeq 1.0$ for this computation. It is believed that ϵ is governed by the global geometry of the collision, not by the viscosity ν. Dimensional analysis suggests the scaling $\epsilon \sim \Gamma/R^2\, g(\sigma_K/R, \theta_0)$.

The contours of $\partial u/\partial x$ in the $y-z$ plane show that, from $t \simeq 2.0$ to $t \simeq 5.5$, $\partial u/\partial x$ has large negative values around $-2.0 \ldots -3.0$ in the part of the collision region that is close to the z axis but that it also has positive values around $1.0 \ldots 2.0$ in the other part. The fusion process is thus not two-dimensional. The vortex tubes corresponding to ω_y get pushed towards each other only in the part of the collision region that is close to the z axis. In particular, it is interesting to notice that half of the newly formed vortex tube corresponding to ω_x resides in a region where $\partial u/\partial x < 0$ but that the other half resides in a region where $\partial u/\partial x > 0$, and that this remains the case during the entire reconnection process and beyond, from $t \simeq 2.0$ to $t \simeq 8.0$.

This investigation is concluded with a discussion of the time scale. The time scale for the fusion process is obtained from the circulation history, Figure J.43, and is $\tau \simeq 3.0$. The viscous time scale $\tau \sim \sigma_K^2/\nu \simeq 16.0$ is definitely not appropriate. The convective time scale $\tau \sim \sigma_K^2/\Gamma \simeq .04$ seems a little bit low. A general time scale which combines the effects of the straining field and viscosity is $\tau \sim f(\epsilon\, \sigma_K^2/\nu)/\epsilon$. The estimate proposed by Schatzle (1987) corresponds to $f(w) \sim \sqrt{w}$, i.e., $\tau \sim \sigma_K/\sqrt{\epsilon\, \nu}$. The estimate obtained from a simple two-dimensional model of the collision of two vortex layers of width σ_K driven toward each other by a straining field ϵ leads to $f(w) \sim \log w$ (Kambe 1983). This estimate is obtained as follows. If the flow is two-dimensional with the same axis as in our computation, one has $v = dy/dt = \epsilon y$ and $u = dx/dt = -\epsilon x$. This integrates to $x = x_0\, e^{-\epsilon t}$. The cancellation of vorticity occurs within a region of extent $\sqrt{\nu/\epsilon}$. If τ is the time it takes a fluid particle to come from the edge σ_K of the vortex layers to that cancellation region, one obtains $\sqrt{\nu/\epsilon} \sim \sigma_K\, e^{-\epsilon \tau}$ which leads to $f(w) \sim \log w$.

If $\epsilon \simeq 1.0$ as discussed above, one obtains, for Schatzle's estimate $\tau \sim 4.0$, and for the log estimate $\tau \sim 1.20$. Both of these estimates are close to the computational value $\tau \simeq 3.0$. Although Schatzle's estimate is numerically closer, one must recall that these are order of magnitude estimates only. It is thought that the log estimate is more correct, simply because it has more physics in it. One must keep in mind however that $\partial v/\partial y$ and $\partial u/\partial x$ are not at all spatially and temporally constant in

the vortex-ring collision problem, and hence that the log estimate is also disputable.

In conclusion, this computation of the fusion of two vortex rings, using the viscous version of the method of regularized vortex particles, captures the physics of the problem, not only at a qualitative level, but also at a quantitative level. In particular, the results agree well with the experimental results of the experiment by Schatzle & Coles (1987). It is also believed that the resolution (or the Reynolds number) could be increased by using many more particles and an $\mathcal{O}(N \log N)$ algorithm.

What about the fission process that occurs in the experiment of Schatzle & Coles? A low resolution computation has been done that includes this process (Winckelmans & Leonard 1988, Chua et al. 1988). The transpose scheme is used and the parameters of the computation are $R = 1.0$, $\Gamma = 1.0$, $s = 3.0$, $\theta_0 = 30°$, $\sigma_R = .125$, $r_{max} = .3125$, $n_c = 2$, $N_s = 25$, $N_\varphi = 52$, $r_l = .0625$, $\sigma = .1562$, $\nu = 5.0 \times 10^{-3}$ and $\Delta t = .075$. It was found necessary to use a relatively large θ_0 to obtain both the fusion and the fission in this particular case with $Re = 200$. For smaller values of θ_0, the fusion occurs but not the fission. The results are shown in Figure J.44 for the particle strength vectors and in Figure J.45 for the diagnostics. This computation is not well resolved because viscous dissipation spreads vorticity to the maximum radius of discretization at an early time. From that point on, the computation essentially corresponds to the time evolution of vortex rings with uniform vorticity core and viscosity is active only when vortex tubes of opposite sign vorticity come in close proximity. For problems where robustness is required and some loss of accuracy may be tolerated, this type of behavior of the method might be of interest. For instance, in the present computation, vortex lines are reconnected, and the particle vorticity field is nearly divergence free for all times. This last point is confirmed by the fact that the curves $\tilde{E}$ and $\tilde{E}_f$ remain very close to each other for all times. The linear impulse is not conserved. As explained in Section 3.5.5, this degradation of the linear impulse is related to the poor discretization of the viscous term.

3.5.7 The problem of the two vortex rings in a "knot" configuration: a test case for the consistency of the method of regularized vortex particles

In this section, the computation of the problem of two vortex rings in a knot configuration when computed with the method of regularized vortex particles is examined.

The motivation for computing this problem is that it is a well defined problem of vortex interactions in three dimensions for which the angular impulse, $\mathbf{A}$, and the helicity, $\mathcal{H} = \int \mathbf{u} \cdot \boldsymbol{\omega}\, d\mathbf{x}$, are non-zero. Recall that both $\mathbf{A}$ and $\mathcal{H}$ vanish in the problem of the fusion of two vortex rings. It is understood that the knot problem is

purely "computational" and cannot be reproduced in the laboratory. Nevertheless, it is an elegant problem that contains some of the features encountered in real flows, such as the reconnection of vortex lines that are not aligned with each other (i.e., with angular impulse) and the presence of vortex lines that are linked (i.e., with helicity, see Moffatt 1969). Last but not least, it is a computational problem that was suggested for years by a drawing stuck to the door of the laboratory of P. R. Schatzle, an invitation from an experimentalist that we could hardly resist (the invitation, not the experimentalist!). This problem was also suggested to A. Leonard in 1975 by S. Corrsin. In what follows, it is referred to as the "knot" problem. Another related problem is the "closed knotted vortex tube" problem (Kida & Takaoka 1987) which also has non-zero helicity.

As will be seen in this section, the knot problem, when computed with the method of vortex particles, highlights some of the serious weaknesses of the method, such as intense vortex stretching, calling for the addition of vortex particles during the course of the computation, and non-zero divergence of the particle vorticity field ω_σ over extended times. This problem also suggests a scheme for the relaxation of $\nabla\cdot\omega_\sigma$ towards zero which is very general and which helps improve the method of regularized vortex particles.

One previous numerical investigation of the problem by Kuwahara (1986) was found. He uses the method of singular vortex particles with the transpose scheme for the stretching of the strength vector. Very few particles are used. The computation is started with 32 vortex particles per ring for a total $N = 64$. A *remeshing scheme* very similar to the one presented in this thesis (see below) is used to add particles wherever vortex stretching is intense. The computation ends with $N = 114$ particles. Diagnostics such as linear impulse I , angular impulse A , energy E_f and helicity $\mathcal{H}$ are also provided. These diagnostics indicate that the computation performs poorly on the conservation of these invariants. The problem is partially due to the poor discretization of the two rings. It will be shown below that the problem is also related to the fact that the particle vorticity field ω_σ has non-zero divergence during the course of the computation.

The present investigation of this problem was done independently of that of Kuwahara. Regularized vortex particles are considered and use is made of the transpose scheme. The discretization is as follows: for each ring, $R = 1.0$ and $\Gamma = 1.0$. The spacing of the rings center to center is $s = 1.0$. Only the center of each ring is discretized. The time step is $\Delta t = .025$, and the core size of the vortex particles is $\sigma = .10$.

Four different computations are compared, all combinations of with and without

remeshing and with and without relaxation of the vorticity divergence.

The *remeshing* is defined as the process of splitting one vortex particle into two wherever vortex stretching becomes too intense. The *relaxation of the vorticity divergence* is defined as a new algorithm which insures that the particle vorticity field ω_σ remains almost divergence free for all times.

First, the remeshing procedure is examined. The strategy is illustrated in Figure J.46. Since vortex particles are isolated elements (as opposed to computational points on a vortex filament), the remeshing process must be local. Recalling that vortex lines move as material lines in an inviscid flow, one assumes that $h(t) \propto |\boldsymbol{\alpha}(t)|$. To satisfy the overlaping condition $\sigma/h > 1$ (typically $\sigma/h \simeq 1.3$), a particle $\boldsymbol{\alpha}$ is split into two particles $\boldsymbol{\alpha}^1$ and $\boldsymbol{\alpha}^2$ when $h(t) \geq tresh\, h(0)$, i.e., when $|\boldsymbol{\alpha}(T)| \geq tresh\, |\boldsymbol{\alpha}(0)|$. Here, the time $t = 0$ is to be understood in a loose sense. It is a reference time which corresponds initially to $t = 0$, but is reset, for each two new particles, every time one particle has been split into two. If the core size σ is a constant for all times, then the constraint of having the same overlap as the inital condition leads to $tresh = 2.0$. If the core size σ is also function of time and is subjected to Equation (3.41), then at remeshing time, $\sigma(T) \leq \sigma(0)/(tresh)^{1/2}$. In this case, if the core size is kept to overlap by the same factor as initially, this leads to $tresh = 2.0^{2/3} = 1.587$. These present computations were conducted with σ constant and $tresh = 2.0$. Finally, a strength and a location must be chosen for each new particle. A natural choice is to assign to the new particles a strength $\boldsymbol{\alpha}/2$ and to locate them at $\mathbf{x} \pm \Delta\mathbf{x}$, where $\Delta\mathbf{x} = crmsh\, \sigma\, \hat{\mathbf{e}}_\alpha$ (with $\hat{\mathbf{e}}_\alpha = \boldsymbol{\alpha}/|\boldsymbol{\alpha}|$). This choice ensures the conservation of the total vorticity, $\sum \boldsymbol{\alpha}$, and of the linear impulse, $\frac{1}{2}\sum \mathbf{x} \wedge \boldsymbol{\alpha}$, but does not conserve the angular impulse, $\frac{1}{2}\sum \mathbf{x} \wedge (\mathbf{x} \wedge \hat{\mathbf{e}}_z)$, in general. A scheme exists that conserves all three linear invariants, but it requires the solution of a set of 9 nonlinear equations for the 9 unknowns $\boldsymbol{\alpha}^1$, $\boldsymbol{\alpha}^2$ and $\Delta\mathbf{x}$. The parameter $crmsh$ is chosen in such a way that the new vortex particles smoothly replace the old one (for instance $crmsh\, \sigma = h(T)/4$). The search for particles that have to be split into two is done every $nrmsh$ time steps.

The procedure of relaxation of the vorticity divergence is now examined. The idea is simple, general and seems to work very well. First, recall that a major problem with the method of vortex particles is that the particle vorticity field ω_σ is not guaranteed to be nearly divergence free for all times (see Section 3.2 and Section 3.3). Of course, the initial field ω_σ is nearly divergence free since the particles are initially nicely aligned as if they were little sections of a vortex tube. There is however no guarantee that the particles will remain aligned for all times. Recall that the method of vortex particles is only solving for an hyperbolic equation (here the vorticity equation) and has no built-in knowledge of the fact that the particle field (here the

	No Remeshing & no relaxation	Remeshing & no relaxation	No remeshing & relaxation	Remeshing & relaxation
Remeshing	no	yes	no	yes
nrmsh		5		5
tresh		2.0		2.0
crmsh		.18		.18
Relaxation of $\nabla\cdot\boldsymbol{\omega}_\sigma$	no	no	yes	yes
nrelax			2	10
N_φ	250	175	250	175
$h(0)$	.025	.036	.025	.036
$N(0)$	500	350	500	250
$N(5.0)$	500	496	500	541

Table 3.2: Parameters for the computation of the knot problem with the method of regularized vortex particles.

particle vorticity field $\boldsymbol{\omega}_\sigma$) should remain divergence free for all times. One way of making sure that $\boldsymbol{\omega}_\sigma$ remains nearly divergence free is to project the velocity field $\mathbf{u}_\sigma$ (which is divergence free) on a grid and to project the curl of that velocity field back onto the particles. This procedure is costly and not convenient since it requires a grid. Recalling however that the curl of the vorticity field is precisely given by $\boldsymbol{\omega}_\sigma^N$ (Section 3.2, Equation (3.39) and Equation (3.40)), a much simpler procedure is proposed, where $\boldsymbol{\omega}_\sigma^N$ is used, without a grid, to reassign the particle strength vectors. The procedure is as follows: Every *nrelax* time steps, one solves for new particle strengths $\boldsymbol{\alpha}^p_{new}(T)$ by imposing that $\boldsymbol{\omega}_\sigma(\mathbf{x}^p(T),T) = \boldsymbol{\omega}_\sigma^N(\mathbf{x}^p(T),T)$, namely by solving the system of linear equations

$$\sum_q \boldsymbol{\alpha}^q_{new}(T)\,\zeta_\sigma(\mathbf{x}^p(T)-\mathbf{x}^q(T)) = \sum_q \left[\boldsymbol{\alpha}^q_{old}(T)\,\zeta_\sigma(\mathbf{x}^p(T)-\mathbf{x}^q(T)) + \nabla\Big(\boldsymbol{\alpha}^q_{old}(T)\cdot\nabla\big(\chi_\sigma(\mathbf{x}^p(T)-\mathbf{x}^q(T))\big)\Big)\right]. \tag{3.95}$$

This system is solved by iteration using the same procedure as for the relaxation of the initial condition (Section 3.5.5, Equation (3.92)).

The parameters that are specific to each of the four computations are summarized in Table 3.2. For all computations, $I_y = -I_z$ with $I = (I_y^2 + I_z^2)^{1/2}$, and $A_y = -A_z$ with $A = (A_y^2 + A_z^2)^{1/2}$. Notice that the linear impulse vector and the

angular impulse vector are aligned. Notice also that there is a natural time scale for the problem, namely $\tau = A^4/I^5 = .07122$. At $t = 0$ one obtains numerically $I(0) = 4.442801$, $A(0) = 3.332101$, $\tilde{E}(0) = \tilde{E}_f(0) = 2.882862$, $\tilde{\mathcal{H}}(0) = 1.999613$, and $\tilde{\mathcal{E}}(0) = \tilde{\mathcal{E}}_f(0) = 799.2296$.

The results of the computations are shown in Figure J.47 through Figure J.50 for plots of the particle strength vectors and in Figure J.51 through Figure J.54 for the diagnostics. As seen in Figure J.47 and Figure J.51, the computation without remeshing and without relaxation of $\nabla\cdot\boldsymbol{\omega}_\sigma$ performs poorly. This is mainly due to the fact the vortex particles become misaligned from the direction of the vortex filament they are supposed to discretize. This phenomenom happens slowly but surely, no matter how many particles are used. It is due to the fact that, when gradients of $\nabla\mathbf{u}$ are present along a vortex tube, the use of the local equation $d\boldsymbol{\alpha}/dt = (\boldsymbol{\alpha}\cdot\nabla)\mathbf{u}_\sigma$ for the particle strength vector does not produce exactly the right amount of stretching and tilting of the strength vector. Of course, this problem does not happen when using vortex filaments because, in that case, the proper vortex stretching and tilting is ensured by the fact that adjacent points on a filament are connected for all times. The diagnostics show that the linear impulse starts degrading when $\boldsymbol{\omega}_\sigma$ starts becoming a poor representation of a divergence free field, i.e., when $\tilde{E}_f \neq \tilde{E}$. The angular impulse and helicity are also poorly conserved. This problem is also related to the non-zero divergence of $\boldsymbol{\omega}_\sigma$.

If the computation with remeshing but without relaxation of $\nabla\cdot\boldsymbol{\omega}_\sigma$ is considered, Figure J.48 and Figure J.52, one obtains roughly the same results. This is to be expected since the replacement of one particle by two particles placed at both ends of the original one does not help reduce $\nabla\cdot\boldsymbol{\omega}_\sigma$, at least when the original particle is not aligned with the direction of the vortex tube. The advantage of using remeshing is however a computational saving in the total number of particles since one does not need to start the computation with as many particles as in the case of no remeshing.

The computation without remeshing but with the relaxation of $\nabla\cdot\boldsymbol{\omega}_\sigma$, Figure J.49 and Figure J.53, is more promising. The particles indeed remain aligned as little sections of a vortex tube, and the computation yields much better results. Notice the creation, at $t \simeq 4.50$ of two new closed vortex filaments as a result of the interaction between the two original rings. It is believed that the outcome of this computation is qualitatively correct. As seen from the diagnostics, the relaxation process keeps $\tilde{E}$ and $\tilde{E}_f$ nearly equal for all times, thus showing that the particle vorticity field is indeed nearly divergence free. The energy however decreases during the course of the computation. The reason is that the relaxation operator, Equation (3.95), is dissipative whenever there are not enough particles to discretize a vortex tube, i.e.,

whenever intense vortex stretching occurs that is not compensated by remeshing. This can easily be seen by inspecting the outcome of one relaxation when applied to a line of vortex particles of core size σ and interspacing h. When $\sigma/h > 1$, the projection operator has little effect(i.e., ω_σ is already a good approximation of ω_σ^N and each particle is like a discretization point on a vortex filament). When $\sigma/h < 1$, the projection operator assigns a new strength to the particles that is smaller then the old one, i.e., $|\alpha_{new}^p(T)| < |\alpha_{old}^p(T)|$. The relaxation operator should thus always be combined with remeshing. The angular impulse, A, and the helicity, $\tilde{\mathcal{H}}$, are slightly better conserved than in the previous two computations, but the improvement is small. The reason for this poor improvement is partially due to the relaxation operator being too dissipative.

Finally, the computation that combines both remeshing and relaxation of $\nabla\cdot\omega_\sigma$, Figure J.50 and Figure J.54, is the most successful one, as expected. Again, the particles remain aligned as little sections of a vortex tube, and the computation leads to the creation of two new closed vortex filaments as a result of the interaction between the original rings. The outcome of this computation is likely to be the most accurate as can be infered from the diagnostics. The linear impulse is almost identically conserved up to $t = 5.0$. The energy $\tilde{E}$ is also almost identically conserved. $\tilde{E}$ and $\tilde{E}_f$ remain very close thus showing that ω_σ is indeed a good representation of a divergence free field. The angular impulse and the helicity are also better conserved than in all other computations.

What about viscous computations? A viscous computation of the same problem was tried with $n_c = 1$, i.e., with 9 particles per cross section. The results appear to be no better than the above, the reason being that the convective time scale during which the violent interaction between the vortex tubes occurs is very short with respect to the viscous time scale. The coarse discretization is unable to capture the physics of the problem. A viscous computation could be done with many more vortex particles, but this effort requires that a $\mathcal{O}(N \log N)$ scheme be implemented.

In conclusion, the use of remeshing combined with the relaxation of $\nabla\cdot\omega_\sigma$ seems to be a good way of solving the inconsistency problems of the method of vortex particles. These improvements can be combined with the explicit treatment of viscosity to yield a method that is consistent, robust and accurate, provided of course that enough vortex particles are used.

Chapter 4

Two-dimensional particles of vorticity gradient: an alternative to the method of contour dynamics

The method of *contour dynamics* introduced by Zabusky, Hughes & Roberts (1979) has been widely used to investigate inviscid two-dimensional flows with piecewise constant vorticity (Zabusky 1981, Zabusky & Overmann 1983, Dritschel 1985, 1986, 1988). In such flows, the velocity at any point in space only depends upon the location of the vortex boundaries and the jump of vorticity across them. The method is thus simple and attractive since it requires only the tracking of the boundaries of the vortex patches evolving under that velocity field.

In this chapter, the method of contour dynamics is generalized to piecewise constant vorticity patches with a smooth vorticity gradient across the boundary. A particle method is also presented that is to the method of contour dynamics what the vortex particle method is to the method of vortex filaments. The evolution equation for the gradient of the vorticity in two-dimensional flows is derived in Section 4.1. The evolution equation for the curl of the vorticity is also given, and it is shown that the method of contour dynamics is actually a method of filaments of vorticity curl. In Section 4.2, The classical method of contour dynamics is reviewed in Section 4.2, and a regularized version of the method with a smooth vorticity gradient across vortex boundaries is derived. In Section 4.3, a method of *particles of vorticity gradient* is developed to solve for the evolution equation for the vorticity gradient of Section 4.1. Both cases of singular and regularized particles are considered, and a viscous method is also presented. A method of *particles of vorticity curl* is also considered to solve for the evolution equation for the vorticity curl of Section 4.1. In Section 4.4, the behavior of the method of contour dynamics and of the method of particles of vorticity gradient with respect to the conservation laws is discussed. (The evaluation of quadratic diagnostics such as energy (i.e., Hamiltonian) and enstrophy is presented in detail in Appendix I.)

Finally, in Section 4.5, some numerical results obtained with the regularized method of particles of vorticity gradient are presented. Both inviscid and viscous

problems are considered: the diffusion of a circular vortex patch of uniform vorticity, and the interaction, inviscid and viscous, of two circular vortex patches of initially uniform vorticity of the same sign.

4.1 An evolution equation for the vorticity gradient in two-dimensional flows

The two-dimensional vorticity equation for an incompressible flow is

$$\frac{\partial \omega}{\partial t} + \nabla\cdot(\omega\,\mathbf{u}) = \nu\,\nabla^2\omega\,, \tag{4.1}$$

where $\mathbf{u}(\mathbf{x},t)$ is the divergence free velocity field and ω is the vorticity field ($\boldsymbol{\omega} = \omega\hat{\mathbf{e}}_z$ with $\omega = \partial v/\partial x - \partial u/\partial y$). If the gradient of Equation (4.1) is taken, and use of the fact that the velocity is divergence free is made, one obtains (Leonard, private communication)

$$\frac{\partial}{\partial t}(\nabla\omega) + \nabla\cdot(\nabla\omega\,\mathbf{u}) = -\left(\nabla\omega\cdot\nabla^T\right)\mathbf{u} + \nu\,\nabla^2(\nabla\omega)\,, \tag{4.2}$$

or in component form,

$$\frac{\partial}{\partial t}\left(\frac{\partial\omega}{\partial x_i}\right) + \frac{\partial}{\partial x_j}\left(\frac{\partial\omega}{\partial x_i}u_j\right) = -\frac{\partial\omega}{\partial x_j}\frac{\partial u_j}{\partial x_i} + \nu\frac{\partial}{\partial x_j}\frac{\partial}{\partial x_j}\left(\frac{\partial\omega}{\partial x_i}\right)\,. \tag{4.3}$$

Another form of Equation (4.2) is given by

$$\frac{\partial}{\partial t}(\nabla\omega\wedge\hat{\mathbf{e}}_z) + \nabla\cdot((\nabla\omega\wedge\hat{\mathbf{e}}_z)\,\mathbf{u}) = ((\nabla\omega\wedge\hat{\mathbf{e}}_z)\cdot\nabla)\,\mathbf{u} + \nu\,\nabla^2(\nabla\omega\wedge\hat{\mathbf{e}}_z)\,, \tag{4.4}$$

where $\nabla\omega\wedge\hat{\mathbf{e}}_z = \nabla\wedge(\omega\,\hat{\mathbf{e}}_z)$ is the curl of the vorticity field. One thus has the remarkable property that, in inviscid two-dimensional flows, lines of the vorticity curl move as material lines. The evolution equation for the curl of the vorticity in two dimensions is thus identical to the evolution equation for the vorticity in three dimensions, Equation (2.4).

In three dimensions, the method of vortex filaments can be used to solve for the inviscid version of Equation (2.4) by treating the vortex filament as a material line (see Chapter 2). The method of vortex particles can also be used to solve for any of the versions (3.14), (3.15) or (3.16) of the vorticity equation, with better results when using version (3.15). Moreover, the regularized method of vortex particles can also be used when viscous diffusion is present (see Chapter 3).

In two dimensions, a filament method has been used to solve for the inviscid version of Equation (4.4) when $\nabla\omega\wedge\hat{\mathbf{e}}_z$ is concentrated on closed filaments, i.e., when

ω is piecewise constant. This is the classical method of contour dynamics. It will be shown that one can design a regularized version of the method of contour dynamics. A method of particles of $\nabla\omega$ will also be introduced to solve for Equation (4.2). Both the singular and the regularized, inviscid or viscous, versions of the method will be developed. It will also be shown that one can use a method of particles of $\nabla\omega \wedge \hat{\mathbf{e}}_z$ to solve for Equation (4.4).

In this chapter, both terms, "method of contour dynamics" and "method of filaments of vorticity curl", are used to refer to the same method.

4.2 The method of contour dynamics or method of filaments of vorticity curl

4.2.1 The classical method of contour dynamics

In the classical method of contour dynamics, the vorticity is concentrated into p closed patches of area $\mathcal{A}^p$, bounded by a closed curve $\mathcal{C}^p(t)$ and of uniform vorticity. The direction of the curve is taken positive counterclockwise. The method consists in convecting the curves $\mathcal{C}^p(t)$ with the velocity induced by the vortex patches. Since the vorticity is constant inside each of these patches, the vorticity gradient is localized on the curves $\mathcal{C}^p(t)$, more specifically,

$$\nabla\wedge(\omega\,\hat{\mathbf{e}}_z) = \nabla\omega(\mathbf{x},t)\wedge\hat{\mathbf{e}}_z = \sum_p \Delta\omega^p \int_{\mathcal{C}^p(t)} \delta(\mathbf{x}-\mathbf{x}^p)\frac{\partial\mathbf{x}^p}{\partial s}\,ds\;, \tag{4.5}$$

where $\Delta\omega^p$ is the jump in ω at $\mathbf{x}^p(s,t)$ (i.e., $\Delta\omega^p = \omega_{left}-\omega_{right}$), $\mathbf{x}^p$ stands for $\mathbf{x}^p(s,t)$, and $\delta(\mathbf{x})$ is the two-dimensional δ-function. The method of contour dynamics is thus a method of filaments of $(\nabla\omega\wedge\hat{\mathbf{e}}_z)$.

Since $\nabla\cdot\mathbf{u} = 0$ and $\omega\,\hat{\mathbf{e}}_z = \nabla\wedge\mathbf{u}$, the velocity is given by the solution of

$$\nabla^2\mathbf{u} = -\nabla\wedge(\omega\,\hat{\mathbf{e}}_z) = -\nabla\omega\wedge\hat{\mathbf{e}}_z\;. \tag{4.6}$$

Recalling that the Green's function for ∇^2 in a two-dimensional unbounded domain is given by $(1/2\pi)\,\log(|\mathbf{x}|/a)$ where a is an arbitrary length scale, one obtains

$$\begin{aligned}
\mathbf{u}(\mathbf{x},t) &= -G(\mathbf{x}) * (\nabla\omega(\mathbf{x},t)\wedge\hat{\mathbf{e}}_z) \\
&= -\frac{1}{2\pi}\int \log\left(\frac{|\mathbf{x}-\mathbf{x}'|}{a}\right)(\nabla\omega(\mathbf{x}',t)\wedge\hat{\mathbf{e}}_z)\,d\mathbf{x}' \\
&= -\frac{1}{2\pi}\sum_p \Delta\omega^p \int_{\mathcal{C}^p(t)} \log\left(\frac{|\mathbf{x}-\mathbf{x}^p|}{a}\right)\frac{\partial\mathbf{x}^p}{\partial s}\,ds \qquad (4.7) \\
&= \frac{1}{2\pi}\sum_p \Delta\omega^p \int_{\mathcal{C}^p(t)} \frac{(\mathbf{x}-\mathbf{x}^p)}{|\mathbf{x}-\mathbf{x}^p|^2}\left((\mathbf{x}-\mathbf{x}^p)\cdot\frac{\partial\mathbf{x}^p}{\partial s}\right)ds\;. \qquad (4.8)
\end{aligned}$$

Equation (4.8) is obtained from Equation (4.7) through integration by parts. It is usually preferred in numerical computations because it is cheaper and numerically easier to handle than Equation (4.7).

It can be shown that the field $\nabla\omega \wedge \hat{\mathbf{e}}_z$ defined by Equation (4.5) is divergence free as it should be. This is so because the integration is done along closed filaments $\mathcal{C}^p(t)$. The velocity field $\mathbf{u}$ is not obtained from taking the curl of a streamfunction, but is obtained from solving Equation (4.6). The fact that $\mathbf{u}$ is divergence free is also only due to the fact that the filaments $\mathcal{C}^p(t)$ are closed curves.

The evolution equation for the contour $\mathcal{C}^p(t)$ is taken as

$$\frac{\partial}{\partial t}\mathbf{x}^p(s,t) = \mathbf{u}(\mathbf{x}^p(s,t),t) \; . \tag{4.9}$$

Notice that, since two adjacent points on a contour are, by definition, connected by the contour, the method automatically ensures the proper stretching of $\nabla\omega \wedge \hat{\mathbf{e}}_z$ in accordance with Equation (4.4). The method of contour dynamics is thus very similar to the method of vortex filaments in three dimensions.

With the method of contour dynamics, there is no need for any regularization of the distribution of $\nabla\omega \wedge \hat{\mathbf{e}}_z$ to obtain a well-behaved velocity field for points on the contour. This fact is in opposition with the method of vortex filaments where one needs a regularization of the vorticity distribution along the filament in order to obtain a well-behaved velocity for points on the filament (see Section 2.2.1 and Section 2.2.2). Indeed, recall that a singular vortex filament has a logarithmically infinite local contribution to the self-induced velocity wherever its curvature is non-zero. Most authors have used the formulation (4.5) through (4.9) to perform numerical computations with the method of contour dynamics (Zabusky 1981, Dritschel 1985, 1986). This however leads to problems such as excessive creation of contour length and subsequent need for *contour surgery* (Dritschel 1988). In Section 4.2.2, a regularized version of the method of contour dynamics is presented that should help solve some of the problems encountered with the classical method.

4.2.2 A regularized version of the method of contour dynamics

A regularized version of the method of contour dynamics, which could also be called *method of regularized filaments of* $\nabla\omega \wedge \hat{\mathbf{e}}_z$, can be obtained by writing

$$\begin{aligned}
(\nabla\wedge(\omega(\mathbf{x},t)\,\hat{\mathbf{e}}_z))_\sigma &= (\nabla\omega)_\sigma(\mathbf{x},t) \wedge \hat{\mathbf{e}}_z \\
&= \zeta_\sigma(\mathbf{x}) * (\nabla\omega(\mathbf{x},t) \wedge \hat{\mathbf{e}}_z) \\
&= \sum_p \Delta\omega^p \int_{\mathcal{C}^p(t)} \zeta_\sigma(\mathbf{x}-\mathbf{x}^p)\,\frac{\partial \mathbf{x}^p}{\partial s}\,ds \; ,
\end{aligned} \tag{4.10}$$

where $\mathbf{x}^p$ stands for $\mathbf{x}^p(s,t)$. Here, $\zeta_\sigma(\mathbf{x})$ is an approximation to the two-dimensional δ-function which is taken as radially symmetric, i.e.,

$$\zeta_\sigma(\mathbf{x}) = \frac{1}{\sigma^2}\,\zeta\left(\frac{|\mathbf{x}|}{\sigma}\right) , \tag{4.11}$$

with the normalization

$$2\pi \int_0^\infty \zeta(\rho)\,\rho\,d\rho = 1 . \tag{4.12}$$

The length scale σ is a core size or cut-off length. By Equation (4.10), the vorticity now makes the transition smoothly from a constant value within the patch bounded by the curve $\mathcal{C}^p(t)$ to another value outside of the patch, the width of the transition region being of $\mathcal{O}(\sigma)$. It can be shown that the field $(\nabla\omega)_\sigma \wedge \hat{\mathbf{e}}_z$ defined by Equation (4.10) is divergence free when σ is a constant for each boundary. This is due to the fact that the boundaries are closed.

The velocity is given by the solution of

$$\nabla^2 \mathbf{u}_\sigma = -(\nabla\omega)_\sigma \wedge \hat{\mathbf{e}}_z . \tag{4.13}$$

First, the function $\chi(\rho)$ is defined such that

$$\zeta(\rho) = \nabla^2\chi(\rho) = \frac{1}{\rho}\frac{d}{d\rho}\left(\rho\frac{d\chi}{d\rho}\right) , \tag{4.14}$$

and

$$\chi_\sigma(\mathbf{x}) = \chi\left(\frac{|\mathbf{x}|}{\sigma}\right) . \tag{4.15}$$

The function $g(\rho)$ which will be needed extensively in what follows is also defined:

$$g(\rho) = \int_0^\rho \zeta(t)\,t\,dt , \tag{4.16}$$

and

$$g_\sigma(\mathbf{x}) = g\left(\frac{|\mathbf{x}|}{\sigma}\right) . \tag{4.17}$$

From the normalization condition (4.12), it follows that $2\pi\,g(\rho) \to 1$ as $\rho \to \infty$. Since $\zeta(\rho)$ is $\mathcal{O}(1)$ for small ρ, $g(\rho)$ is $\mathcal{O}(\rho^2)$ for small ρ. The following relations between $g(\rho)$, $\chi(\rho)$ and $\zeta(\rho)$ will also prove very useful. First, from the definition of $g(\rho)$,

$$\frac{g'(\rho)}{\rho} = \zeta(\rho) . \tag{4.18}$$

Second, from the definition of $g(\rho)$ and $\chi(\rho)$,

$$g(\rho) = \int_0^\rho \zeta(t)\,t\,dt = \int_0^\rho \frac{d}{dt}\left(t\frac{d\chi}{dt}\right)\,dt = \rho\,\chi'(\rho) , \tag{4.19}$$

so that

$$\frac{\chi'(\rho)}{\rho} = \frac{g(\rho)}{\rho^2} \,. \tag{4.20}$$

Finally, from Equation (4.18),

$$\frac{1}{\rho}\frac{d}{d\rho}\left(\frac{g(\rho)}{\rho^2}\right) = \frac{g'(\rho)}{\rho^3} - 2\frac{g(\rho)}{\rho^4} = \frac{1}{\rho^2}\left(\zeta(\rho) - 2\frac{g(\rho)}{\rho^2}\right) \,. \tag{4.21}$$

From Equation (4.20), it follows that $\chi(\rho) = \mathcal{O}(\rho^2)$ for small ρ and that $\chi(\rho) \to \log\rho/(2\pi)$ as $\rho \to \infty$.

Going back to the velocity field which solves Equation (4.13), one obtains

$$\begin{aligned}
\mathbf{u}_\sigma(\mathbf{x},t) &= -G(\mathbf{x}) * ((\nabla\omega)_\sigma(\mathbf{x},t) \wedge \hat{\mathbf{e}}_z) \\
&= -\frac{1}{2\pi}\int \log\left(\frac{|\mathbf{x}-\mathbf{x}'|}{\sigma}\right)((\nabla\omega)_\sigma(\mathbf{x}',t)\wedge\hat{\mathbf{e}}_z)\,d\mathbf{x}' \\
&= -\chi_\sigma(\mathbf{x}) * (\nabla\omega(\mathbf{x},t)\wedge\hat{\mathbf{e}}_z) \\
&= -\sum_p \Delta\omega^p \int_{\mathcal{C}^p(t)} \chi_\sigma(\mathbf{x}-\mathbf{x}^p)\frac{\partial\mathbf{x}^p}{\partial s}\,ds \qquad (4.22) \\
&= \sum_p \Delta\omega^p \int_{\mathcal{C}^p(t)} \frac{g_\sigma(\mathbf{x}-\mathbf{x}^p)}{|\mathbf{x}-\mathbf{x}^p|^2}(\mathbf{x}-\mathbf{x}^p)\left((\mathbf{x}-\mathbf{x}^p)\cdot\frac{\partial\mathbf{x}^p}{\partial s}\right)ds \,. \qquad (4.23)
\end{aligned}$$

Equation (4.23) is obtained from Equation (4.22) through integration by parts. It should be preferred to Equation (4.22) in numerical computation because it is usually cheaper to evaluate numerically. A list of typical regularization functions is given in Table B.2. It is seen that the evaluation of $\chi(\rho)$ is indeed more costly than the evaluation of $g(\rho)$ because it involves the evaluation of a logarithm.

Again, the velocity field $\mathbf{u}_\sigma$ is not obtained from taking the curl of a stream-function but is obtained from solving Equation (4.13). Consequently, there is no guarantee that $\mathbf{u}_\sigma$ is divergence free. It turns out that, because the boundaries $\mathcal{C}^p(t)$ are closed curves, $\mathbf{u}_\sigma$ is divergence free when σ is a constant for each boundary.

Notice that, at large distances compared with σ, the velocity induced by a point on a regularized contour is the same as if the contour were singular since $2\pi\, g(\rho) \to 1$ as $\rho \to \infty$.

Again, as in the classical method of contour dynamics, the evolution equation for the contour $\mathcal{C}^p(t)$ is taken as

$$\frac{\partial}{\partial t}\mathbf{x}^p(s,t) = \mathbf{u}_\sigma(\mathbf{x}^p(s,t),t) \,. \tag{4.24}$$

Of course, other schemes can be used. For instance, if the filaments are convected with some average velocity and if the smoothing $\zeta_\sigma(\mathbf{x})$ is used as average operator, one obtains, following Leonard (1980),

$$\frac{\partial}{\partial t}\mathbf{x}^p(s,t) = \Big(\zeta_\sigma(\mathbf{x}) * \mathbf{u}_\sigma(\mathbf{x},t)\Big)\Big|_{\mathbf{x}=\mathbf{x}^p(s,t)} \,. \tag{4.25}$$

As was the case for the three-dimensional method of filaments of ω, Section 2.2.2, the core size σ of the filaments of $\nabla\omega \wedge \hat{\mathbf{e}}_z$ does not have to be a constant for all filaments and all times. Each filament can be assigned its own core size σ^p which may depend on time $\sigma^p = \sigma^p(t)$. For instance, one can use the model equation

$$\frac{d}{dt}\left(\sigma^p(t)\,\mathcal{L}^p(t)\right) = 0 \tag{4.26}$$

to ensure conservation of the area of vorticity gradient. With that choice, it is then wise to symmetrize the evolution equations by using $\sigma^{pq} = \sigma^{qp}$ where σ^{pq} is the core size used to compute the influence of filament q on filament p and conversely. Indeed, this choice leads to exact conservation of total circulation, linear impulse and angular impulse.

Notice that the use of a core size that also depends on the material coordinate s, $\sigma = \sigma(s,t)$ is a poor choice. Indeed, with this choice, the situation is very similar to the situation encountered with the method of regularized particles of $\nabla\omega$, Section 4.3.3, and the fields $(\nabla\omega)_\sigma \wedge \hat{\mathbf{e}}_z$ and $\mathbf{u}_\sigma$ are not anymore divergence free.

4.3 A particle method for the vorticity gradient

4.3.1 Singular particles of vorticity gradient

The inviscid version of Equation (4.2) is an hyperbolic equation for the vorticity gradient which can be solved using a particle method (see for instance Raviart 1985, 1987). In such a method, one uses particles of vorticity gradient that define the field

$$\nabla\omega(\mathbf{x},t) = \sum_p (\nabla\omega)^p(t)\,S^p\,\delta(\mathbf{x}-\mathbf{x}^p(t)) = \sum_p \boldsymbol{\alpha}^p(t)\,\delta(\mathbf{x}-\mathbf{x}^p(t))\,. \tag{4.27}$$

Notice that an isolated particle has no physical meaning. These particles must be understood as being a discretization of a contour of $\nabla\omega \wedge \hat{\mathbf{e}}_z$, i.e., $\boldsymbol{\alpha}^p(t) \wedge \hat{\mathbf{e}}_z$ is a little section of a contour of $\nabla\omega \wedge \hat{\mathbf{e}}_z$.

From Green's theorem, the condition of vanishing vorticity at infinity gives,

$$0 = \int_{S\to\infty} \omega\, d\mathbf{l} = \int \nabla\omega\, d\mathbf{x} = \sum_p \boldsymbol{\alpha}^p(t)\,, \tag{4.28}$$

a consistency condition to be satisfied for all times. This condition is equivalent to the constraint that, in contour dynamics, the boundaries $\mathcal{C}^p(t)$ must be closed curves.

The velocity is obtained by solving Equation (4.6) with the particle representation of the vorticity gradient. This leads to

$$\mathbf{u}(\mathbf{x},t) \;=\; -G(\mathbf{x}) * (\nabla\omega(\mathbf{x},t) \wedge \hat{\mathbf{e}}_z)$$

$$= -\frac{1}{2\pi}\sum_p \log\left(\frac{|\mathbf{x}-\mathbf{x}^p(t)|}{a}\right)\boldsymbol{\alpha}^p(t)\wedge\hat{\mathbf{e}}_z \tag{4.29}$$

$$\simeq \frac{1}{2\pi}\sum_p \frac{(\mathbf{x}-\mathbf{x}^p(t))}{|\mathbf{x}-\mathbf{x}^p(t)|^2}\left((\mathbf{x}-\mathbf{x}^p(t))\cdot(\boldsymbol{\alpha}^p(t)\wedge\hat{\mathbf{e}}_z)\right). \tag{4.30}$$

Notice that Equation (4.29) is the exact solution of Equation (4.6) using the particles of vorticity gradient. Equation (4.30) is only a direct particle translation of Equation (4.8) and is only "allowed" when the particles are a good representation of a contour of $\nabla\omega\wedge\hat{\mathbf{e}}_z$.

A few remarks have to be made at this point:

- The particle representation of $\nabla\omega\wedge\hat{\mathbf{e}}_z$ is not generally divergence free as it should be. The method is thus inconsistent in some sense because a basis which is not generally divergence free is used to represent a field that should be divergence free for all times. As time evolves, the particle representation of $\nabla\omega\wedge\hat{\mathbf{e}}_z$ could become a very poor representation of a divergence free field.

- One can reconstruct a divergence free field from the particles by writing

$$\begin{aligned}\nabla\omega^N(\mathbf{x},t)\wedge\hat{\mathbf{e}}_z &= \sum_p\Bigg[(\boldsymbol{\alpha}^p(t)\wedge\hat{\mathbf{e}}_z)\,\delta(\mathbf{x}-\mathbf{x}^p(t)) \\ &\qquad -\nabla\left((\boldsymbol{\alpha}^p(t)\wedge\hat{\mathbf{e}}_z)\cdot\nabla\left(\frac{1}{2\pi}\log\left(\frac{|\mathbf{x}-\mathbf{x}^p(t)|}{a}\right)\right)\right)\Bigg] \\ &= \sum_p\Bigg[\left(\delta(\mathbf{x}-\mathbf{x}^p(t))-\frac{1}{2\pi|\mathbf{x}-\mathbf{x}^p(t)|^2}\right)(\boldsymbol{\alpha}^p(t)\wedge\hat{\mathbf{e}}_z) \\ &\qquad +2\,\frac{((\boldsymbol{\alpha}^p(t)\wedge\hat{\mathbf{e}}_z)\cdot(\mathbf{x}-\mathbf{x}^p(t)))}{2\pi|\mathbf{x}-\mathbf{x}^p(t)|^4}(\mathbf{x}-\mathbf{x}^p(t))\Bigg].\end{aligned} \tag{4.31}$$

- The velocity field (4.29) induced by the particles field (4.27) is also not generally divergence free. This is so because it is not obtained from taking the curl of a streamfunction but is obtained from solving Equation (4.6) on the particles. (There is actually no explicit knowledge of the streamfunction in the present formulation!). More specifically,

$$\begin{aligned}\nabla\cdot(\mathbf{u}(\mathbf{x},t)) &= -\frac{1}{2\pi}\sum_p(\boldsymbol{\alpha}^p(t)\wedge\hat{\mathbf{e}}_z)\cdot\nabla\left(\log\left(\frac{|\mathbf{x}-\mathbf{x}^p(t)|}{a}\right)\right) \\ &= -\frac{1}{2\pi}\sum_p\frac{((\boldsymbol{\alpha}^p(t)\wedge\hat{\mathbf{e}}_z)\cdot(\mathbf{x}-\mathbf{x}^p(t)))}{|\mathbf{x}-\mathbf{x}^p(t)|^2}.\end{aligned} \tag{4.32}$$

The divergence of the velocity is small when the particles are aligned as if $\boldsymbol{\alpha}^p\wedge\hat{\mathbf{e}}_z$ were sections of a contour of $\nabla\omega\wedge\hat{\mathbf{e}}_z$. Indeed, if $\nabla\omega\wedge\hat{\mathbf{e}}_z$ is almost divergence free, then Equation (4.6) guarantees that $\mathbf{u}$ is also almost divergence free.

- If the curl of Equation (4.29) is taken, one obtains the vorticity field

$$\begin{aligned}\omega(\mathbf{x},t) &= \frac{1}{2\pi}\sum_p \boldsymbol{\alpha}^p(t)\cdot\nabla\left(\log\left(\frac{|\mathbf{x}-\mathbf{x}^p(t)|}{a}\right)\right)\\ &= \frac{1}{2\pi}\sum_p \frac{(\boldsymbol{\alpha}^p(t)\cdot(\mathbf{x}-\mathbf{x}^p(t)))}{|\mathbf{x}-\mathbf{x}^p(t)|^2}\,, \end{aligned} \tag{4.33}$$

and if the curl of that vorticity field is taken, one obtains

$$\begin{aligned}\nabla(\omega(\mathbf{x},t))\wedge\hat{\mathbf{e}}_z &= \frac{1}{2\pi}\sum_p \nabla\left(\boldsymbol{\alpha}^p(t)\cdot\nabla\left(\log\left(\frac{|\mathbf{x}-\mathbf{x}^p(t)|}{a}\right)\right)\right)\wedge\hat{\mathbf{e}}_z\\ &= \frac{1}{2\pi}\sum_p\left[\frac{1}{|\mathbf{x}-\mathbf{x}^p(t)|^2}(\boldsymbol{\alpha}^p(t)\wedge\hat{\mathbf{e}}_z)\right.\\ &\qquad\left.-2\frac{(\boldsymbol{\alpha}^p(t)\cdot(\mathbf{x}-\mathbf{x}^p(t)))}{|\mathbf{x}-\mathbf{x}^p(t)|^4}((\mathbf{x}-\mathbf{x}^p(t))\wedge\boldsymbol{\alpha}^p(t))\right] \end{aligned} \tag{4.34}$$

This field is divergence free since it is the curl of something. It is however not equal to the field given by Equation (4.31). It is maintained that both fields are very much alike when the particles are a good discretization of $\nabla\omega\wedge\hat{\mathbf{e}}_z$.

In a method of particles of vorticity gradient, the evolution equation for the particle position and strength vector are taken in accordance with Equation (4.2),

$$\frac{d}{dt}\mathbf{x}^p(t) = \mathbf{u}^p(\mathbf{x}^p(t),t)\,, \tag{4.35}$$

$$\begin{aligned}\frac{d}{dt}\boldsymbol{\alpha}^p(t) &= -\left(\boldsymbol{\alpha}^p(t)\cdot\nabla^T\right)\mathbf{u}^p(\mathbf{x}^p(t),t)\\ &= \frac{1}{2\pi}\sum_{\substack{q\\ q\neq p}}\frac{(\mathbf{x}^p(t)-\mathbf{x}^q(t))}{|\mathbf{x}^p(t)-\mathbf{x}^q(t)|^2}((\boldsymbol{\alpha}^p(t)\wedge\boldsymbol{\alpha}^q(t))\cdot\hat{\mathbf{e}}_z)\,, \end{aligned} \tag{4.36}$$

where $\mathbf{u}^p(\mathbf{x},t)$ stands for the velocity field without the contribution of the p particle. The evolution equation (4.36) for the gradient of vorticity does not ensure that the consistency condition (4.28) is satisfied for all times. The method is thus not conservative. One might think that replacing the velocity field (4.29) by the almost equivalent velocity field (4.30) might make the method conservative. Unfortunately, it does not.

4.3.2 Singular particles of vorticity curl

A method of particles of $\nabla\omega$ to solve for Equation (4.2) has been presented above. Because of the problems encountered with this method one might think of using a

method of particles of $\nabla\omega\wedge\hat{\mathbf{e}}_z$ and solve for Equation (4.4) instead, it might be hoped, with more success. In such a method,

$$\nabla\omega(\mathbf{x},t)\wedge\hat{\mathbf{e}}_z=\sum_p((\nabla\omega)^p(t)\wedge\hat{\mathbf{e}}_z)\,S^p\,\delta(\mathbf{x}-\mathbf{x}^p(t))=\sum_p\boldsymbol{\beta}^p(t)\,\delta(\mathbf{x}-\mathbf{x}^p(t))\,. \quad (4.37)$$

The consistency condition is now $\sum_p\boldsymbol{\beta}^p(t)=0$ for all times. With the same procedure as above, one obtains, for the velocity field induced by the particles,

$$\begin{aligned}\mathbf{u}(\mathbf{x},t) &= -\frac{1}{2\pi}\sum_p\log\left(\frac{|\mathbf{x}-\mathbf{x}^p(t)|}{a}\right)\boldsymbol{\beta}^p(t) &(4.38)\\ &\simeq \frac{1}{2\pi}\sum_p\frac{(\mathbf{x}-\mathbf{x}^p(t))}{|\mathbf{x}-\mathbf{x}^p(t)|^2}((\mathbf{x}-\mathbf{x}^p(t))\cdot\boldsymbol{\beta}^p(t))\,. &(4.39)\end{aligned}$$

Again, only Equation (4.38) is the solution of Equation (4.6) using the particle representation of $\nabla\omega\wedge\hat{\mathbf{e}}_z$. Equation (4.39) is only a direct translation of Equation (4.8) and should only be used as long as the particle representation of $\nabla\omega\wedge\hat{\mathbf{e}}_z$ is accurate.

The evolution equations for the particles position and strength vector are now taken in accordance with Equation (4.4)

$$\begin{aligned}\frac{d}{dt}\mathbf{x}^p(t) &= \mathbf{u}^p(\mathbf{x}^p(t),t)\,, &(4.40)\\ \frac{d}{dt}\boldsymbol{\beta}^p(t) &= (\boldsymbol{\beta}^p(t)\cdot\nabla)\,\mathbf{u}^p(\mathbf{x}^p(t),t)\\ &= -\frac{1}{2\pi}\sum_{\substack{q\\ q\neq p}}\frac{((\mathbf{x}^p(t)-\mathbf{x}^q(t))\cdot\boldsymbol{\beta}^p(t))}{|\mathbf{x}^p(t)-\mathbf{x}^q(t)|^2}\boldsymbol{\beta}^q(t)\,, &(4.41)\end{aligned}$$

where $\mathbf{u}^p(\mathbf{x},t)$ stand for the velocity field without the contribution of the p particle. This method does not ensure that the consistency condition (4.28) is satisfied for all times. It is thus also not conservative. Replacing the velocity field (4.38) by the almost equivalent velocity field (4.39) does not make it conservative either.

The method of particles of $\nabla\omega\wedge\hat{\mathbf{e}}_z$ is thus neither better nor worse than the method of particles of $\nabla\omega$. Notice that the two methods are not equivalent. Indeed, Equations (4.2) and (4.4) are only equivalent when $\nabla\cdot\mathbf{u}=0$. Consequently, the method of particles of $\nabla\omega$ that solves for Equation (4.2) is not equivalent for all times to the method of particles of $\nabla\omega\wedge\hat{\mathbf{e}}_z$ that solves for Equation (4.4). Computations that start off with the same discretization (i.e., $\boldsymbol{\beta}^p(0)=\boldsymbol{\alpha}^p(0)\wedge\hat{\mathbf{e}}_z$) might not preserve for all times the orthogonality between $\boldsymbol{\beta}^p(t)$ and $\boldsymbol{\alpha}^p(t)$. The orthogonality is only preserved as long as $\nabla\cdot\mathbf{u}\simeq 0$, i.e., as long as the particle discretization of $\nabla\omega\wedge\hat{\mathbf{e}}_z$ remains almost divergence free.

4.3.3 Regularized particles of vorticity gradient

The regularized version of the method of particles of vorticity gradient is now examined. The necessary smoothing functions have already been introduced in Section 4.2.2. In such a method, one uses regularized particles of vorticity gradient that define the field

$$(\nabla\omega)_\sigma(\mathbf{x},t) = \zeta_\sigma(\mathbf{x}) * \nabla\omega(\mathbf{x},t) = \sum_p \boldsymbol{\alpha}^p(t)\,\zeta_\sigma(\mathbf{x}-\mathbf{x}^p(t))\,. \tag{4.42}$$

The consistency condition (4.28) remains. The velocity field is now obtained by solving Equation (4.13) using the particles. This leads to

$$\begin{aligned}
\mathbf{u}_\sigma(\mathbf{x},t) &= -G(\mathbf{x}) * ((\nabla\omega)_\sigma(\mathbf{x},t) \wedge \hat{\mathbf{e}}_z) \\
&= -\chi_\sigma(\mathbf{x}) * (\nabla\omega(\mathbf{x},t) \wedge \hat{\mathbf{e}}_z) \\
&= -\sum_p \chi_\sigma(\mathbf{x}-\mathbf{x}^p(t))\;\boldsymbol{\alpha}^p(t) \wedge \hat{\mathbf{e}}_z \qquad (4.43) \\
&\simeq \sum_p \frac{g_\sigma(\mathbf{x}-\mathbf{x}^p(t))}{|\mathbf{x}-\mathbf{x}^p(t)|^2}\,(\mathbf{x}-\mathbf{x}^p(t))\,((\mathbf{x}-\mathbf{x}^p(t))\cdot(\boldsymbol{\alpha}^p(t)\wedge\hat{\mathbf{e}}_z))\,. \qquad (4.44)
\end{aligned}$$

Again, only Equation (4.43) is the solution of Equation (4.13) using the particles of vorticity gradient. Equation (4.44) is only a particle translation of Equation (4.23) and is only "allowed" when the particles are a good approximation of a contour of $\nabla\omega \wedge \hat{\mathbf{e}}_z$.

The same remarks that were made in the case of singular particles are relevant here

- The particle field $(\nabla\omega)_\sigma \wedge \hat{\mathbf{e}}_z$ is not generally divergence free.
- One can reconstruct a divergence free field from the particles by writing

$$\begin{aligned}
(\nabla\omega)^N_\sigma(\mathbf{x},t) \wedge \hat{\mathbf{e}}_z &= \sum_p \Big[(\boldsymbol{\alpha}^p(t)\wedge\hat{\mathbf{e}}_z)\,\zeta_\sigma(\mathbf{x}-\mathbf{x}^p(t)) \\
&\qquad -\nabla\Big((\boldsymbol{\alpha}^p(t)\wedge\hat{\mathbf{e}}_z)\cdot\nabla\big(\chi_\sigma(\mathbf{x}-\mathbf{x}^p(t))\big)\Big)\Big] \\
&= \sum_p \Big[\Big(\zeta_\sigma(\mathbf{x}-\mathbf{x}^p(t)) - \frac{g_\sigma(\mathbf{x}-\mathbf{x}^p(t))}{|\mathbf{x}-\mathbf{x}^p(t)|^2}\Big)\,(\boldsymbol{\alpha}^p(t)\wedge\hat{\mathbf{e}}_z) \\
&+ \Big(2\,\frac{g_\sigma(\mathbf{x}-\mathbf{x}^p(t))}{|\mathbf{x}-\mathbf{x}^p(t)|^2} - \zeta_\sigma(\mathbf{x}-\mathbf{x}^p(t))\Big)\,\frac{((\boldsymbol{\alpha}^p(t)\wedge\hat{\mathbf{e}}_z)\cdot(\mathbf{x}-\mathbf{x}^p(t)))}{|\mathbf{x}-\mathbf{x}^p(t)|^2}\,(\mathbf{x}-\mathbf{x}^p(t))\Big]\,.
\end{aligned} \tag{4.45}$$

- The velocity field (4.43) induced by the particles (4.42) is also not generally divergence free. This is so because it is not obtained from taking the curl of

a streamfunction but is obtained from solving Equation (4.13) on the particles. More specifically

$$\begin{aligned}\nabla\cdot(\mathbf{u}_\sigma(\mathbf{x},t)) &= -\sum_p (\boldsymbol{\alpha}^p(t)\wedge\hat{\mathbf{e}}_z)\cdot\nabla\Big(\chi_\sigma(\mathbf{x}-\mathbf{x}^p(t))\Big)\\ &= -\sum_p \frac{g_\sigma(\mathbf{x}-\mathbf{x}^p(t))}{|\mathbf{x}-\mathbf{x}^p(t)|^2}\left((\boldsymbol{\alpha}^p(t)\wedge\hat{\mathbf{e}}_z)\cdot(\mathbf{x}-\mathbf{x}^p(t))\right). \quad (4.46)\end{aligned}$$

Again, when $(\nabla\omega)_\sigma\wedge\hat{\mathbf{e}}_z$ is almost divergence free, Equation (4.13) guarantees that $\mathbf{u}_\sigma$ is also almost divergence free.

- If the curl of Equation (4.43) is taken, one obtains the vorticity field

$$\begin{aligned}\omega_\sigma(\mathbf{x},t) &= \sum_p \boldsymbol{\alpha}^p(t)\cdot\nabla\Big(\chi_\sigma(\mathbf{x}-\mathbf{x}^p(t))\Big)\\ &= \sum_p \frac{g_\sigma(\mathbf{x}-\mathbf{x}^p(t))}{|\mathbf{x}-\mathbf{x}^p(t)|^2}\left(\boldsymbol{\alpha}^p(t)\cdot(\mathbf{x}-\mathbf{x}^p(t))\right), \quad (4.47)\end{aligned}$$

and if the curl of that vorticity field is taken, one obtains

$$\begin{aligned}\nabla(\omega_\sigma(\mathbf{x},t))\wedge\hat{\mathbf{e}}_z &= \sum_p \nabla\Big(\boldsymbol{\alpha}^p(t)\cdot\nabla\Big(\chi_\sigma(\mathbf{x}-\mathbf{x}^p(t))\Big)\Big)\wedge\hat{\mathbf{e}}_z\\ &= \sum_p\Bigg[\frac{g_\sigma(\mathbf{x}-\mathbf{x}^p(t))}{|\mathbf{x}-\mathbf{x}^p(t)|^2}(\boldsymbol{\alpha}^p(t)\wedge\hat{\mathbf{e}}_z)\\ &-\left(2\frac{g_\sigma(\mathbf{x}-\mathbf{x}^p(t))}{|\mathbf{x}-\mathbf{x}^p(t)|^2}-\zeta_\sigma(\mathbf{x}-\mathbf{x}^p(t))\right)\frac{(\boldsymbol{\alpha}^p(t)\cdot(\mathbf{x}-\mathbf{x}^p(t)))}{|\mathbf{x}-\mathbf{x}^p(t)|^2}((\mathbf{x}-\mathbf{x}^p(t))\wedge\boldsymbol{\alpha}^p(t))\Bigg]. \quad (4.48)\end{aligned}$$

This field is divergence free since it is the curl of something. However, it is not equal to the field given by Equation (4.45). Again, it is maintained that both fields are very much alike when the particles are a good discretization of the divergence free field $\nabla\omega\wedge\hat{\mathbf{e}}_z$.

The evolution equations for the particles position and strength vector are taken as

$$\frac{d}{dt}\mathbf{x}^p(t) = \mathbf{u}_\sigma(\mathbf{x}^p(t),t), \quad (4.49)$$

$$\begin{aligned}\frac{d}{dt}\boldsymbol{\alpha}^p(t) &= -\left(\boldsymbol{\alpha}^p(t)\cdot\nabla^T\right)\mathbf{u}_\sigma(\mathbf{x}^p(t),t)\\ &= \sum_q \frac{g_\sigma(\mathbf{x}^p(t)-\mathbf{x}^q(t))}{|\mathbf{x}^p(t)-\mathbf{x}^q(t)|^2}(\mathbf{x}^p(t)-\mathbf{x}^q(t))\left((\boldsymbol{\alpha}^p(t)\wedge\boldsymbol{\alpha}^q(t))\cdot\hat{\mathbf{e}}_z\right). \quad (4.50)\end{aligned}$$

Again, Equation (4.50) does not ensure that the consistency condition (4.28) is satisfied for all times. The method is thus not conservative.

In the same way as for singular particles, one might want to use a method of particles of $\nabla\omega \wedge \hat{\mathbf{e}}_z$ instead of a method of particles of $\nabla\omega$. The method presented in Section 4.3.1 can easily be translated into a regularized version but still remains non conservative.

What about errors? The method presented here is strongly nonlinear because the velocity field depends on the particles. Consequently, a convergence analysis is likely to be as difficult as the convergence analysis for vortex particles in three dimensions. Moreover, it was shown that the method is not consistent for all times. Proceeding nevertheless with a convergence analysis for linear hyperbolic equations (Raviart 1985, 1987), one recalls that the error due to solving an hyperbolic equation with regularized particles is at best $\mathcal{O}(\sigma^r + (h/\sigma)^m)$. The exponent m is related to the number of derivatives that exist of the smoothing function $\zeta(\rho)$. For most of the functions used in practice, m is large so that it is essential that the cores do overlap (i.e., $\sigma/h > 1$) for the second term in the error to vanish as $\sigma \to 0$. The exponent r is related to the moment properties of the smoothing function, that is $\zeta(\rho)$ has to satisfy the integral constraint (4.12) together with

$$\int_0^\infty \zeta(\rho)\,\rho^{1+s}\,d\rho = 0\,, \qquad 2 \le s \le r-1 \qquad s \text{ even}\,, \tag{4.51}$$

$$\int_0^\infty |\zeta(\rho)|\,\rho^{1+r}\,d\rho < \infty\,. \tag{4.52}$$

In particular, it can be shown that $r \ge 2$ as soon as $\int_0^\infty |\zeta(\rho)|\,\rho^3\,d\rho < \infty$. If, moreover, $\zeta(\rho)$ is positive, then $r = 2$.

For instance, the Gaussian smoothing (B.9)

$$\zeta(\rho) = \frac{1}{2\pi}\,e^{-\rho^2/2} \tag{4.53}$$

corresponds to $m = \infty$, $r = 2$. The low order algebraic smoothing (B.11)

$$\zeta(\rho) = \frac{1}{\pi}\,\frac{1}{(\rho^2+1)^2} \tag{4.54}$$

gives $m = \infty$, $r = 0$ because Equation (4.52) is not satisfied. This function may thus be a poor choice because the first component of the error $\mathcal{O}(\sigma^r)$ doesn't vanish as $\sigma \to 0$. The high order algebraic smoothing (B.13)

$$\zeta(\rho) = \frac{2}{\pi}\,\frac{1}{(\rho^2+1)^3} \tag{4.55}$$

corresponds to $m = \infty$, $r = 2$. This smoothing is thus as good the Gaussian smoothing. It is however much easier to use than the Gaussian smoothing. Indeed, the $g(\rho)$ and $\chi(\rho)$ functions associated with the high order algebraic smoothing are much easier to evaluate than the functions associated with the Gaussian smoothing. A list of smoothing functions $\zeta(\rho)$, and their associated $g(\rho)$ and $\chi(\rho)$ functions, is given in Table B.2.

4.3.4 Representation of viscous effects by the redistribution of particle strengths

Despite the weaknesses of the method of particles of vorticity gradient, there is one feature that such a method allows for and that cannot be achieved with a contour method: the possibility of taking into account viscous diffusion. This property is a big advantage of the particle method over the method of contour dynamics. Indeed, with the method of contour dynamics, contours remain contours for all times and cannot undergo contour reconnection unless a sophisticated process of contour surgery is employed (Dritschel 1988).

In the following viscous method of particles of vorticity gradient, the stretching term in Equation (4.2) will be treated in the manner presented in Section 4.3.3. The treatment of the viscous term was already presented in the context of regularized vortex particles, Section 3.3. The analysis presented there is still valid in the present context, with the following changes due to the fact that a function in two dimensions is now considered. Here, the function $\zeta(\rho)$ has to satisfy the integral constraints (4.12), (4.51) and (4.52), together with

$$\int_0^\infty |\zeta'(\rho)|\, \rho^{2+r}\, d\rho = 0\,. \tag{4.56}$$

The function $\eta_\sigma(\mathbf{x})$ is here defined as

$$\eta_\sigma(\mathbf{x}) = \frac{1}{\sigma^4}\,\eta\left(\frac{|\mathbf{x}|}{\sigma}\right) \tag{4.57}$$

with

$$\eta(\rho) = -\frac{\zeta'(\rho)}{\rho}\,. \tag{4.58}$$

With the same steps as in Section 3.3, one obtains, for the viscous method of particles of vorticity gradient,

$$\frac{d}{dt}\mathbf{x}^p(t) = \mathbf{u}_\sigma(\mathbf{x}^p(t),t)\,, \tag{4.59}$$

$$\begin{aligned}\frac{d}{dt}\boldsymbol{\alpha}^p(t) &= -\left(\boldsymbol{\alpha}^p(t)\cdot\nabla^T\right)\mathbf{u}_\sigma(\mathbf{x}^p(t),t)\\ &\quad + 2\,\nu\sum_q\left(S^p\,\boldsymbol{\alpha}^q(t) - S^q\,\boldsymbol{\alpha}^p(t)\right)\eta_\sigma(\mathbf{x}^p(t)-\mathbf{x}^q(t))\,.\end{aligned} \tag{4.60}$$

Notice that the viscous term is conservative.

Again, one can develop a viscous method of particles of $\nabla\omega\wedge\hat{\mathbf{e}}_z$ instead of the present viscous method of particles of $\nabla\omega$.

4.4 The method of filaments of vorticity curl and the method of particles of vorticity gradient with respect to the conservation laws

In this section, the behavior of the method of filaments of vorticity curl (i.e., the method of contour dynamics) and of the method of particles of vorticity gradient with respect to the conservation laws is examined. The conservation laws for two-dimensional unbounded flows are reviewed in detail in Appendix A. The reader is referred to that appendix for a review of some important results.

Since the conservation laws are used as performance diagnostics when doing numerical computations, they are here referred to as *diagnostics*.

The linear diagnostics are first examined. With the singular filaments (4.5), one obtains, using integration by parts,

$$\begin{aligned}
\Omega = \int \omega \, d\mathbf{x} = -\frac{1}{2} \int \mathbf{x} \cdot \nabla\omega \, d\mathbf{x} &= -\frac{1}{2} \sum_p \Delta\omega^p \int_{\mathcal{C}^p(t)} \mathbf{x}^p \cdot \left(\hat{\mathbf{e}}_z \wedge \frac{\partial \mathbf{x}^p}{\partial s} \right) ds \\
&= \frac{1}{2} \sum_p \Delta\omega^p \int_{\mathcal{C}^p(t)} \hat{\mathbf{e}}_z \cdot \left(\mathbf{x}^p \wedge \frac{\partial \mathbf{x}^p}{\partial s} \right) ds \\
&= \sum_p \Delta\omega^p \, \mathcal{A}^p \, , \qquad (4.61)
\end{aligned}$$

where $\mathcal{A}^p$ is the area of the p vortex patch, a constant for all times since the total circulation Ω is conserved,

$$\begin{aligned}
\mathbf{I} = \int \mathbf{x} \wedge (\omega \hat{\mathbf{e}}_z) \, d\mathbf{x} &= \int \mathbf{x} \, (\mathbf{x} \cdot (\nabla\omega \wedge \hat{\mathbf{e}}_z)) \, d\mathbf{x} \\
&= \sum_p \Delta\omega^p \int_{\mathcal{C}^p(t)} \mathbf{x}^p \left(\mathbf{x}^p \cdot \frac{\partial \mathbf{x}^p}{\partial s} \right) ds \, , \qquad (4.62) \\
A = -\frac{1}{2} \int |\mathbf{x}|^2 \, \omega \, d\mathbf{x} &= \frac{1}{2} \int x \, y \left(x \frac{\partial \omega}{\partial y} + y \frac{\partial \omega}{\partial x} \right) d\mathbf{x} \\
&= \frac{1}{2} \sum_p \Delta\omega^p \int_{\mathcal{C}^p(t)} x^p \, y^p \left(x^p \frac{\partial x^p}{\partial s} - y^p \frac{\partial y^p}{\partial s} \right) ds \, . \qquad (4.63)
\end{aligned}$$

With the regularized filaments (4.10), the integrals are evaluated using a polar coordinate system centered at $\mathbf{x}^p$. The above expressions for Ω and $\mathbf{I}$ still hold. The expression for A becomes

$$A = \frac{1}{2} \sum_p \Delta\omega^p \int_{\mathcal{C}^p(t)} x^p \, y^p \left(x^p \frac{\partial x^p}{\partial s} - y^p \frac{\partial y^p}{\partial s} \right) ds - \frac{1}{2} \, C \, \sigma^2 \, \Omega \, , \qquad (4.64)$$

where

$$C = 2\pi \int_0^\infty \zeta(\rho) \, \rho^3 \, d\rho \, . \qquad (4.65)$$

With the high order algebraic smoothing (B.13), $C = 1$. With the low order algebraic smoothing (B.11), C does not converge so that A is not defined unless $\Omega = 0$.

The method of singular filaments of $\nabla\omega\wedge\hat{\mathbf{e}}_z$ (i.e., the classical method of contour dynamics) conserves Ω, $\mathbf{I}$ and A. With the method of regularized filaments of $\nabla\omega \wedge \hat{\mathbf{e}}_z$, these invariants are also conserved provided that $\sigma^p = \sigma^p(t)$ only and that the evolution equation is symmetrized as explained in Section 4.2.2.

The method of particles of $\nabla\omega$ is now examined. For singular particles, one obtains, for the linear diagnostics,

$$\Omega = -\frac{1}{2}\int \mathbf{x}\cdot(\nabla\omega)\,d\mathbf{x} = -\frac{1}{2}\sum_p \mathbf{x}^p\cdot\boldsymbol{\alpha}^p\,, \tag{4.66}$$

$$\mathbf{I} = \int(\hat{\mathbf{e}}_z\cdot(\mathbf{x}\wedge\nabla\omega))\,\mathbf{x}\,d\mathbf{x} = \sum_p(\hat{\mathbf{e}}_z\cdot(\mathbf{x}^p\wedge\boldsymbol{\alpha}^p))\,\mathbf{x}^p\,, \tag{4.67}$$

$$\begin{aligned} A &= \frac{1}{2}\int x\,y\left(x\frac{\partial\omega}{\partial y}+y\frac{\partial\omega}{\partial x}\right)d\mathbf{x} \\ &= \frac{1}{2}\sum_p x^p\,y^p\,(x^p\,\alpha_y^p + y^p\,\alpha_x^p)\,. \end{aligned} \tag{4.68}$$

For regularized particles, the integrals are done using a polar coordinate system centered at $\mathbf{x}^p$. The above expressions for Ω and $\mathbf{I}$ still hold. More specifically,

$$\mathbf{I} = \sum_p(\hat{\mathbf{e}}_z\cdot(\mathbf{x}^p\wedge\boldsymbol{\alpha}^p))\,\mathbf{x}^p - \frac{1}{2}C\,\sigma^2\sum_p\boldsymbol{\alpha}^p\,. \tag{4.69}$$

This expression is identical to Equation (4.67) if the consistency $\sum_p \boldsymbol{\alpha}^p = 0$ is satisfied. For the angular impulse, one obtains

$$A = \frac{1}{2}\sum_p x^p\,y^p\,(x^p\,\alpha_y^p + y^p\,\alpha_x^p) - \frac{1}{2}\,C\,\sigma^2\,\Omega\,. \tag{4.70}$$

The inviscid method of particles of $\nabla\omega$ does not conserve Ω, $\mathbf{I}$ and A. Actually, as seen in Section 4.3.1 and Section 4.3.3, the method does not even guarantee that the consistency condition $\sum_p \boldsymbol{\alpha}^p = 0$ (i.e., $\int\nabla\omega\,d\mathbf{x} = 0$) is satisfied for all times. As also seen in these sections, the use of a method of particles of $\nabla\omega\wedge\hat{\mathbf{e}}_z$ does not improve the situation. For the viscous method, the discretization of the integral approximation of the viscous term is conservative with respect to the consistency condition $\sum_p \boldsymbol{\alpha}^p = 0$. Moreover, the integral operator is conservative with respect to the total vorticity $\sum_p \mathbf{x}^p\wedge\boldsymbol{\alpha}^p$, but the discretization of the integral operator is not. In fact, the situation is very similar to the situation encountered with the three-dimensional method of particles of $\boldsymbol{\omega}$, Section 3.3. The viscous part of the method conserves $\sum_p \boldsymbol{\alpha}^p = 0$ and almost conserves (up to a discretization error of the integral operator) $\sum_p \mathbf{x}^p\wedge\boldsymbol{\alpha}^p$.

The evaluation of the quadratic diagnostics, Hamiltonian E (i.e., kinetic energy when $\Omega = 0$) and enstrophy $\mathcal{E}$ is much more complicated than the evaluation of the linear diagnostics and is presented in detail in Appendix I. That appendix contains a lot of interesting information, such as the derivation of two different formulas for the evaluation of the energy E of a system of filaments of $\nabla\omega \wedge \hat{\mathbf{e}}_z$.

The method of singular filaments of $\nabla\omega \wedge \hat{\mathbf{e}}_z$ conserves E and $\mathcal{E}$. The conservation of $\tilde{E}$ and $\tilde{\mathcal{E}}$ with the method of regularized filaments of $\nabla\omega \wedge \hat{\mathbf{e}}_z$ was not investigated. The method of singular (or regularized) particles of vorticity gradient was also not investigated, but there is numerical evidence that E ($\tilde{E}$) and $\mathcal{E}$ ($\tilde{\mathcal{E}}$) are not generally conserved.

4.5 Numerical results

In this section, some of the numerical results that were obtained with the inviscid and viscous versions of the method of particles of vorticity gradient are presented. The computations that were performed are not of great physical significance but they demonstrate the capabilities and weaknesses of this new method. Two problems are examined: the viscous diffusion of a circular vortex patch of uniform vorticity and the interaction, inviscid and viscous, of two circular vortex patches of initially uniform vorticity of the same sign.

The computations are performed using the high order algebraic smoothing (B.13). As seen in Section 4.3.3, this smoothing $\zeta(\rho)$ has convergence properties that are similar to those of the Gaussian smoothing (B.9) (i.e., $m = \infty$, $r = 2$), but is much easier and cheaper to use. Moreover, the $\eta(\rho)$ function which is used for the treatment of viscous diffusion is strictly positive. This property is a necessary condition for good convergence as seen in Section 3.3. Finally, as seen in Appendix I, this smoothing is the only one for which closed form expressions for the semi-regularized Hamiltonian $\tilde{E}$ and the semi-regularized enstrophy $\tilde{\mathcal{E}}$ can be obtained.

The time integration of the evolution equations for the particles position and strength vector is done using the low storage Runge-Kutta scheme of order 3 (WRK3) introduced by Williamson (1980). The interaction in between particles is done using the $\mathcal{O}(N^2)$ algorithm.

For both computations, $\Omega \neq 0$ and $\mathbf{I} = 0$. Moreover, because of symmetry, the consistency condition $\sum_p \boldsymbol{\alpha}^p = 0$ is trivially satisfied for all times. Thus, the only nontrivial diagnostics are Ω, A, $\tilde{E}$ and $\tilde{\mathcal{E}}$. These diagnostics are computed using the formulas given in Section 4.4 (for the linear diagnostics) and in Appendix I (for the quadratic diagnostics).

4.5.1 The short time diffusion of a circular vortex patch of uniform vorticity

This problem is very simple from a fluid mechanics standpoint but it provides the numerical evidence that the viscous method of particles of vorticity gradient indeed solves for Equation (4.2). The initial condition is as follows. The circle radius is $R = 1.0$. The thickness of the region where $\nabla\omega$ is taken to be non-zero is $\Delta r = .150$. This thickness is discretized using 5 layers of particles, each layer being of thickness $\Delta r/5 = .030$. The distance h between particles in the radial direction is thus $h \simeq .030$. For each layer, $N_\varphi = 200$ particles are used along the circumference so that the typical distance between adjacent particles is also $2\pi R/N_\varphi \simeq .030$. The total number of particles is $N = 1000$. The particle strength is initialized with $\alpha(t = 0) = 100.0/3$ for the middle layer and $\alpha(t = 0) = 0$ for the other 4 layers (2 on each side of the middle layer). This choice gives a vortex patch with uniform vorticity $\omega_0 = (100.0/3) \times (\Delta r/5) = 1.0$ and for which the transition of the vorticity from 1.0 inside the circle to 0 outside is fairly steep.

Notice that there is no vortex stretching stretching in this computation. The particles only have to circle around with the appropriate change in strength vector orientation and the appropriate exchange of strength vector magnitude due to viscous diffusion. Notice also that the computation has to be stopped when viscous diffusion has reached significantly the outer layers. A longer time computation would require more layers of particles. This time could not be achieved because the interaction between particles is done using the $\mathcal{O}(N^2)$ algorithm.

The time integration is done up to $t = 12.5$ with $\Delta t = .05$. This time corresponds to roughly one rotation of the vortex patch since $u_\vartheta(r = R) = \omega_0 R/2 = .50$. The viscosity is chosen so that viscous diffusion reaches the last layer of discretization at about that time. The estimate is based on the one-dimensional spreading of a Gaussian distribution for the vorticity gradient accross the boundary with $\sigma^2 = 2\nu t$ and shows that $\nu = 5.0\ 10^{-5}$ is appropriate. The core size of the particles of $\nabla\omega$ is taken as $\sigma = .08$, which satisfies the overlaping constraint since $h \simeq .03$.

The results are shown in Figure J.57 and Figure J.58. Figure J.57 clearly shows the spreading of the vorticity gradient accross the boundary of the vortex patch. Figure J.58 provides quantitative information that can be compared with theoretical results for conservation laws in two-dimensional unbounded flows (Appendix A). First, the total vorticity Ω is nearly conserved, as it should be, with $\Omega(0) = 3.141593$ and $\Omega(12.5) = 3.140923$. Notice that the value at $t = 0$ corresponds exactly, as it should, to the theoretical value for the uniform vorticity patch with infinite vorticity gradient at the boundary, $\Omega = \omega_0\, \pi R^2$. In what follows, this reference state will be

referred to as the *singular vortex patch.* Notice also that the total vorticity begins to degrade very slightly at $t = 5.0$. As was the case with the viscous method of vortex particles, Chapter 3, Section 3.5, this degradation of total vorticity corresponds to a time when the outer layers are starting to "fill up". More layers would be needed for the particles of these layers to be able to diffuse as well (i.e., give some of their strength to another layer).

The diagnostic related to the angular impulse A also behaves as it should. Indeed, $A/A(0)$ almost follows the straight line predicted by theory, i.e.,

$$\frac{A}{A(0)} = 1 + \left(\frac{\nu\Omega}{-A(0)}\right) t = 1.0 + 1.974723\ 10^{-4}\, t\ . \tag{4.71}$$

In the present computation, one obtains $A(0) = -.7853982 - C\,\sigma^2\,\Omega/2 = -.7954513$. The first term corresponds exactly to the theoretical value for the singular vortex patch, namely $A(0) = -\omega_0\,\pi R^4/4$. The second term is a correction term that comes from the fact that the vortex patch is already diffused a little bit a $t = 0$. Numerically, one obtains, with $\sigma = .08$, $\frac{1}{A(0)}\frac{dA}{dt}(0) = 2.138\ 10^{-4}$ which is close to the exact theoretical value $1.975\ 10^{-4}$ in Equation (4.71). Notice that the particle core size σ is not fully specified by the requirements of the convergence proofs. The convergence proofs only state that it must be bigger than a typical distance between particles, the so-called overlaping condition $\sigma/h > 1$. The strategy that was adopted is to choose the numerical value of σ so that A initially behaves as it should. There is numerical evidence that a choice which is good at $t = 0$ remains good later on. For instance, in this computation, one obtains $A(12.5) = -.7971898$ instead of the theoretical value .7974148 .

The quadratic diagnostics are now examined. The enstrophy for the singular vortex patch is $\mathcal{E}(0) = \omega_0^2\,\pi R^2 = 3.141593$. The numerical values for the semi-regularized enstrophy are $\tilde{\mathcal{E}}(0) = 3.016029$ and $\tilde{\mathcal{E}}(12.5) = 2.985759$. The enstrophy decreases because of viscous diffusion. This decay cannot be compared to a theoretical value because the enstrophy does not decay at a rate proportional to the Hamiltonian E when $\Omega \neq 0$, i.e., when E is not the kinetic energy of the system (recall that the kinetic energy is not defined when $\Omega \neq 0$).

The behavior of the Hamiltonian is now examined. If the streamfunction for the singular vortex patch with uniform vorticity is recalled,

$$\psi = -\frac{\omega_0\, r^2}{4} \ \text{ for } r < R\,; \quad \psi = -\frac{\omega_0\, R^2}{2}\left[\log\left(\frac{r}{R}\right) + \frac{1}{2}\right] \ \text{ for } r > R\,, \tag{4.72}$$

one obtains, for the theoretical value of the Hamiltonian, $E = \frac{1}{2}\int \psi\,\omega\, d\mathbf{x} = -\omega_0^2\,\pi R^4/16 = -.1963495$. However, as explained in Appendix I, the Hamiltonian is only defined

up to a constant times the square of the total circulation when $\Omega \neq 0$. One must thus expect to obtain numerically that $E = -\omega_0^2 \pi R^4/16 - const\,(\omega_0 \pi R^2)^2$ where *const* is unknown. In the present computation, three quantities are evaluated: the semi-regularized particle Hamiltonian $\tilde{E} = \frac{1}{2} \int \mathbf{u}_\sigma \cdot \mathbf{u}\, d\mathbf{x}$ given by Equation (I.31), the singular particle Hamiltonian $E = \frac{1}{2} \int \mathbf{u} \cdot \mathbf{u}\, d\mathbf{x}$ given by Equation (I.16) (with the choice of the arbitrary length scale $a = \sigma$), and the discretization, onto particles, of the Hamiltonian corresponding to singular contour dynamics $E_{cd} = \frac{1}{2} \int \psi\, \omega\, d\mathbf{x}$, Equation (I.40) (also with $a = \sigma$). The numerical results are as follows

- E and E_{cd} are equal with $E(0) = E_{cd}(0) = -1.787353$ and $E(12.5) = E_{cd}(12.5) = -1.787526$. Thereby providing the numerical confirmation that the velocity integral E in which the contribution at ∞ has been discarded is indeed the correct expression for the Hamiltonian even when $\Omega \neq 0$. Moreover, the fact that E and E_{cd} are also equal for all times shows that the particle discretization of $\nabla\omega \wedge \hat{\mathbf{e}}_z$ remains a good discretization of a divergence free field. This is to be expected since there is no stretching in this problem. Finally, one has, for this problem, the numerical value for $const = .1612023$.

- The semi-regularized Hamiltonian is $\tilde{E}(0) = -2.182423$ and $\tilde{E}(12.5) = -2.182410$.

- $\tilde{E}$, E and E_{cd} seem to be conserved, but this is only due to the fact that the time of the computation is short with respect to a global viscous time scale (i.e., $\nu t/R^2 << 1$). The Hamiltonian is indeed not conserved for unbounded viscous flows with non-zero total circulation Ω. For instance, it is easy to show that, for the self-similar Gaussian vortex, $E = -\Omega^2\, [const + (1/8\pi) \log(4\nu t/a^2)]$, so that $dE/dt = -\Omega^2/(8\pi t)$.

In conclusion, this simple computation shows that the viscous method of particles of $\nabla\omega$ is consistent with the equation it is supposed to solve, at least for some time. It also shows that the evaluation of the linear and quadratic diagnostics is correct. The method can thus, in principle, be used for the computation of physical problems where the vorticity gradient is only localized in some regions of the flow. Of course, if it is desired to compute the long time diffusion of a vortex patch, then the method is not well suited because the vorticity gradient is then everywhere. Instead, one should then use the classical method of two-dimensional vortex particles, and add to the method the viscous integral operator that redistributes the circulations in between particles to account for viscous diffusion. This viscous method is easy to implement.

4.5.2 The short time interaction between two vortex patches of uniform and same sign vorticity

In this section, the behavior of the method of particles of $\nabla\omega$ is examined on the problem of the inviscid and viscous interactions between two initially identical circular vortex patches of same sign vorticity. This problem is more complicated and physically more interesting than the problem investigated in Section 4.5.1. First of all, there is a lot of stretching of the patch boundaries to be expected when the two vortex patches strongly interact with each other. Moreover, the fusion process of the vortex patches resulting in the reconnection of lines of $\nabla\omega \wedge \hat{\mathbf{e}}_z$ can only occur if viscosity is present. In fact, the situation is very similar to that encountered with the fusion of two identical vortex rings in three dimensions, Section 3.5. In that case, the fusion process resulting in the reconnection of vortex lines can also only occur if viscosity is present.

The initial condition is as follows. Both vortex patches are identical and are separated by a spacing $s = 2.0$ center to center. The radius of each patch is $R = .75$. The thickness of the region where $\nabla\omega$ is expected to be non-zero is $\Delta r = .125$. This thickness is discretized using 5 layers of particles, each layer being of thickness $\Delta r/5 = .025$. The distance h between particles in the radial direction is thus $h \simeq .025$. For each layer, $N_\varphi = 250$ particles are used along the circumference so that the typical distance between adjacent particles is $2\pi R/N_\varphi \simeq .019$. Thus, there are more particles than are initially needed, but this is done because intense stretching is expected to occur during the course of the computation. The total number of particles is $N = 2500$. The particle strength is initialized with $\alpha(t = 0) = 100.0/2.5$ for the middle layer and $\alpha(t = 0) = 0$ for the other 4 layers (2 on each side of the middle layer). This choice gives a vortex patch with uniform vorticity $\omega_0 = (100.0/2.5) \times (\Delta r/5) = 1.0$.

The viscosity is taken as $\nu = 1.0 \times 10^{-4}$. The core size of the particles is adjusted so as obtain the proper slope for the rate of change of A at time $t = 0$ (see below). It is taken as $\sigma = .065$, which also satisfies the overlaping constraint since $h \simeq .019 \ldots .025$. The time integration is done up to $t = 12.5$ with $\Delta t = .05$.

The results of the inviscid and viscous computations are shown in Figure J.59, Figure J.60 and Figure J.61. Of course, the inviscid computation is done with only one layer of particles. Figure J.59 gives the general picture of the flow. Both inviscid and viscous computations are presented. Notice the intense stretching of lines of $\nabla\omega \wedge \hat{\mathbf{e}}_z$ in the interaction region between the two vortex patches. Both computations have to be stopped because of that intense stretching. The remedy would be to add more particles wherever needed but this was not done in the present computations. Notice also that the situation as far as stretching is concerned is worse for the inviscid case

than for the viscous case. Viscosity helps. Indeed, the viscous interaction between particles of opposite strength vector results in the destruction of steep gradients of $\nabla\omega$ by viscous diffusion, thus leading to the reconnection of lines of $\nabla\omega \wedge \hat{\mathbf{e}}_z$. If it were not for the problems encountered with the excessive stretching, the two patches would probably have merged in a fashion similar to the fusion of vortex rings in three dimensions.

Figure J.60 and Figure J.61 provide the quantitative information, i.e., the diagnostics. Before commenting on the results, the values of the diagnostics at $t = 0$ are first examined. The total vorticity is $\Omega(0) = 3.534292$ as it should be from the theory for the singular patches with $\Omega = 2\,\omega_0\,\pi R^2$. The diagnostic related to the angular impulse A is $A(0) = -2.264156 - C\,\sigma^2\,\Omega(0)/2 = -2.271622$. The first term corresponds exactly to the theoretical value for the singular vortex patches, namely $A(0) = -(\omega_0\,\pi R^2/4)(s^2 + 2\,R^2)$. The second term is a correction term that comes from the fact that the vortex patches are already diffused a little bit at $t = 0$. Numerically, one also obtains, with the choice $\sigma = .065$, $\frac{1}{A(0)}\frac{dA}{dt}(0) = 1.3540 \times 10^{-4}$ which is close to the exact theoretical value $-\nu\,\Omega/A(0) = 1.5558 \times 10^{-4}$. The enstrophy for the singular vortex patches is $\mathcal{E}(0) = 2\,\omega_0^2\,\pi R^2 = 3.534292$. The numerical value for the semi-regularized enstrophy is $\tilde{\mathcal{E}}(0) = 3.381290$. For the Hamiltonian, the value at $t = 0$ can be evaluated using the streamfunction for the singular vortex patch with uniform vorticity, Equation (4.72). It is a matter of simple integration to obtain $E = \frac{1}{2}\int \psi\,\omega\,d\mathbf{x} = -(\omega_0^2\,\pi R^4/2)[\log(s/R) + 3/4] = -.8602391$. Again, as explained in Appendix I, the Hamiltonian is only defined up to a constant times the square of the total circulation when $\Omega \neq 0$. Thus one must expect to obtain numerically that $E = -(\omega_0^2\,\pi R^4/2)[\log(s/R) + 3/4] - const\,(2\,\omega_0\,\pi R^2)^2$ where *const* is unknown. In this computation, one obtains, with the choice of the arbitrary length scale $a = \sigma$, $E(0) = E_{cd}(0) = -2.794289$ and $\tilde{E}(0) = -3.293054$. The fact that $E(0) = E_{cd}(0)$ is again a numerical confirmation that the velocity integral E in which the contribution at ∞ has been discarded is indeed the correct expression for the Hamiltonian even when $\Omega \neq 0$. Finally, for this problem, the numerical value for $const = .1548452$. This value does not correspond to the value obtain in the previous problem, Section 4.5.1.

The time evolution of the diagnostics is also interesting. The inviscid computation seems to do slightly better up to $t = 10.0$ or so, because the diagnostics are better conserved. After $t = 10.0$, the viscous computation seems to perform better. Indeed, the presence of viscous diffusion helps reduce the effects due to the stretching of lines of $\nabla\omega \wedge \hat{\mathbf{e}}_z$ by mutual destruction of particles of opposite orientation, and hence helps reconnect the vortex patches. For instance, the inviscid computation produces different values for E and E_{cd} whereas the viscous computation still produces almost the

same value. This is precisely related to the important stretching not compensated by viscous diffusion and is an indication that the particle field of $\nabla\omega \wedge \hat{\mathbf{e}}_z$ is almost divergence free for the viscous computation and is significantly non divergence free for the inviscid computation.

In conclusion, it was not possible, in the present computation, to complete the interaction of the two vortex patches. It is however thought that it is only a matter of discretization, and that a scheme that is able to handle more particles (i.e., a $\mathcal{O}(N \log N)$ scheme) or a scheme that is able to add particles wherever the stretching is important should solve the problems encountered with the present computation. At this stage, the method is still experimental, and no implementation of such schemes was made.

A little parenthesis on the evaluation of the diagnostics: If, in the problem considered above, the sign of one vortex patch is changed, then an entirely new problem emerges with $\Omega = 0$, $\mathbf{I} \neq 0$ and $A = 0$. Also, since $\Omega = 0$, the kinetic energy is finite and is given by the Hamiltonian E. The time evolution of the two such vortex patches was not computed, but the diagnostics at $t = 0$ were examined. For the singular vortex patches, it is a matter of simple integration to show that $\mathbf{I} = I\,\hat{\mathbf{e}}_x$ with $I = \omega_0\, s\, \pi R^2 = 3.534292$ and that $E = (\omega_0^2\, \pi R^4/2)[\log(s/R) + 1/4] = .6117342$. These are precisely the values obtained with the numerical evaluation of $I(0)$ and $E(0) = E_{cd}(0)$. The numerical evaluation of the diagnostics is thus also correct for problems with $\Omega = 0$. For the semi-regularized energy, one obtains $\tilde{E}(0) = .6077137$.

Chapter 5

Summary and conclusions

Many conclusions that are specific to a chapter are outlined in the result section of that chapter. Some general conclusions are however in order.

- The inviscid method of three-dimensional vortex filaments was investigated, both theoretically and numerically. For multiple-filament computations, convergence was reviewed. For single-filament computations, the modeling of a physical vortex tube by a computational vortex filament was also investigated. In particular, a new regularization scheme was developed that reproduces the dispersion relation of the rectilinear vortex tube of unperturbed core structure (i.e., Kelvin's lowest perturbation mode).

- The method of three-dimensional vortex particles (i.e., *vortex sticks* or *vortons*) was investigated, both numerically and theoretically. Both singular and regularized particles were considered, and convergence of the regularized method was reviewed. The method has consistency problems because the particle vorticity field is not guaranteed to be divergence free for all times. Different evolution equations for the stretching of the strength vector were reviewed, and it was shown that one choice, the *transpose scheme*, leads, with the singular method, to a weak solution of the vorticity equation. This choice was also shown to perform better on the conservation laws for both the singular and the regularized methods.

- A viscous version of the method of regularized vortex particles was developed, using theoretical developements due to Sylvie Mas-Gallic. This method accounts for viscous diffusion by redistributing the strength vectors between particles. The method proved very successful in modeling strong vortex tube interactions where viscosity plays an important role such as the reconnection of vortex tubes of opposite sign vorticity by viscous diffusion. In particular, the fusion of two vortex rings was computed at a Reynolds number of 400, and quantitative information was obtained and compared with experimental data.

- A new three-dimensional regularization function was proposed. It is referred to as the *high order algebraic smoothing.* This smoothing is algebraic, easy to handle in numerical computations and has convergence properties that are as good as those of Gaussian smoothing. The associated functions for the evaluation of the streamfunction and the velocity are also easy to handle. Moreover, this smoothing is the only one known for which closed form expressions for the quadratic diagnostics (energy, helicity and enstrophy) can be obtained.

- The two-dimensional method of contour dynamics was reviewed, and it was shown that the method is actually a method of singular filaments of the vorticity curl. A regularized version of the method was developed. A particle version of the method was also presented. These particles are vector elements of vorticity gradient (particles that are vector elements of the vorticity curl can equally be considered). The particle method is to the method of contour dynamics what the method of vortex particles is to the method of vortex filaments in three dimensions. The particle method presents the same advantages (explicit treatment of viscous diffusion) but suffers also the same consistency problems (the particle vorticity curl is not generally divergence free). Both singular and regularized particles were presented, and a viscous version of the method was also introduced. It was shown numerically that this method can account for the viscous reconnection of lines of vorticity curl (i.e., reconnection of patches of uniform vorticity of the same sign) in a manner similar to the reconnection of vortex lines in three dimensions.

- Diagnostics proved very useful in assessing the accuracy of the numerical computations with respect to known conservation laws. Both linear and quadratic diagnostics were used extensively.

- In three-dimensional inviscid flows, vortex tubes retain their identity (i.e., their circulation) and move as material volumes. The method of vortex filaments, which is based on these simple facts, should be preferred to the method of vortex particles when computing inviscid flows. Vortex filaments are simply more consistent than vortex particles because they insure that the vorticity field is divergence free for all times. Moreover, they are cheaper to use since they only amount to keeping track of computational points on a space curve. In two-dimensional inviscid flows, filaments of the vorticity curl also retain their identity (i.e., the jump of vorticity across them). The method of contour dynamics, which also relies on these facts, should thus be preferred to the method of particles of vorticity gradient or the method of particles of vorticity curl.

- For viscous flows, filament methods cannot generally be used because filaments do not necessarily retain their identity. The viscous method of vortex particles can be used in three dimensions and the viscous method of particles of vorticity gradient (or the viscous method of particles of vorticity curl) can be used in two dimensions. There is numerical evidence that the explicit treatment of viscous diffusion helps solve the consistency problems associated with these vector particle methods by keeping the particle vector field almost divergence free for long times.

- Addition of computational elements (i.e., remeshing) is necessary where stretching is important. In filament methods, the remeshing can be achieved by adding computational points along the filament itself (using the parametric representation of the filament). In vector particle methods, the remeshing can be achieved by splitting a strength vector that is too long into two smaller ones.

- A relaxation scheme that forces the particle representation of the vorticity field to be almost divergence free for all times, regardless of viscous diffusion, was developed and tested numerically. It was shown that this scheme performs successfully when it is combined with the remeshing scheme. This relaxation scheme can easily be applied to the two-dimensional method of particles of vorticity gradient (or particles of vorticity curl).

- All methods investigated in this thesis are in urgent need of fast algorithms for the evaluation of the velocity field (from the vorticity in three dimensions and from the vorticity curl in two dimensions). In particular, it is believed that the combination of the viscous method of vortex particles and of fast algorithms would produce a very powerful tool for the investigation of complex three-dimensional flows.

Appendix A

Conservation laws for two- and three-dimensional incompressible unbounded flows

In what follows, the density is taken as unity.

A.1 Three-dimensional unbounded flows

In the present section, only three-dimensional unbounded flows with zero vorticity at infinity are considered. The total vorticity is therefore zero.

In inviscid flows, there are three linear invariants associated with the conservation of total vorticity, linear impulse and angular impulse

$$\mathbf{\Omega} = \int \boldsymbol{\omega}\, d\mathbf{x} = 0\,, \tag{A.1}$$

$$\mathbf{I} = \int \mathbf{u}\, d\mathbf{x} = \frac{1}{2}\int \mathbf{x}\wedge\boldsymbol{\omega}\, d\mathbf{x}\,, \tag{A.2}$$

$$\mathbf{A} = \int \mathbf{x}\wedge\mathbf{u}\, d\mathbf{x} = \frac{1}{2}\int \mathbf{x}\wedge(\mathbf{x}\wedge\boldsymbol{\omega})\, d\mathbf{x}\,. \tag{A.3}$$

There are also two quadratic invariants associated with the conservation of kinetic energy and helicity

$$E = \frac{1}{2}\int \mathbf{u}\cdot\mathbf{u}\, d\mathbf{x} = \frac{1}{2}\int \boldsymbol{\psi}\cdot\boldsymbol{\omega}\, d\mathbf{x}\,, \tag{A.4}$$

$$\mathcal{H} = \int \boldsymbol{\omega}\cdot\mathbf{u}\, d\mathbf{x}\,. \tag{A.5}$$

E is also referred to as the generalized Hamiltonian.

In viscous unbounded flows, the total vorticity $\mathbf{\Omega} = 0$, the linear impulse $\mathbf{I}$ and the angular impulse $\mathbf{A}$ are still conserved, but the kinetic energy E is not conserved. Indeed, taking the dot product of $\mathbf{u}$ with the momentum equation, and integrating over an unbounded volume, it is easy to show (Lamb 1932 and Batchelor 1967) that

$$\frac{d}{dt}E = -2\,\nu\int e_{ij}e_{ij}\, d\mathbf{x} = -\int \Phi\, d\mathbf{x}\,, \tag{A.6}$$

where $e_{ij} = \frac{1}{2}\left(\frac{\partial u_i}{\partial x_j} + \frac{\partial u_j}{\partial x_i}\right)$. The function Φ is called the dissipation function. From kinematics, it is easy to show (Lamb 1932) that

$$\Phi = \nu\,\boldsymbol{\omega}\cdot\boldsymbol{\omega} - \nu\,\nabla\cdot((\mathbf{u}\cdot\nabla)\mathbf{u})\,, \tag{A.7}$$

so that one obtains, for unbounded flows,

$$\frac{d}{dt}E = -\nu\,\mathcal{E}\,, \tag{A.8}$$

where

$$\mathcal{E} = \int \boldsymbol{\omega}\cdot\boldsymbol{\omega}\,d\mathbf{x}\,, \tag{A.9}$$

and is called the enstrophy. The rate of change of the kinetic energy is thus equal to ($-\nu \times$ enstrophy) and is always negative. Moffatt (1969) has shown that the helicity $\mathcal{H}$ measures the net linkage of vortex lines. Consequently, the helicity is not conserved in viscous flows because of the possibility of reconnection of vortex tubes. Notice that the enstrophy in not conserved in both inviscid or viscous three-dimensional flows because of the stretching of vortex lines. The rate of change of the enstrophy is obtained by taking the dot product of $\boldsymbol{\omega}$ with the vorticity equation (Batchelor 1967). This leads to

$$\begin{aligned}\frac{\partial}{\partial t}\left(\frac{\omega_i\omega_i}{2}\right) + \frac{\partial}{\partial x_j}\left(\frac{\omega_i\omega_i}{2}u_j\right) &= \omega_i\omega_j e_{ij} + \nu\,\omega_i\frac{\partial}{\partial x_j}\frac{\partial\omega_i}{\partial x_j} \\ &= \omega_i\omega_i e_{ij} + \nu\left[\frac{\partial}{\partial x_j}\frac{\partial}{\partial x_j}\left(\frac{\omega_i\omega_i}{2}\right) - \frac{\partial\omega_i}{\partial x_j}\frac{\partial\omega_i}{\partial x_j}\right]\,,\end{aligned} \tag{A.10}$$

so that, integrating over an unbounded volume, one obtains,

$$\frac{d}{dt}\mathcal{E} = 2\int\omega_i\omega_j e_{ij}\,d\mathbf{x} - 2\,\nu\int\frac{\partial\omega_i}{\partial x_j}\frac{\partial\omega_i}{\partial x_j}\,d\mathbf{x}\,. \tag{A.11}$$

A.2 Two-dimensional unbounded flows

In inviscid two-dimensional unbounded flows with vorticity, there are three linear invariants associated with the conservation of total circulation, linear impulse and angular impulse

$$\Omega = \int\omega\,d\mathbf{x}\,, \tag{A.12}$$

$$\mathbf{I} = \int\mathbf{x}\wedge(\omega\hat{\mathbf{e}}_z)\,d\mathbf{x}\,, \tag{A.13}$$

$$A = \frac{1}{2}\int\mathbf{x}\wedge(\mathbf{x}\wedge(\omega\hat{\mathbf{e}}_z))\,d\mathbf{x} = -\frac{1}{2}\int|\mathbf{x}|^2\,\omega\,d\mathbf{x}\,. \tag{A.14}$$

When the total circulation $\Omega = 0$, then $\mathbf{I}$ and A are the linear and angular impulse of the system, i.e., $\mathbf{I} = \int \mathbf{u}\, d\mathbf{x}$ and $A = \hat{\mathbf{e}}_z \cdot \int \mathbf{x} \wedge \mathbf{u}\, d\mathbf{x}$. When $\Omega \neq 0$, then the linear impulse and the angular impulse are not defined because the velocity only decays like $1/r$ as $r \to \infty$. However, Equation (A.13) for $\mathbf{I}$ and Equation (A.14) for A are still well-defined, and they are still invariants.

In inviscid flows, there are also two quadratic invariants associated with the conservation of kinetic energy and enstrophy, (the helicity is zero since $\boldsymbol{\omega} \cdot \mathbf{u} = 0$)

$$E = \frac{1}{2} \int \psi \omega \, d\mathbf{x} \,, \tag{A.15}$$

$$\mathcal{E} = \int \omega \omega \, d\mathbf{x} \,. \tag{A.16}$$

E is usually referred to as the Hamiltonian. When the total circulation $\Omega = 0$, the Hamiltonian E is indeed the kinetic energy of the system, i.e., $E = \frac{1}{2} \int \mathbf{u} \cdot \mathbf{u}\, d\mathbf{x}$. When $\Omega \neq 0$, the total kinetic energy is not defined, but the Hamiltonian E is still well-defined. Notice the difference with three-dimensional inviscid flows for which the enstrophy $\mathcal{E}$ is not conserved because of the stretching of vortex lines.

In viscous two-dimensional unbounded flows with vorticity, Ω and $\mathbf{I}$ are still conserved. A is conserved only when $\Omega = 0$. More specifically, it is easy to show (Dritschel 1985) that

$$\frac{d}{dt}\left(-\frac{1}{2} \int |\mathbf{x}|^2 \omega \, d\mathbf{x}\right) = -\nu \int \omega \, d\mathbf{x} - \int (\mathbf{x} \cdot \mathbf{u}) \omega \, d\mathbf{x} \,. \tag{A.17}$$

The first term is constant since the total circulation is conserved. The second term is shown to vanish from kinematics (using integration by parts). One is thus left with

$$\frac{d}{dt} A(t) = -\nu \, \Omega(t) = -\nu \, \Omega \tag{A.18}$$

which gives, for all times, the surprisingly simple result that A increases linearly in time, i.e.,

$$\frac{A(t)}{A(0)} = 1 + \left(\frac{\nu \, \Omega}{-A(0)}\right) t \,. \tag{A.19}$$

This result is very useful since it can be used in viscous computations with $\Omega \neq 0$ as a check on the treatment of the viscous term.

The enstrophy $\mathcal{E}$ is not conserved in viscous flows. Moreover, when the Hamiltonian E is the kinetic energy of the system (i.e., when $\Omega = 0$), it decays at a rate which is proportional to the enstrophy,

$$\frac{d}{dt} E = -\nu \, \mathcal{E} \,. \tag{A.20}$$

This result is also very useful since it can be used in viscous computations with $\Omega = 0$ as a check on the treatment of the viscous term.

Appendix B

The connection between regularized three-dimensional vortex filaments and regularized two-dimensional vortex particles

The connection between regularized three dimensional vortex filaments and regularized two-dimensional vortex particles is examined. The problem of interest is to find the two-dimensional vorticity distribution that corresponds to the projection, into the plane, of a straight three-dimensional vortex filament perpendicular to the plane. The results of this appendix are used extensively throughout this thesis.

In what follows, the subscript "3" is used for regularization functions of three-dimensional vortex filaments, and the subscript "2" is used for regularization functions of two-dimensional vortex particles.

B.1 The general case

For a regularized three-dimensional vortex filament, one has

$$\begin{aligned} \omega_\sigma(\mathbf{x}) &= \Gamma \int_C \frac{1}{\sigma^3}\,\zeta_3\left(\frac{|\mathbf{x}-\mathbf{x}'|}{\sigma}\right)\frac{\partial \mathbf{x}'}{\partial s'}\,ds' \,, \\ \mathbf{u}_\sigma(\mathbf{x}) &= -\Gamma \int_C \frac{g_3\left(\frac{|\mathbf{x}-\mathbf{x}'|}{\sigma}\right)}{|\mathbf{x}-\mathbf{x}'|^3}(\mathbf{x}-\mathbf{x}')\wedge\frac{\partial \mathbf{x}'}{\partial s'}\,ds' \,, \end{aligned} \tag{B.1}$$

where $\mathbf{x}'$ stands for $\mathbf{x}(s',t)$ and $g_3(\rho) = \int_0^\rho \zeta_3(t)\,t^2\,dt$. If the filament is straight, then the velocity that it induces is circumferential and is obtained by integrating the velocity (B.1) along the filament. If the filament is aligned with the $\hat{\mathbf{e}}_z$ axis, $\mathbf{u}_\sigma(\mathbf{x}) = u_\sigma(r)\,\hat{\mathbf{e}}_\theta$, with

$$u_\sigma(r) = \Gamma \int_{-\infty}^{\infty} \frac{g_3\left(\frac{(r^2+z^2)^{\frac{1}{2}}}{\sigma}\right)}{(r^2+z^2)^{\frac{3}{2}}}\,r\,dz \,, \tag{B.2}$$

where $r = (x^2 + y^2)^{\frac{1}{2}}$ is the distance to the point at which the filament crosses the x-y plane. Making the substitution $t^2 = (r^2 + z^2)/\sigma^2$ in Equation (B.2) leads to

$$u_\sigma(r) = \left(\frac{\Gamma}{r}\right) 2\left(\frac{r}{\sigma}\right)^2 \int_{r/\sigma}^{\infty} \frac{g_3(t)}{t^2\,(t^2 - (r/\sigma)^2)^{\frac{1}{2}}} dt = \Gamma\,\frac{g_2\left(\frac{r}{\sigma}\right)}{r}\,. \tag{B.3}$$

A two-dimensional velocity smoothing function is thus obtained,

$$g_2(\rho) = 2\rho^2 \int_{\rho}^{\infty} \frac{g_3(t)}{t^2(t^2 - \rho^2)^{\frac{1}{2}}} dt\,. \tag{B.4}$$

For the vorticity distribution, one obtains, integrating the vorticity (B.1) along the filament, $\boldsymbol{\omega}_\sigma(\mathbf{x}) = \omega_\sigma(r)\,\hat{\mathbf{e}}_z$, with

$$\begin{aligned} \omega_\sigma(r) &= \Gamma \int_{-\infty}^{\infty} \frac{1}{\sigma^3}\,\zeta_3\left(\frac{(r^2 + z^2)^{\frac{1}{2}}}{\sigma}\right) dz \\ &= \Gamma\,\frac{2}{\sigma^2} \int_{r/\sigma}^{\infty} \frac{t\,\zeta_3(t)}{(t^2 - (r/\sigma)^2)^{\frac{1}{2}}}\,dt = \Gamma\,\frac{1}{\sigma^2}\,\zeta_2\left(\frac{r}{\sigma}\right)\,. \end{aligned} \tag{B.5}$$

A two-dimensional vorticity distribution is thus obtained,

$$\zeta_2(\rho) = 2\int_{\rho}^{\infty} \frac{t\,\zeta_3(t)}{(t^2 - \rho^2)^{\frac{1}{2}}}\,dt\,. \tag{B.6}$$

The two-dimensional functions are related through the circulation condition $g_2(\rho) = \int_0^\rho \zeta_2(t)\,t\,dt$, where $2\pi g_2(\rho)$ is the fraction of circulation within the dimensionless radius ρ. The relations that allow one to find the two-dimensional functions, $\zeta_2(\rho)$ and $g_2(\rho)$, given the three-dimensional functions, $\zeta_3(\rho)$ and $g_3(\rho)$, are thus defined. The following is a very useful formula that gives $g_2(\rho)$ directly from $\zeta_3(\rho)$ (Leonard 1985)

$$\begin{aligned} g_2(\rho) &= 2\rho^2 \int_{\rho}^{\infty} \frac{g_3(t)}{t^2(t^2 - \rho^2)^{\frac{1}{2}}} dt = 2\rho^2 \int_{\rho}^{\infty} \frac{dt}{t^2(t^2 - \rho^2)^{\frac{1}{2}}} \int_0^t \zeta_3(u)u^2 du \\ &= 2\rho^2 \int_{\rho}^{\infty} \frac{dt}{t^2(t^2 - \rho^2)^{\frac{1}{2}}} \left(\frac{1}{4\pi} - \int_t^{\infty} \zeta_3(u)u^2 du\right) \\ &= \frac{1}{2\pi}\rho^2 \int_{\rho}^{\infty} \frac{dt}{t^2(t^2 - \rho^2)^{\frac{1}{2}}} - 2\rho^2 \int_{\rho}^{\infty} \zeta_3(u)u^2 du \int_{\rho}^{u} \frac{dt}{t^2(t^2 - \rho^2)^{\frac{1}{2}}} \\ &= \frac{1}{2\pi} - 2\int_{\rho}^{\infty} \zeta_3(u)\,u\,(u^2 - \rho^2)^{\frac{1}{2}} du\,. \end{aligned} \tag{B.7}$$

B.2 Some examples

The three-dimensional Gaussian smoothing

$$\zeta_3(\rho) = \frac{1}{(2\pi)^{\frac{3}{2}}} e^{-\rho^2/2}\,,$$

$$g_3(\rho) = \frac{1}{4\pi}\left(\operatorname{erf}\left(\frac{\rho}{2^{\frac{1}{2}}}\right) - \left(\frac{2}{\pi}\right)^{\frac{1}{2}} \rho\, e^{-\rho^2/2}\right) , \tag{B.8}$$

gives, using Equation (B.7),

$$\begin{aligned} g_2(\rho) &= \frac{1}{2\pi} - \frac{1}{2^{\frac{1}{2}}\pi^{\frac{3}{2}}}\int_\rho^\infty e^{-t^2/2} t(t^2-\rho^2)^{\frac{1}{2}}\, dt \\ &= \frac{1}{2\pi} - \frac{1}{2^{\frac{1}{2}}\pi^{\frac{3}{2}}} e^{-\rho^2/2}\int_0^\infty e^{-u^2/2} u^2\, du \\ &= \frac{1}{2\pi}\left(1 - e^{-\rho^2/2}\right) , \\ \zeta_2(\rho) &= \frac{1}{\rho}\frac{d}{d\rho} g_2(\rho) = \frac{1}{2\pi} e^{-\rho^2/2} , \end{aligned} \tag{B.9}$$

thus showing that the projection of the three-dimensional Gaussian smoothing gives the two-dimensional Gaussian smoothing.

The three-dimensional low order algebraic smoothing

$$\begin{aligned} \zeta_3(\rho) &= \frac{3}{4\pi}\frac{1}{(\rho^2+1)^{\frac{5}{2}}} , \\ g_3(\rho) &= \frac{1}{4\pi}\frac{\rho^3}{(\rho^2+1)^{\frac{3}{2}}} , \end{aligned} \tag{B.10}$$

gives, using Equation (B.4),

$$\begin{aligned} g_2(\rho) &= \frac{1}{2\pi}\rho^2 \int_\rho^\infty \frac{t}{(t^2+1)^{\frac{3}{2}}}\frac{1}{(t^2-\rho^2)^{\frac{1}{2}}}\, dt \\ &= \frac{1}{2\pi}\rho^2 \int_0^\infty \frac{du}{(u^2+(\rho^2+1))^{\frac{3}{2}}} \\ &= \frac{1}{2\pi}\frac{\rho^2}{\rho^2+1} , \\ \zeta_2(\rho) &= \frac{1}{\rho}\frac{d}{d\rho} g_2(\rho) = \frac{1}{\pi}\frac{1}{(\rho^2+1)^2} , \end{aligned} \tag{B.11}$$

thus showing that the projection of the three-dimensional low order algebraic smoothing gives the two-dimensional low order algebraic smoothing.

The three-dimensional high order algebraic smoothing

$$\begin{aligned} \zeta_3(\rho) &= \frac{15}{8\pi}\frac{1}{(\rho^2+1)^{\frac{7}{2}}} , \\ g_3(\rho) &= \frac{1}{4\pi}\frac{\rho^3\left(\rho^2+\frac{5}{2}\right)}{(\rho^2+1)^{\frac{5}{2}}} , \end{aligned} \tag{B.12}$$

gives, using Equation (B.4) and [43],

$$\begin{aligned}
g_2(\rho) &= \frac{1}{2\pi}\rho^2 \int_\rho^\infty \frac{t\left(t^2+\frac{5}{2}\right)}{(t^2+1)^{\frac{5}{2}}} \frac{1}{(t^2-\rho^2)^{\frac{1}{2}}} dt \\
&= \frac{1}{2\pi}\rho^2 \left[\int_0^\infty \frac{u^2}{(u^2+(\rho^2+1))^{\frac{5}{2}}} du + \left(\rho^2+\frac{5}{2}\right) \int_0^\infty \frac{du}{(u^2+(\rho^2+1))^{\frac{5}{2}}} \right] \\
&= \frac{1}{2\pi}\rho^2 \left[\frac{1}{3}\frac{1}{(\rho^2+1)} + \left(\rho^2+\frac{5}{2}\right)\frac{2}{3}\frac{1}{(\rho^2+1)^2} \right] \\
&= \frac{1}{2\pi}\frac{\rho^2(\rho^2+2)}{(\rho^2+1)^2} , \\
\zeta_2(\rho) &= \frac{1}{\rho}\frac{d}{d\rho} g_2(\rho) = \frac{2}{\pi}\frac{1}{(\rho^2+1)^3} ,
\end{aligned} \tag{B.13}$$

thus showing that the projection of the three-dimensional high order algebraic smoothing gives the two-dimensional high order algebraic smoothing.

Finally, the three-dimensional constant smoothing

$$\zeta_3(\rho) = \begin{cases} \frac{3}{4\pi} & \text{for } \rho < 1 \\ 0 & \text{otherwise} , \end{cases}$$

$$g_3(\rho) = \begin{cases} \frac{1}{4\pi}\rho^3 & \text{for } \rho < 1 \\ \frac{1}{4\pi} & \text{otherwise} , \end{cases} \tag{B.14}$$

gives $\zeta_2(\rho) = 0$ and $g_2(\rho) = 1/2\pi$ for $\rho > 1$. For $\rho < 1$, the use of Equation (B.7) leads to

$$\begin{aligned}
g_2(\rho) &= \frac{1}{2\pi} - \frac{3}{2\pi}\int_\rho^1 t(t^2-\rho^2)^{\frac{1}{2}} dt \\
&= \frac{1}{2\pi}\left(1-(1-\rho^2)^{\frac{3}{2}}\right) , \\
\zeta_2(\rho) &= \frac{1}{\rho}\frac{d}{d\rho} g_2(\rho) = \frac{3}{2\pi}(1-\rho^2)^{\frac{1}{2}} .
\end{aligned} \tag{B.15}$$

In this case, the projection of the three-dimensional constant smoothing does not give the two-dimensional constant smoothing, i.e., the two-dimensional constant vorticity core. This is a surprising result which shows that one must be careful when making the connection between three-dimensional and two-dimensional regularization functions.

There actually exists a three-dimensional smoothing that leads to the two-dimensional constant vorticity core and which was found by trial and error (indeed, finding $g_2(\rho)$ and $\zeta_2(\rho)$ given $g_3(\rho)$ and $\zeta_3(\rho)$ is easy to do using the formulas of Section B.1, but the opposite is difficult !). This special three-dimensional smoothing is given by

$$\zeta_3(\rho) = \begin{cases} \frac{1}{\pi^2}\frac{1}{(1-\rho^2)^{\frac{1}{2}}} & \text{for } \rho < 1 \\ 0 & \text{otherwise} , \end{cases}$$

$$g_3(\rho) = \begin{cases} \frac{1}{2\pi^2}\left(\arcsin\rho - \rho(1-\rho^2)^{\frac{1}{2}}\right) & \text{for } \rho < 1 \\ \frac{1}{4\pi} & \text{otherwise .} \end{cases} \tag{B.16}$$

Notice that this smoothing can be used without problems in the velocity integral (B.1) since $g_3(\rho)$ is $\mathcal{O}(\rho^3)$ for small ρ. Although the three-dimensional vorticity smoothing $\zeta_3(\rho)$ diverges as $\rho \to 1$, the filament vorticity distribution is well-defined since one integrates along the filament as shown in Equation (B.1).The projection of this three-dimensional smoothing is done using Equation (B.7). It leads to $\zeta_2(\rho) = 0$ and $g_2(\rho) = 1/2\pi$ for $\rho > 1$ and to

$$\begin{aligned} g_2(\rho) &= \frac{1}{2\pi} - \frac{2}{\pi^2}\int_\rho^1 \frac{t(t^2-\rho^2)^{\frac{1}{2}}}{(1-t^2)^{\frac{1}{2}}}dt \\ &= \frac{1}{2\pi} - \frac{2}{\pi^2}\int_0^{(1-\rho^2)^{1/2}} \frac{u^2}{((1-\rho^2)-u^2)^{\frac{1}{2}}}du \\ &= \frac{1}{2\pi} - \frac{1}{\pi^2}\left(\frac{\pi}{2}(1-\rho^2)\right) \\ &= \frac{1}{2\pi}\rho^2 , \\ \zeta_2(\rho) &= \frac{1}{\rho}\frac{d}{d\rho}g_2(\rho) = \frac{1}{\pi} \end{aligned} \tag{B.17}$$

for $\rho < 1$. Thus the two-dimensional constant smoothing that corresponds to a constant vorticity core has been recovered.

The regularization functions that were discussed in this appendix are summarized in Tables B.2 and B.1, together with other regularization functions and additional information such as the function $\chi(\rho)$ and the convergence properties (i.e., the exponents m and r).

$\chi(\rho)$	$\zeta(\rho) = -\nabla^2\chi(\rho)$ $= -\frac{(\rho^2\chi'(\rho))'}{\rho^2}$ $= -\frac{(\rho\chi(\rho))''}{\rho}$	$g(\rho) = \int_0^\rho \zeta(t)\, t^2\, dt$	m	r
$\frac{1}{4\pi}\frac{1}{(\rho^2+1)^{1/2}}$	$\frac{3}{4\pi}\frac{1}{(\rho^2+1)^{5/2}}$	$\frac{1}{4\pi}\frac{\rho^3}{(\rho^2+1)^{3/2}}$	∞	0
Low order algebraic; $\zeta(\rho) > 0$, $\eta(\rho) = -\zeta'(\rho)/\rho > 0$; no convergence since $r = 0$; yields low order 2-D algebraic when projected in 2-D.				
$\frac{1}{4\pi}\frac{(\rho^2+3/2)}{(\rho^2+1)^{3/2}}$	$\frac{15}{8\pi}\frac{1}{(\rho^2+1)^{7/2}}$	$\frac{1}{4\pi}\frac{\rho^3(\rho^2+5/2)}{(\rho^2+1)^{5/2}}$	∞	2
High order algebraic; $\zeta(\rho)$, $\eta(\rho) > 0$; yields high order 2-D algebraic.				
$\frac{1}{4\pi}\frac{1}{\rho}\mathrm{erf}\left(\frac{\rho}{2^{1/2}}\right)$	$\frac{1}{(2\pi)^{3/2}} e^{-\rho^2/2}$	$\frac{1}{4\pi}\left(\mathrm{erf}\left(\frac{\rho}{2^{1/2}}\right) - \left(\frac{2}{\pi}\right)^{1/2} \rho\, e^{-\rho^2/2}\right)$	∞	2
Gaussian; $\zeta(\rho)$, $\eta(\rho) > 0$; yields 2-D Gaussian.				
	$\frac{3}{4\pi} e^{-\rho^3}$	$\frac{1}{4\pi}\left(1 - e^{-\rho^3}\right)$	∞	2
$\zeta(\rho) > 0$, $\eta(\rho) \not> 0$.				
	$\frac{3}{4\pi}\,\mathrm{sech}^2(\rho^3)$	$\frac{1}{4\pi}\tanh(\rho^3)$	∞	2
$\zeta(\rho) > 0$, $\eta(\rho) \not> 0$.				
$\frac{1}{4\pi}\left(\frac{1}{\rho}\mathrm{erf}\left(\frac{\rho}{2^{1/2}}\right) + \frac{1}{(2\pi)^{1/2}} e^{-\rho^2/2}\right)$	$\frac{1}{(2\pi)^{3/2}}\left(\frac{5}{2} - \frac{\rho^2}{2}\right) e^{-\rho^2/2}$	$\frac{1}{4\pi}\left(\mathrm{erf}\left(\frac{\rho}{2^{1/2}}\right) - \left(\frac{2}{\pi}\right)^{1/2} \rho\left(1 - \frac{\rho^2}{2}\right) e^{-\rho^2/2}\right)$	∞	4
Super-Gaussian; $\zeta(\rho)$, $\eta(\rho) \not> 0$.				

The functions below have, for $\rho > 1$,				
$\frac{1}{4\pi\rho}$	0	$\frac{1}{4\pi}$		
and, for $\rho < 1$,				
$\frac{1}{8\pi}(3 - \rho^2)$	$\frac{3}{4\pi}$	$\frac{1}{4\pi}\rho^3$	1	2
Constant; does not yield 2-D constant.				
$\frac{1}{2\pi^2}\left(\frac{\arcsin\rho}{\rho} + (1-\rho^2)^{1/2}\right)$	$\frac{1}{\pi^2}\frac{1}{(1-\rho^2)^{1/2}}$	$\frac{1}{2\pi^2}\left(\arcsin\rho - \rho(1-\rho^2)^{1/2}\right)$	–	2
Special smoothing that yields 2-D constant.				

Table B.1: Three-dimensional regularization functions

$\chi(\rho)$	$\zeta(\rho) = \nabla^2\chi(\rho) = \frac{(\rho\chi'(\rho))'}{\rho}$	$g(\rho) = \int_0^\rho \zeta(t)\, t\, dt$	m	r
$\frac{1}{4\pi}\log(\rho^2+1)$	$\frac{1}{\pi}\frac{1}{(\rho^2+1)^2}$	$\frac{1}{2\pi}\frac{\rho^2}{\rho^2+1}$	∞	0
Low order algebraic; $\zeta(\rho) > 0$, $\eta(\rho) = -\zeta'(\rho)/\rho > 0$; no convergence since $r = 0$.				
$\frac{1}{4\pi}\left(\log(\rho^2+1) + \frac{\rho^2}{\rho^2+1}\right)$	$\frac{2}{\pi}\frac{1}{(\rho^2+1)^3}$	$\frac{1}{2\pi}\frac{\rho^2(\rho^2+2)}{(\rho^2+1)^2}$	∞	2
High order algebraic; $\zeta(\rho)$, $\eta(\rho) > 0$.				
$\frac{1}{4\pi}\left(\log\left(\frac{\rho^2}{2}\right) + \mathrm{E}_1\left(\frac{\rho^2}{2}\right)\right)$	$\frac{1}{2\pi}e^{-\rho^2/2}$	$\frac{1}{2\pi}(1 - e^{-\rho^2/2})$	∞	2
Gaussian; $\zeta(\rho)$, $\eta(\rho) > 0$.				
	$\frac{1}{\pi}\mathrm{sech}^2(\rho^2)$	$\frac{1}{2\pi}\tanh(\rho^2)$	∞	2
$\zeta(\rho) > 0$, $\eta(\rho) \not> 0$.				
	$\frac{2}{\pi}\frac{(2-\rho^2)}{(\rho^2+1)^4}$	$\frac{1}{2\pi}\frac{\rho^2(\rho^4+3\rho^2+4)}{(\rho^2+1)^3}$	∞	3
Super-algebraic; $\zeta(\rho)$, $\eta(\rho) \not> 0$.				
$\frac{1}{4\pi}\left(\log\left(\frac{\rho^2}{2}\right) + \mathrm{E}_1\left(\frac{\rho^2}{2}\right) - e^{-\rho^2/2}\right)$	$\frac{1}{2\pi}\left(2 - \frac{\rho^2}{2}\right)e^{-\rho^2/2}$	$\frac{1}{2\pi}\left(1 - \left(1 - \frac{\rho^2}{2}\right)e^{-\rho^2/2}\right)$	∞	4
Super-Gaussian; $\zeta(\rho)$, $\eta(\rho) \not> 0$.				
	$\frac{1}{2\pi}\frac{\mathrm{J}_1(\rho)}{\rho}$	$\frac{1}{2\pi}(1 - \mathrm{J}_0(\rho))$	∞	∞
$\zeta(\rho)$, $\eta(\rho) \not> 0$; spectral like convergence since $r = \infty$.				

The functions below have, for $\rho > 1$,				
$\frac{1}{2\pi}\log\rho$	0	$\frac{1}{2\pi}$		
and, for $\rho < 1$,				
$\frac{1}{4\pi}(\rho^2 - 1)$	$\frac{1}{\pi}$	$\frac{1}{2\pi}\rho^2$	1	2
Constant.				
$\frac{1}{2\pi}\left(\log(1 + (1-\rho^2)^{1/2}) - \frac{1}{3}(1-\rho^2)^{3/2} - (1-\rho^2)^{1/2}\right)$	$\frac{3}{2\pi}(1-\rho^2)^{1/2}$	$\frac{1}{2\pi}(1 - (1-\rho^2)^{3/2})$	2	2
Projection of 3-D constant smoothing.				
	$\frac{1}{\pi\,\mathrm{E}_2(1)}e^{-1/(1-\rho^2)}$	$\frac{1}{2\pi}\left(1 - (1-\rho^2)\frac{\mathrm{E}_2\left(\frac{1}{1-\rho^2}\right)}{\mathrm{E}_2(1)}\right)$	∞	2
Only smoothing which is $\mathcal{C}^\infty$ and of compact support.				

Table B.2: Two-dimensional regularization functions

Appendix C

Mathematical derivations needed in the development of a three-dimensional velocity smoothing that reproduces Kelvin's lowest mode dispersion relation.

The principles that lead to a three-dimensional velocity smoothing that best reproduces Kelvin's lowest mode dispersion relation are outlined in Section 2.4.3.

First, the evaluation of the inverse Fourier transform of $\hat{Q}(l)$ given by Equation (2.117) is examined. The parameter c^2 is real and positive so that $\hat{Q}(l)$ is real for l real. In what follows, the definition of $\hat{Q}(l)$ is extended to the complex plane so as to be able to evaluate the inverse Fourier transform of $\hat{Q}(l)$ using integration in the complex plane [23]. $\hat{Q}(l)$ is first rescaled by writing

$$\hat{P}(l) = \frac{\hat{Q}(2l)}{2} = \frac{1 + l^2 \log l^2}{(c\,l)^4 + (1/2 - 2\gamma)\,l^2 + 1} = \frac{1 + l^2 \log l^2}{c^4 (l^2 + u^2)(l^2 + \bar{u}^2)}\,, \tag{C.1}$$

where

$$\begin{cases} u & = \eta + i\mu, \qquad \eta, \mu \text{ real and positive}, \\ \bar{u} & \text{is the complex conjuguate of } u\,, \\ \xi^2 & = (1 + (1/4 - \gamma)/c^2)/(2\,c^2)\,, \\ \mu^2 & = (1 - (1/4 - \gamma)/c^2)/(2\,c^2)\,. \end{cases}$$

Notice that one needs $c^2 > \gamma - 1/4 = .32722$ for ξ and μ to be real. This inequality will be satisfied because the best fit to Kelvin's dispersion relation occurs at $c^2 = 1.43$. With the above scaling (C.1), it is easy to show that $Q(\rho) = 4\,P(2\rho)$, where $P(\rho)$ is the inverse Fourier transform of $\hat{P}(l)$.

The inverse Fourier transform of $\hat{P}(l)$ is done by considering each term separately, i.e.,

$$\hat{P}(l) = \hat{P}_1(l) + \hat{P}_2(l) = \frac{1}{c^4 (l^2 + u^2)(l^2 + \bar{u}^2)} + \frac{l^2 \log l^2}{c^4 (l^2 + u^2)(l^2 + \bar{u}^2)}\,, \tag{C.2}$$

where the denominator of each term can be factored as

$$(l^2 + u^2)(l^2 + \bar{u}^2) = (l + iu)(l - iu)(l + i\bar{u})(l - i\bar{u})\,. \tag{C.3}$$

First, the inverse Fourier transform of $\hat{P}_1(l)$ is considered,

$$P_1(\rho) = \frac{1}{2\pi c^4} \int_{-\infty}^{\infty} \frac{e^{il\rho}}{(l+iu)(l-iu)(l+i\bar{u})(l-i\bar{u})}\, dl\,. \tag{C.4}$$

Since $\rho > 0$, the contour integral on the contour $\mathcal{C} = \mathcal{C}_1 + \mathcal{C}_2$ as shown in Figure J.19 is considered. The integral on the upper half circle $\mathcal{C}_2$ vanishes as $R \to \infty$ by use of Jordan's Lemma. Making use of the Residue Theorem, one then obtains

$$\begin{aligned} P_1(\rho) &= \frac{i}{c^4}\left[\frac{e^{il\rho}}{(l+iu)(l+i\bar{u})(l-i\bar{u})}\bigg|_{l=iu} + \frac{e^{il\rho}}{(l+iu)(l-iu)(l+i\bar{u})}\bigg|_{l=i\bar{u}}\right] \\ &= \frac{1}{2\,c^4}\frac{1}{(u^2-\bar{u}^2)}\left(\frac{e^{-\rho\bar{u}}}{\bar{u}} - \frac{e^{-\rho u}}{u}\right)\,. \end{aligned} \tag{C.5}$$

The evaluation of the inverse Fourier transform of $\hat{P}_2(l)$ is more difficult. The contour $\mathcal{C} = \mathcal{C}_1 + \mathcal{C}_2 + \mathcal{C}_3 + \mathcal{C}_4$ shown in Figure J.20 is used, and therefore,

$$\begin{aligned} P_2(\rho) &= \frac{1}{2\pi c^4} \int_{-\infty}^{\infty} \frac{l^2 \log l^2\, e^{il\rho}}{(l+iu)(l-iu)(l+i\bar{u})(l-i\bar{u})}\, dl \\ &= \frac{1}{\pi c^4} \Re\left[\int_0^{\infty} \frac{l^2 \log l^2\, e^{il\rho}}{(l+iu)(l-iu)(l+i\bar{u})(l-i\bar{u})}\, dl\right]\,. \end{aligned} \tag{C.6}$$

Notice the two branch cuts of the function $\log l^2$ respectively on the positive and negative real axis. The real part of the integral on $\mathcal{C}_1$ is the integral of interest. The integral on $\mathcal{C}_2$ is shown to vanish as $R \to \infty$ by use of Jordan's Lemma. The integral on $\mathcal{C}_4$ is done using a small quarter circle of radius ϵ and vanishes as $\epsilon \to 0$. Finally, the integral on $\mathcal{C}_3$ gives, with the substitution $l = it$,

$$\int_{\mathcal{C}_3} \cdots dl = \frac{i}{\pi c^4} \int_0^{\infty} \frac{t^2 \log t^2\, e^{-\rho t}}{(t^2-u^2)(t^2-\bar{u}^2)}\, dt - \frac{1}{c^4} \int_0^{\infty} \frac{t^2\, e^{-\rho t}}{(t^2-u^2)(t^2-\bar{u}^2)}\, dt\,. \tag{C.7}$$

The first integral in Equation (C.7) is purely imaginary since it is equal to i times a real integral. It will thus not be of interest. Use of the Residue theorem for the contour integral on $\mathcal{C}$ gives

$$\int_{\mathcal{C}} \cdots dl = \frac{2\,i}{c^4}\, \mathcal{R}es\left(\frac{l^2 \log l^2\, e^{il\rho}}{(l+iu)(l-iu)(l+i\bar{u})(l-i\bar{u})}\right)_{l=i\bar{u}} = -\frac{1}{c^4}\left(\frac{\bar{u}\log_p(-\bar{u}^2)\, e^{-\rho\bar{u}}}{(u^2-\bar{u}^2)}\right), \tag{C.8}$$

where $\log_p$ stands for the principal logarithm. Combining all the terms of interest, one obtains

$$P_2(\rho) = \frac{1}{c^4}\left[\int_0^{\infty} \frac{t^2\, e^{-\rho t}}{(t^2-u^2)(t^2-\bar{u}^2)}\, dt - \Re\left(\frac{\bar{u}\log_p(-\bar{u}^2)\, e^{-\rho\bar{u}}}{(u^2-\bar{u}^2)}\right)\right]\,. \tag{C.9}$$

Adding $P_1(\rho)$ and $P_2(\rho)$ to obtain $P(\rho)$, and recalling that $Q(\rho) = 4\,P(2\rho)$, one finally obtains

$$\begin{aligned} Q(\rho) &= \frac{2}{c^4}\left[\frac{1}{(u^2-\bar{u}^2)}\left(\frac{e^{-2\rho\bar{u}}}{\bar{u}} - \frac{e^{-2\rho u}}{u}\right)\right. \\ &\qquad \left. +2\int_0^\infty \frac{t^2\,e^{-2\rho t}}{(t^2-u^2)(t^2-\bar{u}^2)}\,dt - 2\Re\left(\frac{\bar{u}\log_p(-\bar{u}^2)\,e^{-2\rho\bar{u}}}{(u^2-\bar{u}^2)}\right)\right] . \end{aligned} \tag{C.10}$$

The function $Q(\rho)$ must now be integrated according to Equation (2.114) in order to obtain $q(\rho)$, the three-dimensional velocity smoothing that reproduces Kelvin's lowest mode dispersion relation. Hence,

$$\begin{aligned} \frac{c^4}{2}\frac{4\pi q(\rho)}{\rho} &= -\frac{1}{(u^2-\bar{u}^2)}\int_0^\rho y\left(\frac{e^{-2y\bar{u}}}{\bar{u}} - \frac{e^{-2yu}}{u}\right)dy \\ &\quad -2\int_0^\rho y\left(\int_0^\infty \frac{t^2\,e^{-2yt}}{(t^2-u^2)(t^2-\bar{u}^2)}\,dt\right)dy + 2\Re\left(\frac{\bar{u}\log_p(-\bar{u}^2)}{(u^2-\bar{u}^2)}\int_0^\rho y\,e^{-2y\bar{u}}\,dy\right) \\ &\quad +\text{constant} . \end{aligned} \tag{C.11}$$

The first and third integrals in Equation (C.11) are easy to carry out,

$$\begin{aligned} \int_0^\rho y\,e^{-2y\bar{u}}\,dy &= \frac{1}{4\bar{u}^2}\left(1-(1+2\rho\bar{u})e^{-2\rho\bar{u}}\right) , \\ \int_0^\rho y\left(\frac{e^{-2y\bar{u}}}{\bar{u}} - \frac{e^{-2yu}}{u}\right)dy &= \frac{1}{4(u\bar{u})^3}\left(\bar{u}^3(1+2\rho u)e^{-2\rho u} - u^3(1+2\rho\bar{u})e^{-2\rho\bar{u}}\right) . \end{aligned} \tag{C.12}$$

The second integral in Equation (C.11) is more difficult and is done by interchanging the order of the t and y integral (assuming it converges uniformly, an hypothesis confirmed *a posteriori*). One writes

$$\begin{aligned} 2\int_0^\rho y\left(\int_0^\infty \frac{t^2\,e^{-2yt}}{(t^2-u^2)(t^2-\bar{u}^2)}\,dt\right)dy &= 2\int_0^\infty \frac{t^2}{(t^2-u^2)(t^2-\bar{u}^2)}\left(\int_0^\rho y\,e^{-2yt}\,dy\right)dt \\ &= 2\int_0^\infty \frac{t^2}{(t^2-u^2)(t^2-\bar{u}^2)}\left(\frac{1}{4t^2}\left(1-e^{-2\rho t}\right) - \frac{\rho\,e^{-2\rho t}}{2t}\right)dt \\ &= \frac{1}{2}\int_0^\infty \frac{1}{(t^2-u^2)(t^2-\bar{u}^2)}\,dt - \frac{1}{2}\int_0^\infty \frac{e^{-2\rho t}}{(t^2-u^2)(t^2-\bar{u}^2)}\,dt \\ &\qquad -\rho\int_0^\infty \frac{t\,e^{-2\rho t}}{(t^2-u^2)(t^2-\bar{u}^2)}\,dt . \end{aligned} \tag{C.13}$$

The first integral in Equation (C.13) is done extending the integral from $-\infty$ to ∞ and using contour integration as in Equations (C.4) and (C.5). It leads to

$$\frac{1}{2}\int_0^\infty \frac{1}{(t^2-u^2)(t^2-\bar{u}^2)}\,dt = \frac{i\pi}{4}\frac{(u+\bar{u})}{(u\bar{u})(u^2-\bar{u}^2)} . \tag{C.14}$$

The second integral in Equation (C.13) is done using a partial fraction decomposition of the denominator and recalling the definition of the Exponential Integral of a complex argument

$$\mathrm{E}_1(z) = \int_z^\infty \frac{e^{-t}}{t}\,dt\,, \qquad |arg\, z| < \pi\,. \tag{C.15}$$

It leads to

$$\begin{aligned}
&\frac{1}{2}\int_0^\infty \frac{e^{-2\rho t}}{(t^2-u^2)(t^2-\bar{u}^2)}\,dt \\
&\quad = \frac{1}{4(u^2-\bar{u}^2)}\left[\frac{1}{u}\left(-\int_0^\infty \frac{e^{-2\rho t}}{t+u}\,dt + \int_0^\infty \frac{e^{-2\rho t}}{t-u}\,dt\right)\right. \\
&\qquad\qquad \left. +\frac{1}{\bar{u}}\left(\int_0^\infty \frac{e^{-2\rho t}}{t+\bar{u}}\,dt - \int_0^\infty \frac{e^{-2\rho t}}{t-\bar{u}}\,dt\right)\right] \\
&\quad = \frac{1}{4(u^2-\bar{u}^2)}\left[\frac{1}{u}\left(-e^{2\rho u}\mathrm{E}_1(2\rho u) + e{-}2\rho u\mathrm{E}_1(-2\rho u)\right)\right. \\
&\qquad\qquad \left. +\frac{1}{\bar{u}}\left(e^{2\rho\bar{u}}\mathrm{E}_1(2\rho\bar{u}) - e^{-2\rho\bar{u}}\mathrm{E}_1(-2\rho\bar{u})\right)\right] \\
&\quad = \frac{i}{2(u^2-\bar{u}^2)(u\bar{u})}\,\Im\left(\bar{u}\left(e^{-2\rho u}\mathrm{E}_1(-2\rho u) - e^{2\rho u}\mathrm{E}_1(2\rho u)\right)\right)\,,
\end{aligned} \tag{C.16}$$

where use has been made of the symmetry relation $\mathrm{E}_1(\bar{z}) = \bar{\mathrm{E}}_1(z)$. The third integral in Equation (C.13) is done in a similar way and leads to

$$\begin{aligned}
&\int_0^\infty \frac{t\,e^{-2\rho t}}{(t^2-u^2)(t^2-\bar{u}^2)}\,dt \\
&\quad = \frac{1}{2(u^2-\bar{u}^2)}\left[\int_0^\infty \frac{e^{-2\rho t}}{t+u}\,dt + \int_0^\infty \frac{e^{-2\rho t}}{t-u}\,dt - \int_0^\infty \frac{e^{-2\rho t}}{t+\bar{u}}\,dt - \int_0^\infty \frac{e^{-2\rho t}}{t-\bar{u}}\,dt\right] \\
&\quad = \frac{1}{2(u^2-\bar{u}^2)}\left[e^{2\rho u}\mathrm{E}_1(2\rho u) + e^{-2\rho u}\mathrm{E}_1(-2\rho u) - e^{2\rho\bar{u}}\mathrm{E}_1(2\rho\bar{u}) - e^{-2\rho\bar{u}}\mathrm{E}_1(-2\rho\bar{u})\right] \\
&\quad = \frac{i}{(u^2-\bar{u}^2)}\,\Im\left(e^{2\rho u}\mathrm{E}_1(2\rho u) + e^{-2\rho u}\mathrm{E}_1(-2\rho u)\right)\,.
\end{aligned} \tag{C.17}$$

Combining the integrals appropriately and making some algebraic simplifications, an expression for $q(\rho)$ emerges:

$$\begin{aligned}
c^4\frac{4\pi q(\rho)}{\rho} \;=\; & \frac{1}{2(u^2-\bar{u}^2)(u\bar{u})^3}\left(u^3(1+2\rho\bar{u})e^{-2\rho\bar{u}} - \bar{u}^3(1+2\rho u)e^{-2\rho u}\right) \\
& - \Re\left(\frac{\log_p(-\bar{u}^2)}{(u^2-\bar{u}^2)\bar{u}}(1+2\rho\bar{u})e^{-2\rho\bar{u}}\right) \\
& + \frac{i}{(u^2-\bar{u}^2)}\left[2\rho\,\Im\left(e^{2\rho u}\mathrm{E}_1(2\rho u) + e^{-2\rho u}\mathrm{E}_1(-2\rho u)\right)\right. \\
& \qquad \left. -\frac{1}{(u\bar{u})}\,\Im\left(\bar{u}\left(e^{2\rho u}\mathrm{E}_1(2\rho u) - e^{-2\rho u}\mathrm{E}_1(-2\rho u)\right)\right)\right] \\
& + d\,.
\end{aligned} \tag{C.18}$$

It can be shown that Equation (C.18) is purely real as it should be. The constant d is determined so that $4\pi q(\rho) \to 1$ as $\rho \to \infty$. A tedious asymptotic expansion of $q(\rho)$, using [1]

$$\mathrm{E}_1(z) \sim \frac{e^{-z}}{z}\left(1 - \frac{1}{z} + \frac{1\cdot 2}{z^2} - \frac{1\cdot 2\cdot 3}{z^3} + \cdots\right), \qquad |\arg z| < 3\pi/2\,, \tag{C.19}$$

shows that $d = 0$. An also tedious Taylor series expansion of $q(\rho)$, using [1]

$$\mathrm{E}_1(z) = -\gamma - \log z - \sum_{n=1}^{\infty} \frac{(-1)^n z^n}{n\, n!}, \qquad |\arg z| < \pi\,, \tag{C.20}$$

leads to

$$4\pi q(\rho) = A\,\rho + B\,\rho^3 + \cdots \tag{C.21}$$

for small ρ, with

$$\begin{aligned} A &= \frac{1}{c^4}\left[\frac{(u^2+\bar{u}^2+u\bar{u})}{2(u+\bar{u})(u\bar{u})^3} - \Re\left(\frac{\log_p(-\bar{u}^2)}{(u^2-\bar{u}^2)\bar{u}}\right) + \frac{i\pi}{(u^2-\bar{u}^2)(u\bar{u})}\,\Re(u)\right], \\ B &= \frac{1}{c^4}\left[\frac{-1}{(u+\bar{u})(u\bar{u})} + 2\Re\left(\frac{\bar{u}\log_p(-\bar{u}^2)}{(u^2-\bar{u}^2)}\right) - \frac{2i\pi}{(u^2-\bar{u}^2)}\,\Re(u)\right]. \end{aligned} \tag{C.22}$$

Notice that $q(\rho)$ is $\mathcal{O}(\rho)$ for small ρ, as opposed to classical velocity smoothings that are $\mathcal{O}(\rho^3)$ for small ρ. This point is examined further in Section 2.4.3

The numerical evaluation of the new $q(\rho)$ function is challenging in itself. It is done using complex variables, with $\mathrm{E}_1(z)$ computed using a Taylor series expansion for small z, Equation (C.20), and a continued fraction approximation for large z, with [1]

$$\mathrm{E}_1\left(\frac{1}{z}\right) = e^{-1/z}\,\cfrac{a_0 z}{1+\cfrac{a_1 z}{1+\cfrac{a_2 z}{1+\cdots}}}, \qquad |\arg z| < \pi\,, \tag{C.23}$$

with $a_0 = 1$, $a_{2n} = n$ and $a_{2n+1} = n+1$. The continued fraction is itself evaluated using the method of Padé Approximants [19].

Below is a listing of the Fortran program which evaluates the function $q(\rho)$ for any value of the adjustable parameter c^2. The values of A and B are also evaluated using Equation (C.22). For $c^2 = 1.43$, these values are $A = .8620589$ and $B = -1.176992$.

```
c ***************************************************************************
c
        IMPLICIT COMPLEX*16 (C,Z)
        IMPLICIT REAL*8 (A-B,D-H,O-Y)
        IMPLICIT INTEGER*4 (I-N)
c
        READ(5,*)SQC
        READ(5,*)YFIRST
        READ(5,*)YLAST
        READ(5,*)M
        READ(5,*)EPSI1
        READ(5,*)EPSI2
        READ(5,*)SWITCH
c SQC = c**2 coefficient, Yfirst = first value of y for which to compute q(y)
c YLAST= last value of y for which to compute q(y). M =Total number of points
c for which to compute q(y). EPSI1=accuracy coefficient for the computation
c of the exponential integral function of a complex argument z using a Taylor
c series expansion. EPSI2= same but for the continued fraction approximation.
c SWITCH= that value of abs(z) where we switch from the Taylor series
c expansion to the continued fraction approximation. The continued fraction is
c itself evaluated using the method of Pade Approximants.
c
c The input 1.43, 0., 20., 2001, 1.e-13, 1.e-13 will generate q(y)
c from y =0. to y=20. by deltay=.01 with a lot of accuracy.
c
        RANGE=YLAST-YFIRST
        DELTAY=RANGE/DFLOTJ(M-1)
        PI=3.14159265358979323846264 3
        GAM=.57721566490153286060651 2
        D1=1.
        D2=2.
        D12=1./2.
        D14=1./4.
        ONUL=0.
        ETA=(D1+((D14-GAM)/SQC))/(D2*SQC)
        ETA=DSQRT(ETA)
        EMU=(D1-((D14-GAM)/SQC))/(D2*SQC)
        EMU=DSQRT(EMU)
c
        CU=DCMPLX(ETA,EMU)
        CUSTAR=DCONJG(CU)
        CUSQ=CU*CU
        CUSTSQ=CUSTAR*CUSTAR
        CUCUSTAR=CU*CUSTAR
        CUCUSTARS=CU+CUSTAR
        CUCUSTARM=CU-CUSTAR
        CUSQCUSTSQ=CUSQ-CUSTSQ
c
c Computation of the term in y and y**3 in q(y) for small y's.
c
        C11=(0.,1.)*CUSTAR
        C11=C11*C11
        C11=CDLOG(C11)/(CUSTAR*CUSQCUSTSQ)
c
        A=ETA*PI
        CA=DCMPLX(A,ONUL)
        CA=(CA*(0.,1.))/CUSQCUSTSQ
        CACOEF=CA/(D2*CUCUSTAR)
        CBCOEF=-CA
        PLOG=DREAL(C11)
        CACOEF=CACOEF-(DCMPLX(PLOG)/D2)
        PP=DREAL(C11*CUSTSQ)
        CBCOEF=CBCOEF+DCMPLX(PP)
        CACOEF=CACOEF+((CUSQ+CUCUSTAR+CUSTSQ)/(D2*D2*CUCUSTARS*CUCUSTAR*
```

```
     ~   CUCUSTAR*CUCUSTAR))
         CBCOEF=CBCOEF-(D1/(D2*CUCUSTARS*CUCUSTAR))
         ACOEF=DREAL(CACOEF)
         ACOEF=(ACOEF*D2)/(SQC*SQC)
         BCOEF=DREAL(CBCOEF)
         BCOEF=(BCOEF*D2)/(SQC*SQC)
         WRITE(6,*)ACOEF,BCOEF
C
c Acoef and Bcoef are the coefficients such that q(y)=~ Acoef*y +Bcoef*(y**3)
c + ... for small y.
C
         DO 10 I=1,M
         Y=YFIRST+DFLOTJ(I-1)*DELTAY
         IF(Y.EQ.0.)THEN
         Q=0.
         WRITE(6,*)Y,Q
         GOTO 20
         ENDIF
C
         C1=D2*Y*CU
         C2=CEXPINTG1(C1,EPSI1,EPSI2,SWITCH)
         C3=CDEXP(C1)
         C4=-C1
         C5=CEXPINTG1(C4,EPSI1,EPSI2,SWITCH)
         C6=CDEXP(C4)
         C7=D2*Y*CUSTAR
         C8=CDEXP(-C7)
         C9=(C3*C2-C6*C5)*CUSTAR
         C10=C3*C2+C6*C5
         B9=DIMAG(C9)
         C9=DCMPLX(B9,ONUL)
         B10=Y*DIMAG(C10)
         C10=DCMPLX(B10,ONUL)
         CTERM1=(C9/(D2*CUCUSTAR))-C10
         CTERM1=CTERM1/CUSQCUSTSQ
         CTERM1=CTERM1*(0.,1.)
         CTERM1=-CTERM1
C
         C12=C8*(D1+C7)
         CTERM2=C12*C11
         BTERM2=DREAL(CTERM2)
         CTERM2=DCMPLX(BTERM2,ONUL)
         CTERM2=(-CTERM2)/D2
C
         CTERM3=C12*CU*CUSQ
         CTERM3=CTERM3-(CUSTAR*CUSTSQ*C6*(D1+C1))
         CTERM3=CTERM3/(CUSQCUSTSQ*D2*D2*CUCUSTAR*CUCUSTAR*CUCUSTAR)
C
         CTERM=CTERM1+CTERM2+CTERM3
C
         Q=DREAL(CTERM)
         Q=(D2*Y*Q)/(SQC*SQC)
         WRITE(6,*)Y,Q
20       CONTINUE
10       CONTINUE
         STOP
         END
C
c *************************************************************************
C
         DOUBLE COMPLEX FUNCTION CEXPINTG1(Z,EPSI1,EPSI2,SWITCH)
C
         IMPLICIT COMPLEX*16 (C,Z)
         IMPLICIT REAL*8 (A-B,D-H,O-Y)
```

```
      IMPLICIT INTEGER*4 (I,N)

      GAM=.57721566490153286060606512
      D2=2.
      D1=1.
      ONUL=0.
C
      ABSZ=CDABS(Z)
      IF(ABSZ.LE.SWITCH)GOTO 10
C
C The continued fraction approximation:
C
      ZETA=(1.,0.)/Z
C
      ZEST1=(1.,0.)
C
      K=0
200   K=K+1
      ZEST2=(1.,0.)
      DO 30 I=1,K
      J=(K+1)-I
      FLTJ=DFLOTJ(J)
      JJ=JIDINT((FLTJ+D1)/D2)
      AJ=DFLOTJ(JJ)
C
      ZEST2=(AJ*ZETA*ZEST2)+(1.,0.)
      ZEST2=(1.,0.)/ZEST2
30    CONTINUE
C
      TEST=CDABS((ZEST2-ZEST1))
      ZEST1=ZEST2
      IF(TEST.GE.EPSI2)GOTO 200
C
      ZT=ZEST2*ZETA*CDEXP(-Z)
      GOTO 300
C
C The Taylor series expansion:
C
10    CONTINUE
      SIGN=1.
      ZLOCAL=(1.,0.)
      ZSUM1=(0.,0.)
      DCOEFF=.01
      K=0
100   K=K+1
      SIGN=-SIGN
      FLTK=DFLOTJ(K)
      ZLOCAL=ZLOCAL*(Z/FLTK)
      ZSUM2=ZSUM1+((SIGN*ZLOCAL)/FLTK)
      TEST=CDABS((ZSUM2-ZSUM1)/(ZSUM2+DCOEFF))
      ZSUM1=ZSUM2
      IF(TEST.GE.EPSI1)GOTO 100
      ZT=-ZSUM2-DCMPLX(GAM,ONUL)-CDLOG(Z)
C
300   CONTINUE
      CEXPINTG1=ZT
      RETURN
      END
C
C ***************************************************************************
```

Appendix D

The numerical computation of an infinite periodic vortex filament

A numerical procedure that was originally introduced by Moore (1972) for the computation of finite amplitude perturbations on infinite periodic vortex filaments is described. In the present context, the procedure is modified to account for higher accuracy when the core size σ is not small compared to the wavelength λ. The case of one vortex filament evolving under its own induced velocity is presented. The extension to multiple filaments is straightforward.

Without loss of generality, a vortex filament with a periodicity vector aligned with the x axis, $\boldsymbol{\lambda} = \lambda \hat{\mathbf{e}}_x$ is considered. Then, if s is defined as a material coordinate ranging from -1 to 1 and covering $2p$ wavelengths of the filament as shown in Figure J.21, one obtains, with $\mathbf{x}(s'+m,t) = \mathbf{x}(s',t) + pm\lambda\hat{\mathbf{e}}_x$,

$$\begin{aligned}
\mathbf{u}(\mathbf{x}(s,t),t) &= -\Gamma \int_{-\infty}^{\infty} \frac{g\left(\frac{|\mathbf{x}-\mathbf{x}'|}{\sigma}\right)}{|\mathbf{x}-\mathbf{x}'|^3}(\mathbf{x}-\mathbf{x}') \wedge \frac{\partial \mathbf{x}'}{\partial s'} ds' \\
&= -\Gamma \Bigg[\int_{-1}^{1} \frac{g\left(\frac{|\mathbf{x}-\mathbf{x}'|}{\sigma}\right)}{|\mathbf{x}-\mathbf{x}'|^3}(\mathbf{x}-\mathbf{x}') \wedge \frac{\partial \mathbf{x}'}{\partial s'} ds' \\
&+ \sum_{\substack{m=-\infty \\ m\neq 0}}^{\infty} \int_{-1}^{1} \frac{g\left(\frac{|\mathbf{x}-(\mathbf{x}'+2pm\lambda\hat{\mathbf{e}}_x)|}{\sigma}\right)}{|\mathbf{x}-(\mathbf{x}'+2pm\lambda\hat{\mathbf{e}}_x)|^3}(\mathbf{x}-(\mathbf{x}'+2pm\lambda\hat{\mathbf{e}}_x)) \wedge \frac{\partial \mathbf{x}'}{\partial s'} ds' \Bigg] , \qquad \text{(D.1)}
\end{aligned}$$

where $\mathbf{x}-\mathbf{x}'$ stands for $\mathbf{x}(s,t)-\mathbf{x}(s',t)$. The first integral represents the contribution of $2p$ wavelengths. The second integral represents the contribution of the rest of the filament. p is chosen so that there is no need for a cutoff in the second integral (i.e., $g(\rho) = 1/4\pi$). This is done by requiring that

$$2p\lambda \gg \sigma \, . \qquad \text{(D.2)}$$

If the wavelength of interest λ is much bigger than the core size σ, then it is sufficient to take $p = 1$, i.e., to compute only two wavelengths with the smoothing $g(\rho)$. This is precisely what Moore (1972) did when computing wavelengths much bigger than the core size. Here however, it is desired to be more general and to have the possibility

of computing wavelengths of the order of the core size. This is achieved by increasing the number $2p$ of wavelengths computed with the smoothing $g(\rho)$. Thus,

$$\begin{aligned}\mathbf{u}(\mathbf{x}(s,t),t) &= -\Gamma\left[\int_{-1}^{1}\frac{g\left(\frac{|\mathbf{x}-\mathbf{x}'|}{\sigma}\right)}{|\mathbf{x}-\mathbf{x}'|^3}(\mathbf{x}-\mathbf{x}')\wedge\frac{\partial\mathbf{x}'}{\partial s'}ds'\right.\\ &\left.+\left(\frac{1}{4\pi}\right)\sum_{\substack{m=-\infty\\ m\neq 0}}^{\infty}\int_{-1}^{1}\frac{1}{|\mathbf{x}-(\mathbf{x}'+2pm\lambda\hat{\mathbf{e}}_x)|^3}(\mathbf{x}-(\mathbf{x}'+2pm\lambda\hat{\mathbf{e}}_x))\wedge\frac{\partial\mathbf{x}'}{\partial s'}ds'\right]. \qquad (D.3)\end{aligned}$$

Noticing that the denominator of the second integral is given by

$$\begin{aligned}&|\mathbf{x}-(\mathbf{x}'+2pm\lambda\hat{\mathbf{e}}_x)|^3 =\\ &\qquad\left[|\mathbf{x}-\mathbf{x}'|^2-2(2pm\lambda)\left((\mathbf{x}-\mathbf{x}')\cdot\hat{\mathbf{e}}_x\right)+(2pm\lambda)^2\right]^{\frac{3}{2}}, \qquad (D.4)\end{aligned}$$

one obtains

$$\begin{aligned}\mathbf{u}(\mathbf{x}(s,t),t) &= -\Gamma\left[\int_{-1}^{1}\frac{g\left(\frac{|\mathbf{x}-\mathbf{x}'|}{\sigma}\right)}{|\mathbf{x}-\mathbf{x}'|^3}(\mathbf{x}-\mathbf{x}')\wedge\frac{\partial\mathbf{x}'}{\partial s'}ds'\right.\\ &\left.+\left(\frac{1}{4\pi}\right)\frac{1}{\lambda^2}\int_{-1}^{1}\left[R\left(\frac{\mathbf{x}-\mathbf{x}'}{\lambda}\right)\frac{(\mathbf{x}-\mathbf{x}')}{\lambda}-S\left(\frac{\mathbf{x}-\mathbf{x}'}{\lambda}\right)\hat{\mathbf{e}}_x\right]\wedge\frac{\partial\mathbf{x}'}{\partial s'}ds'\right] \qquad (D.5)\end{aligned}$$

where

$$R(\mathbf{w}) = \sum_{\substack{-\infty\\ m\neq 0}}^{\infty}\frac{1}{[\mathbf{w}\cdot\mathbf{w}-2(2pm)\mathbf{w}\cdot\hat{\mathbf{e}}_x+(2pm)^2]^{\frac{3}{2}}}, \qquad (D.6)$$

$$S(\mathbf{w}) = \sum_{\substack{-\infty\\ m\neq 0}}^{\infty}\frac{2pm}{[\mathbf{w}\cdot\mathbf{w}-2(2pm)\mathbf{w}\cdot\hat{\mathbf{e}}_x+(2pm)^2]^{\frac{3}{2}}}. \qquad (D.7)$$

These infinite series cannot be expressed in terms of elementary functions, but they can be evaluated numerically. Following Moore, a table of R and S is computed for a discrete set of pairs $(\mathbf{w}\cdot\mathbf{w}, \mathbf{w}\cdot\hat{\mathbf{e}}_x)$ and is stored before numerical time integration is started. Then, the value of R and S is computed using bilinear interpolation for the actual $\mathbf{w}$ arising in the computation. The properties $R(-\mathbf{w}) = R(\mathbf{w})$ and $S(-\mathbf{w}) = -S(\mathbf{w})$ allow R and S to be stored only for positive $\mathbf{w}\cdot\hat{\mathbf{e}}_x$. Moreover, since $|\mathbf{w}\cdot\hat{\mathbf{e}}_x| \leq (\mathbf{w}\cdot\mathbf{w})^{\frac{1}{2}}$, R and S are only computed for $0 \leq |\mathbf{w}\cdot\hat{\mathbf{e}}_x| \leq (\mathbf{w}\cdot\mathbf{w})^{\frac{1}{2}}$. This allows for additional savings by storing R_{ij} andS_{ij} in a single matrix $M_{(m+1)\times m}$ with

$$\begin{aligned}R_{ij} &= M(i+1,j)\\ S_{ij} &= M(m+1-i,m+1-j), \qquad (D.8)\end{aligned}$$

for $i = 1,\ldots m$, $j = 1,\ldots m$ and $i \leq j$. The range of $(\mathbf{w}\cdot\mathbf{w})^{\frac{1}{2}}$ for which R and S are computed and stored is the range expected during numerical time integration (typically from 0 to $2p$).

Finally, it is important to notice that, although the range of integration lies over $2p$ wavelengths ($s' \in [-1, 1]$), the dynamics of the filament only need to be computed for one wavelength ($s \in [-\frac{1}{2p}, \frac{1}{2p}]$), as is shown in Figure J.21.

Appendix E

The numerical computation of an infinite, non-periodic vortex filament

A numerical procedure is described which is used to compute the velocity induced by a vortex filament (eventually on itself) which consist of three portions: two semi-infinite colinear filament sections aligned with $\hat{\mathbf{e}}_x$ and one filament section of arbitrary shape that connects smoothly on the two semi-infinite ones (see Figure J.22). If s is a material coordinate along the filament, one has

$$\begin{aligned}
\mathbf{u}(\mathbf{x},t) &= -\Gamma \int_{-\infty}^{\infty} \frac{g\left(\frac{|\mathbf{x}-\mathbf{x}'|}{\sigma}\right)}{|\mathbf{x}-\mathbf{x}'|^3}(\mathbf{x}-\mathbf{x}') \wedge \frac{\partial \mathbf{x}'}{\partial s'} ds' \\
&= -\Gamma \left[\left(\frac{1}{4\pi}\right) \int_{-\infty}^{-1} \frac{(\mathbf{x}-\mathbf{x}')}{|\mathbf{x}-\mathbf{x}'|^3} \wedge \frac{\partial \mathbf{x}'}{\partial s'} ds' + \left(\frac{1}{4\pi}\right) \int_{1}^{\infty} \frac{(\mathbf{x}-\mathbf{x}')}{|\mathbf{x}-\mathbf{x}'|^3} \wedge \frac{\partial \mathbf{x}'}{\partial s'} ds' \right. \\
&\qquad \left. + \int_{-1}^{1} \frac{g\left(\frac{|\mathbf{x}-\mathbf{x}'|}{\sigma}\right)}{|\mathbf{x}-\mathbf{x}'|^3}(\mathbf{x}-\mathbf{x}') \wedge \frac{\partial \mathbf{x}'}{\partial s'} ds' \right], \qquad \text{(E.1)}
\end{aligned}$$

where $\mathbf{x}'$ stands for $\mathbf{x}(s',t)$, and it is assumed that the semi-infinite filament sections are far enough from $\mathbf{x}$ so that there is no need for a smoothing in the Biot-Savart integral (i.e., $g(\rho) = 1/4\pi$). The integral for s' between -1 and 1 is handled numerically in the usual way, using, for instance, parametric cubic splines to represent the filament section $\mathbf{x}(s',t)$ and forcing the splines to connect smoothly on the semi-infinite sections. The other integrals are evaluated analytically. For instance, the velocity contribution of a semi-infinite filament section aligned with $\hat{\mathbf{e}}_x$ and ranging from $x' = -\infty$ to $x' = 0$ gives, for points with $x > 0$,

$$\begin{aligned}
\mathbf{v}(\mathbf{x}) &= -\left(\frac{\Gamma}{4\pi}\right) \int_{-\infty}^{0} \frac{(\mathbf{x}-x'\hat{\mathbf{e}}_x)}{|\mathbf{x}-x'\hat{\mathbf{e}}_x|^3} \wedge \hat{\mathbf{e}}_x dx' \\
&= -\left(\frac{\Gamma}{4\pi}\right)(\mathbf{x} \wedge \hat{\mathbf{e}}_x) \int_{-\infty}^{0} \frac{dx'}{((x-x')^2+(y^2+z^2))^{\frac{3}{2}}} \\
&= -\left(\frac{\Gamma}{4\pi}\right)(\mathbf{x} \wedge \hat{\mathbf{e}}_x) \int_{x}^{\infty} \frac{dx'}{(x''^2+(y^2+z^2))^{\frac{3}{2}}}
\end{aligned}$$

$$= -\left(\frac{\Gamma}{4\pi}\right)(\mathbf{x}\wedge\hat{\mathbf{e}}_x)\frac{1}{(y^2+z^2)}\left(1-\frac{1}{\left(1+\left(\frac{y^2+z^2}{x^2}\right)\right)^{\frac{1}{2}}}\right). \qquad \text{(E.2)}$$

For $(y^2+z^2)/x^2 \geq \epsilon^2$, Equation (E.2) is used. For $(y^2+z^2)/x^2 < \epsilon^2$, it is better to use a Taylor series expansion,

$$\mathbf{v}(\mathbf{x}) = -\left(\frac{\Gamma}{4\pi}\right)(\mathbf{x}\wedge\hat{\mathbf{e}}_x)\frac{1}{2x^2}\left(1-\frac{3}{4}\left(\frac{y^2+z^2}{x^2}\right)\left(1-\frac{5}{6}\left(\frac{y^2+z^2}{x^2}\right)\left(1+\cdots\right)\right)\right). \qquad \text{(E.3)}$$

Using double accuracy, it was found that $\epsilon = 10^{-2}$ is a good choice for switching from Equation (E.2) to Equation (E.3).

An expression similar to Equation (E.2) can be found for the velocity contribution of a semi-infinite filament section aligned with $\hat{\mathbf{e}}_x$, but ranging from $x' = 0$ to $x' = \infty$.

Appendix F

The evolution equations for a set of vortex particles

The evolution equations for the position and strength vector of a set of regularized vortex particles are

$$\begin{aligned}
\frac{d}{dt}\mathbf{x}^p(t) &= \mathbf{u}_\sigma(\mathbf{x}^p(t),t)\,, && \text{(F.1)}\\
\frac{d}{dt}\boldsymbol{\alpha}^p(t) &= (\boldsymbol{\alpha}^p(t)\cdot\nabla)\,\mathbf{u}_\sigma(\mathbf{x}^p(t),t)\,, \quad \text{(classical scheme)}\\
\frac{d}{dt}\boldsymbol{\alpha}^p(t) &= \left(\boldsymbol{\alpha}^p(t)\cdot\nabla^T\right)\mathbf{u}_\sigma(\mathbf{x}^p(t),t)\,, \quad \text{(transpose scheme)}\\
\frac{d}{dt}\boldsymbol{\alpha}^p(t) &= \frac{1}{2}\left(\boldsymbol{\alpha}^p(t)\cdot\left(\nabla+\nabla^T\right)\right)\mathbf{u}_\sigma(\mathbf{x}^p(t),t)\,, \quad \text{(mixed scheme)} && \text{(F.2)}
\end{aligned}$$

for $1 \le p \le N$, with

$$\mathbf{u}_\sigma(\mathbf{x},t) = \sum_q \nabla\left(\chi_\sigma(\mathbf{x}-\mathbf{x}^q)\right)\wedge\boldsymbol{\alpha}^q = -\sum_q \frac{g_\sigma(\mathbf{x}-\mathbf{x}^q)}{|\mathbf{x}-\mathbf{x}^q|^3}(\mathbf{x}-\mathbf{x}^q)\wedge\boldsymbol{\alpha}^q\,. \qquad \text{(F.3)}$$

The classical scheme leads to

$$\begin{aligned}
\frac{d}{dt}\alpha_i^p &= \alpha_l^p\frac{\partial u_i}{\partial x_l} = \alpha_l^p\frac{\partial}{\partial x_l}\left[\sum_q \epsilon_{ijk}\frac{\partial}{\partial x_j}\chi_\sigma(\mathbf{x}-\mathbf{x}^q)\,\alpha_k^q\right]_{\mathbf{x}=\mathbf{x}^p}\\
&= \sum_q \epsilon_{ijk}\,\alpha_l^p\,\alpha_k^q\left(\frac{\partial}{\partial x_l}\frac{\partial}{\partial x_j}\chi_\sigma(\mathbf{x}-\mathbf{x}^q)\right)_{\mathbf{x}=\mathbf{x}^p}\,. \qquad \text{(F.4)}
\end{aligned}$$

Defining $\rho = |\mathbf{x}|/\sigma = (x_m x_m)^{1/2}/\sigma$ with $\frac{\partial\rho}{\partial x_i} = \frac{x_i}{\sigma^2\rho}$, and recalling that $\frac{1}{\rho}\frac{d\chi}{d\rho} = -\frac{g(\rho)}{\rho^3}$, one obtains

$$\begin{aligned}
\frac{\partial}{\partial x_l}\frac{\partial}{\partial x_j}\chi_\sigma(\mathbf{x}) &= \frac{1}{\sigma}\frac{\partial}{\partial x_l}\frac{\partial}{\partial x_j}\chi(\rho) = \frac{1}{\sigma}\frac{\partial}{\partial x_l}\left(\frac{\partial\rho}{\partial x_j}\frac{d\chi}{d\rho}\right)\\
&= \frac{1}{\sigma^3}\frac{\partial}{\partial x_l}\left(\frac{x_j}{\rho}\frac{d\chi}{d\rho}\right) = -\frac{1}{\sigma^3}\frac{\partial}{\partial x_l}\left(x_j\frac{g(\rho)}{\rho^3}\right)\\
&= -\frac{1}{\sigma^3}\left[\frac{g(\rho)}{\rho^3}\delta_{lj} + x_j\frac{\partial\rho}{\partial x_l}\frac{d}{d\rho}\left(\frac{g(\rho)}{\rho^3}\right)\right]\\
&= -\frac{1}{\sigma^3}\left[\frac{g(\rho)}{\rho^3}\delta_{lj} + \frac{x_j x_l}{\sigma^2}\frac{1}{\rho}\frac{d}{d\rho}\left(\frac{g(\rho)}{\rho^3}\right)\right]\,, \qquad \text{(F.5)}
\end{aligned}$$

so that finally, for the classical scheme

$$\frac{d}{dt}\alpha_i^p = -\sum_q \frac{1}{\sigma^3}\epsilon_{ijk}\alpha_l^p\alpha_k^q\left[\frac{g(\rho)}{\rho^3}\delta_{jl} + \frac{1}{\sigma^2\rho}\frac{d}{d\rho}\left(\frac{g(\rho)}{\rho^3}\right)(x_j^p - x_j^q)(x_l^p - x_l^q)\right] ,$$

$$\frac{d}{dt}\boldsymbol{\alpha}^p = -\sum_q \frac{1}{\sigma^3}\left[\frac{g(\rho)}{\rho^3}\boldsymbol{\alpha}^p\wedge\boldsymbol{\alpha}^q + \frac{1}{\sigma^2\rho}\frac{d}{d\rho}\left(\frac{g(\rho)}{\rho^3}\right)(\boldsymbol{\alpha}^p\cdot(\mathbf{x}^p-\mathbf{x}^q))((\mathbf{x}^p-\mathbf{x}^q)\wedge\boldsymbol{\alpha}^q)\right] , \tag{F.6}$$

with $\rho = |\mathbf{x}^p - \mathbf{x}^q|/\sigma$. In a similar way, the transpose scheme gives

$$\frac{d}{dt}\alpha_i^p = \alpha_l^p\frac{\partial u_l}{\partial x_i} = \alpha_l^p\frac{\partial}{\partial x_i}\left[\sum_q \epsilon_{ljk}\frac{\partial}{\partial x_j}\chi_\sigma(\mathbf{x}-\mathbf{x}^q)\,\alpha_k^q\right]_{\mathbf{x}=\mathbf{x}^p} , \tag{F.7}$$

which leads to

$$\frac{d}{dt}\boldsymbol{\alpha}^p = -\sum_q \frac{1}{\sigma^3}\left[-\frac{g(\rho)}{\rho^3}\boldsymbol{\alpha}^p\wedge\boldsymbol{\alpha}^q + \frac{1}{\sigma^2\rho}\frac{d}{d\rho}\left(\frac{g(\rho)}{\rho^3}\right)\Big(\boldsymbol{\alpha}^p\cdot((\mathbf{x}^p-\mathbf{x}^q)\wedge\boldsymbol{\alpha}^q)\Big)(\mathbf{x}^p-\mathbf{x}^q)\right] . \tag{F.8}$$

The combination of the above two schemes gives the mixed scheme

$$\begin{aligned}\frac{d}{dt}\boldsymbol{\alpha}^p &= -\frac{1}{2}\sum_q \frac{1}{\sigma^3}\frac{1}{\sigma^2\rho}\frac{d}{d\rho}\left(\frac{g(\rho)}{\rho^3}\right)\Big[(\boldsymbol{\alpha}^p\cdot(\mathbf{x}^p-\mathbf{x}^q))((\mathbf{x}^p-\mathbf{x}^q)\wedge\boldsymbol{\alpha}^q) \\ &\qquad + \Big(\boldsymbol{\alpha}^p\cdot((\mathbf{x}^p-\mathbf{x}^q)\wedge\boldsymbol{\alpha}^q)\Big)(\mathbf{x}^p-\mathbf{x}^q)\Big] .\end{aligned} \tag{F.9}$$

In the above formulas, the term $\frac{1}{\rho}\frac{d}{d\rho}\left(\frac{g(\rho)}{\rho^3}\right)$ is evaluated by recalling that

$$\frac{1}{\rho}\frac{d}{d\rho}\left(\frac{g(\rho)}{\rho^3}\right) = \frac{1}{\rho^2}\left(\zeta(\rho) - 3\frac{g(\rho)}{\rho^3}\right) . \tag{F.10}$$

The above equations are the ones used in numerical computations when using regularized vortex particles. Notice that the case of singular vortex particles is obtained by setting $g(\rho) = 1$ with $\frac{1}{\rho}\frac{d}{d\rho}\left(\frac{g(\rho)}{\rho^3}\right) = \frac{-3}{\rho^5}$ and by excluding the term $q = p$ from the above sums.

For completeness, the equations obtained with the high order algebraic smoothing function (B.12) and with the explicit treatment of the viscous diffusion as explained in Section 3.3 are given below. Recalling that $\boldsymbol{\alpha}^p = \boldsymbol{\omega}^p\, vol^p$, the evolution equations are

$$\frac{d}{dt}\mathbf{x}^p = -\frac{1}{4\pi}\sum_q \frac{(|\mathbf{x}^p-\mathbf{x}^q|^2 + \frac{5}{2}\sigma^2)}{(|\mathbf{x}^p-\mathbf{x}^q|^2+\sigma^2)^{\frac{5}{2}}}(\mathbf{x}^p-\mathbf{x}^q)\wedge\boldsymbol{\alpha}^q , \tag{F.11}$$

$$\frac{d}{dt}vol^p = 0 , \tag{F.12}$$

$$
\begin{aligned}
\frac{d}{dt}\boldsymbol{\alpha}^p &= \frac{1}{4\pi}\sum_q \Bigg[-\frac{(|\mathbf{x}^p-\mathbf{x}^q|^2+\frac{5}{2}\sigma^2)}{(|\mathbf{x}^p-\mathbf{x}^q|^2+\sigma^2)^{\frac{5}{2}}}\boldsymbol{\alpha}^p\wedge\boldsymbol{\alpha}^q \\
&\quad +3\frac{(|\mathbf{x}^p-\mathbf{x}^q|^2+\frac{7}{2}\sigma^2)}{(|\mathbf{x}^p-\mathbf{x}^q|^2+\sigma^2)^{\frac{7}{2}}}(\boldsymbol{\alpha}^p\cdot(\mathbf{x}^p-\mathbf{x}^q))((\mathbf{x}^p-\mathbf{x}^q)\wedge\boldsymbol{\alpha}^q) \\
&\quad +105\nu\frac{\sigma^4}{(|\mathbf{x}^p-\mathbf{x}^q|^2+\sigma^2)^{\frac{9}{2}}}(vol^p\,\boldsymbol{\alpha}^q - vol^q\,\boldsymbol{\alpha}^p)\Bigg]\,, \text{ (classical scheme)} \\
\frac{d}{dt}\boldsymbol{\alpha}^p &= \frac{1}{4\pi}\sum_q \Bigg[\frac{(|\mathbf{x}^p-\mathbf{x}^q|^2+\frac{5}{2}\sigma^2)}{(|\mathbf{x}^p-\mathbf{x}^q|^2+\sigma^2)^{\frac{5}{2}}}\boldsymbol{\alpha}^p\wedge\boldsymbol{\alpha}^q \\
&\quad +3\frac{(|\mathbf{x}^p-\mathbf{x}^q|^2+\frac{7}{2}\sigma^2)}{(|\mathbf{x}^p-\mathbf{x}^q|^2+\sigma^2)^{\frac{7}{2}}}\Big(\boldsymbol{\alpha}^p\cdot((\mathbf{x}^p-\mathbf{x}^q)\wedge\boldsymbol{\alpha}^q)\Big)(\mathbf{x}^p-\mathbf{x}^q) \\
&\quad +105\nu\frac{\sigma^4}{(|\mathbf{x}^p-\mathbf{x}^q|^2+\sigma^2)^{\frac{9}{2}}}(vol^p\,\boldsymbol{\alpha}^q - vol^q\,\boldsymbol{\alpha}^p)\Bigg]\,, \text{ (transpose scheme)} \\
\frac{d}{dt}\boldsymbol{\alpha}^p &= \frac{1}{4\pi}\sum_q \Bigg[\frac{3}{2}\frac{(|\mathbf{x}^p-\mathbf{x}^q|^2+\frac{7}{2}\sigma^2)}{(|\mathbf{x}^p-\mathbf{x}^q|^2+\sigma^2)^{\frac{7}{2}}}\Big((\boldsymbol{\alpha}^p\cdot(\mathbf{x}^p-\mathbf{x}^q))((\mathbf{x}^p-\mathbf{x}^q)\wedge\boldsymbol{\alpha}^q) \\
&\qquad\qquad +\Big(\boldsymbol{\alpha}^p\cdot((\mathbf{x}^p-\mathbf{x}^q)\wedge\boldsymbol{\alpha}^q)\Big)(\mathbf{x}^p-\mathbf{x}^q)\Big) \\
&\quad +105\nu\frac{\sigma^4}{(|\mathbf{x}^p-\mathbf{x}^q|^2+\sigma^2)^{\frac{9}{2}}}(vol^p\,\boldsymbol{\alpha}^q - vol^q\,\boldsymbol{\alpha}^p)\Bigg]\,. \text{ (mixed scheme)} \qquad \text{(F.13)}
\end{aligned}
$$

Appendix G

The evaluation of quadratic diagnostics when using vortex filaments or vortex particles

In this appendix, the evaluation of quadratic diagnostics such as kinetic energy, helicity and enstrophy is examined when the vorticity is represented with vortex filaments or with vortex particles.

G.1 The singular case

G.1.1 Singular vortex filaments

Singular vortex filaments define the divergence free vorticity field $\boldsymbol{\omega}$ given by Equation (2.10). The divergence free streamfunction $\boldsymbol{\psi}$ is solution of $\nabla^2\boldsymbol{\psi} = -\boldsymbol{\omega}$ and is given by Equation (2.11). The velocity field $\mathbf{u}$ is given by the curl of the streamfunction, Equation (2.12), and is thus also divergence free.

The kinetic energy is given by

$$E = \frac{1}{2}\int \mathbf{u}\cdot\mathbf{u}\,d\mathbf{x} = \frac{1}{2}\int(\nabla\wedge\boldsymbol{\psi})\cdot(\nabla\wedge\boldsymbol{\psi})\,d\mathbf{x}\,. \tag{G.1}$$

Integration by parts leads to

$$\begin{aligned} E &= \frac{1}{2}\int \boldsymbol{\psi}\cdot(\nabla\wedge(\nabla\wedge\boldsymbol{\psi}))\,d\mathbf{x} \\ &= \frac{1}{2}\int \boldsymbol{\psi}\cdot\left(-\nabla^2\boldsymbol{\psi} + \nabla(\nabla\cdot\boldsymbol{\psi})\right)\,d\mathbf{x} \\ &= \frac{1}{2}\int \boldsymbol{\psi}\cdot\boldsymbol{\omega}\,d\mathbf{x} \\ &= \frac{1}{8\pi}\sum_{p,q}\Gamma^p\,\Gamma^q\int_{C^p(t)}\int_{C^q(t)}\frac{1}{|\mathbf{x}^p-\mathbf{x}^q|}\left(\frac{\partial\mathbf{x}^p}{\partial s}\cdot\frac{\partial\mathbf{x}^q}{\partial s'}\right)ds\,ds'\,, \end{aligned} \tag{G.2}$$

since $\nabla^2\boldsymbol{\psi} = -\boldsymbol{\omega}$ and $\nabla\cdot\boldsymbol{\psi} = 0$. Notice that the energy is infinite.

The helicity is given by

$$\begin{aligned} \mathcal{H} &= \int \mathbf{u}\cdot\boldsymbol{\omega}\,d\mathbf{x} \\ &= \frac{1}{4\pi}\sum_{p,q}\Gamma^p\,\Gamma^q\int_{C^p(t)}\int_{C^q(t)}\frac{1}{|\mathbf{x}^p-\mathbf{x}^q|^3}(\mathbf{x}^p-\mathbf{x}^q)\cdot\left(\frac{\partial\mathbf{x}^p}{\partial s}\wedge\frac{\partial\mathbf{x}^q}{\partial s'}\right)ds\,ds'\,. \end{aligned} \tag{G.3}$$

Due to the presence of the cross-product in the integrand, the helicity is finite.

The enstrophy is not defined. Indeed, the evaluation of the expression

$$\mathcal{E} = \int \boldsymbol{\omega} \cdot \boldsymbol{\omega} \, d\mathbf{x} \tag{G.4}$$

amounts to integrating the square of the δ-function.

G.1.2 Singular vortex particles

With singular vortex particles, the particle vorticity field $\boldsymbol{\omega}$ is given by Equation (3.2), and the divergence free Novikov vorticity field $\boldsymbol{\omega}^N$ is given by Equation (3.10). The streamfunction $\boldsymbol{\psi}$ is solution of $\nabla^2\boldsymbol{\psi} = -\boldsymbol{\omega}$ and is given by Equation (3.3). As mentioned in Section 3.1, $\boldsymbol{\psi}$ is not divergence free. Its divergence is given by Equation (3.8). The velocity field $\mathbf{u}$ is given by the curl of the streamfunction $\boldsymbol{\psi}$, Equation (3.4), and is thus divergence free.

The kinetic energy is given by Equation (G.1). Integration by parts leads to

$$\begin{aligned} E &= \frac{1}{2}\int \boldsymbol{\psi} \cdot (\nabla\wedge(\nabla\wedge\boldsymbol{\psi}))\, d\mathbf{x} = \frac{1}{2}\int \boldsymbol{\psi} \cdot \left(-\nabla^2\boldsymbol{\psi} + \nabla(\nabla\cdot\boldsymbol{\psi})\right) d\mathbf{x} \\ &= \frac{1}{2}\int \boldsymbol{\psi} \cdot \boldsymbol{\omega} d\mathbf{x} + \frac{1}{2}\int \boldsymbol{\psi} \cdot \nabla(\nabla\cdot\boldsymbol{\psi}) d\mathbf{x}\,, \end{aligned} \tag{G.5}$$

since $\nabla^2\boldsymbol{\psi} = -\boldsymbol{\omega}$. Notice that, due to the non-zero divergence of the streamfunction $\boldsymbol{\psi}$, the kinetic energy cannot be simply written as

$$E_f = \frac{1}{2}\int \boldsymbol{\psi} \cdot \boldsymbol{\omega} d\mathbf{x} = \left(\frac{1}{8\pi}\right) \sum_{\substack{p,q \\ p\neq q}} \frac{\boldsymbol{\alpha}^p \cdot \boldsymbol{\alpha}^q}{|\mathbf{x}^p - \mathbf{x}^q|}\,, \tag{G.6}$$

where the $q = p$ term has been removed to avoid an infinity in the evaluation of E_f. Equation (G.6) is often mistakenly used to evaluate the kinetic energy of a system of vortex particles. The correct expression is given by Equation (G.1), or equivalently Equation (G.5). Aksman, Novikov and Orszag (1985) obtained the correct expression for the kinetic energy by considering the Fourier transform of the velocity field (3.4) and by integrating Equation (G.1) in Fourier space. They obtained

$$E = \frac{1}{16\pi} \sum_{\substack{p,q \\ p\neq q}} \frac{1}{|\mathbf{x}^p - \mathbf{x}^q|} \left(\boldsymbol{\alpha}^p \cdot \boldsymbol{\alpha}^q + \frac{((\mathbf{x}^p - \mathbf{x}^q)\cdot\boldsymbol{\alpha}^p)}{|\mathbf{x}^p - \mathbf{x}^q|} \frac{((\mathbf{x}^p - \mathbf{x}^q)\cdot\boldsymbol{\alpha}^q)}{|\mathbf{x}^p - \mathbf{x}^q|} \right)\,. \tag{G.7}$$

The meaning of Equation (G.7) will become clear in what follows.

It will be shown that direct integration of Equation (G.1) in the physical space instead of the Fourier space can be done, and that it leads to the same result as Equation (G.7). The advantage of integrating directly in the physical space is that the procedure can easily be extended to the evaluation of the energy of a set of regularized

vortex particles as will be shown in Section G.2.3. Going back to Equation (G.1), one obtains, using suffix notation

$$\begin{aligned} E &= \frac{1}{2}\left(\frac{1}{4\pi}\right)^2 \sum_{\substack{p,q \\ p\neq q}} \epsilon_{ijk}\epsilon_{iln}\alpha_k^p\alpha_n^q \int \frac{\partial}{\partial x_j}\left(\frac{1}{|\mathbf{x}-\mathbf{x}^p|}\right)\frac{\partial}{\partial x_l}\left(\frac{1}{|\mathbf{x}-\mathbf{x}^q|}\right)d\mathbf{x} \\ &= \frac{1}{2}\left(\frac{1}{4\pi}\right)^2 \sum_{\substack{p,q \\ p\neq q}} (\delta_{jl}\delta_{kn}-\delta_{jn}\delta_{kl})\alpha_k^p\alpha_n^q \frac{\partial}{\partial x_j^p}\frac{\partial}{\partial x_l^q}\left(\int \frac{1}{|\mathbf{x}-\mathbf{x}^p|}\frac{1}{|\mathbf{x}-\mathbf{x}^q|}d\mathbf{x}\right) , \end{aligned} \tag{G.8}$$

where use of the symmetry relation $\frac{\partial}{\partial x_i}\left(\frac{1}{|\mathbf{x}-\mathbf{x}^p|}\right) = -\frac{\partial}{\partial x_i^p}\left(\frac{1}{|\mathbf{x}-\mathbf{x}^p|}\right)$ has been made. Taking a local spherical coordinate system centered at $\mathbf{x}^p$, and defining $\mathbf{x}-\mathbf{x}^p = \mathbf{x}'$, $\mathbf{x}-\mathbf{x}^q = \mathbf{x}'+(\mathbf{x}^p-\mathbf{x}^q)$, $d\mathbf{x} = d\mathbf{x}' = dr\, r\, d\theta\, r\sin\theta\, d\phi = -r^2\, dr\, d\mu\, d\phi$ with $\mu = \cos\theta$ and $z = |\mathbf{x}^p-\mathbf{x}^q|$, one obtains

$$\int \frac{1}{|\mathbf{x}-\mathbf{x}^p|}\frac{1}{|\mathbf{x}-\mathbf{x}^q|}d\mathbf{x} = \int_0^{2\pi} d\phi \int_0^{\infty} dr \int_{-1}^{1} d\mu \frac{r}{(r^2+2rz\mu+z^2)^{\frac{1}{2}}} . \tag{G.9}$$

This integral does not converge. However, since only the derivatives of this integral with respect to z are of interest $\left(\frac{\partial}{\partial x_j^p}\int \ldots d\mathbf{x} = \frac{\partial z}{\partial x_j^p}\frac{d}{dz}\int \ldots d\mathbf{x}\right)$, a converging factor that is independent of z can be added to the integral. The following convergent integral is thus considered:

$$\begin{aligned} I &= 2\pi \int_0^{\infty} dr \int_{-1}^{1} d\mu \left(\frac{r}{(r^2+2rz\mu+z^2)^{\frac{1}{2}}}-1\right) \\ &= 2\pi \int_0^{\infty} \left[\frac{(r^2+2rz\mu+z^2)^{\frac{1}{2}}}{z}-\mu\right]_{-1}^{1} dr \\ &= 2\pi \int_0^{\infty} \left(\frac{|r+z|-|r-z|}{z}-2\right) dr \\ &= 2\pi\, z \int_0^{\infty} (|t+1|-|t-1|-2)dt \\ &= 2\pi\, z \int_0^{1} (2t-2)dt = -(2\pi)z . \end{aligned} \tag{G.10}$$

Differentiating I gives

$$\begin{aligned} \frac{\partial}{\partial x_j^p}\frac{\partial}{\partial x_l^q}(-(2\pi)z) &= \frac{\partial}{\partial x_j^p}\left(\frac{\partial z}{\partial x_l^q}\frac{d}{dz}(-2\pi\, z)\right) \\ &= -2\pi\frac{\partial}{\partial x_j^p}\left(\frac{\partial z}{\partial x_l^q}\right) \\ &= 2\pi\frac{\partial}{\partial x_j^p}\left(\frac{(x_l^p-x_l^q)}{z}\right) \\ &= 2\pi\left(\frac{\delta_{jl}}{z}-\frac{(x_j^p-x_j^q)(x_l^p-x_l^q)}{z^3}\right) , \end{aligned} \tag{G.11}$$

so the kinetic energy is finally given by

$$\begin{aligned} E &= \frac{1}{16\pi}\sum_{\substack{p,q\\ p\neq q}}(\delta_{jl}\delta_{kn}-\delta_{jn}\delta_{kl})\alpha_k^p\alpha_n^q\left(\frac{\delta_{jl}}{|\mathbf{x}^p-\mathbf{x}^q|}-\frac{(x_l^p-x_l^q)(x_j^p-x_j^q)}{|\mathbf{x}^p-\mathbf{x}^q|^3}\right) \\ &= \frac{1}{16\pi}\sum_{\substack{p,q\\ p\neq q}}\frac{1}{|\mathbf{x}^p-\mathbf{x}^q|}\left(\boldsymbol{\alpha}^p\cdot\boldsymbol{\alpha}^q+\frac{((\mathbf{x}^p-\mathbf{x}^q)\cdot\boldsymbol{\alpha}^p)}{|\mathbf{x}^p-\mathbf{x}^q|}\frac{((\mathbf{x}^p-\mathbf{x}^q)\cdot\boldsymbol{\alpha}^q)}{|\mathbf{x}^p-\mathbf{x}^q|}\right). \end{aligned} \tag{G.12}$$

The result of Aksman, Novikov and Orszag (1985) has thus been recovered using a completely different method. Notice that Equation (G.12) can be written as

$$\begin{aligned} E &= \frac{1}{16\pi}\sum_{\substack{p,q\\ p\neq q}}\frac{1}{|\mathbf{x}^p-\mathbf{x}^q|}\Bigg[2\boldsymbol{\alpha}^p\cdot\boldsymbol{\alpha}^q \\ &\qquad +\left(\frac{((\mathbf{x}^p-\mathbf{x}^q)\cdot\boldsymbol{\alpha}^p)}{|\mathbf{x}^p-\mathbf{x}^q|}\frac{((\mathbf{x}^p-\mathbf{x}^q)\cdot\boldsymbol{\alpha}^q)}{|\mathbf{x}^p-\mathbf{x}^q|}-\boldsymbol{\alpha}^p\cdot\boldsymbol{\alpha}^q\right)\Bigg]. \end{aligned} \tag{G.13}$$

In this form, the correct expression for the kinetic energy can easily be compared with the wrong expression Equation (G.6). The first term in Equation (G.13) is equal to $\frac{1}{2}\int\boldsymbol{\psi}\cdot\boldsymbol{\omega}\,d\mathbf{x}$. The second term is equal to $\frac{1}{2}\int\boldsymbol{\psi}\cdot\nabla(\nabla\cdot\boldsymbol{\psi})\,d\mathbf{x}$. This term is negligible as long as the vortex particles are aligned as little sections of vortex tubes (i.e., as long as the particle representation Equation (3.2) of a divergence free vorticity field is good). However, when the particles are not aligned as little sections of vortex tubes, then the two expressions (G.6) and (G.13) give different results. As a matter of fact, the difference between the two expressions can be used as a diagnostic to check when the particle representation of the vorticity field becomes a poor representation of a divergence field. This is a numerical tool of great interest because it provides a global indication of the consistency of numerical computations.

Proceeding now with the evaluation of the helicity defined by

$$\mathcal{H}=\int\boldsymbol{\omega}^N\cdot\mathbf{u}\,d\mathbf{x}\,, \tag{G.14}$$

with $\boldsymbol{\omega}^N$ and $\mathbf{u}$ given by (3.10) and (3.4), one obtains

$$\begin{aligned} \mathcal{H} &= \int\left(\sum_p\boldsymbol{\alpha}^p\delta(\mathbf{x}-\mathbf{x}^p)+\nabla\left(\boldsymbol{\alpha}^p\cdot\nabla\left(\frac{1}{4\pi|\mathbf{x}-\mathbf{x}^p|}\right)\right)\right)\cdot \\ &\qquad\left(\sum_q\nabla\left(\frac{1}{4\pi|\mathbf{x}-\mathbf{x}^q|}\right)\wedge\boldsymbol{\alpha}^q\right)d\mathbf{x} \\ &= -\frac{1}{4\pi}\sum_{p,q}\boldsymbol{\alpha}^p\cdot\left(\frac{(\mathbf{x}^p-\mathbf{x}^q)}{|\mathbf{x}^p-\mathbf{x}^q|^3}\wedge\boldsymbol{\alpha}^q\right) \\ &\quad+\left(\frac{1}{4\pi}\right)^2\sum_{p,q}\epsilon_{ijk}\alpha_l^p\alpha_k^q\int\frac{\partial}{\partial x_i}\frac{\partial}{\partial x_l}\left(\frac{1}{|\mathbf{x}-\mathbf{x}^p|}\right)\frac{\partial}{\partial x_j}\left(\frac{1}{|\mathbf{x}-\mathbf{x}^q|}\right)d\mathbf{x}\,. \end{aligned} \tag{G.15}$$

The second term in (G.15) vanishes. Indeed,

$$\begin{aligned}
&\epsilon_{ijk}\alpha_l^p\alpha_k^q \int \frac{\partial}{\partial x_i}\frac{\partial}{\partial x_l}\left(\frac{1}{|\mathbf{x}-\mathbf{x}^p|}\right)\frac{\partial}{\partial x_j}\left(\frac{1}{|\mathbf{x}-\mathbf{x}^q|}\right) d\mathbf{x} \\
&= -\epsilon_{ijk}\alpha_l^p\alpha_k^q \frac{\partial}{\partial x_i^p}\frac{\partial}{\partial x_l^p}\frac{\partial}{\partial x_j^q}\int \frac{1}{|\mathbf{x}-\mathbf{x}^p|}\frac{1}{|\mathbf{x}-\mathbf{x}^q|} d\mathbf{x} \\
&= 2\pi\,\epsilon_{ijk}\alpha_l^p\alpha_k^q \frac{\partial}{\partial x_i^p}\frac{\partial}{\partial x_l^p}\left(\frac{\partial z}{\partial x_j^q}\right) \\
&= 2\pi\,\epsilon_{ijk}\alpha_l^p\alpha_k^q \frac{\partial}{\partial x_i^p}\frac{\partial}{\partial x_l^p}\left(-\frac{\partial z}{\partial x_j^p}\right) = 0\,,
\end{aligned} \tag{G.16}$$

since $\epsilon_{ijk}\frac{\partial}{\partial x_i}\frac{\partial}{\partial x_j} = 0$. One is thus left with the simple formula

$$\mathcal{H} = \frac{1}{4\pi}\sum_{p,q}\frac{(\mathbf{x}^p-\mathbf{x}^q)}{|\mathbf{x}^p-\mathbf{x}^q|^3}\cdot(\boldsymbol{\alpha}^p\wedge\boldsymbol{\alpha}^q)\,. \tag{G.17}$$

Notice that the case $q = p$ is a removable singularity since $\boldsymbol{\alpha}^p\wedge\boldsymbol{\alpha}^p = 0$.

Finally, the enstrophy is not defined. Indeed, the evaluation of the expression

$$\mathcal{E} = \int \boldsymbol{\omega}^N\cdot\boldsymbol{\omega}^N d\mathbf{x} \tag{G.18}$$

leads to a singularity because it amounts to integrating the square of the δ-function.

G.2 The regularized case

G.2.1 A note on quadratic diagnostics and regularized filament or particle methods

Quadratic diagnostics are difficult to evaluate when considering regularized filaments or regularized particles. For instance, the kinetic energy is given by

$$\begin{aligned}
E &= \frac{1}{2}\int \mathbf{u}_\sigma\cdot\mathbf{u}_\sigma d\mathbf{x} = \frac{1}{2}\int(\nabla\wedge\boldsymbol{\psi}_\sigma)\cdot(\nabla\wedge\boldsymbol{\psi}_\sigma)\,d\mathbf{x} \\
&= \frac{1}{2}\int(\nabla\wedge(\boldsymbol{\psi}*\zeta_\sigma))\cdot(\nabla\wedge(\boldsymbol{\psi}*\zeta_\sigma))\,d\mathbf{x}\,,
\end{aligned} \tag{G.19}$$

where $*$ stands for the convolution product. Integrals of the type (G.19) cannot, in general, be done in closed form. Instead, an approximation must be considered in which only one term in the quadratic integrand is regularized. One considers therefore

$$\tilde{E} = \frac{1}{2}\int \mathbf{u}\cdot\mathbf{u}_\sigma d\mathbf{x} = \frac{1}{2}\int(\nabla\wedge\boldsymbol{\psi})\cdot(\nabla\wedge(\boldsymbol{\psi}*\zeta_\sigma))\,d\mathbf{x}\,. \tag{G.20}$$

When using vortex filaments, integrals of the form (G.20) can easily be done in closed form as will be seen in Section G.2.2. When using vortex particles, integrals of that

form can also be done in closed form, at least for some choices of the regularization function $\zeta(\rho)$, as will be shown in Section G.2.3.

$\tilde{E}$ is of course not the energy of the system regularized with $\zeta(\rho)$. Actually, $\tilde{E}$ is the energy of a system regularized with a function $\hat{\zeta}(\rho)$ which is such that $\zeta(\rho) = \hat{\zeta}(\rho) * \hat{\zeta}(\rho)$. This can easily be seen if one recalls the associativity property of the convolution product, and writes

$$\begin{aligned} \tilde{E} &= \frac{1}{2}\int (\nabla\wedge\boldsymbol{\psi})\cdot\left(\nabla\wedge\left(\boldsymbol{\psi} * (\hat{\zeta}_\sigma * \hat{\zeta}_\sigma)\right)\right) d\mathbf{x} \\ &= \frac{1}{2}\int \left(\nabla\wedge(\boldsymbol{\psi} * \hat{\zeta}_\sigma)\right)\cdot\left(\nabla\wedge(\boldsymbol{\psi} * \hat{\zeta}_\sigma)\right) d\mathbf{x} \,. \end{aligned} \tag{G.21}$$

The above suggests the following method for computing the exact energy of a system of regularized filaments or particles. Given $\zeta(\rho)$, find $\tilde{\zeta}(\rho)$ such that $\tilde{\zeta}(\rho) = \zeta(\rho) * \zeta(\rho)$. The energy is then given by

$$E = \frac{1}{2}\int (\nabla\wedge\boldsymbol{\psi})\cdot\left(\nabla\wedge(\boldsymbol{\psi} * \tilde{\zeta}_\sigma)\right) d\mathbf{x} \,. \tag{G.22}$$

Unfortunately, finding $\tilde{\zeta}(\rho)$ from $\zeta(\rho)$ is not always possible. There is actually one case for which $\tilde{\zeta}(\rho)$ can easily be obtained from $\zeta(\rho)$. This is the case of the Gaussian smoothing (B.8) for which the use of the Fourier transform and the convolution theorem leads easily to $\tilde{\zeta}(\rho) = \zeta(\rho/\sqrt{2})$. An exact expression can thus be obtained for the kinetic energy of a system of vortex filaments when the Gaussian smoothing is used. When vortex particles are used, the Gaussian smoothing is unfortunately a case for which Equation (G.22) cannot be integrated in closed form.

In what follows, all quadratic diagnostics will be evaluated using the approximation in which only one term in the quadratic integrand is regularized. It will be understood that this procedure only yields approximate values for the quadratic diagnostics associated with the regularization function $\zeta(\rho)$, and exact values for the diagnostics associated with the regularization function $\hat{\zeta}(\rho)$.

This section is concluded with the following remark. The approximation in which only one term in the quadratic integrand is regularized gives a good approximation to the exact value in the case of the kinetic energy, a fair approximation in the case of the helicity, and a poor approximation in the case of the enstrophy. This is related to the strength of the singularity in the integrand. The integral $\frac{1}{2}\int \mathbf{u}\cdot\mathbf{u}_\sigma \, d\mathbf{x}$ is a good approximation to $\frac{1}{2}\int \mathbf{u}_\sigma\cdot\mathbf{u}_\sigma \, d\mathbf{x}$ in the sense that, as the level of discretization increases (i.e., as the number of filaments or particles is increased) both integrals converge rapidly to the same value. Integrating $\int \boldsymbol{\omega}^N\cdot\mathbf{u}_\sigma \, d\mathbf{x}$ is only a fair approximation to $\int \boldsymbol{\omega}_\sigma^N\cdot\mathbf{u}_\sigma \, d\mathbf{x}$ because the the two integrals converge more slowly to each other as the level of discretization is increased. Finally, integrating $\int \boldsymbol{\omega}^N\cdot\boldsymbol{\omega}_\sigma^N \, d\mathbf{x}$ is a poor

approximation to $\int \boldsymbol{\omega}_\sigma^N \cdot \boldsymbol{\omega}_\sigma^N \, d\mathbf{x}$ because the convergence of the two integrals is very slow.

G.2.2 Regularized vortex filaments

Regularized vortex filaments define the divergence free vorticity field $\boldsymbol{\omega}_\sigma$ given by Equation (2.19). The divergence free streamfunction $\boldsymbol{\psi}_\sigma$ is solution of $\nabla^2 \boldsymbol{\psi}_\sigma = -\boldsymbol{\omega}_\sigma$ and is given by Equation (2.23) with $\nabla^2 \chi(\rho) = -\zeta(\rho)$. The velocity field $\mathbf{u}_\sigma$ is given by the curl of the streamfunction, Equation (2.31), and is thus also divergence free.

The semi-regularized kinetic energy is given by

$$\begin{aligned} \tilde{E} &= \frac{1}{2} \int \mathbf{u}_\sigma \cdot \mathbf{u} \, d\mathbf{x} = \frac{1}{2} \int \boldsymbol{\psi}_\sigma \cdot \boldsymbol{\omega} \, d\mathbf{x} \\ &= \frac{1}{2} \sum_{p,q} \Gamma^p \Gamma^q \int_{\mathcal{C}^p(t)} \int_{\mathcal{C}^q(t)} \chi_\sigma(\mathbf{x}^p - \mathbf{x}^q) \left(\frac{\partial \mathbf{x}^p}{\partial s} \cdot \frac{\partial \mathbf{x}^q}{\partial s'} \right) ds \, ds' \,. \end{aligned} \tag{G.23}$$

This energy is finite since $\chi(\rho)$ is $\mathcal{O}(\rho^2)$ from small ρ.

The semi-regularized helicity is given by

$$\begin{aligned} \tilde{\mathcal{H}} &= \int \mathbf{u}_\sigma \cdot \boldsymbol{\omega} \, d\mathbf{x} \\ &= \sum_{p,q} \Gamma^p \Gamma^q \int_{\mathcal{C}^p(t)} \int_{\mathcal{C}^q(t)} \frac{g_\sigma(\mathbf{x}^p - \mathbf{x}^q)}{|\mathbf{x}^p - \mathbf{x}^q|^3} (\mathbf{x}^p - \mathbf{x}^q) \cdot \left(\frac{\partial \mathbf{x}^p}{\partial s} \wedge \frac{\partial \mathbf{x}^q}{\partial s'} \right) ds \, ds' \,. \end{aligned} \tag{G.24}$$

The semi-regularized enstrophy is given by

$$\begin{aligned} \tilde{\mathcal{E}} &= \int \boldsymbol{\omega}_\sigma \cdot \boldsymbol{\omega} \, d\mathbf{x} \\ &= \sum_{p,q} \Gamma^p \Gamma^q \int_{\mathcal{C}^p(t)} \int_{\mathcal{C}^q(t)} \zeta_\sigma(\mathbf{x}^p - \mathbf{x}^q) \left(\frac{\partial \mathbf{x}^p}{\partial s} \cdot \frac{\partial \mathbf{x}^q}{\partial s'} \right) ds \, ds' \,. \end{aligned} \tag{G.25}$$

G.2.3 Regularized vortex particles

With regularized vortex particles, the particle vorticity field $\boldsymbol{\omega}_\sigma$ is given by Equation (3.30) and the divergence free Novikov vorticity field $\boldsymbol{\omega}_\sigma^N$ is given by Equation (3.39). The streamfunction $\boldsymbol{\psi}_\sigma$ is solution of $\nabla^2 \boldsymbol{\psi}_\sigma = -\boldsymbol{\omega}_\sigma$ and is given by Equation (3.31) with $\nabla^2 \chi(\rho) = -\zeta(\rho)$. As mentioned in Section 3.2, $\boldsymbol{\psi}_\sigma$ is not divergence free. Its divergence is given by Equation (3.38). The velocity field $\mathbf{u}_\sigma$ is given by the curl of the streamfunction $\boldsymbol{\psi}_\sigma$, Equation (3.32), and is thus divergence free.

As mentioned in Section G.2.1, the quadratic diagnostics cannot easily be integrated, even with the approximation in which only one term in the quadratic integral is regularized. There is however one choice of regularization function $\zeta(\rho)$ for which the integrals can be done in closed form: the new high order algebraic smoothing (B.12). This makes the use of this smoothing extremely appealing. Not only does

it have good convergence properties, but it also allows one to find closed form expressions for the quadratic diagnostics, a property not satisfied by any other smoothing known.

The evaluation of the quadratic diagnostics when using the high order algebraic smoothing (B.12) is thus examined. The evaluation of the kinetic energy is first considered, Equation (G.20) or its equivalent expression obtained through integration by parts

$$\begin{aligned}\tilde{E} &= \frac{1}{2}\int \boldsymbol{\psi}_\sigma \cdot (\nabla\wedge(\nabla\wedge\boldsymbol{\psi}))\, d\mathbf{x} = \frac{1}{2}\int \boldsymbol{\psi}_\sigma \cdot \left(-\nabla^2\boldsymbol{\psi} + \nabla(\nabla\cdot\boldsymbol{\psi})\right) d\mathbf{x} \\ &= \frac{1}{2}\int \boldsymbol{\psi}_\sigma \cdot \boldsymbol{\omega}\, d\mathbf{x} + \frac{1}{2}\int \boldsymbol{\psi}_\sigma \cdot \nabla(\nabla\cdot\boldsymbol{\psi})\, d\mathbf{x}\,, \end{aligned} \tag{G.26}$$

since $\nabla^2\boldsymbol{\psi}_\sigma = -\boldsymbol{\omega}_\sigma$. Again, due to the non-zero divergence of the streamfunction, the semi-regularized energy cannot be simply written as

$$\begin{aligned}\tilde{E}_f = \frac{1}{2}\int \boldsymbol{\psi}_\sigma \cdot \boldsymbol{\omega}\, d\mathbf{x} &= \frac{1}{2}\sum_{p,q} \chi_\sigma(\mathbf{x}^p - \mathbf{x}^q)\boldsymbol{\alpha}^p \cdot \boldsymbol{\alpha}^q \\ &= \frac{1}{8\pi}\sum_{p,q} \frac{(|\mathbf{x}^p - \mathbf{x}^q|^2 + \frac{3}{2}\sigma^2)}{(|\mathbf{x}^p - \mathbf{x}^q|^2 + \sigma^2)^{\frac{3}{2}}}\, \boldsymbol{\alpha}^p \cdot \boldsymbol{\alpha}^q\,. \end{aligned} \tag{G.27}$$

Instead, Equation (G.20) must be integrated in closed form. Following the same procedure as in Section G.1.2, one obtains

$$\tilde{E} = \frac{1}{2}\left(\frac{1}{4\pi}\right)^2 \sum_{p,q} (\delta_{jl}\delta_{kn} - \delta_{jn}\delta_{kl}\alpha_k^p\alpha_n^q \frac{\partial}{\partial x_j^p}\frac{\partial}{\partial x_l^q}\left(\int \frac{(|\mathbf{x} - \mathbf{x}^p|^2 + \frac{3}{2}\sigma^2)}{(|\mathbf{x} - \mathbf{x}^p|^2 + \sigma^2)^{\frac{3}{2}}}\frac{1}{|\mathbf{x} - \mathbf{x}^q|}\, d\mathbf{x}\right)\,. \tag{G.28}$$

The evaluation of the integral in Equation (G.28) is done as in Section G.1.2. It leads us to consider the following integral

$$\begin{aligned} I &= 2\pi \int_0^\infty dr \frac{r\left(r^2 + \frac{3}{2}\sigma^2\right)}{(r^2+\sigma^2)^{\frac{3}{2}}} \int_{-1}^1 d\mu \left(\frac{r}{(r^2 + 2rz\mu + z^2)^{\frac{1}{2}}} - 1\right) \\ &= 2\pi \int_0^\infty \frac{r\left(r^2 + \frac{3}{2}\sigma^2\right)}{(r^2+\sigma^2)^{\frac{3}{2}}} \left[\frac{(r^2 + 2rz\mu + z^2)^{\frac{1}{2}}}{z} - \mu\right]_{-1}^1 dr \\ &= 2\pi z \int_0^\infty \frac{t\left(t^2 + \frac{3}{2}a^2\right)}{(t^2+a^2)^{\frac{3}{2}}}(|t+1| - |t-1| - 2)dt \\ &= 2\pi z \int_0^1 \frac{t\left(t^2 + \frac{3}{2}a^2\right)}{(t^2+a^2)^{\frac{3}{2}}}(2t-2)dt\,, \end{aligned} \tag{G.29}$$

with $t = r/z$ and $a = \sigma/z$. The integrals appearing in Equation (G.29) can be

calculated in closed form. Indeed,

$$\begin{aligned}
\int \frac{t\left(t^2+\frac{3}{2}a^2\right)}{\left(t^2+a^2\right)^{\frac{3}{2}}}dt &= \frac{\left(t^2+\frac{1}{2}a^2\right)}{\left(t^2+a^2\right)^{\frac{1}{2}}}, \\
\int \frac{t^2\left(t^2+\frac{3}{2}a^2\right)}{\left(t^2+a^2\right)^{\frac{3}{2}}}dt &= \frac{t\left(t^2+\frac{1}{2}a^2\right)}{\left(t^2+a^2\right)^{\frac{1}{2}}} - \frac{1}{2}t\left(t^2+a^2\right)^{\frac{1}{2}}, \qquad \text{(G.30)}
\end{aligned}$$

so that one obtains

$$\begin{aligned}
I &= 2\pi z\left(a-(1+a^2)^{\frac{1}{2}}\right) = (2\pi)z\left(\frac{\sigma}{z} - \left(1+\left(\frac{\sigma}{z}\right)^2\right)^{\frac{1}{2}}\right) \\
&= 2\pi\sigma\left(1-\left(\rho^2+1\right)^{\frac{1}{2}}\right), \qquad \text{(G.31)}
\end{aligned}$$

with $\rho = z/\sigma = |\mathbf{x}^p - \mathbf{x}^q|/\sigma$. Differentiating I gives

$$\begin{aligned}
\frac{\partial}{\partial x_j^p}\frac{\partial}{\partial x_l^q}(I) &= \frac{\partial}{\partial x_j^p}\left(\frac{\partial\rho}{\partial x_l^q}\frac{dI}{d\rho}\right) \\
&= \frac{\partial^2\rho}{\partial x_j^p \partial x_l^q}\frac{dI}{d\rho} + \frac{\partial\rho}{\partial x_j^p}\frac{\partial\rho}{\partial x_l^q}\frac{d^2I}{d\rho^2} \\
&= 2\pi\left(\frac{\rho}{(\rho^2+1)^{\frac{1}{2}}}\frac{\delta_{jl}}{z} - \frac{\rho^3}{(\rho^2+1)^{\frac{3}{2}}}\frac{(x_j^p-x_j^q)(x_l^p-x_l^q)}{z^3}\right), \qquad \text{(G.32)}
\end{aligned}$$

Use of Equation (G.28) and Equation (G.32) finally leads to the following expression for the semi-regularized energy

$$\begin{aligned}
\tilde{E} = \frac{1}{16\pi}\sum_{p,q}\frac{1}{|\mathbf{x}^p-\mathbf{x}^q|}\Bigg[&2\frac{\rho}{(\rho^2+1)^{\frac{1}{2}}}\boldsymbol{\alpha}^p\cdot\boldsymbol{\alpha}^q \\
&+\frac{\rho^3}{(\rho^2+1)^{\frac{3}{2}}}\left(\frac{((\mathbf{x}^p-\mathbf{x}^q)\cdot\boldsymbol{\alpha}^p)}{|\mathbf{x}^p-\mathbf{x}^q|}\frac{((\mathbf{x}^p-\mathbf{x}^q)\cdot\boldsymbol{\alpha}^q)}{|\mathbf{x}^p-\mathbf{x}^q|} - \boldsymbol{\alpha}^p\cdot\boldsymbol{\alpha}^q\right)\Bigg] \qquad \text{(G.33)}
\end{aligned}$$

It is instructive to compare the correct energy expression (G.33) with the incorrect expression (G.27). The first term in Equation (G.33) is not equal to $\frac{1}{2}\int \boldsymbol{\psi}_\sigma \cdot \boldsymbol{\omega} d\mathbf{x}$, as was the case with singular vortex particles. It is also interesting to note that there is a vortex particle self-energy $(1/16\pi)(\boldsymbol{\alpha}\cdot\boldsymbol{\alpha}/\sigma)$. The two expressions (G.33) and (G.27) give identical results as long as the vortex particles are aligned as little sections of vortex tubes. Also, the difference between the two expressions provides a way of checking the consistency of the numerical computation since the two expressions are different only when $\nabla\cdot\boldsymbol{\omega}_\sigma \neq 0$.

The success of the above derivation strongly depends on the nice integration properties of the high order algebraic smoothing (B.12), such as Equation (G.30). For

most other smoothings, the integrals that appear in expressions of the type (G.29) cannot be done in closed form. Another smoothing that gives a closed form energy expression is the low order algebraic smoothing (B.10), although the result is not as elegant as with the high order algebraic smoothing. Using the same procedure as above, the low order algebraic smoothing leads to

$$\begin{aligned}\tilde{E} &= \frac{1}{16\pi}\sum_{p,q}\frac{1}{|\mathbf{x}^p-\mathbf{x}^q|}\left[2\frac{1}{\rho}\left(\left(\rho^2+1\right)^{\frac{1}{2}}-\frac{\operatorname{arcsinh}\rho}{\rho}\right)\boldsymbol{\alpha}^p\cdot\boldsymbol{\alpha}^q\right.\\ &\quad+\frac{1}{\rho}\left(\left(\rho^2+1\right)^{\frac{1}{2}}+2\frac{1}{\left(\rho^2+1\right)^{\frac{1}{2}}}-3\frac{\operatorname{arcsinh}\rho}{\rho}\right)\\ &\quad\left.\left(\frac{((\mathbf{x}^p-\mathbf{x}^q)\cdot\boldsymbol{\alpha}^p)}{|\mathbf{x}^p-\mathbf{x}^q|}\frac{((\mathbf{x}^p-\mathbf{x}^q)\cdot\boldsymbol{\alpha}^q)}{|\mathbf{x}^p-\mathbf{x}^q|}-\boldsymbol{\alpha}^p\cdot\boldsymbol{\alpha}^q\right)\right], \qquad \text{(G.34)}\end{aligned}$$

with a particle self-energy of $(1/16\pi)(4/3(\boldsymbol{\alpha}\cdot\boldsymbol{\alpha}/\sigma))$.

Proceeding with the evaluation of the helicity, the semi-regularized helicity is taken as

$$\tilde{\mathcal{H}} = \int \boldsymbol{\omega}^N\cdot\mathbf{u}_\sigma\, d\mathbf{x}\,. \qquad \text{(G.35)}$$

With $\boldsymbol{\omega}^N$ and $\mathbf{u}_\sigma$ given by (3.10) and (3.32), one obtains

$$\begin{aligned}\tilde{\mathcal{H}} &= \int\left(\sum_p\boldsymbol{\alpha}^p\delta(\mathbf{x}-\mathbf{x}^p)+\nabla\left(\boldsymbol{\alpha}^p\cdot\nabla\left(\frac{1}{4\pi|\mathbf{x}-\mathbf{x}^p|}\right)\right)\right)\\ &\qquad\cdot\left(\sum_q\nabla\chi_\sigma(\mathbf{x}-\mathbf{x}^q)\wedge\boldsymbol{\alpha}^q\right)d\mathbf{x}\\ &= \sum_{p,q}\boldsymbol{\alpha}^p\cdot(\nabla\chi_\sigma(\mathbf{x}-\mathbf{x}^q)\wedge\boldsymbol{\alpha}^q)\\ &\quad+\frac{1}{4\pi}\sum_{p,q}\epsilon_{ijk}\alpha_l^p\alpha_k^q\int\frac{\partial}{\partial x_i}\frac{\partial}{\partial x_l}\left(\frac{1}{|\mathbf{x}-\mathbf{x}^p|}\right)\frac{\partial}{\partial x_j}\chi_\sigma(\mathbf{x}-\mathbf{x}^q)\,d\mathbf{x}\,. \qquad \text{(G.36)}\end{aligned}$$

As was the case for singular vortex particles, Equation (G.16), it is easy to show that the second term in Equation (G.36) vanishes, so that the simple formula

$$\begin{aligned}\tilde{\mathcal{H}} &= -\sum_{p,q}\boldsymbol{\alpha}^p\cdot\left(\frac{g_\sigma(\mathbf{x}^p-\mathbf{x}^q)}{|\mathbf{x}^p-\mathbf{x}^q|^3}((\mathbf{x}^p-\mathbf{x}^q)\wedge\boldsymbol{\alpha}^q)\right)\\ &= \sum_{p,q}\frac{g_\sigma(\mathbf{x}^p-\mathbf{x}^q)}{|\mathbf{x}^p-\mathbf{x}^q|^3}((\mathbf{x}^p-\mathbf{x}^q)\cdot(\boldsymbol{\alpha}^p\wedge\boldsymbol{\alpha}^q)) \qquad \text{(G.37)}\end{aligned}$$

is obtained. Equation (G.37) is applicable to any smoothing $\zeta(\rho)$, $g(\rho)$. Notice that the motivation for claiming that the $q=p$ term in the enstrophy formula of singular particles (G.17) is a removable singularity is found here. Indeed, any smoothing, no matter how small σ, leads to no contribution of the $q=p$ term since $\boldsymbol{\alpha}^p\wedge\boldsymbol{\alpha}^p=0$.

With the high order algebraic smoothing (B.12), one obtains

$$\tilde{\mathcal{H}} = \frac{1}{4\pi} \sum_{p,q} \frac{\left(|\mathbf{x}^p - \mathbf{x}^q|^2 + \frac{5}{2}\sigma^2\right)}{\left(|\mathbf{x}^p - \mathbf{x}^q|^2 + \sigma^2\right)^{\frac{5}{2}}} \left((\mathbf{x}^p - \mathbf{x}^q) \cdot (\boldsymbol{\alpha}^p \wedge \boldsymbol{\alpha}^q)\right) , \tag{G.38}$$

and, with the low order algebraic smoothing (B.10),

$$\tilde{\mathcal{H}} = \frac{1}{4\pi} \sum_{p,q} \frac{1}{\left(|\mathbf{x}^p - \mathbf{x}^q|^2 + \sigma^2\right)^{\frac{3}{2}}} \left((\mathbf{x}^p - \mathbf{x}^q) \cdot (\boldsymbol{\alpha}^p \wedge \boldsymbol{\alpha}^q)\right) . \tag{G.39}$$

Finally, the evaluation of the semi-regularized enstrophy

$$\tilde{\mathcal{E}} = \int \boldsymbol{\omega}^N \cdot \boldsymbol{\omega}_\sigma^N \, d\mathbf{x} \tag{G.40}$$

is examined. Due to the non-zero divergence of the particle vorticity field, the enstrophy cannot simply be written as

$$\begin{aligned} \tilde{\mathcal{E}}_f = \int \boldsymbol{\omega} \cdot \boldsymbol{\omega}_\sigma \, d\mathbf{x} &= \sum_{p,q} \zeta_\sigma(\mathbf{x}^p - \mathbf{x}^q) \boldsymbol{\alpha}^p \cdot \boldsymbol{\alpha}^q \\ &= \frac{1}{4\pi} \sum_{p,q} \frac{15}{2} \frac{\sigma^4}{\left(|\mathbf{x}^p - \mathbf{x}^q|^2 + \sigma^2\right)^{\frac{7}{2}}} \boldsymbol{\alpha}^p \cdot \boldsymbol{\alpha}^q . \end{aligned} \tag{G.41}$$

Instead, Equation (G.40) must be integrated in closed form. This leads to

$$\begin{aligned} \tilde{\mathcal{E}} &= \int \left(\sum_p \boldsymbol{\alpha}^p \delta(\mathbf{x} - \mathbf{x}^p) + \nabla \left(\boldsymbol{\alpha}^p \cdot \left(\frac{1}{4\pi |\mathbf{x} - \mathbf{x}^p|} \right) \right) \right) \\ &\qquad \cdot \left(\sum_q \boldsymbol{\alpha}^q \zeta_\sigma(\mathbf{x} - \mathbf{x}^q) + \nabla \left(\boldsymbol{\alpha}^q \cdot \nabla \chi_\sigma(\mathbf{x} - \mathbf{x}^q) \right) \right) \\ &= \sum_{p,q} \Bigg[\boldsymbol{\alpha}^p \cdot \boldsymbol{\alpha}^q \zeta_\sigma(\mathbf{x}^p - \mathbf{x}^q) + \boldsymbol{\alpha}^p \cdot \nabla \left(\boldsymbol{\alpha}^q \cdot \nabla \chi_\sigma(\mathbf{x} - \mathbf{x}^q)_{\mathbf{x}=\mathbf{x}^p} \right) \\ &\quad + \frac{1}{4\pi} \alpha_k^p \alpha_i^q \int \frac{\partial}{\partial x_i} \frac{\partial}{\partial x_k} \left(\frac{1}{|\mathbf{x} - \mathbf{x}^p|} \right) \zeta_\sigma(\mathbf{x} - \mathbf{x}^q) d\mathbf{x} \\ &\quad + \frac{1}{4\pi} \alpha_k^p \alpha_l^q \int \frac{\partial}{\partial x_i} \frac{\partial}{\partial x_k} \left(\frac{1}{|\mathbf{x} - \mathbf{x}^p|} \right) \frac{\partial}{\partial x_i} \frac{\partial}{\partial x_l} \chi_\sigma(\mathbf{x} - \mathbf{x}^q) d\mathbf{x} \Bigg] . \end{aligned} \tag{G.42}$$

The integrals in Equation (G.42) are evaluated using the same procedure as for the kinetic energy evaluation and using also

$$\begin{aligned} \int \frac{\partial}{\partial x_i} \frac{\partial}{\partial x_k} \left(\frac{1}{|\mathbf{x} - \mathbf{x}^p|} \right) \zeta_\sigma(\mathbf{x} - \mathbf{x}^q) d\mathbf{x} &= -\int \frac{\partial}{\partial x_k} \left(\frac{1}{|\mathbf{x} - \mathbf{x}^p|} \right) \frac{\partial}{\partial x_i} \zeta_\sigma(\mathbf{x} - \mathbf{x}^q) d\mathbf{x} \\ &= -\frac{\partial}{\partial x_k^p} \frac{\partial}{\partial x_i^q} \int \frac{1}{|\mathbf{x} - \mathbf{x}^p|} \zeta_\sigma(\mathbf{x} - \mathbf{x}^q) d\mathbf{x} , \end{aligned}$$

$$\int \frac{\partial}{\partial x_i}\frac{\partial}{\partial x_k}\left(\frac{1}{|\mathbf{x}-\mathbf{x}^p|}\right)\frac{\partial}{\partial x_i}\frac{\partial}{\partial x_l}\chi_\sigma(\mathbf{x}-\mathbf{x}^q)d\mathbf{x}$$
$$= \frac{\partial}{\partial x_i^p}\frac{\partial}{\partial x_k^p}\frac{\partial}{\partial x_i^q}\frac{\partial}{\partial x_l^q}\int \frac{1}{|\mathbf{x}-\mathbf{x}^p|}\chi_\sigma(\mathbf{x}-\mathbf{x}^q)d\mathbf{x}\,. \qquad \text{(G.43)}$$

The first integral in Equation (G.43) leads one to consider

$$\begin{aligned} I_1 &= (2\pi)\left(\frac{15}{8\pi\sigma^3}\right)\int_0^\infty dr\frac{r}{(r^2+\sigma^2)^{\frac{7}{2}}}\int_{-1}^1 d\mu\left(\frac{r}{(r^2+2rz\mu+z^2)^{\frac{1}{2}}}-1\right) \\ &= \left(\frac{15}{4}\right)\frac{a^4}{z}\int_0^1 \frac{t}{(t^2+a^2)^{\frac{7}{2}}}(2t-2)dt\,, \end{aligned} \qquad \text{(G.44)}$$

with $t = r/z$ and $a = \sigma/z$. The integral appearing in Equation (G.44) can be done in closed form. Indeed,

$$\begin{aligned} \int \frac{t}{(t^2+a^2)^{\frac{7}{2}}}dt &= -\frac{1}{5}\frac{1}{(t^2+a^2)^{\frac{5}{2}}}\,, \\ \int \frac{t^2}{(t^2+a^2)^{\frac{7}{2}}}dt &= \frac{2}{15a^4}\frac{t^3\left(t^2+\frac{5}{2}a^2\right)}{(t^2+a^2)^{\frac{5}{2}}}\,, \end{aligned} \qquad \text{(G.45)}$$

so that finally

$$I_1 = \frac{1}{\sigma}\left(\frac{\rho^2\left(\rho^2+\frac{5}{2}\right)}{(\rho^2+1)^{\frac{5}{2}}}+\frac{3}{2}\left(\frac{1}{(\rho^2+1)^{\frac{5}{2}}}-1\right)\right)\,, \qquad \text{(G.46)}$$

where $\rho = z/\sigma = |\mathbf{x}^p-\mathbf{x}^q|/\sigma$. The second integral in Equation (G.43) leads to consider the same integral I as in the energy evaluation, Equation (G.29). Differentiation of I and I_1 gives

$$\begin{aligned} &-\frac{\partial}{\partial x_k^p}\frac{\partial}{\partial x_i^q}(I_1) \\ &= \frac{1}{\sigma^3}\left(\left(\frac{\rho^2\left(\rho^2+\frac{7}{2}\right)+\frac{5}{2}}{(\rho^2+1)^{\frac{7}{2}}}\right)\delta_{ik}-\frac{3}{\sigma^2}\left(\frac{\rho^2\left(\rho^2+\frac{9}{2}\right)+\frac{7}{2}}{(\rho^2+1)^{\frac{9}{2}}}\right)(x_i^p-x_i^q)(x_k^p-x_k^q)\right)\,, \\ &\frac{\partial}{\partial x_i^p}\frac{\partial}{\partial x_k^p}\frac{\partial}{\partial x_i^q}\frac{\partial}{\partial x_l^q}(I) = \frac{1}{\sigma^3}\left(\frac{\left(\rho^2+\frac{5}{2}\right)}{(\rho^2+1)^{\frac{5}{2}}}\delta_{kl}-\frac{3}{\sigma^2}\frac{\left(\rho^2+\frac{7}{2}\right)}{(\rho^2+1)^{\frac{7}{2}}}(x_k^p-x_k^q)(x_l^p-x_l^q)\right)\,. \end{aligned} \qquad \text{(G.47)}$$

Now all the terms necessary to evaluate Equation (G.42) have been obtained. The final result is given by

$$\begin{aligned} \tilde{\mathcal{E}} &= \frac{1}{4\pi}\sum_{p,q}\frac{1}{\sigma^3}\left[\frac{\left(5-\rho^2\left(\rho^2+\frac{7}{2}\right)\right)}{(\rho^2+1)^{\frac{7}{2}}}\boldsymbol{\alpha}^p\cdot\boldsymbol{\alpha}^q\right. \\ &\qquad \left.+3\frac{\left(\rho^2\left(\rho^2+\frac{9}{2}\right)+\frac{7}{2}\right)}{(\rho^2+1)^{\frac{9}{2}}}\left((\mathbf{x}^p-\mathbf{x}^q)\cdot\boldsymbol{\alpha}^p\right)\left((\mathbf{x}^p-\mathbf{x}^q)\cdot\boldsymbol{\alpha}^q\right)\right]\,, \end{aligned} \qquad \text{(G.48)}$$

with a vortex particle self-enstrophy of $(5/4\pi)(\boldsymbol{\alpha}\cdot\boldsymbol{\alpha}/\sigma^3)$. Again, the succes of the above derivation strongly depends on the integration properties of the high order algebraic smoothing (B.12), such as Equations (G.30) and (G.45). No attempt was made to obtain the expression for the enstrophy when using the low order algebraic smoothing (B.10), but it is doubtful that the necessary integrals can be done in closed form.

The derivation of the expressions for the semi-regularized energy $\tilde{E}$, helicity $\tilde{\mathcal{H}}$ and enstrophy $\tilde{\mathcal{E}}$ of a set of regularized vortex particles is now complete. These expressions are of great interest in numerical computations, especially the expression for the energy $\tilde{E}$. When performing numerical computations, extensive use is made of these quadratic diagnostics, together with the linear diagnostics.

Appendix H

Three-dimensional vortex-dipoles

In this appendix, the use of vortex-dipoles is examined theoretically. The same notation is used as for vortex particles, Sections 3.1 through 3.4. Consequently, many derivations that were presented in detail in these sections are not developed here.

H.1 Singular vortex-dipoles

Singular vortex-dipoles are reviewed in Saffman & Meiron (1986) and define the divergence free velocity field

$$\begin{aligned}\mathbf{u}(\mathbf{x},t) &= \sum_p \left[\boldsymbol{\gamma}^p(t)\,\delta(\mathbf{x}-\mathbf{x}^p(t)) + \nabla\left(\boldsymbol{\gamma}^p(t)\cdot\nabla\left(\frac{1}{4\pi|\mathbf{x}-\mathbf{x}^p(t)|}\right)\right)\right] \\ &= \sum_p \left[\left(\delta(\mathbf{x}-\mathbf{x}^p(t)) - \frac{1}{4\pi|\mathbf{x}-\mathbf{x}^p(t)|^3}\right)\boldsymbol{\gamma}^p(t)\right. \\ &\qquad \left. +3\,\frac{((\mathbf{x}-\mathbf{x}^p(t))\cdot\boldsymbol{\gamma}^p(t))}{4\pi|\mathbf{x}-\mathbf{x}^p(t)|^5}(\mathbf{x}-\mathbf{x}^p(t))\right], \qquad \text{(H.1)}\end{aligned}$$

and the corresponding divergence free vorticity field

$$\begin{aligned}\boldsymbol{\omega}(\mathbf{x},t) = \nabla\wedge\mathbf{u}(\mathbf{x},t) &= \sum_p \nabla\wedge\Big(\boldsymbol{\gamma}^p(t)\,\delta(\mathbf{x}-\mathbf{x}^p(t))\Big) \\ &= \sum_p \nabla\Big(\delta(\mathbf{x}-\mathbf{x}^p(t))\Big)\wedge\boldsymbol{\gamma}^p(t). \qquad \text{(H.2)}\end{aligned}$$

The vector $\boldsymbol{\gamma}^p$ is the strength of the impulsive force necessary to generate such a dipole. The physical significance is that an isolated singular vortex-dipole is an infinitesimal vortex ring with an infinite self-induced velocity.

Singular vortex-dipoles that are aligned along a curve are essentially sections of a cylindrical vortex sheet tube. The dipole strength γ is then proportional to the circulation Γ per unit Lagrangian coordinate (not per unit length!) of the cylindrical vortex sheet and to d^2, the square of the infinitesimal diameter of the cylindrical vortex sheet. On the other hand, $\gamma = \propto \int u\,d\mathbf{x} = \int u\,dS\;l = M\,l$, where M is the volume flow along the curve and l is the distance between adjacent dipoles. Therefore,

$$\gamma \propto \Gamma\,d^2 \propto M\,l\,, \qquad \text{(H.3)}$$

which implies

$$M \propto \frac{\Gamma\, d^2}{l} \,. \tag{H.4}$$

When a straining field locally elongates a cylindrical vortex sheet tube, volume is conserved so that $d^2\, l$ = constant. Since $\mathbf{l}$ is a material line that gets elongated according to $d\mathbf{l}/dt = (\mathbf{l}\cdot\nabla)\,\mathbf{u}$, this implies that d^2 decreases. Recalling that the circulation Γ per unit Lagrangian coordinate is constant, γ decreases. The evolution equations for the vortex-dipole position and strength vector are thus taken as

$$\frac{d}{dt}\mathbf{x}^p(t) = \mathbf{u}(\mathbf{x}^p(t),t)\,, \tag{H.5}$$

$$\frac{d}{dt}\boldsymbol{\gamma}^p(t) = -\left(\boldsymbol{\gamma}^p(t)\cdot\nabla^T\right)\mathbf{u}(\mathbf{x}^p(t),t)\,. \tag{H.6}$$

Equation (H.6) is the equation that gives the correct decreases of the strength vector as will be seen in Section H.4.

The fact that the self-induced velocity of a singular vortex-dipole is infinite makes these dipoles not very useful for numerical computations. The regularized version of these vortex-dipoles is more interesting because the self-induced velocity is finite.

H.2 Regularized vortex-dipoles

Regularized vortex-dipoles define the divergence free velocity field

$$\begin{aligned}
\mathbf{u}_\sigma(\mathbf{x},t) &= \sum_p\Big[\boldsymbol{\gamma}^p(t)\,\zeta_\sigma(\mathbf{x}-\mathbf{x}^p(t)) + \nabla\Big(\boldsymbol{\gamma}^p(t)\cdot\nabla\Big(\chi_\sigma(\mathbf{x}-\mathbf{x}^p(t))\Big)\Big)\Big] \\
&= \sum_p\Bigg[\left(\zeta_\sigma(\mathbf{x}-\mathbf{x}^p(t)) - \frac{g_\sigma(\mathbf{x}-\mathbf{x}^p(t))}{|\mathbf{x}-\mathbf{x}^p(t)|^3}\right)\boldsymbol{\gamma}^p(t) \\
&+ \left(3\,\frac{g_\sigma(\mathbf{x}-\mathbf{x}^p(t))}{|\mathbf{x}-\mathbf{x}^p(t)|^3} - \zeta_\sigma(\mathbf{x}-\mathbf{x}^p(t))\right)\frac{((\mathbf{x}-\mathbf{x}^p(t))\cdot\boldsymbol{\gamma}^p(t))}{|\mathbf{x}-\mathbf{x}^p(t)|^2}(\mathbf{x}-\mathbf{x}^p(t))\Bigg]\,,
\end{aligned} \tag{H.7}$$

and the corresponding divergence free vorticity field

$$\begin{aligned}
\boldsymbol{\omega}_\sigma(\mathbf{x},t) = \nabla\wedge\mathbf{u}_\sigma(\mathbf{x},t) &= \sum_p \nabla\wedge\Big(\boldsymbol{\gamma}^p(t)\,\zeta_\sigma(\mathbf{x}-\mathbf{x}^p(t))\Big) \\
&= \sum_p \nabla\Big(\zeta_\sigma(\mathbf{x}-\mathbf{x}^p(t))\Big)\wedge\boldsymbol{\gamma}^p(t) \\
&= -\sum_p \eta_\sigma(\mathbf{x}-\mathbf{x}^p(t))\,(\mathbf{x}-\mathbf{x}^p(t))\wedge\boldsymbol{\gamma}^p(t)\,.
\end{aligned} \tag{H.8}$$

A regularized vortex-dipole is a fat vortex ring with the velocity field (H.7) and the vorticity field (H.8). Indeed, if a spherical coordinate system centered at $\mathbf{x}^p$, with

$\boldsymbol{\gamma}^p$ aligned with $\theta = 0$ and $\rho = r/\sigma$ is considered, then

$$(\omega_\sigma)_\varphi = \frac{1}{\sigma^5}\,\eta(\rho)\,\gamma\,r\sin\theta\,, \tag{H.9}$$

$$\mathbf{u}_\sigma = \frac{1}{\sigma^3}\left[\left(\zeta(\rho) - \frac{g(\rho)}{\rho^3}\right)\boldsymbol{\gamma} + \left(3\,\frac{g(\rho)}{\rho^3} - \zeta(\rho)\right)\,\gamma\cos\theta\,\hat{\mathbf{e}}_r\right]. \tag{H.10}$$

Figure J.55 illustrates the velocity and vorticity field of a regularized vortex-dipole when the low order algebraic smoothing (B.10) is used. A particularly interesting case is the case in which the Gaussian smoothing (B.8) is used because this case corresponds to the Stokes vortex ring. Indeed, Equations (H.9) and (H.10) give

$$(\omega_\sigma)_\varphi = \frac{1}{(2\pi)^{3/2}\sigma^5}\,e^{-\rho^2/2}\,\gamma\,r\sin\theta\,,$$

$$\mathbf{u}_\sigma = \frac{1}{\sigma^3}\left[\left(\frac{1}{(2\pi)^{3/2}}e^{-\rho^2/2} - \frac{1}{4\pi\rho^3}\left(\mathrm{erf}\left(\frac{\rho}{\sqrt{2}}\right) - \left(\frac{2}{\pi}\right)^{1/2}\rho\,e^{-\rho^2/2}\right)\right)\boldsymbol{\gamma}\right.$$
$$\left. + \left(\frac{3}{4\pi\rho^3}\left(\mathrm{erf}\left(\frac{\rho}{\sqrt{2}}\right) - \left(\frac{2}{\pi}\right)^{1/2}\rho\,e^{-\rho^2/2}\right) - \frac{1}{(2\pi)^{3/2}}e^{-\rho^2/2}\right)\gamma\cos\theta\,\hat{\mathbf{e}}_r\right], \tag{H.11}$$

which are the exact vorticity and velocity fields of the Stokes vortex ring as given by Cantwell (1986) (see also Kambe & Oshima 1975) where $\sigma^2 = 2\,\nu\,t$ and γ is the linear impulse of the ring. This ring is a self-similar solution of the heat equation in spherical coordinates, i.e.,

$$\frac{\partial\omega_\varphi}{\partial t} = \nu\left[\frac{1}{r^2}\frac{\partial}{\partial r}\left(r^2\frac{\partial\omega_\varphi}{\partial r}\right) + \frac{1}{r^2\sin\theta}\frac{\partial}{\partial\theta}\left(\sin\theta\frac{\partial\omega_\varphi}{\partial\theta}\right) - \frac{\omega_\varphi}{r^2\sin^2\theta}\right]$$
$$= \nu\left[\frac{1}{r}\frac{\partial^2}{\partial r^2}\left(r\,\omega_\varphi\right) + \frac{1}{r^2}\frac{\partial}{\partial\theta}\left(\frac{1}{\sin\theta}\frac{\partial}{\partial\theta}\left(\omega_\varphi\sin\theta\right)\right)\right]. \tag{H.12}$$

Regularized vortex-dipoles (i.e., fat vortex rings) aligned along a curve are essentially sections of a fat cylindrical vortex sheet (i.e., a cylindrical vortex sheet of diameter $d << \sigma$ where σ is the thickness of the sheet). Here, d is not infinitesimal, but the discussion on the evolution equation for the strength vector that was presented in Section H.1 still applies. The evolution equations for the position and strength vector of a regularized vortex-dipole are thus taken as

$$\frac{d}{dt}\mathbf{x}^p(t) = \mathbf{u}_\sigma(\mathbf{x}^p(t),t)\,, \tag{H.13}$$

$$\frac{d}{dt}\boldsymbol{\gamma}^p(t) = -\left(\boldsymbol{\gamma}^p(t)\cdot\nabla^T\right)\mathbf{u}_\sigma(\mathbf{x}(t),t)\,. \tag{H.14}$$

The behavior of a cylindrical vortex sheet tube is completely different from the behavior of a vortex tube. A straining field that locally elongates a vortex tube locally increases the value of α according to Equation (3.34). α increases so that the circulation $\Gamma \propto \alpha/l$ is conserved. Vorticity does not leak away from a vortex tube.

On the other hand, a straining field that locally elongates a cylindrical vortex sheet tube locally decreases the value of γ. The volume flow along the tube thus locally decreases since $M \propto \gamma/l$ (γ decreases and l increases!). The volume flow along the tube is not conserved. Fluid is drawn away from the tube at places where the tube gets stretched and is entrained toward the tube at places where the tube gets squeezed. A cylindrical vortex sheet tube is thus not a streamtube.

The evolution equations (H.13) and (H.14) conserve linear impulse but do not conserve angular impulse. (Total vorticity $\mathbf{\Omega} = 0$ and is thus trivially conserved). To investigate these invariants, one first defines the following functions

$$\begin{aligned} f_\sigma(\mathbf{x}) &= \zeta_\sigma(\mathbf{x}) - \frac{g_\sigma(\mathbf{x})}{|\mathbf{x}|^3} , \\ h_\sigma(\mathbf{x}) &= \frac{1}{|\mathbf{x}|^2}\left(3\,\frac{g_\sigma(\mathbf{x})}{|\mathbf{x}|^3} - \zeta_\sigma(\mathbf{x})\right) , \end{aligned} \tag{H.15}$$

and the following notation

$$f^{pq} = f_\sigma(\mathbf{x}-\mathbf{x}^q(t))\Big|_{\mathbf{x}=\mathbf{x}^p(t)} ; \qquad \frac{\partial f^{pq}}{\partial x_i} = \frac{\partial}{\partial x_i} f_\sigma(\mathbf{x}-\mathbf{x}^q(t))\Big|_{\mathbf{x}=\mathbf{x}^p(t)} , \tag{H.16}$$

and similarly for h^{pq} and $\partial h^{pq}/\partial x_i$. Notice that $f^{pq} = f^{qp}$, $h^{pq} = h^{qp}$, $\partial f^{pq}/\partial x_i = -\partial f^{qp}/\partial x_i$ and $\partial h^{pq}/\partial x_i = -\partial h^{qp}/\partial x_i$. Using suffix notation, one obtains, for the evolution equations,

$$\frac{d}{dt}x_i^p = \sum_q f^{pq}\,\gamma_i^q + h^{pq}\left((\mathbf{x}^p-\mathbf{x}^q)\cdot\boldsymbol{\gamma}^q\right)(x_i^p - x_i^q) , \tag{H.17}$$

$$\begin{aligned} \frac{d}{dt}\gamma_i^p &= -\gamma_l^p \frac{\partial}{\partial x_i}\left[\sum_q f_\sigma(\mathbf{x}-\mathbf{x}^q)\,\gamma_l^q + h_\sigma(\mathbf{x}-\mathbf{x}^q)\left((\mathbf{x}-\mathbf{x}^q)\cdot\boldsymbol{\gamma}^q\right)(x_l - x_l^q)\right]_{\mathbf{x}=\mathbf{x}^p} \\ &= -\sum_q\Bigg[\gamma_l^p\gamma_l^q\,\frac{\partial f^{pq}}{\partial x_i} + \frac{\partial h^{pq}}{\partial x_i}\,(x_m^p - x_m^q)\gamma_m^q\,(x_l^p - x_l^q)\gamma_l^p \\ &\qquad + h^{pq}\,\gamma_i^q\,(x_l^p - x_l^q)\gamma_l^p + h^{pq}\,(x_m^p - x_m^q)\gamma_m^q\,\gamma_i^p\Bigg] \\ &= -\sum_q\Bigg[(\boldsymbol{\gamma}^p\cdot\boldsymbol{\gamma}^q)\,\frac{\partial f^{pq}}{\partial x_i} + \left((\mathbf{x}^p-\mathbf{x}^q)\cdot\boldsymbol{\gamma}^p\right)\left((\mathbf{x}^p-\mathbf{x}^q)\cdot\boldsymbol{\gamma}^q\right)\frac{\partial h^{pq}}{\partial x_i} \\ &\qquad + h^{pq}\left(\left((\mathbf{x}^p-\mathbf{x}^q)\cdot\boldsymbol{\gamma}^p\right)\gamma_i^q + \left((\mathbf{x}^p-\mathbf{x}^q)\cdot\boldsymbol{\gamma}^q\right)\gamma_i^p\right)\Bigg] . \end{aligned} \tag{H.18}$$

This gives, for the rate of change of the linear impulse,

$$\begin{aligned} \frac{d}{dt}I_i &= \frac{d}{dt}\left(\frac{1}{2}\sum_p \boldsymbol{\gamma}^p{}_i\right) \\ &= -\frac{1}{2}\sum_{p,q}\Bigg[(\boldsymbol{\gamma}^p\cdot\boldsymbol{\gamma}^q)\,\frac{\partial f^{pq}}{\partial x_i} + \left((\mathbf{x}^p-\mathbf{x}^q)\cdot\boldsymbol{\gamma}^p\right)\left((\mathbf{x}^p-\mathbf{x}^q)\cdot\boldsymbol{\gamma}^q\right)\frac{\partial h^{pq}}{\partial x_i} \end{aligned}$$

$$+h^{pq}\left(((\mathbf{x}^p-\mathbf{x}^q)\cdot\boldsymbol{\gamma}^p)\,\boldsymbol{\gamma}_i^q+((\mathbf{x}^p-\mathbf{x}^q)\cdot\boldsymbol{\gamma}^q)\,\boldsymbol{\gamma}_i^p\right)\Big]$$

$$= 0\,, \tag{H.19}$$

thus showing that the linear impulse is conserved.

For the angular impulse, one considers

$$\frac{d}{dt}\mathbf{A}=\frac{d}{dt}\left(\frac{1}{2}\sum_p \mathbf{x}^p\wedge\boldsymbol{\gamma}^p\right)=\frac{1}{2}\sum_p\left(\frac{d}{dt}\mathbf{x}^p\wedge\boldsymbol{\gamma}^p\right)+\frac{1}{2}\sum_p\left(\mathbf{x}^p\wedge\frac{d}{dt}\boldsymbol{\gamma}^p\right)\,. \tag{H.20}$$

The first term on the rhs of Equation (H.20) is given by

$$\begin{aligned}\frac{1}{2}\sum_p\left(\frac{d}{dt}\mathbf{x}^p\wedge\boldsymbol{\gamma}^p\right) &= -\frac{1}{2}\sum_{p,q}h^{pq}\,\boldsymbol{\gamma}^q\wedge\boldsymbol{\gamma}^p+h^{pq}\,((\mathbf{x}^p-\mathbf{x}^q)\cdot\boldsymbol{\gamma}^q)\,((\mathbf{x}^p-\mathbf{x}^q)\wedge\boldsymbol{\gamma}^p)\\ &= -\frac{1}{2}\sum_{p,q}h^{pq}\,((\mathbf{x}^p-\mathbf{x}^q)\cdot\boldsymbol{\gamma}^q)\,((\mathbf{x}^p-\mathbf{x}^q)\wedge\boldsymbol{\gamma}^p)\\ &\neq 0\end{aligned} \tag{H.21}$$

in general. The second term in Equation (H.20) also does not vanish in general, and the angular impulse is not conserved.

One can also associate to each dipole its own core size $\sigma=\sigma^p$. and make use of the model equation $\sigma^{p\,2}\,l=$ constant which ensures volume conservation. Unfortunately, this requires keeping track of the distance l in between adjacent vortex-dipoles. With that choice, the linear inpulse is still conserved provided the evolution equations are symmetrized, i.e., $\sigma^{pq}=\sigma^{qp}$, where σ^{pq} is the core size that is used to compute the influence of the dipole q on the dipole p and conversely.

H.3 The vortex-dipole as the limit of four vortex particles

It is interesting to notice that a three-dimensional vortex-dipole is the limit of four vortex particles of equal strength magnitude $|\boldsymbol{\alpha}|$ and configured in a fashion that ressembles a vortex ring. This is very similar to two-dimensional vortex-dipoles that are the limit of two vortex blobs of same circulation Γ but opposite sign.

Without loss of generality, the four vortex particles are taken to lie in the $x-y$ plane with positions $\mathbf{x}^p=\mathbf{x}^c\pm(dx/2)\,\hat{\mathbf{e}}_x$, $\mathbf{x}^p=\mathbf{x}^c\pm(dy/2)\,\hat{\mathbf{e}}_y$ as shown in Figure J.56. Each vortex particle has a vorticity field of the form

$$\boldsymbol{\omega}_\sigma^p(\mathbf{x})=\boldsymbol{\alpha}^p\,\zeta_\sigma(\mathbf{x}-\mathbf{x}^p)+\nabla\Big(\boldsymbol{\alpha}^p\cdot\nabla\big(\chi_\sigma(\mathbf{x}-\mathbf{x}^p)\big)\Big)\,. \tag{H.22}$$

The limit of the vorticity field when $dx=dy=d<<\sigma$ is now considered. In that limit, the second term in Equation (H.22) does not contribute to the global vorticity

field. The first term leads to

$$\begin{aligned}
\boldsymbol{\omega}_\sigma(\mathbf{x}) &= -\alpha\,\hat{\mathbf{e}}_y\,\zeta_\sigma\left(\mathbf{x}-(\mathbf{x}^c-(dx/2)\,\hat{\mathbf{e}}_x)\right)+\alpha\,\hat{\mathbf{e}}_y\,\zeta_\sigma\left(\mathbf{x}-(\mathbf{x}^c+(dx/2)\,\hat{\mathbf{e}}_x)\right)\\
&\quad +\alpha\,\hat{\mathbf{e}}_x\,\zeta_\sigma\left(\mathbf{x}-(\mathbf{x}^c-(dy/2)\,\hat{\mathbf{e}}_y)\right)-\alpha\,\hat{\mathbf{e}}_y\,\zeta_\sigma\left(\mathbf{x}-(\mathbf{x}^c+(dy/2)\,\hat{\mathbf{e}}_y)\right)\\
&= -(\alpha\,\hat{\mathbf{e}}_y)\,dx\,\frac{\partial}{\partial x}\zeta_\sigma(\mathbf{x}-\mathbf{x}^c)+(\alpha\,\hat{\mathbf{e}}_x)\,dy\,\frac{\partial}{\partial y}\zeta_\sigma(\mathbf{x}-\mathbf{x}^c)\\
&= \nabla\Big(\zeta_\sigma(\mathbf{x}-\mathbf{x}^c)\Big)\wedge((\alpha\,d)\,\hat{\mathbf{e}}_z)\\
&= -\eta_\sigma(\mathbf{x}-\mathbf{x}^c)\,(\mathbf{x}-\mathbf{x}^c)\wedge\boldsymbol{\gamma}\,, \qquad \text{(H.23)}
\end{aligned}$$

where $\boldsymbol{\gamma}=\gamma\,\hat{\mathbf{e}}_z=(\alpha\,d)\,\hat{\mathbf{e}}_z$ is the strength of the vortex-dipole. Notice that $\alpha\,d\propto\Gamma\,d^2$ where Γ is the circulation of the little vortex ring. This fact makes the connection with Equation (H.3).

In the same way as above, it is easy to show that the limit of the Biot-Savart velocity field induced by the four vortex particles also leads to the velocity field of a regularized vortex-dipole

$$\mathbf{u}_\sigma(\mathbf{x})=\boldsymbol{\gamma}\,\zeta_\sigma(\mathbf{x}-\mathbf{x}^c)+\nabla\Big(\boldsymbol{\gamma}\cdot\nabla\Big(\chi_\sigma(\mathbf{x}-\mathbf{x}^c)\Big)\Big)\,. \qquad \text{(H.24)}$$

H.4 Two-dimensional vortex-dipoles

The motivation for examining two dimensional vortex-dipoles is that, in this case, one can easily obtain the exact expression for the evolution equation of the strength vector. This evolution equation is used to suggest the proper evolution equation for the three-dimensional vortex-dipoles.

In two dimensions, singular vortex-dipoles define the divergence free velocity field

$$\mathbf{u}(\mathbf{x},t)=\sum_p\left[\boldsymbol{\gamma}^p(t)\,\delta(\mathbf{x}-\mathbf{x}^p(t))-\nabla\left(\boldsymbol{\gamma}^p(t)\cdot\nabla\left(\frac{1}{2\pi}\log(|\mathbf{x}-\mathbf{x}^p(t)|)\right)\right)\right]\,, \qquad \text{(H.25)}$$

and the corresponding divergence free vorticity field

$$\boldsymbol{\omega}(\mathbf{x},t)=\nabla\wedge\mathbf{u}(\mathbf{x},t)=\sum_p\nabla\Big(\delta(\mathbf{x}-\mathbf{x}^p(t))\Big)\wedge\boldsymbol{\gamma}^p(t)\,. \qquad \text{(H.26)}$$

To obtain the expression for the divergence free velocity field (H.25), use has been made of the fact that, in two dimensions, $\nabla^2\left(\frac{1}{2\pi}\log|\mathbf{x}|\right)=\delta(\mathbf{x})$.

These singular dipoles are not very useful because their self-induced velocity is infinite. Each singular dipole is a pair of point vortices of same circulation Γ but opposite sign and that are an infinitesimal distance d apart. When singular dipoles are aligned along a curve, they essentially define a singular vortex-dipole sheet. This

sheet is made of two singular vortex sheets of equal but opposite sign circulation per unit Lagrangian coordinate (not per unit length!) and that are an infinitesimal distance d apart.

Regularized vortex-dipoles define the divergence free velocity field

$$\mathbf{u}_\sigma(\mathbf{x},t) = \sum_p \left[\boldsymbol{\gamma}^p(t)\,\zeta_\sigma(\mathbf{x}-\mathbf{x}^p(t)) - \nabla\Big(\boldsymbol{\gamma}^p(t)\cdot\nabla\big(\chi_\sigma(\mathbf{x}-\mathbf{x}^p(t))\big)\Big)\right] , \qquad \text{(H.27)}$$

and the corresponding divergence free vorticity field

$$\begin{aligned}\boldsymbol{\omega}_\sigma(\mathbf{x},t) = \nabla\wedge\mathbf{u}_\sigma(\mathbf{x},t) &= \sum_p \nabla\big(\zeta_\sigma(\mathbf{x}-\mathbf{x}^p(t))\big)\wedge\boldsymbol{\gamma}^p(t) \\ &= -\sum_p \eta_\sigma(\mathbf{x}-\mathbf{x}^p(t))\,(\mathbf{x}-\mathbf{x}^p(t))\wedge\boldsymbol{\gamma}^p(t) . \qquad \text{(H.28)}\end{aligned}$$

Here, $\zeta_\sigma(\mathbf{x})$ is an approximation to the two-dimensional δ-function which is usually taken as radially symmetric, i.e., $\zeta_\sigma(\mathbf{x}) = \zeta(|\mathbf{x}|/\sigma)/\sigma^2$ with $\zeta(\rho)$ a smoothing function such that $2\pi\int_0^\infty \zeta(\rho)\,\rho\,d\rho = 1$. $\eta(\rho) = -\zeta'(\rho)/\rho$ and $\eta_\sigma(\mathbf{x}) = \eta(|\mathbf{x}|/\sigma)/\sigma^4$. The expression for the divergence free velocity field (H.27) has been obtained by defining $\chi(\rho)$ such that $\nabla^2\chi(\rho) = \zeta(\rho)$, and $\chi_\sigma(\mathbf{x}) = \chi(|\mathbf{x}|/\sigma)$.

A list of the regularization functions that are most commonly used is given in Table B.2.

It is easy to see that a regularized vortex-dipole is the limit of two vortex blobs of same circulation Γ but opposite sign as they get close to each other. Indeed, if a pair of vortex blobs at $\mathbf{x}^p = \mathbf{x}^c \pm d\mathbf{x}/2$ as shown in Figure J.56 is considered, then, in the limit $|d\mathbf{x}| << \sigma$, one obtains

$$\begin{aligned}\boldsymbol{\omega}_\sigma(\mathbf{x}) &= \left[\zeta_\sigma\left(\mathbf{x}-(\mathbf{x}^c-d\mathbf{x}/2)\right) - \zeta_\sigma\left(\mathbf{x}-(\mathbf{x}^c+d\mathbf{x}/2)\right)\right]\Gamma\,\hat{\mathbf{e}}_z \\ &= \Big[d\mathbf{x}\cdot\nabla\big(\zeta_\sigma(\mathbf{x}-\mathbf{x}^c)\big)\Big]\,\Gamma\,\hat{\mathbf{e}}_z \\ &= \nabla\big(\zeta_\sigma(\mathbf{x}-\mathbf{x}^c)\big)\wedge(\Gamma(\hat{\mathbf{e}}_z\wedge d\mathbf{x})) \\ &= \nabla\big(\zeta_\sigma(\mathbf{x}-\mathbf{x}^c)\big)\wedge\boldsymbol{\gamma} \\ &= -\eta_\sigma(\mathbf{x}-\mathbf{x}^c)\,(\mathbf{x}-\mathbf{x}^c)\wedge\boldsymbol{\gamma} , \qquad \text{(H.29)}\end{aligned}$$

where $\boldsymbol{\gamma} = \Gamma\,\hat{\mathbf{e}}_z\wedge d\mathbf{x}$ is the strength vector of the dipole. It is also easy to show that the Biot-Savart velocity field induced by the pair of vortex blobs is given by

$$\mathbf{u}_\sigma(\mathbf{x}) = \boldsymbol{\gamma}\,\zeta_\sigma(\mathbf{x}-\mathbf{x}^c) - \nabla\Big(\boldsymbol{\gamma}\cdot\big(\chi_\sigma(\mathbf{x}-\mathbf{x}^c)\big)\Big) . \qquad \text{(H.30)}$$

The velocity field (H.27) and the vorticity field (H.28) of a regularized vortex-dipole are thus recovered. Notice that d is now finite as opposed to the case of singular vortex-dipoles. The only restriction on d is that it is much smaller than σ.

When regularized vortex-dipoles are aligned along a curve, they essentially define a regularized vortex-dipole sheet. This sheet is made of two thick vortex sheets of equal but opposite sign circulation per unit Lagrangian coordinate Γ and that are apart a distance $d << \sigma$, where σ is the thickness of each vortex sheet. The dipole strength γ is proportional to Γd. Also, $\gamma \propto M l$ where M is the volume flow along the curve and l is the distance between adjacent dipoles.

The evolution equation for a regularized vortex-dipole can be found by using the fact that a vortex-dipole is a pair of opposite signs vortex blobs that are close to each other. Then, recalling that Γ is a constant and that $d\mathbf{x}$ is a material line, one can write

$$\begin{aligned} \frac{d}{dt}\boldsymbol{\gamma} = \Gamma \frac{d}{dt}(\hat{\mathbf{e}}_z \wedge d\mathbf{x}) &= \Gamma\, \hat{\mathbf{e}}_z \wedge \frac{d}{dt} d\mathbf{x} \\ &= \Gamma\, \hat{\mathbf{e}}_z \wedge (d\mathbf{x} \cdot \nabla)\mathbf{u} \\ &= \hat{\mathbf{e}}_z \wedge ((\boldsymbol{\gamma} \wedge \hat{\mathbf{e}}_z) \cdot \nabla)\mathbf{u} \\ &= -\left(\boldsymbol{\gamma} \cdot \nabla^T\right)\mathbf{u}\,, \end{aligned} \tag{H.31}$$

where the last equality has been obtained by recalling that $\nabla \cdot \mathbf{u} = 0$ so that $\frac{\partial u}{\partial x}$ can be replaced by $-\frac{\partial v}{\partial y}$ and conversely. This equation is identical to the evolution equation for the vorticity gradient in two dimensions (see Chapter 4, Section 4.1).

The evolution equations for the position and strength vector of a vortex-dipole are thus taken as

$$\frac{d}{dt}\mathbf{x}^p(t) = \mathbf{u}_\sigma(\mathbf{x}^p(t), t)\,, \tag{H.32}$$

$$\frac{d}{dt}\boldsymbol{\gamma}^p(t) = -\left(\boldsymbol{\gamma}^p(t) \cdot \nabla^T\right)\mathbf{u}_\sigma(\mathbf{x}^p(t), t)\,. \tag{H.33}$$

These evolution equations are of course also used when the vortex-dipoles are aligned so as to form a vortex-dipole sheet. Recently, Krasny (1988) has used a combination of a vortex sheet and a vortex-dipole sheet to investigate the time evolution of a periodic shear layer with a wake component

Notice that a vortex-dipole sheet is not a streamtube. Indeed, a straining field that locally elongates a vortex-dipole sheet decreases the value of γ. The volume flow along the tube thus locally decreases since $M \propto \gamma/l$ (γ decreases and l increases!). The volume flow along the dipole sheet is thus not conserved. Fluid goes away from the sheet at places where the sheet gets stretched and is entrained toward the sheet at places where the sheet gets squeezed.

It is a matter of simple algebra to show that the evolution equations (H.32) and (H.33) conserve the linear impulse $\mathbf{I} = \frac{1}{2}\sum_p \boldsymbol{\gamma}^p$ but do not conserve the angular impulse $\mathbf{A} = \frac{1}{2}\sum_p \mathbf{x}^p \wedge \boldsymbol{\gamma}^p$.

If each dipole is assigned its own core size $\sigma = \sigma^p$ which is subjected to the area conservation equation $\sigma^p l = \text{constant}$, then the linear impulse is still conserved provided the evolution equations are symmetrized, i.e., $\sigma^{pq} = \sigma^{qp}$.

Appendix I

The evaluation of quadratic diagnostics when using filaments of vorticity curl or particles of vorticity gradient

In this appendix, the evaluation of quadratic diagnostics such as the the Hamiltonian (i.e., the kinetic energy when $\Omega = 0$) and the enstrophy is examined when the vorticity gradient is represented with filaments of $\nabla\omega \wedge \hat{\mathbf{e}}_z$ or particles of $\nabla\omega$.

I.1 The singular case

I.1.1 Singular filaments of vorticity curl

Singular filaments of $\nabla\omega \wedge \hat{\mathbf{e}}_z$ define the divergence free field, Equation (4.5). The divergence free velocity field is solution of $\nabla^2\mathbf{u} = -\nabla\omega \wedge \hat{\mathbf{e}}_z$ and is given by Equation (4.7).

The evaluation of the Hamiltonian E is delicate. This is due to the fact that the integral $\frac{1}{2}\int \psi\,\omega\,d\mathbf{x}$ cannot be reduced to an integral that involves only velocity and vorticity gradient. Instead, one must solve for the streamfunction and evaluate the integral as is. Recalling that, in two-dimensional flows, the expression for the streamfunction is given by

$$\psi(\mathbf{x}) = -\frac{1}{2\pi}\int \log\left(\frac{|\mathbf{x}-\mathbf{x}'|}{a}\right)\omega(\mathbf{x}')\,d\mathbf{x}'\,, \tag{I.1}$$

one obtains

$$E = -\frac{1}{4\pi}\int\int \log\left(\frac{|\mathbf{x}-\mathbf{x}'|}{a}\right)\omega(\mathbf{x})\,\omega(\mathbf{x}')\,d\mathbf{x}\,d\mathbf{x}'\,. \tag{I.2}$$

Notice that, because of the arbitrariness in the choice of the length scale a when defining the streamfunction ψ, it follows that E is only defined up to some constant times the square of the total circulation Ω. Consequently, E is unique only when it is the kinetic energy of the system, i.e., when $\Omega = 0$.

With singular filaments of $\nabla\omega \wedge \hat{\mathbf{e}}_z$, one obtains

$$\begin{aligned} E &= -\frac{1}{4\pi}\sum_p \Delta\omega^p \int_{\mathcal{A}^p}\left(\sum_q \Delta\omega^q \int_{\mathcal{A}^q} \log\left(\frac{|\mathbf{x}-\mathbf{x}'|}{a}\right) d\mathbf{x}'\right) d\mathbf{x} \\ &= -\frac{1}{4\pi}\sum_{p,q} \Delta\omega^p\,\Delta\omega^q \int_{\mathcal{A}^p}\left(\int_{\mathcal{A}^q} \log\left(\frac{|\mathbf{x}-\mathbf{x}'|}{a}\right) d\mathbf{x}'\right) d\mathbf{x}\,. \end{aligned} \tag{I.3}$$

It is necessary to turn the surface integrals in Equation (I.3) into contour integrals. It must thus be shown that the integrand can be written as the curl of some vector function so that use can be made of Stokes theorem. First, notice that

$$\begin{aligned} \int_{\mathcal{A}} F\left(\frac{|\mathbf{x}|}{a}\right) d\mathbf{x} &= \int_{\mathcal{A}} \hat{\mathbf{e}}_z \cdot \nabla\wedge\left(G\left(\frac{|\mathbf{x}|}{a}\right)(\hat{\mathbf{e}}_z \wedge \mathbf{x})\right) d\mathbf{x} \\ &= \int_C G\left(\frac{|\mathbf{x}|}{a}\right) \hat{\mathbf{e}}_z \cdot (\mathbf{x} \wedge d\mathbf{x})\,, \end{aligned} \tag{I.4}$$

where

$$\rho\, G'(\rho) + 2\, G(\rho) = F(\rho)\,, \tag{I.5}$$

and that

$$\begin{aligned} \int_{\mathcal{A}} x\, F\left(\frac{|\mathbf{x}|}{a}\right) d\mathbf{x} &= \int_{\mathcal{A}} \hat{\mathbf{e}}_z \cdot \nabla\wedge\left(x\, H\left(\frac{|\mathbf{x}|}{a}\right)(\hat{\mathbf{e}}_z \wedge \mathbf{x})\right) d\mathbf{x} \\ &= \int_C x\, H\left(\frac{|\mathbf{x}|}{a}\right) \hat{\mathbf{e}}_z \cdot (\mathbf{x} \wedge d\mathbf{x})\,, \end{aligned} \tag{I.6}$$

where

$$\rho\, H'(\rho) + 3\, H(\rho) = F(\rho)\,, \tag{I.7}$$

and similarly for $\int_{\mathcal{A}} y\, F(|\mathbf{x}|/a)\, d\mathbf{x}$. Using these identities, it is easy to show that

$$\int_{\mathcal{A}} \log\left(\frac{|\mathbf{x}|}{a}\right) d\mathbf{x} = \frac{1}{2}\int_C \left(\log\left(\frac{|\mathbf{x}|}{a}\right) - \frac{1}{2}\right) \hat{\mathbf{e}}_z \cdot (\mathbf{x} \wedge d\mathbf{x})\,, \tag{I.8}$$

$$\int_{\mathcal{A}} x\, d\mathbf{x} = \frac{1}{3}\int_C x\, \hat{\mathbf{e}}_z \cdot (\mathbf{x} \wedge d\mathbf{x})\,, \tag{I.9}$$

$$\int_{\mathcal{A}} x \log\left(\frac{|\mathbf{x}|}{a}\right) d\mathbf{x} = \frac{1}{3}\int_C x \left(\log\left(\frac{|\mathbf{x}|}{a}\right) - \frac{1}{3}\right) \hat{\mathbf{e}}_z \cdot (\mathbf{x} \wedge d\mathbf{x})\,. \tag{I.10}$$

With this knowledge, Equation (I.3) can be written as

$$\begin{aligned} E &= \frac{1}{8\pi}\sum_{p,q} \Delta\omega^p\,\Delta\omega^q\, \hat{\mathbf{e}}_z \cdot \int_{C^q}\left[\int_{\mathcal{A}^p} d\mathbf{x}\left(\log\left(\frac{|\mathbf{x}-\mathbf{x}^q|}{a}\right) - \frac{1}{2}\right)(\mathbf{x}-\mathbf{x}^q)\right] \wedge d\mathbf{x}^q \\ &= \frac{1}{24\pi}\sum_{p,q} \Delta\omega^p\,\Delta\omega^q\, \hat{\mathbf{e}}_z \cdot \int_{C^q}\left[\int_{C^p}\left(\log\left(\frac{|\mathbf{x}^p-\mathbf{x}^q|}{a}\right) - \frac{5}{6}\right)(\mathbf{x}^p-\mathbf{x}^q)\right. \end{aligned}$$

$$(\hat{\mathbf{e}}_z \cdot ((\mathbf{x}^p - \mathbf{x}^q) \wedge d\mathbf{x}^p))\Big] \wedge d\mathbf{x}^q$$

$$= \frac{1}{24\pi} \sum_{p,q} \Delta\omega^p \, \Delta\omega^q \int_{\mathcal{C}^q} \int_{\mathcal{C}^p} \left(\log\left(\frac{|\mathbf{x}^p - \mathbf{x}^q|}{a} \right) - \frac{5}{6} \right) ((\mathbf{x}^p - \mathbf{x}^q) \cdot (\hat{\mathbf{e}}_z \wedge d\mathbf{x}^p))$$
$$((\mathbf{x}^p - \mathbf{x}^q) \cdot (\hat{\mathbf{e}}_z \wedge d\mathbf{x}^q)) . \quad \text{(I.11)}$$

where $d\mathbf{x}^p$ stands for $\partial \mathbf{x}^p / \partial s \, ds$ and $d\mathbf{x}^q$ stands for $\partial \mathbf{x}^q / \partial s' \, ds'$. Using the observation that the area of the vortex patch $\mathcal{A}^q$ is precisely given by $\frac{1}{2} \hat{\mathbf{e}}_z \cdot \int_{\mathcal{C}^q} \mathbf{x}^q \wedge d\mathbf{x}^q$, one can also write, instead of Equation (I.11),

$$E = \frac{1}{8\pi} \sum_{p,q} \Delta\omega^p \, \Delta\omega^q \, \hat{\mathbf{e}}_z \cdot \int_{\mathcal{C}^q} \left[\int_{\mathcal{A}^p} d\mathbf{x} \, \log\left(\frac{|\mathbf{x} - \mathbf{x}^q|}{a} \right) (\mathbf{x} - \mathbf{x}^q) \right] \wedge d\mathbf{x}^q$$
$$- \frac{1}{8\pi} \sum_{p,q} \Delta\omega^p \, \Delta\omega^q \, \mathcal{A}^q \int_{\mathcal{A}^p} d\mathbf{x}$$
$$= \frac{1}{24\pi} \sum_{p,q} \Delta\omega^p \, \Delta\omega^q \int_{\mathcal{C}^q} \int_{\mathcal{C}^p} \left(\log\left(\frac{|\mathbf{x}^p - \mathbf{x}^q|}{a} \right) - \frac{1}{3} \right) ((\mathbf{x}^p - \mathbf{x}^q) \cdot (\hat{\mathbf{e}}_z \wedge d\mathbf{x}^p))$$
$$((\mathbf{x}^p - \mathbf{x}^q) \cdot (\hat{\mathbf{e}}_z \wedge d\mathbf{x}^q))$$
$$- \frac{1}{8\pi} \Omega^2 . \quad \text{(I.12)}$$

The expressions (I.11) and (I.12) are exact expressions for E when using singular contours of $\nabla\omega \wedge \hat{\mathbf{e}}_z$. It is believed that these expressions are new.

The evaluation of the enstrophy $\mathcal{E} = \int \omega \, \omega \, d\mathbf{x}$ is much easier than the evaluation of the Hamiltonian E because the integral can be turned into an integral involving only velocity and vorticity gradient. For singular filaments, one obtains

$$\mathcal{E} = \int \omega \, \omega \, d\mathbf{x} = \int \mathbf{u} \cdot (\nabla\omega \wedge \hat{\mathbf{e}}_z) \, d\mathbf{x}$$
$$= -\frac{1}{2\pi} \sum_{p,q} \Delta\omega^p \, \Delta\omega^q \int_{\mathcal{C}^p(t)} \int_{\mathcal{C}^q(t)} \log\left(\frac{|\mathbf{x}^p - \mathbf{x}^q|}{a} \right) \left(\frac{\partial \mathbf{x}^p}{\partial s} \cdot \frac{\partial \mathbf{x}^q}{\partial s'} \right) ds \, ds' . \quad \text{(I.13)}$$

I.1.2 Singular particles of vorticity gradient

With singular particles, the particle field $\nabla\omega$ is given by Equation (4.27) and is not divergence free. The divergence free field $\nabla\omega^N$ is given by Equation (4.31). The velocity field is solution of $\nabla^2 \mathbf{u} = -\nabla\omega \wedge \hat{\mathbf{e}}_z$ and is given by Equation (4.29). This velocity field is also not divergence free.

The evaluation of the Hamiltonian E is difficult. First, as in contour dynamics, the integral $\frac{1}{2} \int \psi \, \omega \, d\mathbf{x}$ cannot be reduced to an integral that involves only velocity and vorticity gradient. Second, as opposed to contour dynamics, the streamfunction

is unknown and so are its integrals. (Only its derivatives such as the velocity are known!) Thus, the integral $\frac{1}{2}\int \psi\,\omega\,d\mathbf{x}$ cannot be evaluated. One must consider, instead, the velocity integral $\frac{1}{2}\int \mathbf{u}\cdot\mathbf{u}\,d\mathbf{x}$ which only converges when $\Omega = 0$ (in which case it is equivalent to $\frac{1}{2}\int \psi\,\omega\,d\mathbf{x}$).

With singular particles, one has

$$\begin{aligned} E &= \frac{1}{2}\int \mathbf{u}\cdot\mathbf{u}\,d\mathbf{x} \\ &= \frac{1}{8\pi^2}\sum_{p,q}\left(\int \log\left(\frac{|\mathbf{x}-\mathbf{x}^p|}{a}\right)\log\left(\frac{|\mathbf{x}-\mathbf{x}^q|}{a}\right)d\mathbf{x}\right)\boldsymbol{\alpha}^p\cdot\boldsymbol{\alpha}^q\,. \end{aligned} \tag{I.14}$$

For each pair (p,q), the integral is performed using a local polar coordinate system centered at $\mathbf{x}^p$. Notice that the integral does not converge at ∞ (it diverges like $\int^\infty t\,\log^2 t\,dt$). However, when $\Omega = 0$, the sum of all the (p,q) pairs integral converges since $\frac{1}{2}\int \mathbf{u}\cdot\mathbf{u}\,d\mathbf{x}$ converges. The contribution at ∞ may thus be discarded. Defining $\mathbf{x}-\mathbf{x}^p = \mathbf{x}'$, $\mathbf{x}-\mathbf{x}^q = \mathbf{x}' + (\mathbf{x}^p - \mathbf{x}^q)$, $d\mathbf{x} = d\mathbf{x}' = dr\;r\,d\theta$, $z = |\mathbf{x}^p - \mathbf{x}^q|/a$ and $t = r/a$, one obtains

$$\begin{aligned} I &= \int \log\left(\frac{|\mathbf{x}-\mathbf{x}^p|}{a}\right)\log\left(\frac{|\mathbf{x}-\mathbf{x}^q|}{a}\right)d\mathbf{x} \\ &= \frac{a^2}{2}\int_0^\infty dt\,t\,\log t\int_0^{2\pi} d\theta\,\log(t^2+2tz\cos\theta+z^2) \\ &= 2\pi\,a^2\left(\log z\int_0^z dt\,t\,\log t + \int_z^\infty dt\,t\,\log^2 t\right) \\ &= \pi\,a^2\left(\log z\,\left[t^2(\log t - 1/2)\right]_0^z + \left[t^2\,(\log t - 1/2)^2 + t^2\right]_z^\infty\right) \\ &= \frac{\pi}{2}\,a^2\,z^2\,(\log z - 1)\,, \end{aligned} \tag{I.15}$$

where the contribution at ∞ is not taken for the reasons explained above. Finally,

$$E = \frac{1}{16\pi}\sum_{p,q}|\mathbf{x}^p-\mathbf{x}^q|^2\left(\log\left(\frac{|\mathbf{x}^p-\mathbf{x}^q|}{a}\right)-1\right)\boldsymbol{\alpha}^p\cdot\boldsymbol{\alpha}^q\,. \tag{I.16}$$

Notice that the $q = p$ term does not give any contribution even though singular particles have been considered. So far, there is no guarantee that Equation (I.16) is the appropriate integral for $\frac{1}{2}\int \psi\,\omega\,d\mathbf{x}$ when $\Omega \neq 0$. It turns out that it is as will be shown from numerical examples in Section 4.5. So, although this is somewhat of a mystery, it must be true that the process of neglecting the contribution from ∞ in the integral $\frac{1}{2}\int \mathbf{u}\cdot\mathbf{u}\,d\mathbf{x}$ is exactly what needs to be done in order to obtain the correct expression for $\frac{1}{2}\int \psi\,\omega\,d\mathbf{x}$ when $\Omega \neq 0$.

Proceeding now with the evaluation of the enstrophy, and using integration by parts, one obtains

$$\mathcal{E} = \int \omega\,\omega\,d\mathbf{x} = \int \mathbf{u}\cdot(\nabla\omega^N \wedge \hat{\mathbf{e}}_z)\,d\mathbf{x}\,. \tag{I.17}$$

Notice that, due to the non-zero divergence of the particle field $\nabla\omega\wedge\hat{\mathbf{e}}_z$, the enstrophy cannot simply be written as

$$\mathcal{E}_{cd} = \int \mathbf{u}\cdot(\nabla\omega\wedge\hat{\mathbf{e}}_z)\,d\mathbf{x} = -\frac{1}{2\pi}\sum_{\substack{p,q\\ p\neq q}} \log\left(\frac{|\mathbf{x}^p-\mathbf{x}^q|}{a}\right)\,\boldsymbol{\alpha}^p\cdot\boldsymbol{\alpha}^q\,, \qquad \text{(I.18)}$$

where the $q=p$ term has been removed in order to avoid a logarithmic infinity. Equation (I.18) is only valid when the particle discretization of $\nabla\omega\wedge\hat{\mathbf{e}}_z$ is a good representation of a divergence free field. If an expression that is valid for all times is required, Equation (I.17) must be integrated in closed form. To achieve this, the notation $\boldsymbol{\beta}^p=\boldsymbol{\alpha}^p\wedge\hat{\mathbf{e}}_z$ is first defined. One then obtains

$$\begin{aligned}\mathcal{E} &= \int \mathbf{u}\cdot(\nabla\omega^N\wedge\hat{\mathbf{e}}_z)\,d\mathbf{x}\\ &= -\frac{1}{2\pi}\sum_{\substack{p,q\\ p\neq q}} \log\left(\frac{|\mathbf{x}^p-\mathbf{x}^q|}{a}\right)\boldsymbol{\beta}^p\cdot\boldsymbol{\beta}^q\\ &\quad+\left(\frac{1}{2\pi}\right)^2\sum_{\substack{p,q\\ p\neq q}}\int \log\left(\frac{|\mathbf{x}-\mathbf{x}^p|}{a}\right)\beta_j^p\frac{\partial}{\partial x_j}\left(\beta_k^q\frac{\partial}{\partial x_k}\log\left(\frac{|\mathbf{x}-\mathbf{x}^q|}{a}\right)\right)d\mathbf{x}\,.\end{aligned} \qquad \text{(I.19)}$$

The integral in Equation (I.19) is written as

$$\begin{aligned}&\sum_{\substack{p,q\\ p\neq q}}\beta_j^p\,\beta_k^q\int\log\left(\frac{|\mathbf{x}-\mathbf{x}^p|}{a}\right)\frac{\partial}{\partial x_j}\frac{\partial}{\partial x_k}\log\left(\frac{|\mathbf{x}-\mathbf{x}^q|}{a}\right)d\mathbf{x}\\ &\quad=-\sum_{\substack{p,q\\ p\neq q}}\beta_j^p\,\beta_k^q\int\frac{\partial}{\partial x_j}\log\left(\frac{|\mathbf{x}-\mathbf{x}^p|}{a}\right)\frac{\partial}{\partial x_k}\log\left(\frac{|\mathbf{x}-\mathbf{x}^q|}{a}\right)d\mathbf{x}\\ &\quad=-\sum_{\substack{p,q\\ p\neq q}}\beta_j^p\,\beta_k^q\frac{\partial}{\partial x_j^p}\frac{\partial}{\partial x_k^q}\int\log\left(\frac{|\mathbf{x}-\mathbf{x}^p|}{a}\right)\log\left(\frac{|\mathbf{x}-\mathbf{x}^q|}{a}\right)d\mathbf{x}\,,\end{aligned} \qquad \text{(I.20)}$$

where use has been made of the symmetry relation $\frac{\partial}{\partial x_i}\log\left(\frac{|\mathbf{x}-\mathbf{x}^p|}{a}\right)=-\frac{\partial}{\partial x_i^p}\log\left(\frac{|\mathbf{x}-\mathbf{x}^p|}{a}\right)$. Recalling Equation (I.15) for the integral I appearing in Equation (I.20), one proceeds with

$$\begin{aligned}\frac{\partial}{\partial x_j^p}\frac{\partial}{\partial x_k^q}(I) &= \frac{\partial}{\partial x_j^p}\left(\frac{\partial z}{\partial x_k^q}\frac{d}{dz}(I)\right)\\ &= \pi\,a^2\frac{\partial}{\partial x_j^p}\left(-\frac{(x_k^p-x_k^q)}{a^2\,z}\,z(\log z-1/2)\right)\\ &= -\pi\left(\delta_{jk}(\log z-1/2)+\frac{(x_k^p-x_k^q)(x_j^p-x_j^q)}{a^2\,z^2}\right)\,.\end{aligned} \qquad \text{(I.21)}$$

All the elements necessary to evaluate the enstrophy have been derived. Recalling that $\boldsymbol{\beta}^p = \boldsymbol{\alpha}^p \wedge \hat{\mathbf{e}}_z$, one finally obtains

$$\begin{aligned}\mathcal{E} &= -\frac{1}{2\pi}\sum_{\substack{p,q\\p\neq q}} \log\left(\frac{|\mathbf{x}^p-\mathbf{x}^q|}{a}\right)\boldsymbol{\alpha}^p\cdot\boldsymbol{\alpha}^q \\ &\quad + \frac{1}{4\pi}\sum_{\substack{p,q\\p\neq q}}\left[\left(\log\left(\frac{|\mathbf{x}^p-\mathbf{x}^q|}{a}\right)-\frac{1}{2}\right)\boldsymbol{\alpha}^p\cdot\boldsymbol{\alpha}^q \right. \\ &\qquad \left. + \frac{(\hat{\mathbf{e}}_z\cdot((\mathbf{x}^p-\mathbf{x}^q)\wedge\boldsymbol{\alpha}^p))(\hat{\mathbf{e}}_z\cdot((\mathbf{x}^p-\mathbf{x}^q)\wedge\boldsymbol{\alpha}^q))}{|\mathbf{x}^p-\mathbf{x}^q|^2}\right]. \qquad \text{(I.22)}\end{aligned}$$

Notice the difference between this exact result and the approximation (I.18). Of course, the second term in the exact result is small when the particles discretization of $\nabla\omega\wedge\hat{\mathbf{e}}_z$ is still a good representation of a divergence free field. It is useful to keep track of both expressions when doing numerical computations because their difference gives an indication of how consistent the computation is.

I.2 The regularized case

For regularized filaments or particles methods, it is necessary to smooth only one term in the integrand of a quadratic diagnostic in order to obtain a closed form expression for the integral. The approximation of a quadratic diagnostic by smoothing only one term in the integrand was discussed in the context of vortex particles, Section G.2.1, but applies equally well in the present context. The reader is referred to Section G.2.1 for the justification of such a procedure.

I.2.1 Regularized filaments of vorticity curl

Regularized filaments of $\nabla\omega\wedge\hat{\mathbf{e}}_z$ define the divergence free field $(\nabla\omega)_\sigma\wedge\hat{\mathbf{e}}_z$, Equation (4.10). The divergence free velocity field is solution of $\nabla^2\mathbf{u}_\sigma = -(\nabla\omega)_\sigma\wedge\hat{\mathbf{e}}_z$ and is given by Equation (4.22) with $\nabla^2\chi(\rho)=\zeta(\rho)$.

The evaluation of the diagnostics is done using the same procedure as for singular filaments, Section I.1.1.

The evaluation of the Hamiltonian is first considered. ω is taken constant within each patch, but a regularized streamfunction is now considered. The semi-regularized Hamiltonian is thus defined as

$$\begin{aligned}\tilde{E} &= \frac{1}{2}\int\psi_\sigma\,\omega\,d\mathbf{x} \\ &= -\frac{1}{2}\int\int\chi_\sigma(\mathbf{x}-\mathbf{x}')\,\omega(\mathbf{x})\,\omega(\mathbf{x}')\,d\mathbf{x}\,d\mathbf{x}'\end{aligned}$$

$$= -\frac{1}{2}\sum_p \Delta\omega^p \int_{A^p}\left(\sum_q \Delta\omega^q \int_{A^q} \chi_\sigma(\mathbf{x}-\mathbf{x}')\,d\mathbf{x}'\right) d\mathbf{x}\,. \qquad \text{(I.23)}$$

Again, it is necessary to turn the surface integrals in Equation (I.23) into contour integrals. This cannot easily be done for an arbitrary smoothing function $\zeta(\rho)$. There is however one smoothing for which this can be done in closed form: the high order algebraic smoothing (B.13) which has a corresponding $\chi(\rho)$ function given by

$$\chi(\rho) = \frac{1}{4\pi}\left(\log(\rho^2+1) + \frac{\rho^2}{\rho^2+1}\right)\,. \qquad \text{(I.24)}$$

Using the relations (I.4) through (I.7), and defining $\rho = |\mathbf{x}|/\sigma$, it can be shown that

$$\int_A \left(\log(\rho^2+1) + \frac{\rho^2}{\rho^2+1}\right) d\mathbf{x} = \frac{1}{2}\int_C \log(\rho^2+1)\,\hat{\mathbf{e}}_z\cdot(\mathbf{x}\wedge d\mathbf{x})\,, \qquad \text{(I.25)}$$

$$\int_A x\,\log(\rho^2+1)\,d\mathbf{x} = \frac{1}{3}\int_C x\,\left(\log(\rho^2+1) + 2\,\frac{(\rho-\arctan\rho)}{\rho^3} - \frac{2}{3}\right)\hat{\mathbf{e}}_z\cdot(\mathbf{x}\wedge d\mathbf{x})\,, \qquad \text{(I.26)}$$

so that Equation (I.23) becomes

$$\begin{aligned}\tilde{E} &= \frac{1}{8\pi}\sum_{p,q}\Delta\omega^p\,\Delta\omega^q\,\hat{\mathbf{e}}_z\cdot\int_{C^q}\left[\int_{A^p} d\mathbf{x}\,\frac{1}{2}\log\left(\frac{|\mathbf{x}-\mathbf{x}^q|^2}{\sigma^2}+1\right)(\mathbf{x}-\mathbf{x}^q)\right]\wedge d\mathbf{x}^q \\ &= \frac{1}{24\pi}\sum_{p,q}\Delta\omega^p\,\Delta\omega^q\int_{C^q}\int_{C^p}\left(\frac{1}{2}\log\left(\frac{|\mathbf{x}^p-\mathbf{x}^q|^2}{\sigma^2}+1\right)+\frac{\left(\frac{|\mathbf{x}^p-\mathbf{x}^q|}{\sigma}-\arctan\left(\frac{|\mathbf{x}^p-\mathbf{x}^q|}{\sigma}\right)\right)}{\left(\frac{|\mathbf{x}^p-\mathbf{x}^q|}{\sigma}\right)^3}-\frac{1}{3}\right) \\ &\qquad ((\mathbf{x}^p-\mathbf{x}^q)\cdot(\hat{\mathbf{e}}_z\wedge d\mathbf{x}^p))\,((\mathbf{x}^p-\mathbf{x}^q)\cdot(\hat{\mathbf{e}}_z\wedge d\mathbf{x}^q))\,. \qquad \text{(I.27)}\end{aligned}$$

The evaluation of the semi-regularized enstrophy is now considered. Again, the integral for the enstrophy can be reduced to an integral involving only velocity and vorticity gradient and is thus easy to perform, namely,

$$\begin{aligned}\tilde{\mathcal{E}} &= \int \omega_\sigma\,\omega\,d\mathbf{x} = \int \mathbf{u}_\sigma\cdot(\nabla\omega\wedge\hat{\mathbf{e}}_z)\,d\mathbf{x} \\ &= -\sum_{p,q}\Delta\omega^p\,\Delta\omega^q\int_{C^p(t)}\int_{C^q(t)}\chi_\sigma(\mathbf{x}^p-\mathbf{x}^q)\left(\frac{\partial\mathbf{x}^p}{\partial s}\cdot\frac{\partial\mathbf{x}^q}{\partial s'}\right)ds\,ds'\,. \qquad \text{(I.28)}\end{aligned}$$

I.2.2 Regularized particles of vorticity gradient

With regularized particles, the particle field $(\nabla\omega)_\sigma$ is given by Equation (4.42) and is not divergence free. The divergence free field $(\nabla\omega)_\sigma^N$ is given by Equation (4.45). The velocity field is solution of $\nabla^2\mathbf{u}_\sigma = -(\nabla\omega)_\sigma\wedge\hat{\mathbf{e}}_z$ and is given by Equation (4.43) with $\nabla^2\chi(\rho) = \zeta(\rho)$. This velocity field is also not divergence free.

The evaluation of the diagnostics is done using the same procedure as with singular particles, Section I.1.2

For the Hamiltonian, the following semi-regularized velocity integral is examined:

$$\begin{aligned}\tilde{E} &= \frac{1}{2}\int \mathbf{u}_\sigma \cdot \mathbf{u}\, d\mathbf{x} \\ &= \frac{1}{8\pi^2}\sum_{p,q}\left(2\pi \int \chi_\sigma(\mathbf{x}-\mathbf{x}^p)\,\log\left(\frac{|\mathbf{x}-\mathbf{x}^q|}{\sigma}\right) d\mathbf{x}\right)\boldsymbol{\alpha}^p\cdot\boldsymbol{\alpha}^q\,. \end{aligned} \tag{I.29}$$

The integral in parenthesis cannot be done in general. Only in the case of the high order algebraic smoothing (B.13) could a closed form expression for that integral be obtained. Indeed, if that smoothing is considered,

$$\begin{aligned} I &= 2\pi \int \chi_\sigma(\mathbf{x}-\mathbf{x}^p)\,\log\left(\frac{|\mathbf{x}-\mathbf{x}^q|}{\sigma}\right) d\mathbf{x} \\ &= \frac{\sigma^2}{4}\int_0^\infty dt\, t\left(\log(t^2+1)+\frac{t^2}{t^2+1}\right)\int_0^{2\pi} d\theta\,\log(t^2+2tz\cos\theta+z^2) \\ &= \pi\,\sigma^2\left[\log z\int_0^z dt\, t\left(\log(t^2+1)+\frac{t^2}{t^2+1}\right)\right. \\ &\qquad\left. +\int_z^\infty dt\, t\,\log t\left(\log(t^2+1)+\frac{t^2}{t^2+1}\right)\right] \\ &= \frac{\pi}{2}\sigma^2\left[\log z\,\left[t^2\,\log(t^2+1)\right]_0^z\right. \\ &\qquad\left. +\left[t^2\log t\,\log(t^2+1)-\frac{1}{2}(t^2+1)(\log(t^2+1)-1)\right]_z^\infty\right] \\ &= \frac{\pi}{4}\sigma^2\,(z^2+1)\,(\log(z^2+1)-1)\,, \end{aligned} \tag{I.30}$$

where the contribution at ∞ is again not taken. One thus finally obtains

$$\tilde{E} = \frac{1}{32\pi}\sum_{p,q}(|\mathbf{x}^p-\mathbf{x}^q|^2+\sigma^2)\left(\log\left(\frac{|\mathbf{x}^p-\mathbf{x}^q|^2}{\sigma^2}+1\right)-1\right)\boldsymbol{\alpha}^p\cdot\boldsymbol{\alpha}^q\,. \tag{I.31}$$

Again, it turns out that Equation (I.31) is the appropriate expression for E even when $\Omega = 0$. Numerical evidence of this fact is given in Section 4.5.

The evaluation of the semi-regularized enstrophy is now considered,

$$\tilde{\mathcal{E}} = \int \omega_\sigma\,\omega\, d\mathbf{x} = \int \mathbf{u}_\sigma\cdot(\nabla\omega^N\wedge\hat{\mathbf{e}}_z)\, d\mathbf{x}\,. \tag{I.32}$$

Again, due to the non-zero divergence of the particle field $(\nabla\omega)_\sigma\wedge\hat{\mathbf{e}}_z$, the semi-regularized enstrophy cannot be simply written as

$$\tilde{\mathcal{E}}_{cd} = \int \mathbf{u}_\sigma\cdot(\nabla\omega\wedge\hat{\mathbf{e}}_z)\, d\mathbf{x} = -\sum_{p,q}\chi_\sigma(\mathbf{x}^p-\mathbf{x}^q)\,\boldsymbol{\alpha}^p\cdot\boldsymbol{\alpha}^q\,. \tag{I.33}$$

where the $q = p$ term does not make any contribution since $\chi(\rho) = \mathcal{O}(\rho^2)$ for small ρ. Equation (I.33) is only an approximation to $\tilde{\mathcal{E}}$ that is valid as long as the the particle discretization of $(\nabla\omega)_\sigma \wedge \hat{\mathbf{e}}_z$ is still a good representation of a divergence free field. The exact expression for $\tilde{\mathcal{E}}$ is obtained by writing, with the same notation as for singular particles,

$$\begin{aligned}\tilde{\mathcal{E}} &= \int \mathbf{u}_\sigma \cdot (\nabla\omega^N \wedge \hat{\mathbf{e}}_z)\, d\mathbf{x} \\ &= -\sum_{p,q} \chi_\sigma(\mathbf{x}^p - \mathbf{x}^q)\, \boldsymbol{\beta}^p \cdot \boldsymbol{\beta}^q \\ &\quad + \left(\frac{1}{2\pi}\right)^2 \sum_{p,q} \int 2\pi \chi_\sigma(\mathbf{x} - \mathbf{x}^p)\, \beta_j^p \frac{\partial}{\partial x_j}\left(\beta_k^q \frac{\partial}{\partial x_k} \log\left(\frac{|\mathbf{x} - \mathbf{x}^q|}{a}\right)\right) d\mathbf{x}\,.\end{aligned} \tag{I.34}$$

The integral in Equation (I.34) is written as

$$\begin{aligned}&\sum_{p,q} \beta_j^p\, \beta_k^q \int 2\pi\, \chi_\sigma(\mathbf{x} - \mathbf{x}^p) \frac{\partial}{\partial x_j}\frac{\partial}{\partial x_k} \log\left(\frac{|\mathbf{x} - \mathbf{x}^q|}{a}\right) d\mathbf{x} \\ &\qquad = -2\pi \sum_{p,q} \beta_j^p\, \beta_k^q \frac{\partial}{\partial x_j^p}\frac{\partial}{\partial x_k^q} \int \chi_\sigma(\mathbf{x} - \mathbf{x}^p)\, \log\left(\frac{|\mathbf{x} - \mathbf{x}^q|}{a}\right) d\mathbf{x}\,,\end{aligned} \tag{I.35}$$

In general, the integral appearing in Equation (I.35) cannot be done in closed form. However, if the high order algebraic smoothing is considered, then the integral can be done and is given by I, Equation (I.30). Therefore,

$$\begin{aligned}\frac{\partial}{\partial x_j^p}\frac{\partial}{\partial x_k^q}(I) &= \frac{\pi}{2}\sigma^2 \frac{\partial}{\partial x_j^p}\left(-\frac{(x_k^p - x_k^q)}{\sigma^2\, z} z \log(z^2+1)\right) \\ &= -\pi\left(\delta_{jk}\frac{1}{2}\log(z^2+1) + \frac{(x_k^p - x_k^q)(x_j^p - x_j^q)}{\sigma^2(z^2+1)}\right)\,.\end{aligned} \tag{I.36}$$

Notice how compact the result is. This is due to the nice integration properties of the high order algebraic smoothing. All the elements necessary to obtain the exact semi-regularized enstrophy have been derived, and

$$\begin{aligned}\tilde{\mathcal{E}} &= -\frac{1}{2\pi}\sum_{p,q}\frac{1}{2}\left(\log\left(\frac{|\mathbf{x}^p - \mathbf{x}^q|^2}{\sigma^2} + 1\right) + \frac{|\mathbf{x}^p - \mathbf{x}^q|^2}{|\mathbf{x}^p - \mathbf{x}^q|^2 + \sigma^2}\right) \boldsymbol{\alpha}^p \cdot \boldsymbol{\alpha}^q \\ &\quad + \frac{1}{4\pi}\sum_{p,q}\left[\frac{1}{2}\log\left(\frac{|\mathbf{x}^p - \mathbf{x}^q|^2}{\sigma^2} + 1\right) \boldsymbol{\alpha}^p \cdot \boldsymbol{\alpha}^q \right. \\ &\qquad \left. + \frac{(\hat{\mathbf{e}}_z \cdot ((\mathbf{x}^p - \mathbf{x}^q) \wedge \boldsymbol{\alpha}^p))(\hat{\mathbf{e}}_z \cdot ((\mathbf{x}^p - \mathbf{x}^q) \wedge \boldsymbol{\alpha}^q))}{|\mathbf{x}^p - \mathbf{x}^q|^2 + \sigma^2}\right]\,.\end{aligned} \tag{I.37}$$

Again, the second term in this exact result is small as long as the divergence of the particle representation of $(\nabla\omega)_\sigma \wedge \hat{\mathbf{e}}_z$ is small. In numerical computations, it is interesting to keep track of both expressions, Equation (I.33) and Equation (I.37), because their difference is an indication of how consistent the computation is.

I.3 Some important remarks

A few remarks concerning the above evaluation of the Hamiltonian E (or $\tilde{E}$):

- The evaluation of E with singular particles of $\nabla\omega$ does not rely on the fact that particles are used instead of contours. Consequently, another exact expression for the Hamiltonian when using singular filaments of $\nabla\omega \wedge \hat{\mathbf{e}}_z$ (i.e., contour dynamics) was found, and which is totally equivalent to Equation (I.11), namely

$$E = \frac{1}{16\pi} \sum_{p,q} \Delta\omega^p \, \Delta\omega^q \int_{\mathcal{C}^q} \int_{\mathcal{C}^p} |\mathbf{x}^p - \mathbf{x}^q|^2 \left(\log\left(\frac{|\mathbf{x}^p - \mathbf{x}^q|}{a} \right) - 1 \right) d\mathbf{x}^p \cdot d\mathbf{x}^q \, . \tag{I.38}$$

  Notice how different the two expressions are. It is remarkable that Equation (I.38) which involves only dot products of elements of contours ($d\mathbf{x}^p \cdot d\mathbf{x}^q$) is equivalent to Equation (I.11) which involves dot products of relative positions and elements of contours ($((\mathbf{x}^p - \mathbf{x}^q) \cdot d\mathbf{x}^p)((\mathbf{x}^p - \mathbf{x}^q) \cdot d\mathbf{x}^q)$).

- The evaluation of $\tilde{E}$ with regularized particles of $\nabla\omega$ does not rely on the fact that particles are used instead of contours. Consequently, an expression for $\tilde{E}$ was also found for regularized filaments of $\nabla\omega \wedge \hat{\mathbf{e}}_z$, namely

$$\begin{aligned} \tilde{E} \;=\; & \frac{1}{32\pi} \sum_{p,q} \Delta\omega^p \Delta\omega^q \int_{\mathcal{C}^p} \int_{\mathcal{C}^q} (|\mathbf{x}^p - \mathbf{x}^q|^2 + \sigma^2) \\ & \left(\log\left(\frac{|\mathbf{x}^p - \mathbf{x}^q|^2}{\sigma^2} + 1 \right) - 1 \right) d\mathbf{x}^p \cdot d\mathbf{x}^q \, . \end{aligned} \tag{I.39}$$

  This expression is equivalent to Equation (I.27) since, in general, $\frac{1}{2} \int \psi_\sigma \, \omega \, d\mathbf{x} = \frac{1}{2} \int \mathbf{u}_\sigma \cdot \mathbf{u} \, d\mathbf{x}$.

- The converse of the above is not true. The evaluation of E with singular filaments of $\nabla\omega \wedge \hat{\mathbf{e}}_z$ relies on the fact that contours are used instead of particles. In other words, Equation (I.16) and the discretization onto particles of Equation (I.11), using $\boldsymbol{\alpha} = \hat{\mathbf{e}}_z \wedge (\omega \, d\mathbf{x})$,

$$E_{cd} \simeq \frac{1}{24\pi} \sum_{p,q} \left(\log\left(\frac{|\mathbf{x}^p - \mathbf{x}^q|}{a} \right) - \frac{5}{6} \right) ((\mathbf{x}^p - \mathbf{x}^q) \cdot \boldsymbol{\alpha}^p)((\mathbf{x}^p - \mathbf{x}^q) \cdot \boldsymbol{\alpha}^q) \, , \tag{I.40}$$

  are not equivalent. Equation (I.40) is not equal to E when a particle representation of $\nabla\omega$ is understood. Of course, the two expressions are identical as long as the particles are aligned as if $\boldsymbol{\alpha} \wedge \hat{\mathbf{e}}_z$ were a discretization of a contour of $\nabla\omega \wedge \hat{\mathbf{e}}_z$. In numerical computations with particles of $\nabla\omega$, it is interesting to keep track of both quantities because their difference is an indication of how well the particle method is doing.

- The same remark applies to Equation (I.31) and the discretization onto particles of Equation (I.27), $\tilde{E}_{cd}$.

References

[1] Abramowitz, M. & Stegun, I. E. 1972. *Handbook of Mathematical Functions, Applied Mathematics Series* **55**, Nat. Bur. Stand., 10th ed.

[2] Agishtein, M. E. & Migdal, A. A. 1986. Computer simulation of three-dimensional vortex dynamics. *Modern Physics Letters A* **1** (3), 221-30.

[3] Aksman, M. J., Novikov, E. A. & Orszag, S. A. 1985. Vorton method in three-dimensional hydrodynamics. *Phys. Rev. Letters* **54** (22), 2410-13.

[4] Anderson, C. & Greengard, C. 1984. On vortex methods. *SIAM J. Numer. Anal.* **22**, 413.

[5] Anderson, C. 1986. A method of local corrections for computing the velocity field due to a distribution of vortex blobs. *J. Comput. Phys.* **62**, 111-23.

[6] Appel, A. 1985. An efficient program for many-body simulation. *SIAM J. Sci. Stat. Comput.* **6**, 85-103.

[7] Aref, H. & Flinchem, E. P. 1984. Dynamics of a vortex filament in a shear flow. *J. Fluid Mech.* **148**, 477-97.

[8] Arms, R. J. & Hama, F. R. 1965. Localized-induction concept on a curved vortex and motion of an elliptical vortex ring. *Phys. Fluids* **8**, 553-59.

[9] Ashurst, W. T. 1979. Numerical simulation of turbulent mixing layers via vortex dynamics. In *Turbulent Shear Flows I*, Eds. F. Durst et al.: Springer-Verlag, 402-13 (Also *Sandia Nat. Labs, Livermore*, SAND77-8612).

[10] Ashurst, W. T. 1983. Large eddy simulation via vortex dynamics. *AIAA 6th Comput. Fluid Dyn. Conf.*, Danvers, Mass., AIAA-83-1879-CP.

[11] Ashurst, W. T. & Meiburg, E. 1985. Three-dimensional shear layers via vortex dynamics, *Sandia Nat. Labs, Livermore*, SAND85-8777.

[12] Ashurst, W. T. & Meiron, D. I. 1987. Numerical study of vortex reconnection. *Phys. Rev. Letters* **58** (16), 1632-35.

[13] Batchelor, G. K. 1967. *An Introduction to Fluid Dynamics.* Cambridge University Press.

[14] Beale, J. T. & Majda, A. 1981. Rates of convergence for viscous splitting of the Navier-Stokes equations. *Math. Comput.* **37**, 243-59.

[15] Beale, J. T. & Majda, A. 1982a. Vortex methods, I: convergence in three dimensions. *Math. Comput.* **39**, 1-27.

[16] Beale, J. T. & Majda, A. 1982b. Vortex methods, II: higher order accuracy in two and three dimensions. *Math. Comput.* **39**, 29-52.

[17] Beale, J. T. 1986a. On the accuracy of vortex methods at large times. *Proceedings of the Workshop on Computational Fluid Dynamics and Reacting Flows*, I.M.A. Univ. of Minnesota.

[18] Beale, J. T. 1986b. A convergent 3-D vortex method with grid-free stretching. *Math. Comput.* **46**, 401-23 and S15-20.

[19] Bender, C. M. & Orszag, S. A. 1978. *Advanced Mathematical Methods for Scientists and Engineers.* McGraw-Hill.

[20] Betchov, R. 1965. On the curvature and torsion of an isolated vortex filament. *J. Fluid Mech.* **22**, 471-79.

[21] Cantaloube, B. & Huberson, S. 1984. A vortex point method for calculating inviscid incompressible flows around rotary wings. *Rech. Aérosp.* **6**, 19-31.

[22] Cantwell, B. J. 1986. Viscous starting jets. *J. Fluid Mech.* **173**, 159-89.

[23] Carrier, G. F., Krook, M. & Pearson, C. E. 1983. *Functions of a Complex Variable: theory and technique.* Hod Books, Ithaca, N.Y.

[24] Chen, H. L. & Oshima, K. 1988. Numerical analysis of reconnection of vortex rings. *Inst. Space and Astron. Sci. Rep. SP* **6**, 3-12.

[25] Choquin, J.-P. 1987. Simulation numérique d'écoulements tourbillonnaires de fluides incompressibles par des méthodes particulaires. *Thèse de Doctorat.* Université Paris VI.

[26] Choquin, J.-P. & Cottet, G.-H. 1988. Sur l'analyse d'une classe de méthodes de vortex tridimensionnelles. *C. R. Acad. Sci. Paris* **306**, Série I, 739-42.

[27] Choquin, J.-P. & Huberson, S. 1988. Particle simulation of viscous flow. Submitted to *Computers and Fluids.*

[28] Chua, K., Leonard, A., Pepin, F. & Winckelmans, G. 1988. Robust vortex methods for three-dimensional incompressible flows. *Proceedings of the Symposium on Recent Developments in Comput. Fluid Dynamics, ASME Winter Annual Meeting*, Chicago, Illinois, AMD-Vol.95.

[29] Cieśliński, J. 1986. Exact solution to the localized-induction-approximation equation modeling smoke ring motion. *Phys. Rev. Letters* **57** (13), 1507-10.

[30] Cottet, G.-H. 1982. Méthode particulaire pour l'équation d'Euler dans le plan. *Thèse de 3 ème cycle.* Université Paris VI.

[31] Cottet, G.-H. 1987. Sur l'analyse des méthodes particulaires pour certain problèmes non linéaires. *Thèse d'Etat.* Université Pierre et Marie Curie, Paris.

[32] Cottet, G.-H. 1988. A new aproach for the analysis of vortex methods in two and three dimensions, *Ann. Inst. Henri Poincaré* **5**, 227-85.

[33] Cottet, G.-H. & Mas-Gallic, S. 1983. A particle method to solve transport-diffusion equations - Part I: the linear case. *Centre de Math. Appl., Ecole Polytechnique, Palaiseau, France*, Internal Report **115**. (Submitted to *Num. Math.*).

[34] Cottet, G.-H. & Mas-Gallic, S. 1987. A particle method to solve transport-diffusion equations - Part II: the Navier-Stokes. *Centre de Math. Appl., Ecole Polytechnique, Palaiseau, France*, Internal Report **158**. (Submitted to *Num. Math.*) .

[35] Crow, S. C. 1970. Stability theory for a pair of trailing vortices. *AIAA J.* **8**, 2172-79.

[36] Degond, P. & Mas-Gallic, S. 1988a. The weighted particle method for convection-diffusion equations - Part I: the case of an isotropic viscosity. Submitted to *Math. Comput.*

[37] Degond, P. & Mas-Gallic, S. 1988b. The weighted particle method for convection-diffusion equations - Part II: the anisotropic case. Submitted to *Math. Comput.*

[38] Dritschel, D. G. 1985. The stability and energetics of corotating uniform vortices. *J. Fluid Mech.* **157**, 95-134.

[39] Dritschel, D. G. 1986. The nonlinear evolution of rotating configurations of uniform vorticity. *J. Fluid Mech.* **172**, 157-82.

[40] Dritshel, D. G. 1988. Contour surgery: a topological reconnection scheme for extended integrations using contour dynamics. *J. Comput. Phys.* **77**, 240-66.

[41] Fraenkel, L. E. 1970. On steady vortex rings of small cross-section in an ideal fluid. *Proc. R. Soc. London Ser. A* **316**, 29-62.

[42] Fraenkel, L. E. 1972. Examples of steady vortex rings of small cross-section in an ideal fluid. *J. Fluid Mech.* **51** (1), 119-35.

[43] Gradshteyn, I. S. & Ryzhik, I. M. 1980. *Tables of Integrals, Series and Products.* Academic Press.

[44] Greengard, C. 1986. Convergence of the vortex filament method. *Math. Comput.* **47**, 387-98.

[45] Greengard, L. & Rokhlin, V. 1987. A fast algorithm for particle simulations. *J. Comput. Phys.* **73**, 325-48.

[46] Greengard, C. & Thomann, E. 1988. Singular vortex systems and weak solutions of the Euler equations. *Phys. Fluids* **31** (10), 2810-13.

[47] Hama, F. R. 1962. Progressive deformation of a curved vortex filament by its own induction. *Phys. Fluids* **5**, 1156-62.

[48] Hama, F. R. 1963. Progressive deformation of a perturbed line vortex filament. *Phys. Fluids* **6**, 526-34.

[49] Hasimoto, H. 1972. A soliton on a vortex filament. *J. Fluid Mech.* **51** (3), 477-85.

[50] Huberson, S. 1986. Etude numérique et asymptotique de noyaux tourbillonaires. *Thèse d'Etat.* Université Paris VI.

[51] Inoue, O. 1985. Vortex simulation of turbulent mixing layer. *AIAA J.* **23**(3),367-73.

[52] Izutsu, N., Oshima, K. & Oshima, Y. 1987. Experimental study of interacting vortex rings. *Inst. Space and Astron. Sci. Rep. SP* **5**, 3-13.

[53] Jones, D. S. 1966. *Generalized Functions.* MacGraw-Hill.

[54] Kambe, T. & Oshima, Y. 1975. Generation and decay of viscous vortex rings. *J. Phys. Soc. Japan* **38** (1), 271-80.

[55] Kambe, T. 1983. A class of exact solutions of two-dimensional viscous flows. *J. Phys. Soc. Japan* **52** (3), 834-41.

[56] Kelvin, Lord 1880. Vibrations of a columnar vortex. *Phil. Mag.* **10**, 155-68.

[57] Kida, S. & Takaoka, M. 1987. Bridging in vortex reconnection. *Phys. Fluids* **30** (10), 2911-14.

[58] Krasny, R. 1988. A vortex-dipole sheet model for a wake. Submitted to *Phys. Fluids.*

[59] Kuwahara, S. 1986. Studies on vortex motion based on the dividing vorton model. *Inst. Space Space and Astron. Sci. Rep. SP* **4**, 11-21.

[60] Lamb, H. 1932. *Hydrodynamics.* Cambridge University Press, 6th ed.

[61] Leonard, A. 1975. Numerical simulation of interacting, three-dimensional vortex filaments. *Proceedings of the Fourth International Conference on Numerical Methods in Fluid Dynamics*, Colo. Heidelberg: Springer-Verlag, 245-50.

[62] Leonard, A. 1980a. Vortex simulation of three-dimensional spotlike disturbances in a laminar boundary layer. In *Turbulent Shear Flows II.* Berlin/Heidelberg: Springer-Verlag, 67-77.

[63] Leonard, A. 1980b. Vortex methods for flow simulation. *J. Comput. Phys.* **37**, 289-335.

[64] Leonard, A. 1981. Turbulent structures in wall-bounded shear flows observed via three-dimensional numerical simulations. In *the Role of Coherent Structures in Modelling Turbulence and Mixing.* Heidelberg: Springer-Verlag, 119-45.

[65] Leonard, A. 1985. Computing three-dimensional incompressible flows with vortex elements. *Ann. Rev. Fluid Mech.* **17**, 523-59.

[66] Leibovich, S. & Ma, H. Y. 1983. Soliton propagation on vortex cores and the Hasimoto soliton. *Phys. Fluids* **26**, 3173-79.

[67] Mas-Gallic, S. 1987. Contribution à l'analyse numérique des méthodes particulaires. *Thèse d'Etat.* Université Paris VI.

[68] Meiburg, E. & Lasheras, J. C. 1986. Comparison between experiments and numerical simulations of three-dimensional plane wakes. *Phys. Fluids* **30**(3), 623-25.

[69] Meiron, D. I., Ashurst, W. T., Orszag, S. A. & Shelley, M. 1988. Numerical study of vortex reconnection. *Proceedings of the SIAM Workshop on Vortex Dynamics*, Leesburg, Virginia.

[70] Moffatt, H. K. 1969. The degree of knottedness of tangled vortex lines. *J. Fluid Mech.* **35**, 117-29.

[71] Moore, D. W. & Saffman, P. G. 1971. Structure of a line vortex in an imposed strain. In *Aircraft Wake Turbulence* (ed. Olsen, Goldburg & Rogers), 339-54. Plenum Press.

[72] Moore, D. W. 1972. Finite amplitude waves on aircraft trailing vortices. *Aeronaut. Q.* **23**, 307-14.

[73] Moore, D. W. & Saffman, P. G. 1972. The motion of a vortex filament with axial flow. *Philos. Trans. R. Soc. London Ser. A* **272**, 403-29.

[74] Moore, D. W. & Saffman, P. G. 1975. The instability of a straight vortex filament in a strain field. *Proc. R. Soc. London Ser. A* **346**, 413-25.

[75] Mosher, M. C. 1985. A method for computing three-dimensional vortex flows. *Z. Flugwiss. Weltraumforsch.* **9** (3), 125-33.

[76] Nakamura, Y., Leonard, A. & Spalart, P. R. 1982. Vortex simulation of an inviscid shear layer. *AIAA/ASME 3rd Joint Thermophysics, Fluids, Plasma and Heat Tranfer Conference*, St. Louis, Missouri, AIAA-82-0948.

[77] Norbury, J. 1973. A family of steady vortex rings. *J. Fluid Mech.* **53** (3), 417-31.

[78] Novikov, E. A. 1983. Generalized dynamics of three-dimensional vortical singularities (vortons). *Sov. Phys. JETP* **57** (3), 566-69.

[79] Pierrehumbert, R. T. 1986. Remarks on a paper by Aref and Flinchem. *J. Fluid Mech.* **163**, 21-26.

[80] Pumir, A. & Kerr, R. M. 1987. Numerical simulation of interacting vortex tubes. *Phys. Rev. Letters* **58** (16), 1636-39.

[81] Pumir, A. & Siggia, E. D. 1987. Vortex dynamics and the existence of solutions to the Navier-Stokes equations. *Phys. Fluids* **30** (6), 1606-26.

[82] Raviart, P.-A. 1985. An analysis of particle methods. In *Numerical Methods in Fluid Dynamics* (ed. F. Brezzi), Lecture Notes in Mathematics **1127**, 243-324, Springer-Verlag.

[83] Raviart, P.-A. 1987. *Méthodes Particulaires.* Summer School of Numerical Analysis, C.E.A., I.N.R.I.A. & E.D.F., Centre d'Etude du Bréau-sans-Nappe, France.

[84] Rehbach, C. 1973a. Calcul d'écoulements autour d'ailes sans épaisseur avec nappes tourbillonnaires évolutives. *Rech. Aérosp.* **2**, 53-61. (English translations: NASA TT-F 1583 (1973) and ESRO TT 6 (1974)).

[85] Rehbach, C. 1973b. Etude numérique de nappes tourbillonnaires issues d'une ligne de décollement près du bord d'attaque. *Rech. Aérosp.* **6**, 325-30. (English translation: ESA TT 306 (1976)).

[86] Rehbach, C. 1978. Numerical calculation of three-dimensional unsteady flows with vortex sheets. AIAA 16th Aerospace Sci. Meet., Huntsville, Alabama, AIAA-78-28047.

[87] Robinson, A. C. & Saffman, P. G. 1984. Three-dimensional stability of an elliptical vortex in a straining field. *J. Fluid Mech.* **142**, 451-66.

[88] Rosenhead, L. 1930. The spread of vorticity in the wake behind a cylinder. *Proc. R. Soc. London Ser. A* **127**, 590-612.

[89] Saffman, P. G. 1970. The velocity of viscous vortex rings. *Stud. Appl. Math.* **49**, 371-80.

[90] Saffman, P. G. & Baker, G. R. 1979. Vortex interactions. *Ann. Rev. Fluid Mech.* **11**, 95-122.

[91] Saffman, P. G. 1978. The number of waves on unstable vortex rings. *J. Fluid Mech.* **84** (4), 625-39.

[92] Saffman, P. G. & Meiron, D. I. 1986. Difficulties with three-dimensional weak solutions for inviscid incompressible flow. *Phys. Fluids* **29** (8), 2373-75.

[93] Sante Da Rios, L. 1906. Sul moto d'un liquido indefinito con un filello vorticoso di forma qualunque. *Circ. Rend. Mat. Palermo* **22**, 117-35.

[94] Schatzle, P. R. 1987. An experimental study of fusion of vortex rings. *Ph. D. thesis*, California Institute of Technology.

[95] Shirayma, S. & Kuwahara, K. 1984. Vortex method in three-dimensional flows. *Proceedings of the Ninth International Conference on Numerical Methods in Fluid Dynamics*, Springer-Verlag.

[96] Siggia, E. D. 1984. Collapse and amplification of a vortex filament. *Phys. Fluids* **28** (3), 794-805.

[97] Spalart, P. R. & Leonard, A. 1981. Computation of separated flows by a vortex tracing algorithm. AIAA 14th Fluid and Plasma Dynamics Conference, Palo Alto, CA., AIAA-81-1246.

[98] Spalart, P. R. 1982. Numerical simulation of separated flows. *Ph. D. thesis*, Univ. of California, Berkeley.

[99] Spalart, P. R., Leonard, A. & Baganoff, D. 1983. Numerical simulation of separated flows. Nasa Ames Research Center, NASA TM-84328.

[100] Stanaway, S. K., Cantwell, B. J. & Spalart, P. R. 1988. Navier-Stokes simulations of axisymmetric vortex rings. *AIAA 26th Aerospace Sci. Meet.*, Reno, Nevada, AIAA-88-0318.

[101] Takaki, R. & Hussain, A. K. M. H. 1986. Theoretical study of strong interaction of vortex filaments. *Inst. Space and Astron. Sci. Rep. SP* **4**, 3-10.

[102] Tsai, C.-Y. & Widnall, S. E. 1976. The stability of short waves on a straight vortex filament in a weak externally imposed strain field. *J. Fluid Mech.* **73**, 721-33.

[103] Van Dyke, M. 1982. *An Album of Fluid Motion.* Stanford, California: Parabolic Press.

[104] Vaskin, V. É. 1966. Motion of a three-dimensional diffusing vortex tube in an incompressible viscous fluid. *Soviet Physics - Doklady* **10** (12), 1135-37.

[105] Whitham, G. B. 1974. *Linear and Nonlinear Waves.* New York: Wiley.

[106] Widnall, S. E., Bliss, D. B. & Tsai, C.-Y. 1974. The instability of short waves on a vortex ring. *J. Fluid Mech.* **66**, 35-47.

[107] Widnall, S. E. & Tsai, C.-Y. 1977. The instability of the thin vortex ring of constant vorticity. *Philos. Trans. R. Soc. London Ser. A* **287**, 273-305.

[108] Williamson, J. H. 1980. Low-storage Runge-Kutta schemes. *J. Comput. Phys.* **35**, 48-56.

[109] Winckelmans, G. & Leonard, A. 1988a. Weak solutions of the three-dimensional vorticity equation with vortex singularities. *Phys. Fluids* **31** (7), 1838-39.

[110] Winckelmans, G. & Leonard, A. 1988b. Improved vortex methods for three-dimensional flows. *Proceedings of the SIAM Workshop on Vortex Dynamics*, Leesburg, Virginia.

[111] Yamashita, A. & Oshima, Y. 1988. Vortex filament simulation for the crosslinking rings. *Inst. Space and Astron. Sci. Rep. SP* **6**, 13-18.

[112] Zabusky, N. J., Hughes, M. H. & Roberts, K. V. 1979. Contour dynamics for the Euler equations in two dimensions. *J. Comput. Phys.* **30**, 96-106.

[113] Zabusky, N. J. 1981. Recent developments in contour dynamics for the Euler equations. *Ann. NY Acad. Sci.* **373**, 160-70.

[114] Zabusky, N. J. & Overman, E. A. 1983. Regularization of contour dynamical algorithms - 1. Tangential regularization. *J. Comput. Phys.* **52**, 351-73.

Appendix J

Figures

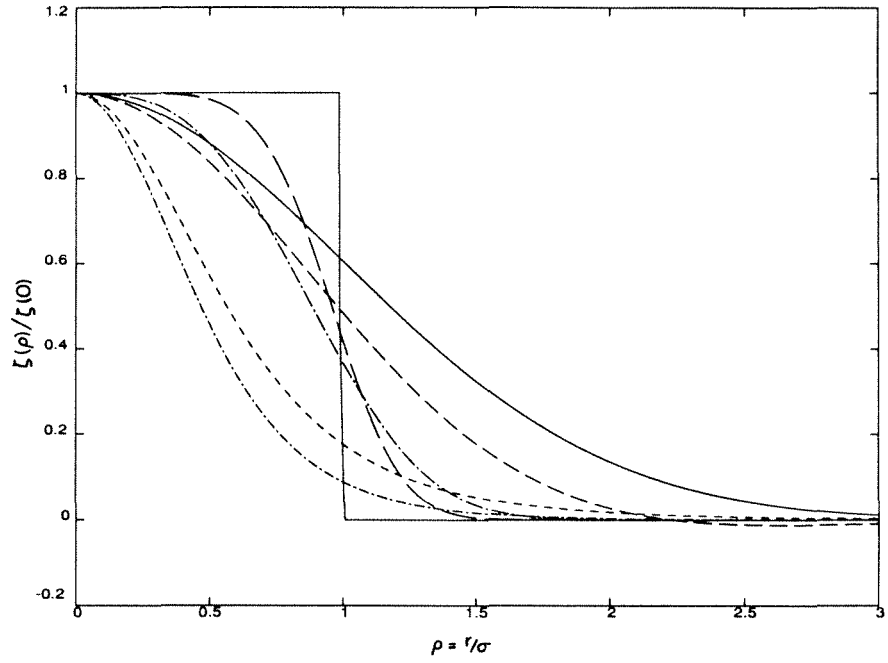

Figure J.1: Some three-dimensional regularization functions: low order algebraic (short dash), high order algebraic (short chain-dot), Gaussian (solid), $e^{-\rho^3}$ (long chain-dot), $\mathrm{sech}^2(\rho^3)$ (long dash), Super-Gaussian (medium dash), constant (dot).

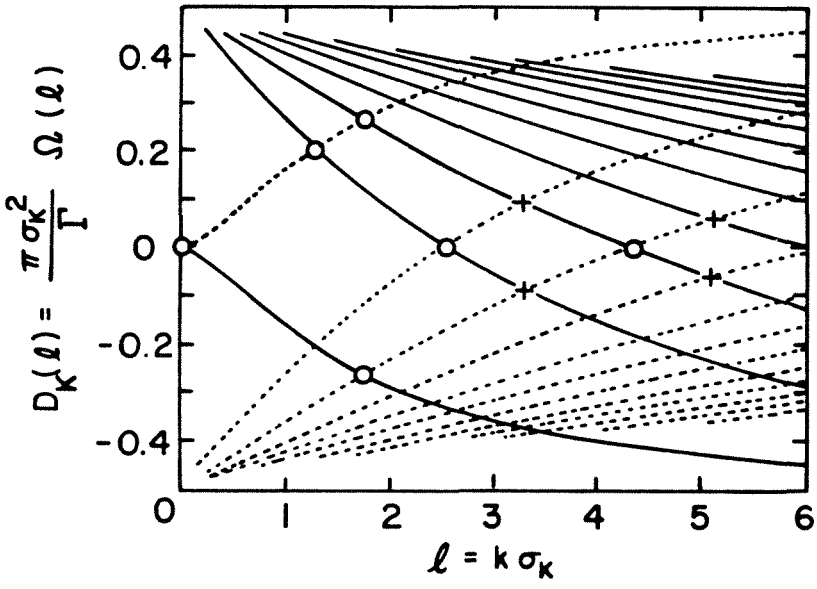

Figure J.2: Roots of the dispersion relation for angular mode $m = +1$ (dot) and $m = -1$ (solid) for rectilinear vortex with uniform vorticity core. Circles indicate unstable crossing points and crosses stable crossing points in weak strain. (From Robinson & Saffman 1984).

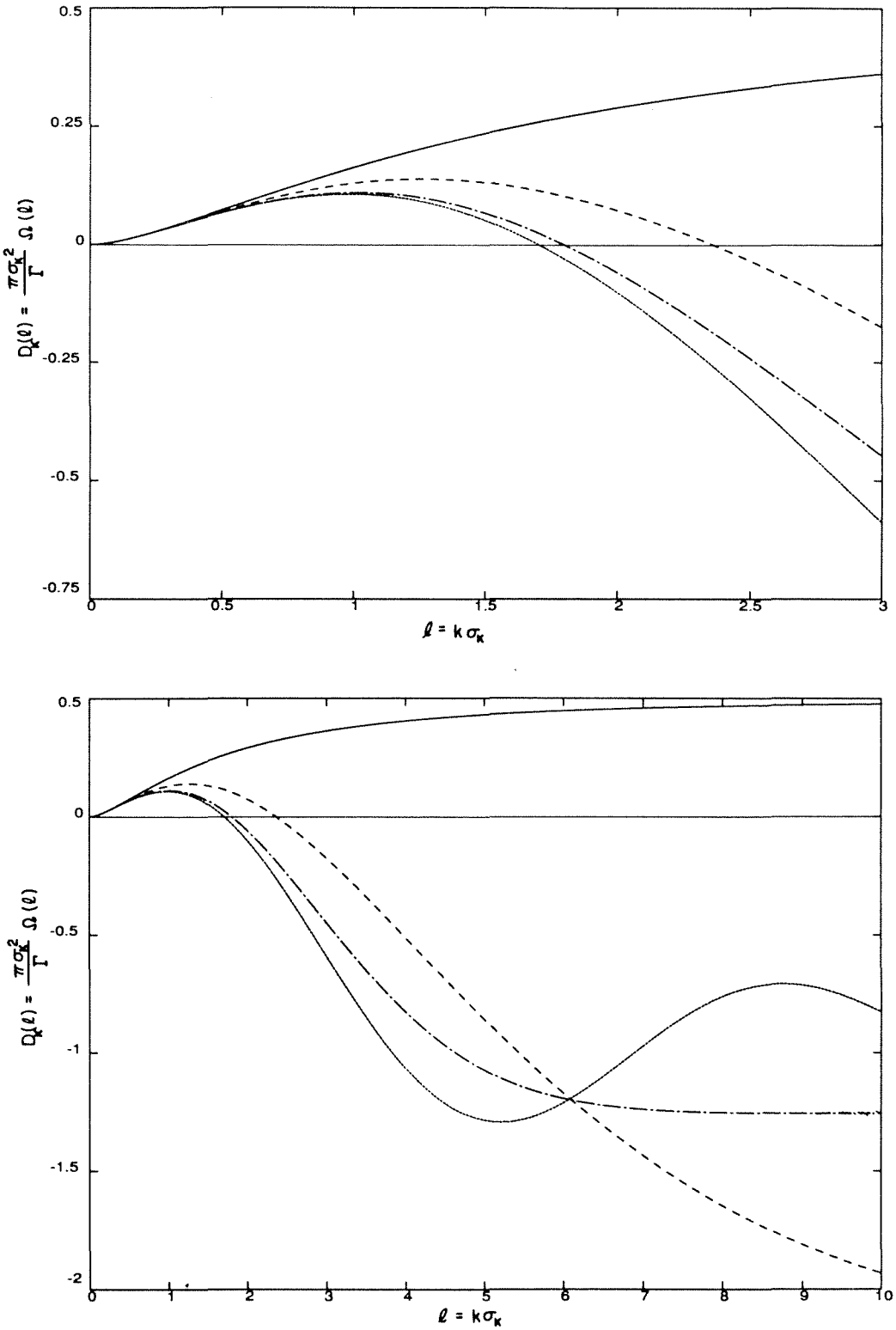

Figure J.3: Dispersion relation for a rectilinear vortex. Exact result for uniform vortex (solid). Vortex filaments using low order algebraic smoothing with $\beta = e^{-3/4}$ (dash), Gaussian with $\beta = (1/2^{1/2})\, e^{(\gamma/2-3/4)}$ (chain-dot), constant with $\beta = (1/2)\, e^{7/12}$ (dot).

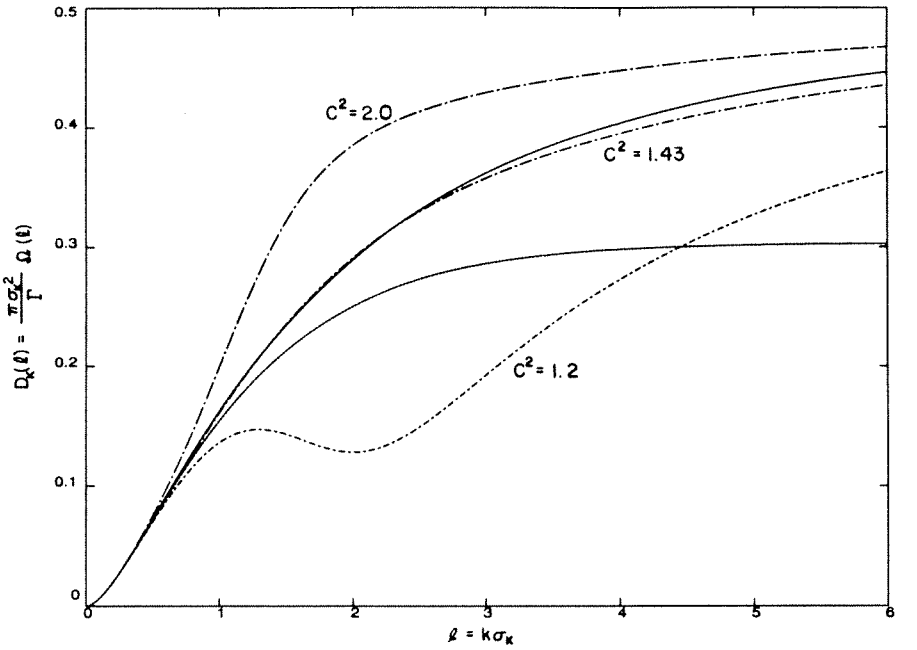

Figure J.4: Dispersion relation for a rectilinear vortex. Exact result of Kelvin (1880) for uniform vortex (solid). Approximation of exact result for different values of c^2 (chain-dot). Exact result for regularized vortex filament using the new simple algebraic velocity smoothing $q(\rho)$ with $\beta = e^{1/4}$ (dot).

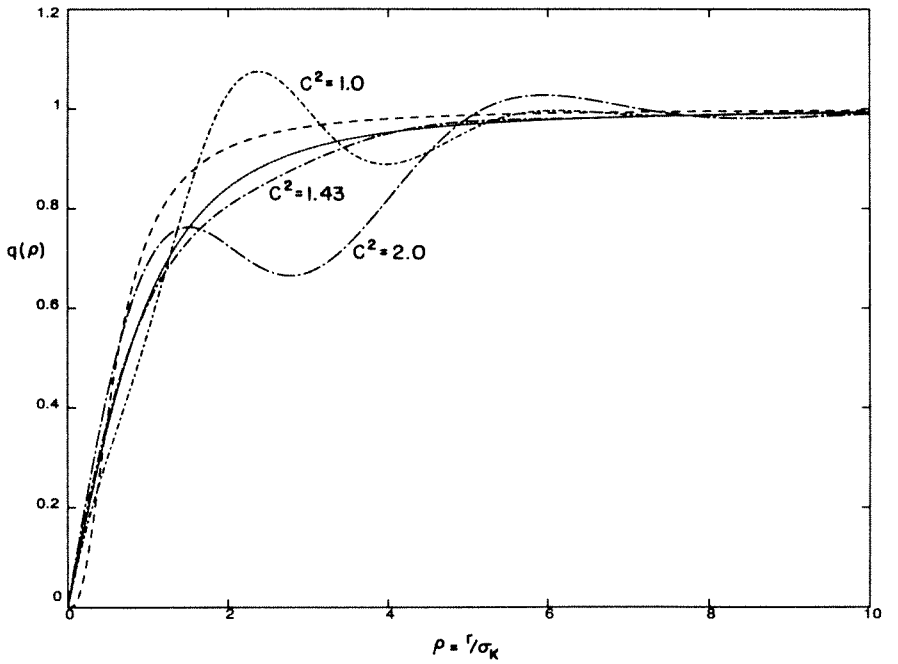

Figure J.5: New velocity smoothings $q(\rho)$: new velocity smoothing that reproduces the approximation of Kelvin's exact result (chain-dot), new simple algebraic velocity smoothing with $\beta = e^{1/4}$ (dot). For comparison, low order algebraic smoothing $g(\rho)$ with $\beta = e^{-3/4}$ (dash).

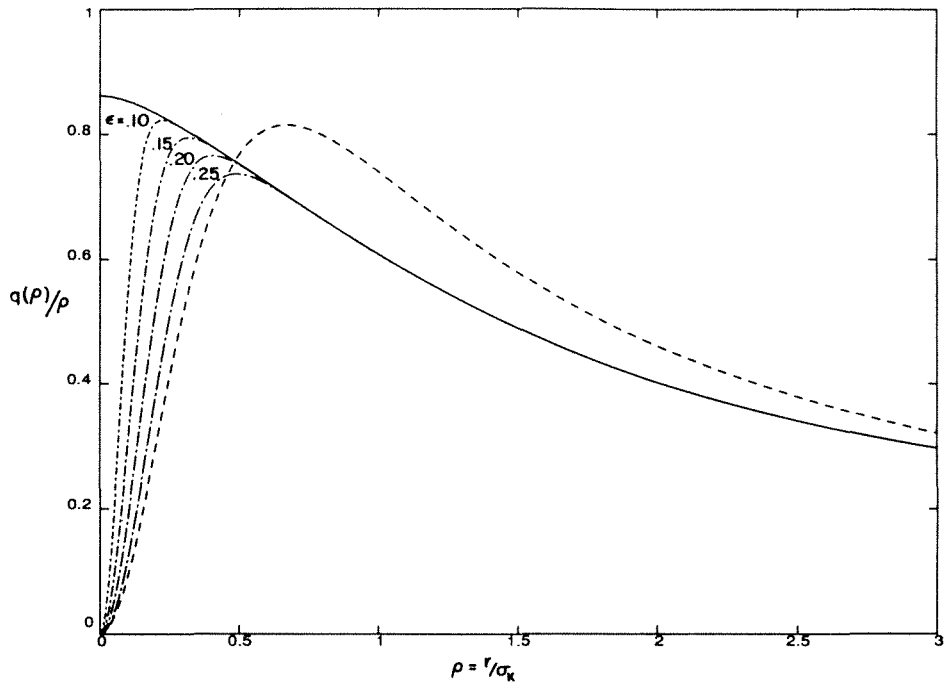

Figure J.6: Numerical decoupling of the new velocity smoothing $q(\rho)$: $q(\rho)/\rho$ (solid), $q_\epsilon(\rho)/\rho$ for different values of ϵ (chain-dot). For comparison, low order algebraic smoothing $g(\rho)/\rho$ with $\beta = e^{-3/4}$ (dash).

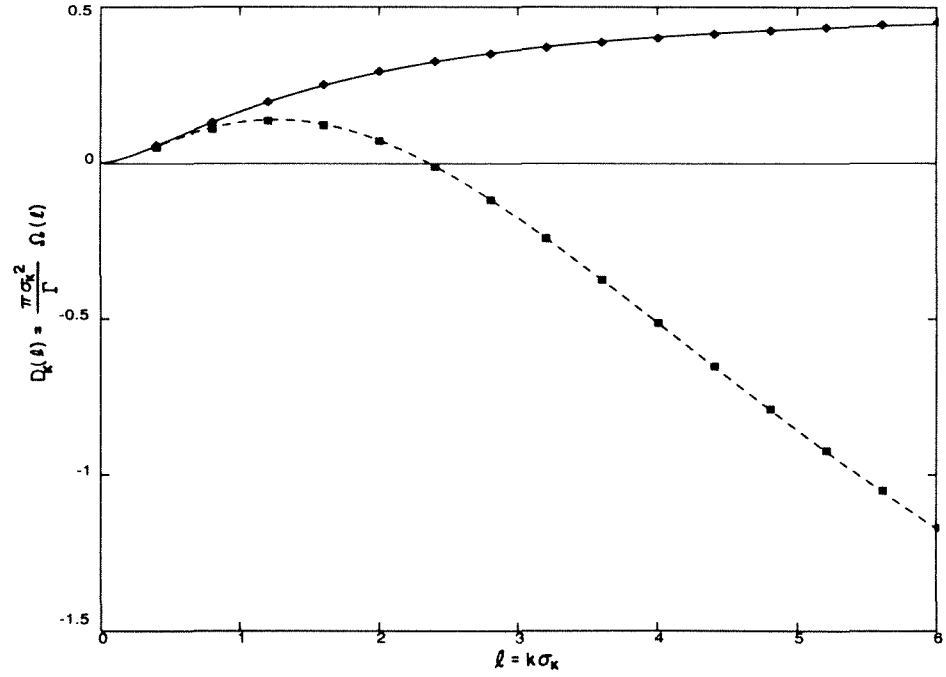

Figure J.7: Dispersion relation for a rectilinear vortex. Exact result of Kelvin (1880) (solid) and numerical results with new velocity smoothing $q(\rho)$ (diamond). Exact result for low order algebraic smoothing $g(\rho)$ and $\beta = e^{-3/4}$ (dash) and numerical results (square).

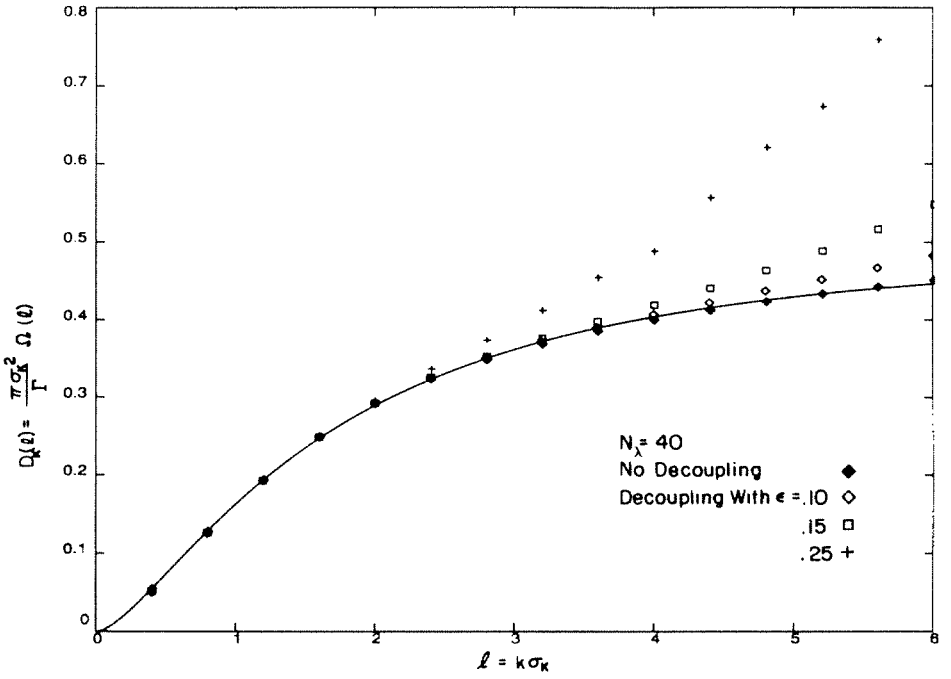

Figure J.8: Dispersion relation for a rectilinear vortex. Exact result of Kelvin (1880) (solid). Numerical results using new velocity smoothing $q(\rho)$ with fixed N_λ and different values of ϵ (symbols).

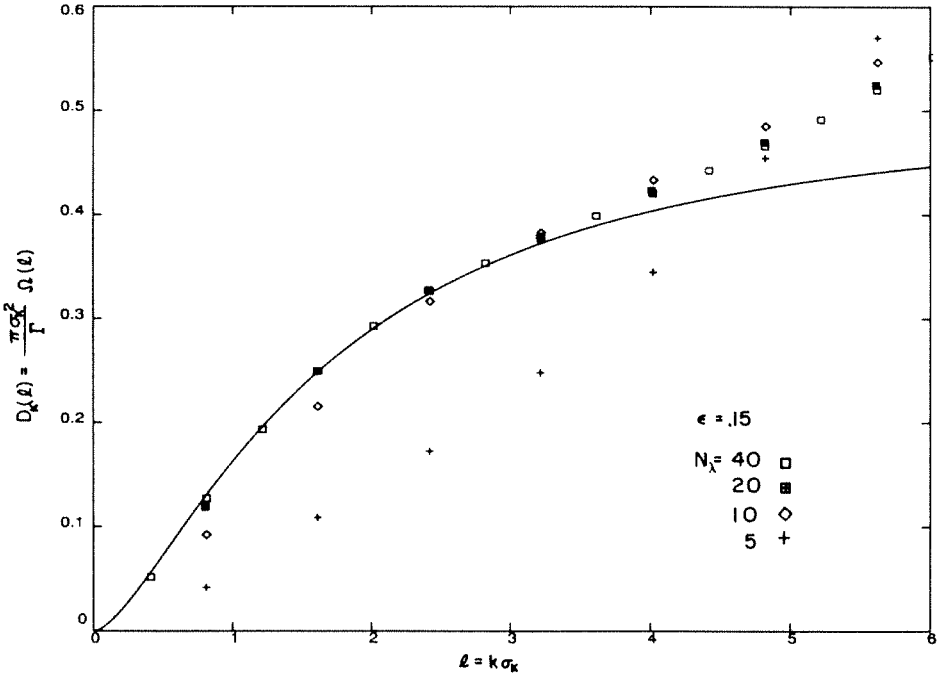

Figure J.9: Dispersion relation for a rectilinear vortex. Exact result of Kelvin (1880) (solid). Numerical results using new velocity smoothing $q(\rho)$ with fixed ϵ and different values of N_λ (symbols).

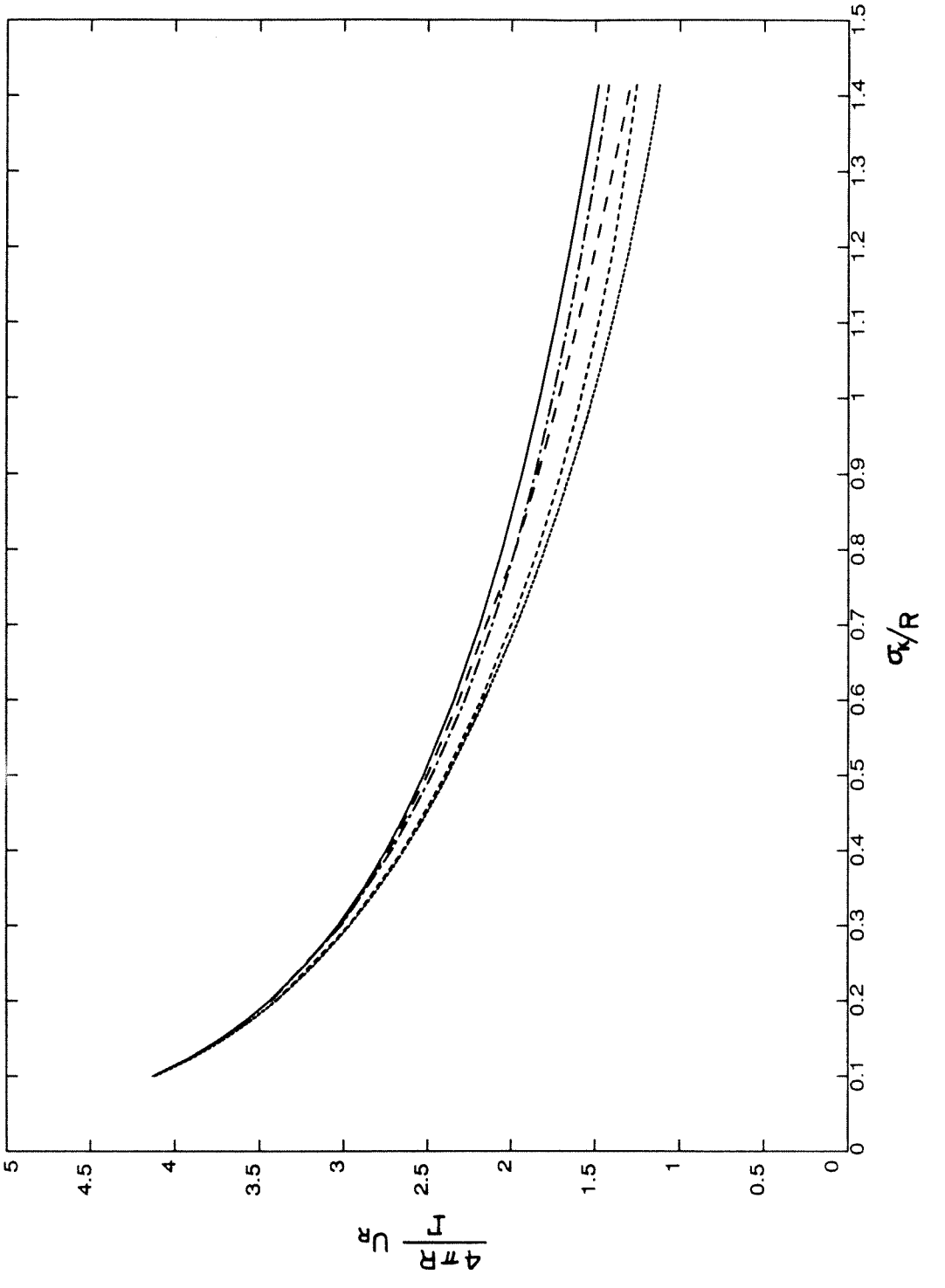

Figure J.10: Velocity of a vortex ring. Lamb's asymptotic result for uniform vorticity core (solid), Fraenkel's asymptotic result (dot), Norbury's numerical result (short dash), low order algebraic $g(\rho)$ (dash) and new $q(\rho)$ (chain-dot).

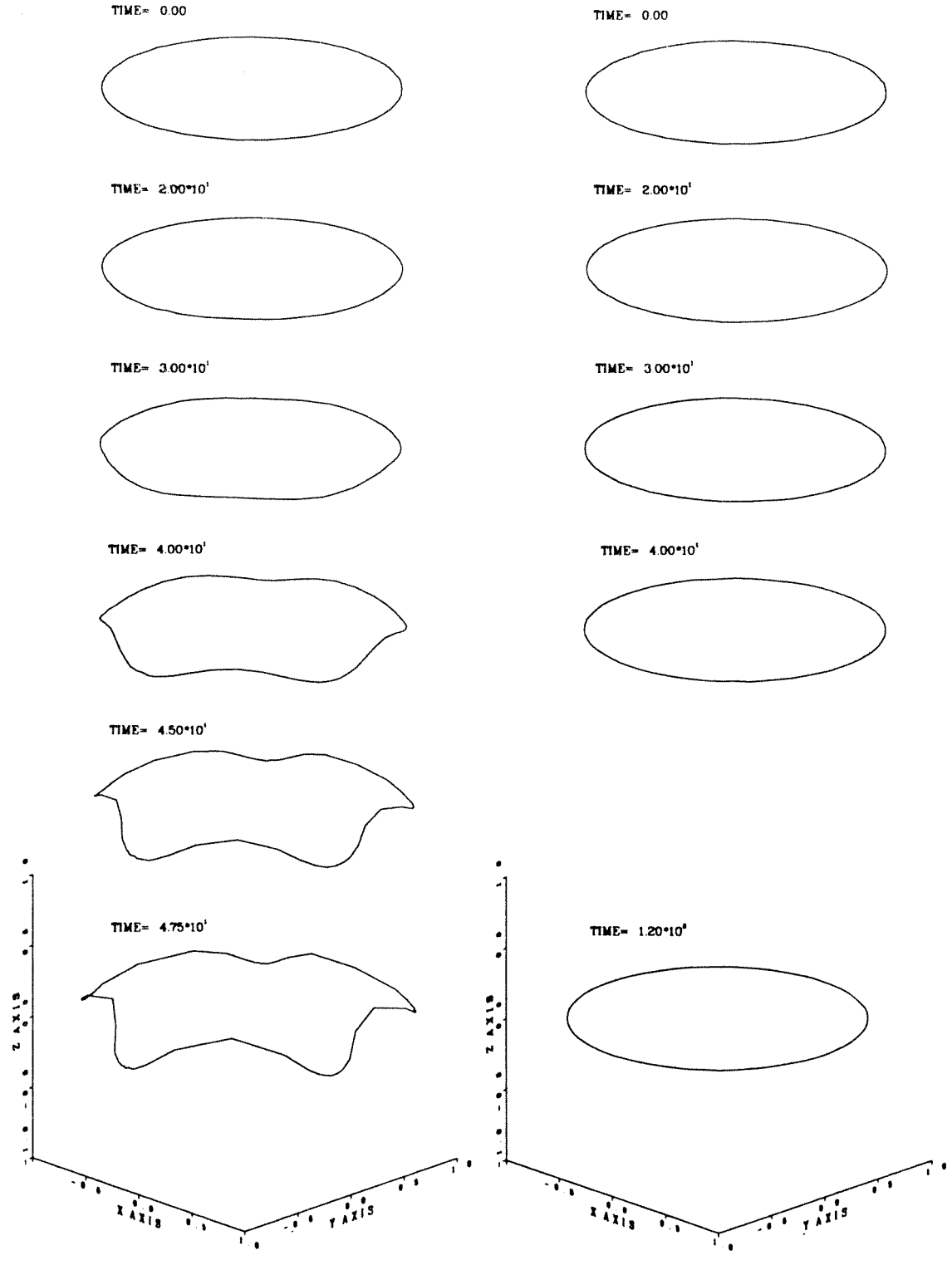

Figure J.11: Stability of a single-filament vortex ring ($\Gamma = 1.0$, $R = 1.0$, $\sigma_K = .50$): low order algebraic velocity smoothing $g(\rho)$ with $\beta = e^{-3/4}$ (left), new smoothing $q(\rho)$ (right).

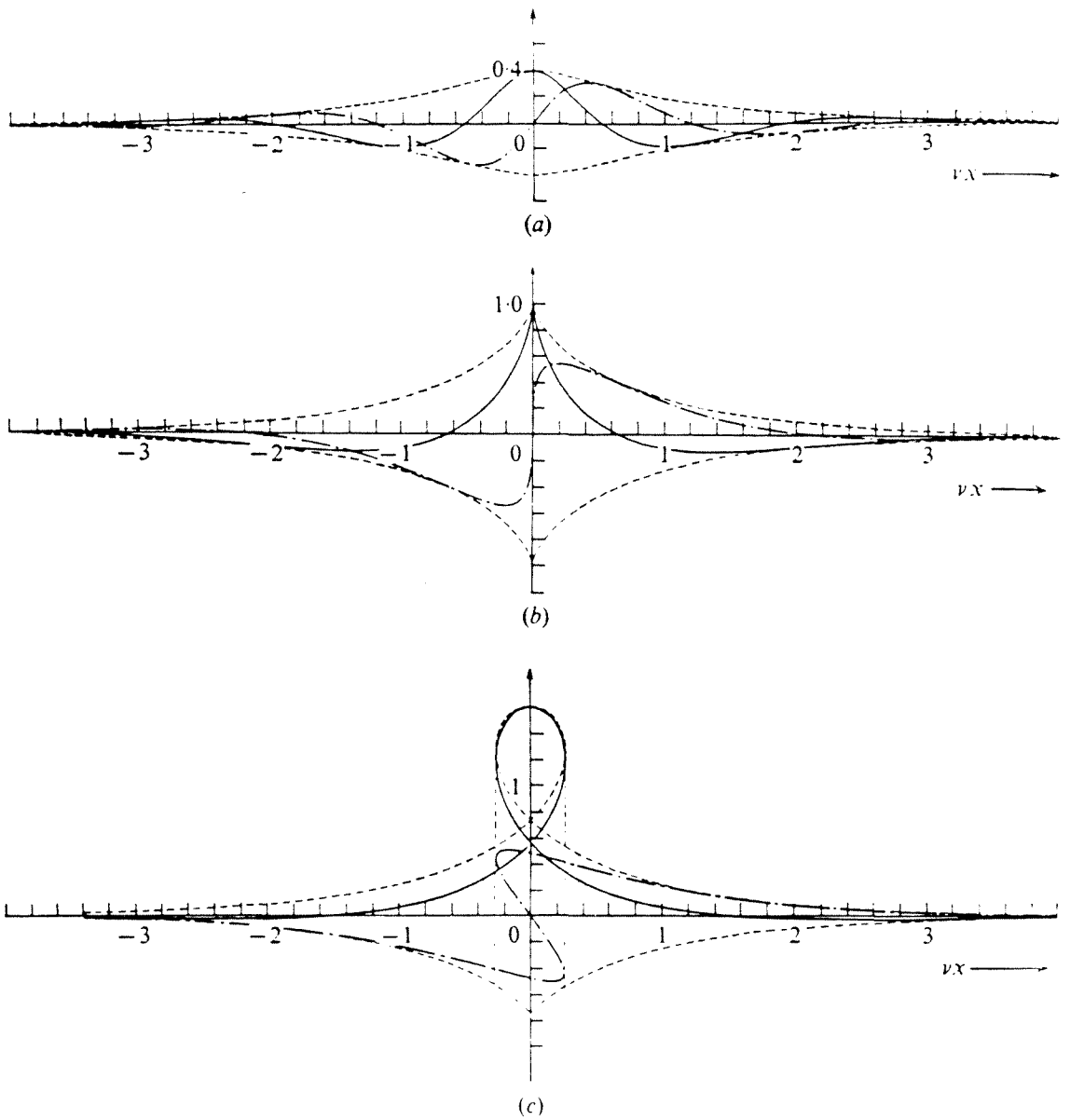

Figure J.12: The Hasimoto soliton for different values of the torsion parameter: (a) $T = 2.0$, (b) $T = 1.0$, (c) $T = .50$ (from Hasimoto 1972).

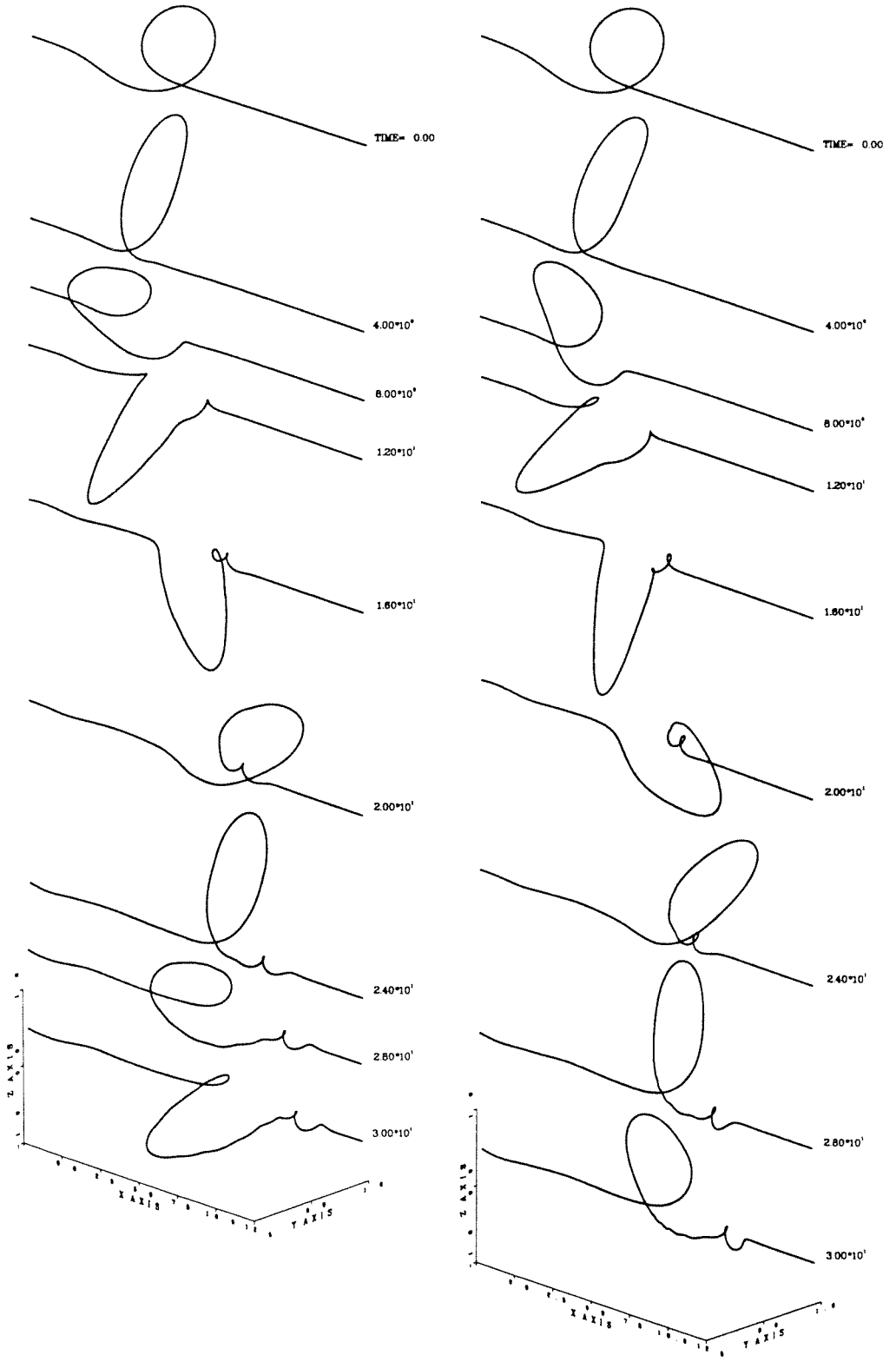

Figure J.13: Perspective view of a solitary wave on a filament evolving under the full Biot-Savart velocity ($\Gamma = 1.0$, $T = .50$, $\sigma_K = .20$): low order algebraic smoothing $g(\rho)$ with $\beta = e^{-3/4}$ (left), new smoothing $q(\rho)$ (right).

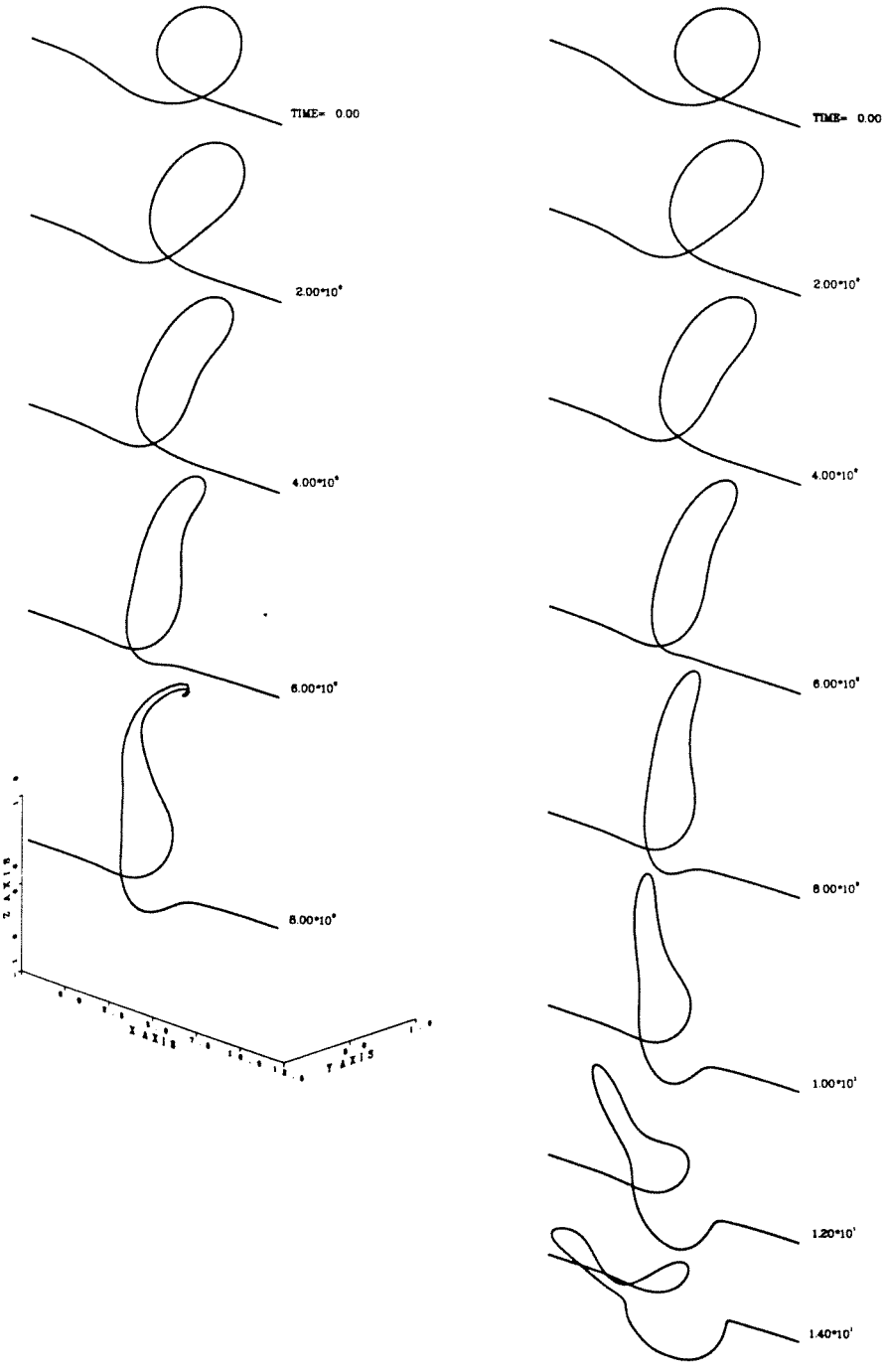

Figure J.14: Perspective view of a solitary wave on a filament evolving under the full Biot-Savart velocity ($\Gamma = 1.0$, $T = .50$, $\sigma_K = .40$): low order algebraic smoothing $g(\rho)$ with $\beta = e^{-3/4}$ (left), new smoothing $q(\rho)$ (right).

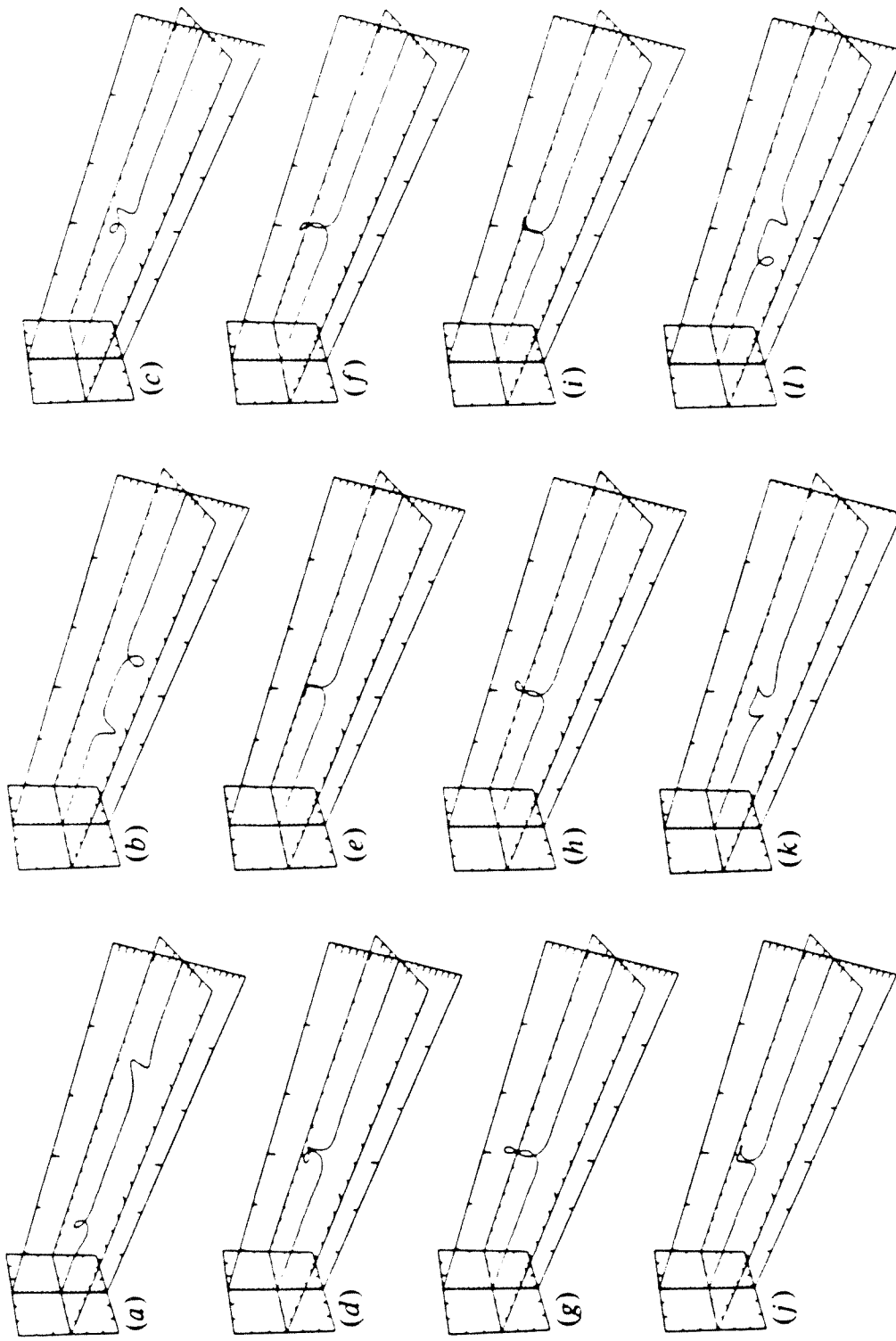

Figure J.15: Perspective view of the collision of opposite but otherwise identical solitons on a filament evolving under LIA. Frames not uniformly spaced in time (from Aref & Flinchem 1984).

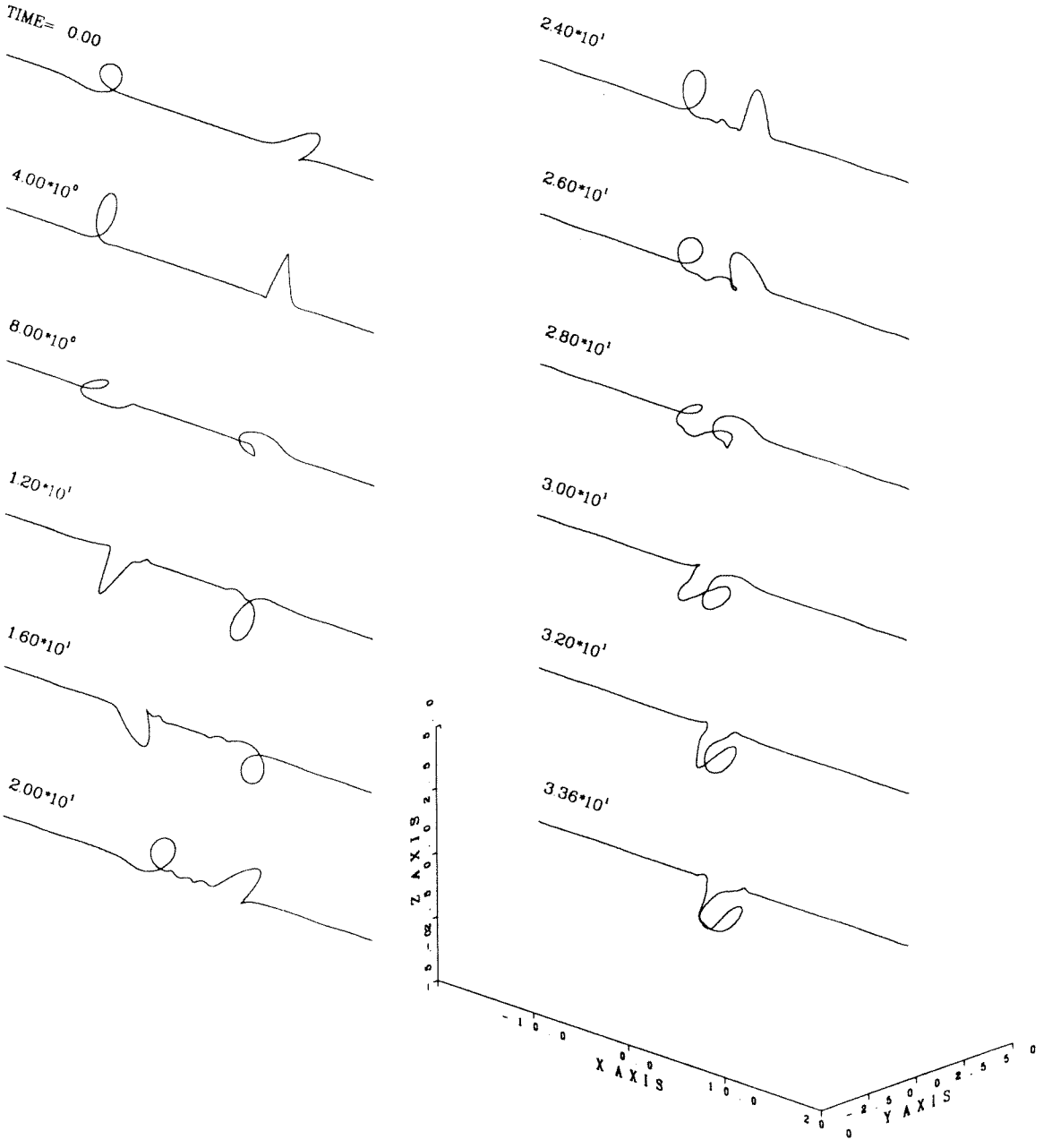

Figure J.16: Perspective view of the collision of opposite but otherwise identical solitary waves on a filament evolving under the full Biot-Savart velocity. ($\Gamma = 1.0$, $T = .50$, $\sigma_K = .10$, new velocity smoothing $q(\rho)$).

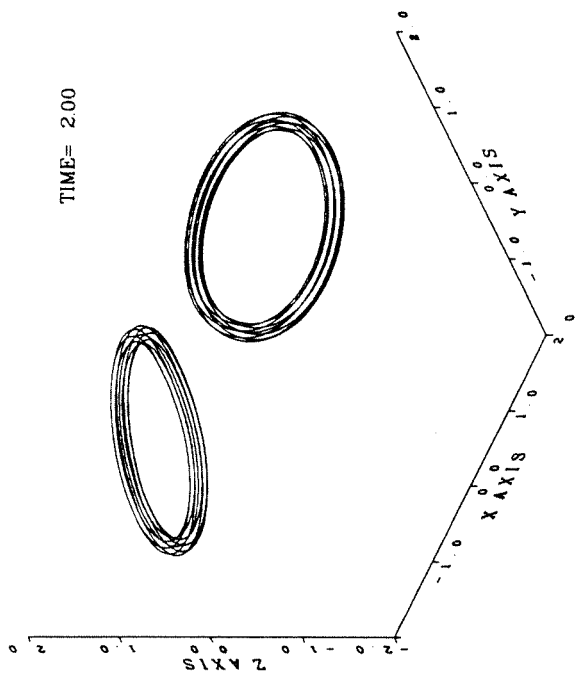
TIME= 2.00
X AXIS
Y AXIS
Z AXIS

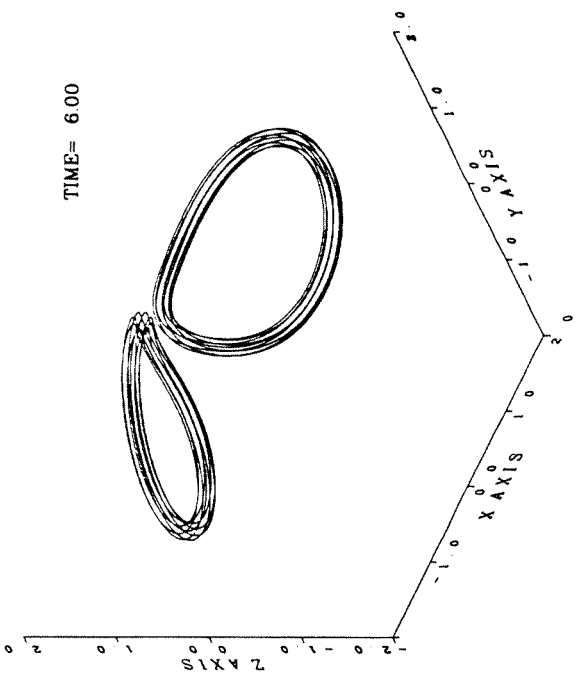
TIME= 6.00
X AXIS
Y AXIS
Z AXIS

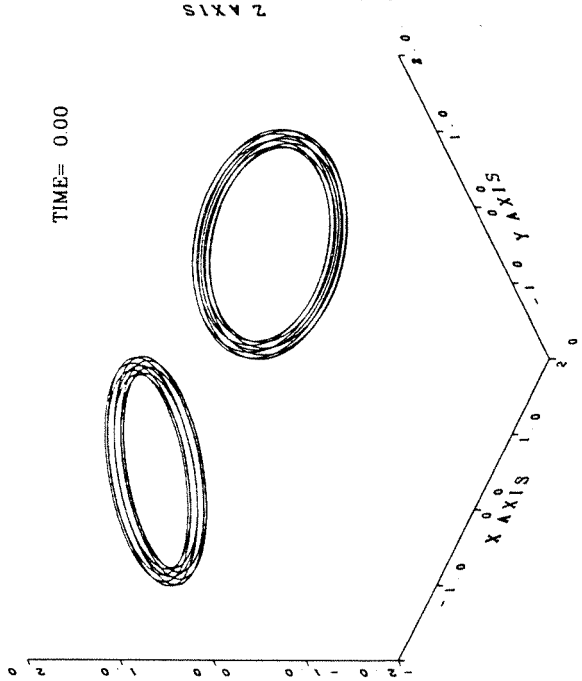
TIME= 0.00
X AXIS
Y AXIS
Z AXIS

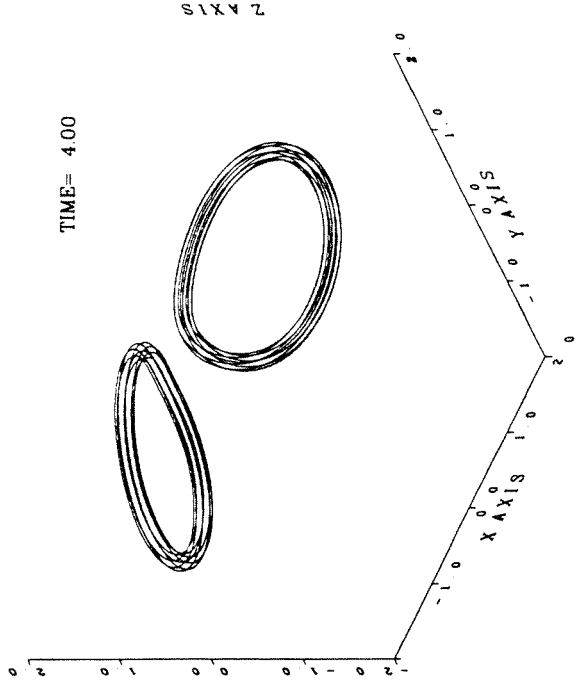
TIME= 4.00
X AXIS
Y AXIS
Z AXIS

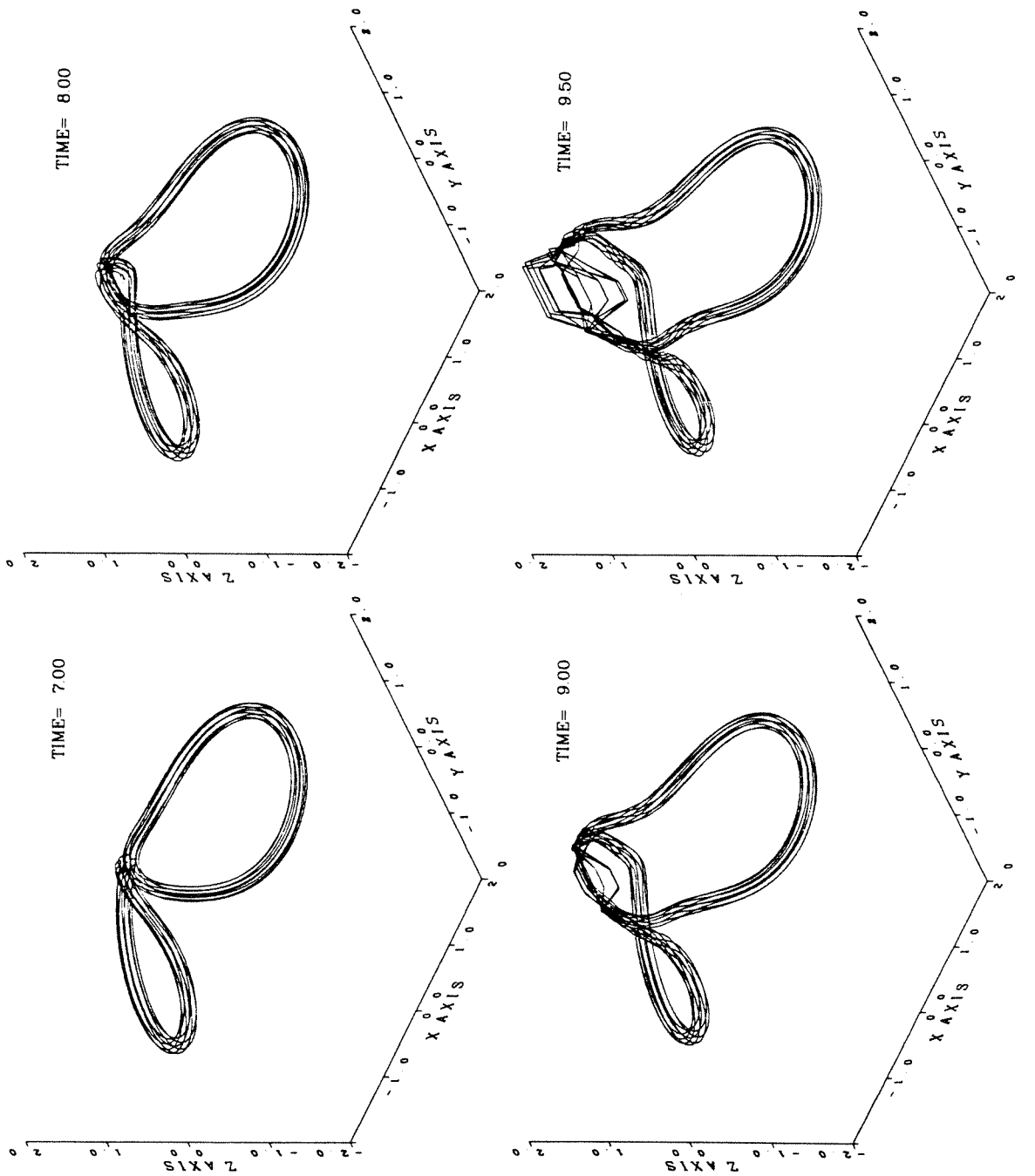

Figure J.17: The fusion of two vortex rings computed with the method of regularized vortex filaments. Perspective view of the filaments.

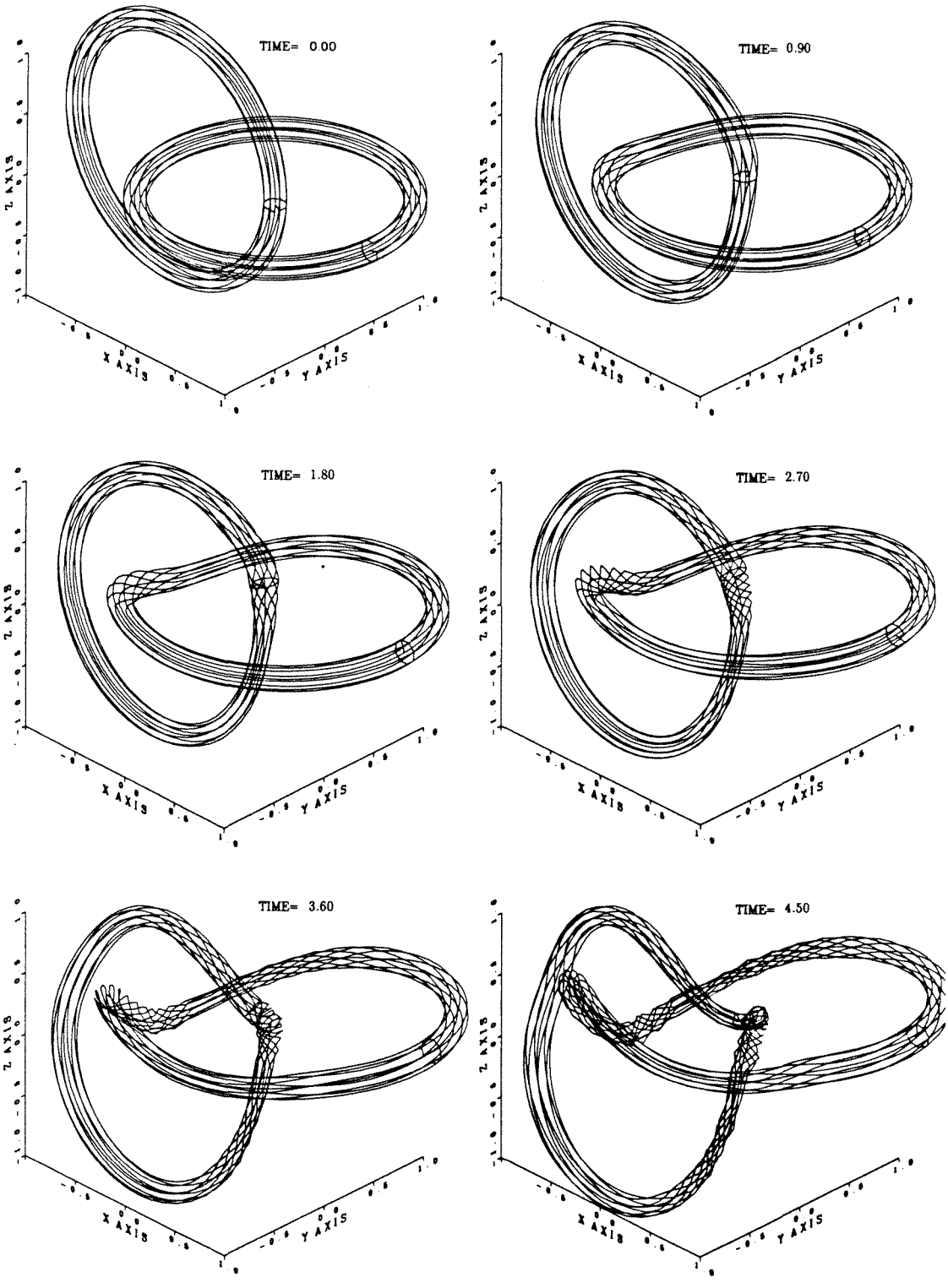
TIME= 0.00
TIME= 0.90
TIME= 1.80
TIME= 2.70
TIME= 3.60
TIME= 4.50
Z AXIS
X AXIS
Y AXIS

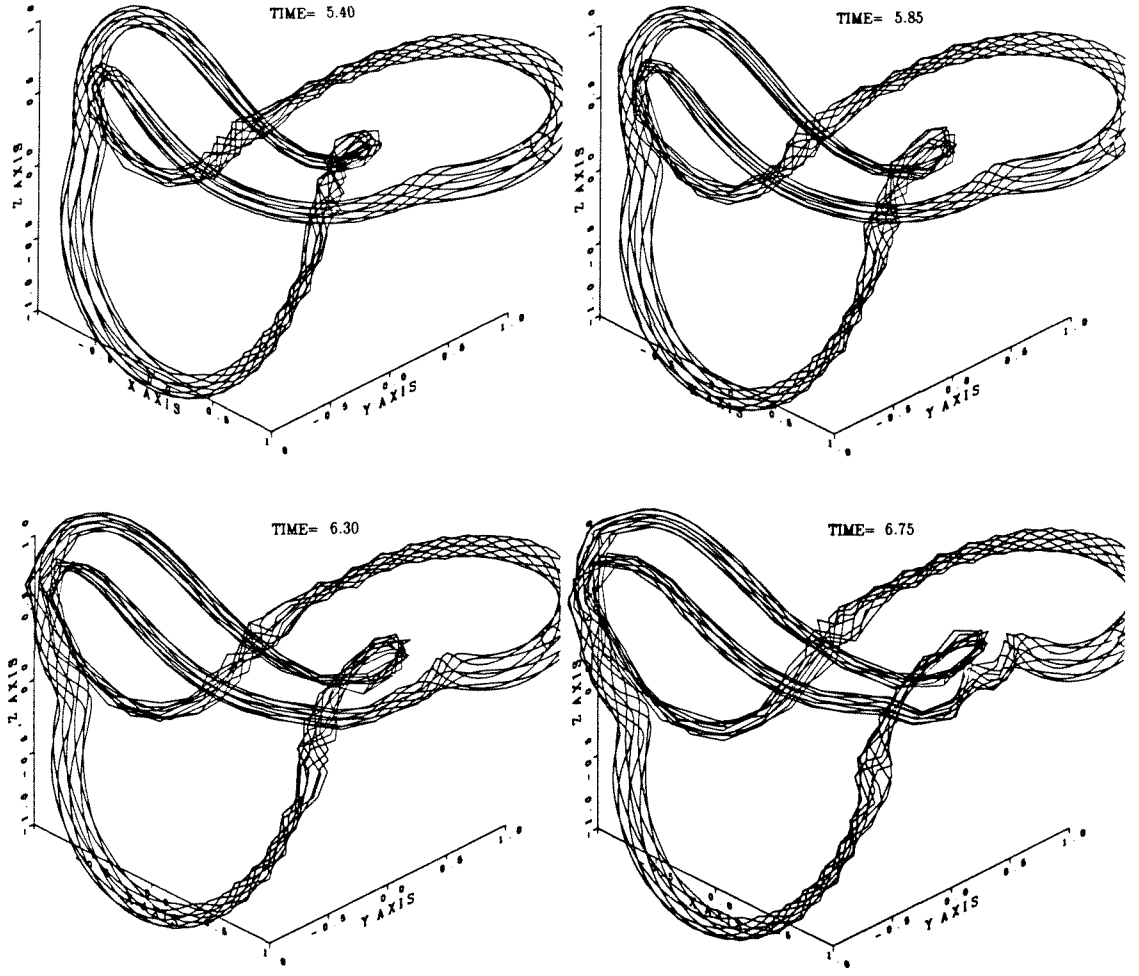

Figure J.18: The "knot" problem computed with the method of regularized vortex filaments. Perspective view of the filaments.

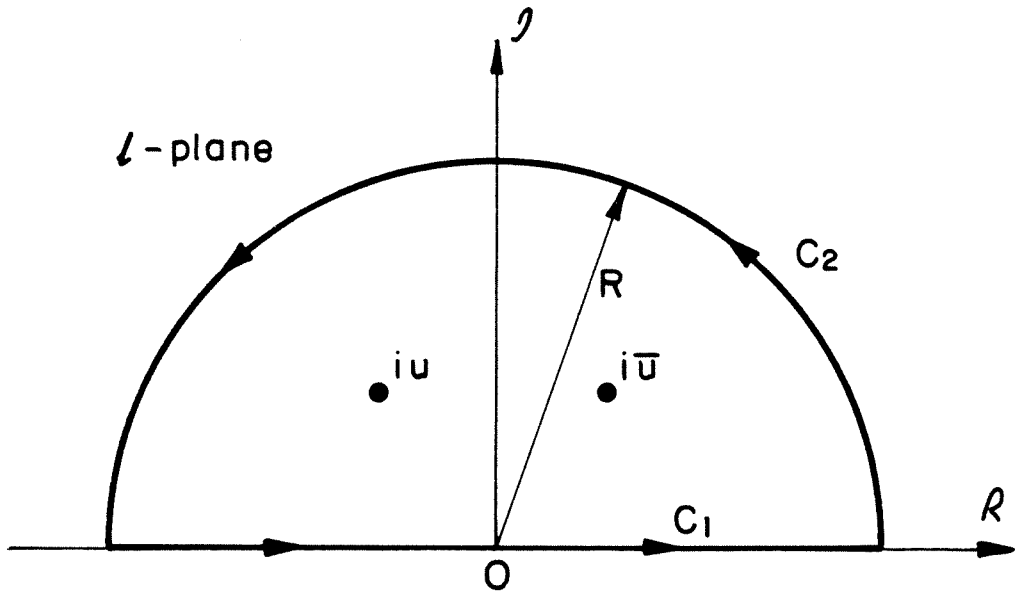

Figure J.19: Contour of integration for the evaluation of the inverse Fourier transform of $\hat{P}_1(l)$.

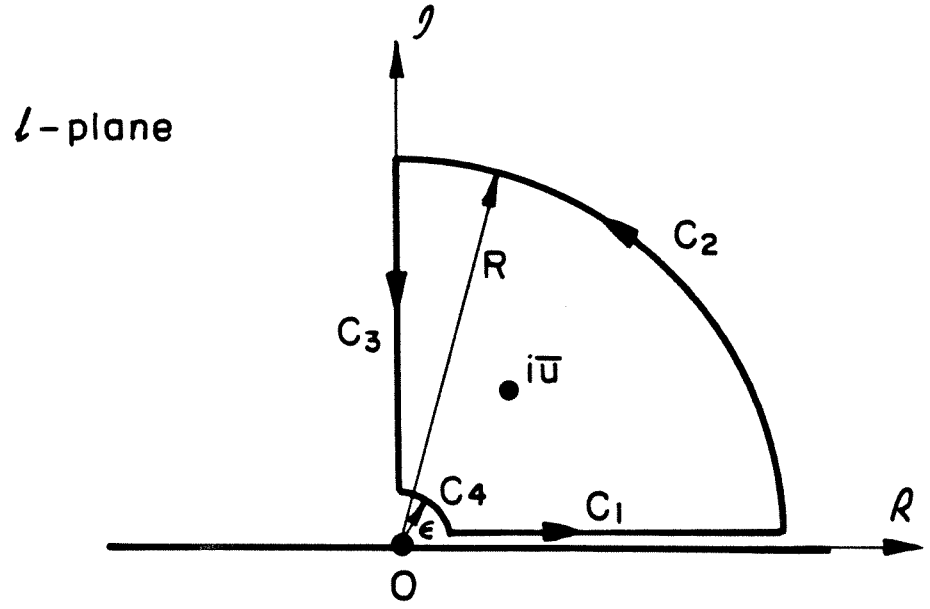

Figure J.20: Contour of integration for the evaluation of the inverse Fourier transform of $\hat{P}_2(l)$.

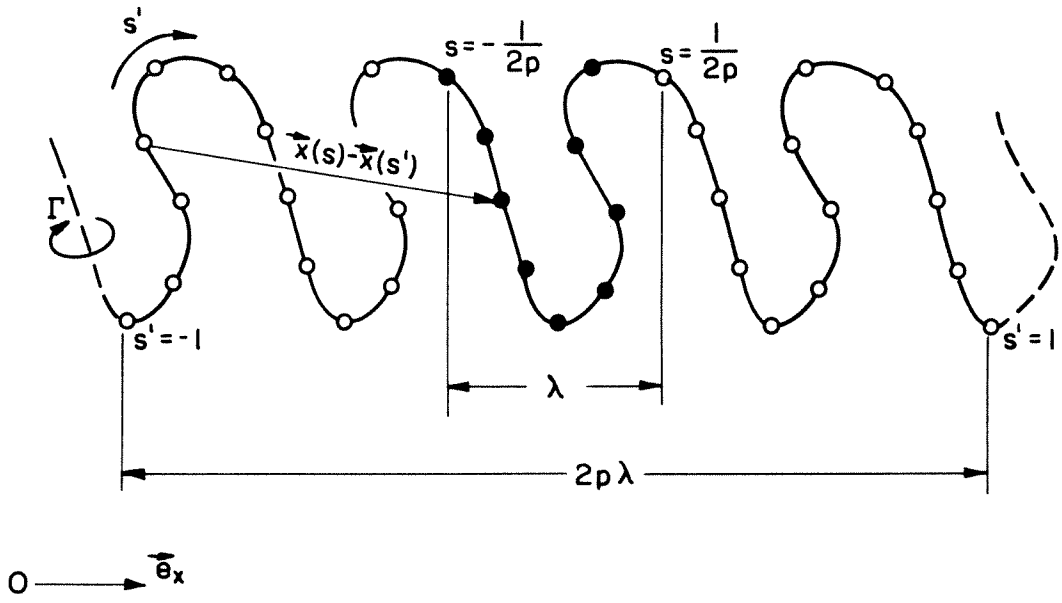

Figure J.21: The computation of an infinite periodic vortex filament.

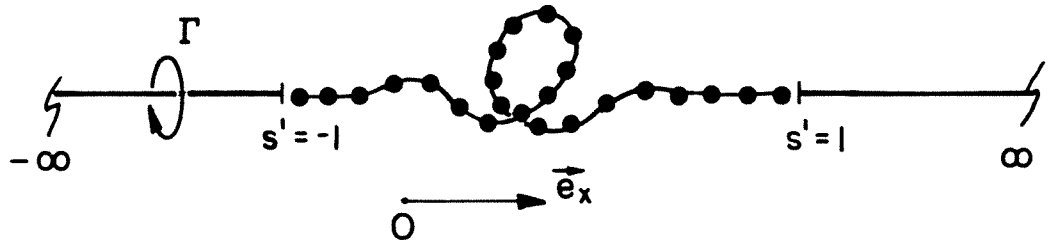

Figure J.22: The computation of an infinite non-periodic vortex filament.

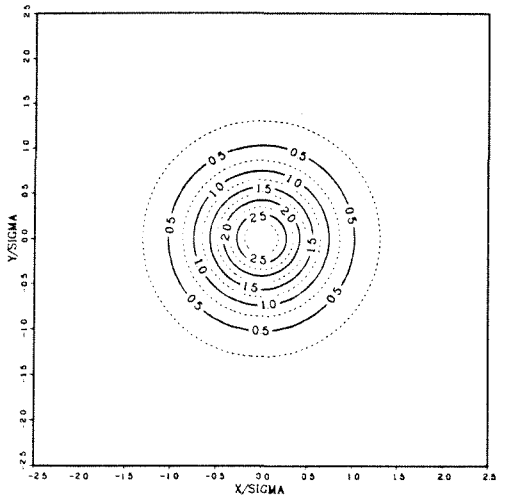

$|\omega_\sigma|$

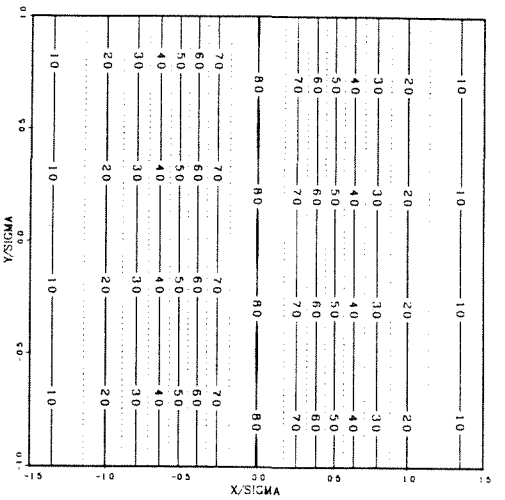

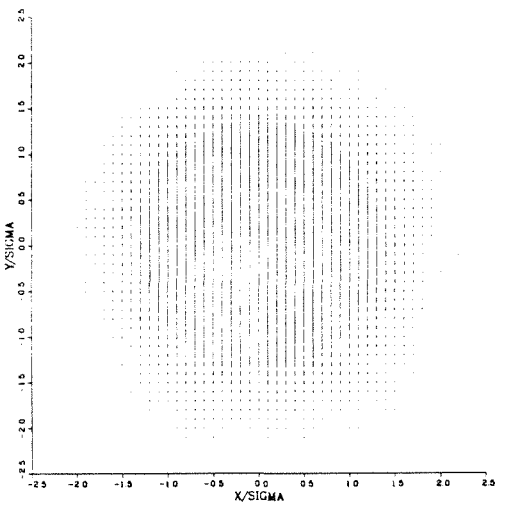

ω_σ

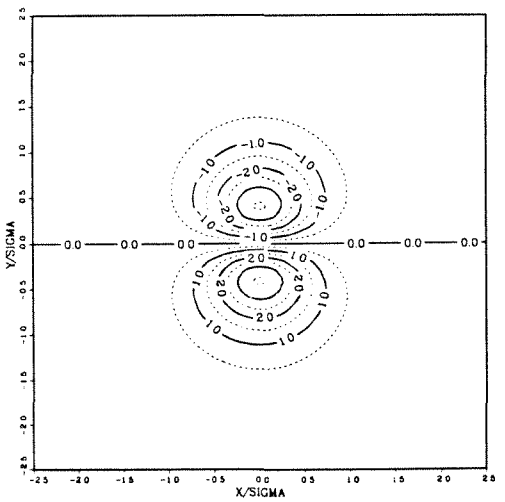

$\nabla \cdot \omega_\sigma$

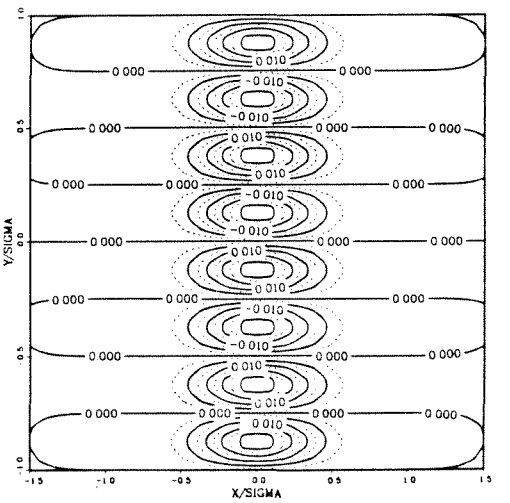

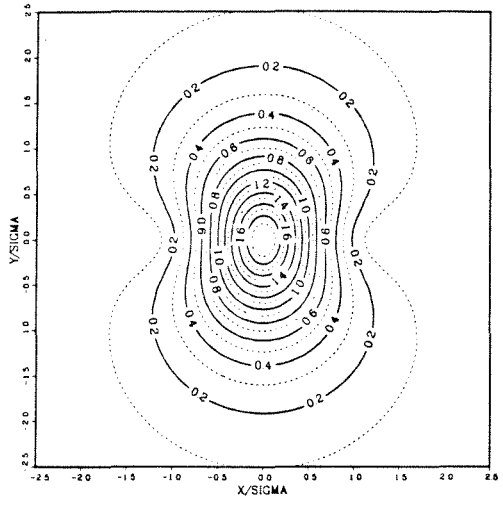

$|\omega_\sigma^N|$

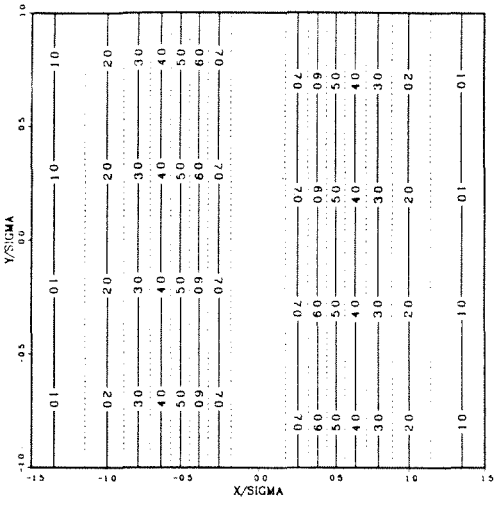

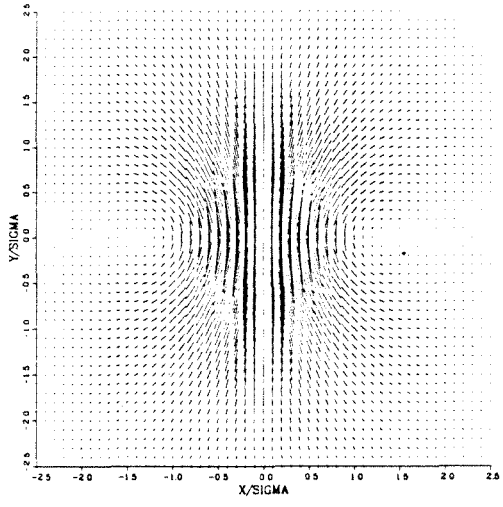

ω_σ^N

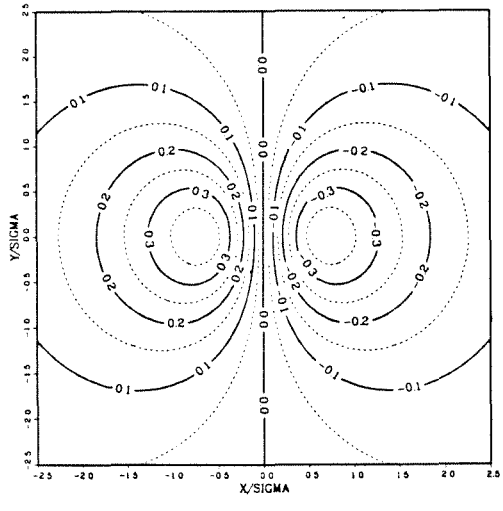

$(u_\sigma)_\varphi$

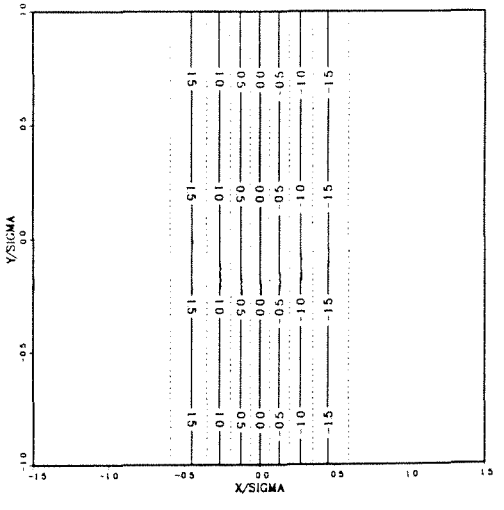

Figure J.23: Vorticity and velocity fields for an isolated regularized vortex particle (left) and for a infinite array of particles with $\sigma/h = 2.0$ (right) (The low order algebraic smoothing has been used).

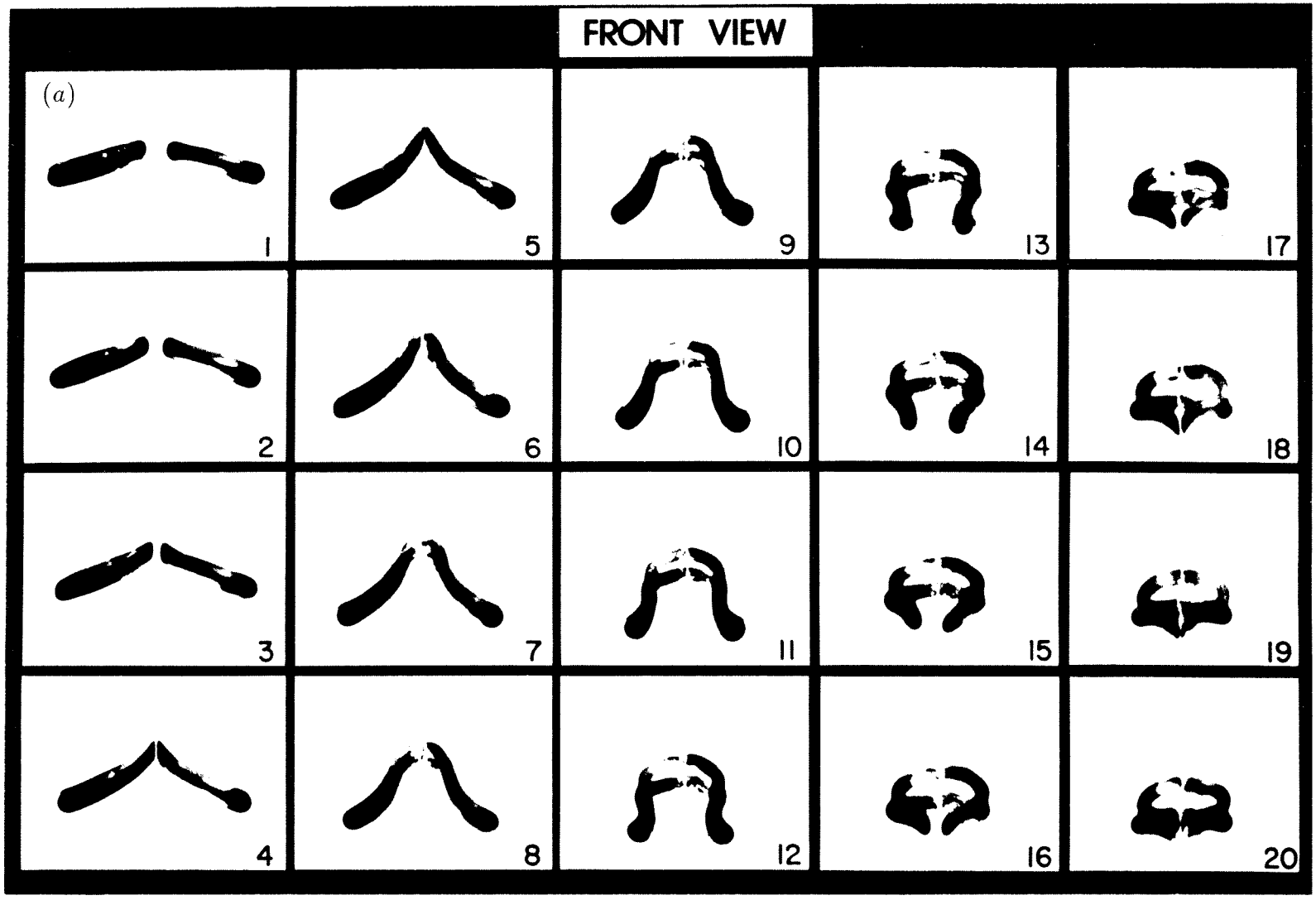
FRONT VIEW
(a)
1
2
3
4
5
6
7
8
9
10
11
12
13
14
15
16
17
18
19
20

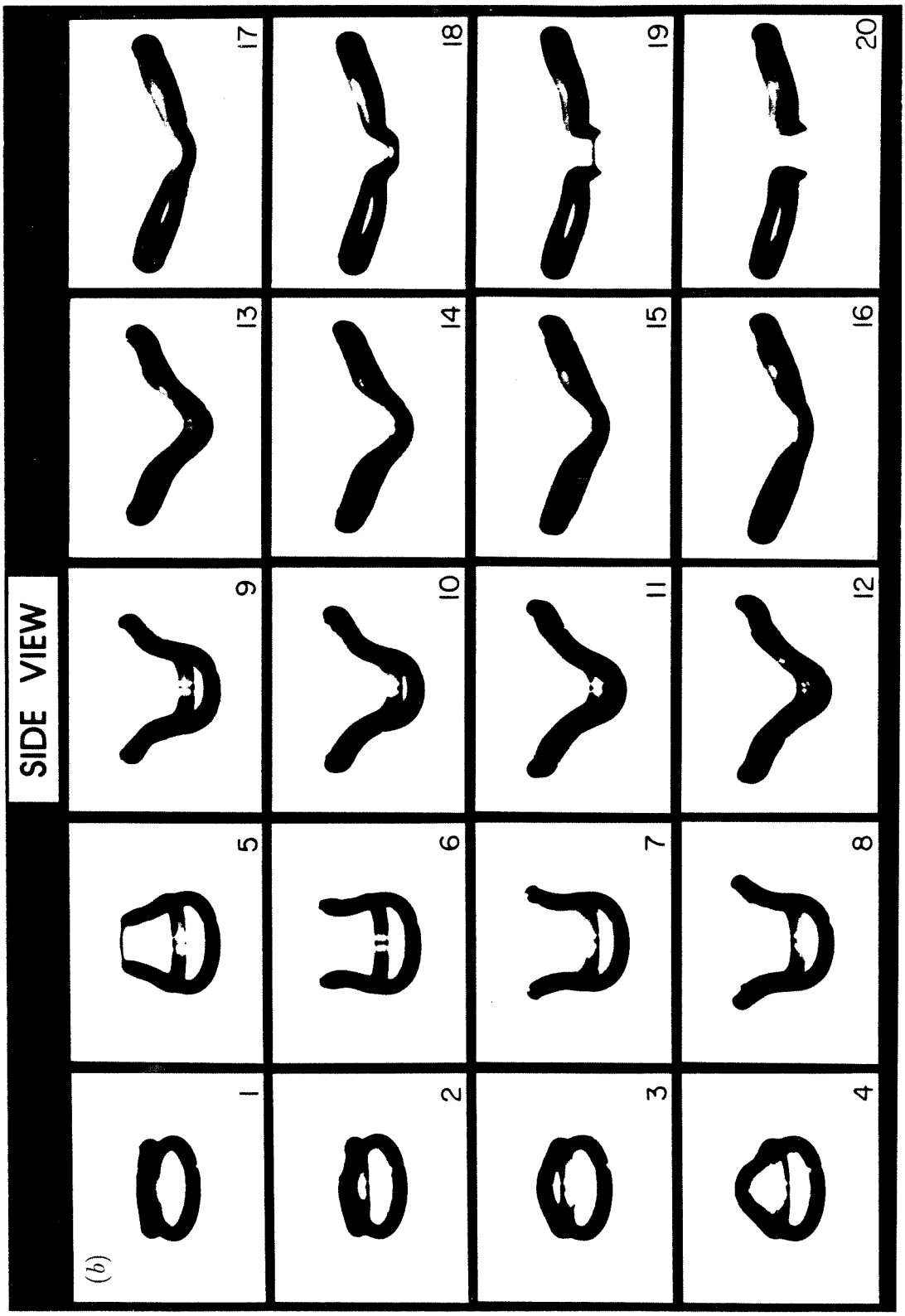

Figure J.24: The fusion and fission of two laminar vortex rings in water. Dye is used as a marker. (a) front view, (b) side view. Photographs from Schatzle (1987) and private communication.

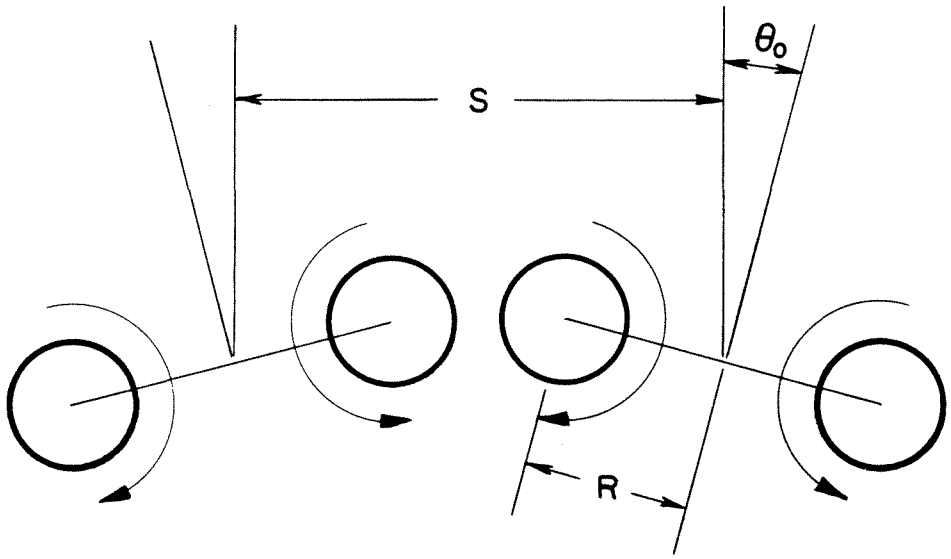

Figure J.25: Initial condition for the computation of the fusion of two vortex rings.

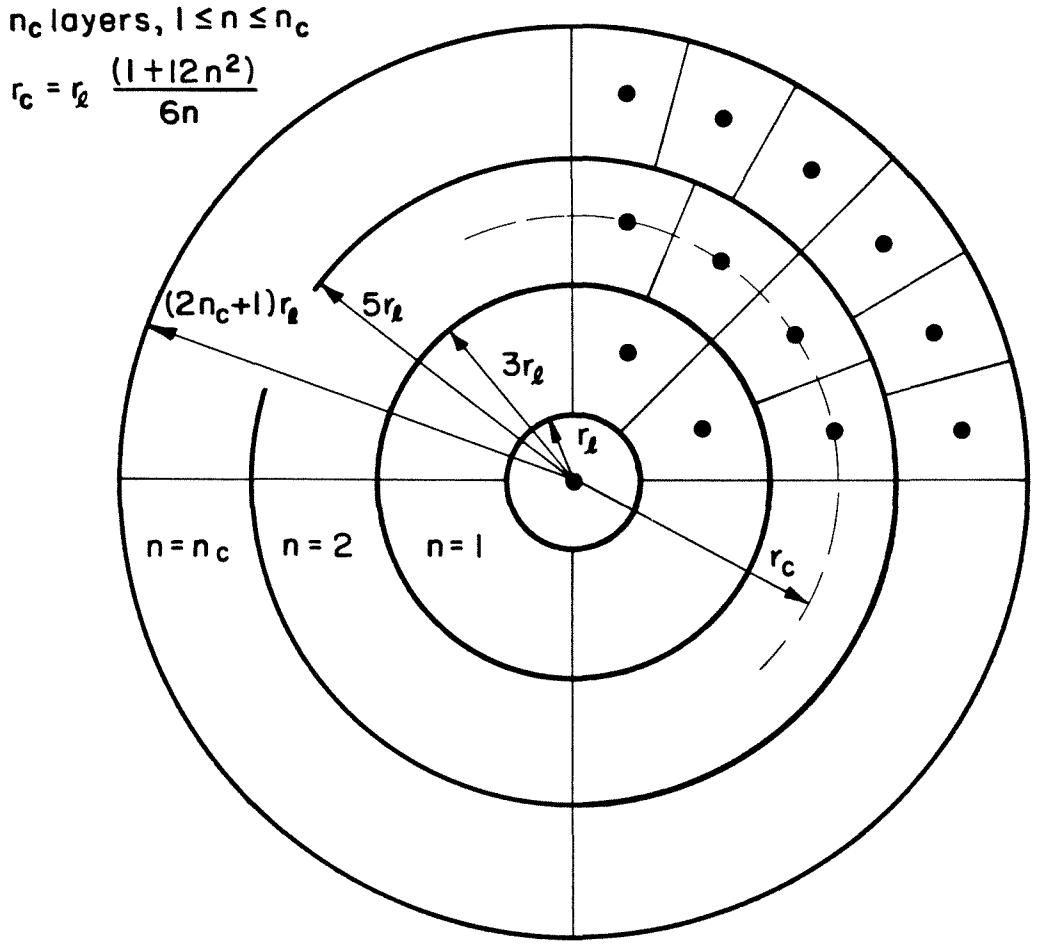

Figure J.26: Discretization of the core of a vortex tube. Each cell has an equal area $\pi\, r_l^2$.

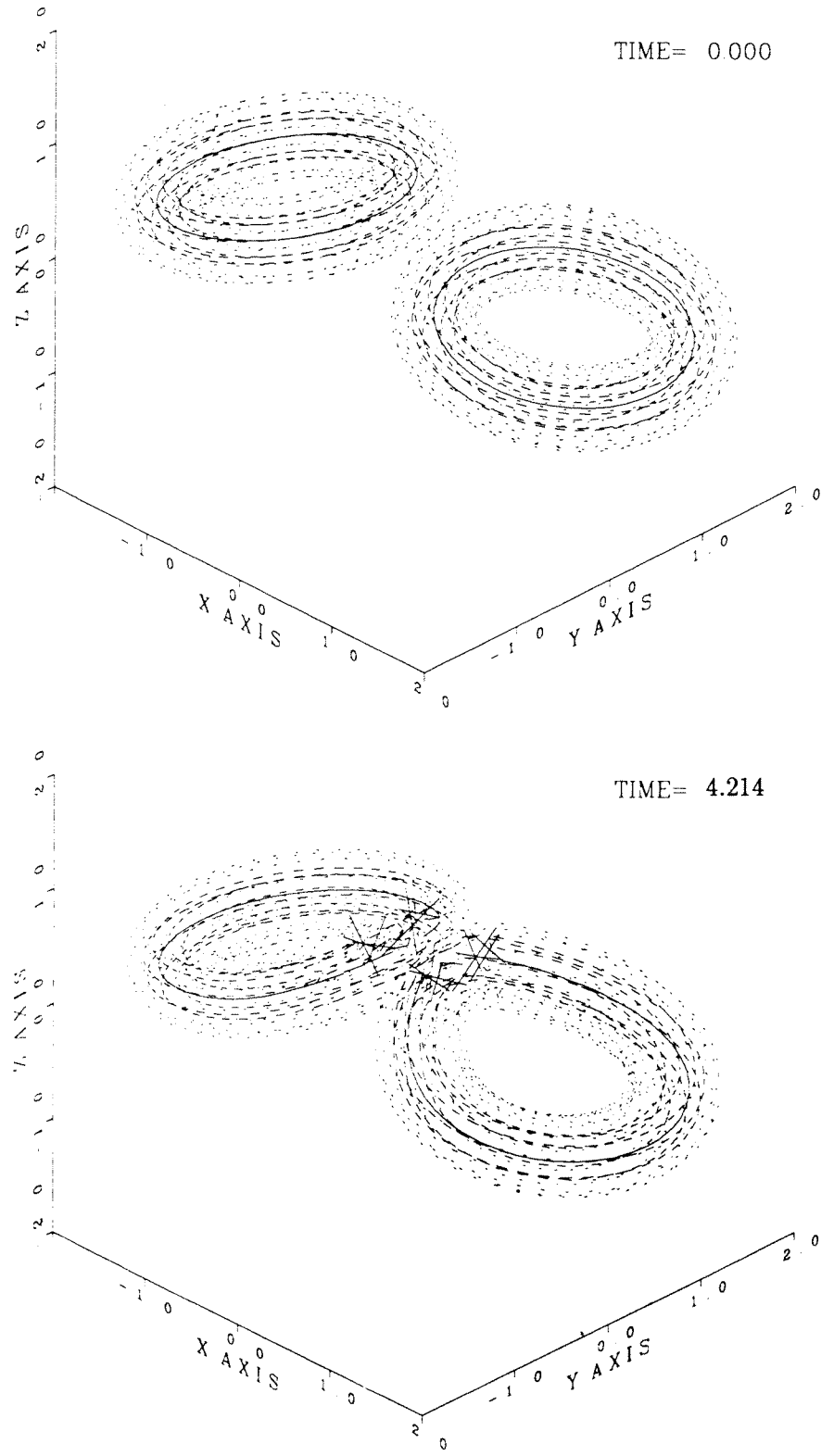

Figure J.27: The fusion of two vortex rings computed with the method of singular vortex particles and using the transpose scheme. Perspectives view of the particle strength vectors α^p.

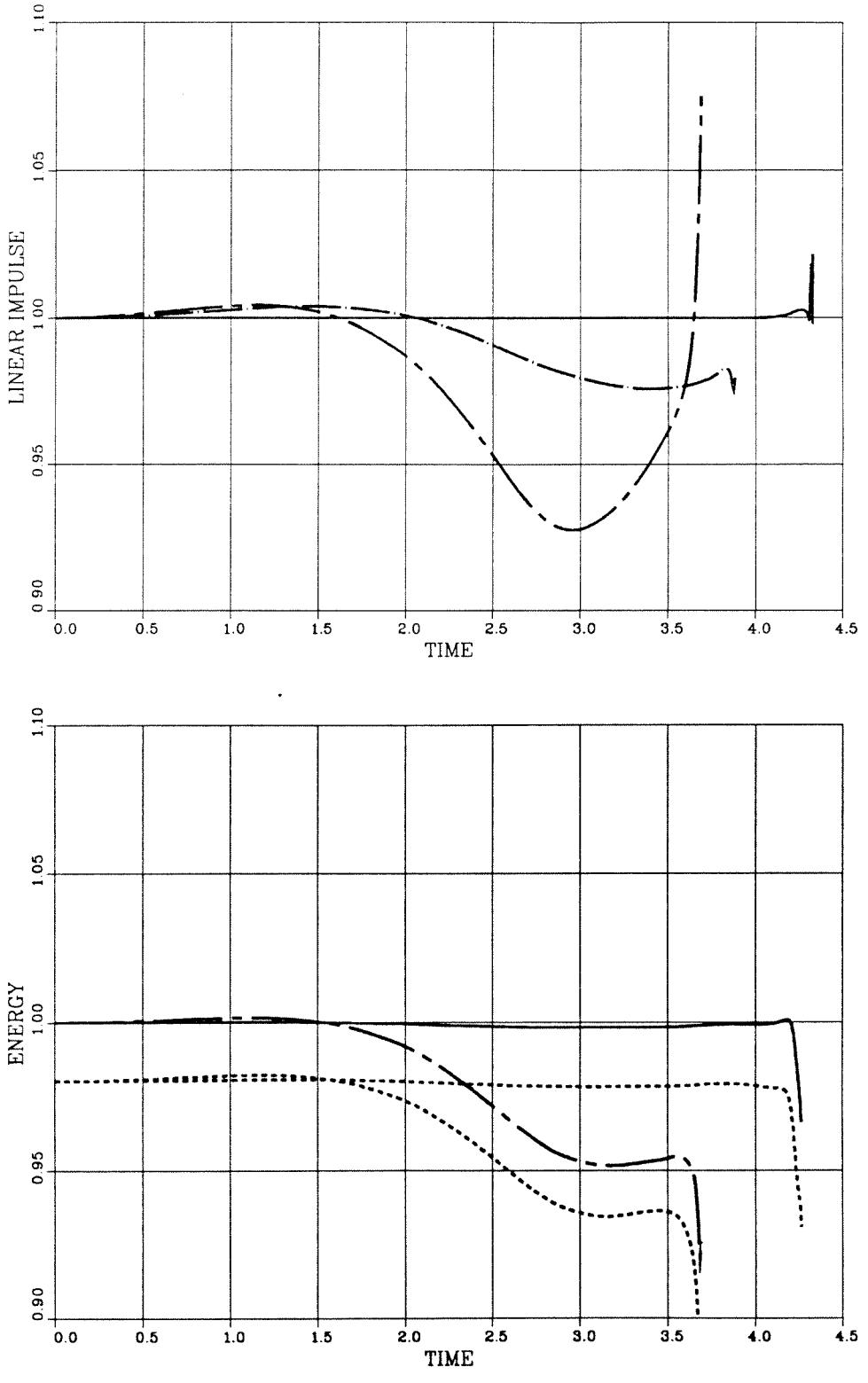

Figure J.28: The fusion of two vortex rings computed with the method of singular vortex particles. Diagnostics I, E and E_f (dash). Transpose scheme (solid), classical scheme (chain-dash) and mixed scheme (chain-dot).

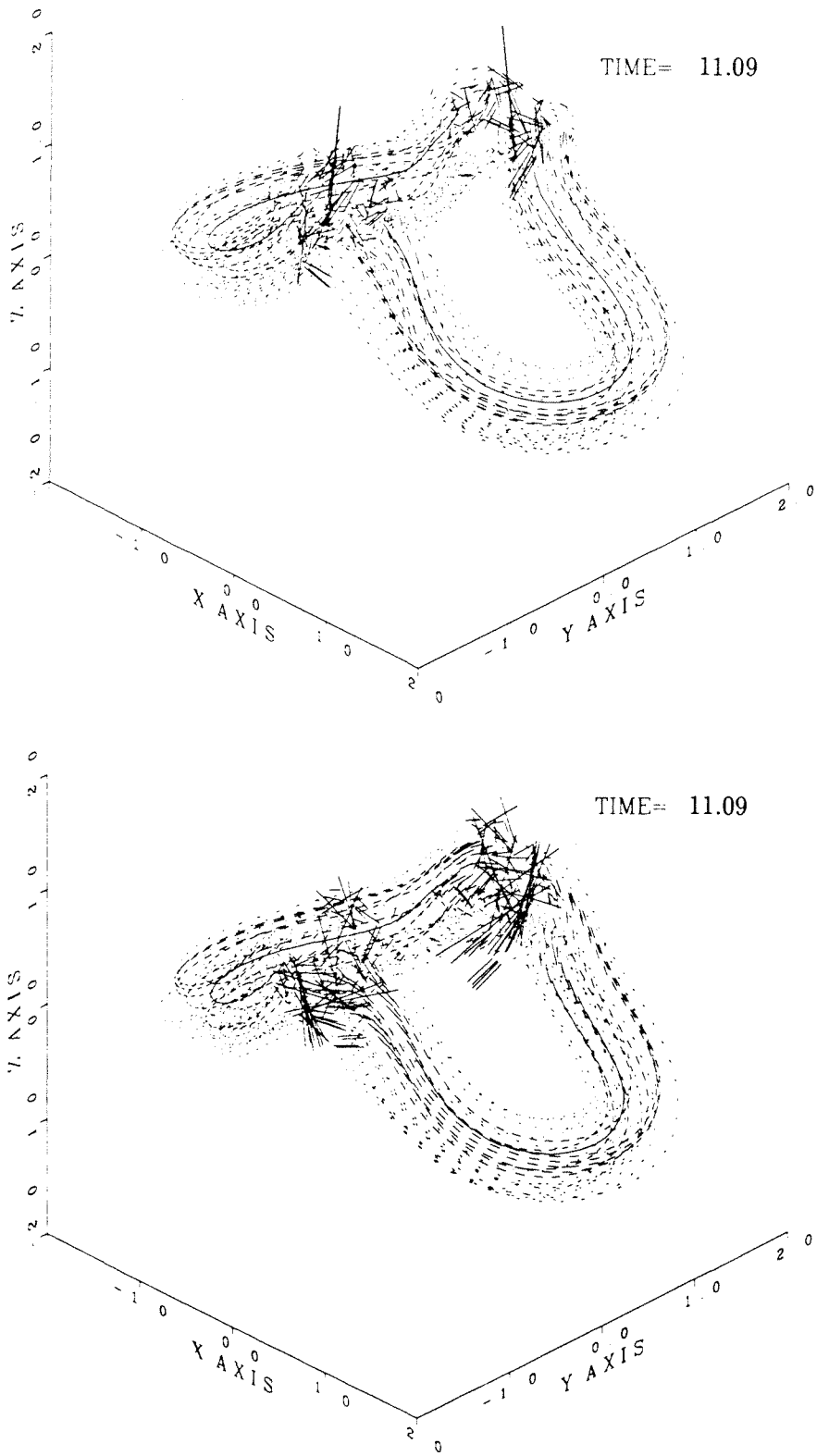

Figure J.29: The fusion of two vortex rings computed with the inviscid method of regularized vortex particles. Perspectives view of the particle strength vectors α^p: (a) classical scheme, (b) transpose scheme.

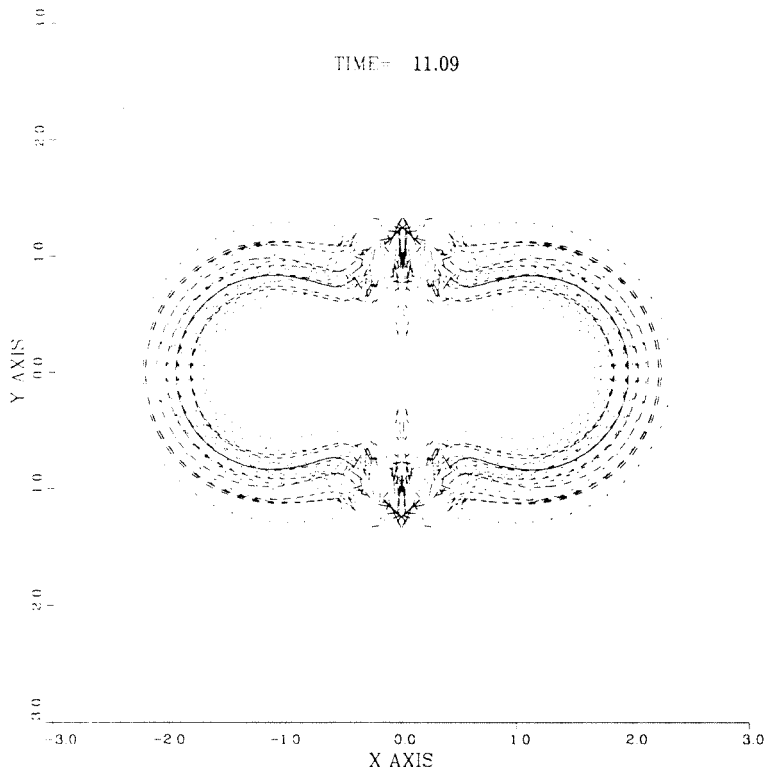

(a)

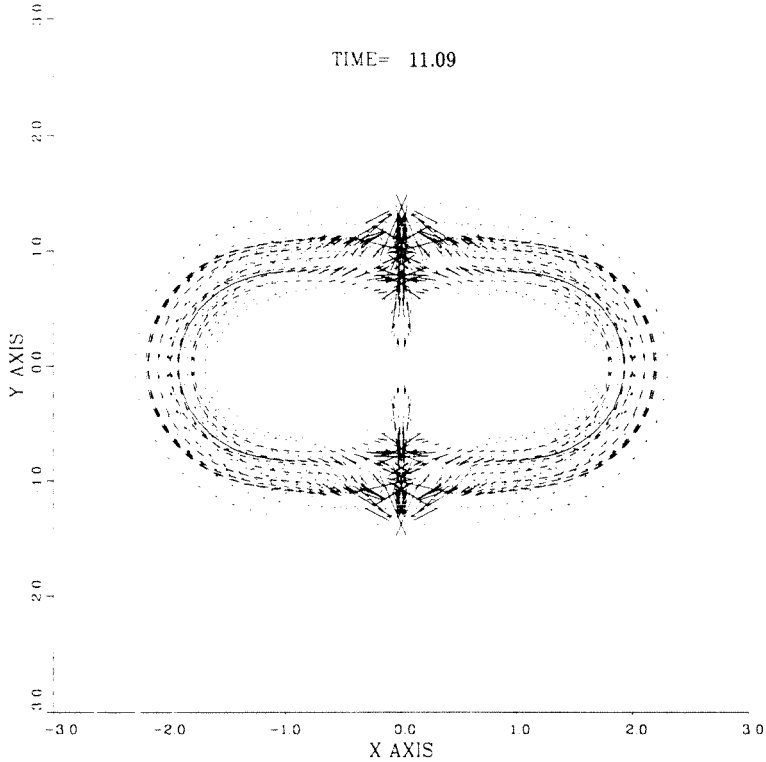

(b)

Figure J.30: The fusion of two vortex rings computed with the inviscid method of regularized vortex particles. $x - y$ projection of the particle strength vectors α^p: (a) classical scheme, (b) transpose scheme.

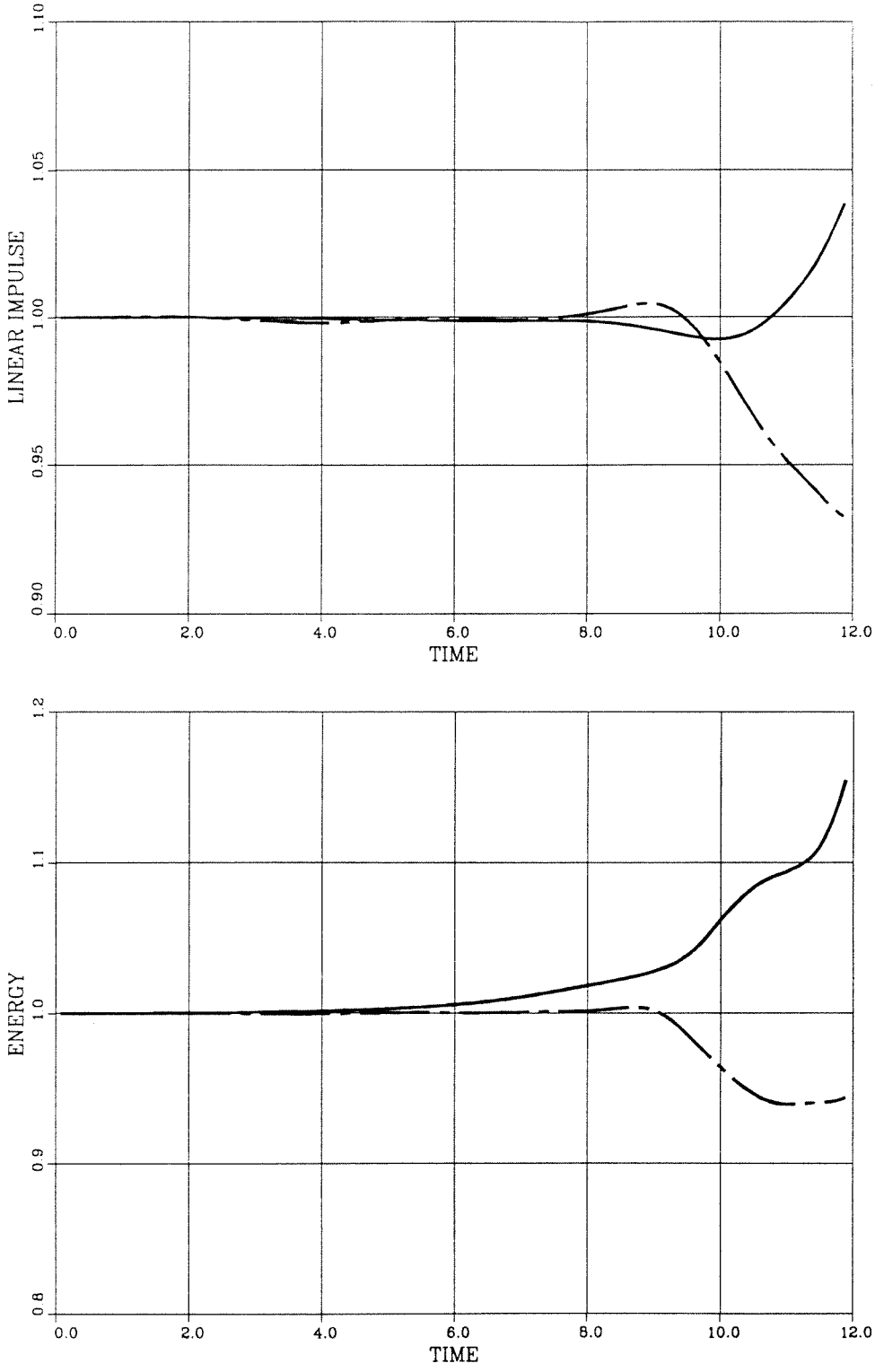

Figure J.31: The fusion of two vortex rings computed with the inviscid method of regularized vortex particles. Diagnostics I, E_f. Transpose scheme (solid), classical scheme (chain-dash).

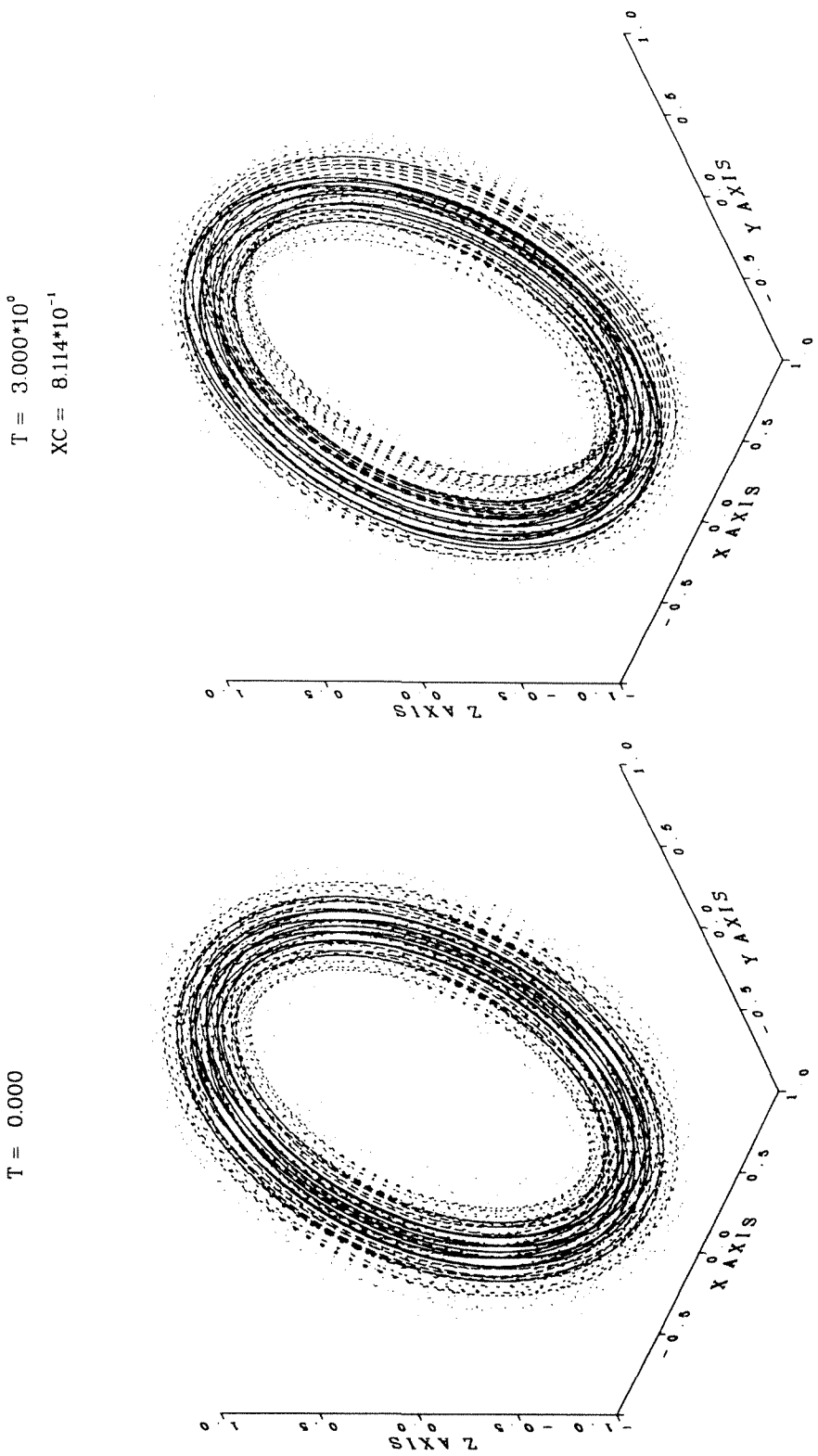

Figure J.32: The single vortex ring computed with the inviscid method of regularized vortex particles. $n_c = 5$. Perspective view of the particle strength vectors α^p.

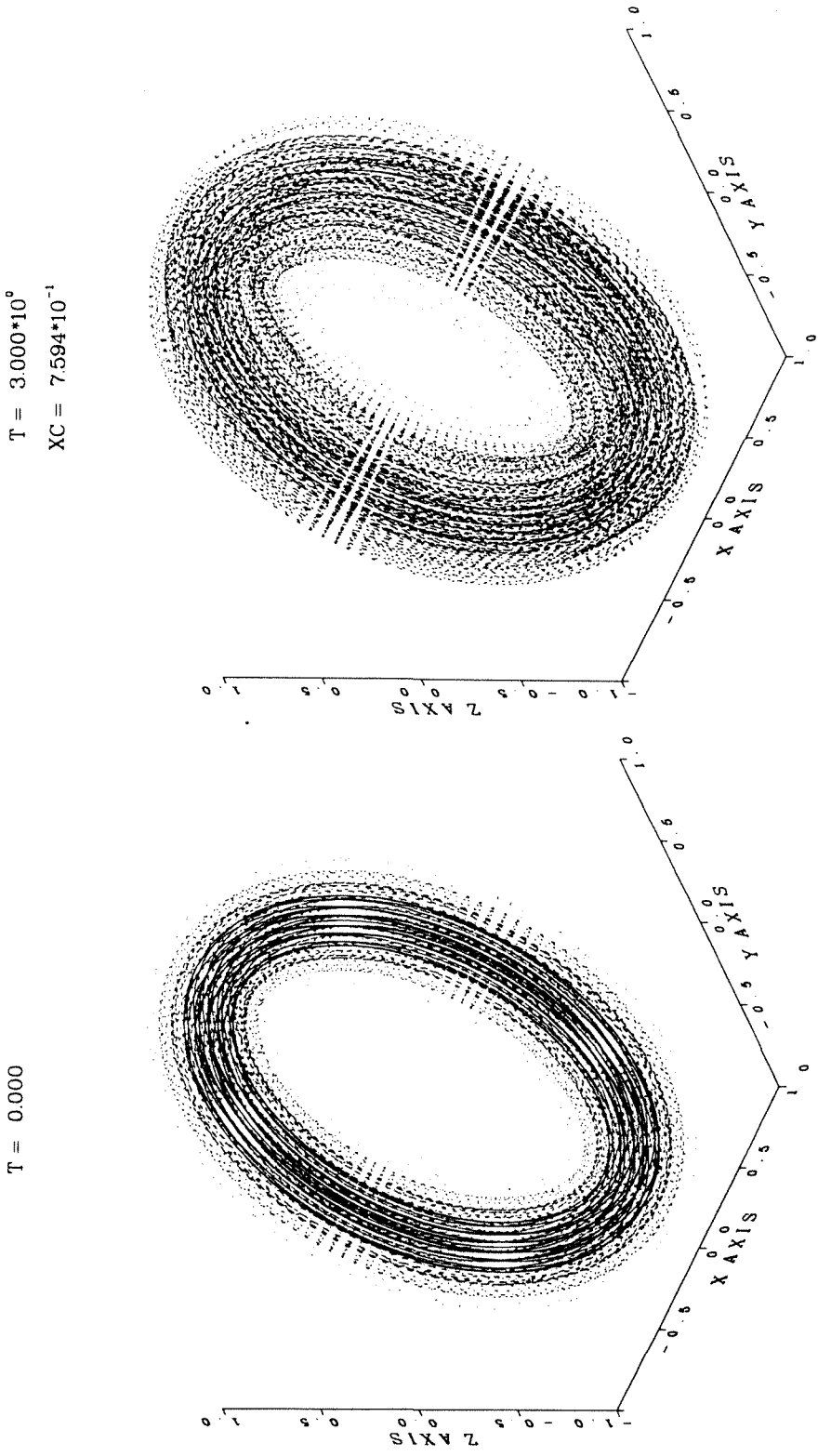

Figure J.33: The single vortex ring computed with the viscous method of regularized vortex particles. $Re = 400$ and $n_c = 6$. Perspective view of the particle strength vectors α^p.

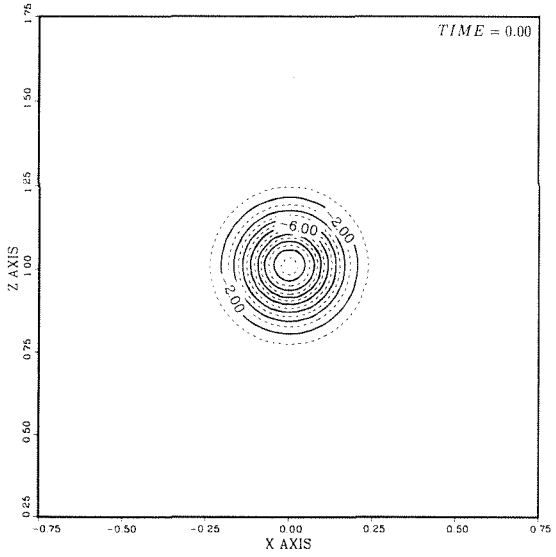
TIME = 0.00
-6.00
-2.00
-2.00
Z AXIS
X AXIS
0.25
0.50
0.75
1.00
1.25
1.50
1.75
-0.75
-0.50
-0.25
0.00
0.25
0.50
0.75

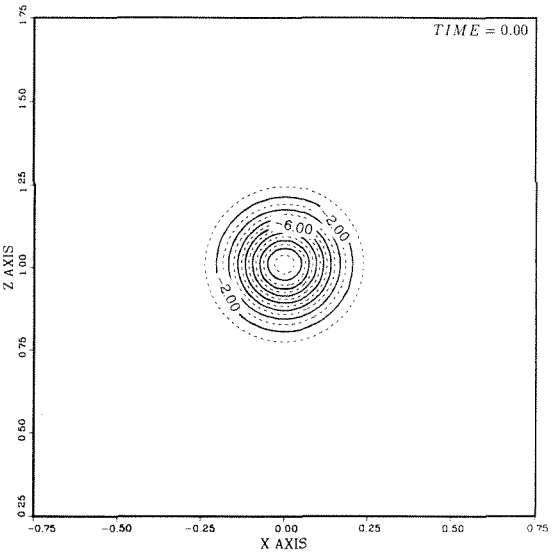
TIME = 0.00
-6.00
-2.00
-2.00
Z AXIS
X AXIS
0.25
0.50
0.75
1.00
1.25
1.50
1.75
-0.75
-0.50
-0.25
0.00
0.25
0.50
0.75

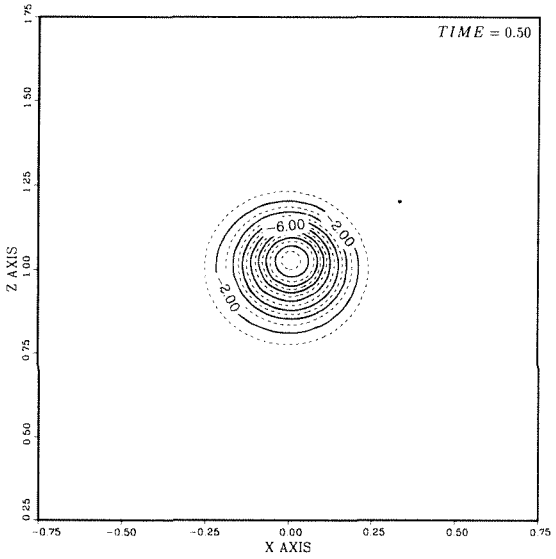
TIME = 0.50
-6.00
-2.00
-2.00
Z AXIS
X AXIS
0.25
0.50
0.75
1.00
1.25
1.50
1.75
-0.75
-0.50
-0.25
0.00
0.25
0.50
0.75

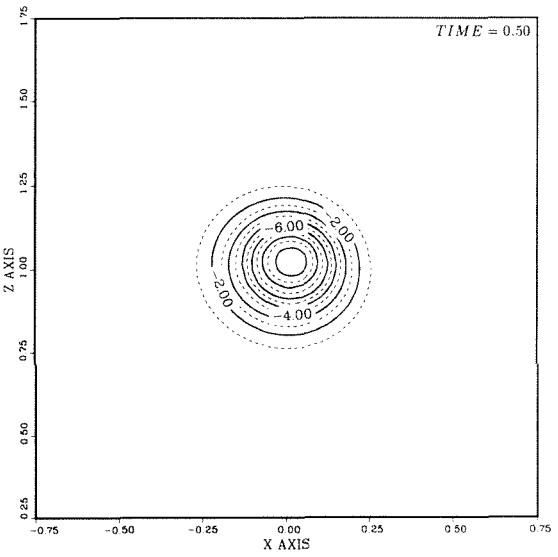
TIME = 0.50
-6.00
-2.00
-2.00
-4.00
Z AXIS
X AXIS
0.25
0.50
0.75
1.00
1.25
1.50
1.75
-0.75
-0.50
-0.25
0.00
0.25
0.50
0.75

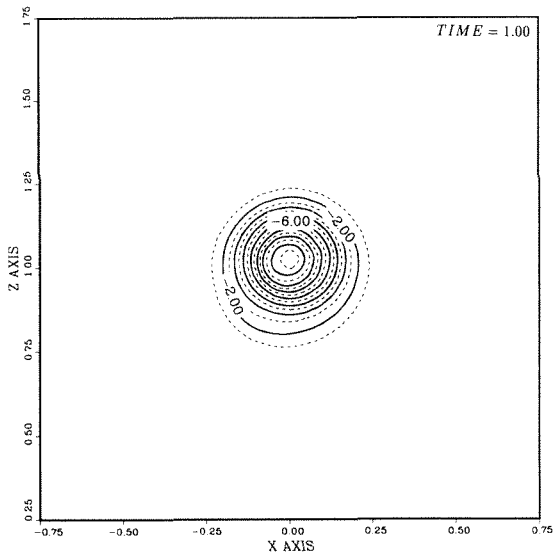
TIME = 1.00
-6.00
-2.00
-2.00
Z AXIS
X AXIS
0.25
0.50
0.75
1.00
1.25
1.50
1.75
-0.75
-0.50
-0.25
0.00
0.25
0.50
0.75

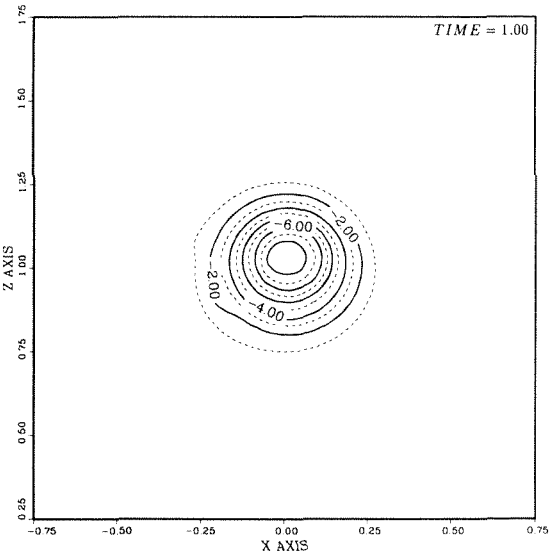
TIME = 1.00
-6.00
-2.00
-2.00
-4.00
Z AXIS
X AXIS
0.25
0.50
0.75
1.00
1.25
1.50
1.75
-0.75
-0.50
-0.25
0.00
0.25
0.50
0.75

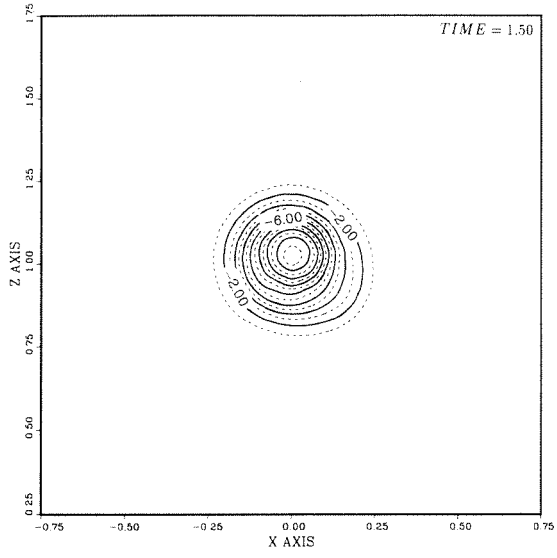
TIME = 1.50
-6.00
-2.00
-2.00
Z AXIS
X AXIS

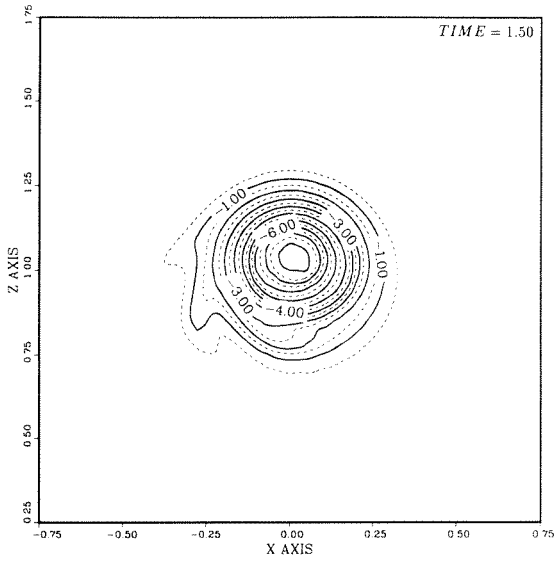
TIME = 1.50
-1.00
-6.00
-3.00
-1.00
-3.00
-4.00
Z AXIS
X AXIS

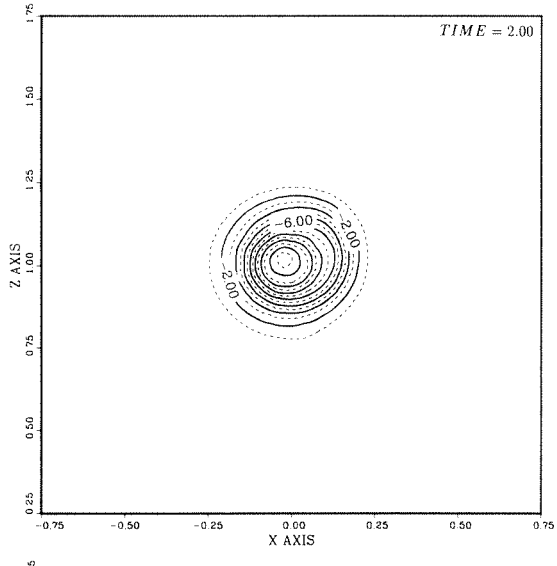
TIME = 2.00
-6.00
-2.00
-2.00
Z AXIS
X AXIS

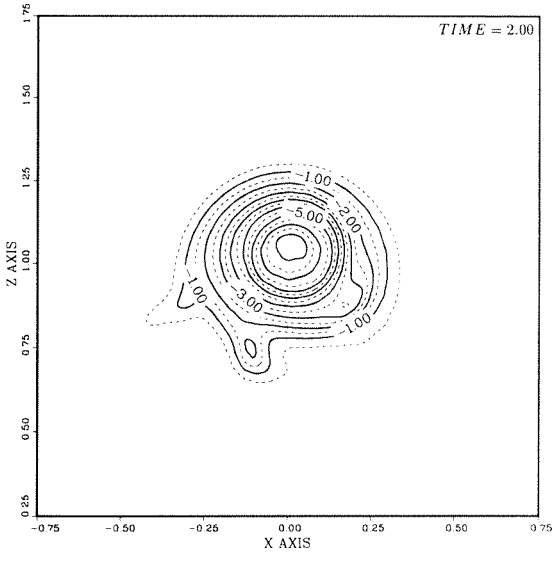
TIME = 2.00
-1.00
-5.00
-2.00
-1.00
-3.00
-1.00
Z AXIS
X AXIS

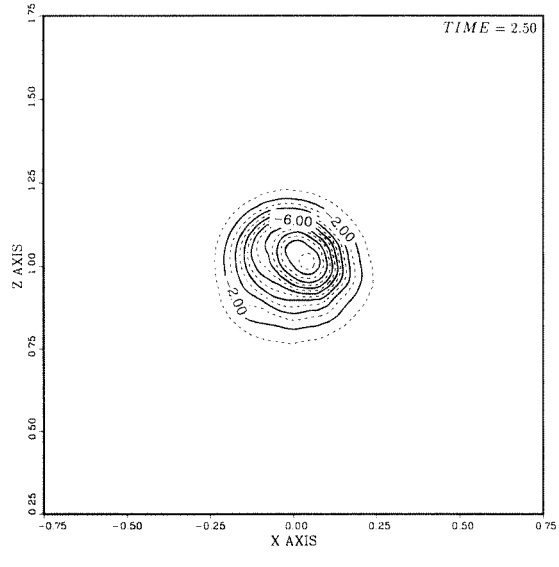
TIME = 2.50
-6.00
-2.00
-2.00
Z AXIS
X AXIS

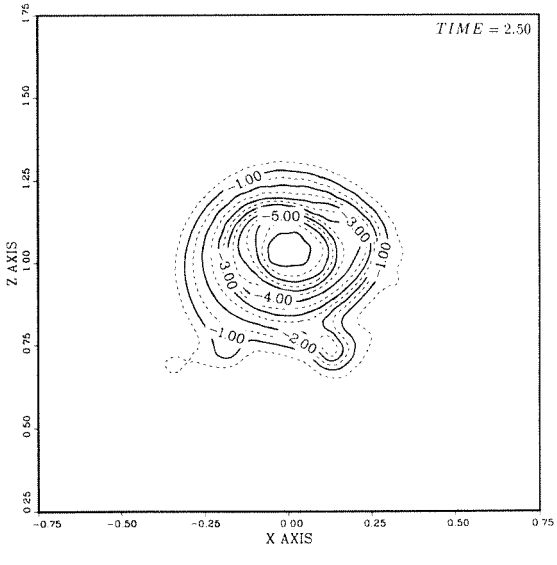
TIME = 2.50
-1.00
-5.00
-3.00
-1.00
-3.00
-4.00
-1.00
-2.00
Z AXIS
X AXIS

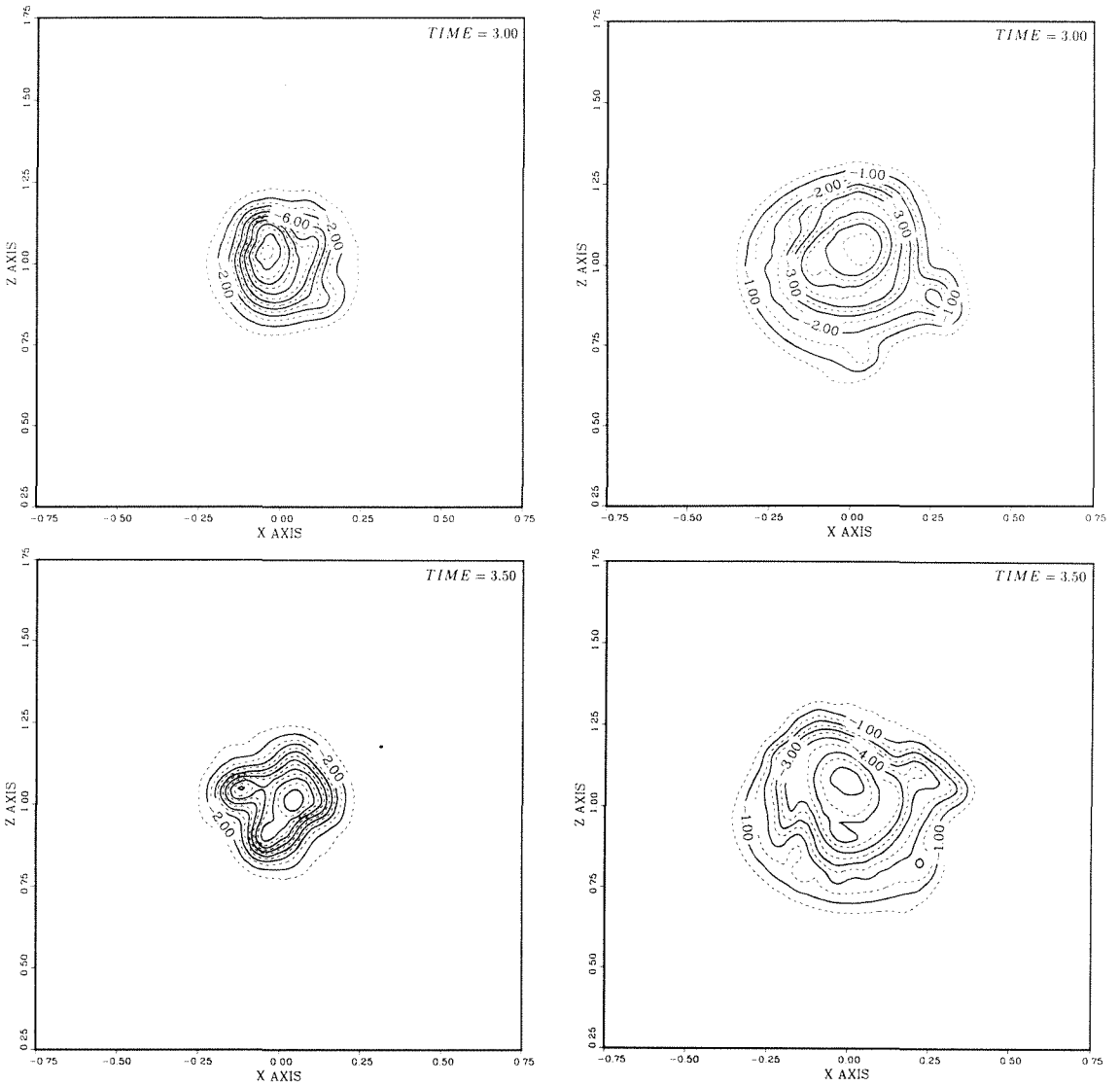

Figure J.34: The single vortex ring computed with the method of regularized vortex particles. Vorticity contours: inviscid with $n_c = 5$ (left), viscous with $Re = 400$ and $n_c = 6$ (right).

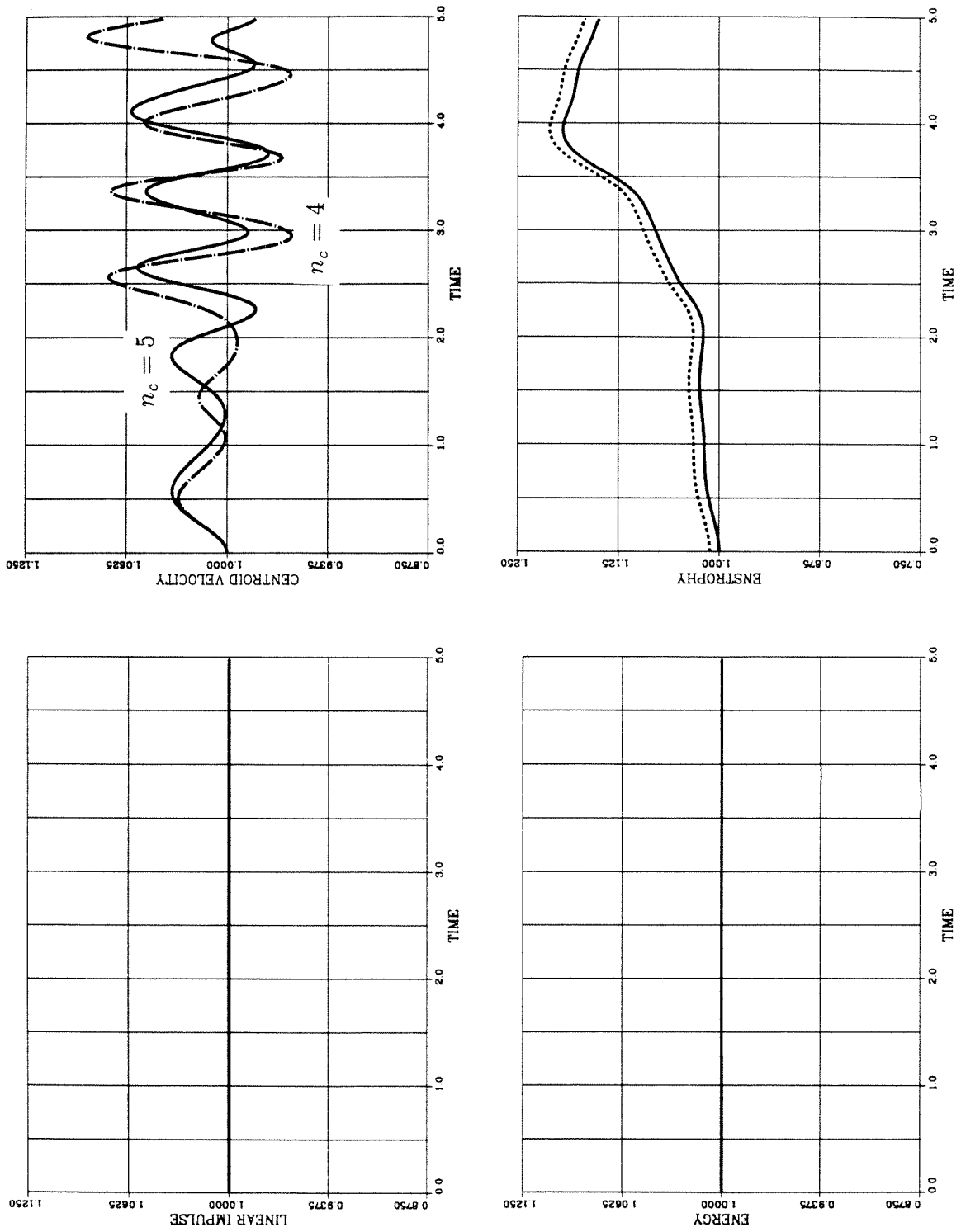

Figure J.35: The single vortex ring computed with the inviscid method of regularized vortex particles. $n_c = 5$. Diagnostics I, dX_c/dt, $\tilde{E}$ (solid) and $\tilde{E}_f$ (dash), $\tilde{\mathcal{E}}$ (solid) and $\tilde{\mathcal{E}}_f$ (dash).

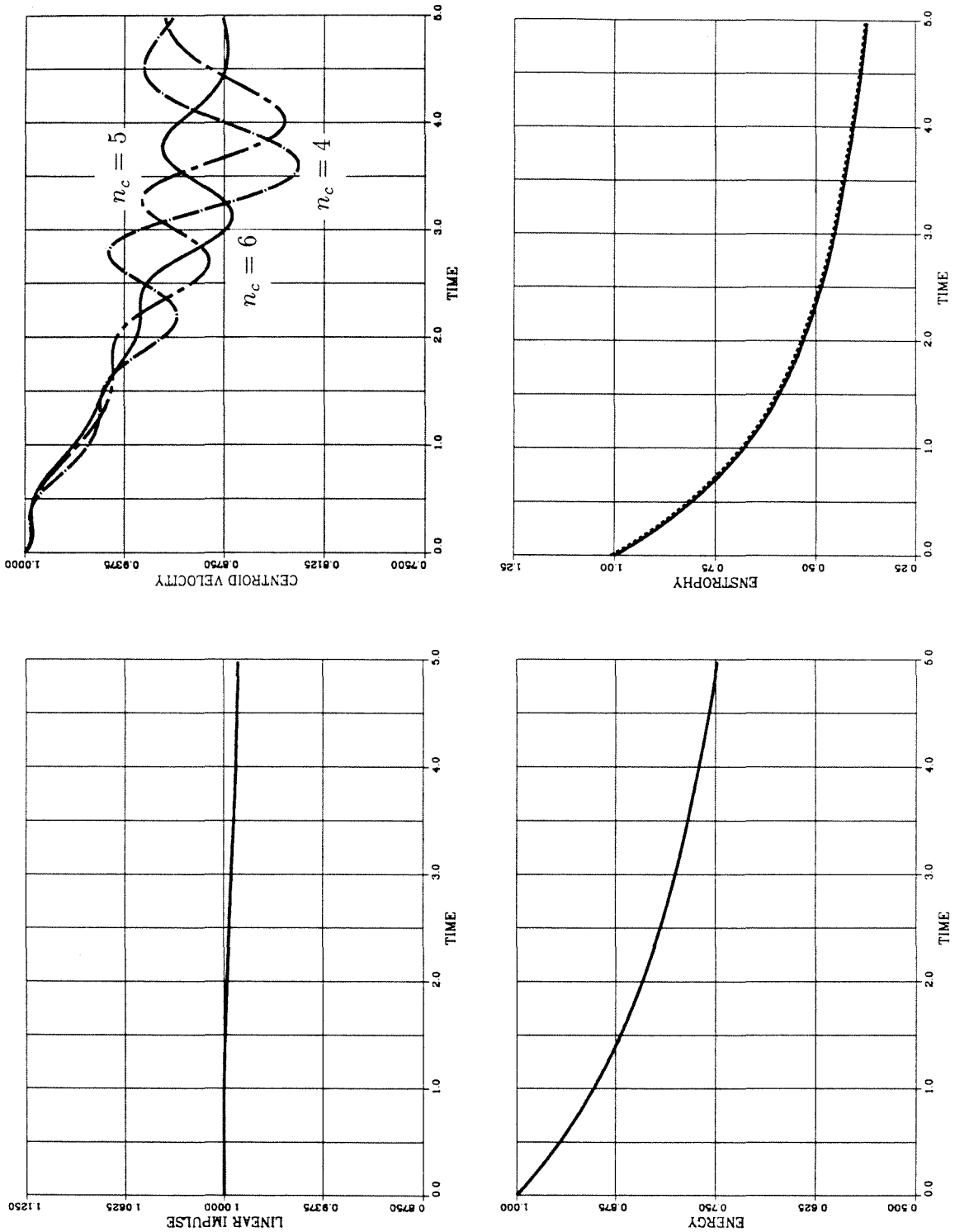

Figure J.36: The single vortex ring computed with the viscous method of regularized vortex particles. $Re = 400$ and $n_c = 6$. Diagnostics I, dX_c/dt, $\tilde{E}$ (solid) and $\tilde{E}_f$ (dash), $\tilde{\mathcal{E}}$ (solid) and $\tilde{\mathcal{E}}_f$ (dash).

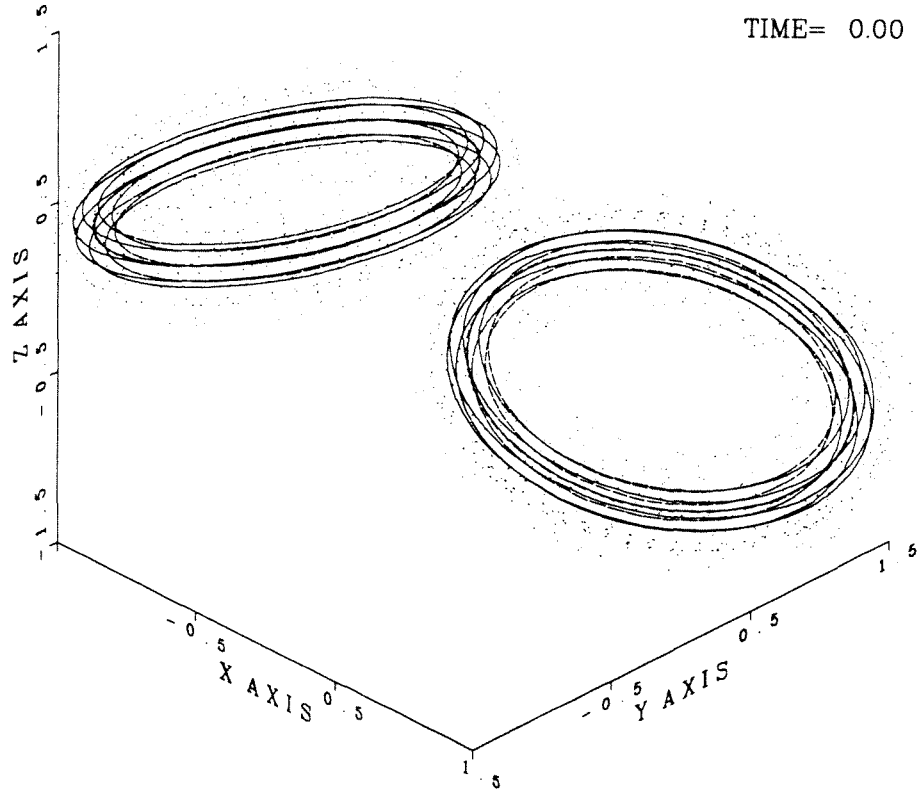
TIME= 0.00
Z AXIS
1.5
0.5
-0.5
-1.5
X AXIS
-0.5
0.5
1.5
Y AXIS
-0.5
0.5
1.5

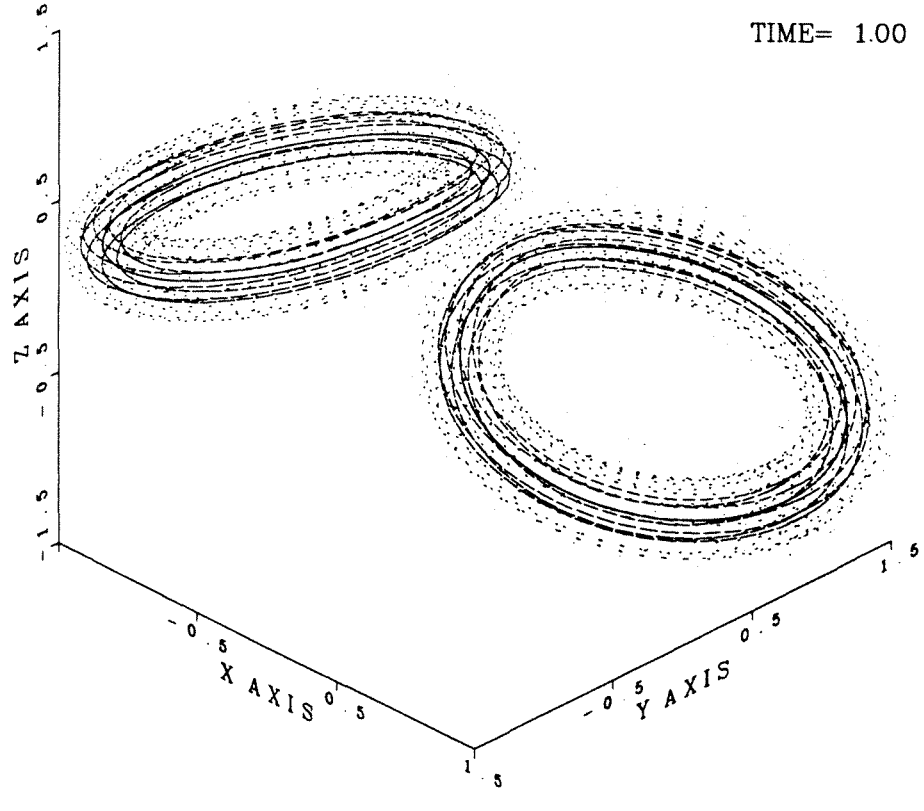
TIME= 1.00
Z AXIS
1.5
0.5
-0.5
-1.5
X AXIS
-0.5
0.5
1.5
Y AXIS
-0.5
0.5
1.5

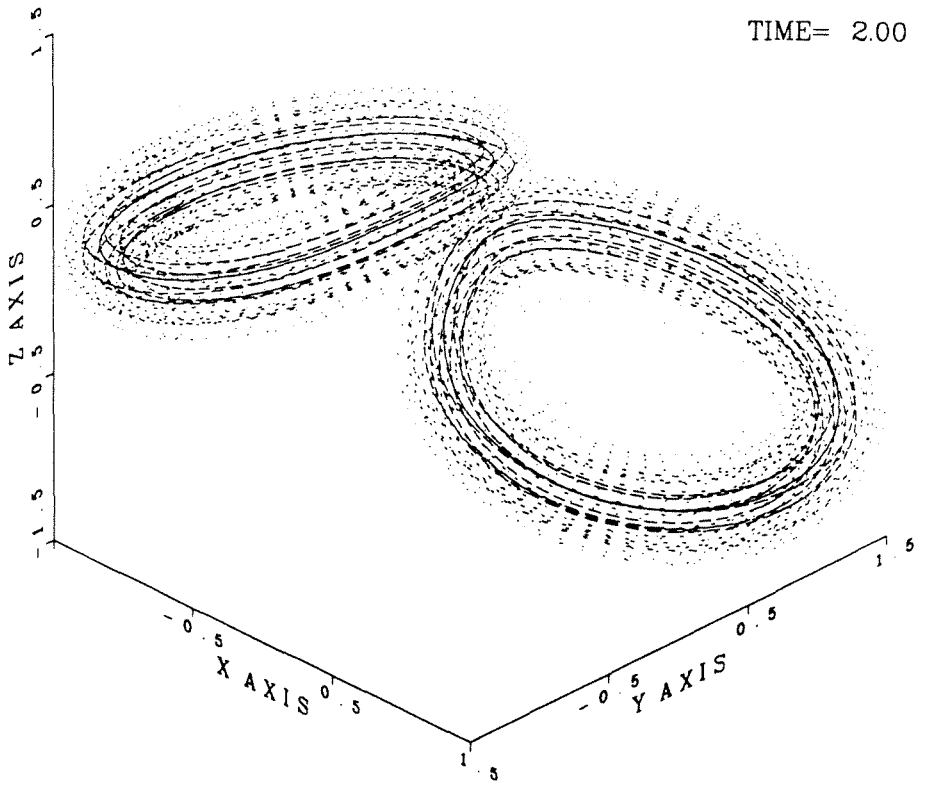
TIME= 2.00
Z AXIS
1.5
0.5
-0.5
-1.5
X AXIS
-0.5
0.5
1.5
Y AXIS
-0.5
0.5
1.5

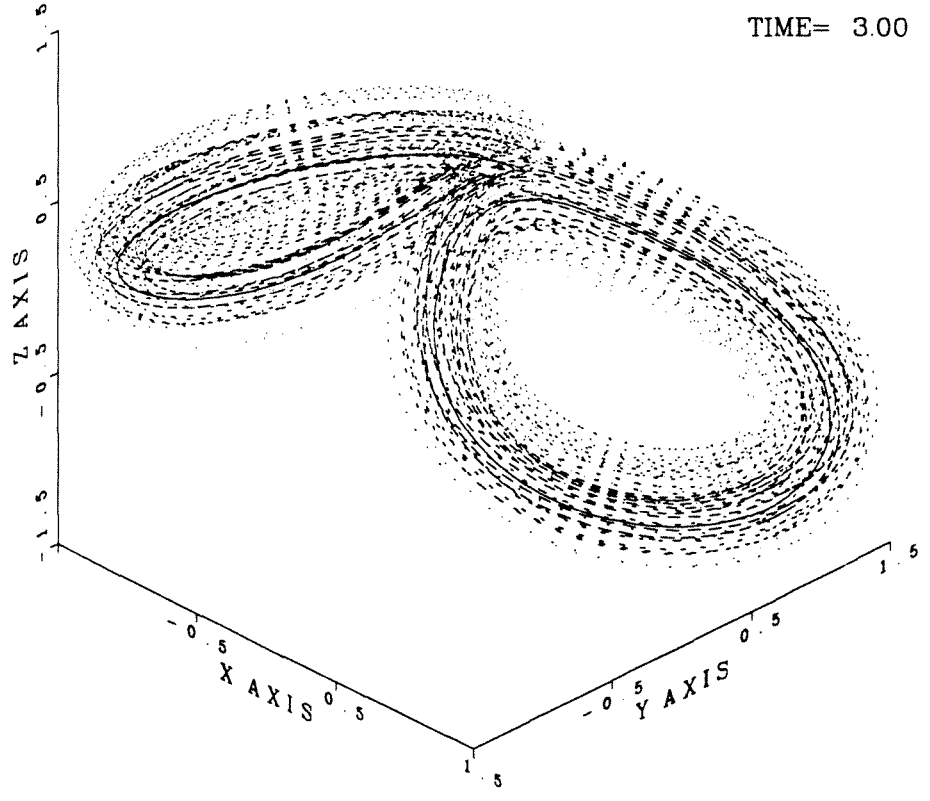
TIME= 3.00
Z AXIS
1.5
0.5
-0.5
-1.5
X AXIS
-0.5
0.5
1.5
Y AXIS
-0.5
0.5
1.5

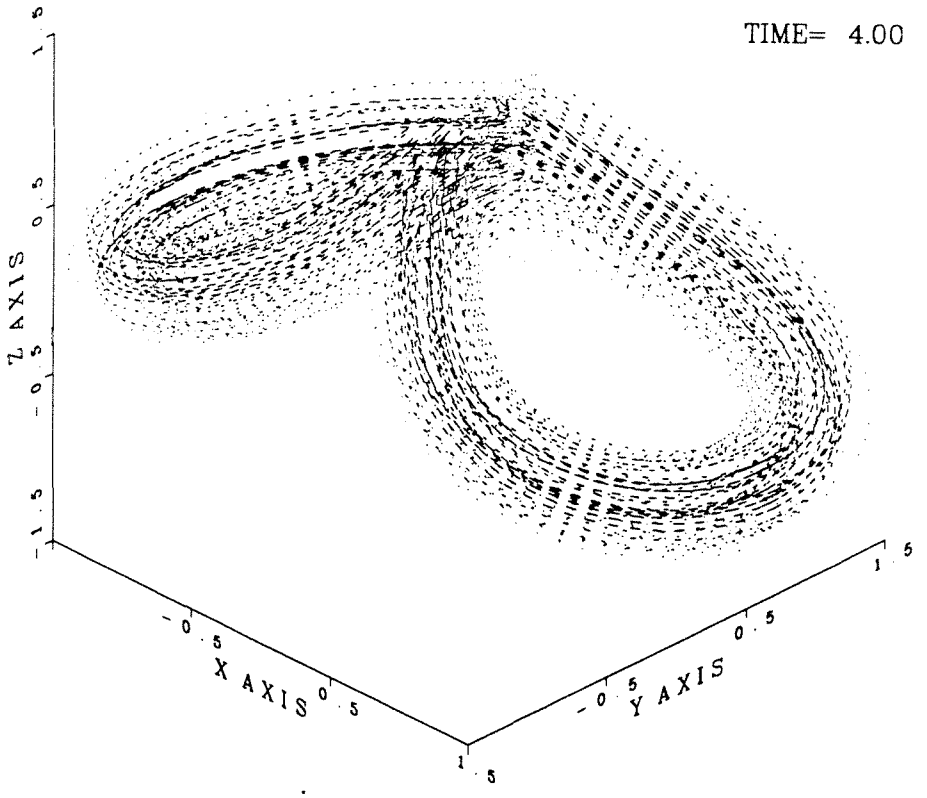
TIME= 4.00
Z AXIS
X AXIS
Y AXIS

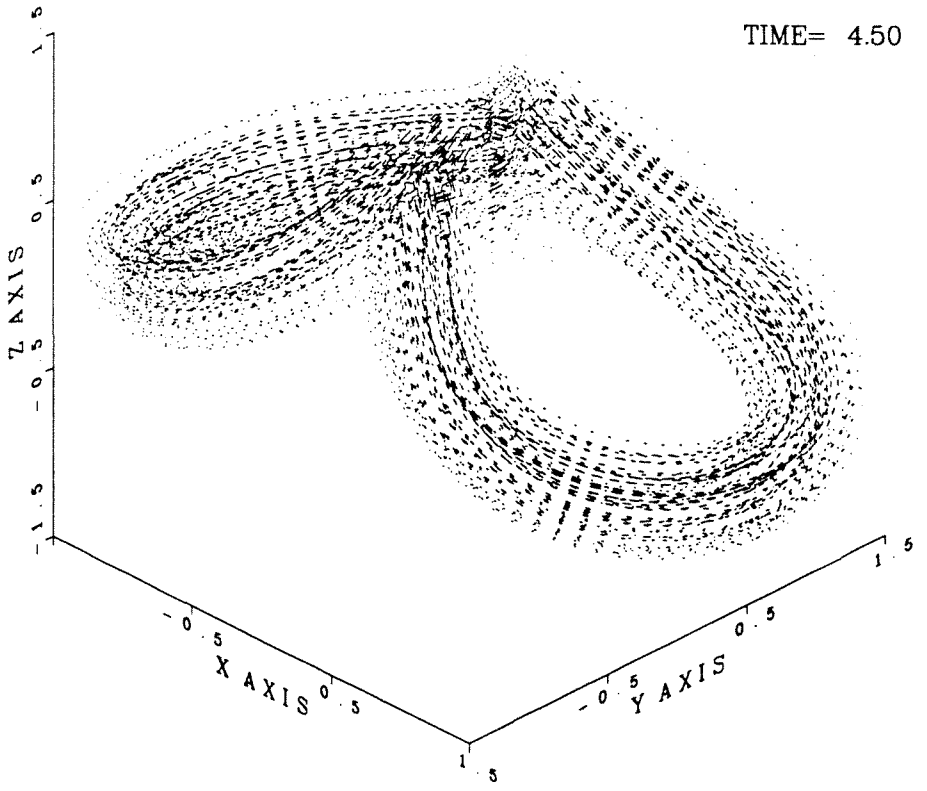
TIME= 4.50
Z AXIS
X AXIS
Y AXIS

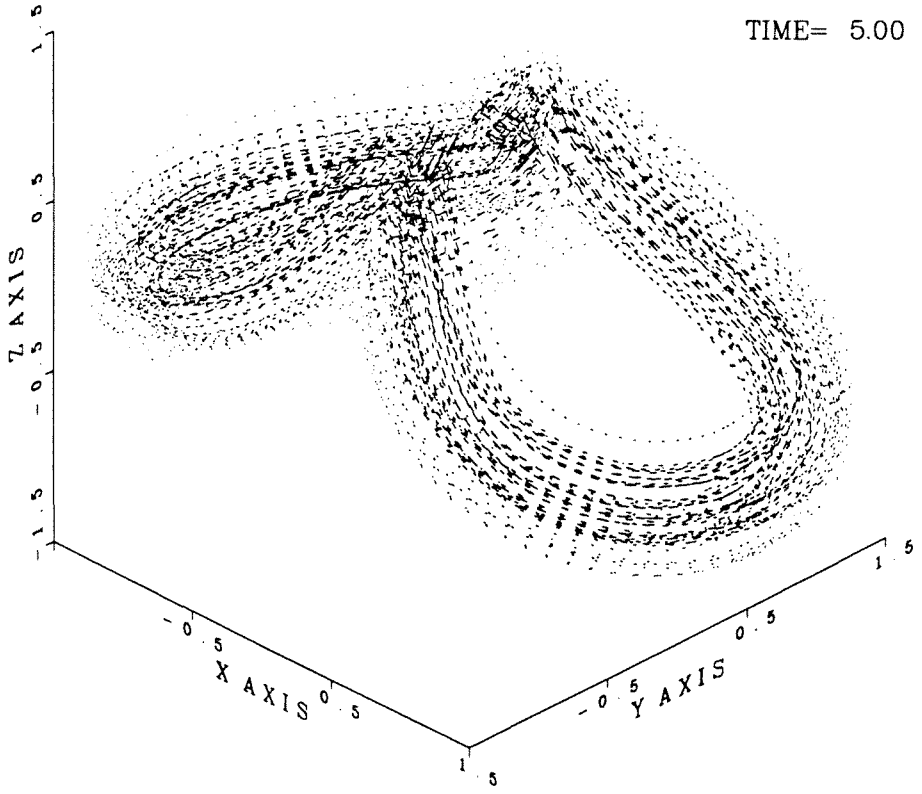
TIME= 5.00
Z AXIS
1.5
0.5
-0.5
-1.5
X AXIS
-0.5
0.5
Y AXIS
-0.5
0.5
1.5

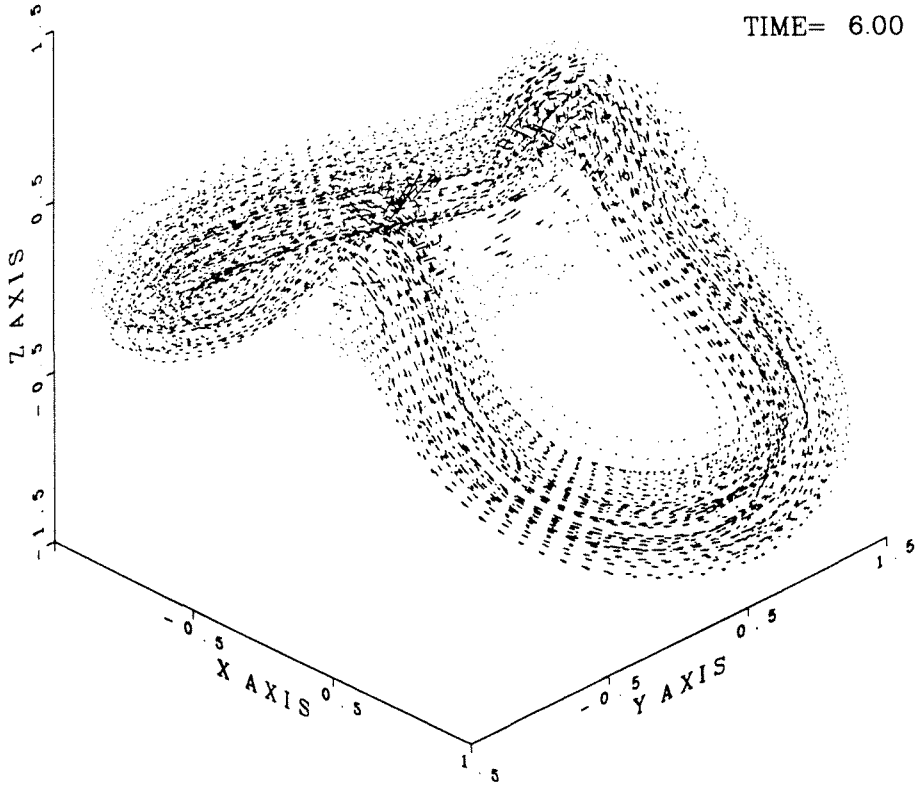
TIME= 6.00
Z AXIS
1.5
0.5
-0.5
-1.5
X AXIS
-0.5
0.5
Y AXIS
-0.5
0.5
1.5

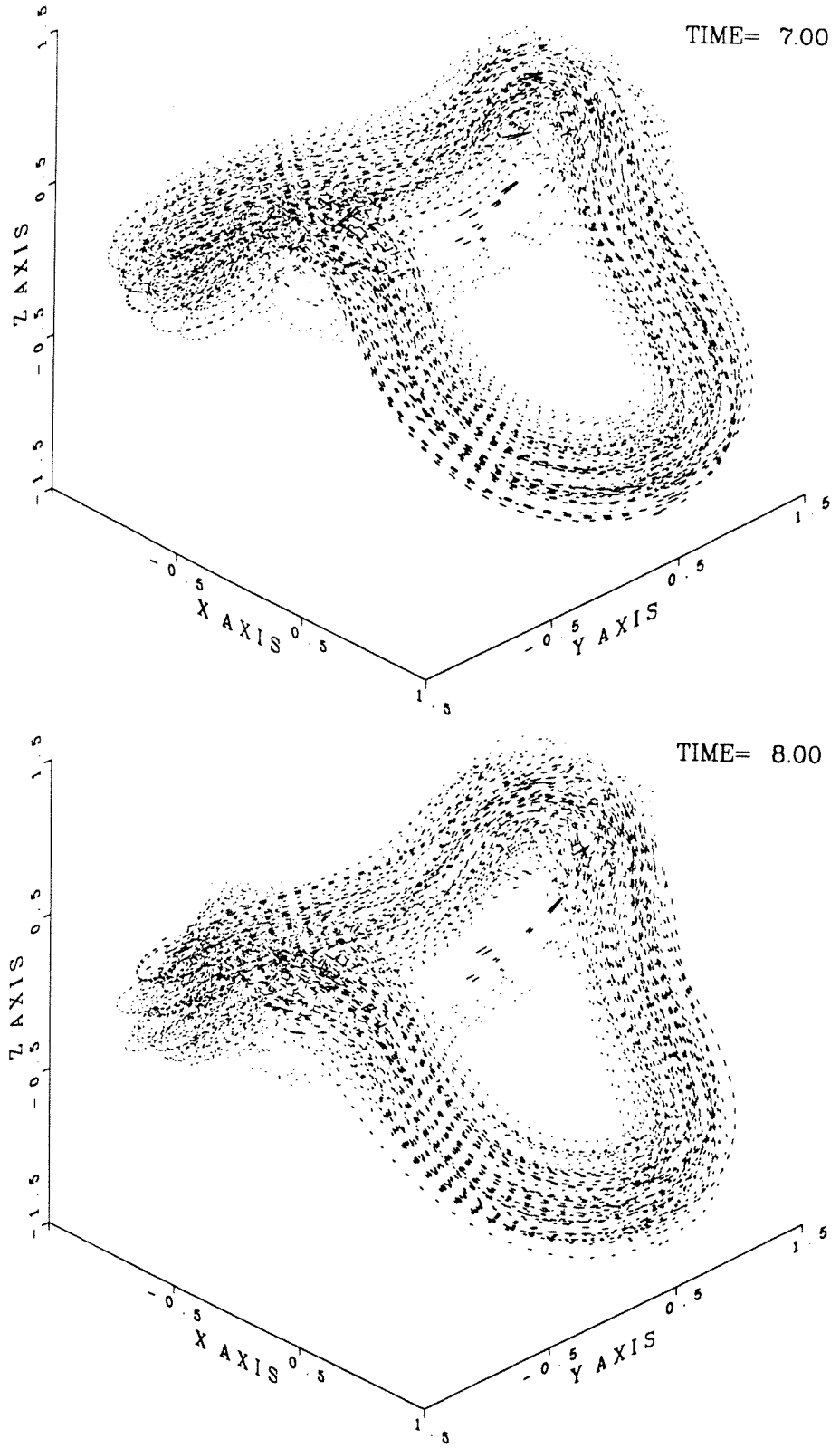

Figure J.37: The fusion of two vortex rings computed with the viscous method of regularized vortex particles. $Re = 400$. Perspective view of the particle strength vectors α^p.

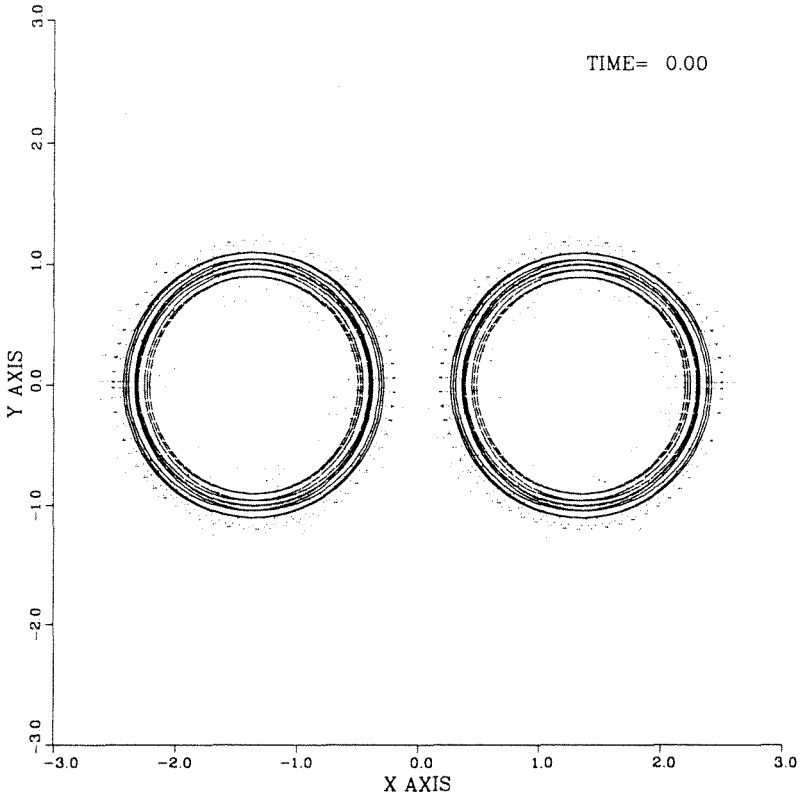
TIME= 0.00
Y AXIS
X AXIS
3.0
2.0
1.0
0.0
-1.0
-2.0
-3.0

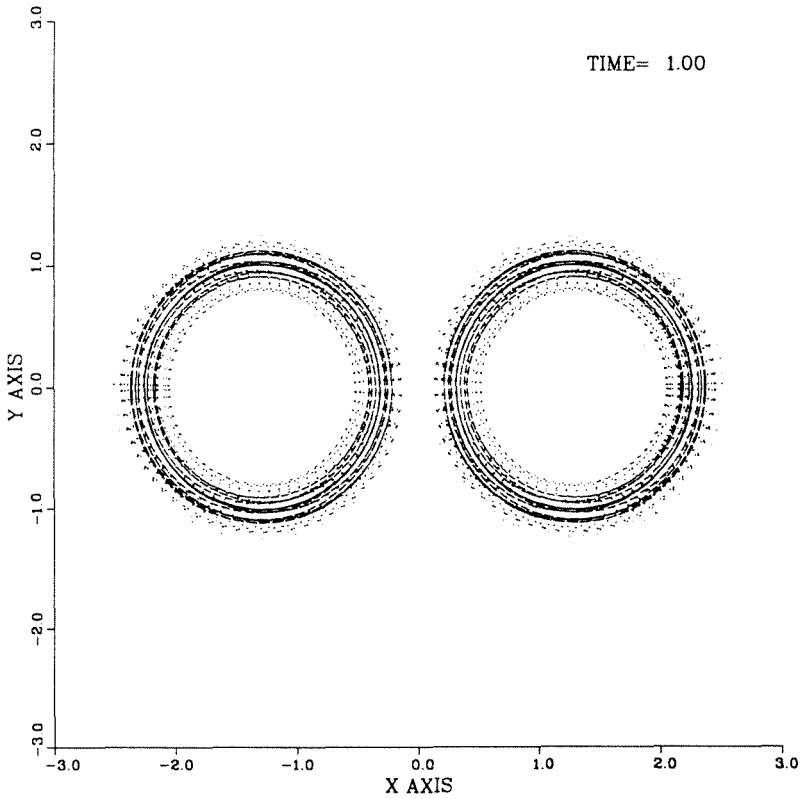
TIME= 1.00
Y AXIS
X AXIS
3.0
2.0
1.0
0.0
-1.0
-2.0
-3.0

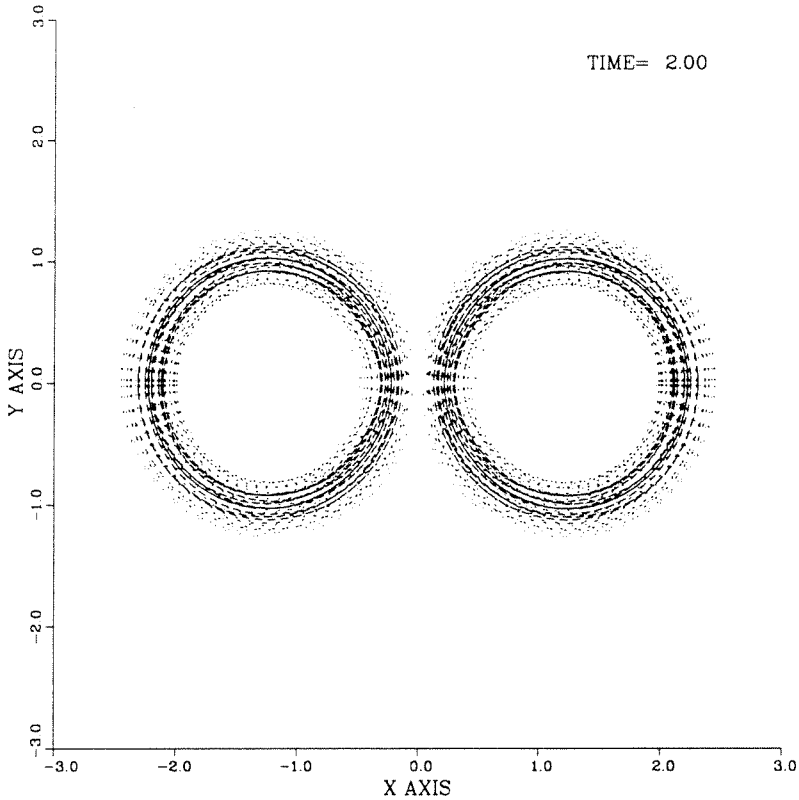
TIME= 2.00
Y AXIS
X AXIS
3.0
2.0
1.0
0.0
-1.0
-2.0
-3.0

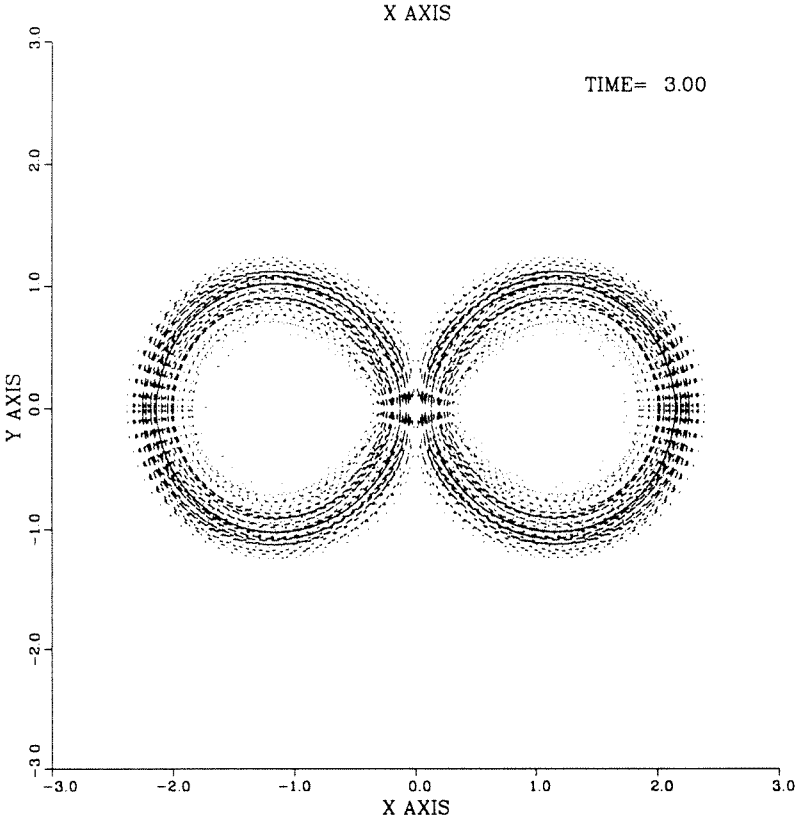
TIME= 3.00
Y AXIS
X AXIS
3.0
2.0
1.0
0.0
-1.0
-2.0
-3.0

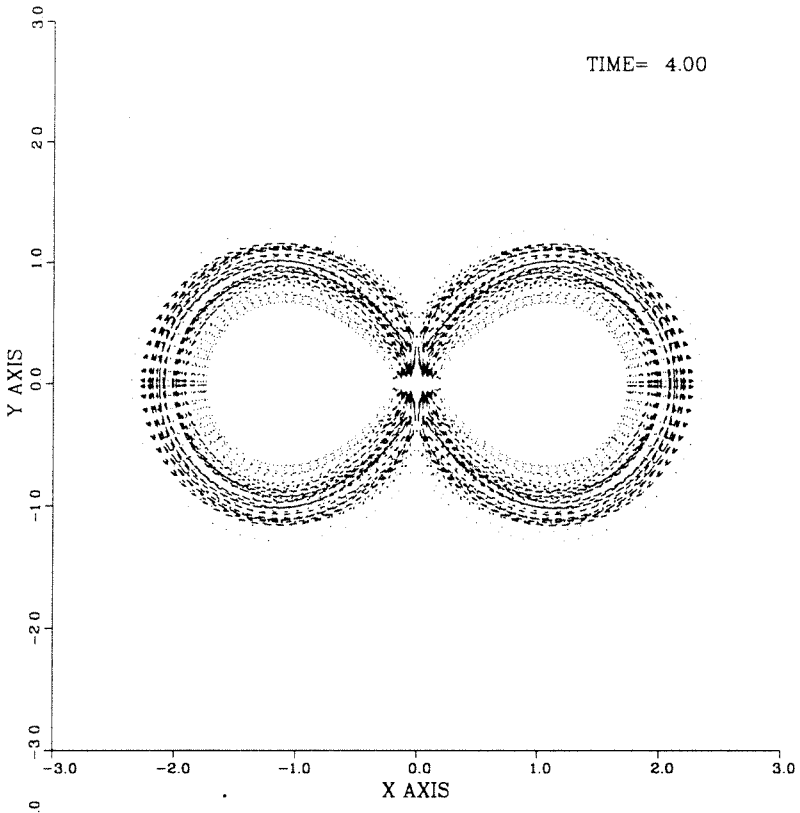
TIME= 4.00
Y AXIS
X AXIS
3.0
2.0
1.0
0.0
-1.0
-2.0
-3.0

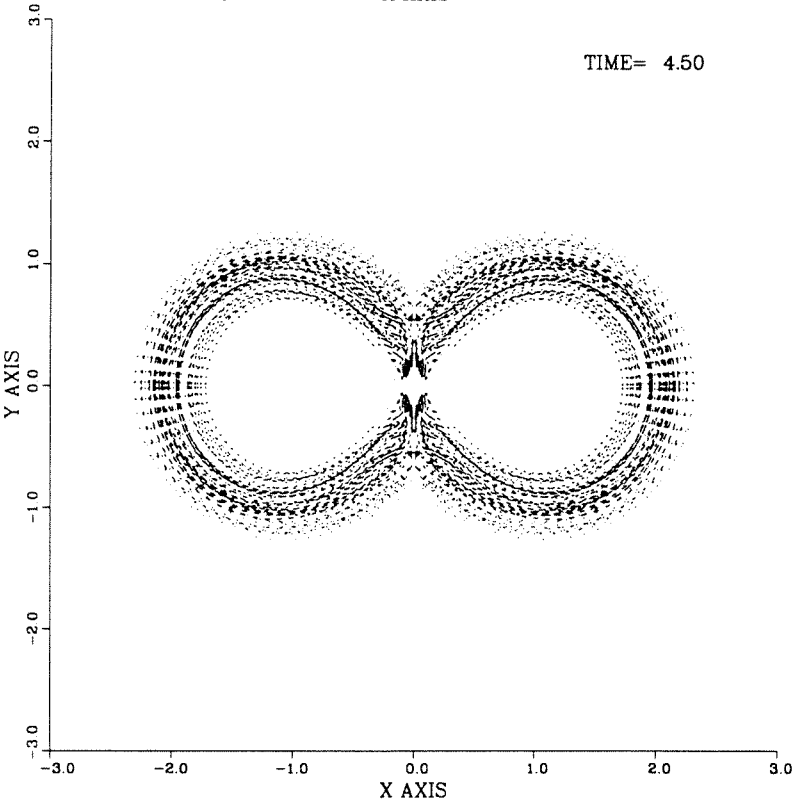
TIME= 4.50
Y AXIS
X AXIS
3.0
2.0
1.0
0.0
-1.0
-2.0
-3.0

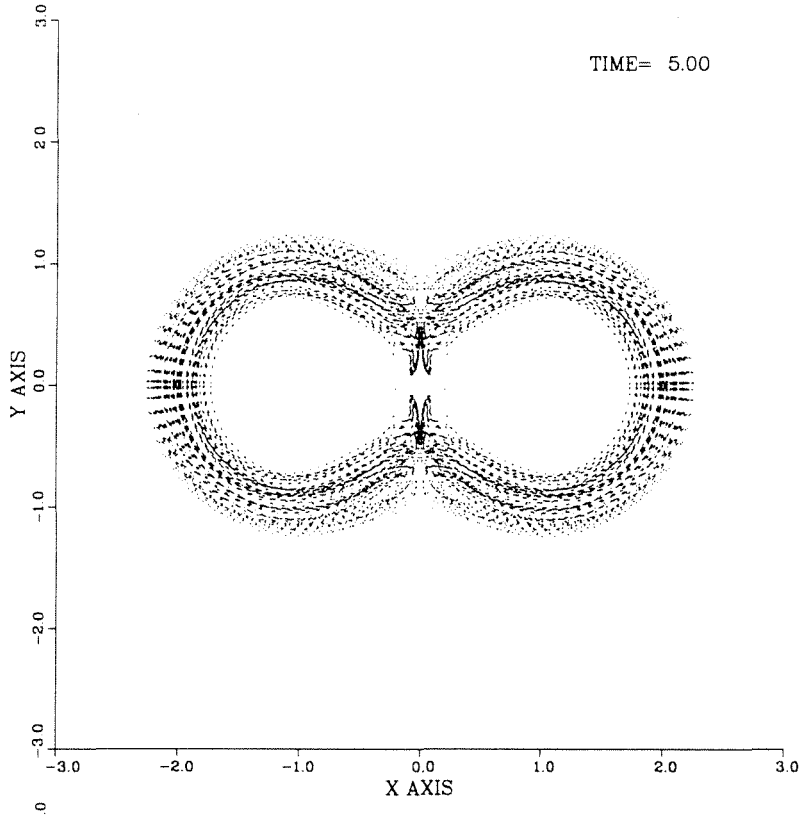
TIME= 5.00
Y AXIS
X AXIS
3.0
2.0
1.0
0.0
-1.0
-2.0
-3.0

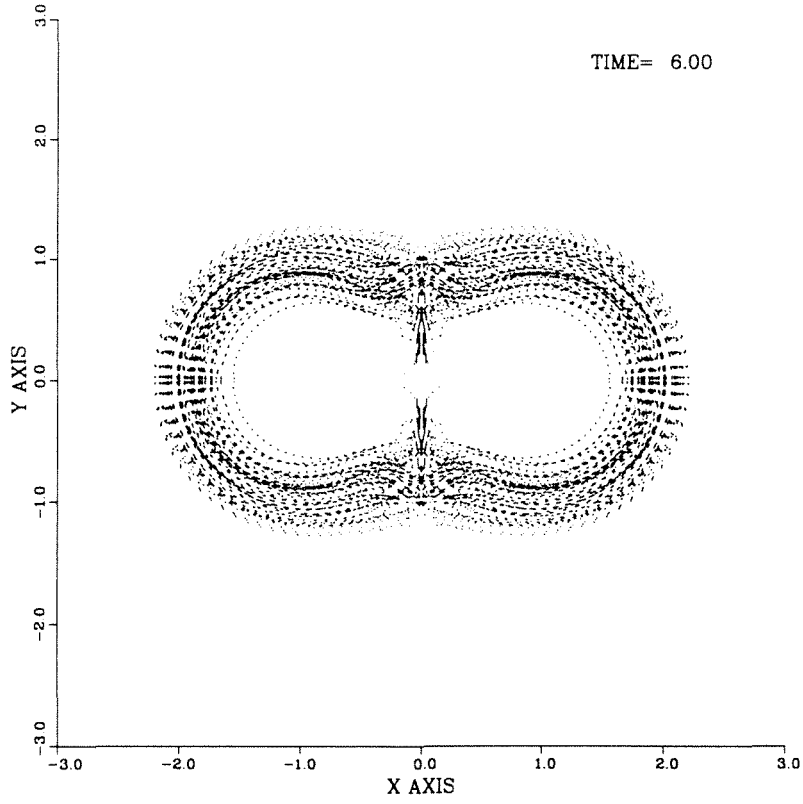
TIME= 6.00
Y AXIS
X AXIS
3.0
2.0
1.0
0.0
-1.0
-2.0
-3.0

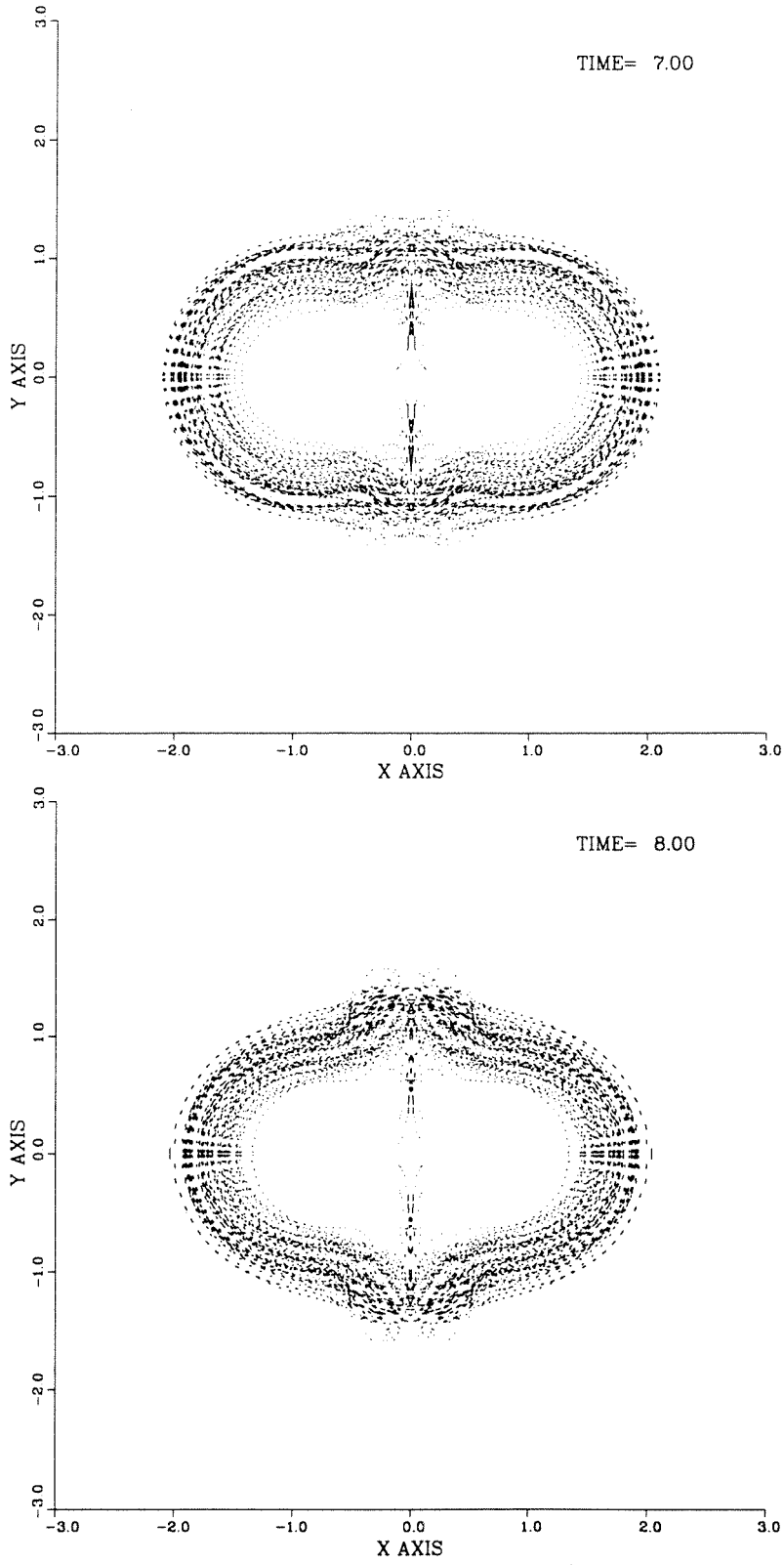

Figure J.38: The fusion of two vortex rings computed with the viscous method of regularized vortex particles. $Re = 400$. $x - y$ projection of the particle strength vectors α^p.

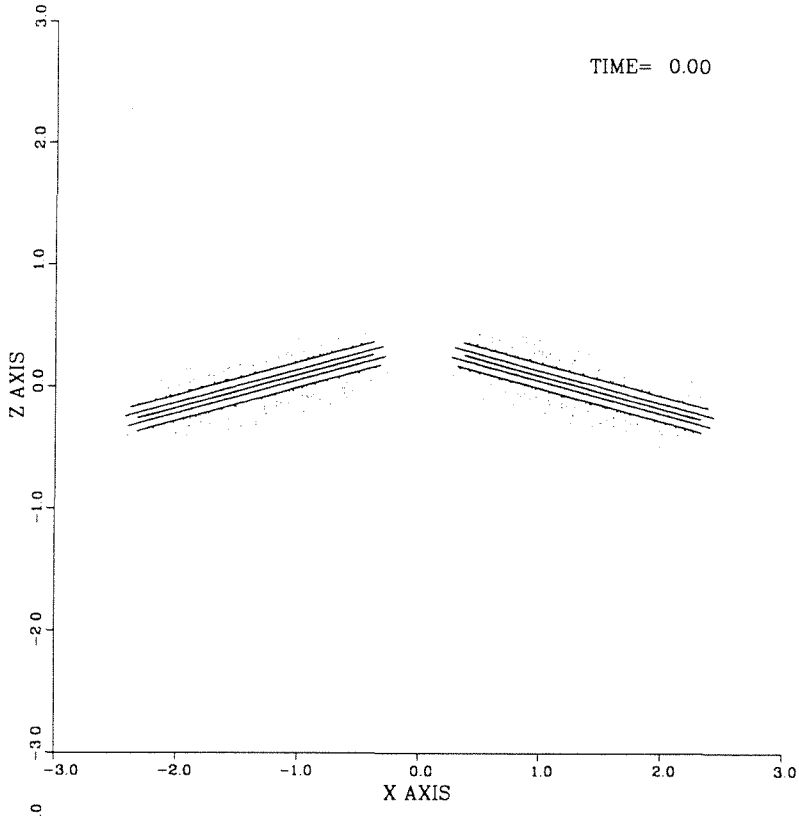
TIME= 0.00
Z AXIS
X AXIS
3.0
2.0
1.0
0.0
-1.0
-2.0
-3.0

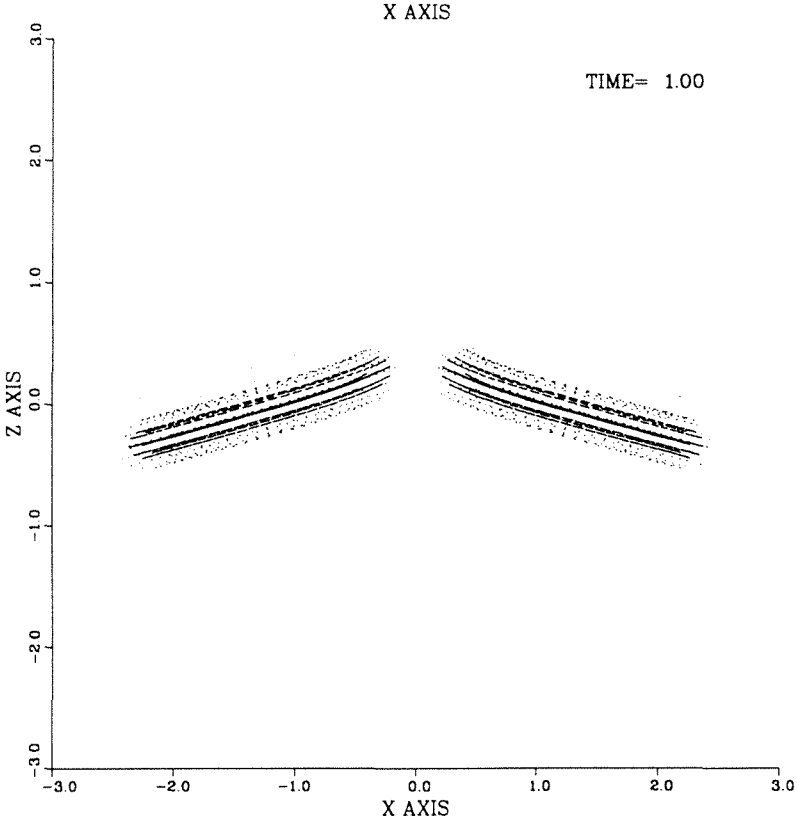
TIME= 1.00
Z AXIS
X AXIS
3.0
2.0
1.0
0.0
-1.0
-2.0
-3.0

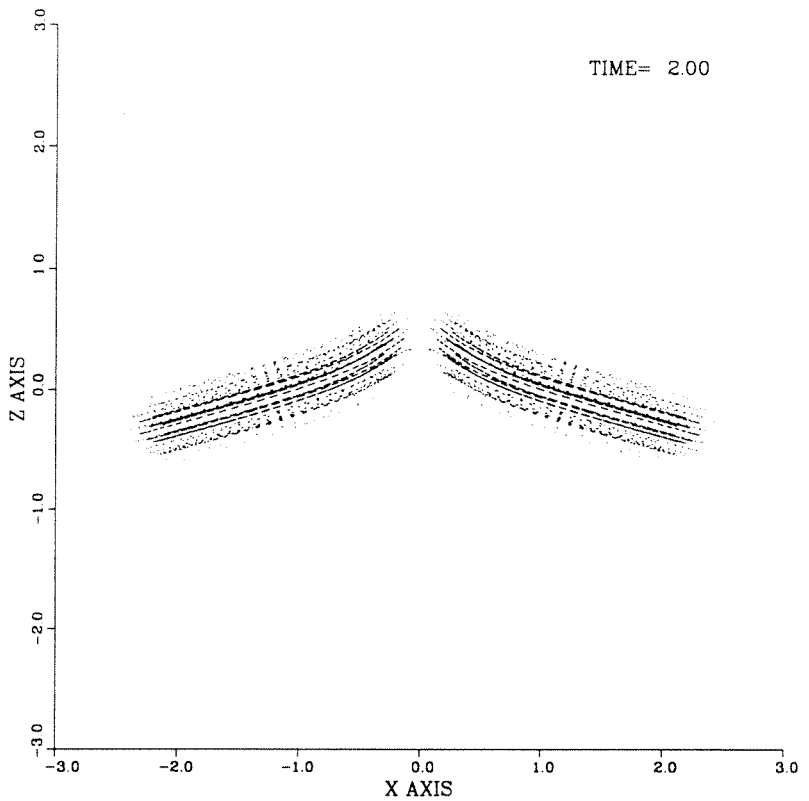
TIME= 2.00
Z AXIS
X AXIS
3.0
2.0
1.0
0.0
-1.0
-2.0
-3.0

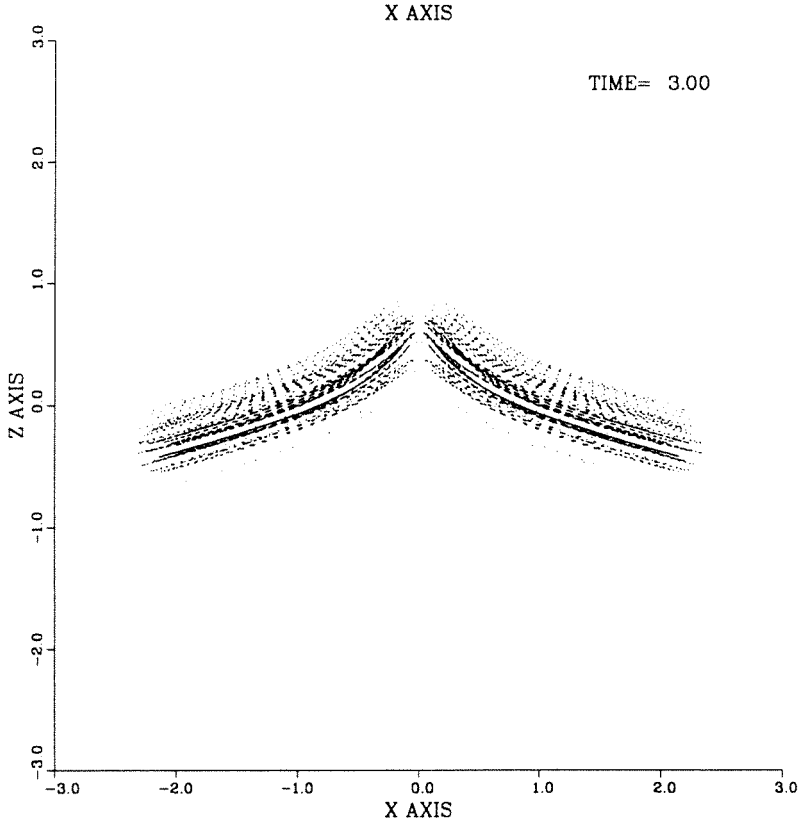
TIME= 3.00
Z AXIS
X AXIS
3.0
2.0
1.0
0.0
-1.0
-2.0
-3.0

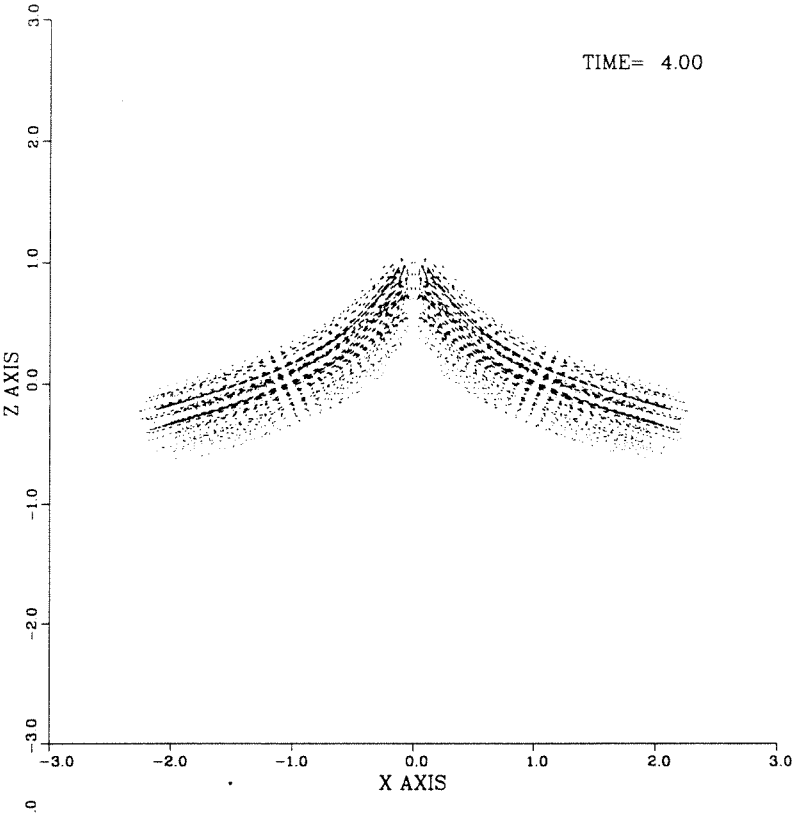
TIME= 4.00
Z AXIS
X AXIS
3.0
2.0
1.0
0.0
-1.0
-2.0
-3.0

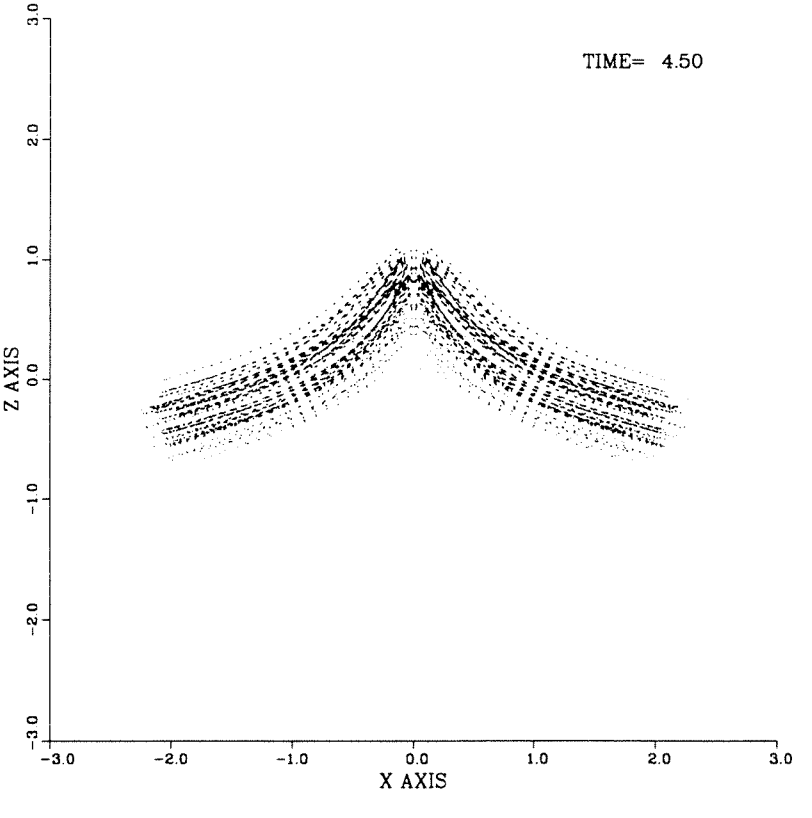
TIME= 4.50
Z AXIS
X AXIS
3.0
2.0
1.0
0.0
-1.0
-2.0
-3.0

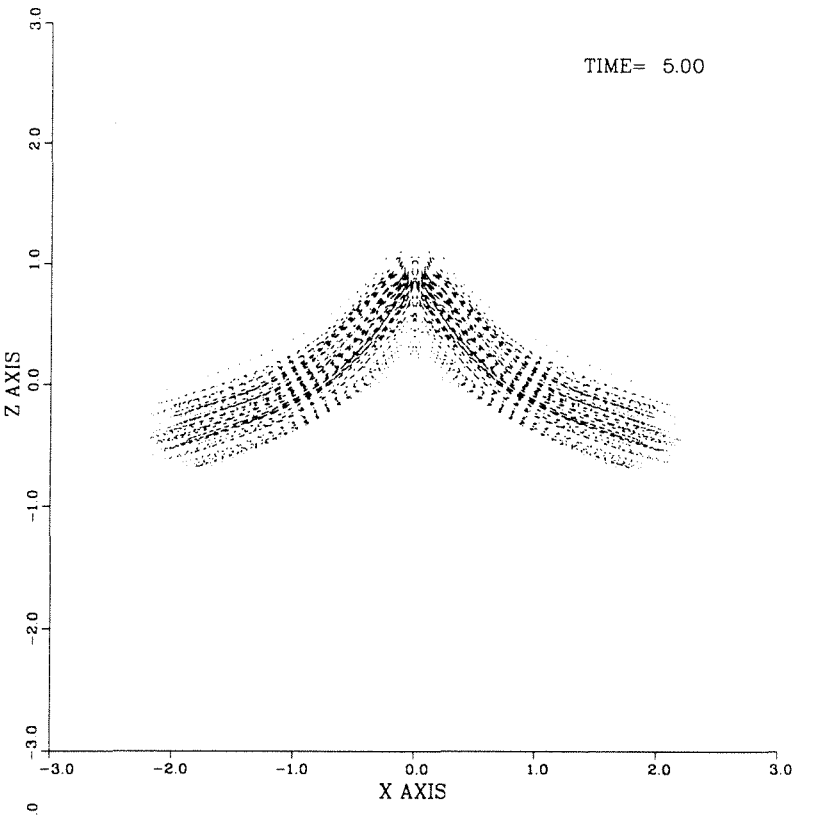
TIME= 5.00
Z AXIS
X AXIS
3.0
2.0
1.0
0.0
-1.0
-2.0
-3.0

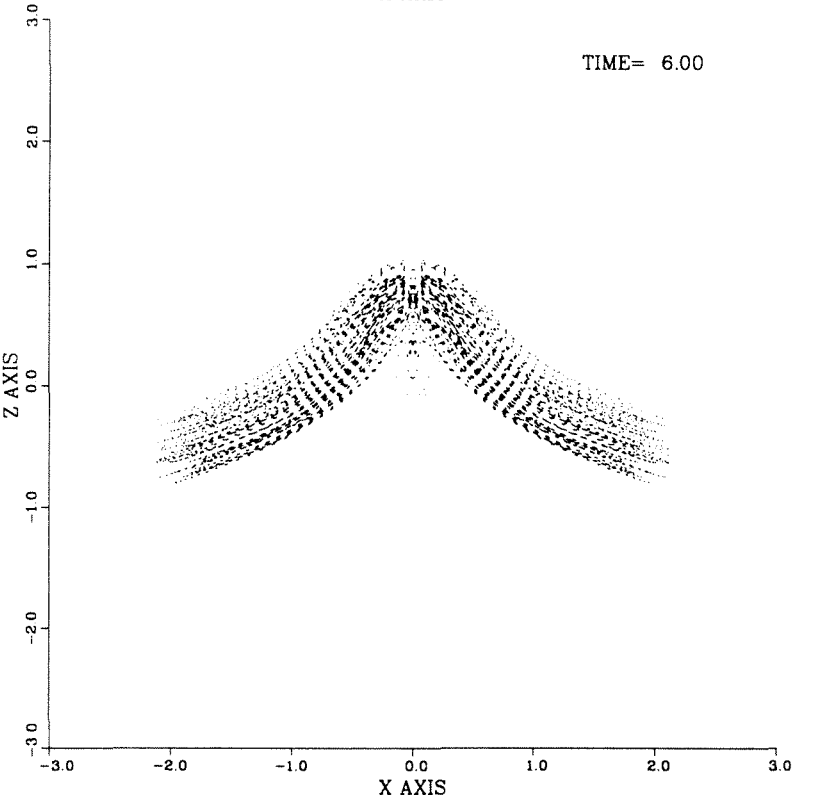
TIME= 6.00
Z AXIS
X AXIS
3.0
2.0
1.0
0.0
-1.0
-2.0
-3.0

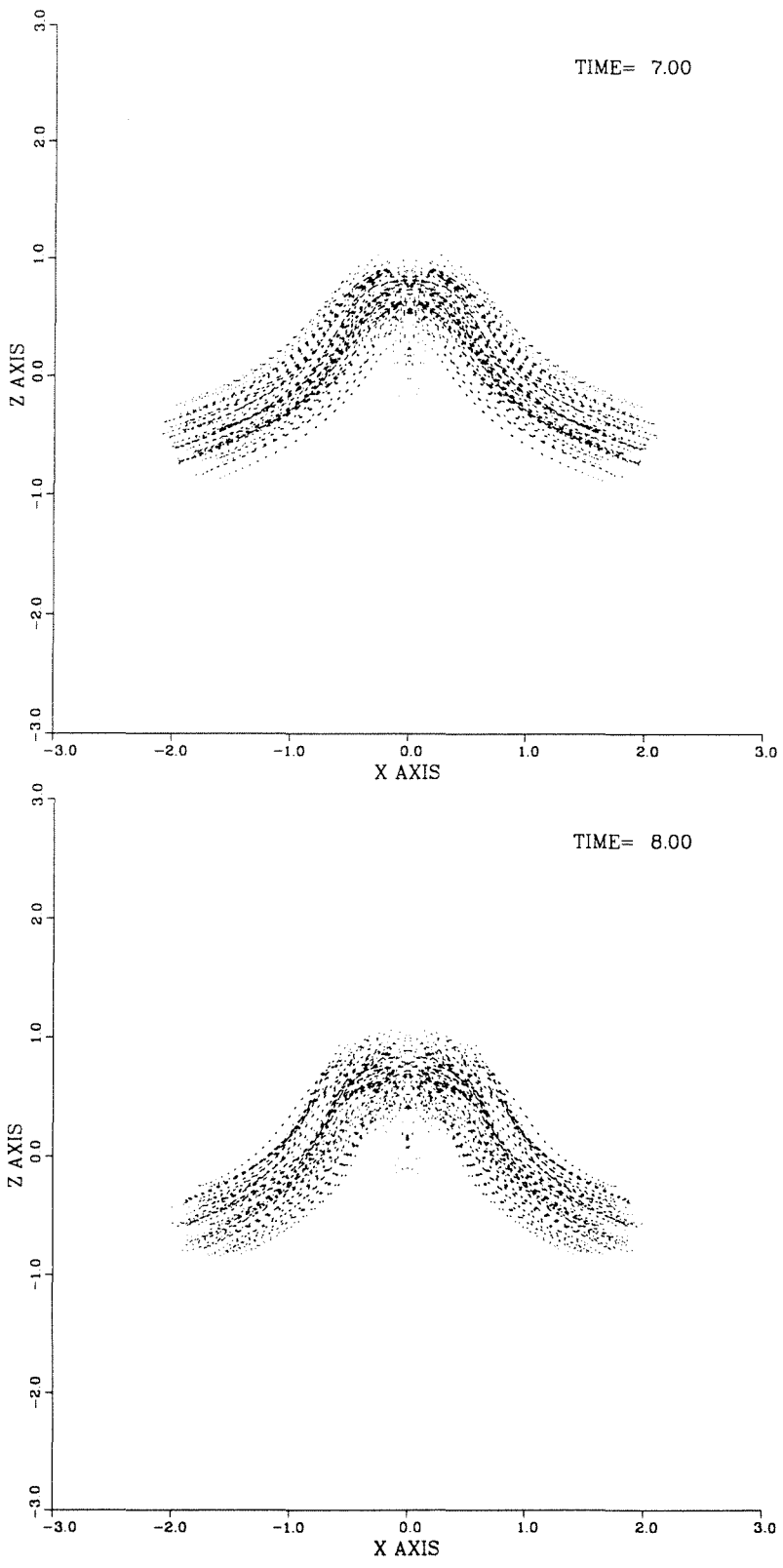

Figure J.39: The fusion of two vortex rings computed with the viscous method of regularized vortex particles. $Re = 400$. $x - z$ projection of the particle strength vectors α^p.

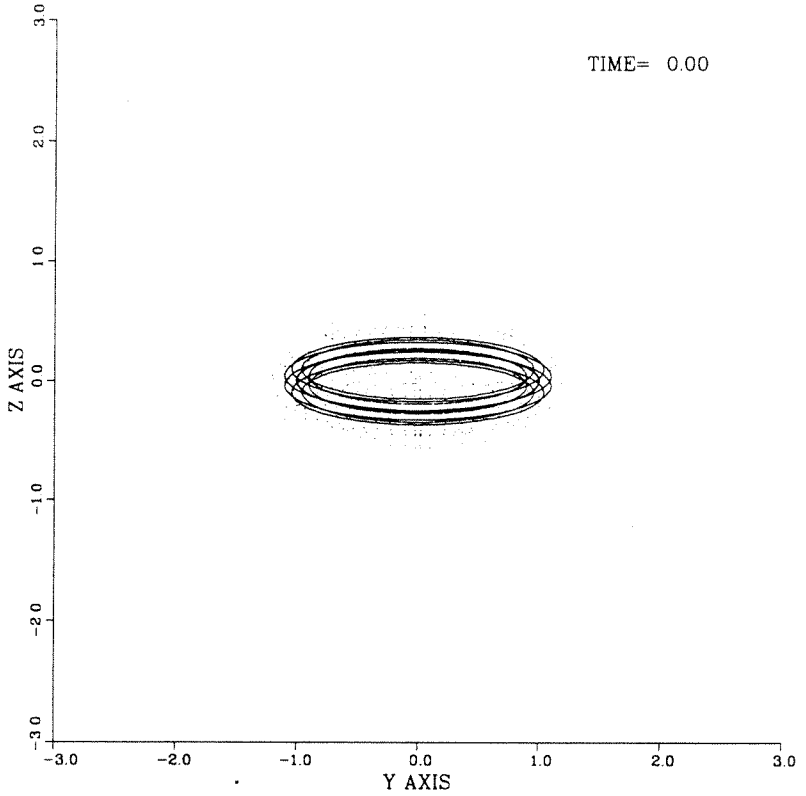
TIME= 0.00
Z AXIS
Y AXIS
3.0
2.0
1.0
0.0
-1.0
-2.0
-3.0

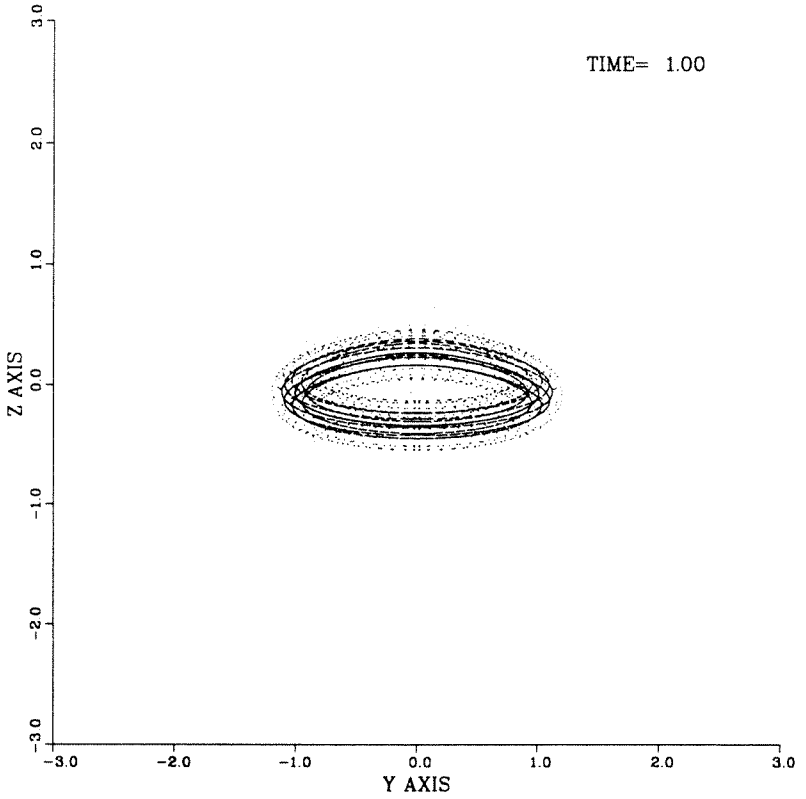
TIME= 1.00
Z AXIS
Y AXIS
3.0
2.0
1.0
0.0
-1.0
-2.0
-3.0

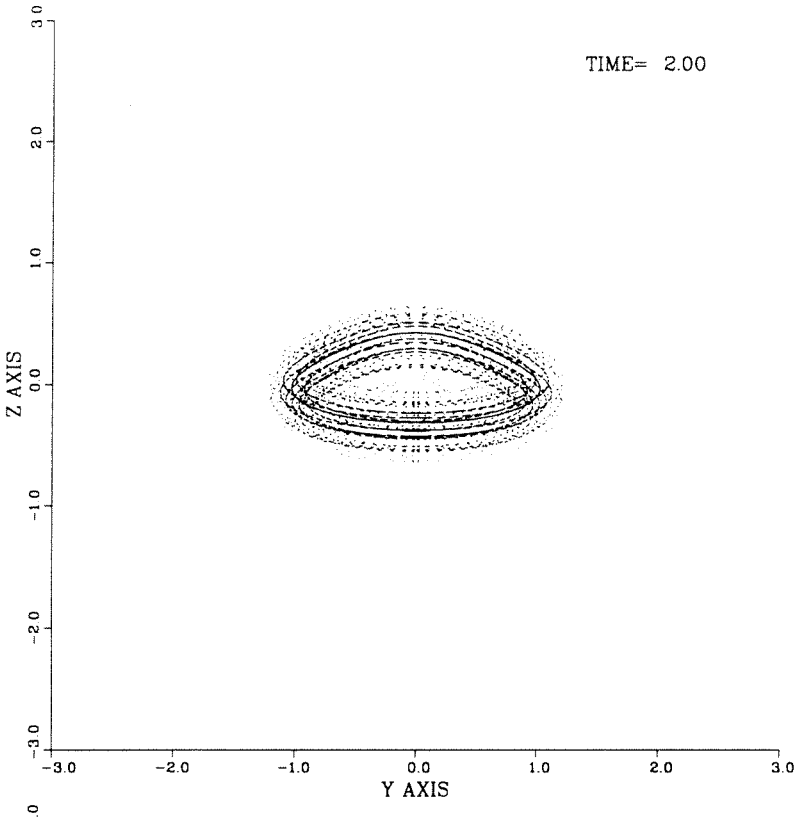
TIME= 2.00
Z AXIS
Y AXIS
3.0
2.0
1.0
0.0
-1.0
-2.0
-3.0

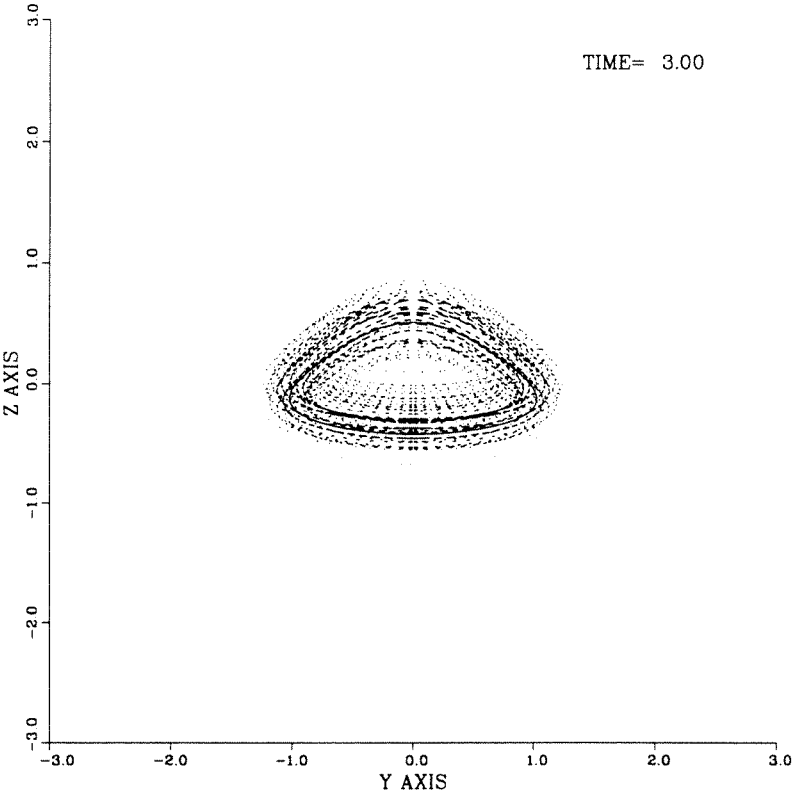
TIME= 3.00
Z AXIS
Y AXIS
3.0
2.0
1.0
0.0
-1.0
-2.0
-3.0

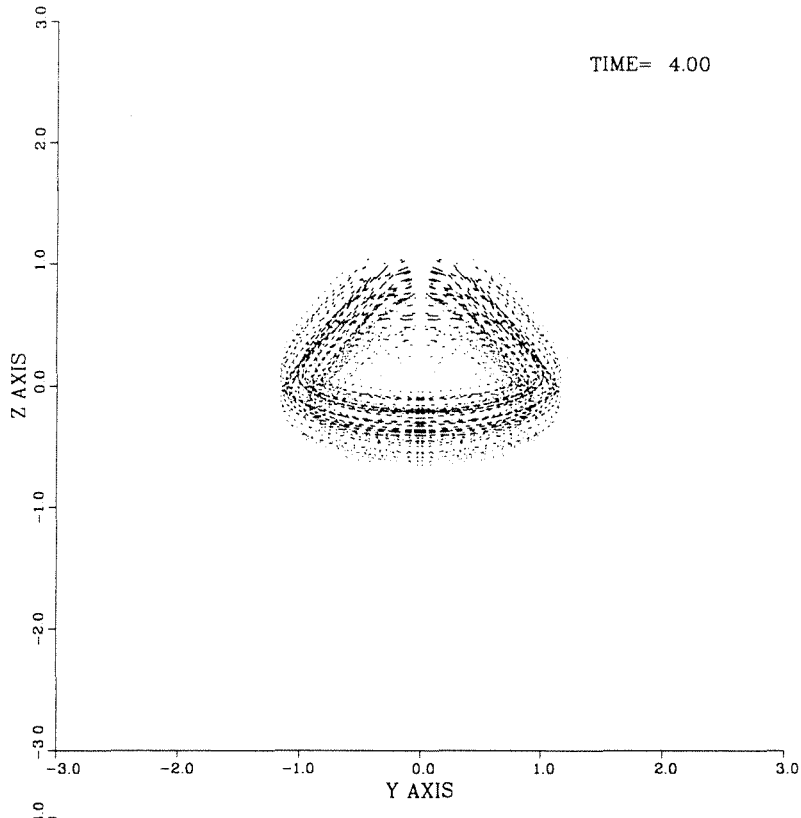
TIME= 4.00
Z AXIS
Y AXIS
3.0
2.0
1.0
0.0
-1.0
-2.0
-3.0

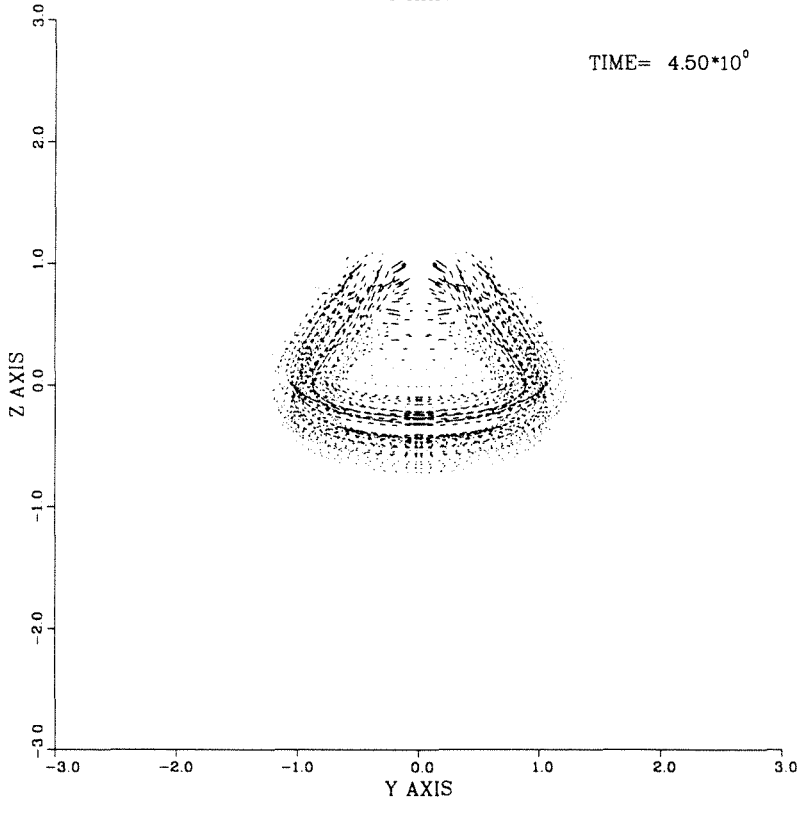
TIME= 4.50*10^0
Z AXIS
Y AXIS
3.0
2.0
1.0
0.0
-1.0
-2.0
-3.0

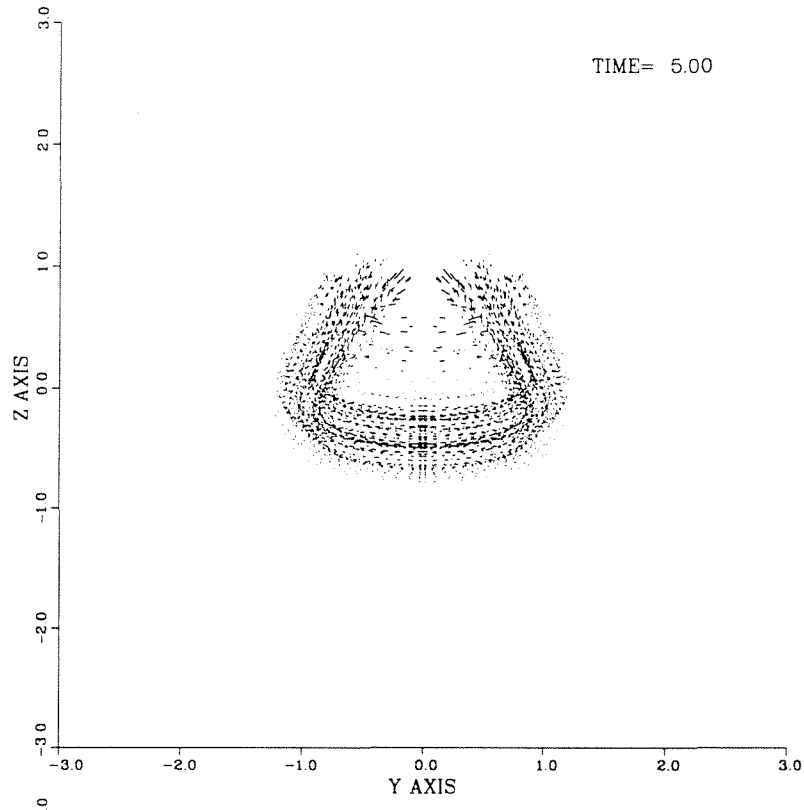
TIME= 5.00
Z AXIS
Y AXIS
3.0
2.0
1.0
0.0
-1.0
-2.0
-3.0

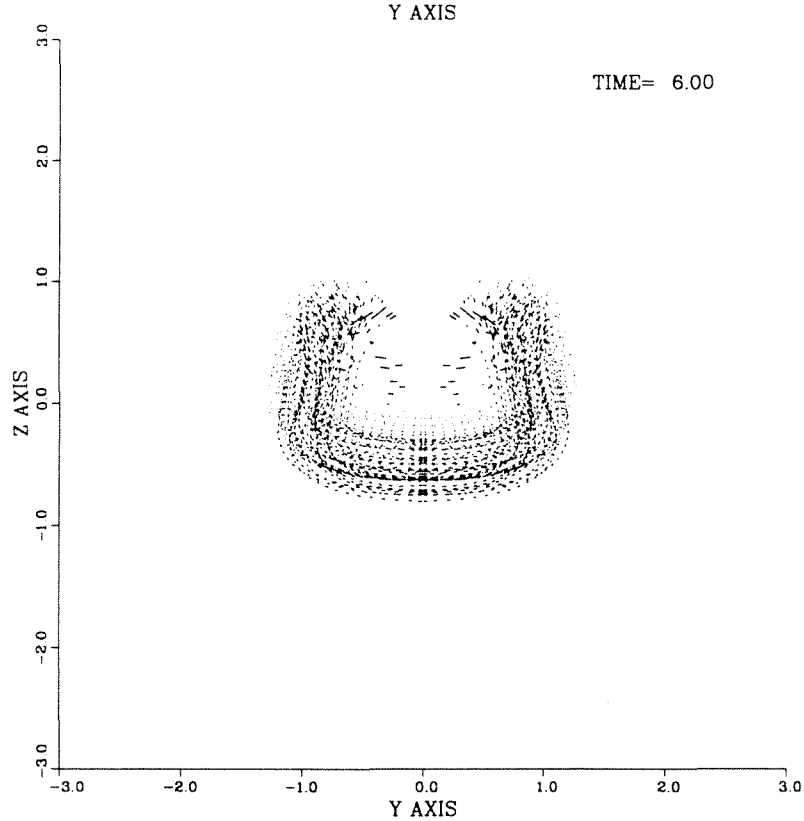
TIME= 6.00
Z AXIS
Y AXIS
3.0
2.0
1.0
0.0
-1.0
-2.0
-3.0

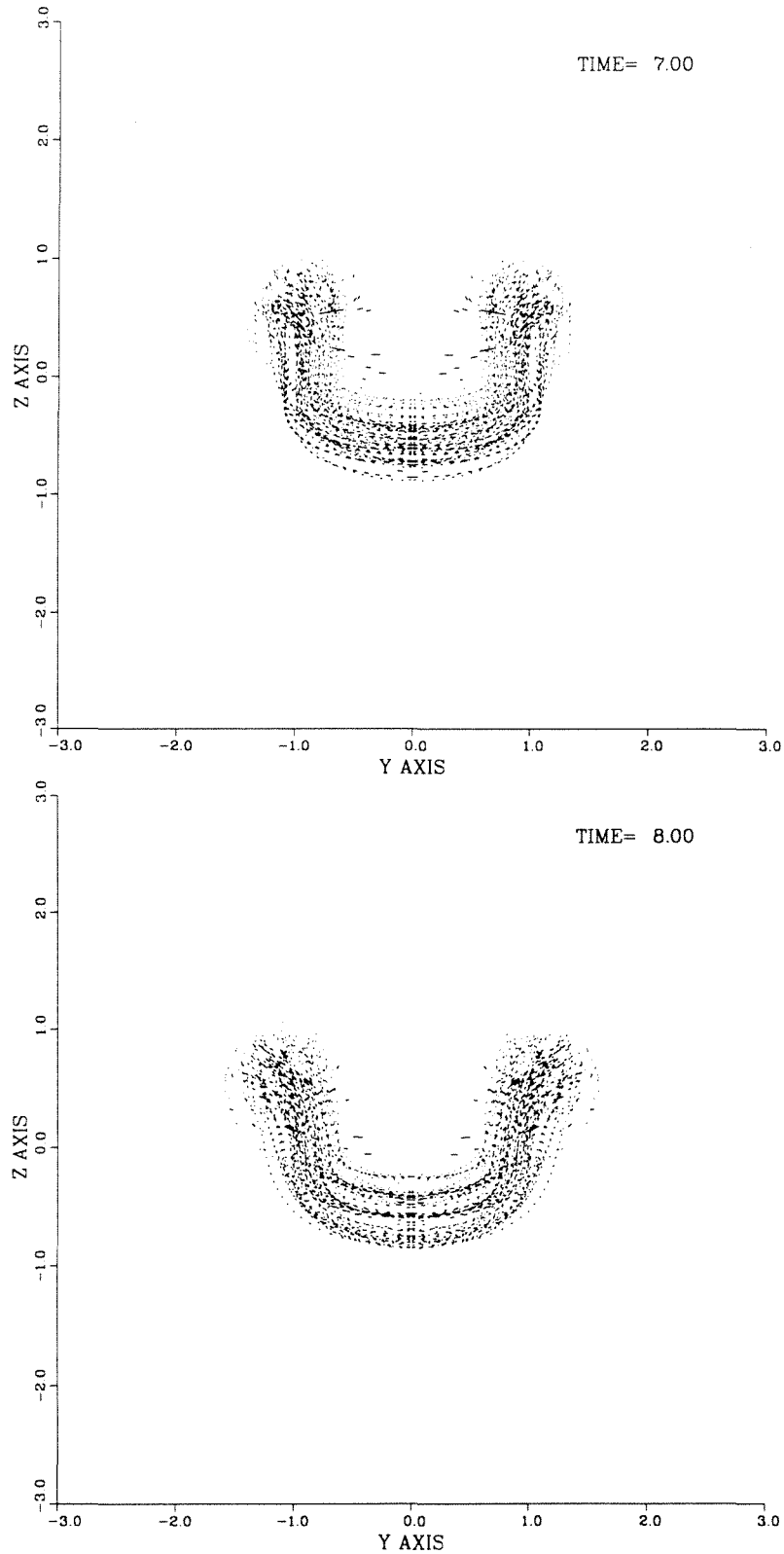

Figure J.40: The fusion of two vortex rings computed with the viscous method of regularized vortex particles. $Re = 400$. $y - z$ projection of the particle strength vectors α^p.

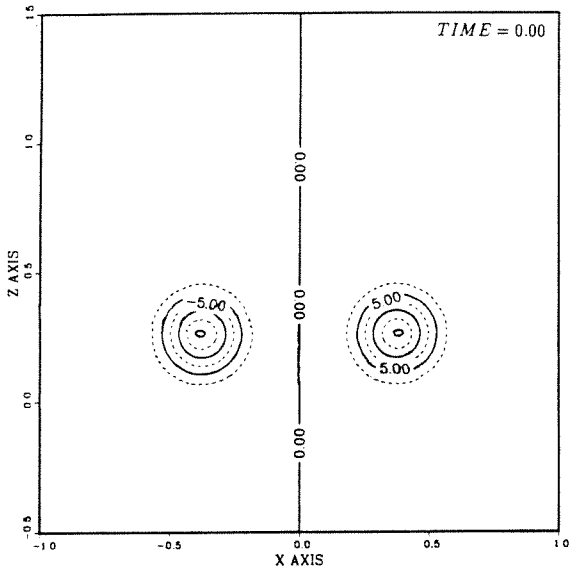
TIME = 0.00
Z AXIS
X AXIS
5.00
5.00
5.00
0.00
0.00
0.00

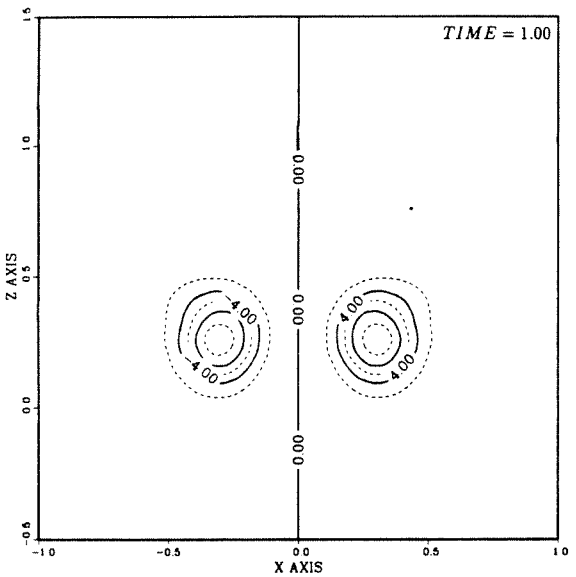
TIME = 1.00
Z AXIS
X AXIS
4.00
4.00
4.00
4.00
0.00
0.00
0.00

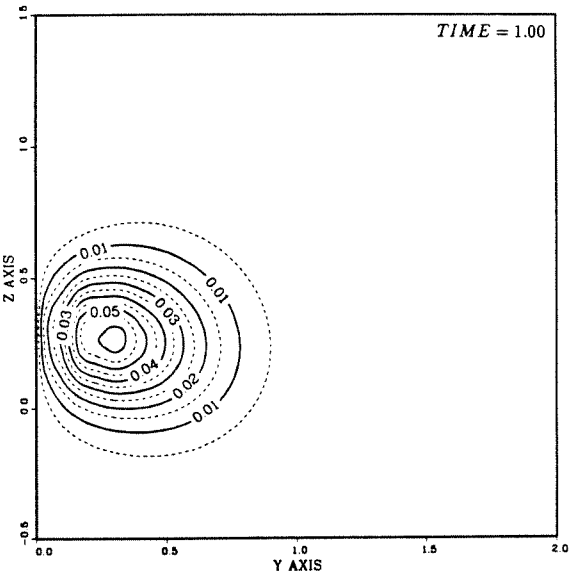
TIME = 1.00
Z AXIS
Y AXIS
0.01
0.01
0.01
0.02
0.02
0.03
0.03
0.03
0.04
0.05

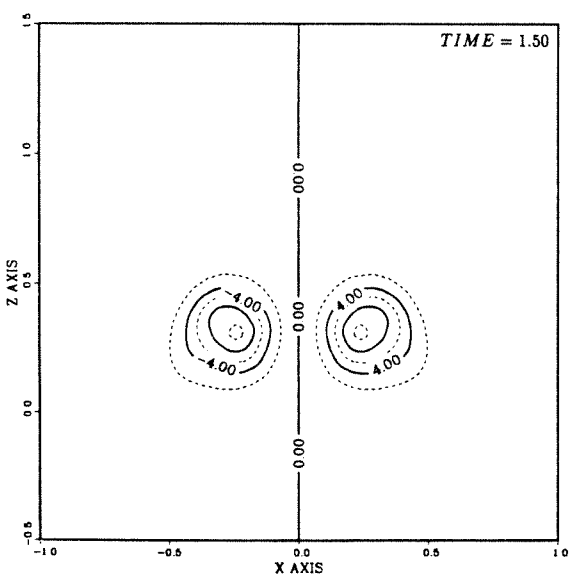
TIME = 1.50
Z AXIS
X AXIS
4.00
4.00
4.00
4.00
0.00
0.00
0.00

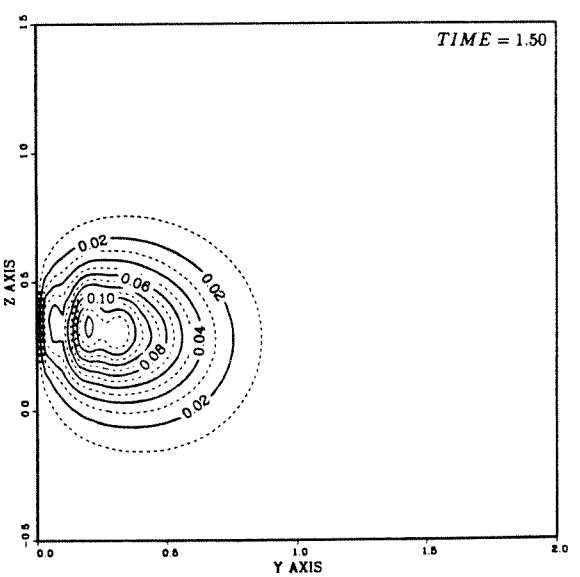
TIME = 1.50
Z AXIS
Y AXIS
0.02
0.02
0.02
0.04
0.04
0.06
0.08
0.10

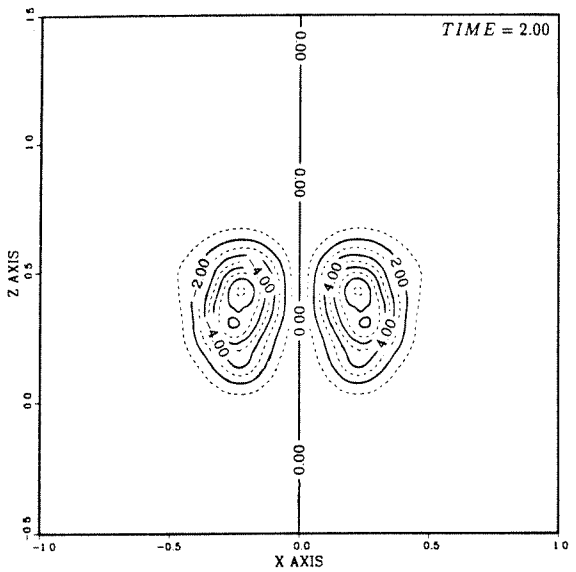
TIME = 2.00
Z AXIS
X AXIS
0.00
-2.00
-4.00
2.00
4.00

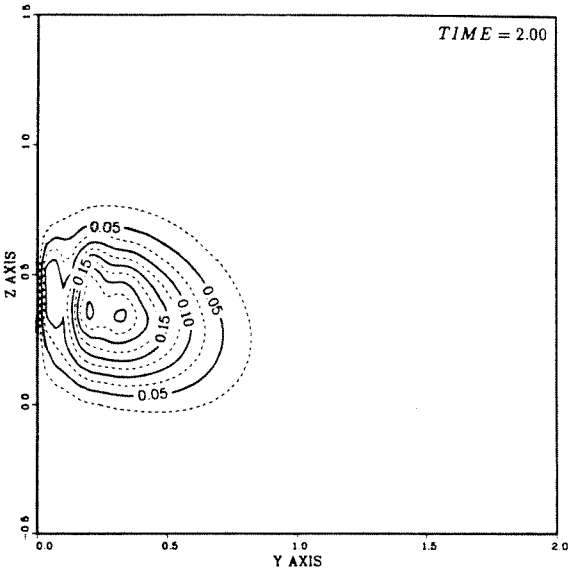
TIME = 2.00
Z AXIS
Y AXIS
0.05
0.10
0.15

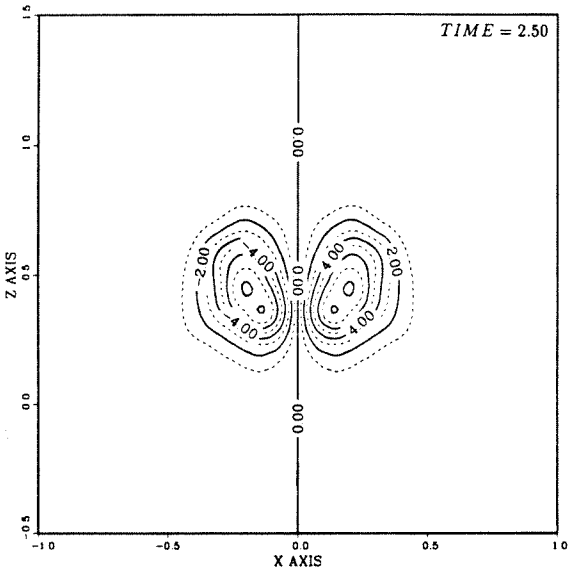
TIME = 2.50
Z AXIS
X AXIS
0.00
-2.00
-4.00
2.00
4.00

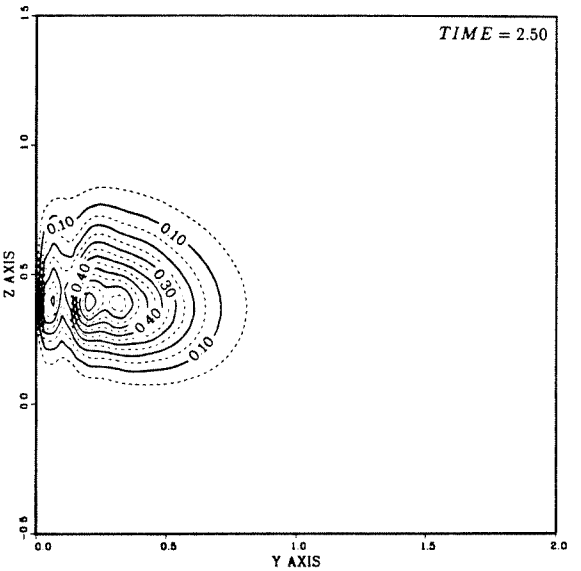
TIME = 2.50
Z AXIS
Y AXIS
0.10
0.30
0.40

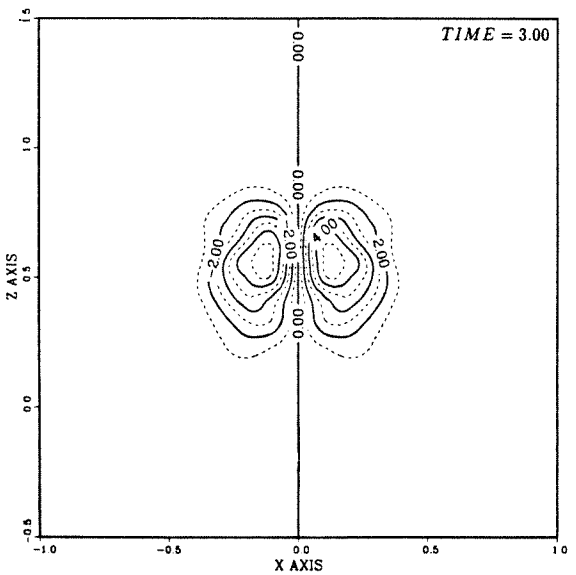
TIME = 3.00
Z AXIS
X AXIS
0.00
-2.00
-4.00
2.00
4.00

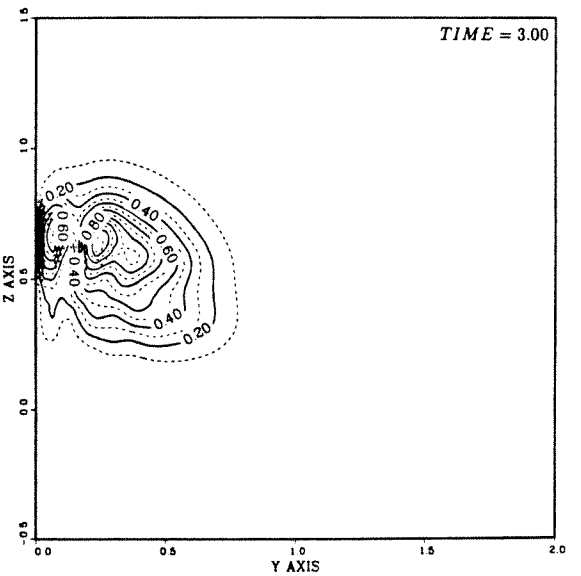
TIME = 3.00
Z AXIS
Y AXIS
0.20
0.40
0.60
0.80

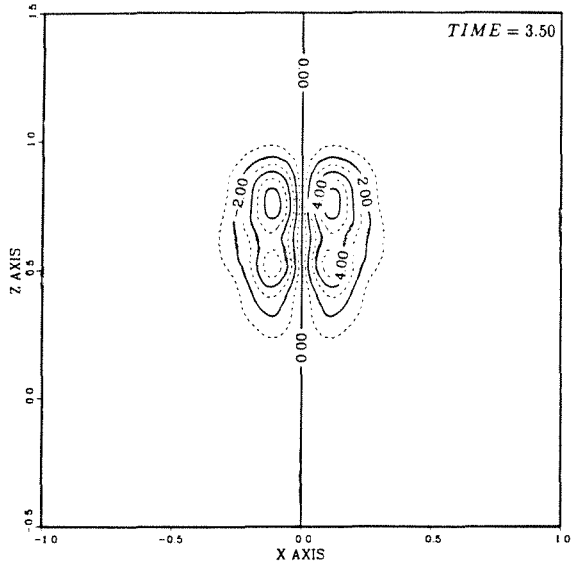
TIME = 3.50
Z AXIS
X AXIS

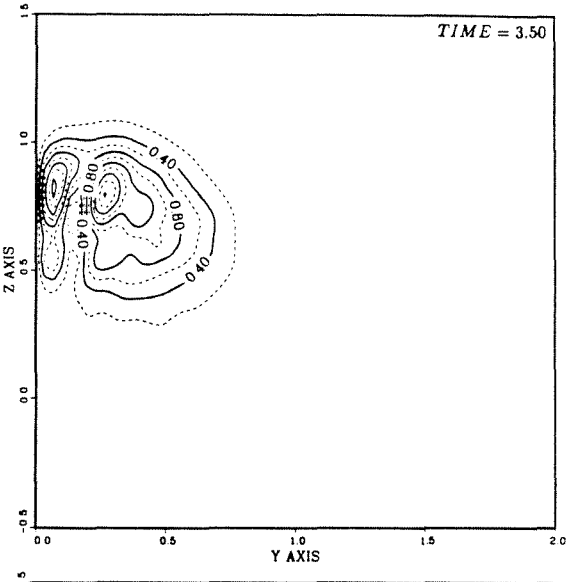
TIME = 3.50
Z AXIS
Y AXIS

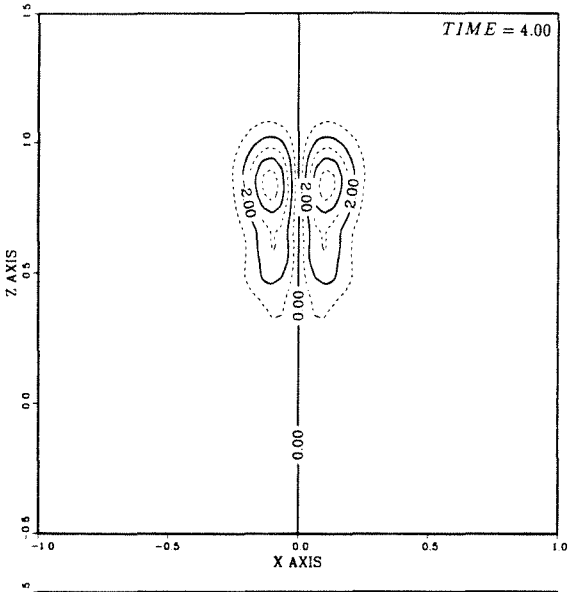
TIME = 4.00
Z AXIS
X AXIS

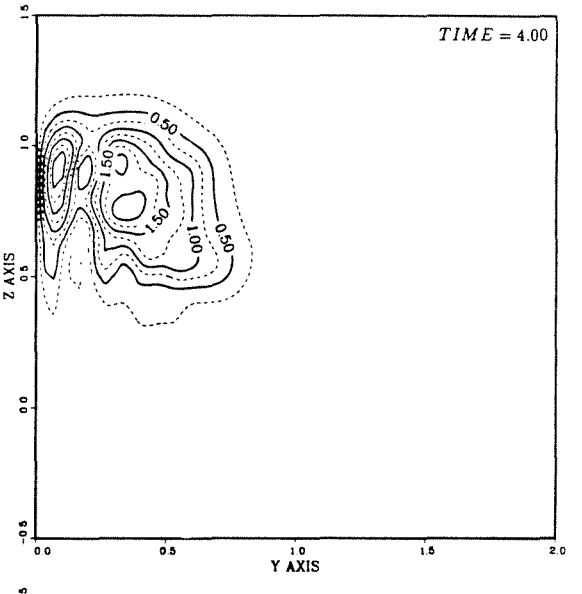
TIME = 4.00
Z AXIS
Y AXIS

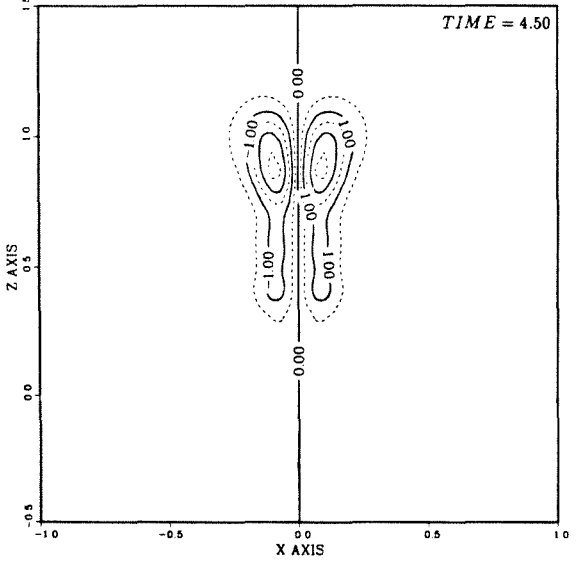
TIME = 4.50
Z AXIS
X AXIS

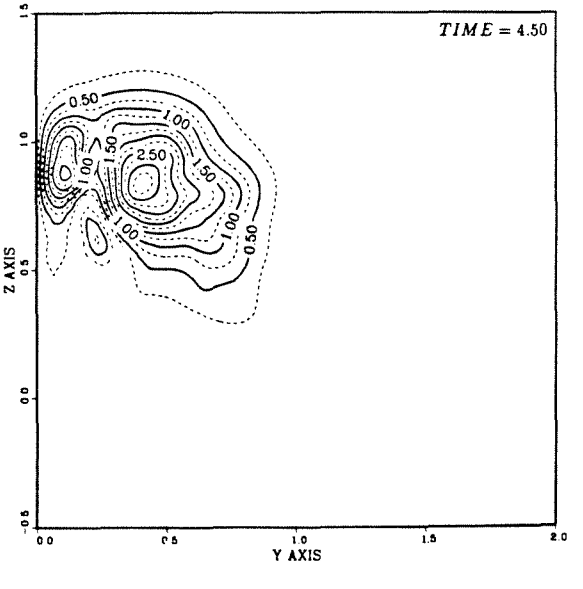
TIME = 4.50
Z AXIS
Y AXIS

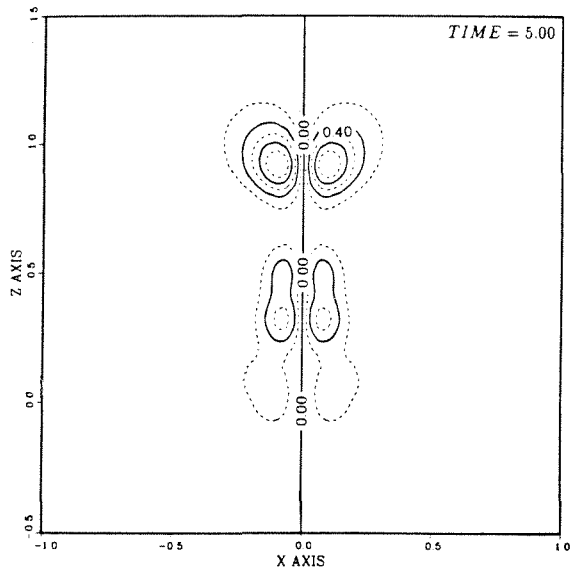
TIME = 5.00
Z AXIS
X AXIS
0.00
0.40

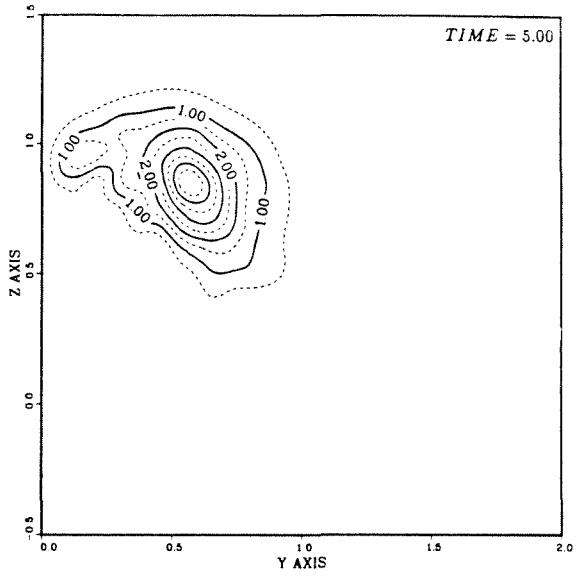
TIME = 5.00
Z AXIS
Y AXIS
1.00
2.00

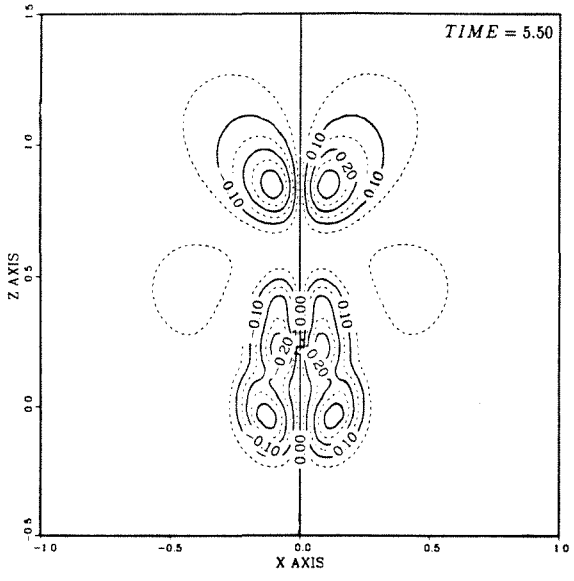
TIME = 5.50
Z AXIS
X AXIS
0.10
0.20
0.00

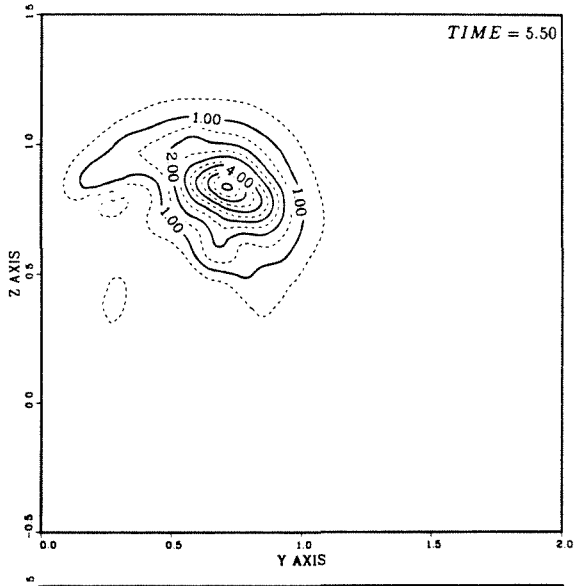
TIME = 5.50
Z AXIS
Y AXIS
1.00
2.00
4.00

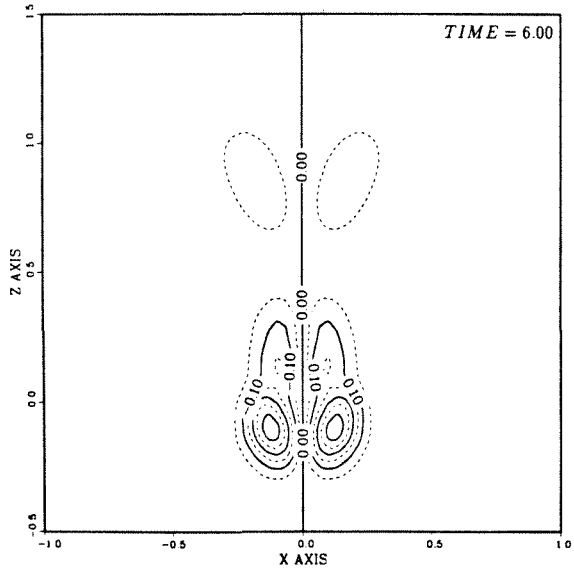
TIME = 6.00
Z AXIS
X AXIS
0.00
0.10

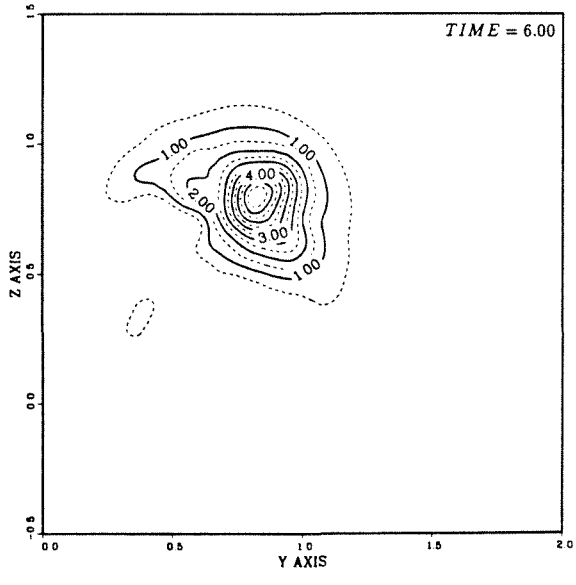
TIME = 6.00
Z AXIS
Y AXIS
1.00
2.00
4.00
3.00

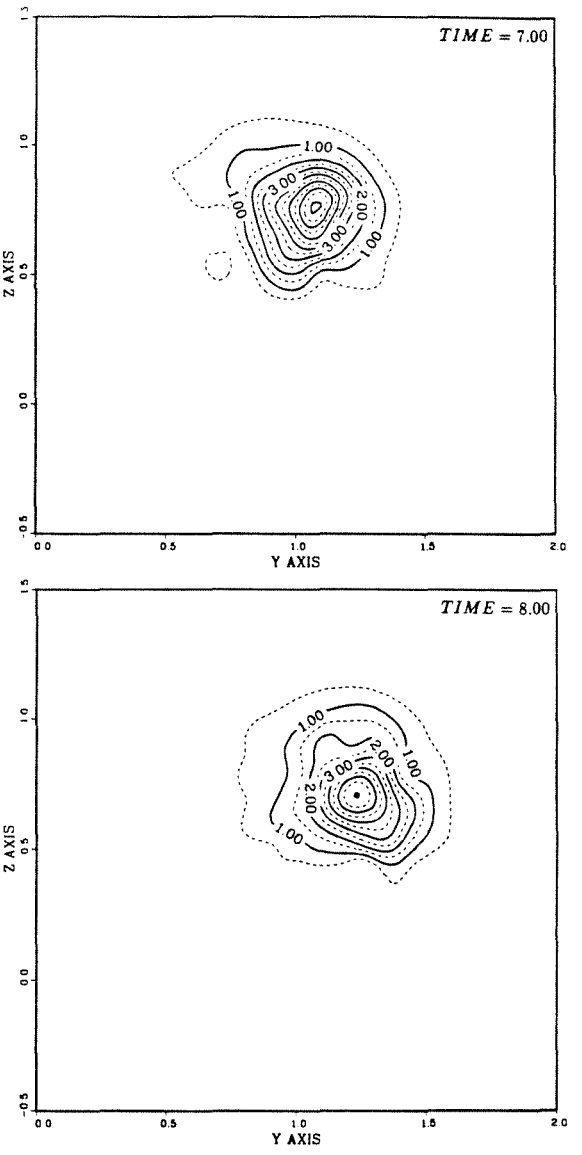

Figure J.41: The fusion of two vortex rings computed with the viscous method of regularized vortex particles. $Re = 400$. Contours of out of plane vorticity: ω_y in $x - z$ plane (left), ω_x in $y - z$ plane (right).

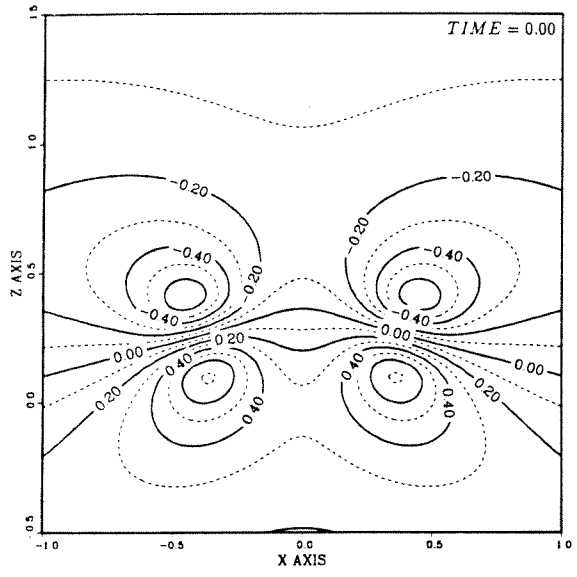
TIME = 0.00
Z AXIS
X AXIS

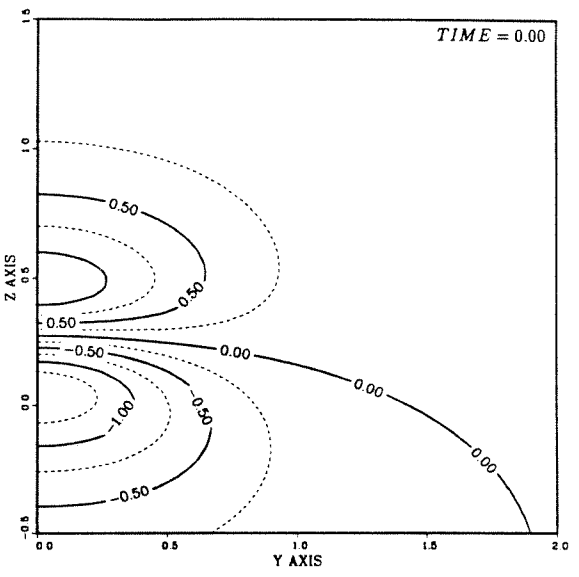
TIME = 0.00
Z AXIS
Y AXIS

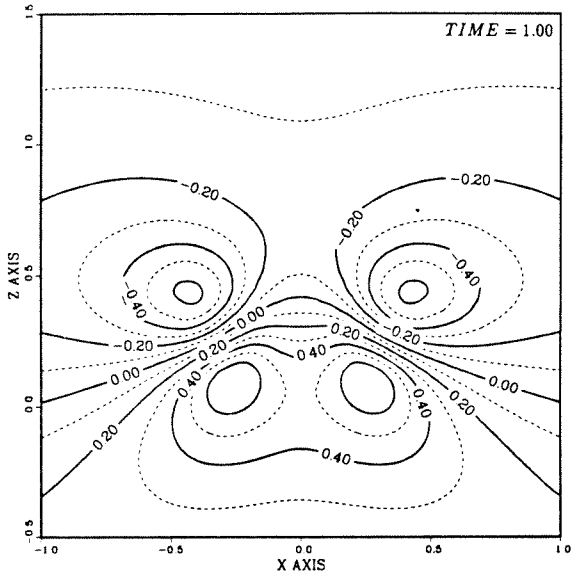
TIME = 1.00
Z AXIS
X AXIS

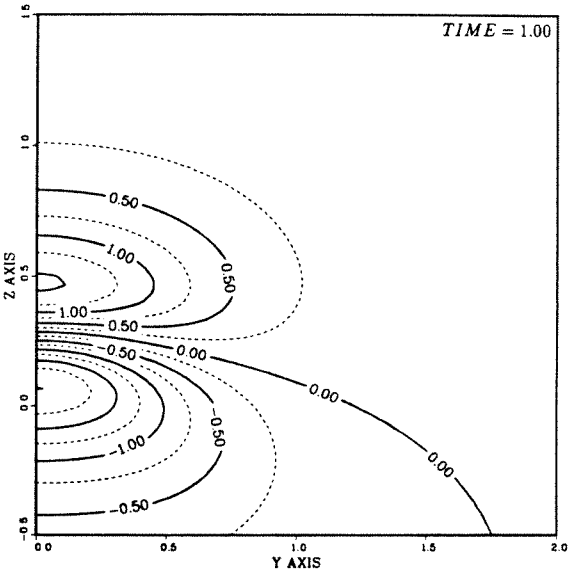
TIME = 1.00
Z AXIS
Y AXIS

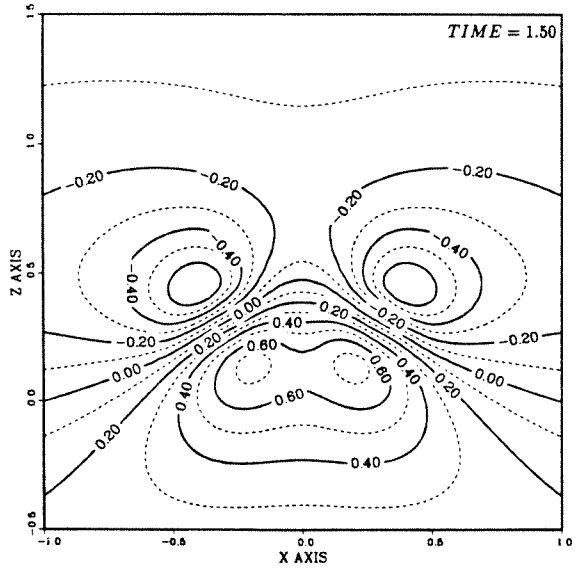
TIME = 1.50
Z AXIS
X AXIS

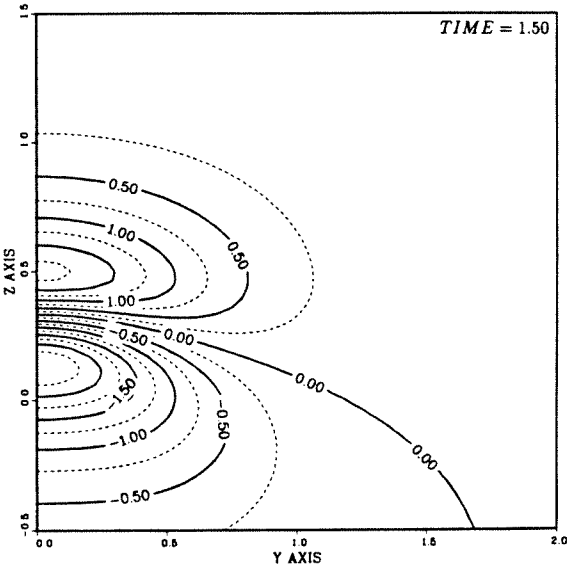
TIME = 1.50
Z AXIS
Y AXIS

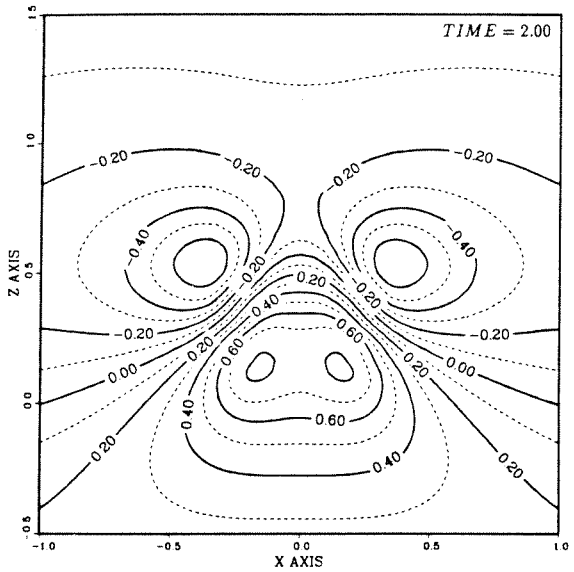
TIME = 2.00
Z AXIS
X AXIS

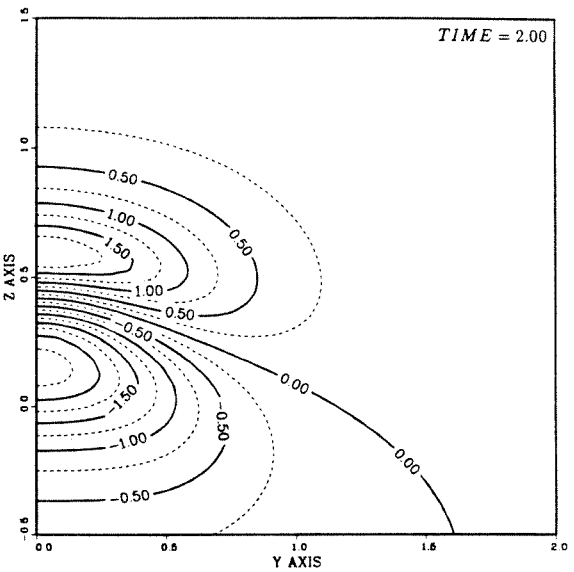
TIME = 2.00
Z AXIS
Y AXIS

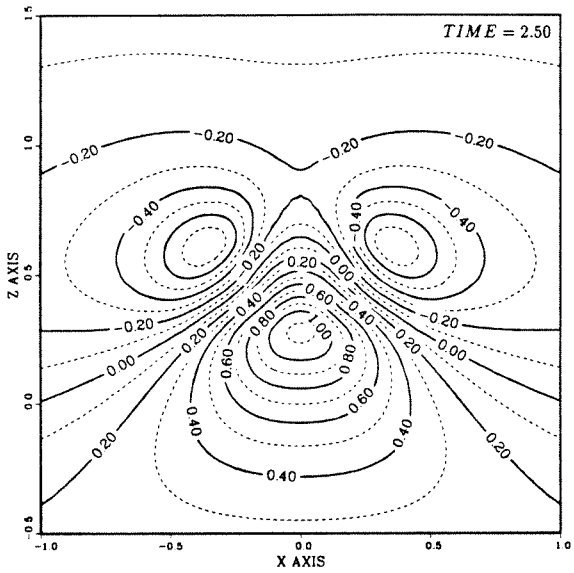
TIME = 2.50
Z AXIS
X AXIS

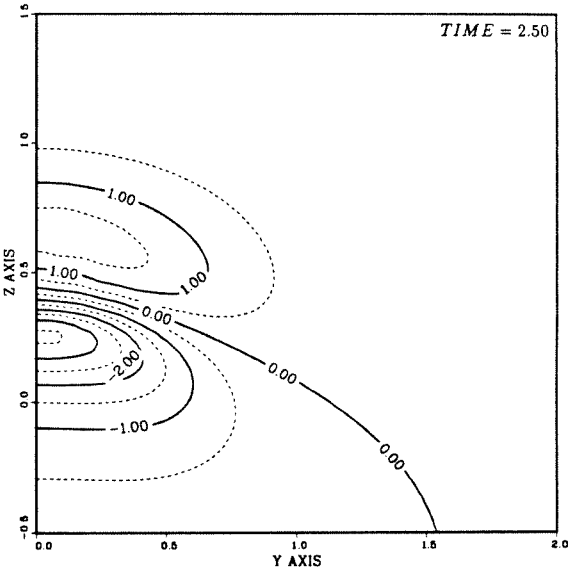
TIME = 2.50
Z AXIS
Y AXIS

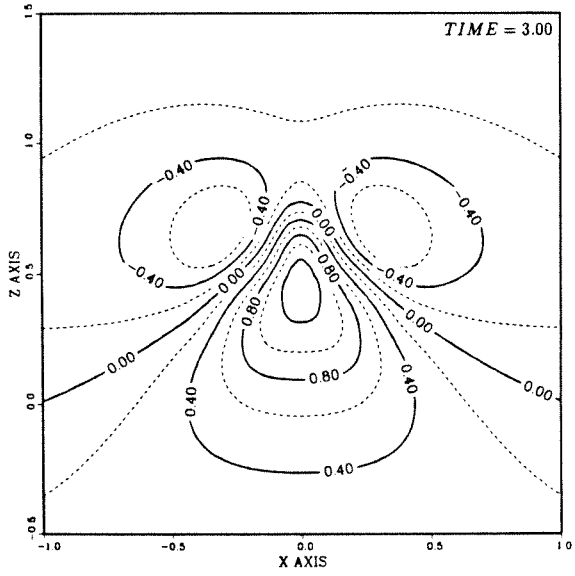
TIME = 3.00
Z AXIS
X AXIS

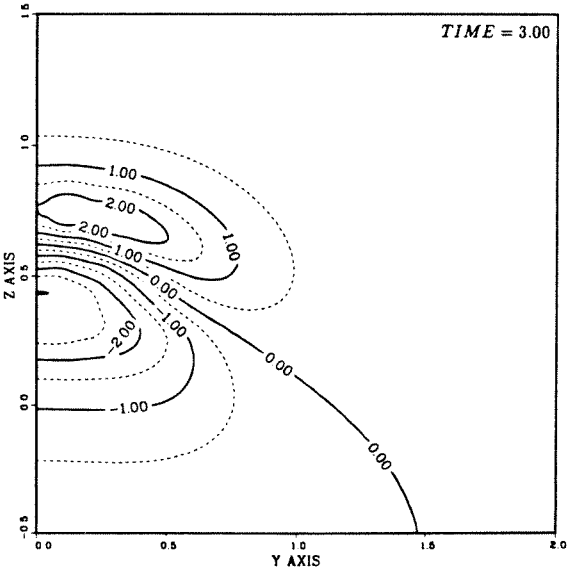
TIME = 3.00
Z AXIS
Y AXIS

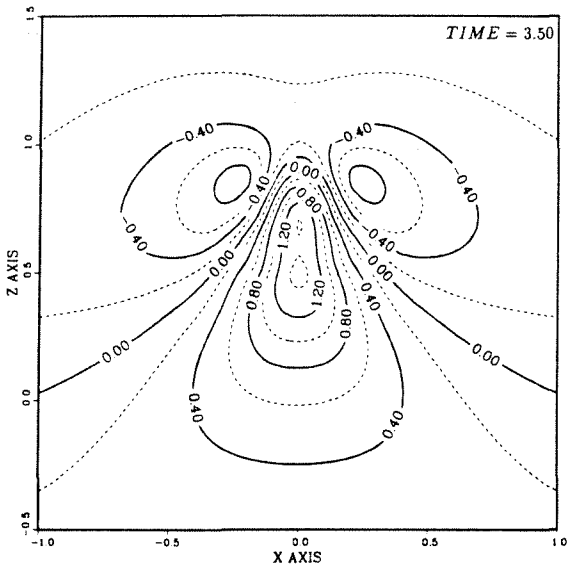
TIME = 3.50
Z AXIS
X AXIS

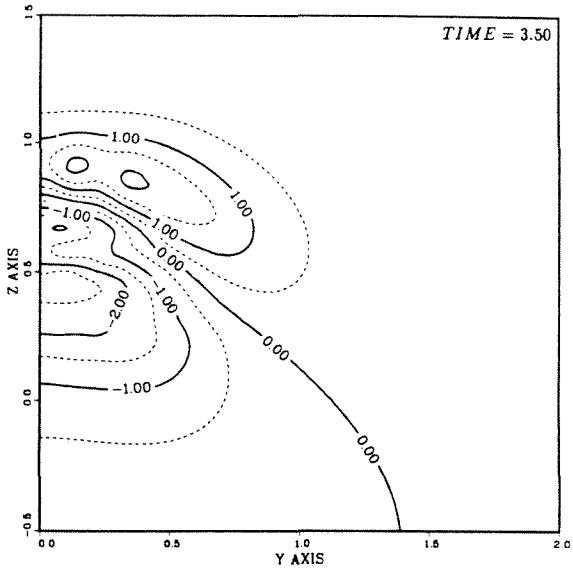
TIME = 3.50
Z AXIS
Y AXIS

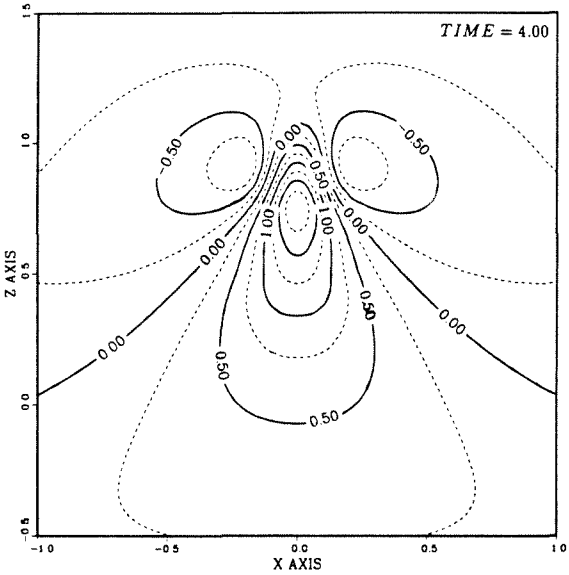
TIME = 4.00
Z AXIS
X AXIS

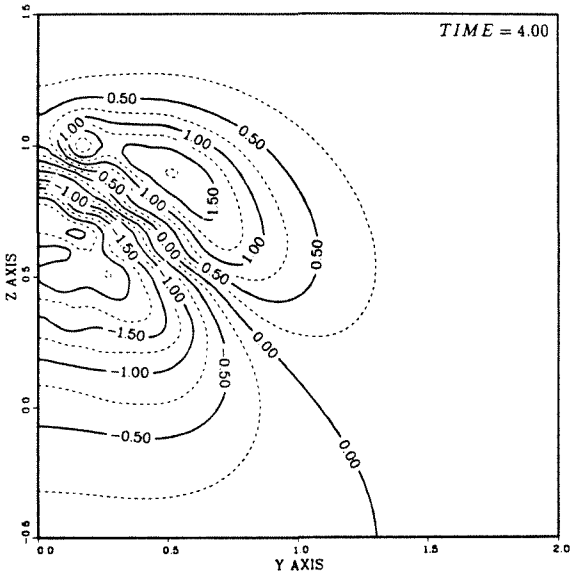
TIME = 4.00
Z AXIS
Y AXIS

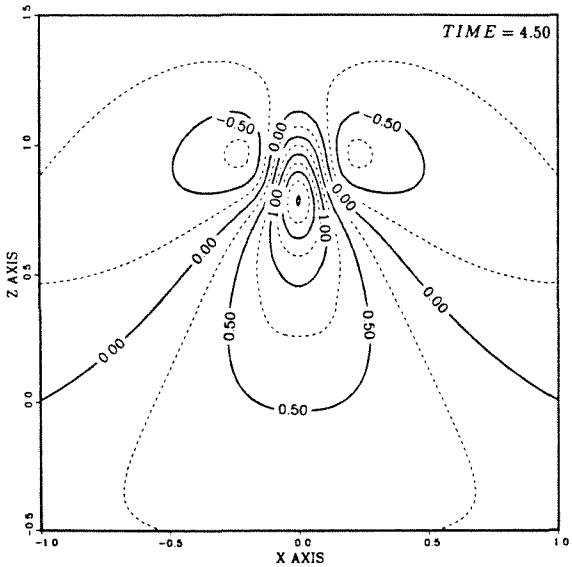
TIME = 4.50
Z AXIS
X AXIS

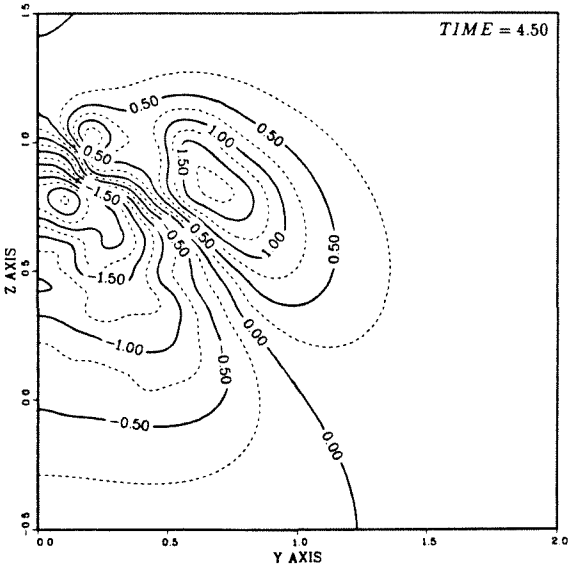
TIME = 4.50
Z AXIS
Y AXIS

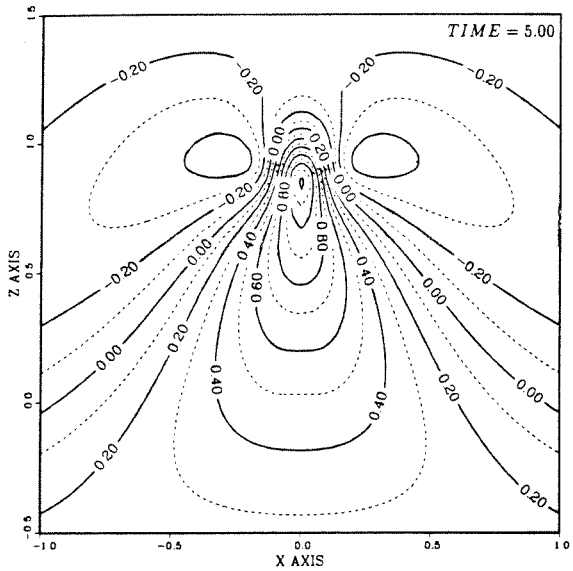
TIME = 5.00
Z AXIS
X AXIS

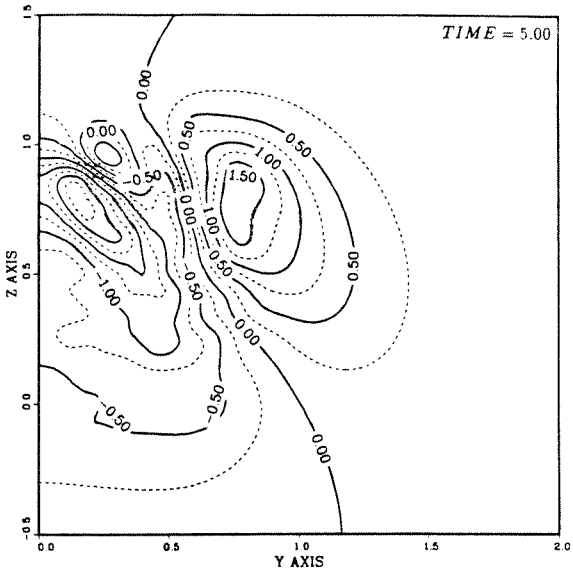
TIME = 5.00
Z AXIS
Y AXIS

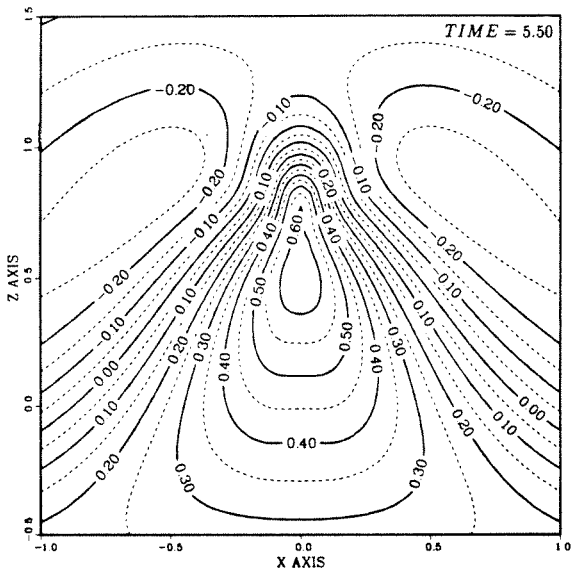
TIME = 5.50
Z AXIS
X AXIS

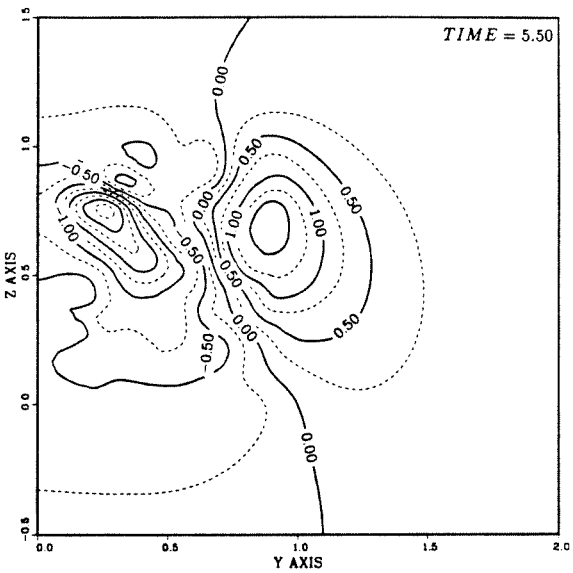
TIME = 5.50
Z AXIS
Y AXIS

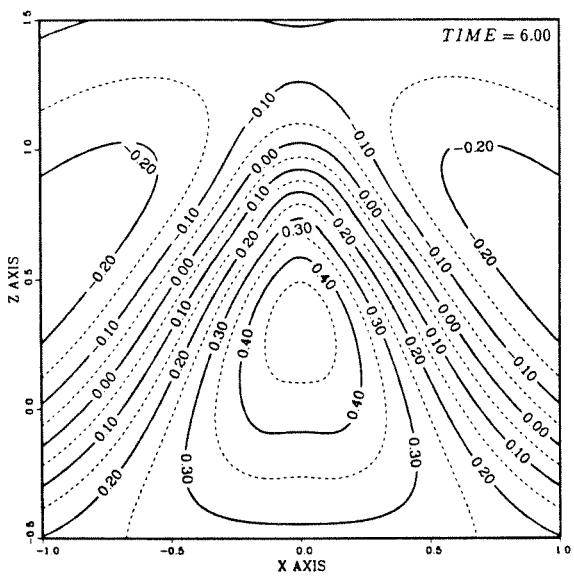
TIME = 6.00
Z AXIS
X AXIS

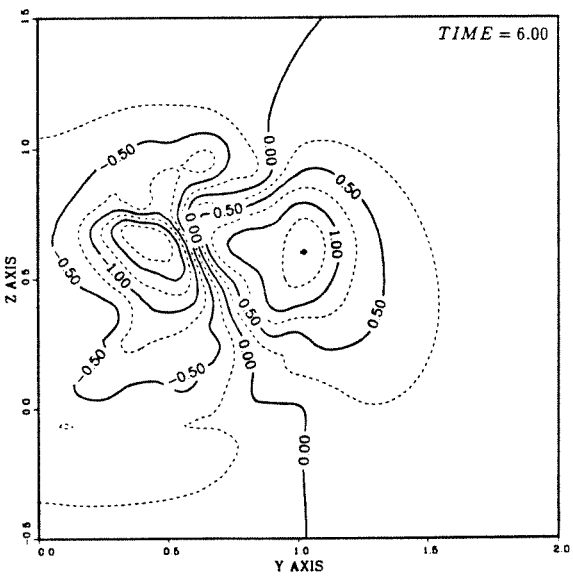
TIME = 6.00
Z AXIS
Y AXIS

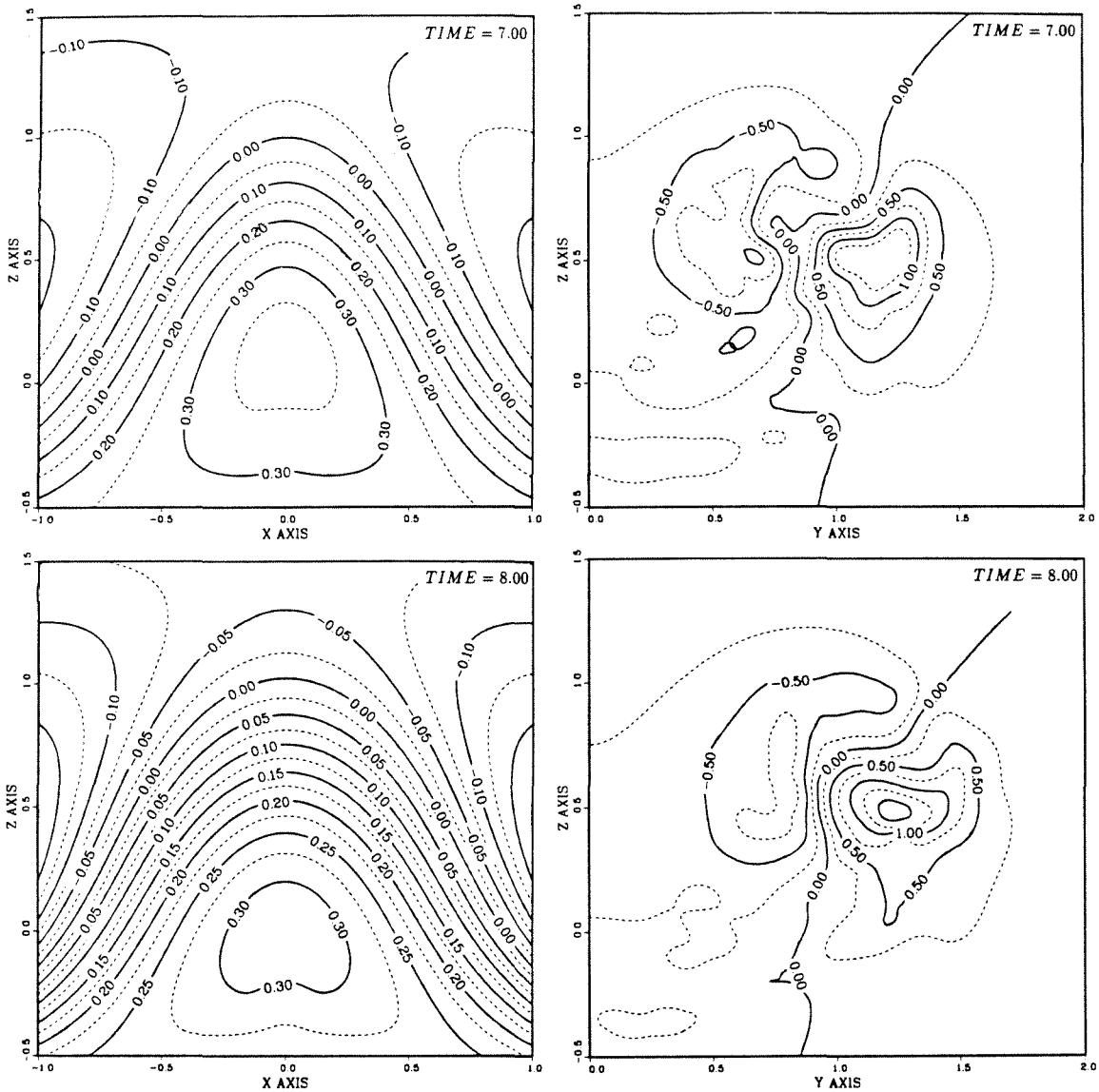

Figure J.42: The fusion of two vortex rings computed with the viscous method of regularized vortex particles. $Re = 400$. Contours of out of plane strain-rate: $\partial v/\partial y$ in $x - z$ plane (left), $\partial u/\partial x$ in $y - z$ plane (right).

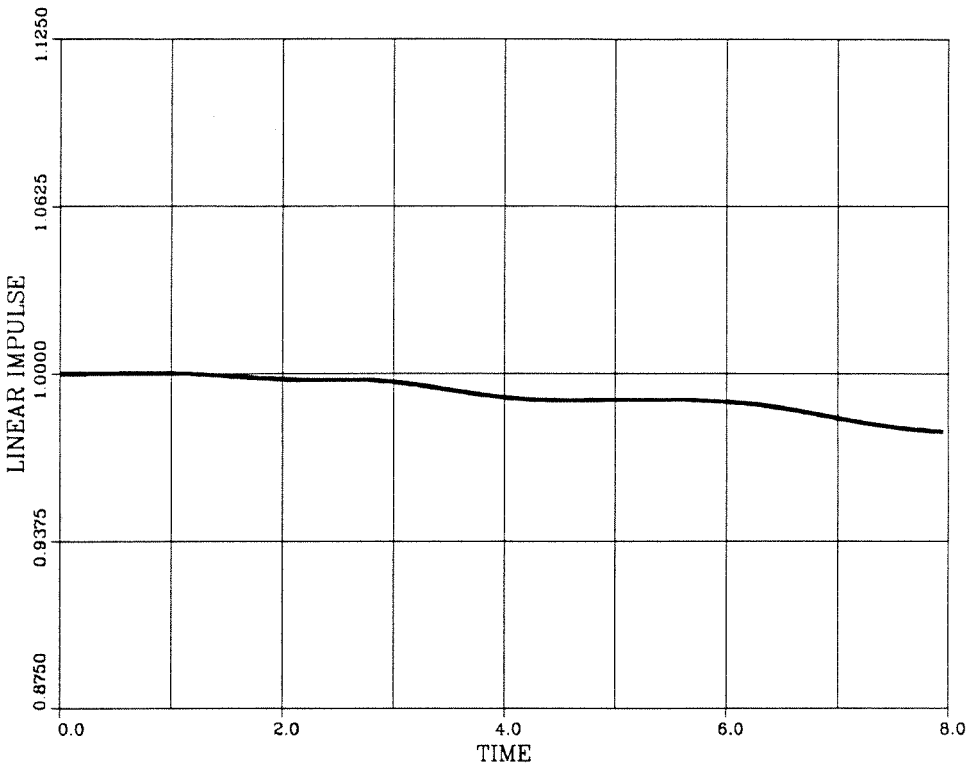
LINEAR IMPULSE
1.1250
1.0625
1.0000
0.9375
0.8750
0.0
2.0
4.0
6.0
8.0
TIME

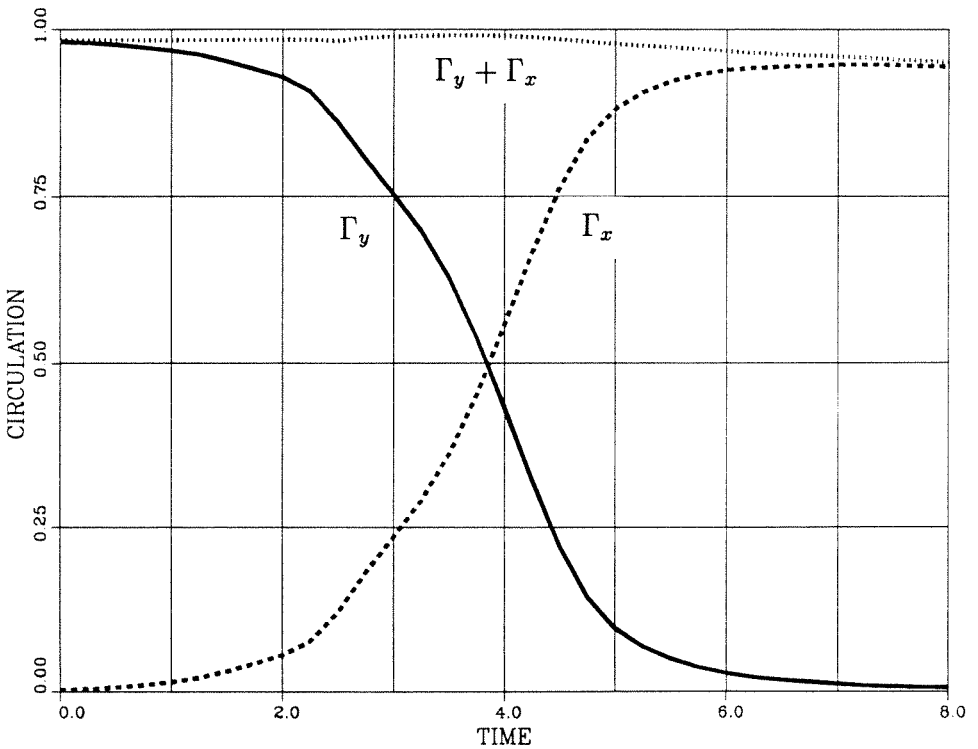
CIRCULATION
1.00
0.75
0.50
0.25
0.00
$\Gamma_y + \Gamma_x$
Γ_y
Γ_x
0.0
2.0
4.0
6.0
8.0
TIME

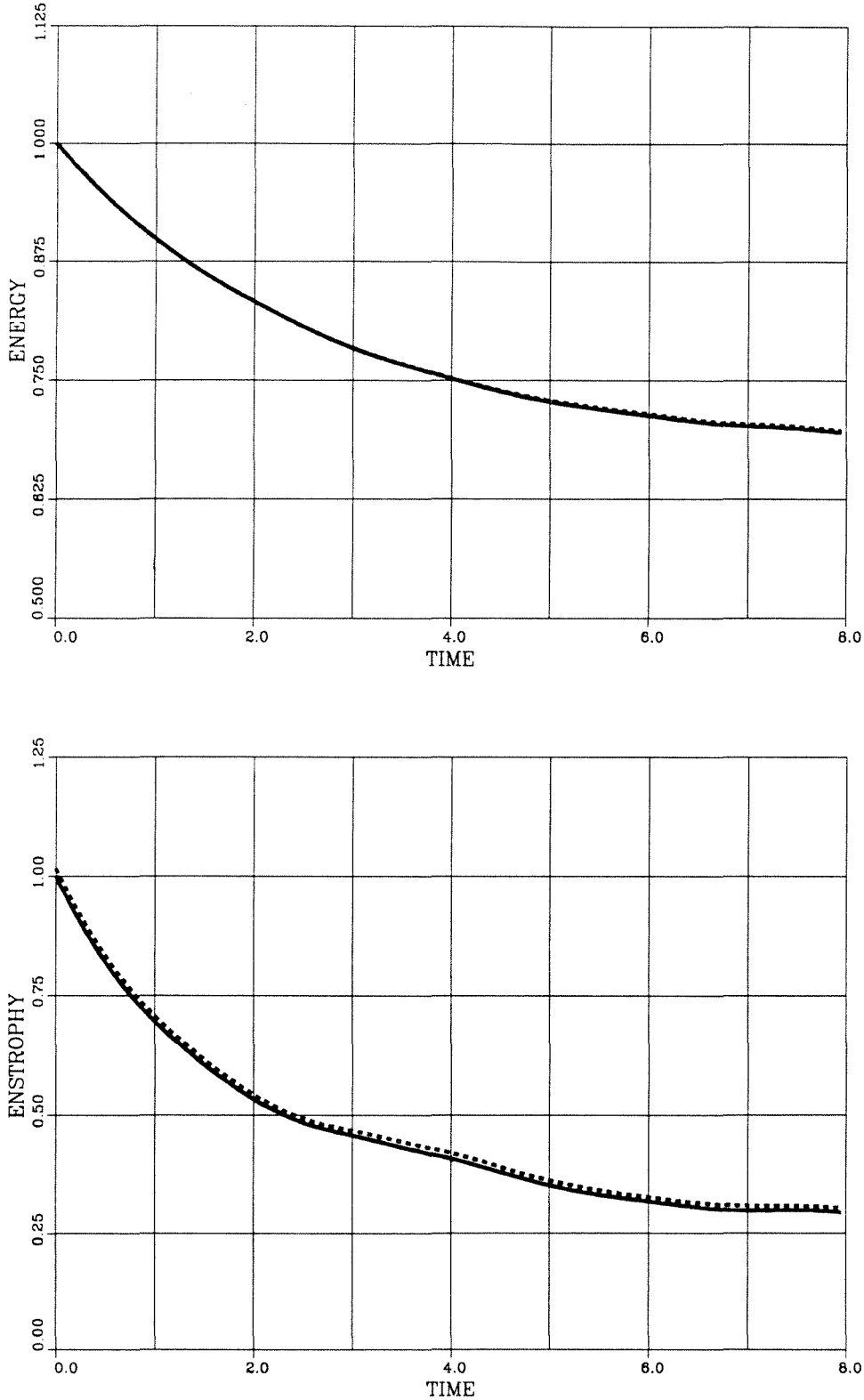

Figure J.43: The fusion of two vortex rings computed with the viscous method of regularized vortex particles. $Re = 400$. Diagnostics I, Γ, $\tilde{E}$ (solid) and $\tilde{E}_f$ (dash), $\tilde{\mathcal{E}}$ (solid) and $\tilde{\mathcal{E}}_f$ (dash).

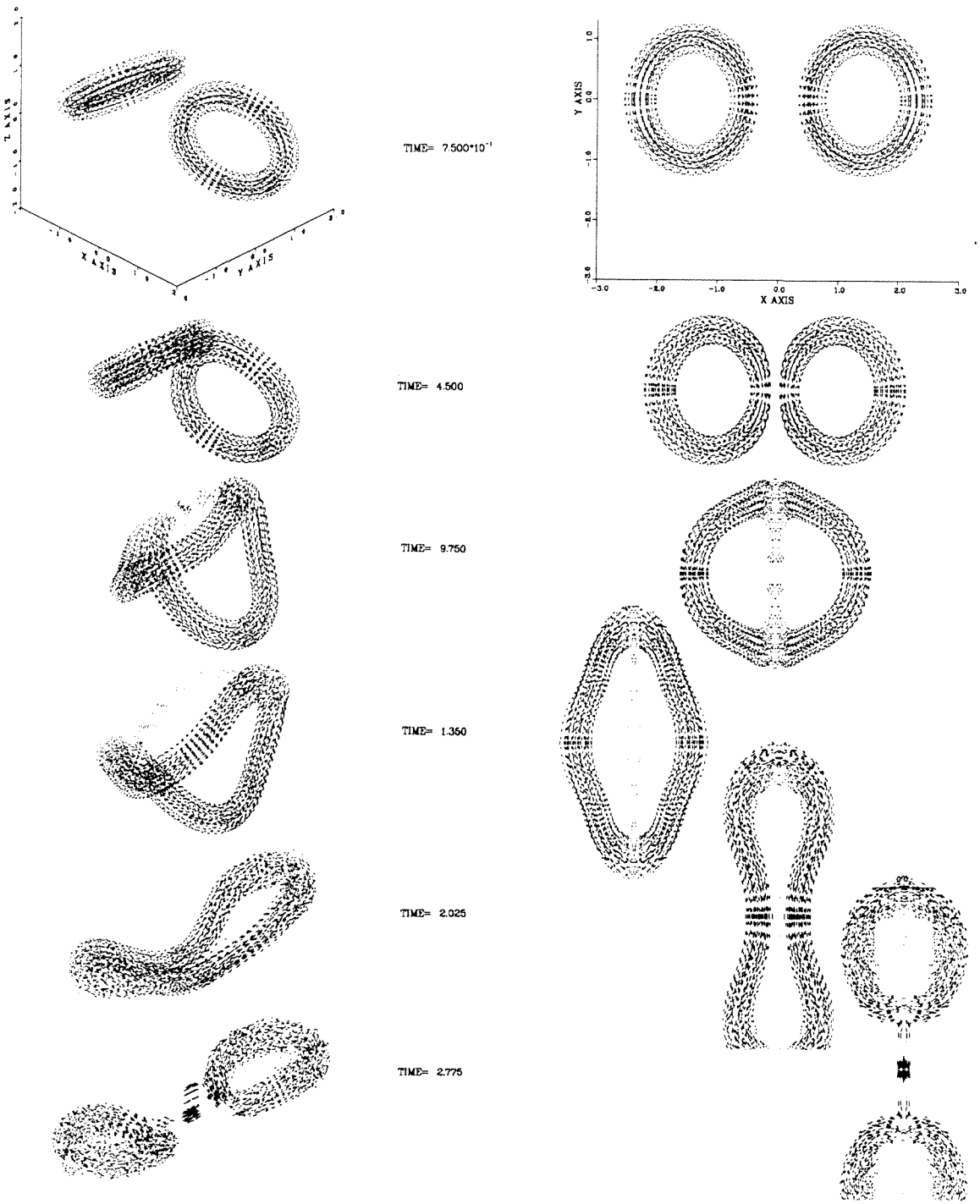

Figure J.44: The fusion and fission of two vortex rings computed with the viscous method of regularized vortex particle. Low resolution computation with transpose scheme. Perspective view of the particle strength vectors α^p.

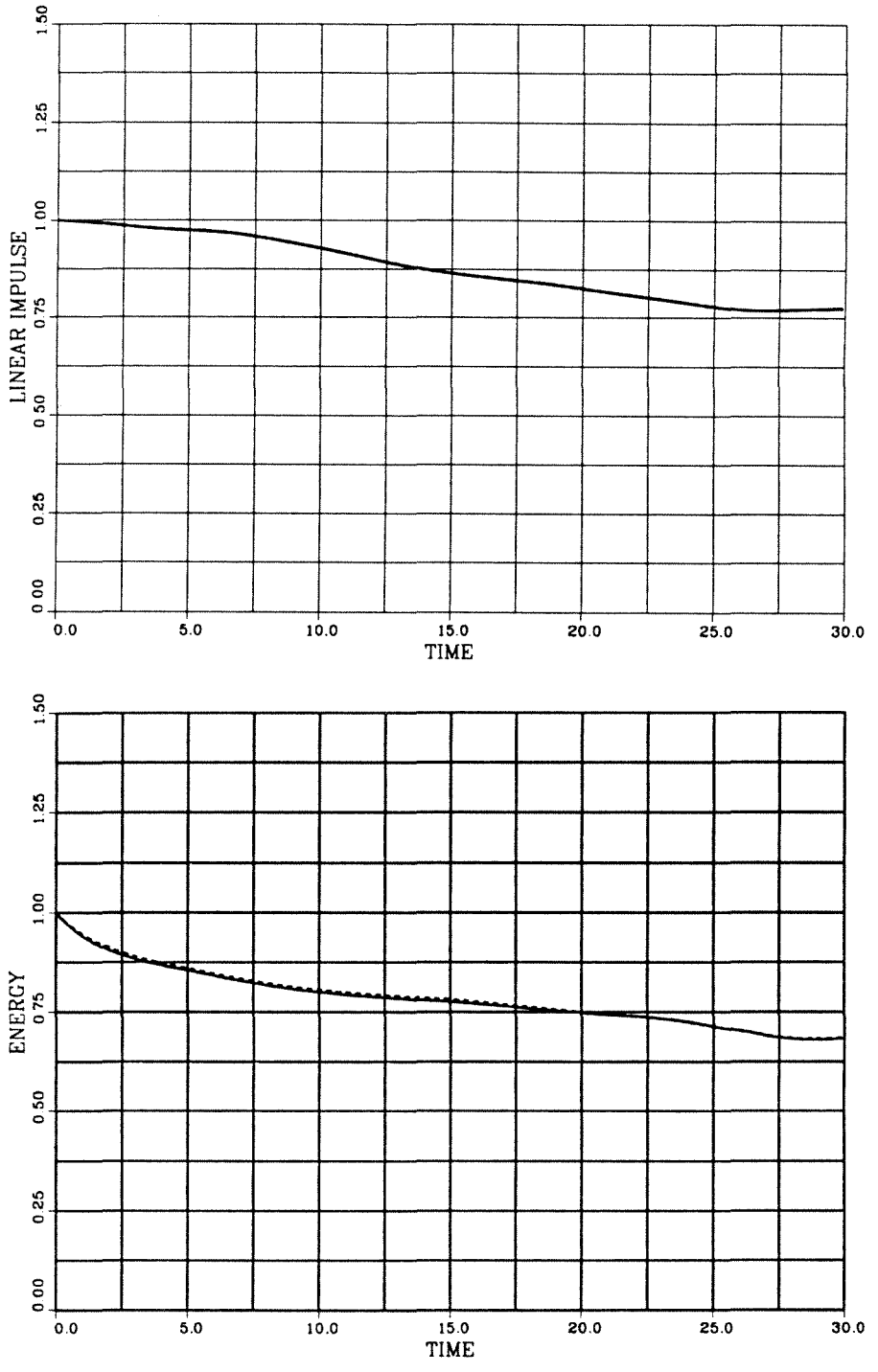

Figure J.45: The fusion and fission of two vortex rings computed with the viscous method of regularized vortex particle. Low resolution computation with transpose scheme. Diagnostics I, $\tilde{E}$ (solid) and $\tilde{E}_f$ (dash).

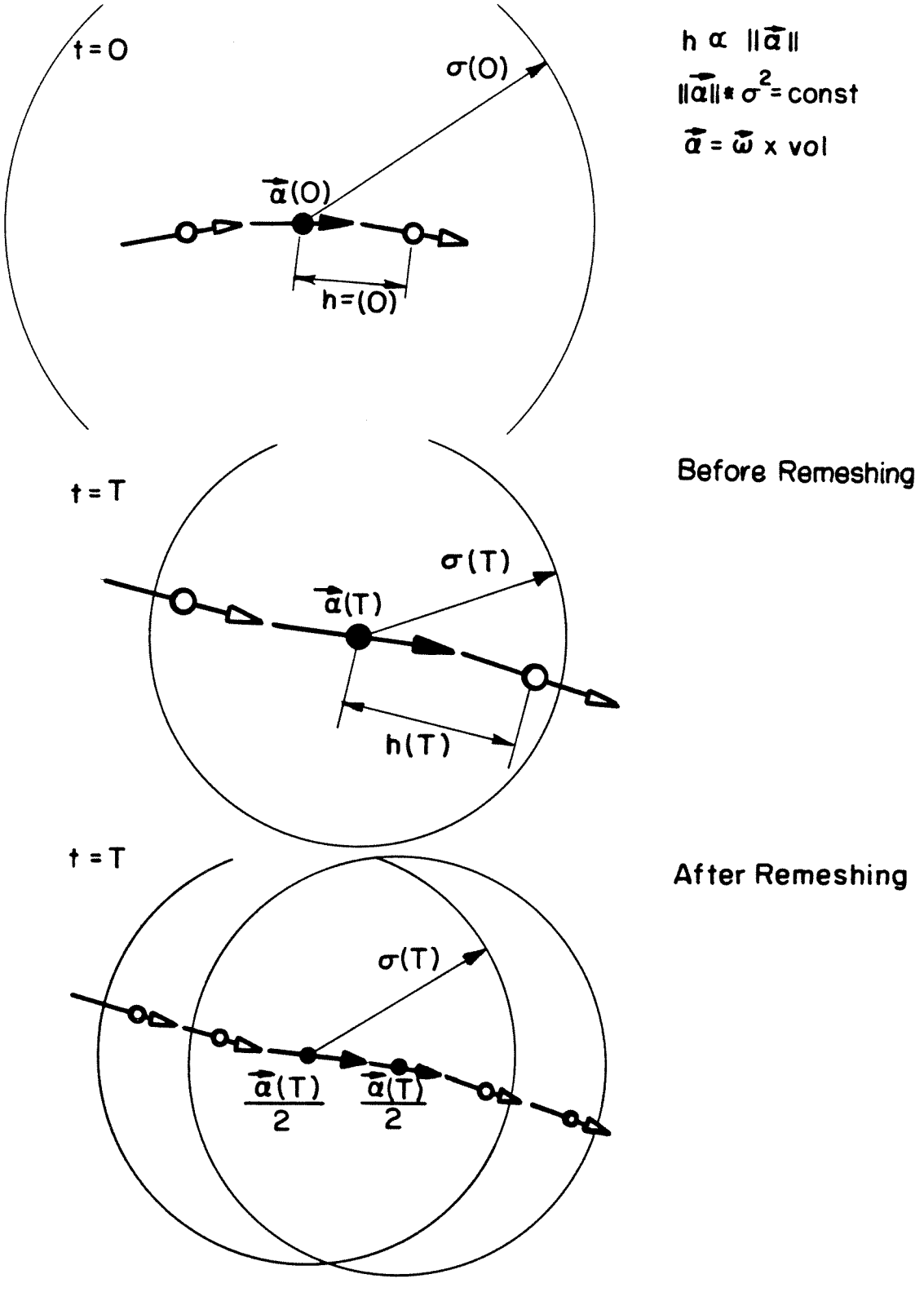

Figure J.46: Remeshing strategy for regularized vortex particles.

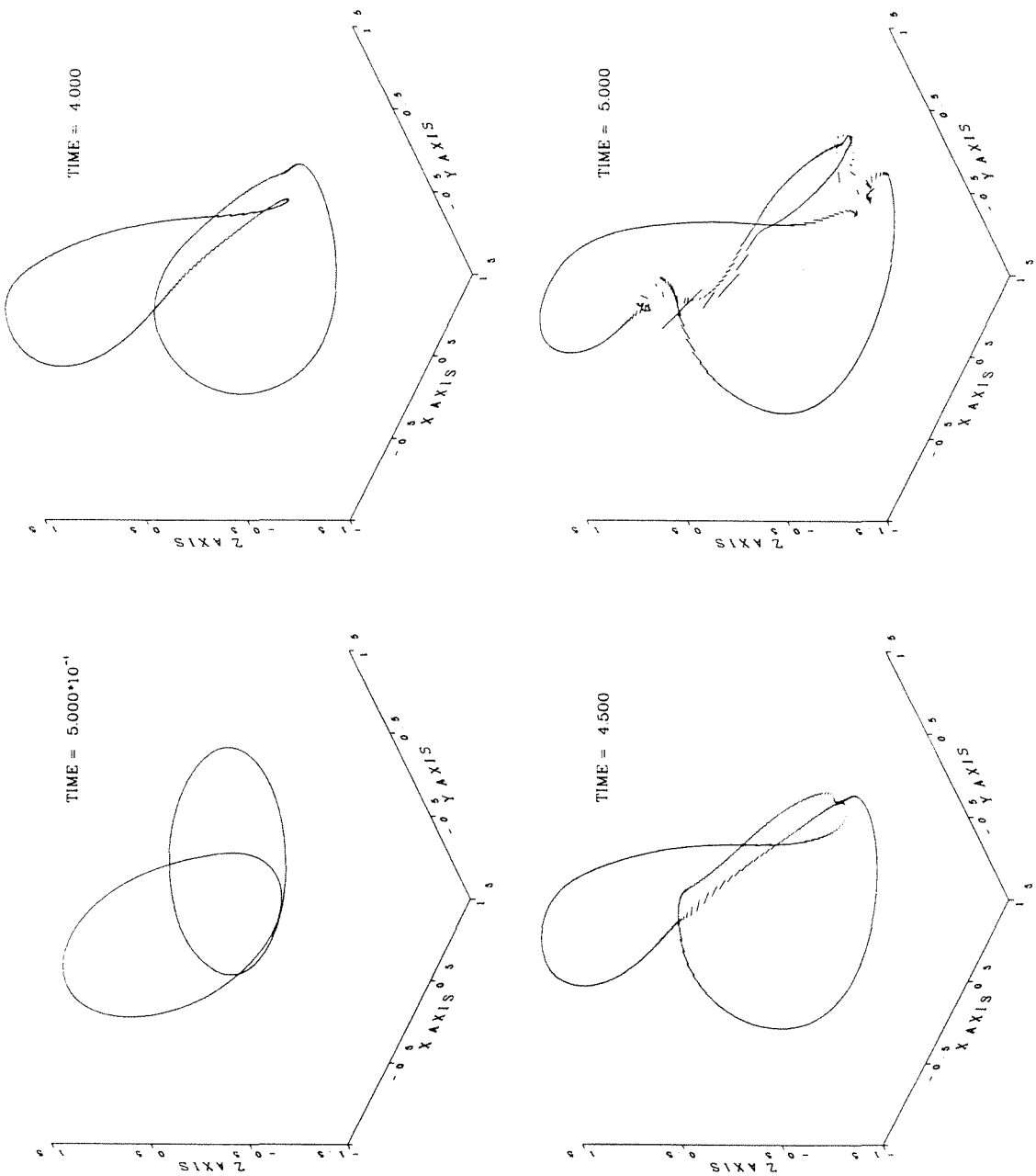

Figure J.47: The "knot" problem computed with the method of regularized vortex particles. No remeshing and no relaxation of the vorticity divergence. Perspective view of the particle strength vectors α^p.

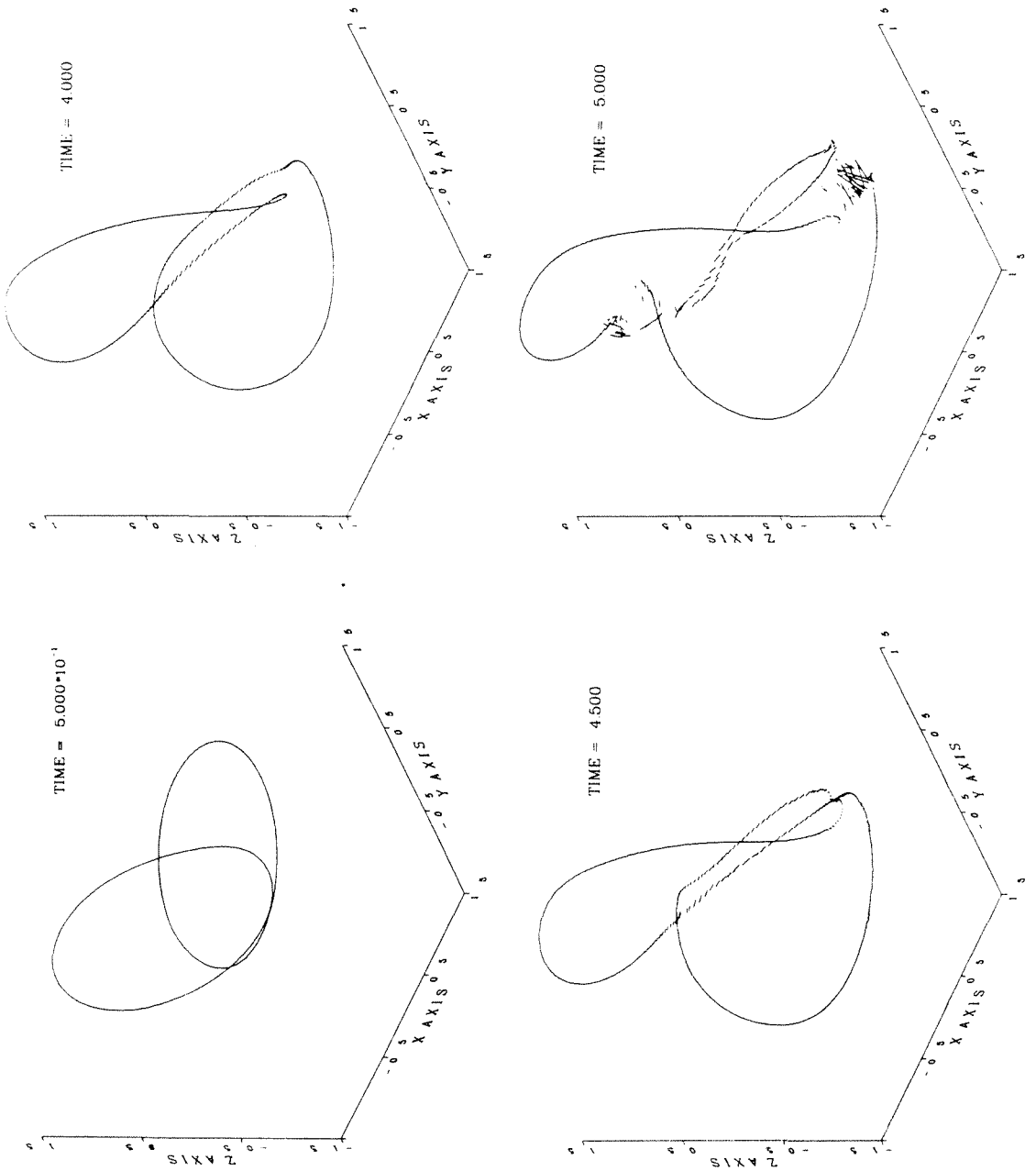

Figure J.48: The "knot" problem computed with the method of regularized vortex particles. Remeshing but no relaxation of the vorticity divergence. Perspective view of the particle strength vectors α^p.

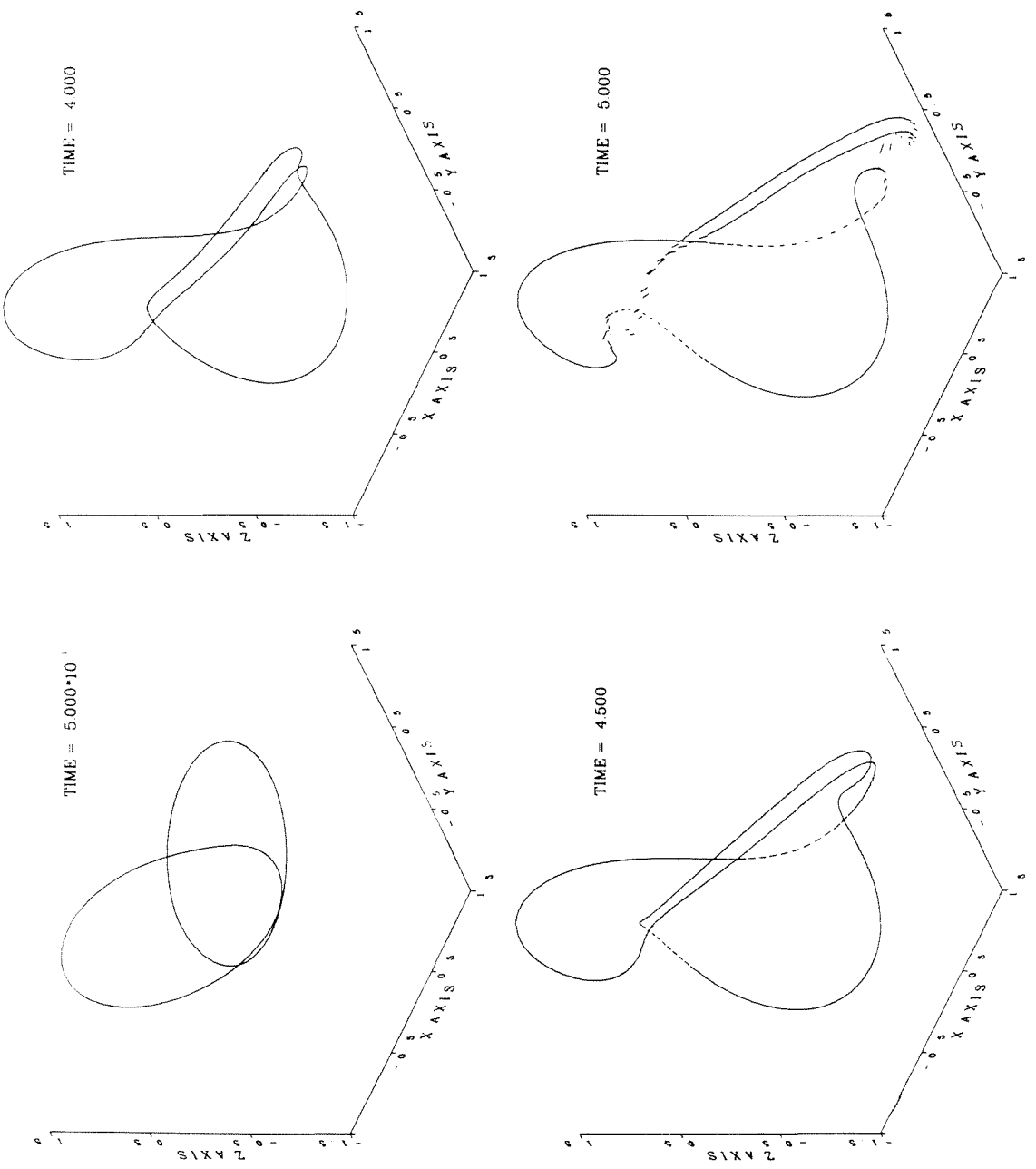

Figure J.49: The "knot" problem computed with the method of regularized vortex particles. No remeshing but relaxation of the vorticity divergence. Perspective view of the particle strength vectors α^p.

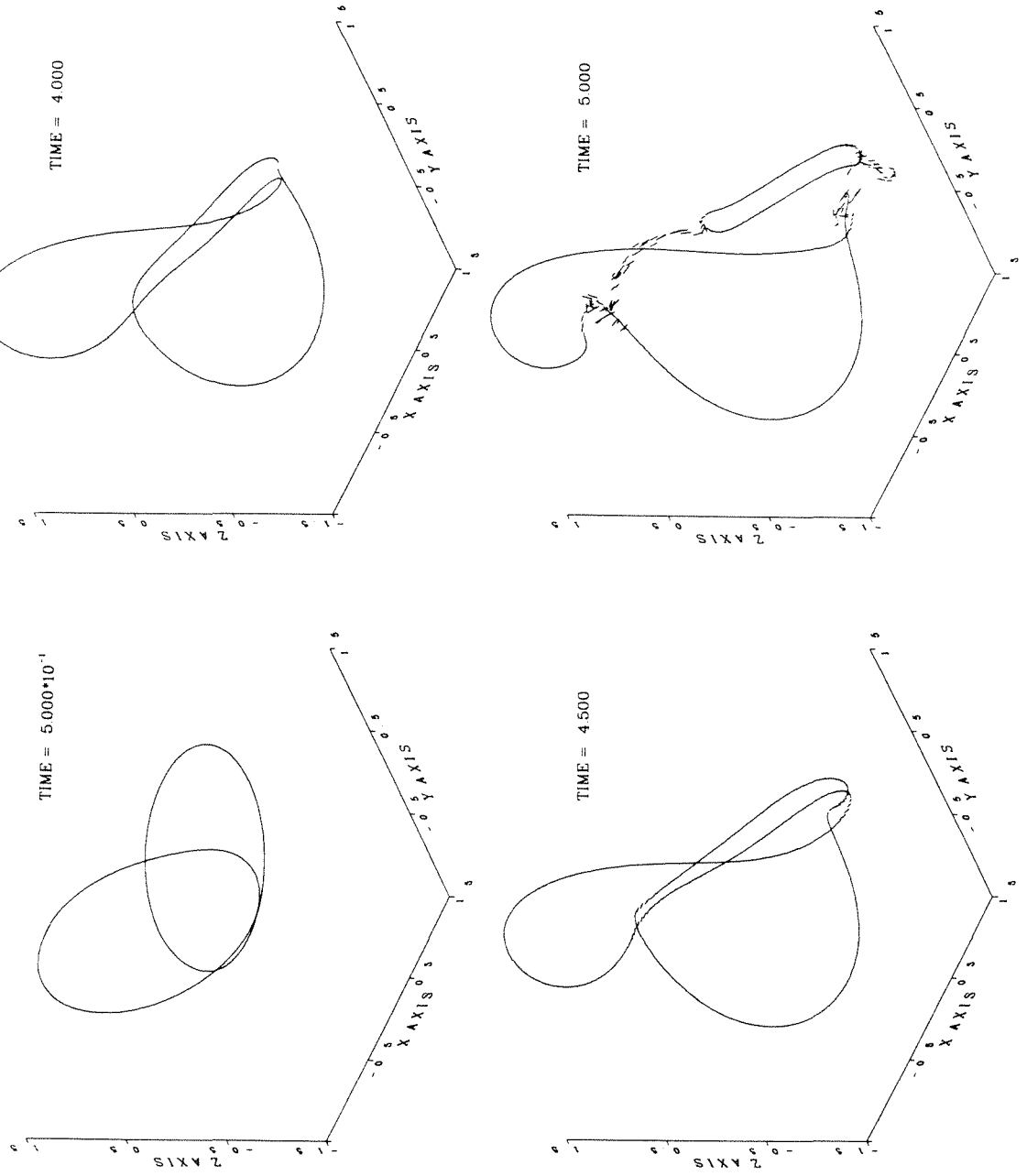

Figure J.50: The "knot" problem computed with the method of regularized vortex particles. Remeshing and relaxation of the vorticity divergence. Perspective view of the particle strength vectors α^p.

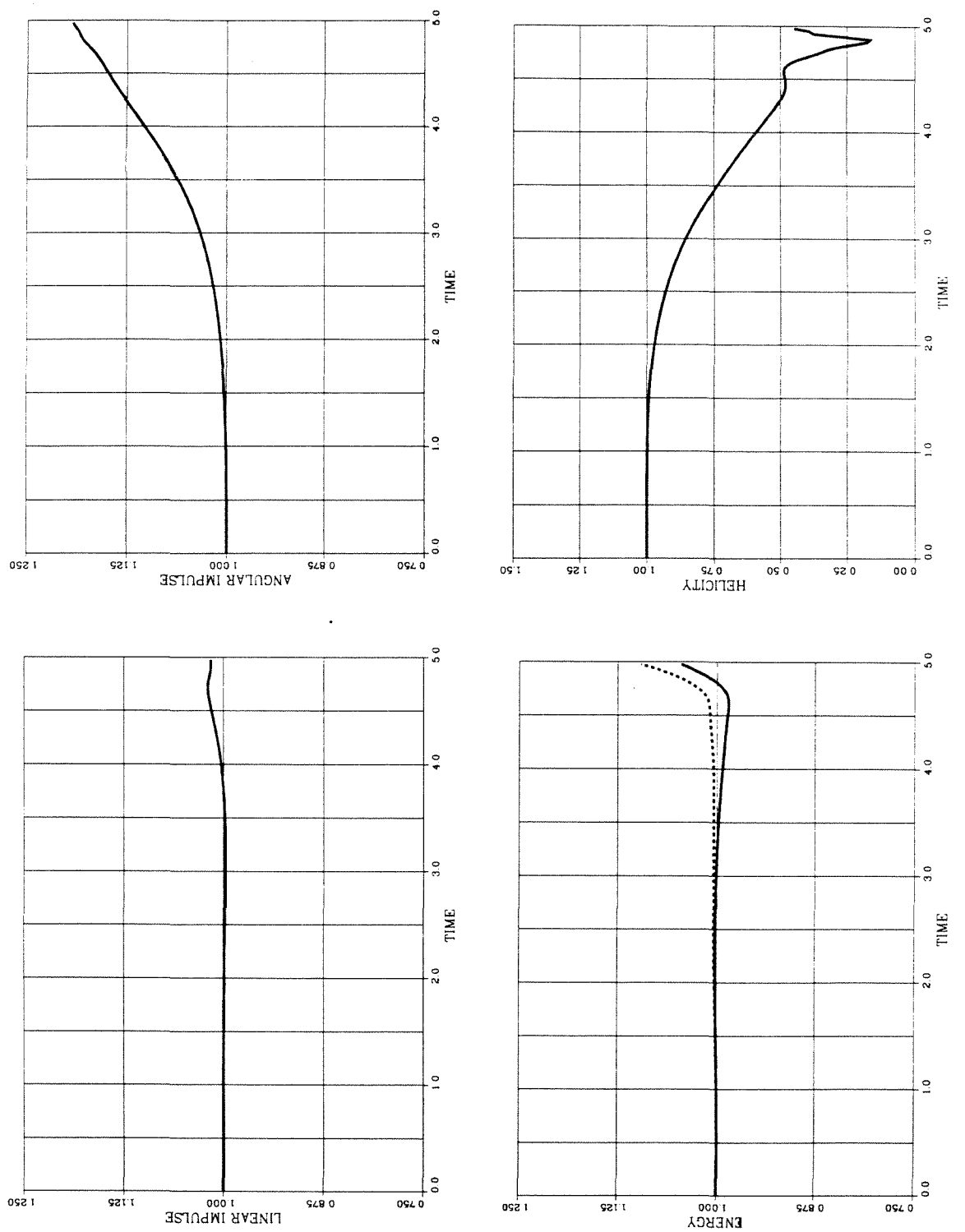

Figure J.51: The "knot" problem computed with the method of regularized vortex particles. No remeshing and no relaxation of the vorticity divergence. Diagnostics I, A, $\tilde{E}$ (solid) and $\tilde{E}_f$ (dash), $\tilde{\mathcal{H}}$.

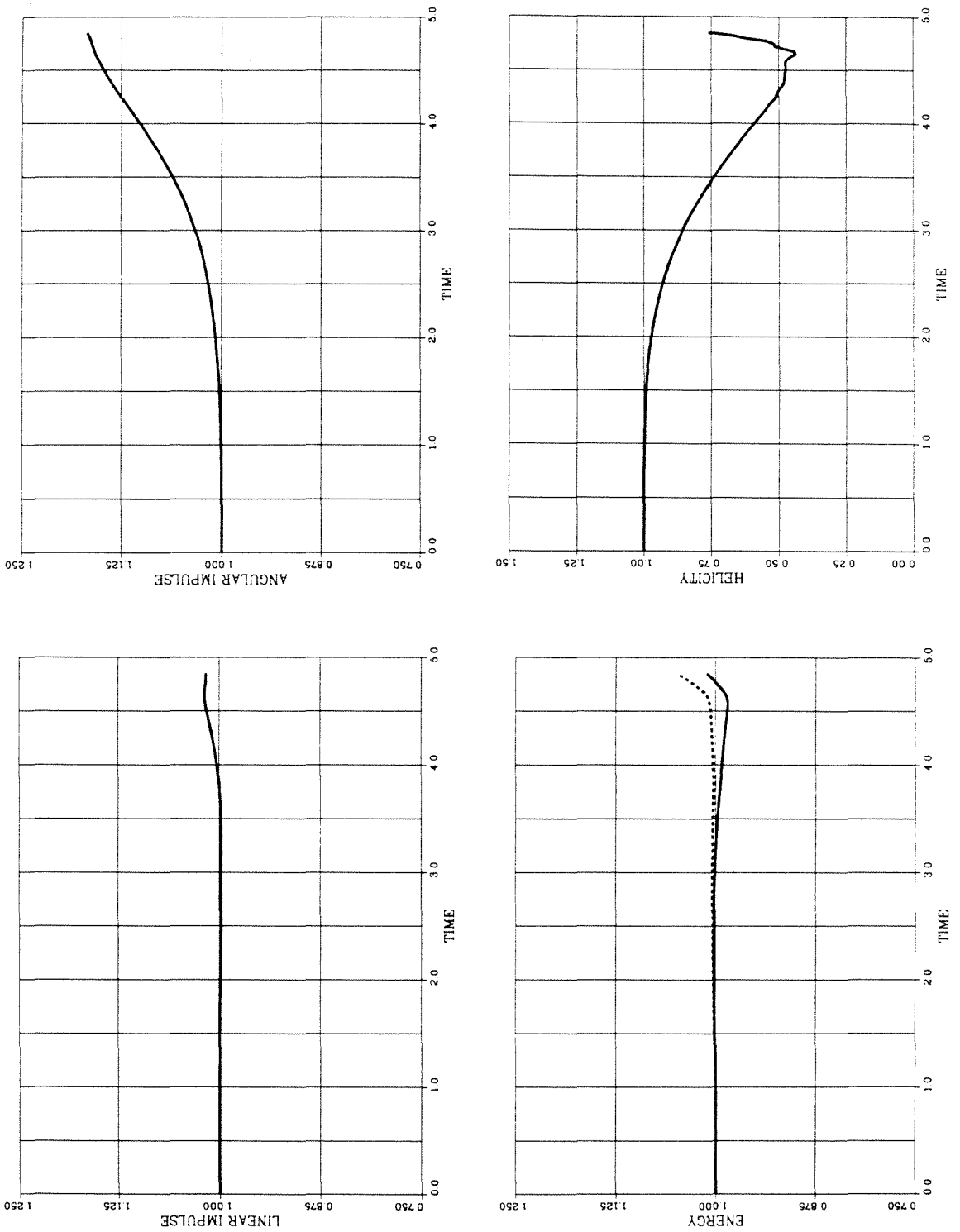

Figure J.52: The "knot" problem computed with the method of regularized vortex particles. Remeshing but no relaxation of the vorticity divergence. Diagnostics I, A, $\tilde{E}$ (solid) and $\tilde{E}_f$ (dash), $\tilde{\mathcal{H}}$.

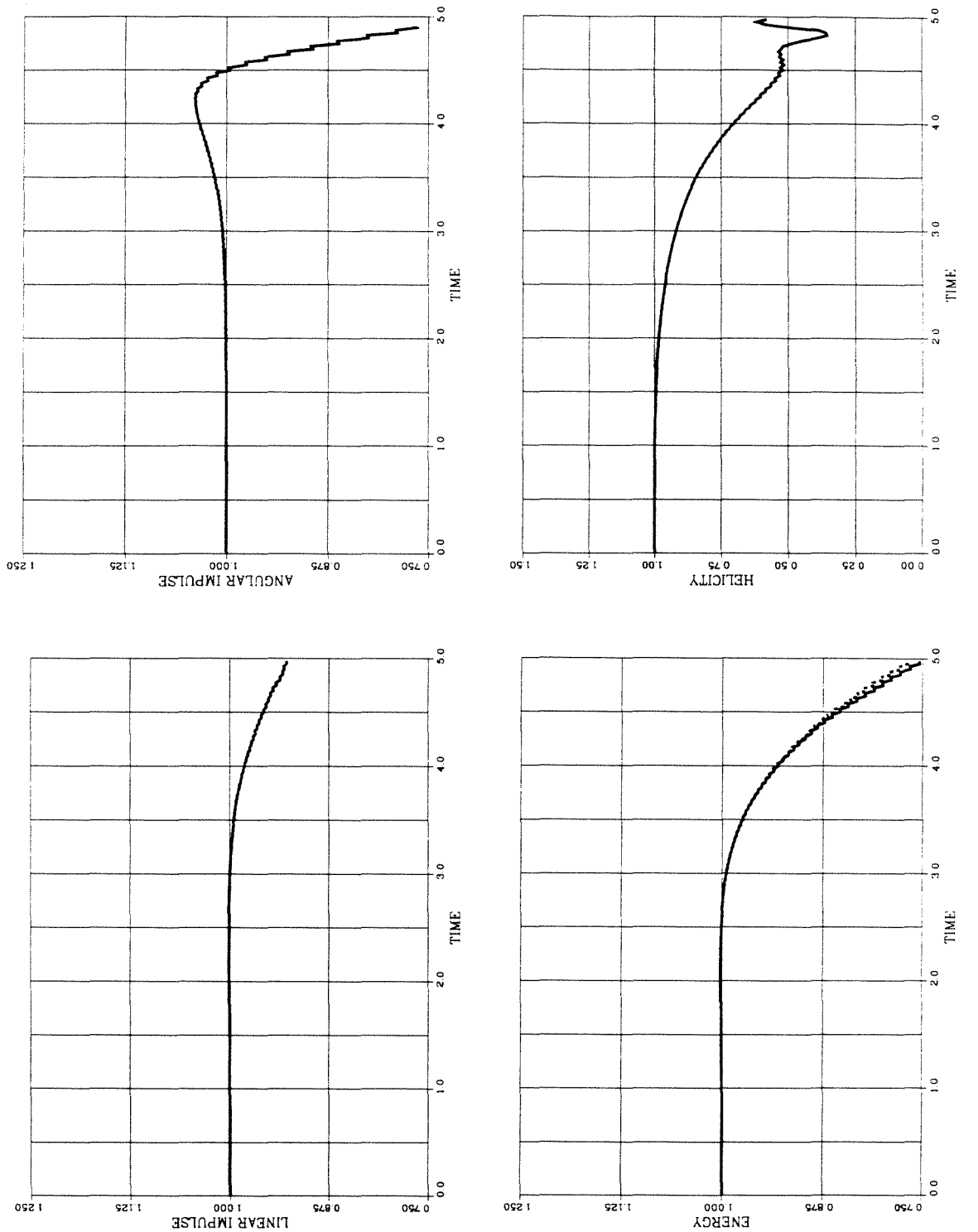

Figure J.53: The "knot" problem computed with the method of regularized vortex particles. No remeshing but relaxation of the vorticity divergence. Diagnostics I, A, $\tilde{E}$ (solid) and $\tilde{E}_f$ (dash), $\tilde{\mathcal{H}}$.

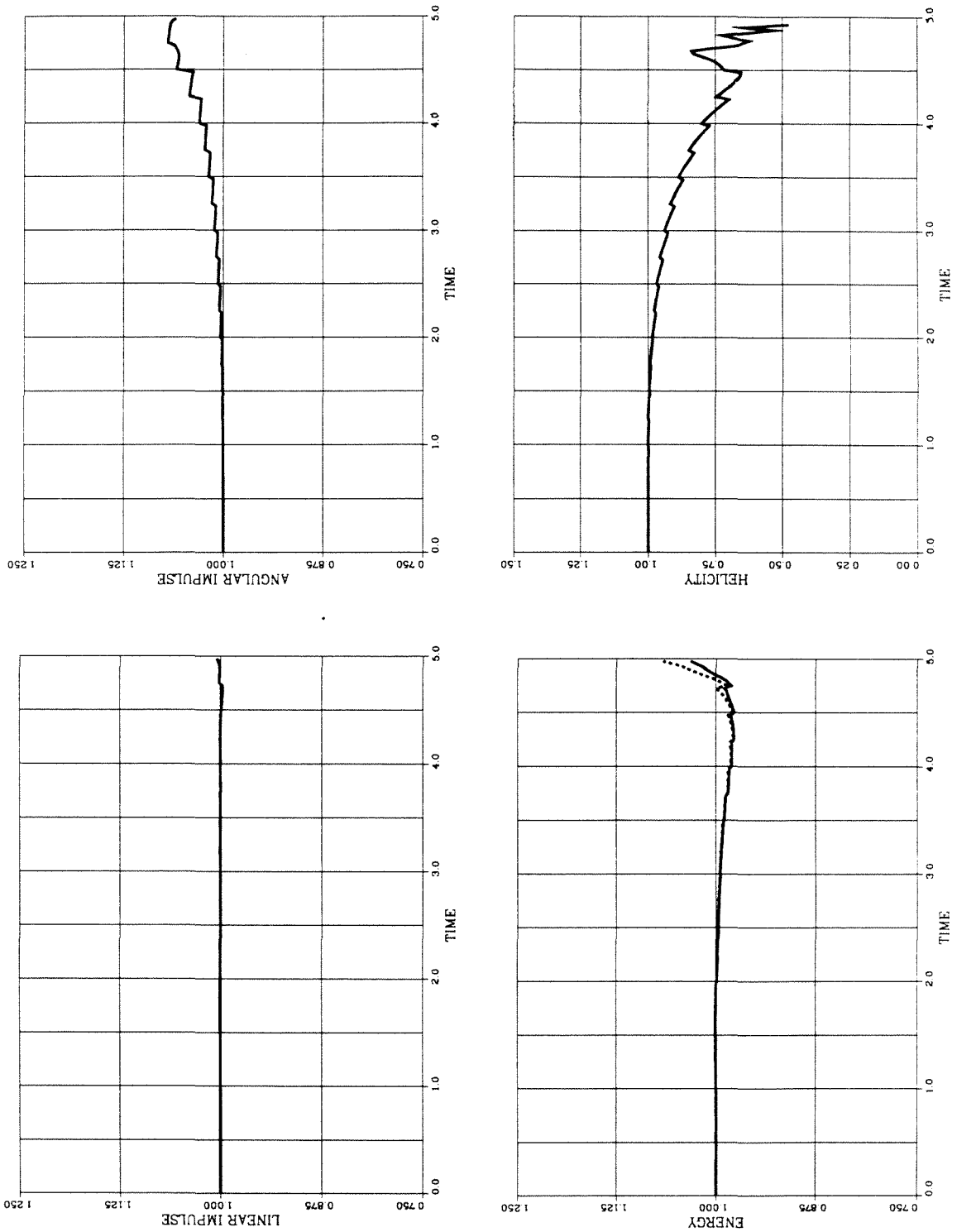

Figure J.54: The "knot" problem computed with the method of regularized vortex particles. Remeshing and relaxation of the vorticity divergence. Diagnostics I, A, $\tilde{E}$ (solid) and $\tilde{E}_f$ (dash), $\tilde{\mathcal{H}}$.

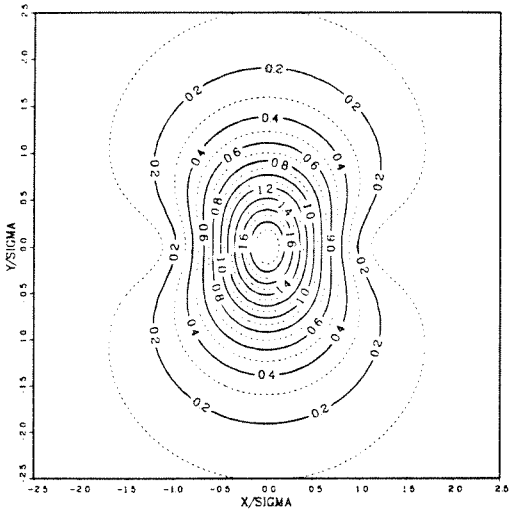

$|\mathbf{u}_\sigma|$

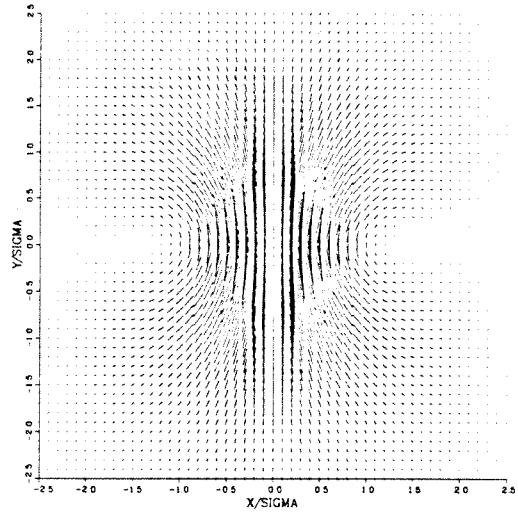

$\mathbf{u}_\sigma$

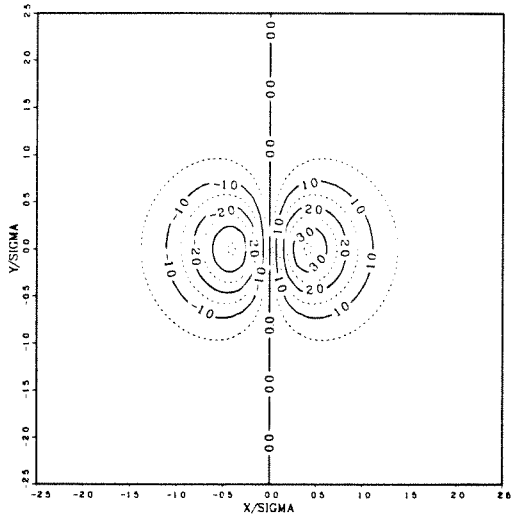

$(\omega_\sigma)_\varphi$

Figure J.55: Vorticity and velocity fields for an isolated three-dimensional regularized vortex-dipole (The low order algebraic smoothing has been used).

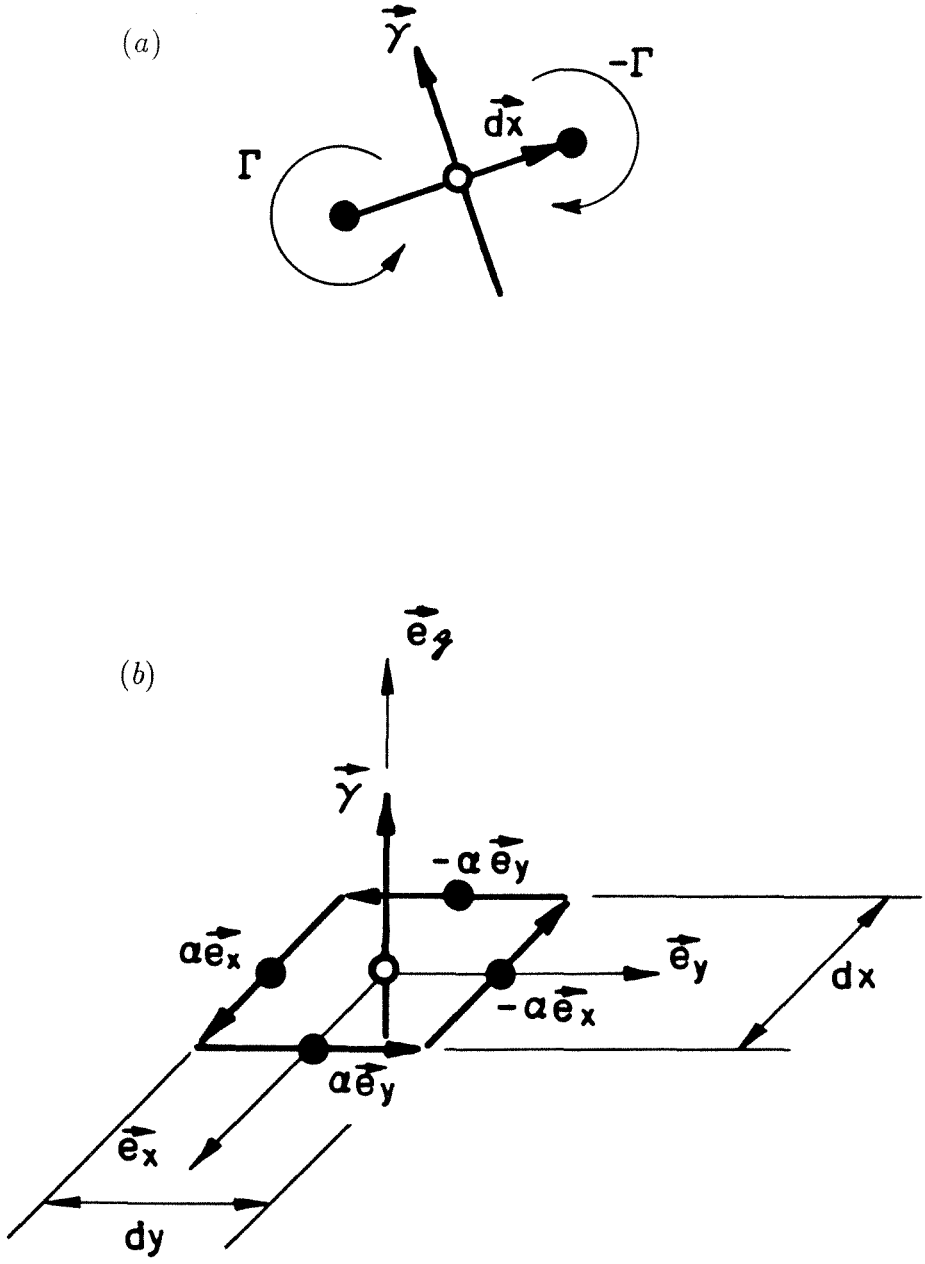

Figure J.56: (a) Two-dimensional regularized vortex-dipole as the limit of two two-dimensional regularized vortex particles. (b) Three-dimensional regularized vortex-dipole as the limit of four three-dimensional regularized vortex particles.

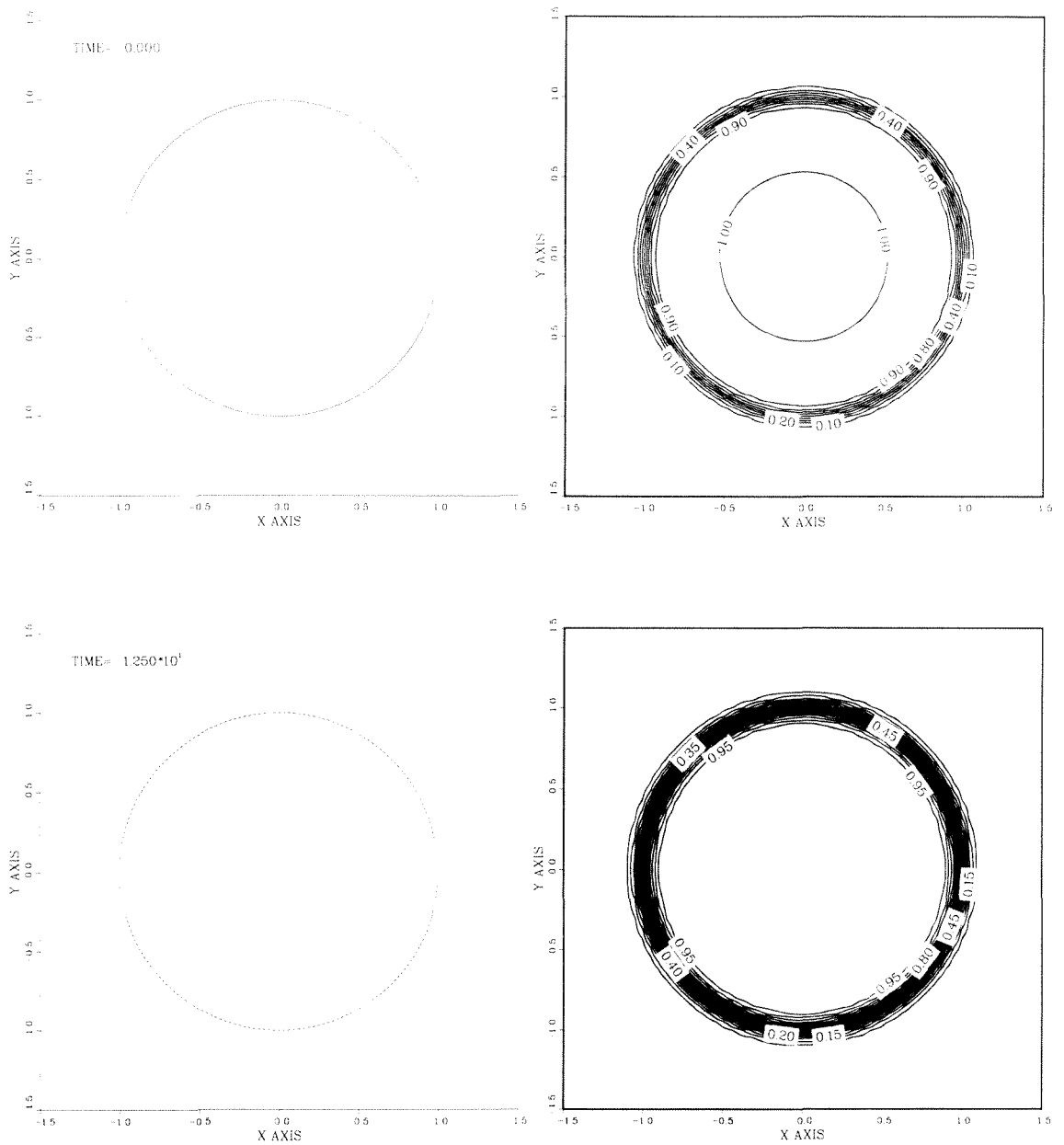

Figure J.57: The short time diffusion of a circular vortex patch of uniform vorticity computed with the method of regularized particles of vorticity gradient: Vectors $\alpha^p \wedge \hat{\mathbf{e}}_z$ (left) , Vorticity contours (right).

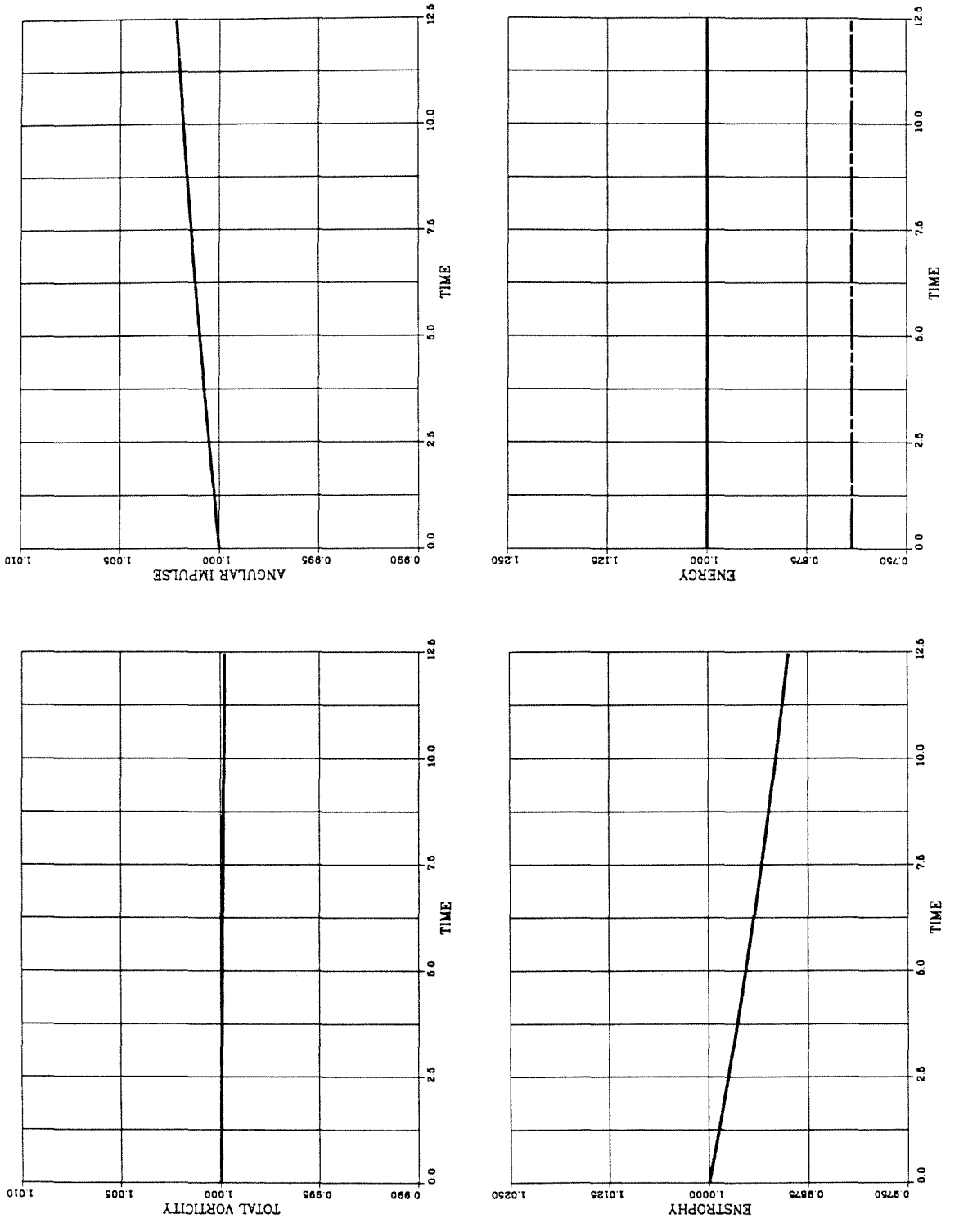

Figure J.58: Diagnostics for the short time diffusion of a circular vortex patch of uniform vorticity computed with the method of regularized particles of vorticity gradient: Ω, A, $\tilde{\mathcal{E}}$, $\tilde{E}$ (solid), E (dash) and E_{cd} (chain-dash).

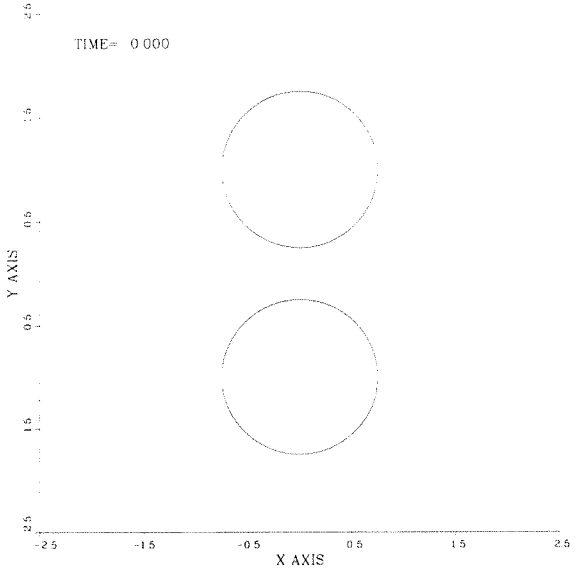
TIME= 0.000
Y AXIS
X AXIS
2.5
1.5
0.5
-0.5
-1.5
-2.5

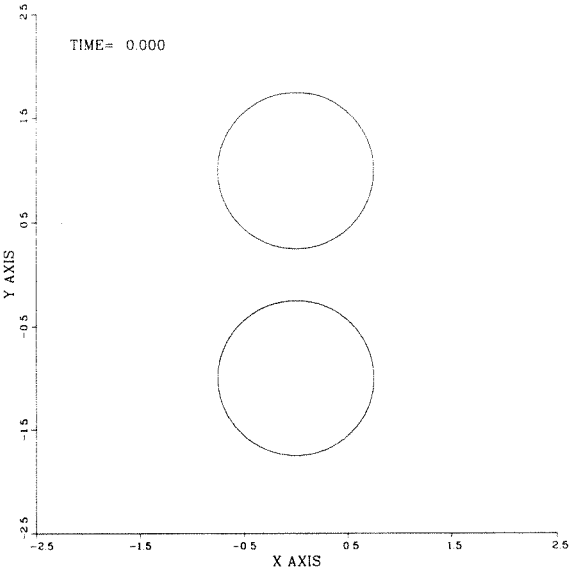
TIME= 0.000
Y AXIS
X AXIS
2.5
1.5
0.5
-0.5
-1.5
-2.5

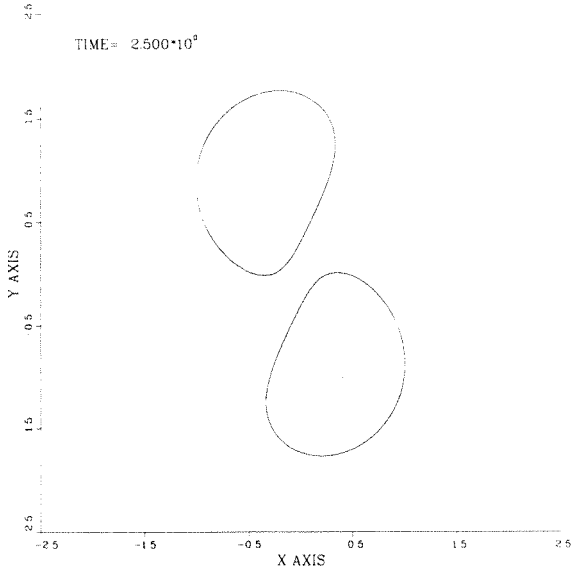
TIME= 2.500*10^0
Y AXIS
X AXIS
2.5
1.5
0.5
-0.5
-1.5
-2.5

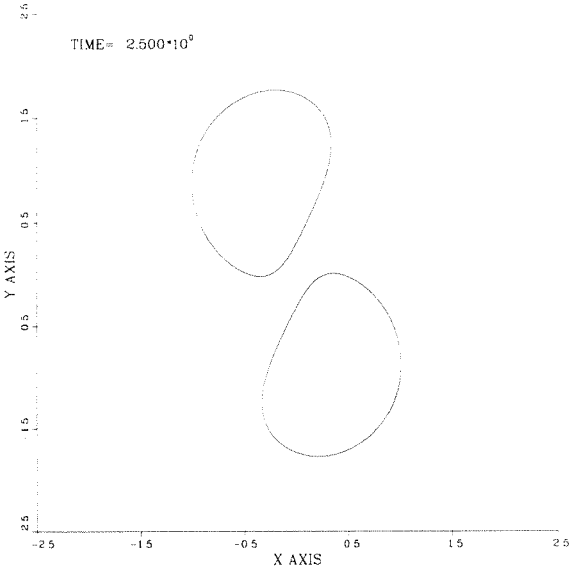
TIME= 2.500*10^0
Y AXIS
X AXIS
2.5
1.5
0.5
-0.5
-1.5
-2.5

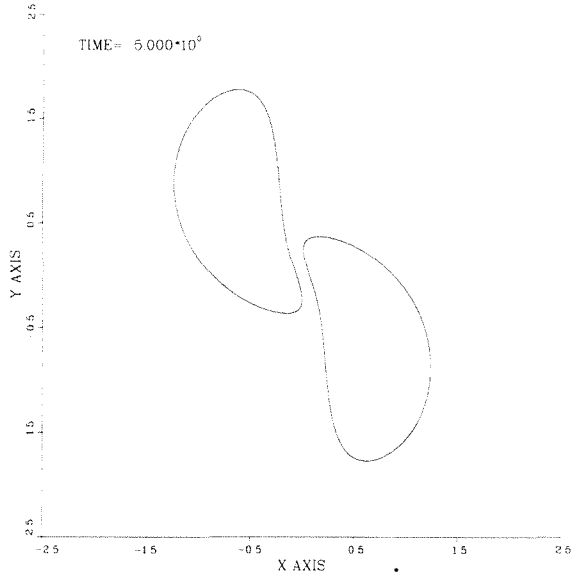
TIME= 5.000*10^0
Y AXIS
X AXIS
-2.5
-1.5
-0.5
0.5
1.5
2.5

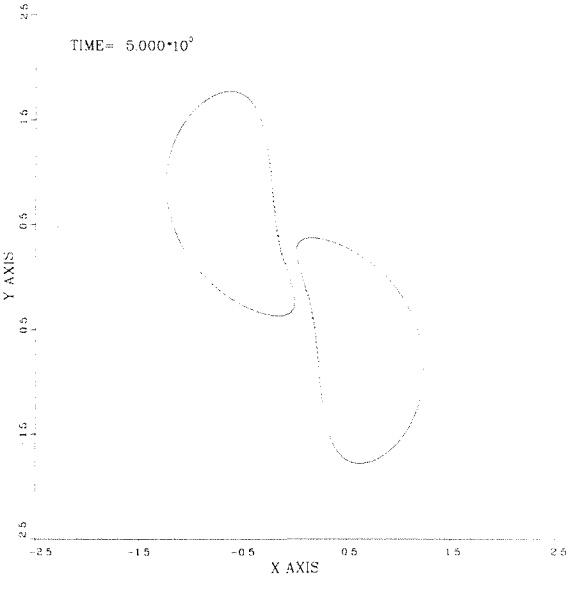
TIME= 5.000*10^0
Y AXIS
X AXIS
-2.5
-1.5
-0.5
0.5
1.5
2.5

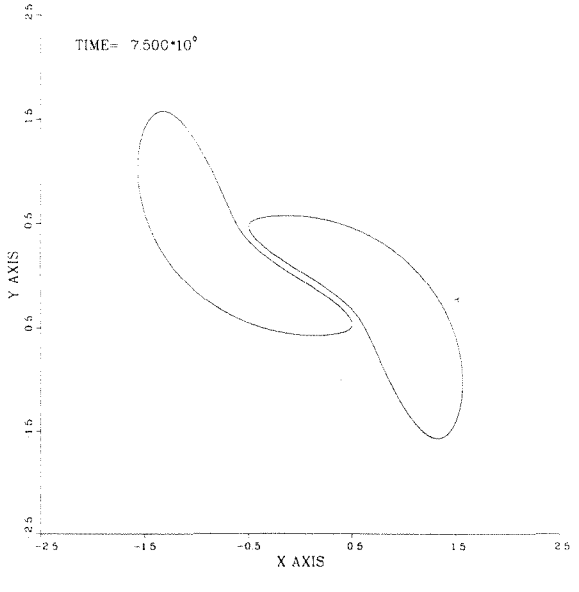
TIME= 7.500*10^0
Y AXIS
X AXIS
-2.5
-1.5
-0.5
0.5
1.5
2.5

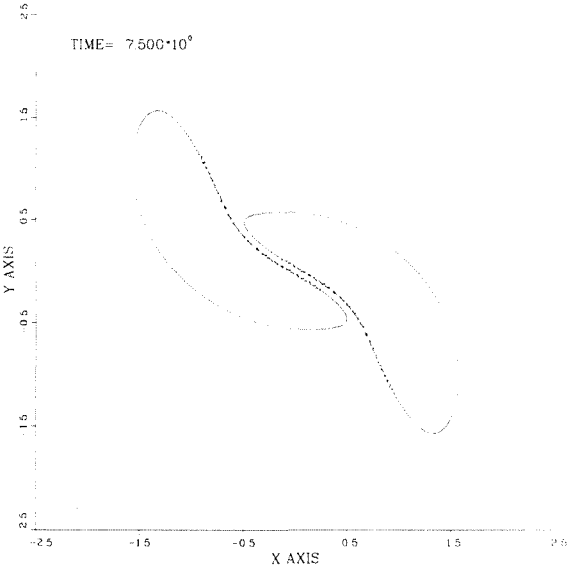
TIME= 7.500*10^0
Y AXIS
X AXIS
-2.5
-1.5
-0.5
0.5
1.5
2.5

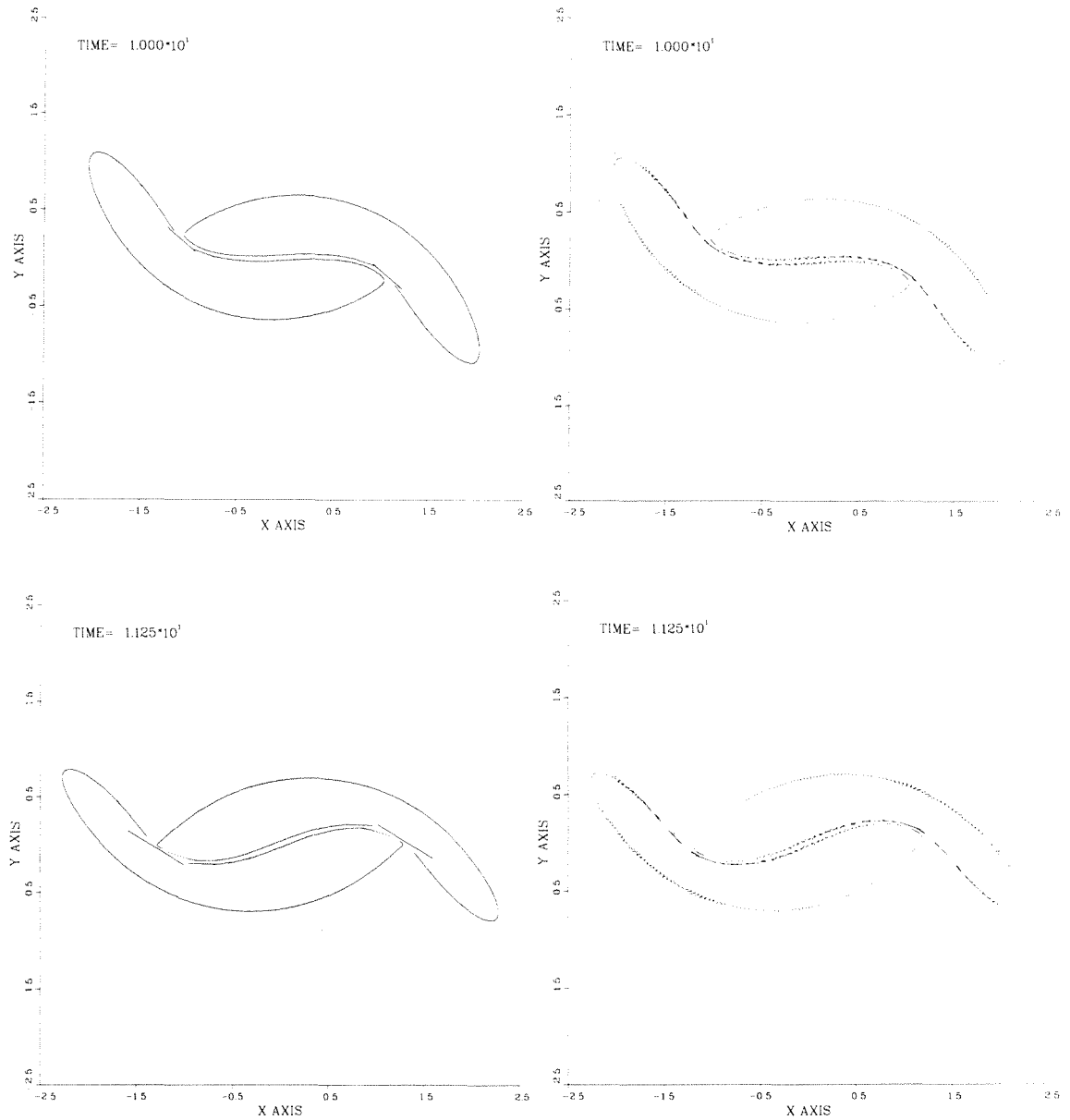

Figure J.59: The short time interaction between two vortex patches of uniform and same sign vorticity computed with the method of regularized particles of vorticity gradient. Vectors $\alpha^p \wedge \hat{\mathbf{e}}_z$: inviscid (left), viscous (right).

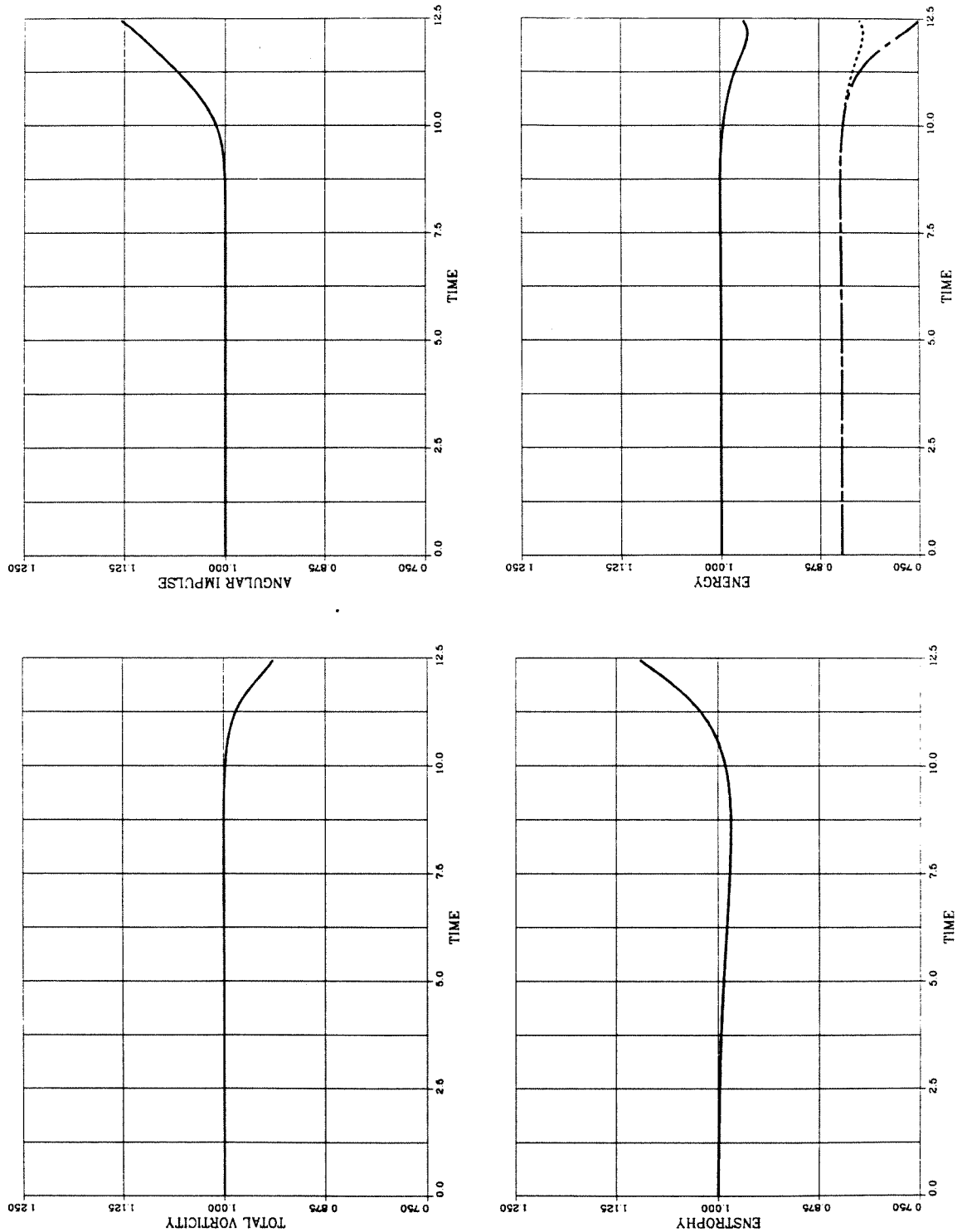

Figure J.60: Diagnostics for the short time inviscid interaction between two vortex patches of uniform and same sign vorticity computed with the method of regularized particles of vorticity gradient: Ω, A, $\tilde{\mathcal{E}}$, $\tilde{E}$ (solid), E (dash) and E_{cd} (chain dash).

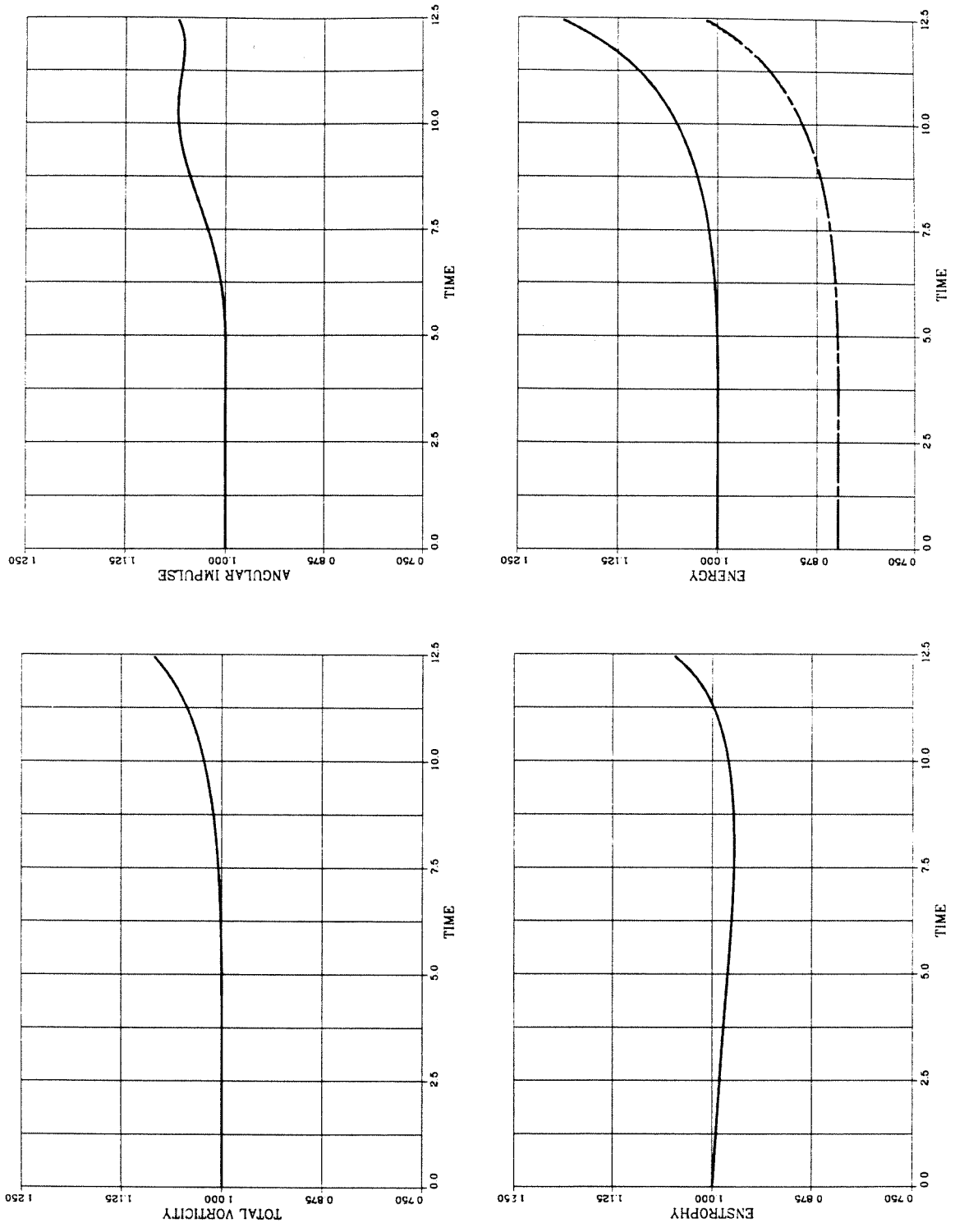

Figure J.61: Diagnostics for the short time viscous interaction between two vortex patches of uniform and same sign vorticity computed with the method of regularized particles of vorticity gradient: Ω, A, $\tilde{\mathcal{E}}$, $\tilde{E}$ (solid), E (dash) and E_{cd} (chain dash).